UNIVERSITY OF THE
WITWATERSRAND,
JOHANNESBURG

DESIGN AND SYNTHESIS OF CHRONIC WOUND HEALING COLLAGEN PEPTIDE MIMICS

NTLAMA FRANCIS LESOTHO

DECLARATION

I, Ntlama Lesotho, declare that this thesis is my own unaided work. From its inception to completion, it has been supervised solely by Dr Maya Mellisa Makatini. It is submitted for examination for the degree of Doctor of Philosophy at the University of Witwatersrand. It has not been submitted before for any degree or examination at any other University. Any other work employed to help explain different concepts in this thesis is duly referenced.

March 2024

Date

Ntlama Francis Lesotho

March 2024

Date

Dr Maya Mellisa Makatini

(Supervisor)

DEDICATION

I dedicate this thesis to my late loving parents, Mr. Malefetsane Peter Lesotho and Mrs. Maliokhoane Mary Lesotho.

PUBLICATIONS

Lesotho N, Peme T, Makatini M. Design, synthesis, and characterization of type I collagen mimetic peptides. *J Pept Sci.* 2023;e3531. doi:10.1002/psc.3531

ACKNOWLEDGEMENTS

My precious Father, my Lord and God, thank you for the glory, excellence and love you deposited in me. I am so thankful I did not disappoint you. Countless times you said to me, “do not be afraid, neither be dismayed for I am with you. I will not fail you nor forsake you” (**Joshua 1:6**).

Dr. Maya, my supervisor, thank you. All the sacrifices you went through, particularly towards the end of this journey will forever remain indelible and etched on my mind. Many thanks for your benevolence, support, encouragement and motivation.

My beloved family, thank you so much for your patience and love. Malesotho, my beloved wife, even this storm was not strong enough to create a gulf between me and you, thank you. Nosizwe and Joel, my lovely children, thank you for always cheering me on. I love you big.

Ausi Puleng, Ausi Thandiwe, Abuti Sehloho and Abuti Manterna, it is finally done. Thank you for endless encouragement, and love. I owe you one.

Dr. Peme thank you for being there all the time I needed help. You have been awesome. To the rest of my colleagues, Dr. Thando, Priscilla Nyembe, Ntombizanele Ngqinayo, Khanani Machumele, Refilwe Moepye and Thapelo Mbhele, thank you. You have been so tolerant and loving towards me. May the Lord bless you.

To everyone in the stores, Mr. David Moloto and Mr. Valoyi, thank you for making this journey a lot easier for me. You never failed to smile back whenever I got to your office. You are an asset to the School of Chemistry.

Prof. Nqosa Mahao and Prof. Mosito, thank you so much for your unwavering support and confidence you have always had in me. Your support has been invaluable to say the least. A hearty ‘thank you’ for making it possible for me.

This research was made a lot easier because of the generous financial contributions of National University of Lesotho, National Manpower Development Secretariat, The National Research Foundation (NRF) Thuthuka award (Gun 117975) and CSUR award (Gun 138081) and The Witwatersrand University.

ABSTRACT

The South African wound care management market is expecting a compound annual growth rate (CAGR) of 6.75%. The numbers are expected to further increase because South Africa has the highest number (4.6 million) of people living with diabetes in Africa. Annually approximately 2% of patients with diabetes develop diabetic foot ulcers and hence chronic wounds. Many chronic wound patients must deal with the financial burden, as many current wound treatment options are expensive, ineffective, and inconvenient.

Intervention in the form of synthetic collagen mimetic peptides has been limited due to cytotoxicity and susceptibility to protease degradation. These challenges have, for an ardent time affected the clinical and commercial development of synthetic wound healing peptides. The aim of the current study is to develop novel wound healing peptides by derivatizing bioactive peptides into selective and protease stable peptidomimetics. All the synthesized peptides are meant to mimic the function of collagen type I. Thus, the designed peptides comprise of the *retro*- integrin binding type I collagen motif, -GFOGER-, the DGD tripeptide for attraction of growth factors, the *retro*- tripeptides Thr-Thr-Lys (TTK), Gly-His-Lys (GHK), Gln-Pro-Arg (QPR) and Glu-Glu-Met (EEM) to stimulate collagen production.

The importance of collagen is evidenced by the fact that it features in all four stages of wound healing. This therefore means, its inclusion in any biomaterial meant to curb chronicity in wound healing is indispensable. With this approach, the biomaterial would overcome the challenge of excess matrix metalloproteinases (MMPs), which degrade both viable and nonviable collagen used in the wound healing process. It would further provide a collagen-based wound scaffold that compensates for the loss of collagen required for proper tissue regeneration. The applications of collagens in wound healing are immense. Due to its material properties, and apparent effectiveness, collagen has the potential to be utilized as an unprecedented treatment protocol for chronic, slow-healing wounds.

Sixteen palmitate and adamantane collagen mimetic peptides were designed and successfully synthesized using the solid-phase peptide synthesis strategy. Eight of the sixteen peptides comprise of lipophilic moieties (adamantane and palmitic acid) for improved membrane permeability and different collagen inducing *retro*-tripeptides namely, TTK, GHK, QPR and

EEM (*retro*-DGD-GG-GFOGER-GG-TTK-Adamantane (NL010)/palmitate (NL009), *retro*-DGD-GG-GFOGER-GG-GHK-Adamantane/palmitate, *retro*-DGD-GG-GFOGER-GG-QPR-Adamantane/palmitate and *retro*-DGD-GG-GFOGER-GG-EEM-Adamantane/palmitate). Another eight are control peptides without the *retro*-tripeptides (*retro*-DGRGOF-Adamantane/palmitate, *retro*-GOP-GFOGER-GOP-Adamantane/palmitate, *retro*-GG-GFOGER-GG-Adamantane/palmitate and *retro*-DGD-GG-GFOGER-GG-Adamantane (NL008)/palmitate).

The tertiary structure and secondary features (folding patterns) of the peptides were determined using the Nuclear Magnetic Resonance (NMR) and Circular Dichroism (CD). From NMR experiments, medium-range couplings were detected for NL010 and NL009, suggesting a possibility of *alpha* helices. Temperature ^{1}H NMR experiment for the peptide DGRGOF-Adamantane proved the presence of *cis* and *trans* geometric isomers. CD experiments revealed that NL009 mainly has α-helix while NL010 mainly consists of a parallel conformation.

Synthesis of adamantane and palmitate peptides with enhanced integrin binding was accomplished by incorporation of *para*-fluorophenylalanine in place of phenylalanine in the peptide *retro*-GG-GFOGER-GG-Adamantane/palmitate. The peptides were obtained in low yields but with increased hydrophobicity.

Structural features for the improvement of the stability of the peptides against protease degradation were accomplished by the synthesis of peptoids and *N*-methylated peptides. The peptoids were synthesized in low yields but with increased hydrophobicity.

The efficacy of NL009 and NL010 in wound healing was tested both *in vitro* and *in vivo*. In the former, the efficiency of both NL009 and NL010 in inducing migration of cells in a scratch wound was accentuated by hyaluronic acid. In *in vivo* studies, NL010 performed better than NL009. However, NL010 was outperformed by a comparator, Puramatrix®

The peptides have the ability to induce migration of cells and therefore have an ability to create an environment needed for proper wound healing. The peptides could be used in place of native collagen and bring about proper healing of wounds.

THESIS OUTLINE

The study is presented in ten parts. **Chapter I** consists of the introduction, literature review, design and the study hypothesis.

Chapter II, the first part of this study provides a formal description of the design and synthesis of novel palmitate collagen I mimetic peptides, DGD-GG-GFOGER-GG-TTK/GHK/QPR/EEM-palmitate. Nuclear magnetic resonance (NMR) spectroscopy is utilized to elucidate the tertiary structure while the secondary structure of the peptides is determined by employments of circular dichroism (CD). NMR spectroscopy revealed that the peptides have a partial α-helical structure. CD measurements further confirmed that the adamantane collagen I mimetic peptides mainly exist in the α-helical structural conformation.

Chapter II consists of a publication made in Journal of Peptide Science (Lesotho N, Peme T, Makatini M. Design, synthesis and characterization of type I collagen mimetic peptides. J Pept Sci. 2023;e3531. doi:10.1002/psc.3531)

The second part, **Chapter III,** describes the design and synthesis of collagen mimetic peptides synthesized in first part of the study, however, with a lipophilic cage moiety that possesses a much-reduced surface area (cage moiety), adamantane. In comparison with the palmitate collagen mimetic peptides in first part of the study, these peptides are synthesized with relatively lower yield. CD experiments reveal that the peptides mainly have parallel *beta* sheet conformation.

The third part, **Chapter IV** of the study describes the structural elucidation of adamantane collagen I mimetic peptides synthesized in the second part of the study using NMR spectroscopy. NMR spectroscopy revealed that the adamantane collagen I mimetic peptide *retro*-DGD-GG-GFOGER-GG-TTK has a partial α-helical structure.

Chapter V, the fourth section, describes the design and synthesis of fluorinated adamantane and palmitate peptides by incorporation of *para*-fluorophenylalanine. Fluorine in *para* position of benzene ring of phenylalanine increases electron density of the ring, thereby improves its interaction with the integrin. Introduction of fluorine improves the hydrogen

bonding interaction between the peptide and the integrin's asparagine and glutamine. Peptides are synthesized with low yields, albeit with increased hydrophobicity.

Chapter VI, the fifth section of the thesis describes the design and synthesis of adamantane and palmitic acid collagen mimetic peptides with structural modifications for improved resistance towards protease degradation. Among the synthesized collagen mimetic peptides are the peptoids and *N*-methylated peptides. In peptoids, resistance is built by the 'transfer' of the 'R' groups of amino acids from an *alpha* carbon to the amide nitrogen, to protect the hydrolysis of the amide bond. In *N*-methylated collagen mimetic peptides, the binding of the protease to the peptide is made difficult or impossible by steric hindrance. Methyl group is introduced on nitrogen of the amide bond to sterically protect the peptide bond against protease activity. The yields in these reactions are low mainly due to acylation reaction that involves a sterically hindered secondary amine.

The sixth part, **Chapter VII** of the study describes application of the peptides *retro*-DGD-GG-GFOGER-GG-Adamantane (NL008), *retro*-DGD-GG-GFOGER-GG-TTK-Palmitate (NL009) and *retro*-DGD-GG-GFOGER-GG-TTK (NL010) in *in vitro* studies. In a scratch wound assay, the peptides displayed the ability to induce migration of cells. Migration of cells was further enhanced by the presence of hyaluronic acid. In *in vivo* study, peptides are tested for their ability to induce wound closure inflicted on rodents. NL010 outperformed NL009. However, NL010 performed less efficiently in comparison to the comparator Puramatrix®.

Chapter VIII consists of a conclusion, the experimental is outlined in **Chapter IX** and **Chapter X** is the appendix.

LIST OF TABLES

Chapter I

Table 1.1: Wound dressings (Part 1 of 2) 14

Table 1.2: Wound dressings (Part 2 of 2) 15

Chapter II

Table 1: Percentage yields and mass spectrometry data of peptides 36

Table 2: Estimated secondary structure content of the palmitate pepides 38

Table 3: Long-range coupling obtained from the ROESY spectrum 38

Chapter III

Table 3.1: Yields of the synthesized control and growth factor based peptides 55

Table 3.2: Estimated secondary structure content of the adamantane peptides 58

Chapter IV

Table 4.1: TOCSY spin systems and ROESY dipeptides 69

Table 4.2: Characterisation table for *retro*-DGD-GG-GFOGER-GG-TTK-Adamantane 71

Table 4.3: Determination of tertiary structure of *retro*-DGD-GG-GFOGER-GG-TTK-Adamantane 74

Chapter V

Table 5.1: Yields of *retro-para*-fluorophenylalanine peptides 83

Chapter VI

Table 6.1: Yields of synthesized peptoids 94

Table 6.2: Yields of synthesized reference peptoids 96

Table 6.3: Yields of synthesized D-Peptides 98

Table 6.4: Yields of oxazolidinone amino acids 100

Table 6.5: Yields of *N*-methylated amino acids 104

Table 6.6: Yields of synthesis of singly substituted *retro-N*-methylated peptides 106

Table 6.7: Yields of synthesized doubly substituted *retro-N*-methylated peptides 106

Chapter IX

Table 9.1: Characterization table of *retro*-GG-GFOGER-GG-Adamantane.....141

Table 9.2: Characterization table of *retro*-DGD-GG-GFOGER-GG-Adamantane.....145

Table 9.3: Characterization table of *retro*-DGD-GG-GFOGER-GG-TTK-Palmitate.....150

Table 9.4: *Retro*-DGD-GG-GFOGER-GG-TTK-Adamantane characterization table.....155

Chapter X

Table 10.1: TOCSY/ROESY amide and *alpha* protons chemical shifts of *retro*-GG-GFOGER-GG-Adamantane.....244

Table 10.2: Correlations between dipeptides observed in the ROESY spectrum of *retro*-GG-GFOGER-GG-Adamantane 245

Table 10.3: Tertiary structure determination of *retro*-GG-GFOGER-GG-Adamantane.....245

Table 10.4: ROESY correlations of dipeptide of NL008 246

Table 10.5: TOCSY/ROESY amide and *alpha* proton chemical shifts of *retro*-DGD-GG-GFOGER-GG-Adamantane 247

Table 10.6: ROESY correlations for the tertiary structure determination of *retro*-DGD-GG-GFOGER-GG-Adamantane 247

Table 10.7*:* Amide proton interactions in *retro*-DGD-GG-GFOGER-GG-TTK-Adamantane. ..248

Table 10.8: TOCSY/ROESY amide and *alpha* protons correlations of NL009 249

Table 10.9: Helix content of *retro*-DGD-GG-GFOGER-GG-TTK-Palmitate. 250

Table 10.10*:* Helix content of *retro*-DGD-GG-GFOGER-GG-GHK-Palmitate 250

Table 10.11*:* Helix content of *retro*-DGD-GG-GFOGER-GG-QPR-Palmitate. 251

Table 10.12*:* Helix content of *retro*-DGD-GG-GFOGER-GG-EEM-Palmitate 251

Table 10.13*:* Helix content of *retro*-DGD-GG-GFOGER-GG-TTK-Adamantane 251

Table 10.14*:* Helix content of *retro*-DGD-GG-GFOGER-GG-GHK-Adamantane.....252

Table 10.15*:* Helix content of *retro*-DGD-GG-GFOGER-GG-EEM-Adamantane.....252

LIST OF SCHEMES

Chapter II

SCHEME 1 General scheme for the synthesis of palmitate peptides 35

SCHEME 2 Conversion of *cis* to *trans* isomer 37

Chapter III

Scheme 3.1: Formation of pyrroglutamic acid 49

Scheme 3.2: Cyclization products of glutamic acid 49

Scheme 3.3: O-acylation followed by O-N migration after amino deprotection 52

Chapter V

Scheme 5.1: Protection of *para*-fluorophenylalanine. 78

Scheme 5.2: Coupling reaction of *para*-fluorophenylalanine to the tripeptide *retro*-GG-G-NH_2 81

Scheme 5.3: Binding peptide synthetic route 83

Chapter VI

Scheme 6.1: The general synthetic procedure for the synthesis of peptide-peptoid derivatives 93

Scheme 6.2*:* General scheme for the synthesis of *retro*-D-peptides 98

Scheme 6.3: Synthesis of Fmoc-Phe-OH 100

Scheme 6.4: Proposed mechanism for cyclisation of Fmoc-amino acid 101

Scheme 6.5: Reductive amination of 5-oxazolidinone 102

LIST OF FIGURES

Chapter I

Figure 1.1: General structure of an integrin 3
Figure 1.2: Extracellular I-Domain 4
Figure 1.3: Unliganded and liganded conformations of integrin 5
Figure 1.4: Coordination of the metal – unliganded conformation 6
Figure 1.5: Collagen-integrin I-domain macromolecular complex 7
Figure 1.6: Cell adhesion molecule (CAM) mediation in cell-to-cell binding 8
Figure 1.7: Unliganded and liganded conformations with no I domain on β subunit 9
Figure 1.8: Sequence homology for integrin transmembrane and cytoplasmic domains 10
Figure 1.9: Primary, secondary and tertiary structure of collagen 13
Figure 1.10: Phenylalanine interactions (Discovery studio software program) 18
Figure 1.11: Hydroxyproline interactions 18
Figure 1.12: Glutamic acid interactions 19
Figure 1.13: Arginine interaction with aspartic acid 19
Figure 1.14: Arginine interaction with histidine 20
Figure 1.15: Structures of the polyanionic DGD and the GG-DGD peptides. 21
Figure 1.16: *retro*-DGD-GG-GFOGER-GG-XYZ-Adamantate peptide. 22

Chapter II

Figure 1: General structure of collagen mimetic peptide 36
Figure 2: Geometric isomers of the peptides 36
Figure 3: Sections of ^{1}H NMR spectra at different temperatures 36
Figure 4: *retro*-DGD-GG-GFOGER GG-TTK-palmitate circular dichroism 37

Chapter III

Figure 3.1: General structure of wound healing peptide 41
Figure 3.2: Mass spectrum of the thirteen amino acid sequence before the addition of the *retro*-tripeptides TTK/GHK/QPR/EEM 45
Figure 3.3: HPLC test chromatogram 2 46

Figure 3.4: Comparison of crude high resolution mass spectra of *retro*-DGD-GG-GFOGER-GG-GHK-Adamantane (**A**) and *retro*-DGD-GG-GFOGER-GG-Adamantane (**B**).....48
Figure 3.5: Comparison of crude high resolution mass spectra of *retro*-DGD-GG-GFOGER-GG-EEM-Adamantane (**A**) and *retro*-DGD-GG-GFOGER-GG-Adamantane (**B**). 50
Figure 3.6: Comparison of crude high resolution mass spectra of *retro*-DGD-GG-GFOGER-GG-QPR-Adamantane (**A**) and *retro*-DGD-GG-GFOGER-GG-Adamantane (**B**).....51
Figure 3.7: Comparison of crude high resolution mass spectra of *retro*-DGD-GG-GFOGER-GG-TTK-Adamantane (**A**) and *retro*-DGD-GG-GFOGER-Adamantane (**B**) 53
Figure 3.8: Comparison of steric hindrance around the carbonyl group of adamantane carboxylic acid versus palmitic acid. 55
Figure 3.9: Circular dichroism spectrum of *retro*-DGD-GG-GFOGER-GG-TTK-Adamantane ...58

Chapter IV

Figure 4.1: Collagen mimetic peptide – *retro*-DGD-GG-GFOGER-GG-TTK-Adamantane. 63
Figure 4.2: ^{1}H NMR spectrum of *retro*-DGD-GG-GFOGER-GG-TTK-Adamantate 64
Figure 4.3: Amide Section of TOCSY spectrum of *retro*-DGD-GG-GFOGER-GG-TTK-Adamantate 66
Figure 4.4: ROESY spectrum of *retro*-DGD-GG-GFOGER-GG-TTK-Adamantane.....68
Figure 4.5: *Alpha*-amide section of ROESY spectrum.....69
Figure 4.6: *retro*-DGD-GG-GFOGER-GG-TTK-Adamantane.....71

Chapter V

Figure 5.1: Phenylalanine interactions.....76
Figure 5.2: Structure of *retro*- *para*-fluorophenylalanine adamantane peptide 77
Figure 5.3: ^{1}H NMR of Fmoc-*para*-fluoro phenylalanine.....79
Figure 5.4: Structure of Fmoc-*para* fluoro-phenylalanine 79
Figure 5.5: Section of ^{1}H NMR spectrum of Fmoc-*para*-fluoro phenylalanine 80
Figure 5.6: Mass spectrum of crude *retro*-GG-G[*para*-fluoroPhe]OGER-GG-NH_2.....82
Figure 5.7: Mass spectrum of *retro*-GG-G[*para*-F-Phe]OGER-GG-Adamantane and -Palmitate peptides 85

Chapter VI

Figure 6.1: *retro*-GG-GFOGER-GG-Adamantane peptoid 90

Figure 6.2: Structural differences between the normal *N*– substituted glycine (oligo–NSG) peptoid and oligo-*N*-substituted alanine (oligo-NSA) backbones 91

Figure 6.3: Structure of the *retro*-reference peptoid 95

Figure 6.4: *retro*-GG-G_DFOG_DER-GG-Adamantane D-Peptide 97

Figure 6.5: Mass spectrum of phenylalanine oxazolidinone 100

Figure 6.6: Side products of acylation reaction of arginine 102

Figure 6.7: Mass spectrum of crude *N*-methylated Fmoc-phenylalanine 103

Figure 6.8: Singly substituted *retro*-*N*-methylated peptide 104

Figure 6.9: Doubly substituted *retro*-*N*-methylated adamantane peptide 105

Chapter VII

Figure 7.1: Palmitate collagen mimetic peptide 109

Figure 7.2: A: Chemical structure of the NL009, NL010 and NL008 CMP 110

Figure 7.3: Graphical depiction of the experimental design 114

Figure 7.4: Bacterial and fungal evaluation of the treatments on agar plates using the streaking method 115

Figure 7.5: Cytotoxicity assays to assess cell viability 118

Figure 7.6: NL008, NL009 and NL010 scratch closure rates 119

Figure 7.7: NL008, NL009 and NL010 scratch closure rates on the 3T3 cell line 120

Figure 7.8: 7-day study of three rats treated with the negative control, HAgel, NL010-HAgel and the market comparator 121

Figure 7.9: 14-day study of three rats treated with the negative control, HAgel, NL010-HAgel and the market comparator 122

LIST OF ABBREVIATIONS

Acids

HCL	Hydrochloric acid
PTSA	*p*-Toluenesulfonic acid
TFA	Trifluoroacetic acid
TFMSA	trifluoromethanesulfonic acid

Coupling reagents

DIC	*N, N*'-Diisopropylcarbodiimide
DIPEA	Diisopropylethylamine
HATU	O-(7-Azabenzotriazole-1-yl)-*N, N, N'N'*-tetramethyluronium hexafluorophosphate
HBTU	(2-(1H-Benzotriazol-1-yl)-1,1,3,3-tetramethyluronium hexafluorophosphate, Hexafluorophosphate Benzotriazole TetramethylUronium)
HOAt	1-Hydroxy-7-azabenzotriazole
HOBt	Hydroxybenzotriazole

Protecting groups

Boc	*tert*-Butyloxycarbonyl
Fmoc	9-Fluorenylmethlyoxycarbonyl
Fmoc-OSu	N-(9-Fluorenylmethoxycarbonyloxy) succinimide
Mbh	4,4'-Dimethoxybenzhydryl
Mtr	4-Methoxy-2,3,6-trimethylbenzenesulfonyl
Pbf	2,2,4,6,7-Pentamethyldihydrobenzofuran-5-sulfonyl
Pmc	2,2,5,7,8-Pentamethylchroman-6-sulfonyl
tBu	*tert*-Butyl
tButhio	*tert*-Butylthio
trt	Triphenylmethyl

Solvents

ACN	Acetonitrile
DCM	Dichloromethane
DMF	dimethyl formaamide
DMSO	Dimethylsuphoxide
IPA	Isopropanol
MeOH	Methanol

Other reagents

EDT	ethanedithiol
$MgSO_4$	Anhydrous magnesium sulphate
MTT	3-(4,5-Dimethylthiazol-2-yl)-2,5-diphenyltetrazoliumbromide
$NaHCO_3$	Sodiumhydrogencarbonate
TES	Triethylsilane
TIS	Triisopropylsilane

Nuclear Magnetic Resonance

δ	Chemical shift
m	Multiplet
COSY	Correlation Spectroscopy
DEPT-135 -	Distortionless Enhancement by Polarization Transfer
HSQC	Heteronuclear Single Quantum Correlation
HMBC	Heteronuclear Multiple Bond Correlation
TOCSY	Total Correlation Spectroscopy
ROESY	Rotating-frame nuclear Overhauser Effect correlation Spectroscopy

AA	Amino acid
AMP	Antimicrobial Peptides
CAM	Cellular Adhesion Molecules

CD	Circular dichroism
CMP	Collagen Mimetic Peptides
ECM	Extracellular Matrix
EGF	Epidermal Growth Factor
ESI	Electron Spray Ionization
FGF	Fibroblast Growth Factor
HA	Hyaluronic acid
HAgel	Hyaluronic acid hydrogel
HRMS	High Resolution Mass Spectrometry
LCMS	Liquid Chromatography- Mass Spectrometry
mg	milligram
min	minute
mL	milliliter
mM	millimolar
MMP	Metalloproteinases
M	molar
MS	mass spectrometry
m/z	mass charge
NL009-HAgel	NL009 collagen mimetic peptide hyaluronic acid hydrogel
NL010-HAgel	NL010 collagen mimetic peptide hyaluronic acid hydrogel
p-fluoro-Phe	*para* fluorophenylalanine
PDGF	Platelet Derived Growth Factor
SPPS	Solid Phase Peptide Synthesis
TGF-β	Transforming Growth Factor-β
TLC	Thin Layer Chromatography
UHPLC-MS	Ultra High-Performance Liquid Chromatography – Mass Spectrometry
VEGF	Vascular Endothelial Growth Factor

TABLE OF CONTENTS

DECLARATION ..... **ii**

DEDICATION ..... **iii**

PUBLICATIONS ..... **iv**

ACKNOWLEDGEMENTS ..... **v**

LIST OF TABLES ..... **x**

LIST OF SCHEMES ..... **xii**

LIST OF FIGURES ..... **xiii**

LIST OF ABBREVIATIONS ..... **xvi**

CHAPTER I **1**

INTRODUCTION **1**

1.1 CHRONIC WOUND HEALING 1

1.2 INTEGRIN 2

1.3 COLLAGEN 10

1.4 WOUND CARE AND DRESSINGS 13

1.5 COLLAGEN MIMETIC PEPTIDES 17

1.6 STRUCTURE DETERMINATION OF PEPTIDES 24

1.7 AIM OF STUDY 25

1.8 REFERENCES 26

CHAPTER II **33**

1. INTRODUCTION 33
2. DESIGN OF PEPTIDE MIMICS 36
3. PEPTIDE SYNTHESIS 36
4. GEOMETRIC ISOMERS 35
5. DGD-GG-GFOGER-GG-TTK-PALMITATE SECONDARY STRUCTURE 37
6. NMR TERTIARY STRUCTURE ELUCIDATION 37
7. ROESY EXPERIMENT 38
8. CONCLUSION 38

CHAPTER III **40**

SYNTHESIS OF GROWTH FACTOR-BASED PEPTIDES CONJUGATED TO ADAMANTANE **40**

3.1 PEPTIDE SYNTHESIS 42

3.2 RESULTS AND DISCUSSION 54

3.3 CIRCULAR DICHROISM 56
3.4 CONCLUSION 60
3.5 REFERENCES 60
CHAPTER IV 63
STRUCTURE DETERMINATION OF ADAMANTANE PEPTIDES 63
4.1 RESULTS AND DISCUSSION 64
4.2 CONCLUSION 74
4.3 REFERENCES 75
CHAPTER V 76
BINDING PEPTIDES 76
5.1 SYNTHESIS 77
5.2 RESULTS AND DISCUSSION 78
5.3 SYNTHESIS OF *para*-FLUORO PHENYLALANINE PEPTIDES 80
5.4 RESULTS AND DISCUSSION 83
5.5 CONCLUSION 86
5.6 REFERENCES 87
CHAPTER VI 89
SYNTHESIS OF PEPTIDOMIMETICS WITH IMPROVED PROTEOLYTIC STABILITY 89
6.1 RESULTS AND DISCUSSION 89
6.2 CONCLUSION 107
6.3 REFERENCES 107
CHAPTER VII 109
BIOLOGICAL STUDIES 109
7.1 BIOLOGICAL TESTS 111
7.2 In vivo STUDIES 113
7.3 RESULTS 117
7.4 CONCLUSION 122
7.5 REFERENCES 123
CHAPTER VIII 124
CONCLUSION 124
8.1 REFERENCES 126
CHAPTER IX 127

EXPERIMENTAL 127
9.1 GENERAL INFORMATION 127
9.2 INSTRUMENTATION 127
9.3 GENERAL TECHNIQUES 128
9.4 GENERAL PROCEDURES 129
9.5 SUMMARY OF SYNTHESIZED COMPOUNDS 136
9.6 MASS SPECTRA OF SELECTED PEPTIDES 178
9.7 NMR SPECTRA OF SELECTED PEPTIDES 208
9.8 CIRCULAR DICHROISM (CD) OF SELECTED PEPTIDES 240
APPENDIX 244
10.1 CHARACTERIZATION TABLES 244
10.2 CIRCULAR DICHROISM 250
10.3 SUPPLEMENTARY INFORMATION FOR THE PUBLISHED ARTICLE 253

CHAPTER I

INTRODUCTION

1.1 CHRONIC WOUND HEALING

The normal wound healing process comprises of four stages, namely, haemostasis, inflammation, proliferation, and maturation. However, not all wounds successfully go through these stages of healing. If the process of wound healing gets stuck in any of the mentioned phases, the process of healing gets botched. Wounds that fail to heal within three months under standard care are referred to as chronic wounds.[1–8]

Chronic wound healing subjects the patient to significant discomfort and distress thereby adversely affecting the quality of life of the patient. It is common in patients with cardiopulmonary disease, peripheral vascular disease, immune system deficiencies, diabetes and obesity.[9–11] Pressure ulcers (PUs), diabetic foot ulcers (DFUs), and leg ulcers (LUs) such as venous leg ulcers, arterial leg ulcers and ulcers of mixed aetiology are prevalent types of chronic wounds.[8]

For every 100 000 people within the age group 45 – 65, and those above 75 there are respectively about 120 and 800 patients reported to be afflicted by chronic wound disease.[12] Clearly, the elderly population is more vulnerable to chronic wound healing. It is reported that the disease afflicts about 1% of the European population and millions across the globe.

About 2.8 million in the USA[13] and 4 million people in Germany[12] are afflicted by this disease. In consideration of this high number of patients, clearly chronic wound healing incurs massive health care costs amounting to billions of dollars. The amount of money allocated to the treatment of chronic wound disease is indicative of the gravity of this disease. In the UK, France, and Germany, about 1.3 to 2% of the total annual healthcare cost is apportioned to the treatment of venous leg ulcers.[12] In Germany, approximately 5 billion Euros is spent annually on chronic wound disease[14] whilst the USA spent $2.3 billion in 2005 on advanced wound care products. The figures, in terms of money, continued to rise annually at a rate of 12.3% to $4.6 billion in 2011.[14] In South Africa, the South Africa Wound Care Management Industry has witnessed a compound annual growth rate (CAGR) in chronic wounds of 6.7% since 2019.

Stalled wounds can have a devastating impact on patient well-being that reaches far beyond the healthcare system and can compound healthcare costs. They have an adverse effect on the quality of life and create a significant economic burden.[15]

Among many factors that could possibly contribute towards the chronicity of wounds is the malfunction or absence of the extracellular matrix macromolecules. Inappropriate concentrations shift in the balance and lack of activity of factors such as resident skin cells, blood mononuclear cells, cytokines, chemokines, extracellular matrix, growth factors, and other regulatory molecules that take part in the proper wound healing process could negatively affect any of the stages of wound healing. The stuck wound healing process may further be exacerbated by infection.[9,10]

Although not as common as stalled inflammation, impaired angiogenesis can also result in chronic hypoxia and inadequate micronutrient delivery thereby causing chronic wound healing. This impaired wound healing has been reported in diabetic ulcers, venous insufficiency ulcers, and ischemic ulcers.[16,17] The characteristic features of chronic wounds are elevated levels of matrix metalloproteinases (MMPs) and proinflammatory cytokines. At elevated levels, matrix metalloproteinases digest the healthy ECM, including collagen, as well as the growth factors. Depleted amounts of collagen and growth factors cause the inflammatory stage to stall, and proliferation fails to proceed.

Collagen employed in wound healing is mainly produced by the fibroblast cells. Collagen is produced subsequent to its interaction with the specific integrin on the surface of the fibroblasts.

1.2 INTEGRIN

Integrins are heterodimeric non-covalently associated cell-surface and transmembrane glycoproteins. They belong to a family called cell adhesion receptors.[18] This family falls under cell adhesion molecules (CAM).

1.2.1 Classification of integrins

Integrins are made up of 18 α and 8 β different subunits which combine to form 24 distinct integrin heterodimers in mammals.[19] There are integrins which bind only to collagen, this specific binding of integrins is dictated by extracellular domains of the α and β integrin subunits. There are eight classes of integrin. One class that comprises integrins $\alpha_1\beta_1$, $\alpha_2\beta_1$, $\alpha_{10}\beta_1$, $\alpha_{11}\beta_1$, specifically binds collagen.[20]

Categorically, collagen type I binds to $\alpha_2\beta_1$ integrin on the surface of the fibroblast to produce more collagen at the wound site.

1.2.2 Structure of Integrins

As shown in Figure 1.1 below, integrins consist of two heterodimeric α and β polypeptide chains. These proteins are found embedded in cell membranes and protrude both into the cytoplasm and on the surface of the cells. In both subunits, there are three distinct domains, the short cytoplasmic tail, the transmembrane domain, and the large glycosylated extracellular domain.[21] Although the two subunits are not necessarily identical, they seem to be related to each other.[22,23]

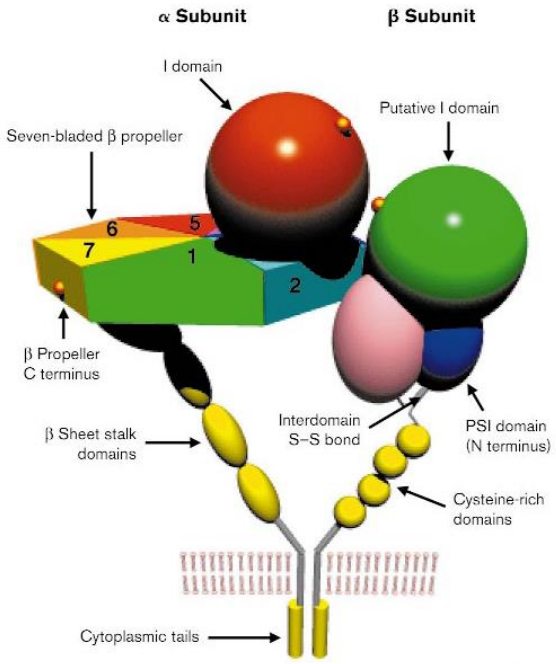

Figure 1.1: General structure of an integrin.[9]

1.2.2.1 Extracellular domain

The N-terminal of the two subunits consists of large globular domains. The α-subunit consists of tandem repeats which fold into seven bladed β-propeller structure.[24] Between blade 2 and 3 there is an insertion called the I-domain. This segment consists of about two hundred amino acids.[25]

The I-domain adopts Rossman type fold. The central part of the I-domain is occupied by six β-strands. Five of these strands are parallel while one is anti-parallel to other strands. The β strands are surrounded by seven α-helices.[26] The two are connected to each other by loops. Above the β-strands is a region called

metal ion dependent adhesion site (MIDAS). This region is occupied by divalent metal cations such as Co^{2+}, Mg^{2+}, Mn^{2+}. The structure of the I-domain is shown in the Figure 1.2.

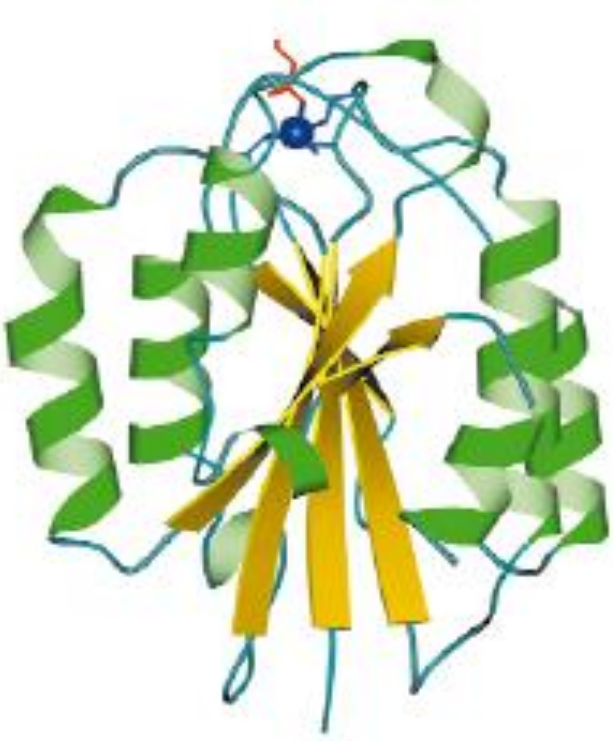

Figure 1.2: Extracellular I-Domain.[27]

The β-subunit on the other hand has putative I-domain which rests on two PSI domains. Also, this domain consists of 200 amino acids. This observation suggests that putative I-domain possibly adopts a Rossman fold type structure like α-subunit domain.[22]

1.2.2.2 Conformations of I-domain

There are two possible conformations of integrins, closed-unliganded and open-liganded conformations. In closed-unliganded conformation, there is no extracellular matrix protein-cell interaction, and the integrin is bent towards the cell membrane as shown in Figure 1.3 (a).

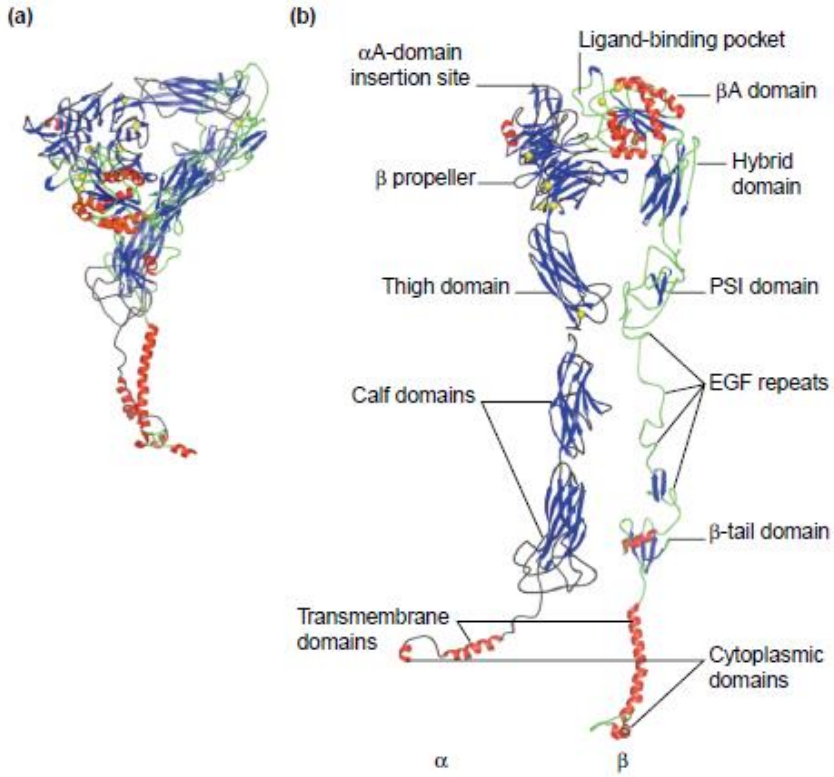

Figure 1.3: (a) Unliganded and (**b**) liganded conformations of integrin.[22]

Furthermore, in closed unliganded conformation, the amino acids of the loops linking α-helices and the β-strands interact via their side chains directly or indirectly through water with the divalent metal cation, thus holding the metal ion in place.[26] The divalent metal ion has an octahedral arrangement with two serine residues (S153 and S155) and aspartic acid (D151) and three water molecules. Threonine and another aspartic acid indirectly interact with the metal via water molecules as shown in Figure 1.4.

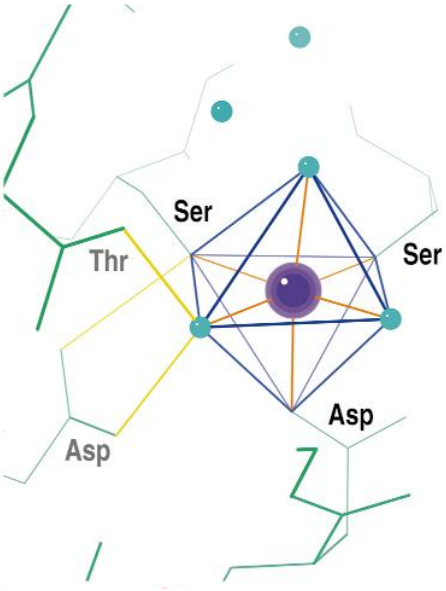

Figure 1.4: Coordination of the metal – unliganded conformation.[27]

Open liganded conformation is attained as a result of the interaction between collagen and the I-domain. Interaction of collagen through glutamic acid to the divalent metal ion is accompanied by change in coordination. Aspartic acid which was directly coordinated to the metal now indirectly interacts with the divalent metal ion through water molecules. Though the two serine residues are still coordinated, the number of water molecules also gets reduced to two from three as threonine also directly coordinates to the metal. It appears that the divalent metal ion can only coordinate to one acidic residue at a time.[27]

Figure 1.5 (a) and (b) below show interaction of collagen via glutamic acid. In the figure, (a) shows simple interaction with the metal while (b) shows the octahedral arrangement of the metal divalent ion with collagen and the amino acids of the loops in the MIDAS region.

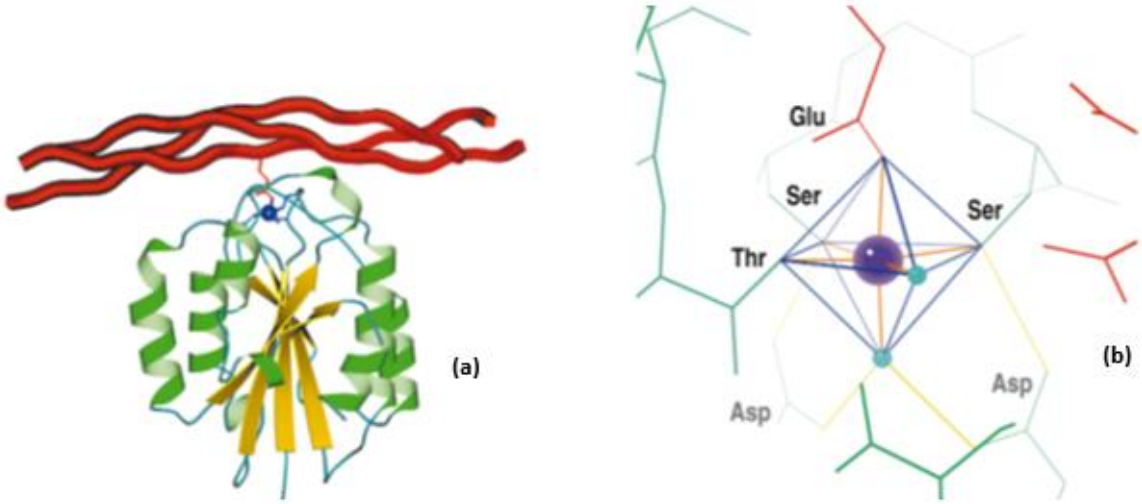

Figure 1.5: Collagen-integrin I-domain macromolecular complex.[27]

The figure above shows the collagen triple-helix GFOGER motif's interaction with the metal ion in the metal ion dependent adhesion site region of the I-domain. The triple-helical configuration is maintained throughout the length of the entire peptide.[28–31]

Integrins can transduce signals either from inside the cell to the extracellular matrix or vice versa. With this ability, integrins can link the cytosketal system with the extracellular matrix. Integrins can convert between active (adhesive) state and inactive (non-adhesive). Large extracellular domains of integrins attach cells to other cells or binds cells to the extracellular matrix proteins such as collagen.[32] Figure 1.6 below shows the interaction of two cells mediated by the integrin.

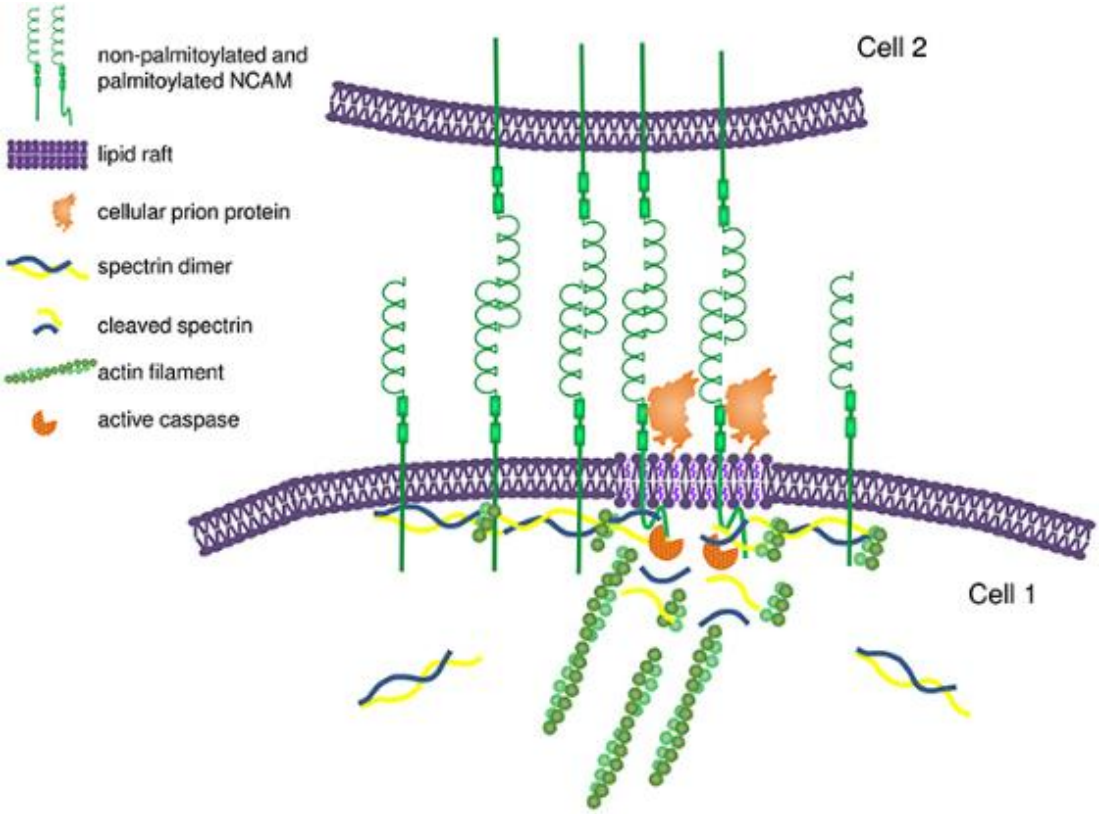

Figure 1.6: Cell adhesion molecule (CAM) mediation in cell-to-cell binding.[33]

Outside-in signaling

When extracellular matrix proteins such as collagen interact with the divalent metal ion, a signal is transduced into the cell, often, to the nucleus. During synthesis of collagen type I, the GFOGER motif of collagen interacts with the $\alpha_2\beta_1$ to transduce signals to the nucleus to synthesize collagen. This is an example of outside-in signaling.[34]

Inside-out signaling

The cytoskeletal proteins such as kindlins and talin interact with the short cytoplasmic tails and increase or decrease the affinity of the extracellular domain to the extracellular matrix proteins. Upon interaction with the cytoplasmic tails of integrin, the conformation changes from inactive (bent) to active (extended). In this position, integrin interacts easily with the ligand as shown in Figure 1.7.[20]

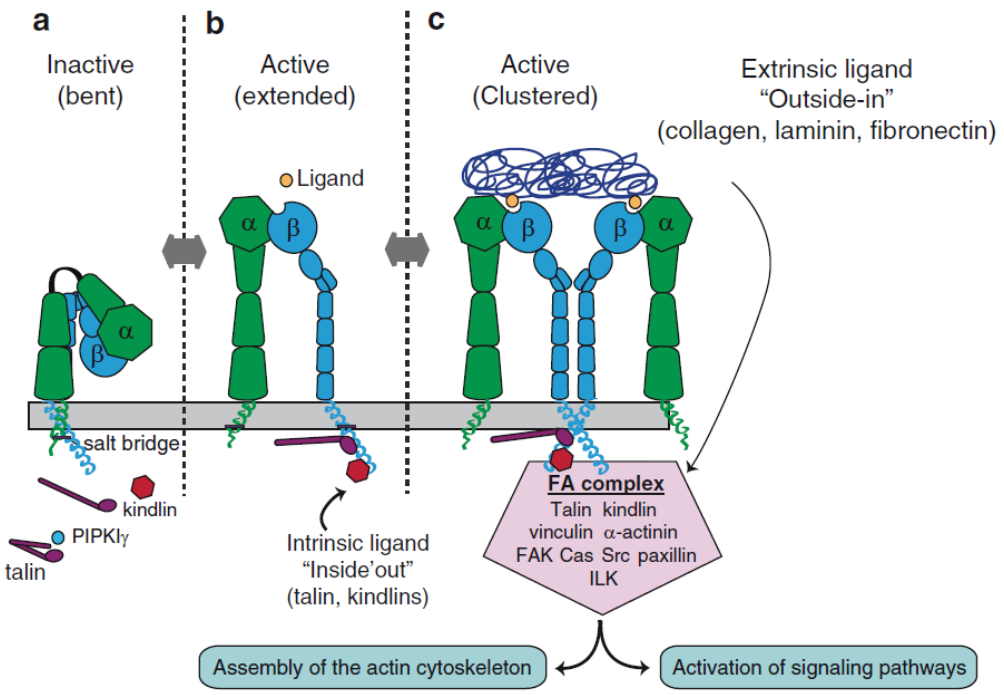

Figure 1.7: Unliganded and liganded conformations with no I domain on β subunit.[20]

1.2.2.3 Transmembrane Domain

Transmembrane domain is a structure that consists of about 25–29 amino acids. These amino acids form α-helices. The same helices may combine and coil about each other to form a homodimer. Two different helices form heterodimers in the same manner.[21]

In an example of different β subunits (β_1, β_2, β_3, β_5 and β_7) forming heterodimers with α_{IIb} subunit, it was revealed that the two transmembrane subunits are tightly packed through glycine-glycine interactions (shown in gold in Figure 1.8).[20] Furthermore, a putative salt bridge was observed in a region just outside the transmembrane domain. The salt bridge is formed between arginine and aspartic acid in all the $\alpha_{IIb}\beta$ integrins. Respectively, talins and kindlins bind to two proximal and distal highlighted in red, NpxxY and NxxY in Figure 1.8.

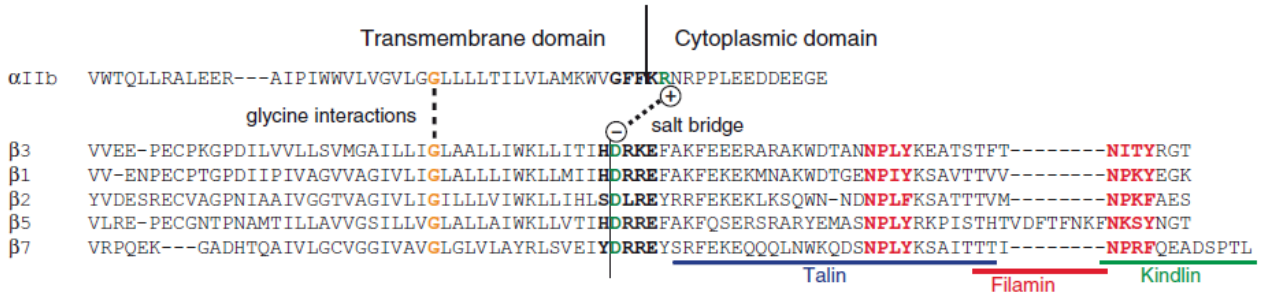

Figure 1.8: Sequence homology for integrin transmembrane and cytoplasmic domains.[20]

All the integrin transmembrane subunits that are inactive tightly pack together to form a complex. There is a coiled coil interaction between the canonical GXXXG dimerization motifs within the transmembrane domains.

1.2.2.4 Cytoplasmic Domain

The α and β subunits of the cytoplasmic tails are very short. This mainly stems from the very fact that these domains are each made up of only about ten to seventy amino (except β_4 which comprises over a thousand amino acids). While the α subunits are so divergent, the β subunits have been discovered to be relatively homologous. The highly reserved region in α subunit, the GFFKR and the HDR(R/K)E forms a salt bridge between amine of arginine and the side chain of aspartic acid. The salt bridge helps maintain the integrin in an inactive low affinity state.[18]

1.3 COLLAGEN

Collagen is an extracellular matrix protein that consists of three parallel left-handed *alpha* helical chains. The chains are in polyproline II-type helical configuration and coil about each other right-handedly in one residue stagger to form a right-handed triple helix. It is the most abundant structural protein in humans that constitutes a third of total protein and therefore a prominent constituent of the extracellular matrix. It comprises three quarters of dry weight of the skin,[35,36] and is found in abundance in the connective tissue of all animals.[37,38] In mammals, collagen characterized by fibres is a main constituent of skin, bone, tendon, cartilage and teeth.

1.3.1 Classification

In vertebrates, forty-six polypeptide chains constitute twenty-eight different types of collagen.[39,40] Collagen types I, II, III, V, XI, XXIV and XXV are fibril forming collagens.[38] Type I and III are particularly important in wound healing.

1.3.2 Collagen Structure

1.3.2.1 Primary and secondary structure

Linear sequence of amino acids forms the primary structure. A protein derives its unique physiological functions from its unique sequence of amino acids. For instance, the sequence -Gly-Phe-Hyp-Gly-Glu-Arg- is recognized specifically by the integrin $\alpha_2\beta_1$ to trigger collagen synthesis. Without this sequence wound healing would be stalled due to the absence of collagen.

The secondary structure has to do with the orientation of the protein. This is highly influenced by the conformations of the individual amino acid residues comprising the protein. Proteins can take up different orientations which are connected to different functions. The secondary structure of proteins consists of α-helix, β-sheet and the loops.[41]

1.3.2.2 Alpha helix

Alpha helix is a right-handed helix whose amide proton (NH) forms a hydrogen bond with carbonyl oxygen (C=O) located four amino acids away. The amide proton and carbonyl oxygen are roughly parallel to the helical axis, that is, they are oriented in the same direction thereby rendering the whole structure positive on the N-terminus and C-terminus negative. Side chain groups point outwards from the helix. Respectively, glycine and proline, due to the absence of the side chain and amide protons destabilize *alpha* helix.[42]

1.3.2.3 Beta sheets

Beta sheets consist of a set of side-by-side polypeptide chains. The chains may run all in the same direction and hence parallel to each other or in alternate directions (anti-parallel configurations). Respectively, the polypeptide chains that are parallel and those that alternate are referred to as parallel pleated sheet and antiparallel pleated sheet. The *anti*-parallel *beta* sheets are more stable. Side chains point alternately above and below the plane of the *beta*-sheet. Each strand is made up of six amino acids

and more. In both configurations, however, the CO and NH groups of neighboring chains are hydrogen bonded.[43]

1.3.2.4 Loops and turns

Loops connect *alpha*-helices and *beta* sheets. They are found on surfaces of proteins and usually contain hydrophilic residues. Turns are loops with less than five amino acids. As with the *alpha* helix and the *beta* sheets, amino acid residues are hydrogen bonded to each other, albeit, between amino acids that are three residues away. Proline and glycine are prevalent in *beta* turns.

1.3.2.5 Tertiary structure

This is the third level of protein organization. Polypeptide chains secondary structure tend to fold and form hydrophobic interactions, disulfide bridges, salt bridges, etc. thereby causing the formation of motifs and domains.[41]

1.3.2.6 Quaternary structure

This level describes the organization of subunits in a protein with multiple subunits (oligomeric proteins). The subunits are held together by non-covalent interactions. Oligomeric proteins are more stable than dissociated subunits. Active sites are often made up of amino acid residues from different subunits. Quaternary and tertiary structures are often affected by ligand (substrate or inhibitor) binding.[41]

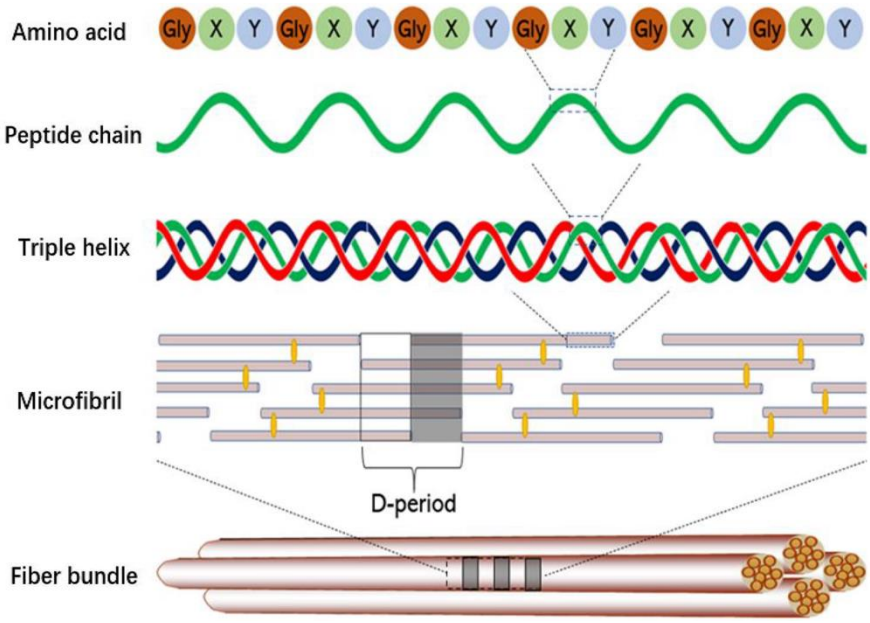

Figure 1.9: Primary, secondary and tertiary structure of collagen.[44]

1.4 WOUND CARE AND DRESSINGS

One major form of intervention in chronic wound healing impasse has always been to use collagen-embedded wound dressings. Prior to employment of dressing product and treatment, accurate diagnosis of wound aetiology followed by appropriate dressing selection must be made.[36,37] Key considerations towards holistic wound care include knowledge of dressing products and their properties and dressing selection skills.[23]

An ideal wound dressing is intended to shield the wound from the external surroundings, absorb wound exudate, reduce inflammation, clear out pathogens and promote healing. Model dressings are non-toxic, non-allergenic, non-adherent and should allow effortless dressing changes without further disruption.

Other factors worth considering when choosing a dressing include the following;

i. Peri-wound skin protection
ii. Effective bacterial barrier formation
iii. Wound shape conformation
iv. Application and removal minimal pain
v. Toxic or irritant extractables free
vi. Non-biodegradable fibers producing
vii. Optimal temperature and pH preserving[45]

Current commercially available dressing materials and topical antiseptics are shown in Table 1.1.

Table 1.1: Wound dressings (Part 1 of 2).[45]

Dressing	Dressing property	Type of chronic wound
Film	Occlusive, moisture retentive, infection protective, can cause fluid collection.[46] Helps promote re-epithelialization	Superficial wounds[47]
Hydrogels	Wound hydrating, liquefy hard eschar and slough.[48] Autolytic debridement aids removal of excess exudate. Forms a physical barrier and promotes epithelialization and cell migration.	Wounds with slough and deep or tunnelling wounds.[49]
Hydrocolloids	Autolytic debridement augments angiogenesis, granulation tissue formation and healing. It is occlusive, very absorbent and has a waterproof backing.[50] Consists of gel-forming agents inside a wafer of dressing. Acts as a scab, allows the body to retain healing fluids.	Superficial and granulating wounds[51]
Alginates	Good absorbent, haemostatic, moist retentive, may require secondary dressing.[52] Minimizes bacterial infections, promotes rapid re-epithelialization and granulation tissue formation.	Exudative and deep or tunnelling wounds.[53]
Hydrofibers	Form a gel upon interaction with wound exudate. It is thrice as effective as absorbent alginates.[54]	Exudative and deep or tunnelling wounds.[55]
Foams	Could either be hydrophobic or hydrophilic. Silicone membrane permits wound and periwound protection. Provides thermal insulation and are moist retentive.	Wounds with moderate-to-heavy exudate and granulating wounds.[56]

Table 1.2: Wound dressings (Part 2 of 2).[45]

Dressing	Dressing property	Contribution to wound healing
Polymeric membrane Dressing (PMD)	Has semipermeable polyurethane film backing on hydrophilic polyurethane membrane matrix with porous structure that exudates fluid from wounds.[57]	Cleanses wounds and expedite healing. Promotes moist wound healing conditions in superficial, exudative and granulating wounds.[58]
Protease lowering dressings	Remove slough, aim chronic wound exudate proteases sequestration.[59]	Promotes granulation tissue formation.[60] Employed in wounds with slough.
Silver	Silver ions produce the antimicrobial effect, reduce infection, and prevent infection after metalloproteinases within wounds. It promotes wound healing.[61]	Employed in infected or colonized wounds. Helps prevent excessive granulation tissue. [62]
Iodine	Cadexomer iodine kills both gram-positive and gram-negative bacteria, fungi and is moisture retentive. It promotes absorption of fluid, exudate, debris, and bacteria. [63]	Employed in infected or colonized wounds.[64]

1.4.1 Collagen dressings

All collagen dressings employed in wound healing hitherto were aimed at diverting the MMP's from digesting healthy ECM. The idea is to have the MMP's focus on the collagen in the dressing thereby leaving the endogenous native collagen and ECM to proceed with the wound healing process. Collagen attracts and activates fibroblasts and may provide an organism with scaffolding effect resulting in wound healing. It plays a chemotactic role in all the stages of wound healing.[65] Collagen dressing types employed in wound healing come in different forms as shown below;

i. Powders
ii. Gels or pastes
iii. Gel impregnated
iv. Cavity wound fill
v. Standard-size wound dressing pads
vi. With and without adhesive borders

Collagen contained in these dressings may be native (with intact triple helix) or denatured or reconstituted collagen (gelatin).[65]

1.4.2 Limitations of available methods

The major limitation with wound dressings is that they cannot be labelled as ideal for all wounds.[66] For example some wound dressings can adhere to the wound bed making it difficult to remove and leaving residues in the wound bed. The dressings can produce odour which can be mistaken for infection and cannot handle heavily draining wounds.[67] Thus a clinician or trained person is always needed to determine the appropriate dressing for each wound type. Although a lot of progress has been made in the design of dressings since 1962 when Winter *et al.* noticed that occluded wounds required less time for epithelialization,[68] still, dressing alone is not sufficient. Wound healing is a complex process that requires a holistic, interdisciplinary, and cost-effective approach, hence the need for effective biological agents.

Topical antiseptics are available in various forms, but many have been proven to have cytotoxic properties[68,69] and some such as mupirocin have shown an incidence of resistance at a very high rate of 11-65%.[68] The clinical challenge of treating infected wounds with traditional antibiotics and bio-platforms has been growing steadily and has now plateaued, thus, generating the need for a paradigm shift in wound care. With regards to biological agents, most published research has been done by small laboratories. Although there are some clear benefits seen in clinical investigations[70] there is still a great need for further investigations in this area. That is, despite years of research into wound healing there is still a lack of effective biological agents for the treatment of chronic wounds,[15] hence a need for further research.

Several bio-platforms containing the following classes of biomaterials have been reported for wound healing of both acute and chronic wounds; collagen based biopolymers, silk biomaterials, marine-derived[71] and nanofiber-based biomaterials that mimic the ECM.[72] Among these wound healing approaches, peptides with wound healing properties have emerged and have demonstrated potential chronic wound management.[73] Wound healing promoting peptides have been embedded into biomaterials and this has resulted in a nascent approach for the design of regenerative biomaterials.[74,75]

The bioactivity of peptides is dependent on their size, conformation, net charge, charge distribution within the peptide and their hydrophobic nature.[76,77] Additional factors affecting the activity and application of peptides include the route of delivery, concentration at the target, toxicity, stability of the peptide (physiochemical and milieu influenced) and stability maintenance.[77]

1.5 COLLAGEN MIMETIC PEPTIDES

Collagen mimetic peptides (CMPs) are synthetic collagen peptides employed as tools to study collagen. CMP's help give an insight into the structure, molecular properties, and various interactions of collagen. Knowledge of the molecular structure of collagen is fundamental and therefore an essential prerequisite to understanding its function.[42]

Studying collagen involves synthesizing the peptides and testing them both *in vivo* and *in vitro* with the aim of developing novel collagen mimetic drugs. In synthesizing collagen mimetic peptides, specificity is important because collagen can carry out many functions. If, for instance, a need to synthesize a drug that would trigger synthesis of collagen arises, focus should strictly be on type I collagen. Next, the amino acid sequence in type I collagen that acts as a ligand should be established. Once these two are established then collagen can be mimicked and tested.

The current study focuses on mimicking collagen type I involvement in wound healing. The aim is to synthesize peptide drugs that would combat chronic wound healing. To achieve the latter, peptides that invoke the presence of macromolecules that play a role in wound healing such as growth factors and collagen were designed.

1.5.1 Collagen mimetic peptide design

1.5.1.1 Selection of the binding motif- based on the Interactions of collagen type I with the integrin.

Type I collagen has a GFOGER motif with which it interacts with integrins $\alpha_2\beta_1$, $\alpha_1\beta_1$, $\alpha_{10}\beta_1$, $\alpha_{11}\beta_1$. Benzene ring of phenylalanine (F8, Figure 1.10) has an electron density due to resonance in the π-system. Respectively, the negatively charged cloud interacts with cation π (NH_3^+) and anion π (COO^-) of glutamine (Q215) and asparagine (N154) via Van de Walls forces, the hydrophobic interaction as shown in Figure 1.10.

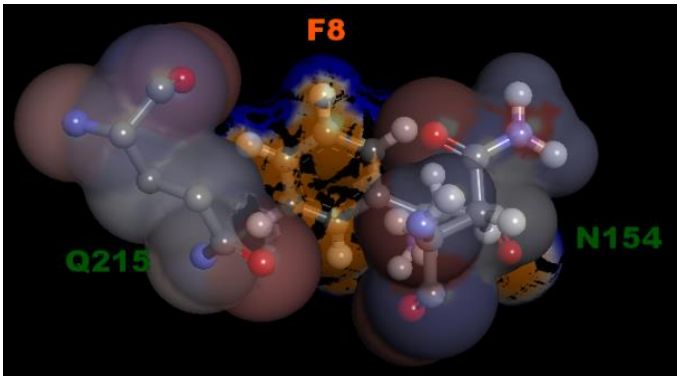

Figure 1.10: Phenylalanine interactions[78] drawn using Discovery studio software program.[79]

Hydroxyproline (X9, Figure 1.11) interacts with asparagine (N154) via hydrogen bonding. Oxygen of the carbonyl group of hydroxyproline interacts electrostatically with NH_3^+ of asparagine. Figure 1.11 shows the hydrogen bonding in discussion.

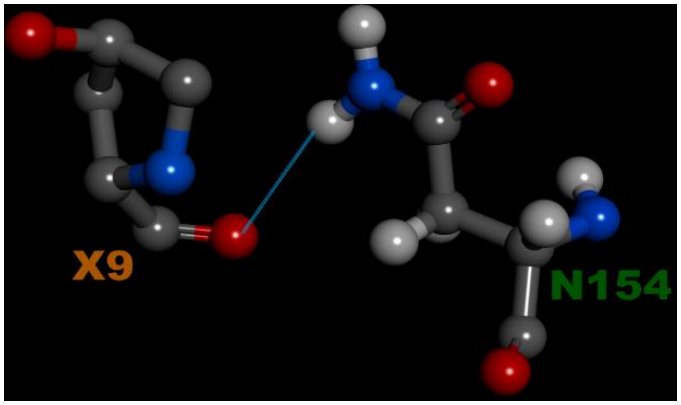

Figure 1.11: Hydroxyproline interactions.[78]

Figure 1.12 shows how glutamic acid (E11) interacts via its oxygen of the carboxylic acid with the divalent metal ion (Co^{2+}, Mg^{2+} or Mn^{2+}) in the MIDAS region of the integrin. This interaction induces a change in conformation of the integrin and is called outside-in signaling. Glutamic acid also forms a salt bridge with the side chains of threonine (T221) through hydrogen bonding.

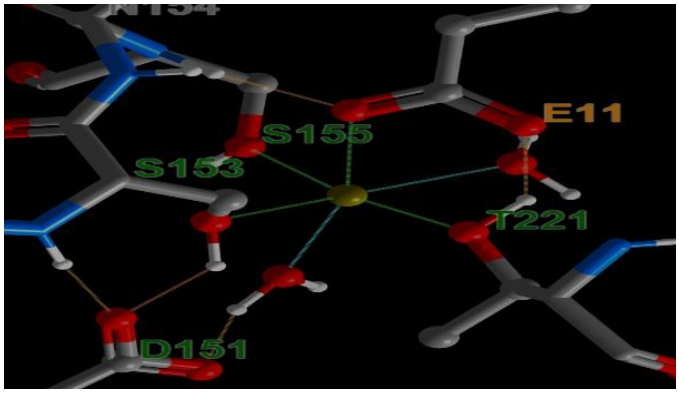

Figure 1.12: Glutamic acid interactions.[78]

Arginine (R12, Figure 1.13) forms three bonds with aspartic acid (D219). The carbonyl oxygen of aspartic acid forms two hydrogen bonds with the guanidyl group of arginine at the same time. The hydrogen bond between C = NH_2^+ and the carbonyl oxygen of aspartic acid forms the salt bridge. The same oxygen of aspartic acid also forms hydrogen bond with the *alpha* C = NH of the guanidyl group. The third hydrogen bond involves the backbone aspartic acid carbonyl oxygen and the NH of arginine.

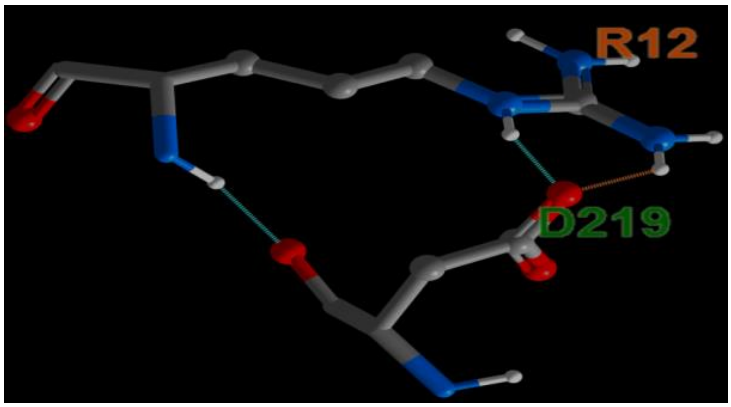

Figure 1.13: Arginine interaction with aspartic acid.[78]

Figure 1.14 depicts interaction of arginine (R12) with histidine. Arginine employs its backbone carbonyl oxygen to form a hydrogen bond with NH of histidine (H258).

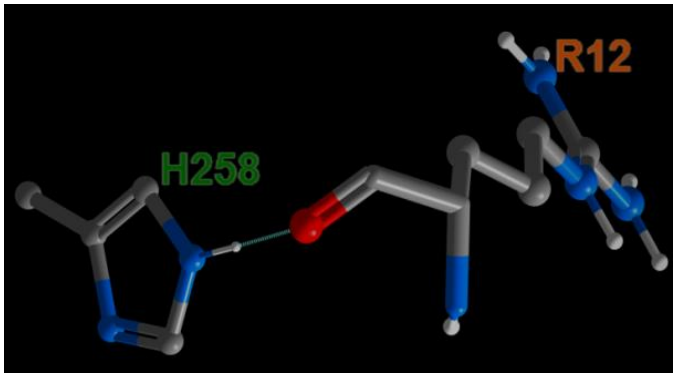

Figure 1.14: Arginine interaction with histidine.[78]

Furthermore, the *retro*-tripeptides, TTK, GHK, QPR and EEM would be employed mainly to stimulate collagen production.

1.5.2 Growth factor inducing tripeptides

Growth factors are hormone-like molecules that interact with specific receptors to control and regulate each phase of wound healing.[37] The tissue repair process is initiated immediately after injury by the release of various growth factors, cytokines, and low-molecular-weight compounds from the serum of injured blood vessels and from degranulating platelets. Growth factors are polypeptides that control the growth, differentiation, and metabolism of cells. Various growth factors that are released at the wound site are presumed to be essential for wound healing. These include epidermal growth factor (EGF), fibroblast growth factor (FGF), keratinocyte growth factor (KGF), transforming growth factor (TGF) and vascular endothelial growth factor (VEGF).[38] Tripeptide, DGD would be employed mainly to enhance binding to collagen and to attract vascular endothelial growth factors.

1.5.3 Lipophilic molecules

The collagen mimetic peptides that exist today have limitations such as poor membrane permeability and are susceptible to being degraded by proteases.[80–82] To improve membrane permeability palmitic acid (fatty acid) and cage moieties such as adamantane were incorporated into the peptide sequences. Palmitic acid has been reported to be a good mitochondrial permeability transition promoter and various cosmetics companies have designed anti-aging creams with peptides coupled to palmitic acids.[83] Adamantane (cage) derivatives have been previously reported to enhance the biological activity,[84] membrane permeability and retard biodegradation when incorporated into biologically active molecules.[85]

1.5.4 The design of growth factor-based collagen mimetic peptides

The sequence consists of two parts, part A which is made up of anionic growth factor attracting amino acids and part B with collagen inducing or signalling amino acids. The aim was to construct a novel sequence.

Part A

Based on the glutamic acid polyanionic peptides reported by Wang *et al*[101] that can attract endothelial growth factors (VEGFs) by charge-charge interactions the Asp-Gly-Asp (DGD) sequence was created and the Asp was utilized instead of the Glu and separated with a glycine residue. The sequence will be synthesized on a 2-chlorotrityl chloride resin (Asp-Gly-Asp-resin) to afford an extra negative charge from the free carboxylic group after the cleavage. Two Gly-Gly residues were also added as a spacer, Figure 1.15.

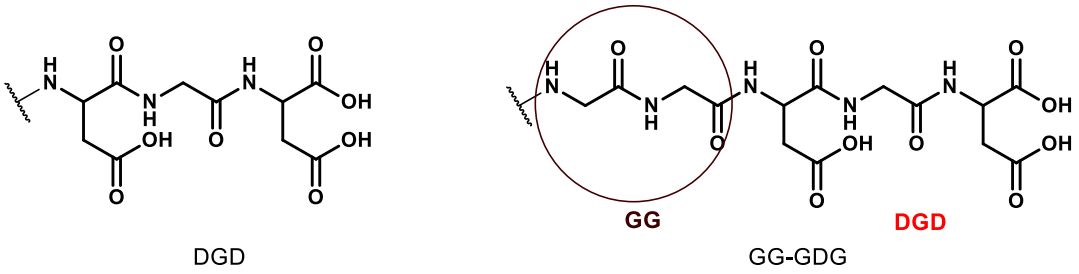

Figure 1.15: Structures of the polyanionic DGD and the GG-DGD peptides.

Part B

Amino acids present in the collagen integrin-binding motif Gly-Phe-Hyp-Gly-Glu-Arg- (GFOGER), a spacer GG and more amino acids that can signal collagen such as Thr-Thr-Lys (TTK), Gly-His-Lys (GHK), Gln-Pro-Arg (QPR), and Glu-Glu-Met (EEM) were selected and sequences, for example GFOGER-GG-TTK were designed. Since the Arg is positively charged and will interfere with the anionic growth factor attracting region the GFOGER-GG-TTK sequence was coupled to the resin-attached peptide (GG_DGD) from the Gly-Phe-Hyp side of the sequence which is hydrophobic. This resulted in the peptide being joined retro to its original sequence. According to the literature,[102] retro peptides have not shown any negative effects.

The complete design of the growth factor-based peptide was based on the following:

i. To improve membrane permeability using fatty acids and cage moieties such as palmitic acid and adamantane would be utilized.[40,42]

ii. Incorporation of poly-anionic (DGD) amino acids to attract growth factors (VEGFs) and enhance binding to collagen fibre through charge-charge interactions.[48,49]

iii. Addition of the *retro*-collagen integrin-binding motif *retro*-Gly-Phe-Hyp-Gly-Glu-Arg (*retro*-GFOGER).

iv. Minimization of steric hindrance on either side of the integrin recognition sequence (*retro*-GFOGER) by inclusion of (GG) sequence as spacers.

v. Incorporation of the *retro* sequences, Thr-Thr-Lys (TTK), Gly-His-Lys (GHK), Gln-Pro-Arg (QPR) and Glu-Glu-Met (EEM) which have been proven to stimulate collagen production.[49]

The proposed structure of the peptide would be as shown in Figure 1.16 below.

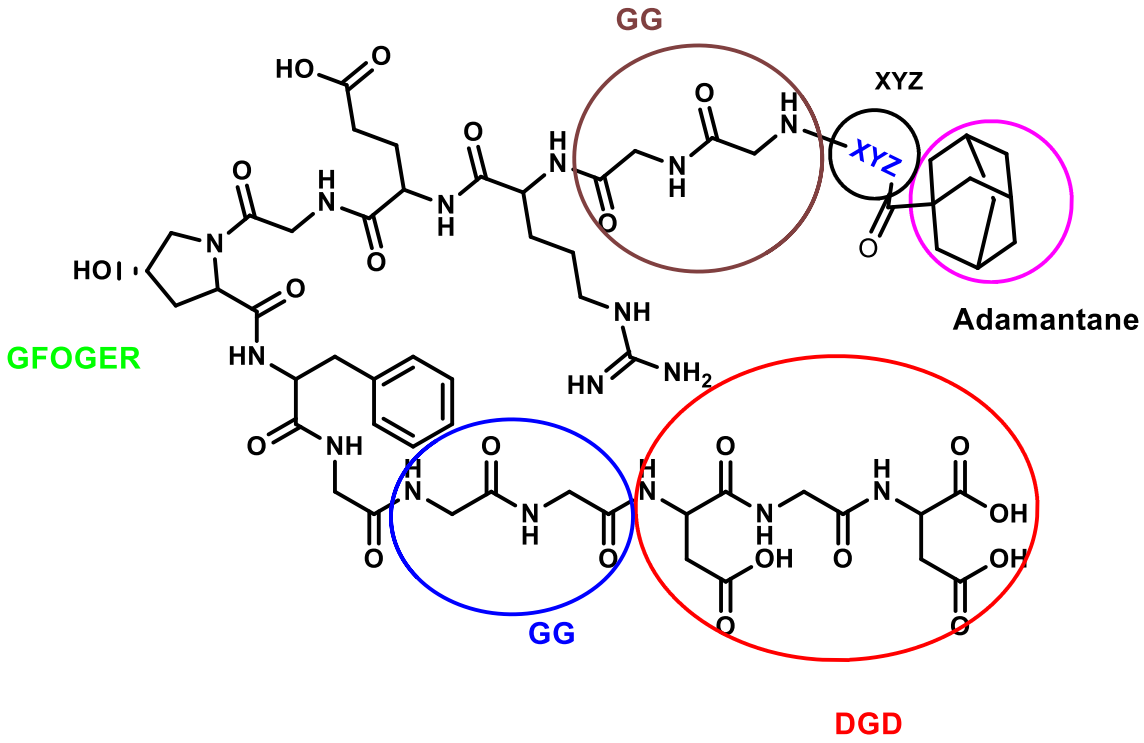

Figure 1.16: *retro*-DGD-GG-GFOGER-GG-XYZ-Adamantate peptide.

1.5.5 Design of protease stable peptidomimetic

1.5.5.1 N-Methylated peptides

N-Methylated peptides are peptides which possess *N*-methyl substituted peptide amide bonds. Since proteases break peptide bonds by binding to specific amino acid sequences in a peptide and catalyse their hydrolysis,[80–82] introduction of a methyl group would sterically hinder binding of the protease. Without binding to a particular sequence of amino acids, peptide bonds would be robust to survive

enzymatic degradation by protease.[86,87] Incorporation of *N*-methylated amino acids into a peptide modifies the peptide backbone thereby reducing its hydrophobicity.[88,89] Substitution of amide proton with a methyl group changes the configuration of the peptide bond from *trans* to *cis*. This decreases the affinity of the peptide to bind to the peptidase's active site.

1.5.5.2 D-Peptides

Proteases cleave peptide bonds of L-peptides because of the compatibility they have with such peptides in terms of the stereochemistry. D amino acids have also been reported to induce an exceptional specificity of the immune response hence many researchers are applying them in the design of vaccines.[90]

1.5.5.3 Peptoids

Peptoids are oligomers of *N*-substituted glycines. The side chain of all amino acids that make up peptoids are on the nitrogen of the amide bond.[91] This means there are two *alpha* hydrogens, and the amide proton is substituted by the side chain of the respective amino acid. This renders peptoids flexible in that hydrogen bonding, which aids in the stability of the peptide, no longer exists. Unlike in other polypeptides, in peptoids, there is loss of main chain chirality.[92,93] Figure 1.17 below shows the difference between peptide and peptoids.

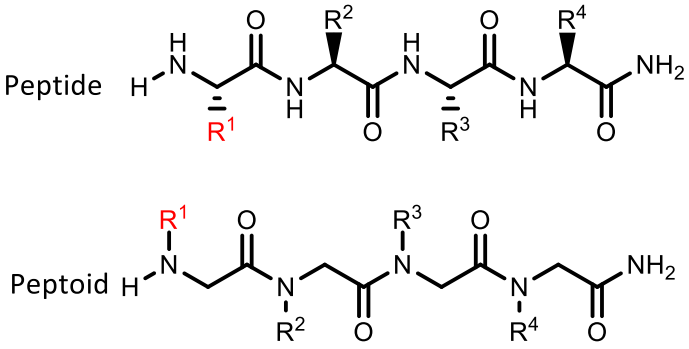

Figure 1.17: Peptide versus peptoid chain.

Another factor which contributes to the flexibility of peptoids is formation of tertiary amide bonds. Formation of tertiary peptide bond is accompanied by high population of both *cis* and *trans* isomers.[94] Presence of the side chain on the nitrogen of amide bond and attainment of *cis*-isomers make these oligomers resistant to enzymatic degradation.[95] The peptidomimetics are presented in chapters 4 and 5.

1.6 STRUCTURE DETERMINATION OF PEPTIDES

1.6.1 Nuclear magnetic resonance (NMR) spectroscopy

Nuclear magnetic resonance (NMR) spectroscopy is key in the determination of structure and various aspects of proteins and biological macromolecules. Chemical shifts are used to probe regions of secondary structures and therefore long-range coupling experiments such as nuclear overhauser spectroscopy (NOESY) or rotating-frame NOE spectroscopy (ROESY) are utilized. Chemical shift values are influenced by many factors such as the presence of an α-helix or β-sheet.[96]

1.6.1.1 Two-Dimensional NMR spectroscopy

Two main mechanisms are employed towards determination of the structure of peptides. Firstly, scalar coupling (through-bond coupling) which involves experiments such as COSY and TOCSY.[97] The magnitude of interactions of two protons depends on the intervening bonds between the two protons. The second important type of interaction is dipolar. This involves direct through space interaction of protons. This type of experiment is called NOESY or ROESY.[96] Combination of COSY, TOCSY and ROESY is fundamental in determination of secondary structure of peptides.[98] TOCSY experiment gives different spin systems of different amino acid that comprise a peptide. Spin systems help distinguish between different amino acids. Each amino acid has a unique spin system.[98] This is because there is no scalar coupling across the peptide bond.

1.6.1.2 Nuclear overhauser effect

ROESY or NOESY afford data about relative three-dimensional locations of different residues in protein sequences. That is, they report on pairwise distances between protons and the comparative positioning of the different protons in a peptide structure.[97] Dipolar interactions depend on the proximity of interacting protons. This experiment is important in the elucidation of peptides since it provides information about two amino acids that are coupled to each other.[97]

1.6.1.3 Circular dichroism

Circular dichroism (CD) is the difference in absorption of left-handed circularly polarized light and right-handed circularly polarized light by chiral molecules containing one or more light-absorbing groups (chromophores).[99] By far the most widespread use of CD spectroscopy is to identify protein secondary structure content. Secondary structure elements generate a CD spectrum due to the chirality of the peptide backbone when scanning in the far-UV. Tertiary structure elements are revealed when scanning

in the near-UV as CD signals are generated predominantly from aromatic side chains (tryptophan, tyrosine, and phenylalanine).[100]

1.7 AIM OF STUDY

The aim of this study is to design and synthesize membrane permeable, protease stable collagen mimetic peptides and peptidomimetics that can bind to the integrin and induce wound healing.

1.7.1 Objectives:

- To develop synthetic procedures for the synthesis of collagen mimetic peptides using the solid phase peptide synthesis technique.
- To increase membrane permeability by conjugating highly lipophilic moieties to the peptide sequence.
- To incorporate D-amino acids into the peptide sequence to induce specificity and increase stability.
- To synthesize peptide-peptoids hybrids with improved metabolic stability
- To incorporate *N*-methylated amino acids to improve resistance to proteolysis
- To determine the 3-dimensional structure of the peptides using the nuclear magnetic resonance (NMR) spectroscopy and circular dichroism experiments.

1.7.2 Hypothesis:

Since collagen type I plays a crucial role in wound healing, single stranded peptidomimetic derived from amino acid sequences of collagen I can be designed and synthesised to bind to the integrin and stimulate the production of collagen required to promote wound healing.

1.7.3 Research question:

Can amino acid sequences derived from collagen be used to design novel chronic wound healing peptidomimetics?

1.8 REFERENCES

(1) Schreml, S.; Szeimies, R.-M.; Prantl, L.; Landthaler, M.; Babilas, P. Wound Healing in the 21st Century. *J Am Acad Dermatol* **2010**, *63* (5), 866–881.

(2) Diegelmann, R. F.; Evans, M. C. Wound Healing: An Overview of Acute, Fibrotic and Delayed Healing. *Front biosci* **2004**, *9* (1), 283–289.

(3) Taylor, J. E.; Laity, P. R.; Hicks, J.; Wong, S. S.; Norris, K.; Khunkamchoo, P.; Johnson, A. F.; Cameron, R. E. Extent of Iron Pick-up in Deforoxamine-Coupled Polyurethane Materials for Therapy of Chronic Wounds. *Biomaterials* **2005**, *26* (30), 6024–6033.

(4) Percival, S. L.; Bowler, P.; Woods, E. J. Assessing the Effect of an Antimicrobial Wound Dressing on Biofilms. *Wound repair and regen* **2008**, *16* (1), 52–57.

(5) Zhao, R.; Liang, H.; Clarke, E.; Jackson, C.; Xue, M. Inflammation in Chronic Wounds. *Int J Mol Sci* **2016**, *17* (12), 2085.

(6) Iqbal, A.; Jan, A.; Wajid, M. A.; Tariq, S. Management of Chronic Non-Healing Wounds by Hirudotherapy. *World J Plast Surg* **2017**, *6* (1), 9.

(7) Nunan, R.; Harding, K. G.; Martin, P. Clinical Challenges of Chronic Wounds: Searching for an Optimal Animal Model to Recapitulate Their Complexity. *Dis Model Mech* **2014**, *7* (11), 1205–1213.

(8) Snyder, R. J. Treatment of Nonhealing Ulcers with Allografts. *Clin Dermatol* **2005**, *23* (4), 388–395.

(9) Uluer, E. T.; Vatansever, H. S.; Kurt, F. O. Wound Healing and Microenvironment. *Wound Healing: Stem Cells Repair and Restorations, Basic and Clinical Aspects* **2018**, 67–77.

(10) Gabriel, A.; Barrett, C.; Cullen, B.; Hodges, D.; Lee, W.; Snyder, R.; Speyrer, M.; Suski, M.; Dick, S.; Thomason, H. A. Infection and Inflammation in the Wound Environment: Addressing Issues of Delayed Wound Healing With Advanced Wound Dressings. *Wounds* **2020**, *32* (1 Suppl), S1–S17.

(11) Sen, C. K. Human Wounds and Its Burden: An Updated Compendium of Estimates. *Adv Wound Care (New Rochelle)* **2019**, *8* (2), 39–48.

(12) Patel, N. P.; Granick, M. S.; Kanakaris, N. K.; Giannoudis, P. v; Werdin, F.; Rennekampff, H.-O. Comparison of Wound Education in Medical Schools in the United States, United Kingdom, and Germany. *Eplasty* **2008**, *8*.

(13) Page, J. C.; Newswander, B.; Schwenke, D. C.; Hansen, M.; Ferguson, J. Retrospective Analysis of Negative Pressure Wound Therapy in Open Foot Wounds with Significant Soft Tissue Defects. *Adv Skin Wound Care* **2004**, *17* (7), 354–364.

(14) Graham, I. D.; Harrison, M. B.; Shafey, M.; Keast, D. Knowledge and Attitudes Regarding Care of Leg Ulcers. Survey of Family Physicians. *Can Fam Physician* **2003**, *49* (7), 896–902.

(15) Richmond, N. A.; Maderal, A. D.; Vivas, A. C. Evidence-based Management of Common Chronic Lower Extremity Ulcers. *Dermatol Ther* **2013**, *26* (3), 187–196.

(16) Honnegowda, T. M.; Kumar, P.; Udupa, E. G. P.; Kumar, S.; Kumar, U.; Rao, P. Role of Angiogenesis and Angiogenic Factors in Acute and Chronic Wound Healing. *Plast Aesthet Res* **2015**, *2*, 243–249.

(17) Lemraski, E. G.; Jahangirian, H.; Dashti, M.; Khajehali, E.; Sharafinia, S.; Rafiee-Moghaddam, R.; Webster, T. J. Antimicrobial Double-Layer Wound Dressing Based on Chitosan/Polyvinyl Alcohol/Copper: In Vitro and in Vivo Assessment. *Int J Nanomedicine* **2021**, *16*, 223.

(18) Bella, J.; Kolatkar, P. R.; Marlor, C. W.; Greve, J. M.; Rossmann, M. G. The Structure of the Two Amino-Terminal Domains of Human ICAM-1 Suggests How It Functions as a Rhinovirus Receptor and as an LFA-1 Integrin Ligand. *Proc Natl Acad Sci* **1998**, *95* (8), 4140–4145.

(19) Casasnovas, J. M.; Stehle, T.; Liu, J.; Wang, J.; Springer, T. A. A Dimeric Crystal Structure for the N-Terminal Two Domains of Intercellular Adhesion Molecule-1. *Proc Natl Acad Sci* **1998**, *95* (8), 4134–4139.

(20) Manakan, B. S.; Roy, Z. Integrin Structure and Function. In *Cell-Extracellular matrix interactions in cancer*; Zent, R., Pozzi, A., Eds.; Springer Science, **2010**; pp 19–41.

(21) WR, B. Cosman B: Histologic Basis of Keloid and Hypertrophic Scar Differentiation: Clinicopathologic Correlation. *Arch Pathol* **1966**, *82*, 65.

(22) Humphries, M. J.; McEwan, P. A.; Barton, S. J.; Buckley, P. A.; Bella, J.; Mould, A. P. Integrin Structure: Heady Advances in Ligand Binding, but Activation Still Makes the Knees Wobble. *Trends Biochem Sci* **2003**, *28* (6), 313–320.

(23) Brauchle, M.; Fässler, R.; Werner, S. Suppression of Keratinocyte Growth Factor Expression by Glucocorticoids in Vitro and during Wound Healing. *J Invest Dermatol* **1995**, *105* (4), 579–584.

(24) Dowsett, C.; von Hallern, B. The Triangle of Wound Assessment: A Holistic Framework from Wound Assessment to Management Goals and Treatments. *Wounds Int* **2017**, *8* (4), 34–39.

(25) Pierce, G. F.; Mustoe, T. A.; Altrock, B. W.; Deuel, T. F.; Thomason, A. Role of Platelet-derived Growth Factor in Wound Healing. *J Cell Biochem* **1991**, *45* (4), 319–326.

(26) Casasnovas, J. M.; Stehle, T.; Liu, J.; Wang, J.; Springer, T. A. A Dimeric Crystal Structure for the N-Terminal Two Domains of Intercellular Adhesion Molecule-1. *Proc Natl Acad Sci* **1998**, *95* (8), 4134–4139.

(27) Bella, J.; Berman, H. M. Integrin-Collagen Complex: A Metal-Glutamate Handshake. *Structure* **2000**, *8* (6), R121 – R126.

(28) Lee, J.-O.; Rieu, P.; Arnaout, M. A.; Liddington, R. Crystal Structure of the A Domain from the Subunit of Integrin CR3 (CD11 b/CD18). *Cell* **1995**, *80* (4), 631–638.

(29) Qu, A.; Leahy, D. J. The Role of the Divalent Cation in the Structure of the I Domain from the CD11a/CD18 Integrin. *Structure* **1996**, *4* (8), 931–942.

(30) Macri, L.; Clark, R. A. F. Tissue Engineering for Cutaneous Wounds: Selecting the Proper Time and Space for Growth Factors, Cells and the Extracellular Matrix. *Skin Pharmacol Physiol* **2009**, *22* (2), 83–93.

(31) Cooper, D. M.; Yu, E. Z.; Hennessey, P.; Ko, F.; Robson, M. C. Determination of Endogenous Cytokines in Chronic Wounds. *Ann Surg* **1994**, *219* (6), 688.

(32) Humphries, J. D.; Byron, A.; Humphries, M. J. Integrin Ligands at a Glance. *J Cell Sci* **2006**, *119* (19), 3901–3903.

(33) Leshchyns'ka, I.; Sytnyk, V. Reciprocal Interactions between Cell Adhesion Molecules of the Immunoglobulin Superfamily and the Cytoskeleton in Neurons. *Front Cell Dev Biol* February 16, **2016**, *4* (9), 1 – 10.

(34) Koivisto, L.; Heino, J.; Häkkinen, L.; Larjava, H. Integrins in Wound Healing. *Adv Wound Care (New Rochelle)* **2014**, *3* (12), 762–783.

(35) Veit G, Kobbe B, Keene DR, Paulsson M, Koch M, Wagener R. Collagen XXVIII, a Novel von Willebrand Factor A Domain-Containing Protein with Many Imperfections in the Collagenous Domain. *J Biol Chem* **2006**,281, 3494–3504.

(36) Brinckmann J. Collagens at a Glance. *Top Curr Chem* 2005;247:1—-6.

(37) Myllyharju, J. Prolyl 4-Hydroxylases, the Key Enzymes of Collagen Biosynthesis. *Matrix Biol* **2003**, *22* (1), 15–24.

(38) Prockop, D. J.; Kivirikko, K. I. Collagens: Molecular Biology, Diseases, and Potentials for Therapy. *Annu Rev Biochem* **1995**, *64* (1), 403–434.

(39) Kagan, H. M.; Li, W. Lysyl Oxidase: Properties, Specificity, and Biological Roles inside and Outside of the Cell. *J Cell Biochem* **2003**, *88* (4), 660–672.

(40) Dölz, R.; Engel, J. Nucleation, Propagation, and Direction of Triple Helix Formation in Collagens I, III, and IV and in Gelatin as Monitored by Electron Microscopy a. *Ann N Y Acad Sci* **1990**, *580* (1), 421–424.

(41) Samantha Chui. Sequence Motif Identification; **2004**.

(42) Shoulders, M. D.; Raines, R. T. Collagen Structure and Stability. *Annu Rev Biochem* **2009**, *78*, 929.

(43) Nowick, J. S. Exploring β-Sheet Structure and Interactions with Chemical Model Systems. *Acc. Chem. Res.* **2008**, *41* (10), 1319–1330.

(44) He, X.; Xie, L.; Zhang, X.; Lin, F.; Wen, X.; Teng, B. The Structural Characteristics of Collagen in Swim Bladders with 25-Year Sequence Aging: The Impact of Age. *Appl Sci (Switzerland)* **2021**, *11* (10).

(45) Sood, A.; Granick, M. S.; Tomaselli, N. L. Wound Dressings and Comparative Effectiveness Data. *Adv Wound Care (New Rochelle)* **2014**, *3* (8), 511–529.

(46) Dhivya, S.; Padma, V. V.; Santhini, E. Wound Dressings–a Review. *Biomedicine (Taipei)* **2015**, *5* (4), 1–5.

(47) Debra, J. B.; Cheri, O. Wound Healing: Technological Innovations and Market Overview. *Technology Catalysts International Corporation* **1998**, *2*, 1–185.

(48) Jones, V.; Milton, T. When and How to Use Hydrogels. *Nurs Times* **2000**, *96* (23 Suppl), 3–4.

(49) Powers, J. G.; Morton, L. M.; Phillips, T. J. Dressings for Chronic Wounds. *Dermatol Ther* **2013**, *26* (3), 197–206.

(50) Ramundo, J.; Gray, M. Enzymatic Wound Debridement. *J Wound Ostomy Continence Nurs* **2008**, *35* (3), 273–280.

(51) Dabiri, G.; Damstetter, E.; Phillips, T. Choosing a Wound Dressing Based on Common Wound Characteristics. *Adv Wound Care (New Rochelle)* **2016**, *5* (1), 32–41.

(52) Sayag, J.; Lieaume, S.; Bohbot, S. Healing Properties of Calcium Alginate Dressings. *J Wound Care* **1996**, *5* (8), 357–362.

(53) Falanga, V.; Lindholm, C.; Carson, P. A.; Panuncialman, J.; Mamakos, L.; Tiziana, L. N.; Falanga, J. K. *Text Atlas of Wound Management*; CRC Press, **2012**.

(54) Bello, Y. M.; Phillips, T. J. Management of Venous Ulcers. *J Cutan Med Surg* **1998**, *3*, S1–6.

(55) Fonder, M. A.; Lazarus, G. S.; Cowan, D. A.; Aronson-Cook, B.; Kohli, A. R.; Mamelak, A. J. Treating the Chronic Wound: A Practical Approach to the Care of Nonhealing Wounds and Wound Care Dressings. *J Am Acad Dermatol* **2008**, *58* (2), 185–206.

(56) Nielsen, J.; Fogh, K. Clinical Utility of Foam Dressings in Wound Management: A Review. *Chronic Wound Care Manag. Res* **2015**, *2*, 31.

(57) KIM, Y.-J.; LEE, S.-W.; HONG, S.-H.; LEE, H.-K.; KIM, E.-K. The Effects of PolyMem (R) on the Wound Healing. *J Korean Soc Plast Reconstr Surg* **1999**, 1165–1172.

(58) Benskin, L. L. L. PolyMem® Wic® Silver® Rope: A Multifunctional Dressing for Decreasing Pain, Swelling, and Inflammation. *Adv Wound Care (New Rochelle)* **2012**, *1* (1), 44–47.

(59) Edwards, J. V.; Howley, P. S. Human Neutrophil Elastase and Collagenase Sequestration with Phosphorylated Cotton Wound Dressings. *Journal of Biomedical Materials Research Part A: An Official Journal of The Society for Biomaterials, The Japanese Society for Biomaterials, and The Australian Society for Biomaterials and the Korean Society for Biomaterials* **2007**, *83* (2), 446–454.

(60) Cullen, B.; Smith, R.; Mcculloch, E.; Silcock, D.; Morrison, L. Mechanism of Action of PROMOGRAN, a Protease Modulating Matrix, for the Treatment of Diabetic Foot Ulcers. *Wound Repair Regen* **2002**, *10* (1), 16–25.

(61) Lansdown, A. B. G. Silver I: Its Antibacterial Properties and Mechanism of Action. *J Wound Care* **2002**, *11* (4), 125–130.

(62) Leaper, D. Appropriate Use of Silver Dressings in Wounds: International Consensus Document. *Int Wound J* **2012**, *9* (5), 461.

(63) Zhou, L. H.; Nahm, W. K.; Badiavas, E.; Yufit, T.; Falanga, V. Slow Release Iodine Preparation and Wound Healing: In Vitro Effects Consistent with Lack of in Vivo Toxicity in Human Chronic Wounds. *Br. J. Dermatol.* **2002**, *146* (3), 365–374.

(64) Drosou, A.; Falabella, A.; Kirsner, R. S. Antiseptics on Wounds: An Area of Controversy. *Wounds* **2003**, *15* (5), 149–166.

(65) Kadler, K. E.; Baldock, C.; Bella, J. Boot--Handford, R. P. Collagens at a Glance. *J Cell Sci* **1955**, *120*.

(66) Myllyharju, J.; Kivirikko, K. I. Collagens, Modifying Enzymes and Their Mutations in Humans, Flies and Worms. *TRENDS in Genetics* **2004**, *20* (1), 33–43.

(67) Beck, K.; Boswell, B. A.; Ridgway, C. C.; Bächinger, H. P. Triple Helix Formation of Procollagen Type I Can Occur at the Rough Endoplasmic Reticulum Membrane. *J. Biol. Chem.* **1996**, *271* (35), 21566–21573.

(68) Myllyharju, J.; Kivirikko, K. I. Collagens, Modifying Enzymes and Their Mutations in Humans, Flies and Worms. *TRENDS Genet* **2004**, *20* (1), 33–43.

(69) Canty, E. G.; Kadler, K. E. Procollagen Trafficking, Processing and Fibrillogenesis. *J Cell Sci* **2005**, *118* (7), 1341–1353.

(70) McLaughlin, S. H.; Bulleid, N. J. Molecular Recognition in Procollagen Chain Assembly. *Matrix Biology* **1998**, *16* (7), 369–377.

(71) Claverie, M.; McReynolds, C.; Petitpas, A.; Thomas, M.; Fernandes, S. Marine-Derived Polymeric Materials and Biomimetics: An Overview. *Polymers (Basel)* **2020**, *12* (5), 1002.

(72) Vasita, R.; Katti, D. S. Nanofibers and Their Applications in Tissue Engineering. *Int J Nanomedicine* **2006**, *1* (1), 15.

(73) Hosoyama, K.; Lazurko, C.; Muñoz, M.; McTiernan, C. D.; Alarcon, E. I. Peptide-Based Functional Biomaterials for Soft-Tissue Repair. *Front Bioeng Biotechnol* **2019**, 205.

(74) Girotti, A.; Reguera, J.; Rodríguez-Cabello, J. C.; Arias, F. J.; Alonso, M.; Testera, A. M. Design and Bioproduction of a Recombinant Multi (Bio) Functional Elastin-like Protein Polymer Containing Cell Adhesion Sequences for Tissue Engineering Purposes. *J Mater Sci Mater Med* **2004**, *15* (4), 479–484.

(75) Chen, F.-M.; Liu, X. Advancing Biomaterials of Human Origin for Tissue Engineering. *Prog Polym Sci* **2016**, *53*, 86–168.

(76) Collier, J. H.; Segura, T. Evolving the Use of Peptides as Biomaterials Components. *Biomaterials* **2011**, *32* (18), 4198.

(77) Varanko, A.; Saha, S.; Chilkoti, A. Recent Trends in Protein and Peptide-Based Biomaterials for Advanced Drug Delivery. *Adv Drug Deliv Rev* **2020**, *156*, 133–187.

(78) Discovery Studio. Client 16.1.0. San Diego, CA, USA.

(79) Biovia, D. S. Discovery Studio Modeling Environment. *Release* **2017**.

(80) Leitinger, B.; Hohenester, E. Mammalian Collagen Receptors. *Matrix Biol.* April **2007**, pp 146–155.

(81) Beck, K.; Brodsky, B. Supercoiled Protein Motifs: The Collagen Triple-Helix and the a-Helical Coiled Coil. *J. Struct. Biol*. **1998,** *122* (1 - 2), 17 - 29.

(82) Okuyama, K. Revisiting the Molecular Structure of Collagen. *Connect Tissue Res*. **2008**, pp 299–310.

(83) Zhao, X.; Zhang, X.; Liu, D. Collagen Peptides and the Related Synthetic Peptides: A Review on Improving Skin Health. *J. Funct. Foods*. Elsevier Ltd November 1, **2021**.

(84) Štimac, A.; Šekutor, M.; Mlinarić-Majerski, K.; Frkanec, L.; Frkanec, R. Adamantane in Drug Delivery Systems and Surface Recognition. *Molecules*. MDPI AG February 1, **2017**.

(85) Chee, F. C.; Guy, A.; Biggin, P. C. Distribution and Dynamics of Adamantanes in a Lipid Bilayer. *Biophys J* **2008**, *95* (12), 5627–5636.

(86) Hruby, V. J.; Balse, P. M. Conformational and Topographical Considerations in Designing Agonist Peptidomimetics from Peptide Leads. *Curr. Med. Chem*. **2000**, *7* (9).

(87) Bruno, B. J.; Miller, G. D.; Lim, C. S. Basics and Recent Advances in Peptide and Protein Drug Delivery. *Ther Deliv*. November **2013**, pp 1443–1467.

(88) Adessi, C.; Soto, C. Converting a Peptide into a Drug: Strategies to Improve Stability and Bioavailability. *Curr. Med. Chem*. **2002,** *9* (9), 963 – 978.

(89) Werle, M.; Bernkop-Schnürch, A. Strategies to Improve Plasma Half Life Time of Peptide and Protein Drugs. *Amino Acids*. June **2006**, pp 351–367. https://doi.org/10.1007/s00726-005-0289-3.

(90) Seia, M.; Zisman, E. Different Roles of D-amino Acids in Immune Phenomena. *The FASEB J* **1997**, *11* (6), 449–456.

(91) Zuckermann, R. N. Peptoid Origins. *Biopolymers*. **2011**, pp 545–555.

(92) Corson, A. E.; Armstrong, S. A.; Wright, M. E.; McClelland, E. E.; Bicker, K. L. Discovery and Characterization of a Peptoid with Antifungal Activity against Cryptococcus Neoformans. *ACS Med Chem Lett* **2016**, *7* (12), 1139–1144.

(93) Mas-Moruno, C.; Cruz, L. J.; Mora, P.; Francesch, A.; Messeguer, A.; Pérez-Payá, E.; Albericio, F. Smallest Peptoids with Antiproliferative Activity on Human Neoplastic Cells. *J Med Chem* **2007**, *50* (10), 2443–2449.

(94) Chongsiriwatana, N. P.; Patch, J. A.; Czyzewski, A. M.; Dohm, M. T.; Ivankin, A.; Gidalevitz, D.; Zuckermann, R. N.; Barron, A. E. Peptoids That Mimic the Structure, Function, and Mechanism of Helical Antimicrobial Peptides. *Proc Natl Acad Sci* **2008**, *105* (8), 2794–2799.

(95) Uchida, M.; McDermott, G.; Wetzler, M.; le Gros, M. A.; Myllys, M.; Knoechel, C.; Barron, A. E.; Larabell, C. A. Soft X-Ray Tomography of Phenotypic Switching and the Cellular Response to Antifungal Peptoids in Candida Albicans. *Proc Natl Acad Sci* **2009**, *106* (46), 19375–19380.

(96) Mielke, S. P.; Krishnan, V. V. Characterization of Protein Secondary Structure from NMR Chemical Shifts. *Prog Nucl Magn Reson Spectrosc* April 5, **2009**, pp 141–165.

(97) Zerbe, O.; Bader, R. Peptide NMR.

(98) Logan, T. M. Macromolecular NMR Spectroscopy; **2005**.

(99) Woody, W. R. [4] Circular Dichroism. *Methods Enzymol* **1995**, *246*, 34–71.

(100) Dinitto, J. M.; Kenney, J. M. Noise Characterization in Circular Dichroism Spectroscopy. *Appl Spectrosc* **2012**, *66* (2), 180–187.

(101) Wang, A. Y.; Leong, S.; Liang, Y. C.; Huang, R. C. C.; Chen, C. S.; Yu, M. S. Immobilization of Growth Factors on Collagen Scaffolds Mediated by Polyanionic Collagen Mimetic Peptides and Its Effect on Endothelial Cell Morphogenesis. *Biomacromolecules* **2008**, *9* (10), 2929–2936.

(102) Czechowicz, P.; Jaśkiewicz, M.; Neubauer, D.; Gościniak, G.; Kamysz, W. Anticandidal Activity of Omiganan and Its Retro Analog Alone and in Combination with Fluconazole. *Probiotics Antimicrob. Proteins* **2021**, *13*, 1173–1182.

CHAPTER II

DOI: 10.1002/psc.3531

RESEARCH ARTICLE

Journal of PeptideScience WILEY

Design, synthesis, and characterization of type I collagen mimetic peptides

Ntlama Lesotho | Thabo Peme | Maya Makatini

Molecular Sciences Institute, School of Chemistry, University of the Witwatersrand, Johannesburg, South Africa

Correspondence
Maya Makatini, Molecular Sciences Institute, School of Chemistry, University of the Witwatersrand, Private Bag 3, PO WITS, Johannesburg 2050, South Africa.
Email: maya.makatini@wits.ac.za

Funding information
National University of Lesotho; National Manpower Development Secretariat; National Research Foundation, Grant/Award Numbers: 117975, 138081

The current wound-healing collagen mimetic peptides (CMPs) have limitations such as poor membrane permeability and protease susceptibility. Herein, the solid-phase peptide synthesis of CMPs containing the integrin binding motif GFOGER is reported. The peptide sequences also consist of lipophilic moieties (adamantane and palmitic acid) for improved membrane permeability and different collagen-inducing tripeptides, namely, Thr-Thr-Lys (TTK), Gly-His-Lys (GHK), Gln-Pro-Arg (QPR), and Glu-Glu-Met (EEM). The synthesized peptides were successfully characterized and purified using liquid chromatography-mass spectrometry and preparative high-performance liquid chromatography techniques, respectively. The palmitic acid moiety increased the hydrophobic nature of the peptides, and they were retained longer on the stationary material of the reverse phase C-18 column. The three-dimensional parallel-strand helical structure of peptide DGD-GG-GFOGER-GG-TTK-palmitate was obtained using nuclear magnetic resonance spectroscopy and circular dichroism. The synthesized peptides have the desired helical structure, which can promote integrin binding.

KEYWORDS
Adamantine, collagen mimetic peptides, collagen-inducing peptides, growth factors, integrin-binding motif, palmitic acid, parallel helix

1 | INTRODUCTION

The integrin $\alpha_2\beta_1$ *alpha* I-domain is the primary ligand binding region and has the receptors that interact with collagen.[1] Integrin $\alpha_1\beta_1$ and $\alpha_2\beta_1$ are the major integrin receptors for the recognition of type I collagen, which contains the GFOGER amino acid sequence. The GFOGER has been identified as the major binding motif of collagen I. It has been reported that the binding of collagen to the integrins involves the collagen carboxyl-divalent cations coordination at the top of the I-domain and the glutamate is the source of this carboxyl. The glycine (G) amino acid is vital for the folding of the triple helix.[2] Hydroxyproline (O) is responsible for hydrogen bonding and stereoelectronic effect during binding with the integrin.[3,4] Phenylalanine allows for hydrophobic interaction.[3] The peptide sequence of interest should mimic the GFOGER collagen motif sequence. To enhance the tissue repair process, tripeptides' signaling growth factors can be added to the sequence.[5]

Growth factors are hormone-like molecules that interact with specific receptors to control and regulate each phase of wound heal-ing.[6] The tissue repair process is initiated immediately after injury by the release of various growth factors, cytokines, and low molecular-weight compounds from the serum of injured blood vessels and from degranulating platelets. Growth factors are polypeptides that control the growth, differentiation, and metabolism of cells. Various growth factors that are released at the wound site are pre-sumed to be essential for wound healing. These include epidermal growth factor (EGF), fibroblast growth factor (FGF), keratinocyte growth factor (KGF), transforming growth factor (TGF), and vascular endothelial growth factor (VEGF).[7]

2 | DESIGN OF PEPTIDE MIMICS

The collagen mimetic peptides (CMPs) that exist today have limitations such as poor membrane permeability and are susceptible to protease degradation. To improve membrane permeability, palmitic acid (fatty acid) and cage moieties such as adamantane were incorporated into the peptide sequences. Palmitic acid has been reported to be a good mitochondrial permeability transition promoter, and various cosmetics companies have designed anti-aging creams with peptides coupled with palmitic acids.[8] Adamantane (cage) derivatives have been previously reported to enhance biological activity,[9] membrane permeability, and retard biodegradation when incorporated into biologically active molecules.[10]

The designed peptides comprise lipophilic moieties, the integrin-binding type I collagen motif, -GFOGER-, the DGD tripeptide for attraction of growth factors,[5] the tripeptides Thr-Thr-Lys (TTK), Gly-His-Lys (GHK), Gln-Pro-Arg (QPR), and Glu-Glu-Met (EEM) to stimulate collagen production (Figure 1).[11]

The GG dipeptides on either side of the collagen motif act as spacers, meant to reduce the steric hindrance around the GFOGER motif. With all these modifications implemented, the envisaged peptide structure is shown in Figure 1.

Thus, this study involves the design and synthesis of novel membrane permeating wound healing CMPs coupled to collagen-inducing tripeptide sequences.

3 | PEPTIDE SYNTHESIS

Eight palmitate peptides and one control adamantane peptide (DGRGOF-adamantane) were synthesized, using the solid-phase peptide synthesis strategy. Chlorotrityl resin (600 mg) was weighed into a reaction vessel. The resin was first activated with thionyl chloride (2 ml) and dry DCM (10 ml) overnight at room temperature. After filtering and washing the resins with dry DCM (4 ml x 5), the first amino acid Fmoc-Asp(OtBu)-OH (0.987 g, 0.2 M) was attached to the resin through the C-terminal. This amino acid was first dissolved in dry DCM. Thereafter, DIPEA (2.0 ml, 1 M) was added. The resultant reaction mixture was gently mixed by bubbling nitrogen gas into the reaction for 45 min. After the coupling of the Fmoc-Asp(OtBu)-OH, the resin was washed with DMF (3 x 5 ml), followed by DCM (3 x 5 ml) to remove excess reagents and by-products.

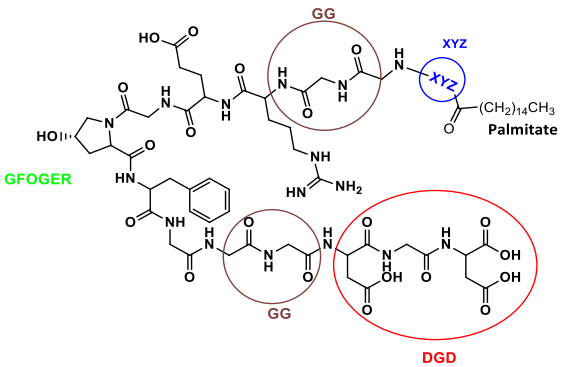

FIGURE 1 General structure of collagen mimetic peptide; XYZ can either be TTK/GHK/QPR/EEM.

A 20% piperidine solution (10 ml) was added twice for 5 min to remove the protecting group, and the reaction was mixed by bubbling a gentle stream of nitrogen gas. The resin was then washed with DMF (3 x 5 ml), followed by DCM (3 x 5 ml) to remove excess reagents.

The second amino acid Fmoc-Gly-OH (0.429 g, 0.12 M) was coupled to the resin attached amino acid by using a coupling reagent HBTU (0.519 g, 0.11 M) and DIPEA (1.26 ml, 0.6 M) as the base. The resultant reaction mixture was gently mixed by bubbling nitrogen gas into the reaction for 45 min. The resin was washed with DMF (3 x 5 ml), followed by DCM (3 x 5 ml) to remove excess reagents. The same coupling process was utilized to couple all the other amino acids.

The adamantane carboxylic acid (0.260 g, 0.12 M) or palmitic acid (0.369 g, 0.12 M) were prepared in DMF (10.74 ml). These solutions were added to the resin-bound peptides along with HBTU (0.519 g, 0.11 M) and DIPEA (1.26 ml, 0.6 M). The washing procedures are similar to the one above. The cleavage of the peptide from the resin was achieved by reacting the resin bound peptides with a solution of 95% TFA, 2.5% water, and 2.5% TIS for 3 h with gentle shaking. The cleavage solution was filtered off, and the resin was washed with 5 ml of TFA, and the filtrate was poured into 50 ml centrifuge tubes. Cold diethyl ether was added to the filtered solution upon which a white precipitate of the crude peptide was formed. The samples were centrifuged at 5,000 rpm for 10 min. The step was repeated three times with cold diethyl ether. The general scheme for the synthesis of CMPs is shown in Scheme 1.

Each peptide was dissolved in acetonitrile and a few drops of formic acid for the mass spectral analysis. The successful synthesis of the peptides was evidenced by ultra-high performance liquid chromatography-mass spectrometry as shown in Table 1.

All the control peptides were eluted after 8 min with a high percentage (85%) of acetonitrile (HPLC gradient elution method 5–95% acetonitrile in 14 min).

This observation was attributed to the non-polar aliphatic chain ($-[CH_2]_{14}CH_3$) of palmitic acid, which can form strong hydrophobic interactions with the C-18 hydrocarbon chain. The hydrophobicity is more pronounced in DGRGOF-palmitate. The DGRGOF peptides were not derived from collagen 1 but were designed from the well-researched integrin binding RGD[12] peptide sequence to be used as a control; hence, its conformational structure could be different and potentially favor stronger interactions with the stationary phase. This behavior might indicate that the palmitate peptides will have a good affinity for the cell wall membrane lipids, hence improved membrane permeability.

According to Table 1, longer peptides coupled to palmitic acid have shorter retention times. An increase in the length of the peptides resulted in an increase in the hydrophilicity of the peptides. This could be attributed to the introduction of polar amino acids.

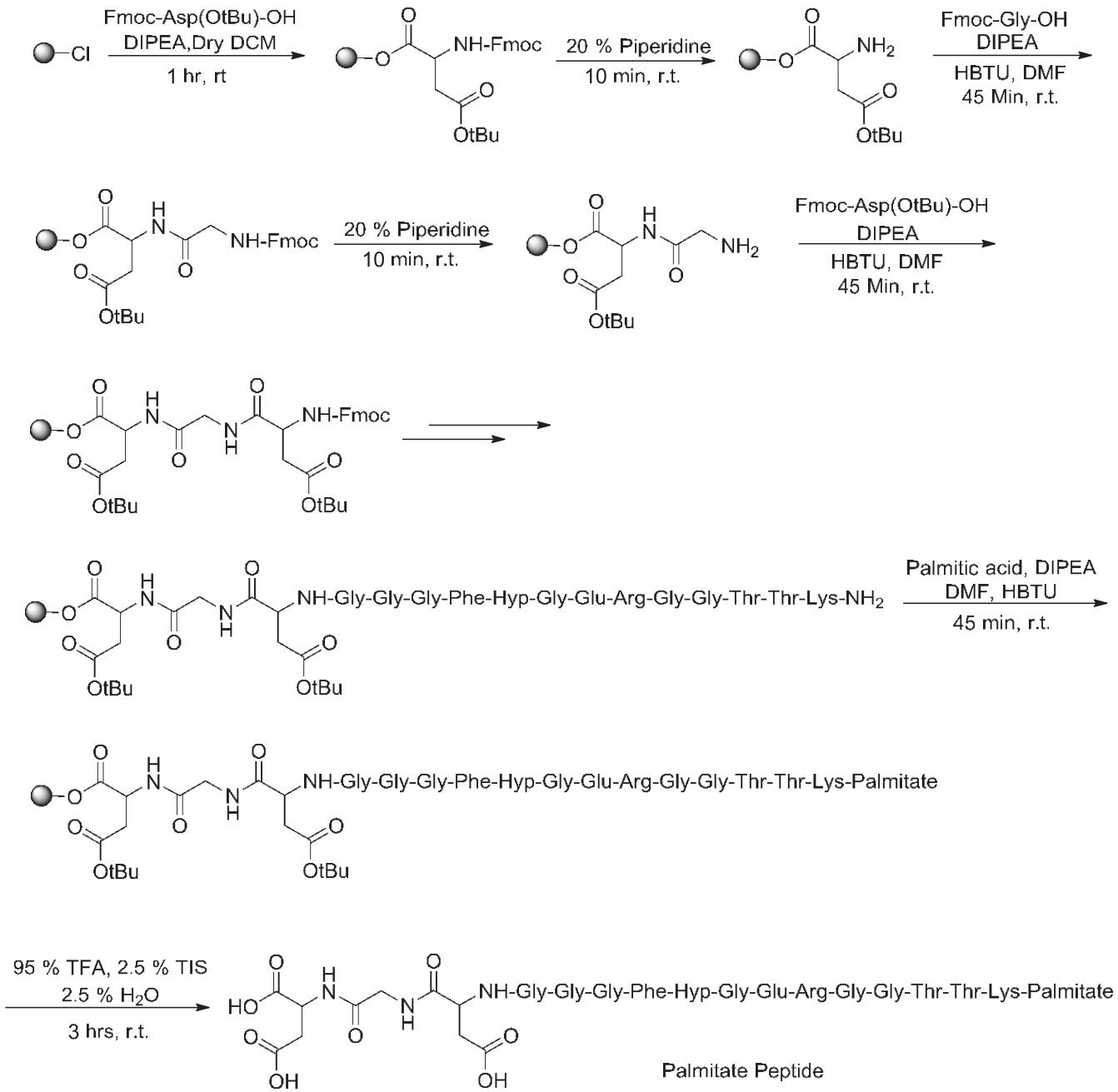

SCHEME 1 General scheme for the synthesis of palmitate peptides.

The DGD-GG-GFOGER-GG-TTK and DGD-GG-GFOGER-GG-QPR have almost the same retention times, DGD-GG-GFOGER-GG-GHK-palmitate is relatively more hydrophilic, and DGD-GG-GFOGER-GG-GG-EEM-palmitate is more hydrophobic. The EEM amino acid sequence is acidic, while the other tripeptides TTK, GHK, and QPR are basic; hence, the presence of basic residues might reduce membrane permeability but improve aqueous solubility.

Comparison of the control palmitate peptides GOP-GFOGER-GOP-, GG-GFOGER-GG-, and DGD-GG-GFOGER-GG- further reveals that the tripeptides, GOP, and DGD and the dipeptide GG possibly do not have any observable influence in terms of the polarity of the peptides as all the peptides elute at approximately the same time

4 | GEOMETRIC ISOMERS

Another observation that was made from mass spectrometry (Table 1) is that peptides seem to exist as conformers. The peaks appear to be slightly split, and the resulting peaks have the same molecular weight. The peak splitting is however not observed in DGD-GG-GFOGER-

TABLE 1 Percentage yields and mass spectrometry data of peptides.

Control peptide	Palmitate-tripeptide	Calculated mass (g/mol)	Experimental mass (g/mol)	Yield (%)	Retention time (min)
DGRGOF-palmitate	-	901.5273 ($C_{44}H_{71}N_9O_{11}$)	902.5413 $[M + H]^+$	43	9.61
DGRGOF-adamantane	-	825.4021 ($C_{39}H_{55}N_9O_{11}$)	826.4111 $[M + H]^+$	39	5.79
GOP-GFOGER-GOP-palmitate	-	1,449.7868 ($C_{69}H_{107}N_{15}O_{19}$)	1,451.7978 $[M + H]^+$	36	Peak 1 = 8.00 Peak 2 = 8.20
GG-GFOGER-GG-palmitate	-	1,143.6288 ($C_{53}H_{85}N_{13}O_{15}$)	1,144.6346 $[M + H]^+$	31	Peak 1 = 8.30 Peak 2 = 8.40
DGD-GG-GFOGER-GG-palmitate	-	1,430.7042 ($C_{63}H_{98}N_{16}O_{22}$)	1,431.7201 $[M + H]^+$	31	Peak 1 = 8.33 Peak 2 = 8.4
-	DGD-GG-GFOGER-GG-TTK-	1,760.8945 ($C_{77}H_{124}N_{20}O_{27}$)	881.4604 $[M + 2H]^{2+}$	32	6.42
-	DGD-GG-GFOGER-GG-GHK	1,752.8795 ($C_{77}H_{120}N_{22}O_{25}$)	877.4499 $[M + 2H]^{2+}$	28	6.00
-	DGD-GG-GFOGER-GG-QPR	1,811.9166 ($C_{79}H_{125}N_{23}O_{26}$)	907.0723 $[M + 2H]^{2+}$	14	6.54
-	DGD-GG-GFPGER-GG-EEM	1,819.8298 ($C_{78}H_{121}N_{19}O_{29}S$)	1,821.8628 $[M + H]^+$	34	9.00

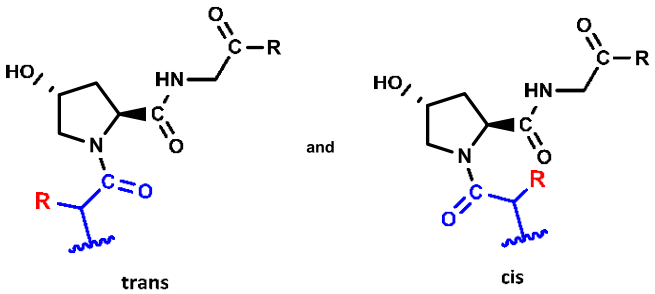

FIGURE 2 Geometric isomers of the peptides.

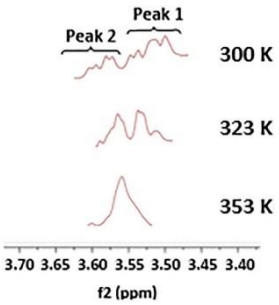

FIGURE 3 Sections of ^{1}H NMR spectra at different temperatures.

GG-TTK-palmitate, DGD-GG-GFOGER-GG-GHK-palmitate, and DGD-GG-GFOGER-GG-QPR-palmitate, suggesting that longer peptides are restricted and cannot rotate easily to form isomers.

The presence of conformers can be attributed to hydroxyproline and proline (the imino acids), which have a secondary amine group. These amino acids couple with other amino acids to form tertiary amides, which have a high population of both *cis* and *trans* geometric isomers as shown in Figure 2.[2]

In addition to α-helix, or fully extended conformation, proline and hydroxyproline derivatives may give rise to geometric isomers of the same peptide.[13] In most cases, the *trans* isomer is favored over the *cis* isomer.[2] The reason for the latter is that the *cis* isomer places the R groups of the two connected amino acids near each other as shown in Figure 2.

To prove the existence of geometric conformers, ^{1}H NMR temperature experiment for the peptide DGRGOF-adamantane was conducted. The proton spectrum, Figure 3 showed two distinct *alpha* protons at 3.50 and 3.60 ppm, which belong to the *trans* and *cis* isomers.

At 300 K, the two conformers of the peptide in DMSO-d_6 were detected independently. At 323 K, the signals for the two conformers were still individually detected, although the two signals had moved closer together to form a distorted doublet. Eventually, the two signals coalesced to a single peak at 3.55 ppm at a coalescence temperature, T_C, of 353 K. When the NMR experiment is conducted at elevated temperatures, the two peaks appear to coalesce to form one peak, thereby indicating rotation of the amide bond, possibly that of *cis* isomer to attain a different more stable *trans* configuration. The result of the experiment, done at 300, 323, and 353 K, is shown in Figure 3.

The two peaks appear to be distinct at 300 and 323 K because an amide bond has a double bond character and therefore not free to rotate. The supplied energy helps to overcome the energy barrier responsible for the existence of *cis* conformer, and all the peptides attain the same *trans* conformation (Scheme 2).[14,15]

Orientation of the amide bond is important in terms of the stability of the peptide. All the peptide bonds in collagen triple helix are

trans.[2] This means that the formation of *cis* amide bonds by the tertiary amide is a disadvantage because *cis* amide bonds cannot form stable triple helices. That is, all the *cis* amide bonds must first be converted to *trans* to form triple helices. Only when in *trans* orientation the carbonyl oxygen of the subsequent amino acid residue (O_{i-1}) can donate electron density into the antibonding orbital of the carbonyl ($C_i = O_i$) of hydroxyproline (n ! π*), reinforcing the stability of the peptide.[16,17]

5 | SECONDARY STRUCTURE ELUCIDATION OF DGD-GG-GFOGER-GG-TTK-PALMITATE

The secondary structure of DGD-GG-GFOGER-GG-TTK-palmitate was elucidated employing the circular dichroism experiment. Furthermore, the NMR experiment was used to elucidate the three-dimensional structure.

The spectrum of DGD-GG-GFOGER-GG-TTK-palmitate has two strong bands characteristic of an alpha-helical structure as shown in Figure 4.

The chromatogram shows two strong negative bands at 208 and 222 nm, which are characteristic of an alpha helix configuration.[18,19] Parallel beta strands were also detected (Table 2). This is in line with the natural structural conformation of collagen, which comprises of a right-handed bundle of three parallel, left-handed polyproline II-type helices.[2] The peptide DGD-GG-GFOGER-GG-QPR-palmitate also exhibits a similar secondary structure of a parallel stranded helix. The more basic DGD-GG-GFOGER-GG-GHK-palmitate sequence and the more acidic DGD-GG-GFOGER-GG-GG-EEM-palmitate peptides exhibit a higher content of the helical conformation and the stable antiparallel strand arrangement. These peptides have managed to form a dominant consistent helical conformation, especially DGD-GG-GFOGER-GG-GHK-palmitate.

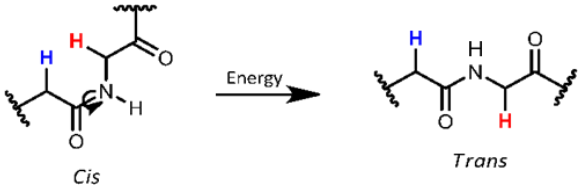

SCHEME 2 Conversion of *cis* to *trans* isomer.

6 | NMR TERTIARY STRUCTURE ELUCIDATION OF DGD-GG-GFOGER-GG-TTK-PALMITATE

6.1 | ^{1}H NMR

The tertiary structure of DGD-GG-GFOGER-GG-TTK-palmitate peptide (Table 3) was elucidated, and the full characterization is shown in Table S1.

TOCSY experimental result, as depicted in Figures S40 and S41, reveals that there are 15 spin systems. The presence of cross peaks in the methyl region of the spectrum is indicative of the spin system of threonine. It is the only amino acid that has the methyl group in the peptide DGD-GG-GFOGER-GG-TTK-palmitate. The threonine spin system has only three peaks due to the interaction of *alpha* with *beta* and *gamma* methyl protons.

A spin system that has only one cross peak and, in which the observed peak is in the α-region (3.5–4.6 ppm) of the TOCSY spectrum, is characteristic of glycine. The spin system of lysine was identifiable by its six cross peaks. In terms of the arrangement of the peaks, lysine has $A_2(F_2T_2)MTX$ spin system.[20] The arrangement of peaks in the spin system, in order of decreasing chemical shift, is $H^{\alpha} > H^{\varepsilon} > H^{\beta} > H^{\beta} > H^{\delta} > H^{\gamma}$.[21]

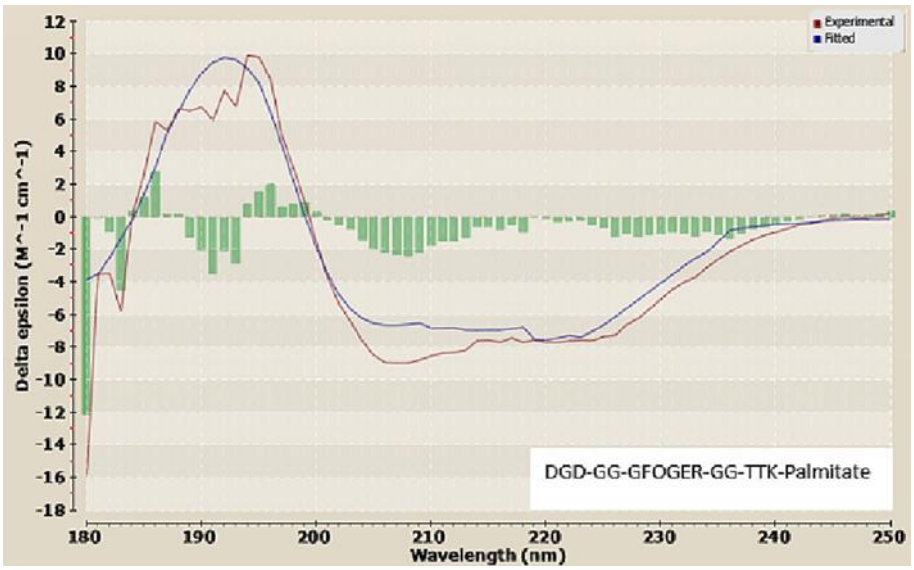

FIGURE 4 DGD-GG-GFOGER GG-TTK-palmitate circular dichroism spectrum.

Peptide	Helix (%)	Antiparallel (%)	Parallel (%)	Turn (%)	Other (%)
DGD-GG-GFOGER-GG-TTK-Palmitate	28.3	0.0	29	0	42.7
DGD-GG-GFOGER-GG-GHK-Palmitate	74.0	11.1	0.0	14.9	0.0
DGD-GG-GFOGER-GG-QPR-Palmitate	34.0	4.5	24.5	0.0	37.1
DGD-GG-GFOGER-GG-EEM-Palmitate	52.5	12.3	0.0	4.3	30.9

TABLE 2 Estimated secondary structure content of the palmitate pepides.

Hyp-Arg (α-helix)	Expected interaction	Observed interaction	Coupling range
$d_{\alpha\beta}(i, i + 3)$	4.74, (2.56, 2.44)	4.75, 2.56; 4.74, 2.40	Medium
$d_{\alpha N}(i, i + 3)$	4.74, 7.73	4.74, 7.73	Medium
$d_{NN}(i, i + 3)$	8.14, 7.73	8.14, 7.71	Medium
$d_{\alpha N}(i, i + 4)$	4.74, 8.02	Not observable	-

TABLE 3 Long-range coupling obtained from the ROESY spectrum.

An ambiguity is observed regarding glutamic acid, hydroxyproline, and arginine. The spin systems for these amino acid residues all have five peaks. That is, the length of the spin system is the same; they all have the $A_2(T_2)MPX$ system.[20] However, glutamic acid is distinguish-able from these amino acid residues in that, in order of decreasing chemical shift, hydroxyproline and arginine are the same, both having $H^{\alpha} > H^{\delta} > H^{\beta} > H^{\beta} > H^{\gamma}$.

Glutamic acid was identifiable by its characteristic pattern of cross peaks, having AM (PT)X system.[20] All the protons on both the beta and gamma carbons are different in terms of chemical shift; therefore, the spin system has five peaks. In order of decreasing chemical shift, there is $H^{\alpha} > H^{\gamma} > H^{\gamma} > H^{\beta} > H^{\beta}$. Hydroxyproline and arginine were distinguished from one another using the ROESY experiment.

7 | ROESY EXPERIMENT

The alpha-amide section of the ROESY spectrum shown in Figure S44 and expanded in Figure S45 facilitated the identification of the dipeptides and he primary structure of the peptide DGD-GG-GFOGER-GG-TTK-palmitate.

Since amino acids that are at a distance from each other can have their protons within 5 Å, mainly due to their preferred conformation, it is, therefore, possible to observe an interaction between amino acid residues that are four amino acids apart from each other. Some of the conformations that can bring protons that are three or four amino acid residues apart include α-helix, bent, or random conformation. Such interactions are indicated in Table 3. The demonstrated interactions, therefore, prove that the structure of the peptide is alpha helix as indicated earlier by the circular dichroism experiment.

8 | CONCLUSION

Eight designed CMPs were successfully synthesized using the SPPS strategy. The alpha-helical structure of the DGD-GG-GFOGER-GG-TTK-palmitate peptide was successfully derived from the ROESY and circular dichroism experiments.

The existence of *trans* isomers, antiparallel/parallel stranded heli-cal conformations, indicates that there is a possibility of the synthe-sized peptides forming a triple helical structure that resembles collagen. Attainment of the helix that mimics collagen further implies that this peptide can interact with the integrin the same way as colla-gen would.

AUTHOR CONTRIBUTIONS

Maya Makatini was involved in the conceptualization, formal analysis, funding acquisition, investigation, methodology, project administration, supervision, writing-review and editing, and making available resources needed for the project. Ntlama Lesotho acquired and curated all the data, wrote the original draft, and performed the formal analysis, investigation, and methodology in the lab. Thabo Peme was involved in the analysis and writing-review and editing.

ACKNOWLEDGEMENTS

The National University of Lesotho and the National Manpower Development Secretariat are acknowledged for their financial assistance, the National Research Foundation (NRF) Thuthuka Award (Gun 117975) and CSUR Award (Gun 138081) for funding, the Wits mass spectrometry team Dr Eric Morifi, Dr Izak Kotze for his assistance with NMR experiments, Dr Ikechukwu Achilonu, and Prof Yasien Sayed for their assistance with CD experiments.

CONFLICT OF INTEREST STATEMENT

The authors declare that they have no known competing interests.

ORCID

Maya Makatini iD https://orcid.org/0000-0001-7280-0945

REFERENCES

1. Bella J, Berman HM. Integrin-collagen complex: a metal-glutamate handshake. *Structure*. 2000;8(6):R121-R126. doi:10.1016/S0969-2126(00)00153-2
2. Shoulders MD, Raines RT. Collagen structure and stability. *Annu Rev Biochem*. 2009;78(1):929-958. doi:10.1146/annurev.biochem.77. 032207.120833
3. Emsley J, Knight CG, Farndale RW, Barnes MJ, Liddington RC. Struc-tural basis of collagen recognition by integrin A2β1. *Cell*. 2000;101(1): 47-56. doi:10.1016/S0092-8674(00)80622-4
4. Leitinger B, Hohenester E. Mammalian collagen receptors. *Matrix Biol*. 2007;26(3):146-155. doi:10.1016/j.matbio.2006.10.007
5. Wang AY, Leong S, Liang YC, Huang RCC, Chen CS, Yu SM. Immobili-zation of growth factors on collagen scaffolds mediated by polyanio-nic collagen mimetic peptides and its effect on endothelial cell morphogenesis. *Biomacromolecules*. 2008;9(10):2929-2936. doi:10. 1021/bm800727z
6. David L, Steed MD. The role of growth factors in wound healing. *Surg Clin N Am*. 1997;77(3):575-586. doi:10.1016/S0039-6109(05) 70569-7
7. Park JW, Hwang SR, Yoon IS. Advanced growth factor delivery sys-tems in wound management and skin regeneration. *Molecules*. 2017; 22(8):1259. doi:10.3390/molecules22081259
8. Zhao X, Zhang X, Liu D. Collagen peptides and the related synthetic peptides: a review on improving skin health. *J Funct Foods*. 2021;86: 104680. doi:10.1016/j.jff.2021.104680
9. Stimac A, Sekutor M, Mlinaric-Majerski K, Frkanec L, Frkanec R. Ada-mantane in drug delivery systems and surface recognition. *Molecules*. 2017;22(2):297. doi:10.3390/molecules22020297
10. Chee FC, Guy A, Biggin PC. Distribution and dynamics of adaman-tanes in a lipid bilayer. *Biophys J*. 2008;95(12):5627-5636. doi:10. 1529/biophysj.108.139477
11. Errante F, Ledwon P, Latajka R, Rovero P, Papini AM. Cosmeceutical peptides in the framework of sustainable wellness economy. *Front Chem*. 2020;8:969. doi:10.3389/fchem.2020.572923
12. Ludwig BS, Kessler H, Kossatz S, Reuning U. Rgd-binding integrins revisited: how recently discovered functions and novel synthetic ligands (re-)shape an ever-evolving field. *Cancer*. 2021;13(7):1711. doi:10.3390/cancers13071711
13. Fischer G. Chemical aspects of peptide bond isomerisation. *Chem Soc Rev*. 2000;29(2):119-127. doi:10.1039/a803742f
14. Isaac N. *Physical Organic Chemistry*. 2nded. Longman Group UK. Limited; 1995
15. Hu X, Zhang W, Carmichael I, Serianni AS. Amide *cis-trans* isomeriza-tion in aqueous solutions of methyl N-formyl-d-glucosaminides and methyl N-acetyl-d-glucosaminides: chemical equilibria and exchange kinetics. *J Am Chem Soc*. 2010;132(13):4641-4652. doi:10.1021/ja9086787
16. DeRider ML, Wilkens SJ, Waddell MJ, et al. Collagen stability: insights from NMR spectroscopic and hybrid density functional computational investigations of the effect of electronegative substituents on prolyl ring conformations. *J Am Chem Soc*. 2002;124(11):2497-2505. doi:10. 1021/ja0166904
17. Hinderaker MP, Raines RT. An electronic effect on protein structure. *Protein Sci*. 2003;12(6):1188-1194. doi:10.1110/ps.0241903
18. Koslowski A, Sreerama N, Woody RW. Circular dichroism of peptides and proteins. In: Berova N, Woody RW, Nakanishi K, eds. *Circular Dichroism: Principles and Applications*. Willy-VCH Press; 2000.
19. Greenfield N, Fasman G. Computed circular dichroism spectra for the evaluation of protein conformation. *Biochem*. 1969;8(10):4108-4116. doi:10.1021/bi00838a031
20. Zerbe O, Bader R. Peptide NMR. Personal communication
21. Cavanagh J, Fairbrother WJ, Palmer AG, Skelton NJ, Rance M. *Protein NMR Spectroscopy: Principles and Practice*. 2nd ed. Academic Press; 2006.

SUPPORTING INFORMATION

Additional supporting information can be found online in the Support-ing Information section at the end of this article.

How to cite this article: Lesotho N, Peme T, Makatini M. Design, synthesis, and characterization of type I collagen mimetic peptides. *J Pept Sci*. 2023;e3531. doi:10.1002/psc.3531

CHAPTER III

SYNTHESIS OF GROWTH FACTOR-BASED PEPTIDES CONJUGATED TO ADAMANTANE

The chapter describes the successful solid-phase peptide synthesis of adamantane conjugated collagen type I mimetic peptides. The synthesized peptides were characterized using the ultra-high performance liquid chromatography-mass spectrometry. Geometric and conformational isomers were elucidated using the nuclear magnetic resonance spectroscopy and circular dichroism techniques.

The design of the palmitate peptides is described in detail in Chapter 2. In this chapter, the adamantane derivatives are described and are made up of the following components: 1. The adamantane moiety, a caged structured compound that has been reported to have good membrane permeability and to retard biodegradation when incorporated into biologically active molecules.[1] 2. A tripeptide, DGD employed mainly to enhance binding to collagen and to attract vascular endothelial growth factors. 3. The GG dipeptide on either side of the collagen binding motif (*retro*-GFOGER) that acts as a spacer to reduce steric hindrance. 4. The *retro*-tripeptides, TTK, GHK, QPR and EEM employed mainly to stimulate collagen production. With all these modifications implemented, the envisaged peptide structure is shown below.

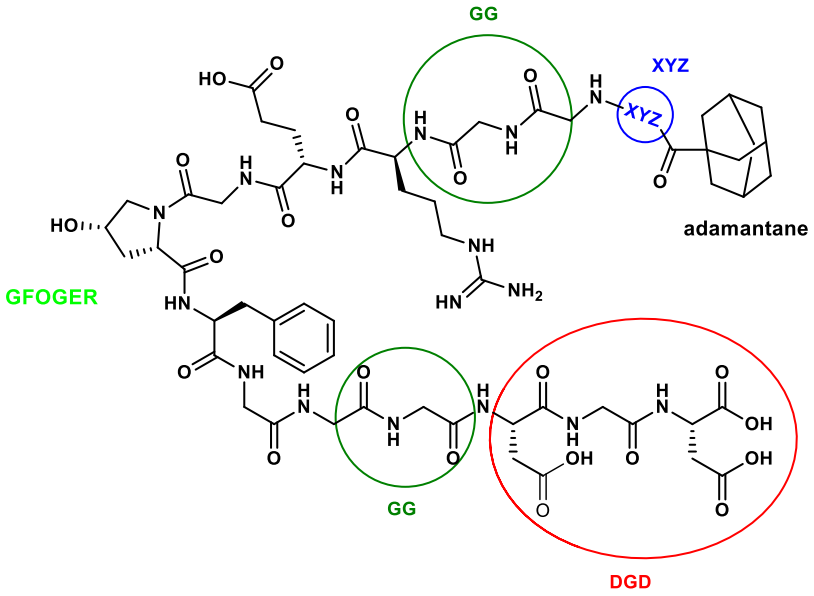

Figure 3.1: General structure of wound healing peptide, XYZ can either be *retro*-TTK/GHK/QPR/EEM.

Collagen mimetic peptides are applied to the skin where they carry out their primary function in the extracellular matrix. Hence, permeability through the skin is crucial and of prime importance. The lipid bilayer has a largely non-polar interior; therefore, non-polar molecules are more permeable than polar molecules. In addition, the smaller the molecule, the easier it is for it to cross the membrane.[1]

The palmitic acid collagen mimetic peptides in the previous chapter and the adamantane collagen mimetic peptides presented here are similar in structure apart from the palmitic acid and adamantane moieties. Both moieties are utilized to facilitate membrane permeability since they are fatty acids.[2–4] Palmitic acid is a linear fatty acid while adamantane is a cage-structured compound. Neither have distinctive functional groups.

Adamantane has gained much attention in the field of medicinal chemistry and has been dubbed the 'lipophilic bullet'.[5] It has widely been explored in pharmaceutics such as chemotherapeutics, anabolic steroids, antivirals and anti-diabetic agents. Adamantane modifications are chosen to enhance lipophilicity and the stability of drugs, thereby improving their pharmacokinetic profile.[5] Several adamantane derived drugs are available in the market and they all show diverse biological properties such as antiviral,[6] antibacterial,[7] antifungal,[7] and anti-inflammatory properties.[8]

Adamantane derivatives have elastase inhibitory effect. Elastase is an enzyme that breaks down elastin, an elastic fibre that, together with collagen, determine the mechanical properties of connective tissue.[8]

Adamantane moiety is highly lipophilic, stress-free bulky cyclic hydrocarbon and incorporation of this moiety into several molecules results in compounds with improved biological availability. Therefore, adamantane was incorporated into the designed peptides and the 3-D structures of both palmitate and adamantane peptides were elucidated in order to understand the structure-activity relationship.

3.1 PEPTIDE SYNTHESIS

Four adamantane collagen type I mimetic peptides and one control adamantane peptide (DGRGOF-Adamantane) were synthesised, using the solid phase peptide synthesis strategy. Chlorotrityl resin (600 mg) was weighed into a reaction vessel. The resin was first activated with thionyl chloride (2 mL) in dry DCM (10 mL) overnight at room temperature. After filtering and washing the resins with dry DCM (4mL x 5), the first amino acid (Fmoc-Asp(OtBu)-OH) was attached to the resin through the C-terminal. Fmoc-Asp(OtBu)-OH (0.987 g, 0.2 M) was dissolved in DCM (10 mL). To the latter was added DIPEA (2.0 mL, 1M) and the resultant mixture was added to the resin. The reaction mixture was gently mixed by bubbling nitrogen gas into the reaction for 45 minutes. After the coupling of the Fmoc-Asp(O*t*Bu)-OH, the resin was washed with DMF (3 × 5 mL) followed by DCM (3 × 5 mL) to remove excess reagents and by-products. A 20% piperidine solution (10 mL) was added to the resin and bubbled with nitrogen for five minutes twice to remove the protecting group. The resin was then washed with DMF (3 × 5 mL) followed by DCM (3 × 5 mL) to remove excess reagents.

The second amino acid Fmoc-Gly-OH (0.429 g, 0.12M) was coupled to the resin attached amino acid by using a coupling reagent HBTU (0.519 g, 0.11 M) and DIPEA (1.26 mL, 0.6 M) as the base. The resultant reaction mixture was gently mixed by bubbling nitrogen gas into the reaction for 45 minutes. The resin was washed with DMF (3 × 5 mL) followed by DCM (3 × 5 mL) to remove excess reagents. The same coupling process was utilized to couple all the other amino acids. The adamantane (0.260 g, 0.12 M) was prepared in DMF (10.74 mL). The

solutions were added to the resin-peptides along with HBTU (0.519 g, 0.11 M) and DIPEA (1.26 mL, 0.6 M). The washing procedures are similar to the ones above.

For all these adamantane reactions, a strict order of addition of reagents was observed. That is, the amino acid was first dissolved in DMF. Secondly, DIPEA was added and allowed for a while to react with the amino acid residue. To activate the acid, a stoichiometric amount of HBTU was added and the reaction mixture was left to stir to allow the reaction of the carboxylate anion and HBTU to proceed for about 10 minutes before the solution was added to the resin. This step was taken in order to avoid guanidinylation, a reaction in which HBTU reacts with the deprotected amine of the amino acid on the peptide on the resin.[9]

As part of coupling reaction monitoring, the Ninhydrin test was utilized. Two test tubes labelled 'S' and 'R' were utilized. To test tube 'S' was added approximately 15 beads of resin from a reaction mixture while test tube 'R' was left empty. Three drops of each reagent A, B and C prepared as described in Chapter IX section 9.4.12 (general procedure L) were added to both test tubes. The test tubes were heated in a water bath at 110°C for 5 minutes. If the solution of test tube S, relative to R, was light blue, and the beads dark blue, it meant the coupling was incomplete and the coupling had to be redone. For the dark blue solution with colourless beads, the coupling reaction was given more time to complete. If upon testing, colourless or faint blue colour was obtained, the reaction was stopped, and the next step of the synthesis was performed. The reaction had to be redone in cases where, in comparison with the contents of flask 'R', the solution would be observed to be intense blue and all the beads blue also. In the case where there was uncertainty, HPLC was used to confirm the successful coupling of amino acid residues. For hydroxyproline (secondary amines), an indication of completion of the coupling reaction was evidenced by a less intense red brown colour.

The mass spectrum of the thirteen amino acid sequence (*retro*-DGD-GG-GFOGER-GG-) before the addition of the *retro*-tripeptides TTK/GHK/QPR/EEM is shown in Figure 3.2. The desired mass of 1355.5926 m/z was observed along with impurities therefore the coupling reagent was changed from HBTU to (O-(7-Azabenzotriazole-1-yl)-N, N, N'N'-tetramethyluronium hexafluorophosphate (HATU). Although HATU is normally used to couple amino acids or peptides that are sterically hindered,[10] in this instance, it was mainly employed due to its efficacy and the ability to facilitate coupling without epimerization.[11,12] The difference between the two coupling reagents is in terms of the stability of the activated intermediate which is stabilized by hydrogen bonding from the extra nitrogen that the HATU reagent possesses.[13]

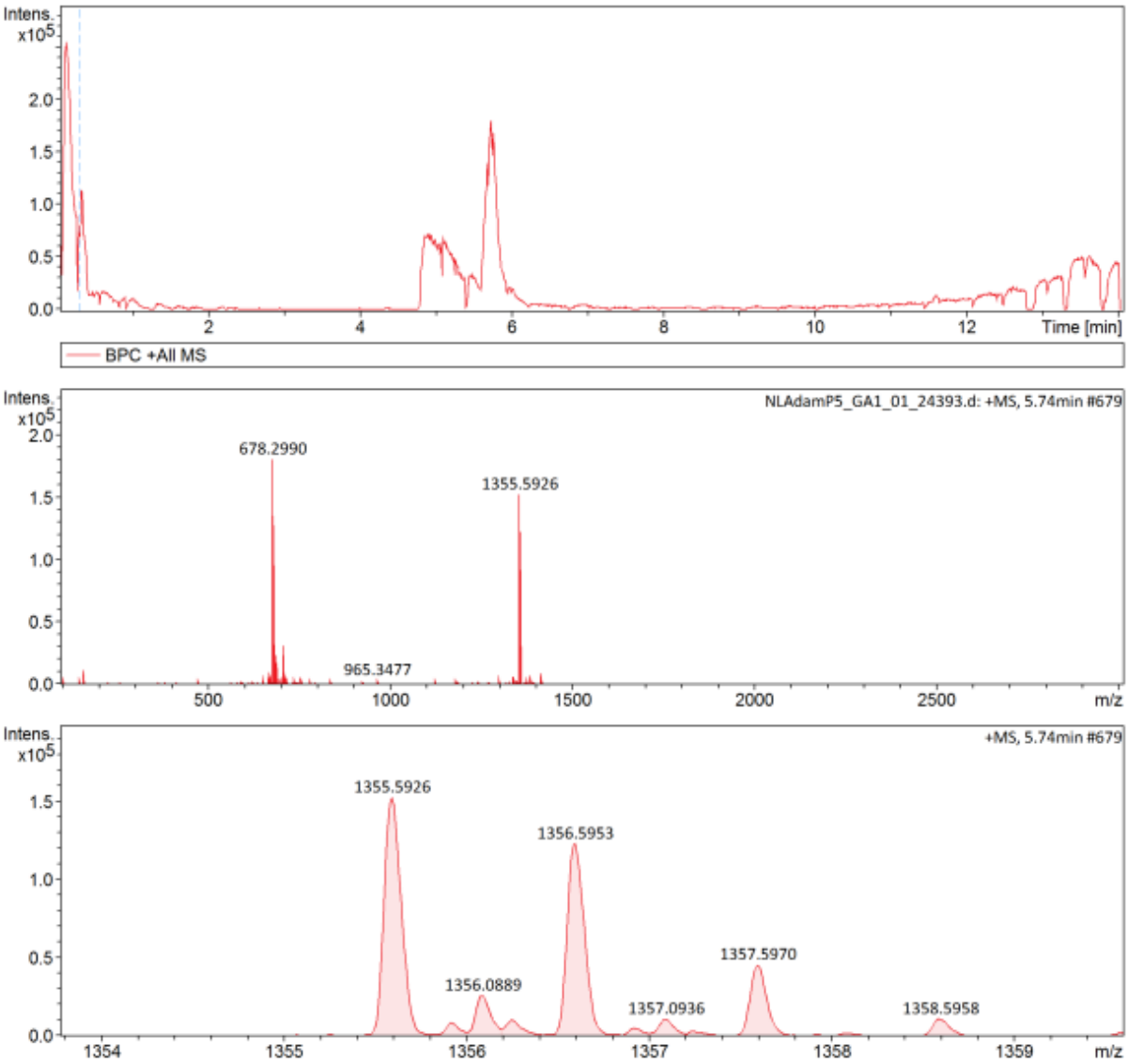

Figure 3.2: Mass spectrum of the thirteen amino acid sequence before the addition of the *retro*-tripeptides TTK/GHK/QPR/EEM**.**

After the employment of HATU, fewer impurities were observed (Figure 3.3) but the ones that were present had the same mass as the ones observed in Figure 3.2.

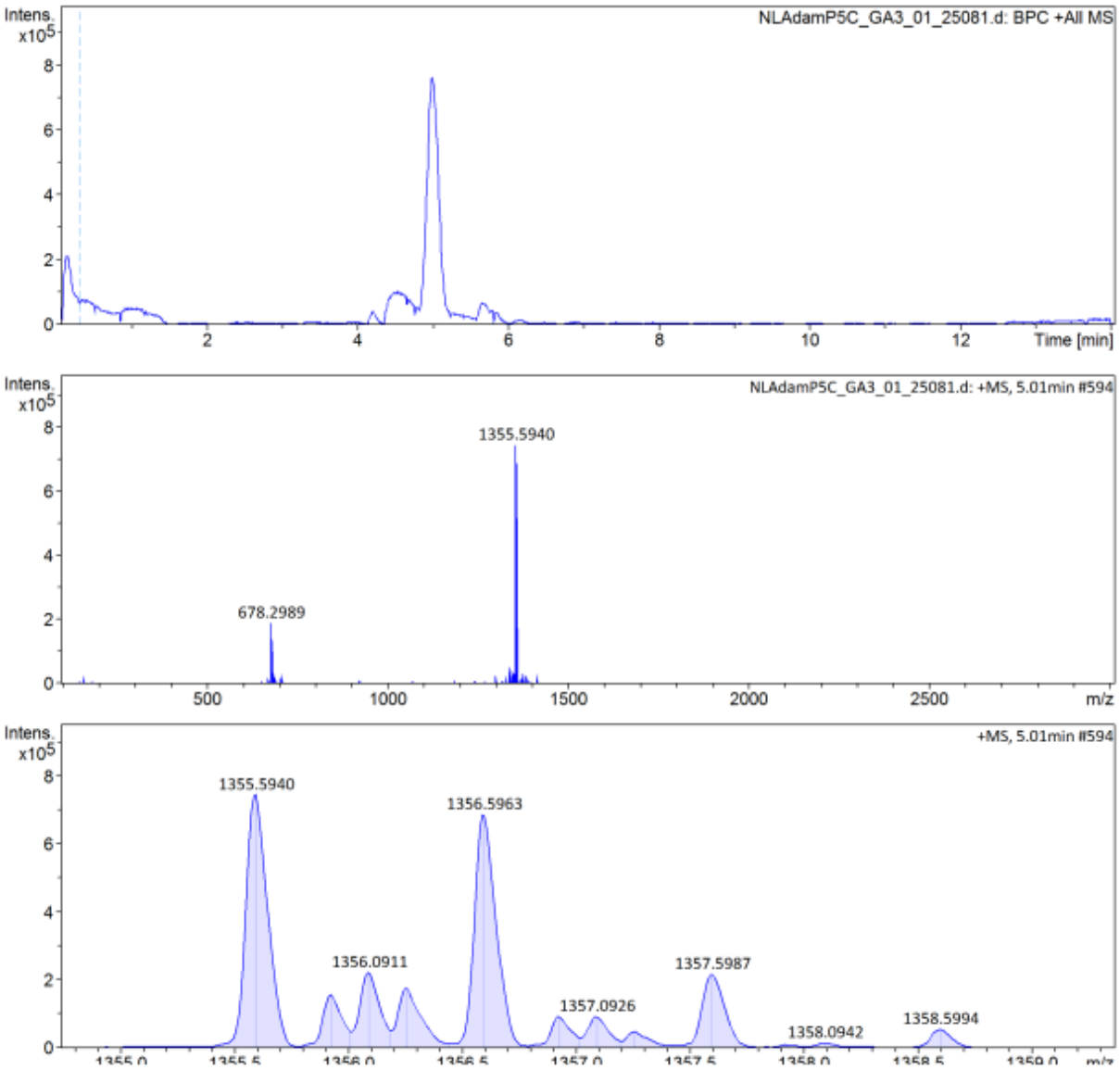

Figure 3.3: HPLC test chromatogram 2.

One observation made during coupling reactions was that phenylalanine took an exceptionally long period of time to couple to hydroxyproline. Due to this observation, double coupling had to be done. This was also influenced by the observation from Ninhydrin Test indicating 'incomplete coupling'. The difficult coupling of phenylalanine to hydroxyproline could have been induced by steric hindrance.

The cleavage of the peptide from the resin was achieved by reacting the resin bound peptides with a solution of 95 % TFA, 2.5 % water and 2.5 % TIS for 3 hours with gentle shaking. The cleavage solution was filtered off and the resin was washed with 5 mL of TFA and the filtrate was poured into 50 mL centrifuge tubes. Cold diethyl ether was added to the filtered solution

upon which a white precipitate of the crude peptide was formed. The samples were centrifuged at 5000 rpm for 10 minutes. The step was repeated 3 times with cold diethyl ether.

The choice of the cleavage mixture was dictated by the amino acid composition of the peptide. Care was taken not to expose the peptides to cleavage reagents for extended periods of time, that is, time for cleavage was considered an important factor. Lastly, appropriate scavengers and reaction conditions were also chosen to avoid modification or destruction of the peptides.

The fact that methionine and histidine have acid labile side chains, after their deprotection, meant time of exposure of these amino acids had to be taken into consideration. Furthermore, the choice of the cocktail mixture was also influenced by the sensitive imidazole ring of histidine which, in extended periods of time could be acylated.[10] For peptides that have arginine, methionine and histidine (*retro*-DGD-GG-GFOGER-GG-GHK- and *retro*-DGD-GG-GFOGER-GG-EEM-), the time for the cleavage was strictly three hours. This amount of time was observed to be suitable for the mentioned peptides.

The high resolution mass spectra for crude peptides are compared in Figures 3.4, 3.5, 3.6 and 37 and show the formation of minimum impurities from the *retro*-DGD-GG-GFOGER-GG-Adamantane.

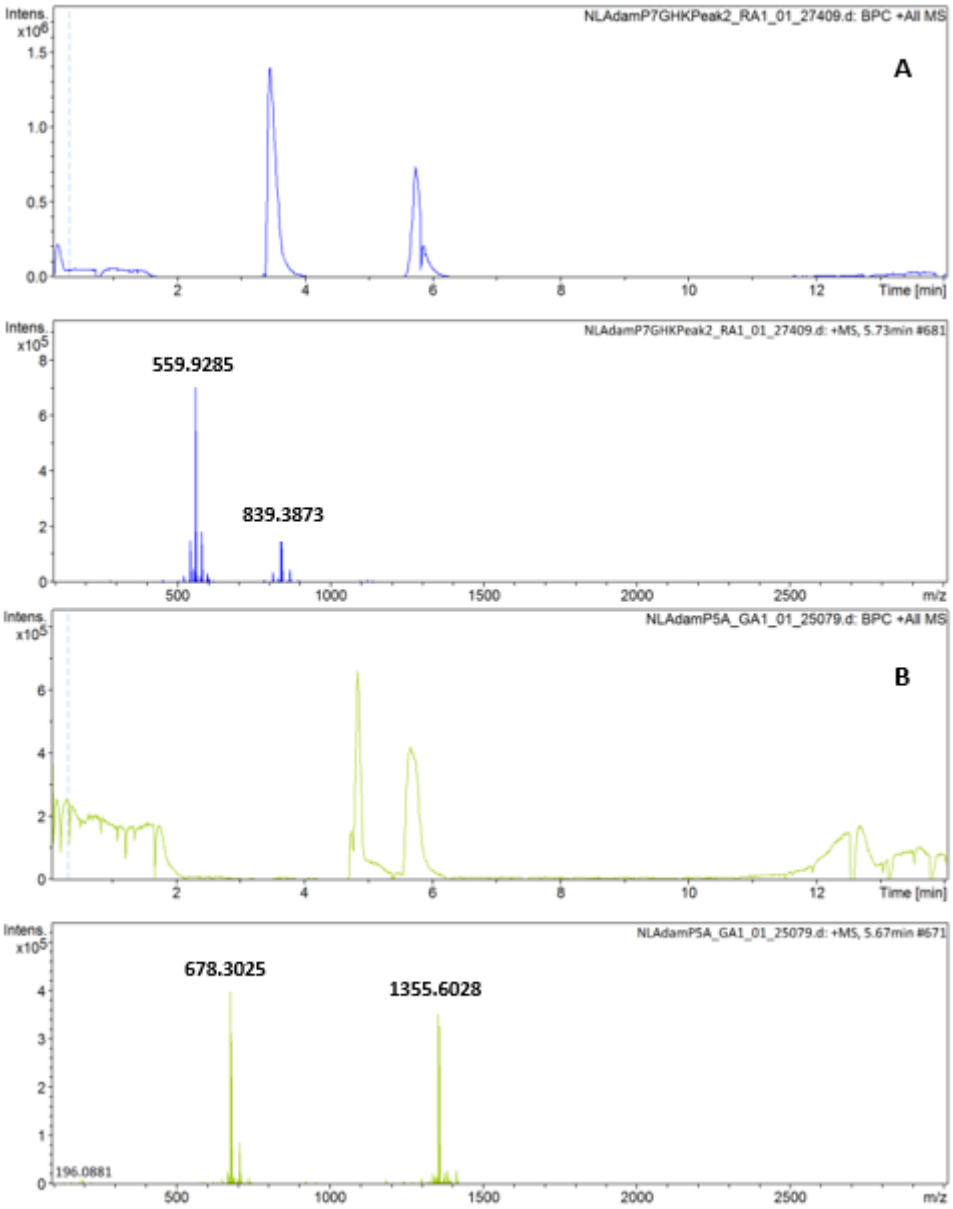

Figure 3.4: Comparison of crude high resolution mass spectra of *retro*-DGD-GG-GFOGER-GG-GHK-Adamantane (**A**) and *retro*-DGD-GG-GFOGER-GG-Adamantane (**B**).

(i) Possible side reactions from Glutamic acid (E)-Glutamic acid (E)-Methionine (M) of the *retro*-DGD-GG-GFOGER-GG-EEM peptide.

Due to the ability of glutamic acid to form both five and six-membered rings, it is involved in numerous side reactions. Cyclization may be induced either by an activated γ-carboxyl group or heating. Cyclization to form five-membered rings takes place under two conditions;

(a) when γ-carboxylic group is activated

(b) when glutamic acid is heated.[11]

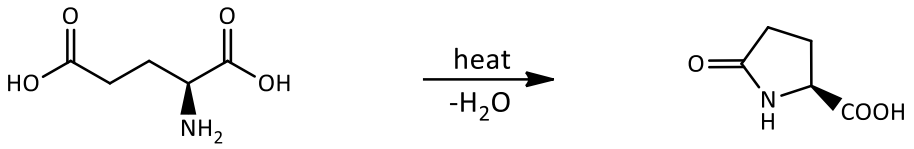

(*S*)-2-aminopentanedioic acid (*S*)-5-oxopyrrolidine-2-carboxylic acid

Scheme 3.1: Formation of pyrroglutamic acid.

In addition to the pyrrolidinones, N-protected glutamic acid can also cyclize to form six-membered rings (Scheme 3.2).

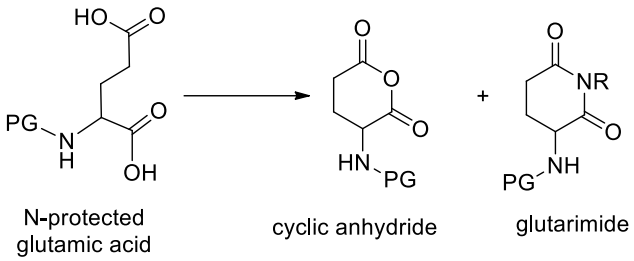

Scheme 3.2: Cyclization products of glutamic acid.

Only for the two peptides, *retro*-DGD-GG-GFOGER-GG-EEM-Adamantane and -Palmitate was the cocktail mixture containing 1, 2-ethanedithiol (EDT) utilized (94 % TFA, 2.0 % water and 2.0 % TIS, 2.0 % EDT) for cleavage from the resin. This was mainly to prevent methionine oxidation to methionine sulfoxide. The addition of EDT resulted in fewer impurities. The spectra for the crude peptides are compared in Figure 3.5 and show the formation of minimum impurities from the DGD-GG-GFOGER-GG-Adamantane.

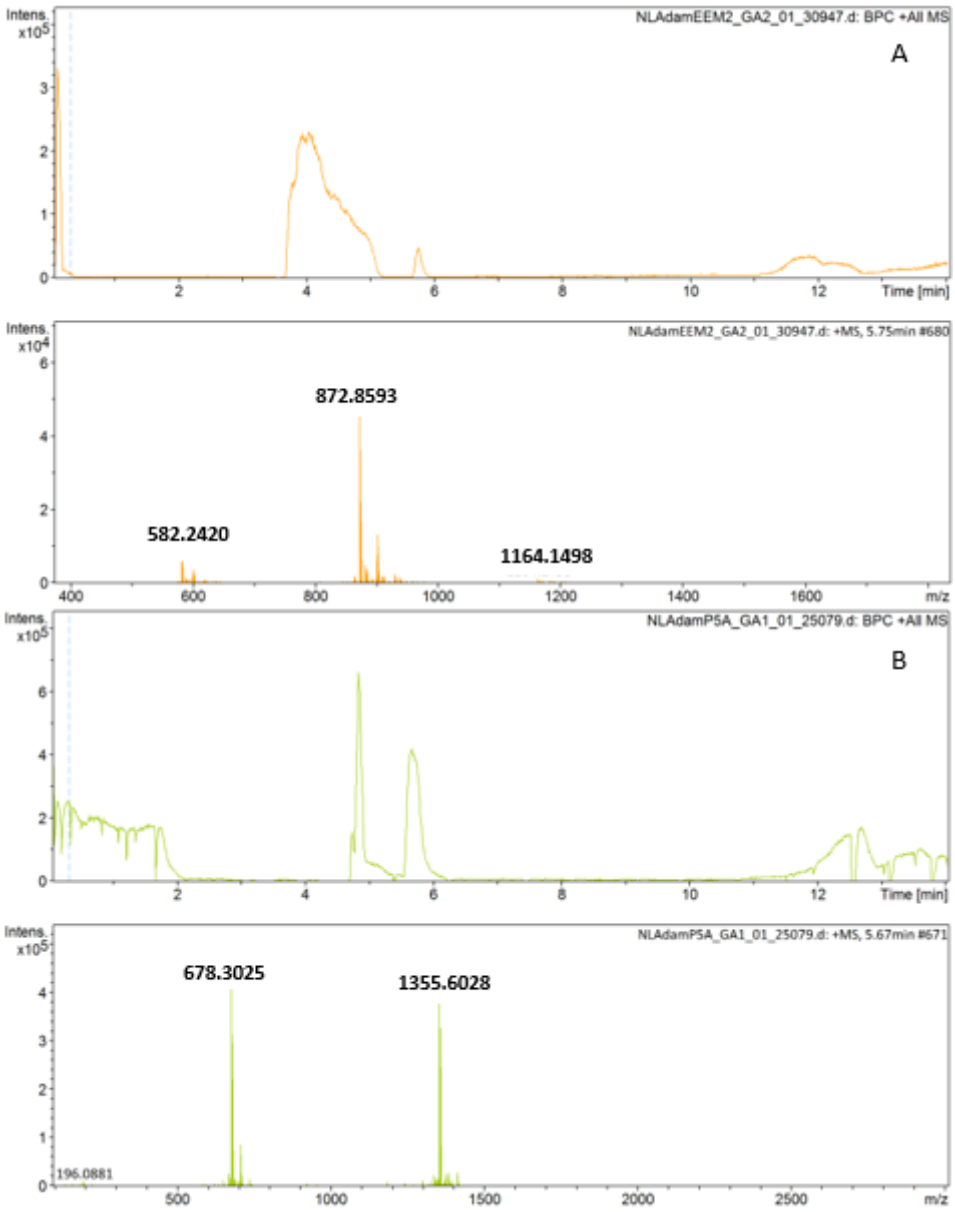

Figure 3.5: Comparison of crude high resolution mass spectra of *retro*-DGD-GG-GFOGER-GG-EEM-Adamantane (**A**) and *retro*-DGD-GG-GFOGER-GG-Adamantane (peak 678.3025) (**B**).

The peptide *retro*-DGD-GG-GFOGER-GG-QPR was successfully cleaved with a solution of 95 % TFA, 2.5 % water and 2.5 % TIS in 3 hours, the mass spectrum is shown below.

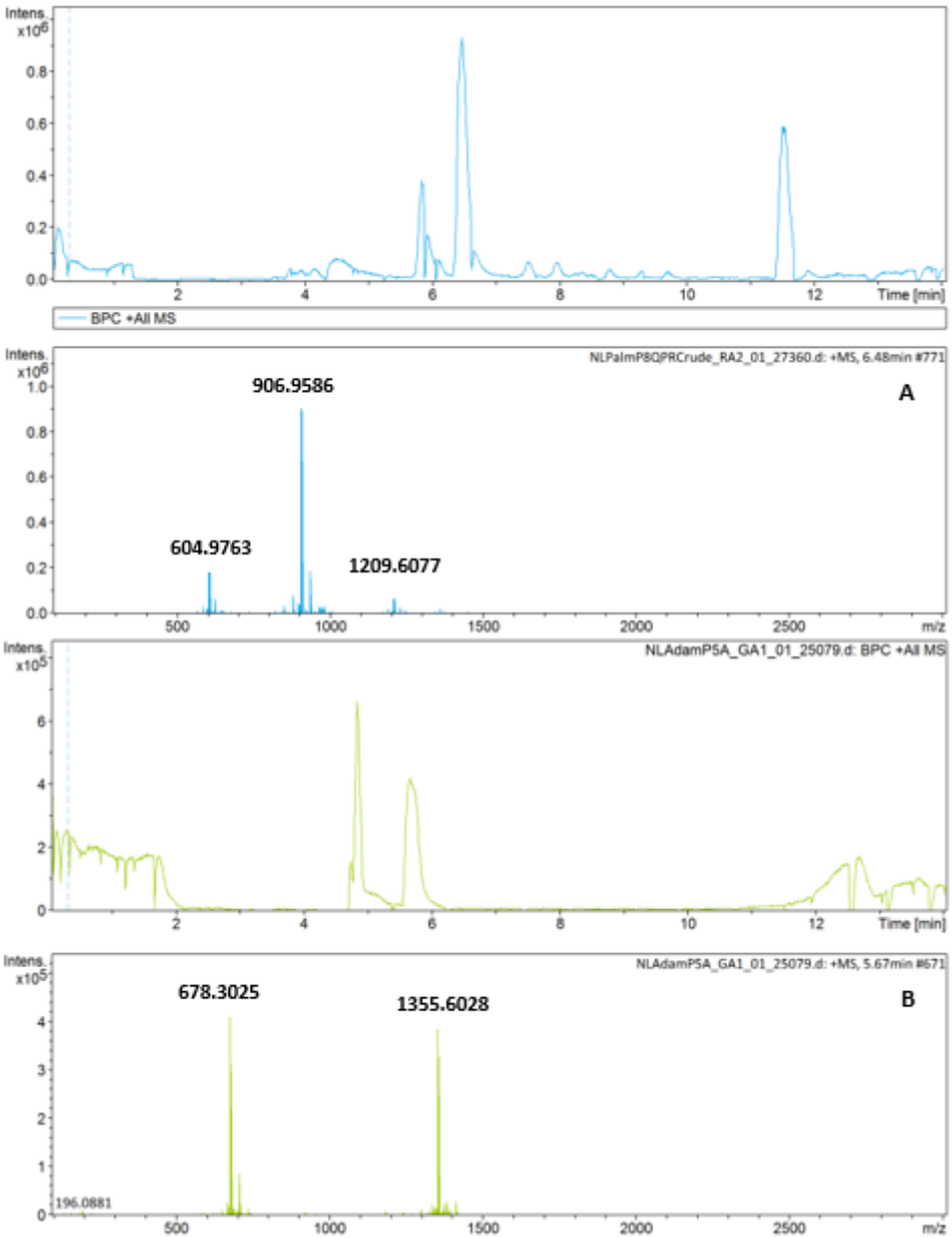

Figure 3.6: Comparison of crude high resolution mass spectra of *retro*-DGD-GG-GFOGER-GG-QPR-Adamantane (**A**) and *retro*-DGD-GG-GFOGER-GG-Adamantane (peak 678.3025) (**B**).

(ii) Possible side reaction from Threonine (T)-Threonine (T)-Lysine (K) of DGD-GG-GFOGER-GG-TTK peptides.

The side chain of threonine can undergo reactions such as dehydration or *O*-acylation followed by *O*-*N* migration if the OH group is unprotected. Therefore, peptides containing threonine residues can undergo acid catalysed acyl *N* – *O* shift during cleavage (Scheme 3.3).[12]

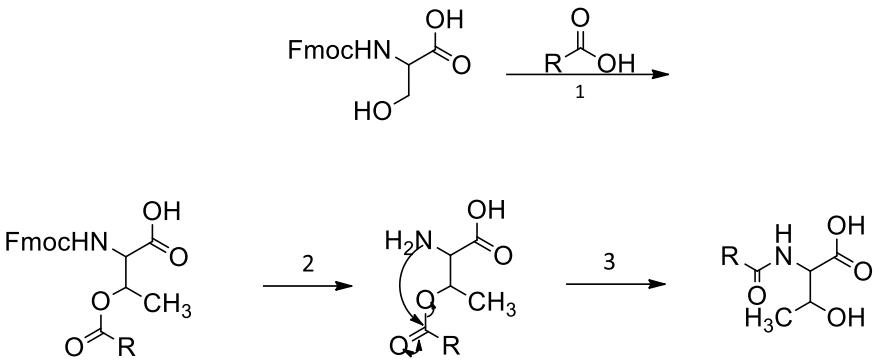

Scheme 3.3: O-acylation followed by O-N migration after amino deprotection. (1) O-acylation (2) Amino protecting group removal (3) O-N migration.

The peptide *retro*-DGD-GG-GFOGER-GG-QPR was successfully cleaved with a solution of 95 % TFA, 2.5 % water and 2.5 % TIS in 3 hours, the mass spectrum is shown below.

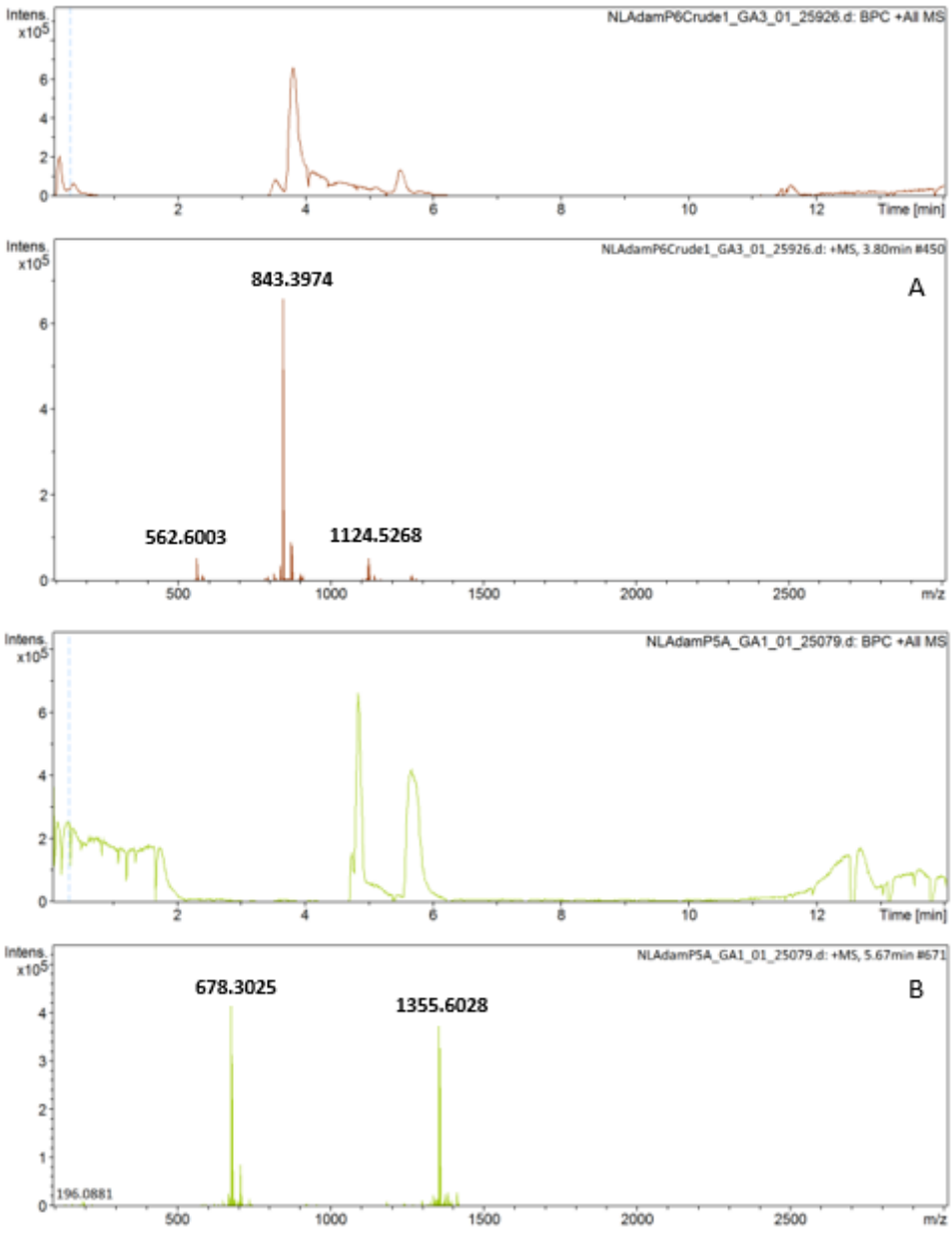

Figure 3.7: Comparison of crude high resolution mass spectra of *retro*-DGD-GG-GFOGER-GG-TTK-Adamantane (peak 843.3974) (**A**) and *retro*-DGD-GG-GFOGER-Adamantane (peak 678.3025) (**B**).

Respectively, the chromatograms for the purified peptides *retro*-DGD-GG-GFOGER-GG-Adamantane, *retro*-DGD-GG-GFOGER-GG-GHK-Adamantane, *retro*-DGD-GG-GFOGER-GG-QPR-Adamantane, *retro*-DGD-GG-GFOGER-GG-EEM-Adamantane and *retro*-DGD-GG-GFOGER-GG-TTK-Adamantane are presented in chapter IX sections 9.6.8, 9.6.12, 9.6.14, 9.6.16 and 9.6.10. After isolation, the peptides were purified using preparatory high performance liquid chromatography and the method is outlined in chapter IX section 9.4.14.

3.2 RESULTS AND DISCUSSION

The results obtained from the mass spectrometry experiments and the yields of the adamantane peptides are shown in Table 3.1. The differences in retention times of the peptides were used to identify the peptides that are more hydrophobic. According to the results in Table 3.1, *retro*-DGD-GG-GFOGER-GG-GHK- and *retro*-DGD-GG-GFOGER-GG-QPR-Adamantane peptides are relatively more polar than *retro*-DGD-GG-GFOGER-GG-TTK- and *retro*-DGD-GG-GFOGER-GG-EEM-Adamantane. Since all the amino acids that make up the *retro*-tripeptide TTK are relatively polar, it would be expected that *retro*-DGD-GG-GFOGER-GG-TTK-Adamantane peptide would have a shorter retention time. From these results, it could be deduced that structural conformations also play a role in the manner in which the peptides interact with the stationary phase. Tripet *et al*, discovered that enhancement or reduction of hydrophobicity of peptide as expressed by its reverse-phase HPLC retention time could be related to its conformation.[13,14] The structural conformation of the peptide *retro*-DGD-GG-GFOGER-GG-TTK is fully elucidated using CD and NMR in the next chapter. The longer retention of *retro*-DGD-GG-GFOGER-GG-EEM-Adamantane was attributed to the acidic nature of the *retro*-tripeptide EEM since the more hydrophilic *retro*-tripeptides consist of two basic amino acid residues (G**HK**) or a basic residue and an amide side chain (**Q**P**R**) which are polar than a carboxylic group. The same trend was observed in Chapter II, the palmitate-peptides with basic residues were more hydrophilic.

Increased hydrophobicity usually results in improved membrane permeability but positively charged amino acids normally bind to the negatively charged phospholipids of the cell wall and this can also improve membrane permeability.[15,16] Hence the peptides will be tested in the future using the parallel artificial membrane permeability assay (PAMPA) to determine the best tripeptide polarity for improved membrane permeability for this class of compounds.

Table 3.1: Yields of the synthesized control and growth factor based peptides.

Integrin binding motif from collagen III	Growth Factor Based peptide	Calculated Mass (g/mol)	Experimental Mass (g/mol)	Yield (%)	Retention Time (min)
retro-DGRGOF-Adamantane	-	825.4021 ($C_{39}H_{55}N_9O_{11}$)	826.4111 $[M + H]^+$	39	Peak 1 = 5.79 Peak 2 = 5.85
-	*retro*-DGD-GG-GFOGER-GG-TTK- Adamantane	842.3847 $C_{72}H_{108}N_{20}O_{27}$	843.3929 $[M + H]^+$	30	6.01
-	*retro*-DGD-GG-GFOGER-GG-GHK- Adamantane	838.3772 $C_{72}H_{104}N_{22}O_{25}$	839.2885 $[M + H]^+$	21	3.52
-	*retro*-DGD-GG-GFOGER-GG-QPR- Adamantane	867.8979 $C_{74}H_{109}N_{23}O_{26}$	868.9049 $[M + H]^+$	12	3.87
-	*retro*-DGD-GG-GFOGER-GG-EEM- Adamantane	871.8523 $C_{73}H_{105}N_{19}O_{29}S$	872.8559 $[M + H]^+$	23	5.98

According to Table 3.1, the peptides were synthesized with low yields. It must further be noted that these yields are even lower than the yields obtained for the palmitate derivatives in Chapter II. Since the difference is only in the lipophilic moiety on the N-terminal of the peptides, it could be inferred that the difference in yields could be due to steric hindrance imparted by adamantane carboxylic acid. Figure 3.8 is meant to portray the ease of access between the two fatty acids.

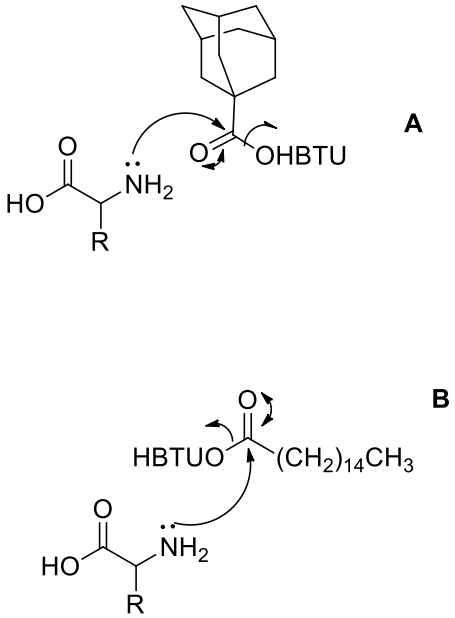

Figure 3.8: Comparison of steric hindrance around the carbonyl group of adamantane carboxylic acid versus palmitic acid.

Relative to palmitic acid in (B), acylation reactions involving adamantane (A) leads to low reaction yields. The reason could be the cage structure of adamantane. Unlike in (B), the carbonyl carbon in (A) is bonded to a tertiary carbon. Effectively, the carbonyl carbon in adamantane is in the vicinity of three methylene groups. This causes the electron deficient carbon to be not easily accessible. On the contrary, the carbonyl carbon in palmitic acid is in the vicinity of only one methylene group. This means the electron deficient carbon is more accessible.

Zhou, N. I. *et al* has reported that adamantane rigid cage moiety protects nearby functional groups from metabolic cleavage and thereby enhancing its stability and distribution in the blood plasma.[13, 18] In this instance, it is protecting the carbonyl group, a deleterious effect in terms of reaction yield.

3.3 CIRCULAR DICHROISM

There are two possible configurations of peptide bonds, *trans* or *cis*.[17] All amino acids with exception of proline and its derivatives prefer the *trans* configuration mainly because of stability.[19] The *trans* peptide bonds between amino acids lead to the formation of a stable collagen triple helix structure.[18] With proline, however, *cis* is preferred because when the peptide bond is *trans*, there is more steric strain. The proline's cyclic R-group influences the type of conformation attained by the amide bond. The R-group of proline and that of the subsequent amino acid are positioned in close proximity when the proline adopts the *trans* conformation. As a result, proline prefers the *cis* conformation due to the much-reduced hindrance.[19] The two configurations do not result in the same circular dichroism spectrum and hence the spectrum can be used to identify the synthesized configuration.[20] According to the results obtained in the NMR experiments reported in Chapter II the *cis* and *trans* isomers of the compounds exist simultaneously unless the sample is introduced to higher temperatures therefore the CD experiment could not be used to identify the presence of either the *cis* or *trans* as both exist.

Considering, for example, the type I collagen motif -GFOGER-, if hydroxyproline has *trans* peptide bond configuration with glycine, then there is a high possibility that oxygen of the

peptide bond between phenylalanine and hydroxyproline will donate electron density from its non-bonding electron pair into the antibonding orbital ($n \rightarrow \pi^*$) of the carbonyl carbon of peptide bond of hydroxyproline and glycine. That is, the negative band at about 222 nm is indicative of the electronic transition from amide carbonyl oxygen lone pair orbital, *n*, to the π^* ($n \rightarrow \pi^*$) orbital.[21]

Another strong negative band is observed at 208 and a positive band at 190 nm. In an α-helix, these bands respectively are indicative of an exciton splitting of electronic transition of the peptide amide bond from π to non-bonding π orbital ($\pi \rightarrow \pi^*$).[22,23] That is, from a given spectrum, it is possible to tell if a given peptide has an α-helix structure or not. However, it must be noted that different conformations may exist all at the same time in each peptide. A peptide may not have one exclusive secondary structure.

In consideration of the Fasman standard spectra,[24] the spectrum in Figure 3.9 has secondary structural features that are characteristic of an α-helix peptide.[25,26]

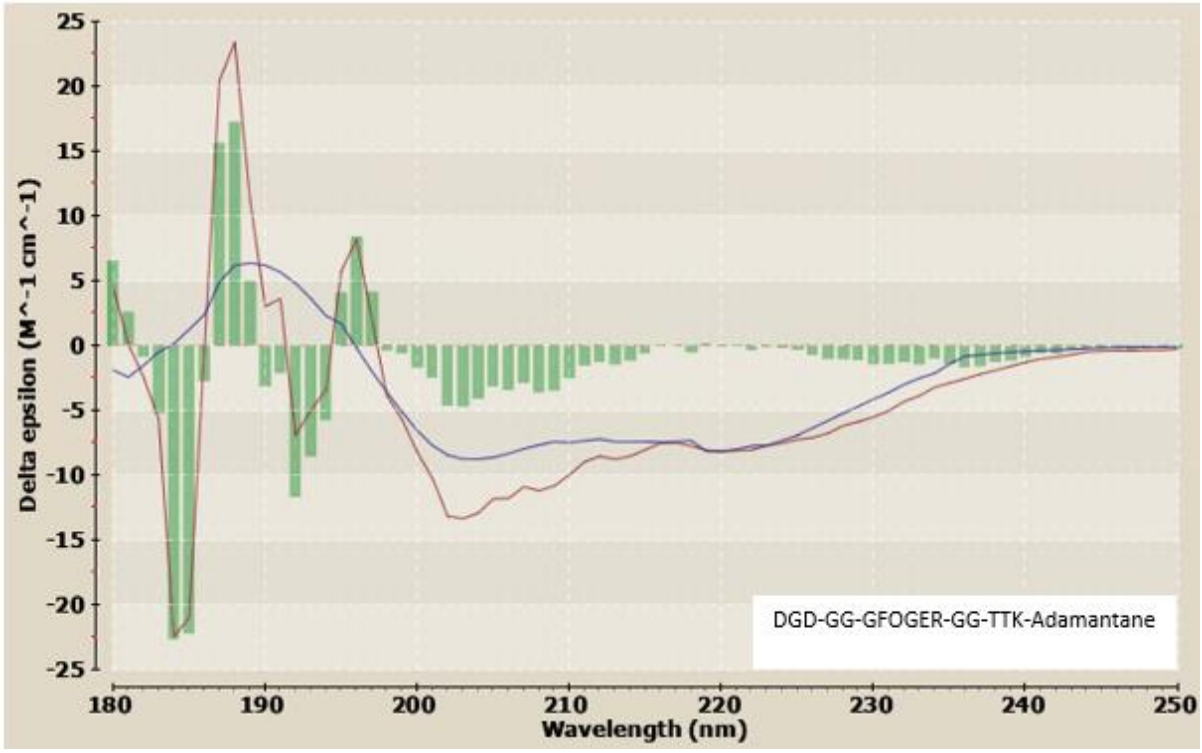

Figure 3.9: Circular dichroism spectrum of *retro*-DGD-GG-GFOGER-GG-TTK-Adamantane. Red line = Experimental; blue line = Fitted.

Not all the synthesized growth-factor based peptides have the same content of secondary structural conformations. Some of the peptides formed mainly antiparallel *beta* sheets while others formed parallel *beta* sheets. The parallel arrangement is in line with the natural structural conformation of collagen which comprises of a right-handed bundle of three parallel, left-handed polyproline II-type helices.[18] The secondary structures of the peptides are shown in Table 3.2.

Table 3.2: Estimated secondary structure content of the adamantane peptides.

Peptide	Helix (%)	Antiparallel (%)	Parallel (%)	Turn (%)	Other (%)
retro-DGD-GG-GFOGER-GG-TTK-Adamantane	18.1	6.5	35.0	0	40.4
retro-DGD-GG-GFOGER-GG-GHK-Adamantane	45.5	0	7.1	0	47.4
retro-DGD-GG-GFOGER-GG-EEM-Adamantane	50.7	35.8	0	13.6	0

From the results in Table 3.2, it could be inferred that adamantane does not exclusively influence the type of conformation of the peptides. The only difference in the peptides in Table 3.1 is in the *retro*-tripeptides TTK, GHK and EEM. This, therefore, suggests that the

observed different secondary conformation content of peptides could mainly be influenced by the different sequences of amino acids of the tripeptides.

Relative to *retro*-DGD-GG-GFOGER-GG-TTK-Adamantane, it was observed that *retro*-GHK and *retro*-EEM tripeptides favour the formation of the *alpha* helical structure of the peptides. Furthermore, the *retro*-tripeptide, TTK does not favour the formation of the *alpha* helix but on the contrary the parallel conformation. The *retro*-TTK palmitate derivative reported in Chapter II also had the lowest content of the *alpha* helical conformation.

The relatively high content of 'turn' conformation in *retro*-EEM peptide could not be explained since the tripeptide contains neither proline nor glycine. Furthermore, *retro*-EEM is the only peptide that does not have parallel conformations. Within the protein structure, there are turn motifs, which are commonly categorized as α, β, γ, δ and π-turns. The most common motif is the β-turn, which consists of four amino acids including proline and glycine. Proline's cyclic R-group induces sharper conformational bends due to its preferred *cis* conformation while the small R-group (-H) of glycine allows tighter packing of the amino acids. These structural features of proline and glycine favour the turn structure in the protein molecule.[27] The rigid structure of the R-group of proline can considerably change the 3-dimensional structure of the peptide and is found in regions of the proteins where turns and folds occur.[28]

When comparing the circular dichroism spectra of adamantane derivatives to the spectra of the palmitate derivatives reported in Chapter II, it was noted that adamantane is mainly parallel, whereas palmitate is mainly α-helical (Chapter II). Therefore, the palmitic acid and adamantane moieties carboxylic acids are influencing the secondary structure of the peptides. The peptides assemble differently because of the attached fatty acids. If the fatty acid moieties influence the assembly of the peptides, surely their peptide derivatives would function differently as the orientation of the peptides is important in terms of the function.

In a study by Aloisi, M. *et al.* involving adamantane based heteropeptides, circular dichroism proved that the admantane peptides are able to fold into recurring chiral cyclic conformations stabilized by intramolecular hydrogen bonding.[32] Molecular dynamics simulations on the

other hand indicated that the adamantane oligomers populated compact conformations, with a subset forming cyclic geometries by hydrogen bonding.[32]

The desire to know the tertiary structure of adamantane peptides, therefore, compelled us to carry NMR experiment to elucidate the structure utilizing the chemical shifts as explained in the following Chapter IV.

3.4 CONCLUSION

Adamantane collagen type I mimetic peptides were successfully synthesized. The peptides exist as a mixture of conformations, with parallel and α-helix conformations being more dominant.

3.5 REFERENCES

(1) Chee, F. C.; Guy, A.; Biggin, P. C. Distribution and Dynamics of Adamantanes in a Lipid Bilayer. *Biophys J* **2008**, *95* (12), 5627–5636.

(2) Hosoyama, K.; Lazurko, C.; Muñoz, M.; McTiernan, C. D.; Alarcon, E. I. Peptide-Based Functional Biomaterials for Soft-Tissue Repair. *Front Bioeng Biotechnol* **2019**, *7* (205), 1 – 19.

(3) Xu, Y.; Kirchner, M. Collagen Mimetic Peptides. *Bioengineering*. MDPI AG January 1, **2021**, 1–24.

(4) Grillaud, M.; Bianco, A. Multifunctional Adamantane Derivatives as New Scaffolds for the Multipresentation of Bioactive Peptides. *J. Pept. Sci.* John Wiley and Sons Ltd May 1, **2015**, 330–345.

(5) Wanka, L.; Iqbal, K.; Schreiner, P. R. The Lipophilic Bullet Hits the Targets: Medicinal Chemistry of Adamantane Derivatives. *Chem. Rev.* May 8, **2013**, pp 3516–3604.

(6) Davies, W. L.; Grunert, R. R.; Haff, R. F.; McGahen, J. W.; Neumayer, E. M.; Paulshock, M.; Watts, J. C.; Wood, T. R.; Hermann, E. C.; Hoffmann, C. E. Antiviral Activity of 1-Adamantanamine (Amantadine). *Science (1979)* **1964**, *144*, 862–863.

(7) Orzeszko, A.; Gralewska, R.; Staroœciak, B. J.; Kazimierczuk, Z. Synthesis and Antimicrobial Activity of New Adamantane Derivatives ; *Acta Biochimica Polonica*, **1999,** *47*(1), 87 – 94.

(8) Jimenez-Jimenez, F. J.; Alonso-Navarro, H.; Garcia-Martin, E.; Agundez, J. A. G. Anti-Inflammatory Effects of Amantadine and Memantine: Possible Therapeutics for the Treatment of Covid-19? *J Pers Med* **2020**, *10* (4), 217.

(9) Vrettos, E. I.; Sayyad, N.; Mavrogiannaki, E. M.; Stylos, E.; Kostagianni, A. D.; Papas, S.; Mavromoustakos, T.; Theodorou, V.; Tzakos, A. G. Unveiling and Tackling Guanidinium Peptide Coupling Reagent Side Reactions towards the Development of Peptide-Drug Conjugates. *RSC Adv* **2017**, *7* (80), 50519–50526.

(10) Atherton, E. Solid Phase Peptide Synthesis. *A practical Approach* **1989**.

(11) Feinberg, R. S.; Merrifield, R. B. Modification of Peptides Containing Glutamic Acid by Hydrogen Fluoride-Anisole Mixtures.-Acylation of Anisóle or the Glutamyl Nitrogen. *J. Am. Chem. Soc.* **1975**, *97* (12), 3485 – 3496.

(12) Le-Nguyen, D.; Heitz, A.; Castro, B. Renin Substrates. Part 2. Rapid Solid Phase Synthesis of the Ratine Sequence Tetradecapeptide Using BOP Reagent. *J. Chem. Soc., Perkin Trans 1* **1987**, 1915–1919.

(13) Tripet, B.; Cepeniene, D.; Kovacs, J. M.; Mant, C. T.; Krokhin, O. V.; Hodges, R. S. Requirements for Prediction of Peptide Retention Time in Reversed-Phase High-Performance Liquid Chromatography: Hydrophilicity/Hydrophobicity of Side-Chains at the N- and C-Termini of Peptides Are Dramatically Affected by the End-Groups and Location. *J Chromatogr A* **2007**, *1141* (2), 212–225.

(14) Zhou NE; Mant CT; Hodges RS. Effect of Preferred Binding Domains on Peptide Retention Behavior in Reversed-Phase Chromatography: Amphipathic Alpha Helices. *Peptide Res* **1990**, *3* (1), 8 – 20.

(15) Marie, E.; Sagan, S.; Cribier, S.; Tribet, C. Amphiphilic Macromolecules on Cell Membranes: From Protective Layers to Controlled Permeabilization. *J. Membr. Biol.* **2014**, *247* (9), 861–881.

(16) Milletti, F. Cell-Penetrating Peptides: Classes, Origin, and Current Landscape. *Drug Discov Today* **2012**, *17* (15–16), 850–860.

(17) Robinson, S. W.; Afzal, A. M.; Leader, D. P. Bioinformatics: Concepts, Methods, and Data. In Handbook of Pharmacogenomics and Stratified Medicine; Padmanabhan, S., Ed.; *Academic Press*, **2014**; pp 259–287.

(18) Shoulders, M. D.; Raines, R. T. Collagen Structure and Stability. *Annu Rev Biochem* **2009**, *78*, 929.

(19) Schultz, D. A.; Friedman, A. M.; White, M. A.; Fox, R. O. The Crystal Structure of the Cis-Proline to Glycine Variant (P114G) of Ribonuclease A. *Protein Sci.* **2005**, *14* (11), 2862–2870.

(20) Gillard, R. D. Circular Dichroism and Configuration of Complexes of Amino Acids. In *Proceedings of the Royal Society of London. Series A, Mathematical and Physical Sciences*; **1967**, *297* (1448), 134–140.

(21) Matsuo, K.; Yonehara, R.; Gekko, K. Secondary-Structure Analysis of Proteins by Vacuum-Ultraviolet Circular Dichroism Spectroscopy. *J Biochem* **2004**, *135* (3), 405–411.

(22) Woody, W. R. [4] Circular Dichroism. *Methods Enzymol* **1995**, *246*, 34–71.

(23) Koslowski, A.; Sreerama, N.; Woody, R. W. Circular Dichroism of Peptides and Proteins. In *Circular dichroism: Principles and Applications*; Berova, N., Woody, R. W., Nakanishi, K., Eds.; *Willy-VCH Press*: **2000**, 55–95.

(24) Greenfield, N.; Fasman, G. Computed Circular Dichroism Spectra for the Evaluation of Protein Conformation. *Biochemistry* **1969**, *8* (10), 4108–4116.

(25) Holzwarth, G.; Doty, P. The Ultraviolet Circular Dichroism of Polypeptides. *J. Am. Chem. Soc.* **1965**, *87* (2), 218–228.

(26) Corrêa, D.; Henrique, C.; Ramos, I.; Corrêa, D. H. A.; Ramos, C. H. I. The Use of Circular Dichroism Spectroscopy to Study Protein Folding, Form and Function Protein Stability, Folding and Misfolding View Project Studies with Human Tissue Kallikrein View Project The Use of Circular Dichroism Spectroscopy to Study Protein Folding, Form and Function. *Afr. J. Biochem. Res* **2009**, *3* (5), 164–173.

(27) Wikipedia contributors. *Protein folding*. Wikipedia, The Free Encyclopedia.

(28) Wikipedia contributors. *Rossmann fold*. Wikipedia, The Free Encyclopedia.

(29) Štefica Horvat; Kata Mlinarić-Majerski; Ljubica Glavaš-Obrovac; Andreja Jakas; Jelena Veljković; Saška Marczi; Goran Kragol; Maja Roščić; Marija Matković; Andrea Milostić-Srb. Tumor-Cell-Targeted Methionine-Enkephalin Analogues Containing Unnatural Amino Acids: Design, Synthesis, and in Vitro Antitumor Activity. *J. Med. Chem.* **2006**, *49* (11), 3136–3142.

(30) Roscic, M.; Sabljic, V.; Mlinaric-Majerski, K.; Tefica Horvat, S. In Vitro Enzymatic Stabilities of Methionine-Enkephalin Analogues Containing an Adamantane-Type Amino Acid. *Croatica Chemical Acta,* **2008**, *81*(4), 637 – 640.

(31) Štimac, A.; Šekutor, M.; Mlinarić-Majerski, K.; Frkanec, L.; Frkanec, R. Adamantane in Drug Delivery Systems and Surface Recognition. *Molecules*. MDPI AG February 1, **2017**.

(32) Aloisi, A.; Christensen, N.; Sørensen, K.; Guilbaud, C.; Jensen, K.; Bianco, A. Synthesis and Characterization of Adamantane-Containing Heteropeptides with a Chirality Switch. *European J Org Chem* **2020** (7), 2020.

CHAPTER IV

STRUCTURE DETERMINATION OF ADAMANTANE PEPTIDES

The chapter describes the elucidation of the tertiary structure of collagen mimetic peptide, *retro*-DGD-GG-GFOGER-GG-TTK-Adamantane (NL010). The structure is elucidated using 2D NMR spectroscopy experiments. The structure of the peptide is shown in Figure 4.1.

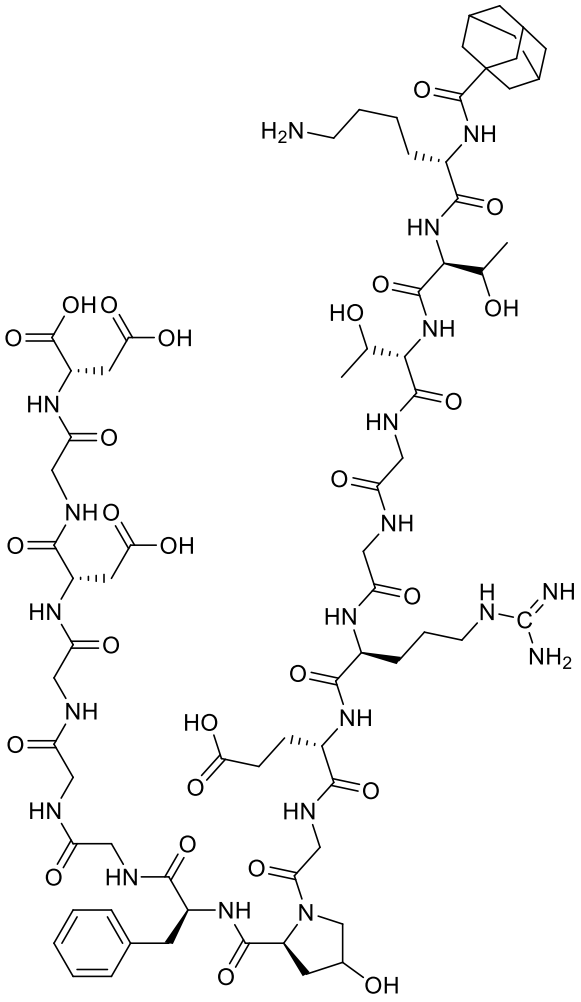

Figure 4.1: Collagen mimetic peptide – *retro*-DGD-GG-GFOGER-GG-TTK-Adamantane.

4.1 RESULTS AND DISCUSSION

4.1.1 Nuclear Magnetic Resonance (NMR)

4.1.1.1 ^{1}H NMR

The ^{1}H NMR spectrum of the collagen mimetic peptide, *retro*-DGD-GG-GFOGER-GG-TTK-Adamantane is shown in Figure 4.2. The spectrum displays a number of protons in the aliphatic, *alpha*, aromatic and amide region of the spectrum.

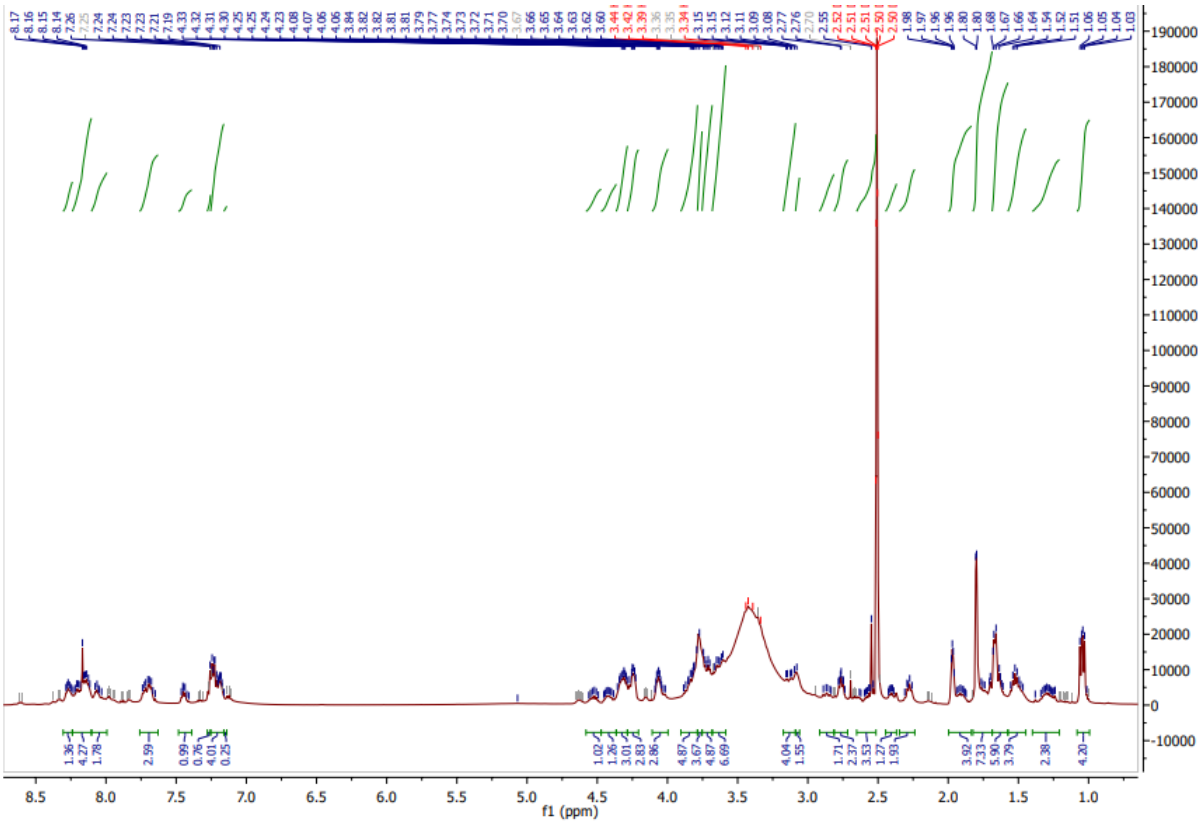

Figure 4.2: ^{1}H NMR spectrum of *retro*-DGD-GG-GFOGER-GG-TTK-Adamantate.

With the aid of ^{13}C NMR, DEPT 135, COSY, HSQC and HMBC, full characterization of the peptide was accomplished.

The amide region consists of fifteen protons instead of the calculated sixteen. The discrepancy is due to the hydroxyproline tertiary amide nitrogen which lacks an amide proton. The number of amide protons is indicative of the number of amino acid residues that make up a peptide since there is one amide proton for each amino acid residue.

The COSY experiment was utilized to confirm the assignment of the *alpha* protons that make up a spin system because of the 1,3-through bond interaction between the amide and *alpha* protons. In a case where one amide proton interacts with two *alpha* protons instead of one, the amino acid was identified as glycine.

Identification of several amino acids was however accomplished through the TOCSY experiment which revealed different spin systems. Spins systems are unique to different amino acids and hence were employed to identify amino acids. The amide section of the TOCSY spectrum is shown in Figure 4.3.

4.1.1.2 TOCSY experiment

All the cross peaks in the TOCSY experiment are due to protons of the same spin system. It shows the interaction between two protons that interact with each other through bonds.[1,2] The amide proton in the TOCSY experiment can interact with another proton connected by a long-range coupling. The experiment correlates all protons of a spin system regardless of how far the protons are from each other.[3] Because of the latter, TOCSY can show almost all the protons that make up the side chains of the amino acids.

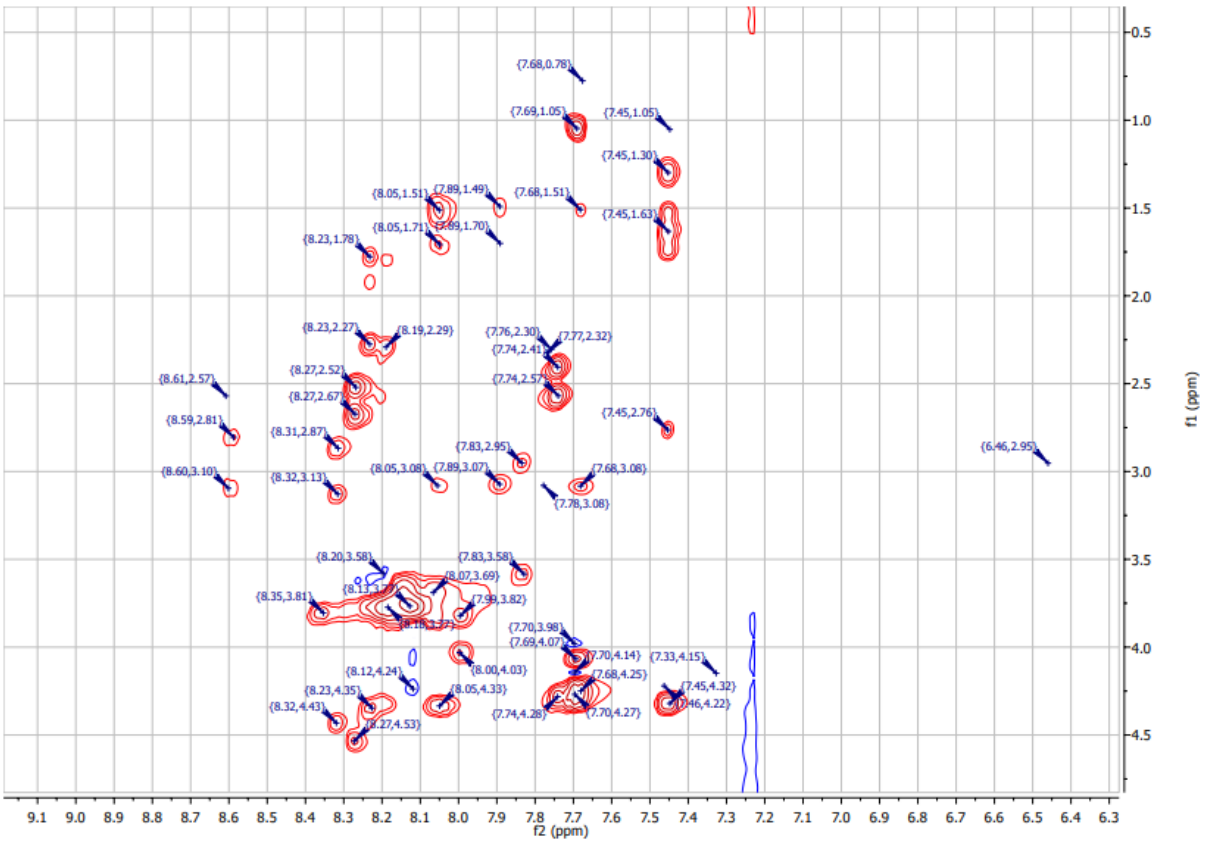

Figure 4.3: Amide Section of TOCSY spectrum of *retro*-DGD-GG-GFOGER-GG-TTK-Adamantate.

The presence of the cross peaks in the methyl region of the spectrum is indicative of the spin system of threonine. It is the only amino acid that has the methyl group in the peptide sequence of *retro*-DGD-GG-GFOGER-GG-TTK-Adamantane. Its spin systems with amide resonance peaks at 8.14 and 1.04 ppm have only three peaks due to the interaction of *alpha* with *beta* and *gamma* methyl protons.

Spin systems with chemical shifts of 8.53, 8.36, 8.13, 8.15, 8.32, 7.69, 8.12 ppm that have only one cross peak in the α-region (3.5 – 4.6 ppm) of the TOCSY spectrum, are characteristic of glycine. The amide proton of glycine is always split into a triplet because of the two neighboring *alpha* protons. The peptides have five glycine amino acids and they were differentiated from each other using the ROESY spectrum, Table 4.1.

The spin system of lysine was identifiable by its six cross peaks. In terms of the arrangement of the peaks, lysine has a $A_2(F_2T_2)$MTX spin system.[4] The arrangement of peaks in the spin system, in order of decreasing chemical shift is $H^{\alpha} > H^{\varepsilon} > H^{\beta} > H^{\beta} > H^{\delta} > H^{\gamma}$.[4] Lysine was therefore attributed to the spin system with an amide proton at 7.45 ppm.

An ambiguity was observed regarding glutamic acid, hydroxyproline and arginine. The spin systems for these amino acid residues all have five peaks. That is, the length of the spin system is the same, they all have the $A_2(T_2)$MPX system. However, glutamic acid is distinguishable from these amino acid residues in that, in order of decreasing chemical shift, hydroxyproline and arginine are the same, both having $H^{\alpha} > H^{\delta} > H^{\beta} > H^{\beta} > H^{\gamma}$. Therefore, glutamic acid was identifiable by its characteristic pattern of cross peaks, having AM(PT)X system. All the protons on both the *beta* and *gamma* carbons are different in terms of chemical shift, therefore the spin system has five peaks. In order of decreasing chemical shift, there is $H^{\alpha} > H^{\gamma} > H^{\gamma} > H^{\beta} > H^{\beta}$. Hydroxyproline and arginine were distinguished from one another using the ROESY experiment, Figure 4.5, Table 4.1.

4.1.1.3 ROESY experiment

ROESY experiment shows dipeptides that exist within a given peptide. While TOCSY shows one spin system, ROESY combines two spin systems because there is a scalar coupling between *i* and *i* – 1 amino acid residues.

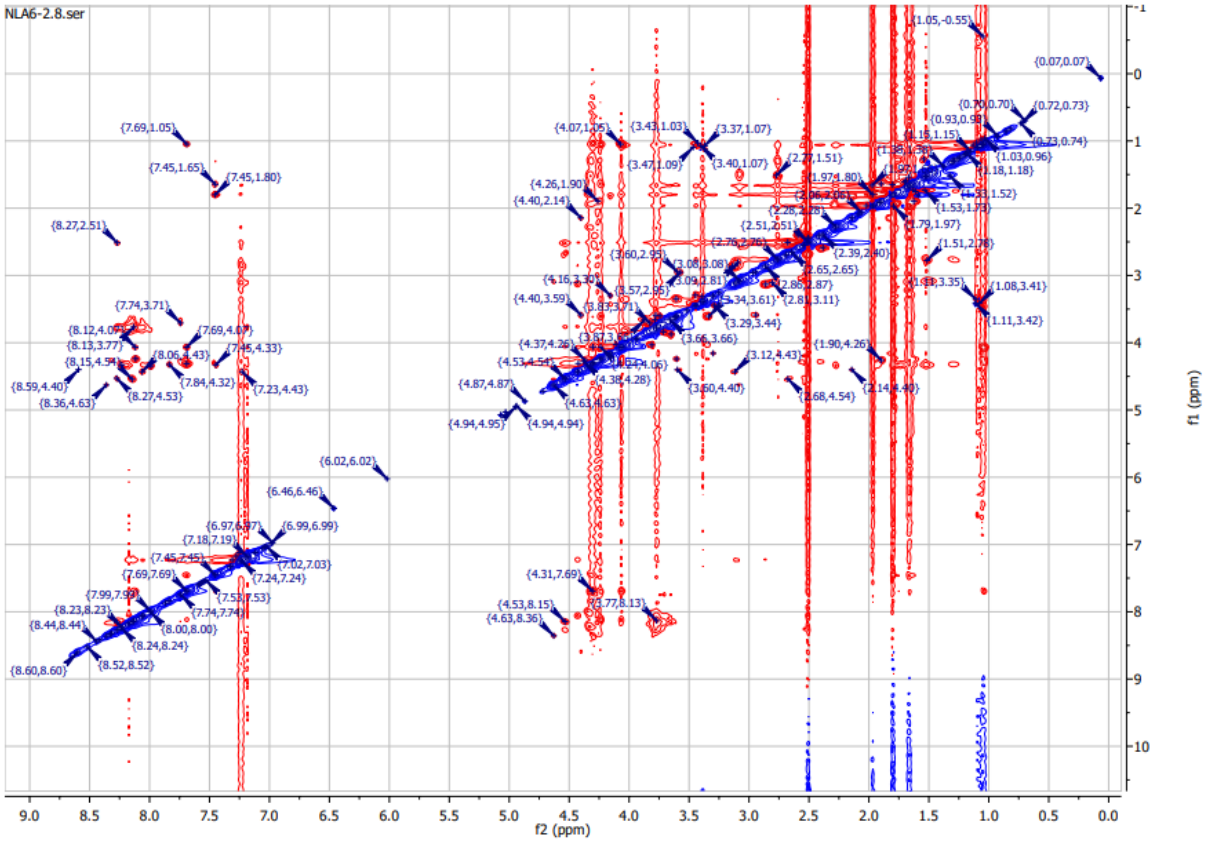

Figure 4.4: ROESY spectrum of *retro*-DGD-GG-GFOGER-GG-TTK-Adamantane.

All the *alpha* protons of the spin systems identified in the TOCSY experiment were observed in ROESY experimental spectrum. The *alpha* proton of self-amino acid residue interacted with the *alpha* proton of the next coupled amino acid as shown in the *alpha*-amide section of ROESY spectrum in Figure 4.5.

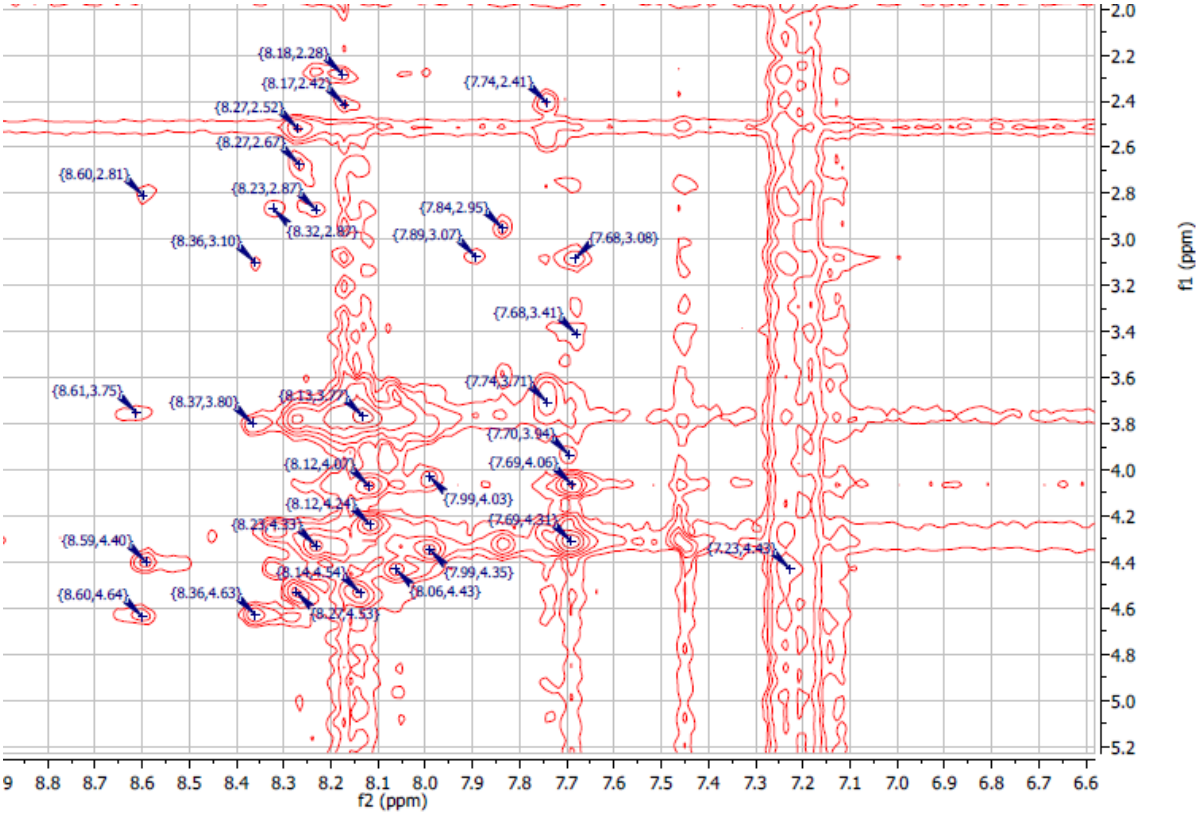

Figure 4.5: *Alpha*-amide section of ROESY spectrum.

Since ROESY spectrum displays existing dipeptides within a peptide, the *alpha* region of its spectrum consists of two *alpha* protons. One cross-peak is reflective of the *alpha* proton of the self-amino acid residue (*i*) while the other is from a neighbouring amino acid residue (*i* – 1). Table 4.1 shows existing dipeptides in the collagen mimetic peptide *retro*-DGD-GG-GFOGER-GG-TTK-Adamantane.

Table 4.1: TOCSY spin systems and ROESY dipeptides.

TOCSY Spin System		**ROESY**		**Dipeptide**
H^{α}	**H^{β}, H^{γ}, H^{δ} ,H^{ϵ}**	**$H^{\alpha}1$, $H^{\alpha}2$**	**H^{β}, H^{γ}, H^{δ}, H^{ϵ}**	
4.63	3.10, 2.80	4.63, 4.41	3.10, 2.80	Asp-Gly
4.41	3.10, 2.80	4.41, 4.63	3.10, 2.80	Gly-Asp
4.63	3.10, 2.80	4.63, 3.80	3.10, 2.80	Asp-Gly
3.80	-	3.80, 3.77	-	Gly-Gly
3.77	-	3.77, 4.54	-	Gly-Gly

TOCSY Spin System		ROESY		Dipeptide
4.54	-	4.54, 4.66	2.86, 3.13, 7.12, 7.26, 7.19	Gly-Phe
4.66	2.86, 3.13, 7.12, 7.26, 7.19	4.66, 4.43	2.86, 3.13, 7.12, 7.26, 7.19, 1.90, 4.23, 3.61	Phe-Hyp
4.43	1.92, 4.23, 3.61	4.43, 4.27	1.92, 4.39, 3.61	Hyp-Gly
4.27	-	4.27, 4.33	2.56, 2.44	Gly-Glu
4.33	2.56, 2.44	4.33, 4.31	2.56, 2.44, 3.00, 1.51, 1.91,	Glu-Arg
4.31	3.00, 1.51, 1.91	4.31, 4.07	3.00, 1.51, 1.91	Arg-Gly
4.07	-	4.07, 4.24	-	Gly-Gly
4.24	-	4.24, 3.82	4.05, 0.94	Gly-Thr
3.82	4.05, 0.94	3.82, 3.82	4.05, 0.94	Thr-Thr
3.82	4.05, 0.94	3.82, 4.35	4.05, 0.94, 1.92, 1.51, 1.33, 2.76	Thr-Lys
4.35	1.92, 1.51, 1.33, 2.76	4.35	1.92, 1.51, 1.33, 2.76	-

After the assignment of the dipeptides, the full peptide was characterized using ^{13}C NMR, DEPT 135, COSY, HSQC and HMBC, as shown in Table 4.2.

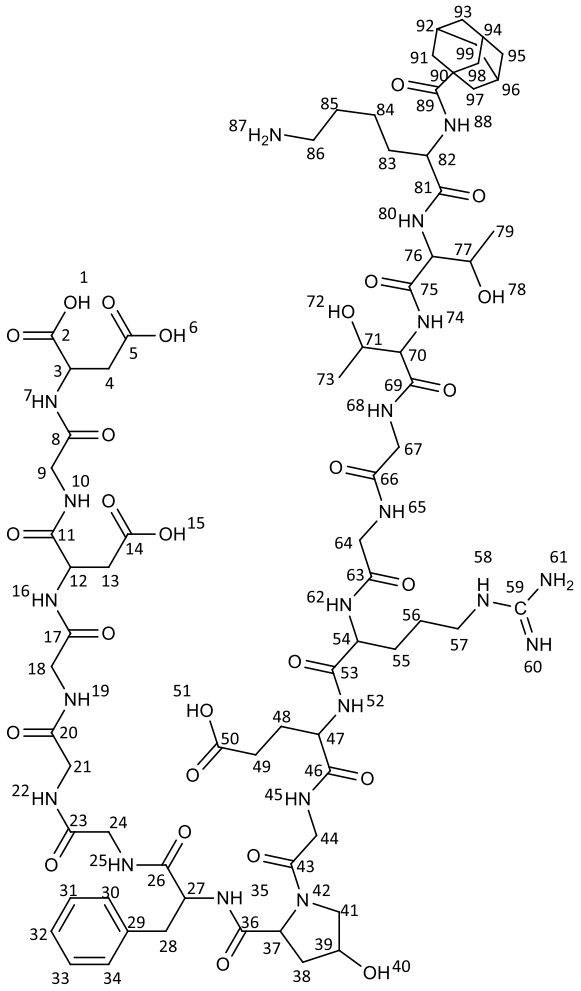

Figure 4.6: *retro*-DGD-GG-GFOGER-GG-TTK-Adamantane.

Table 4.2: Characterisation table for *retro*-DGD-GG-GFOGER-GG-TTK-Adamantane.

No.	δ ^{1}H	δ ^{13}C	δ COSY	δ HSQC	δ HMBC
1	11.0	-	-	-	-
2	-	-	-	-	165.63, 4.63-
3	4.63	54.22	4.63, 8.60	4.63, 54.22	4.63, 165.63
4	2.81	40.77	2.81, 4.63	2.81, 40.77	2.81,54.66
5	-	-	-	-	170.30, 2.83-
6	11.0	-	-	-	-
7	8.60	-	8.59, 4.63	-	8.56, 171.72
8	-	-	-	-	166.73, 4.41
9	4.41	54.47	4.41, 8.54	4.41, 54.47	4.41, 166.68

No.	δ ^{1}H	δ ^{13}C	δ COSY	δ HSQC	δ HMBC
10	8.54	-	8.54, 4.41	-	8.54, 179.77
11	-	-	-	-	165.63, 4.63
12	4.63	54.22	4.63, 8.60	4.63, 54.22	4.63,135.63
13	2.81	40.77	4.63, 2.81	2.81, 40.77	2.81, 54.66
14	-	-	-	-	170.30, 2.83-
15	11.0	-	-	-	
16	8.60	-	8.60, 4.63	-	8.60, 171.15
17	-	-	-	-	171.97, 3.80
18	3.80	49.33	3.80, 8.36	3.80, 49.33	3.80, 171.97
19	8.36	-	8.36, 3.80	-	8.36, 163.90
20	-	-	-	-	169.85, 3.77-
21	3.77	44.91	3.77, 8.13	3.77, 44.91	3.77, 169.88
22	8.13	-	8.13, 3.77	-	8.13, 171.26
23	-	-	-	-	171.48, 4.54-
24	4.54	50.22	4.54, 8.15	4.54, 50.22	4.54, 171.36
25	8.15	-	8.15, 4.54	-	8.15, 177.49
26	-	-	-	-	171.34, 4.66-
27	4.66	58.53	4.66, 8.14	4.66, 58.64	4.66, 178.07
28	2.85	38.25	2.81, 4.65	2.85, 38.25	2.85, 179.66
29	-	138.19	-	-	138.19, 7.19
30	7.14	127.84	7.14, 7.27	7.14, 126.71	7.14, 126.71,
31	7.27	129.49	7.27, 7.17	7.27, 129.39	-
32	7.17	126.15	7.17, 7.27	7.17, 128.86	-
33	7.27	129.49	7.27, 7.17	7.27, 129.39	-
34	7.14	127.84	7.14, 7.27	7.14, 126.71	7.14, 126.71
35	8.14	-	8.14, 4.66	-	8.14, 171.16
36	-	-	-	-	172.69, 4.43
37	4.43	54.47	4.43, 8.32	4.43, 54.47	4.53, 171.85
38	1.90	37.53	1.90, 4.23	1.90, 37.53	1.89, 69.04
39	4.23	69.03	4.23, 3.61	4.23, 69.03	4.23, 67.03
40	3.58	-	-	-	3.55, 69.21
41	3.61	54.48	3.61, 4.23	3.61, 54.48	3.62, 65.08
42	-	-	-	-	-
43	-	-	-	-	-
44	4.27	49.35	4.27, 8.32	4.27, 49.35	4.27, 172.20
45	8.32	-	8.32, 4.27	-	8.32, 175.43
46	-	-	-	-	172.31, 4.32
47	4.33	52.51	4.33, 8.23	4.33, 52.51	4.33, 172.03
48	2.53	40.16	2.53, 4.20	2.53, 40.16	2.53, 49.32
49	3.05	40.77	3.05, 2.52	3.05, 40.77	2.02, 40.16
50	-	-	-	-	165.94, 3.04-
51	11.0	-	-	-	
52	8.23	-	8.23, 4.33	-	8.23, 170.07
53	-	-	-	-	170.55, 4.31-
54	4.31	52.51	4.31, 7.69	4.31, 52.51	4.31, 172.29
55	1.89	28.03	1.89, 4.31	1.89, 52.68	1.92, 169.12

No.	δ ^{1}H	δ ^{13}C	δ COSY	δ HSQC	δ HMBC
56	1.51	59.42	1.51, 1.89	1.51, 59.42	1.51, 28.03
57	3.00	55.35	3.02, 1.51	3.02, 55.35	3.02, 59.42
58	8.82	-	8.82, 3.07	-	8.82, 55.35
59	-	-	-	-	156.80, 8.82
60	-	-	-	-	-
61	-	-	-	-	-
62	7.69	-	7.69, 4.31	-	7.69, 170.62
63	-	-	-	-	174.00, 4.07
64	4.06	52.60	4.06, 7.69	4.06, 52.60	4.06, 170.53
65	7.69	-	7.69, 4.07	-	7.69, 170.62
66	-	-	-	-	170.88, 4.23
67	4.24	58.76	4.24, 8.12	4.24, 58.76	4.24, 171.09
68	8.12	-	8.12, 4.24	-	8.12, 173.58
69	-	-	-	-	169.58, 3.82-
70	3.82	52.90	3.82, 7.99	3.82, 52.90	3.82, 169.68
71	4.04	66.87	3.82, 4.04	4.04, 66.87	4.04,
72	4.32	-	-	-	4.32, 66.87
73	1.04	19.79	1.04, 4.04	1.04, 19.79	1.04, 66.87
74	7.79	-	7.79, 3.82	-	7.79, 179.67
75	-	-	-	-	169.58, 3.82--
76	3.82	52.90	3.82, 7.99	3.82, 52.90	3.82, 169.58
77	4.04	66.87	3.82, 4.04	4.04, 66.87	4.04,
78	4.32				4.32, 66.87
79	1.04	19.79	1.04, 4.04	1.04, 19.79	1.04, 66.87
80	7.79	-	7.79, 3.82	-	7.79, 179.67
81	-	-	-	-	-
82	4.35	59.45	4.35, 7.99	4.35, 59.45	4.35, 172.31
83	7.99	-	7.99, 4.35	-	7.99, 179.67
84	1.88	37.91	1.88, 4.29	1.88, 37.91	1.88, 37.23
85	1.57	37.65	1.57, 1.88	1.57, 37.65	1.57, 36.64
86	1.73	29.14	1.73, 1.57	1.73, 29.14	1.73, 40.50
87	2.27	31.08	2.27, 1.73	2.27, 31.08	2.27, 25.33
88	-	-	-	-	-
89	-	-	-	-	178.05, 1.60
90	-	36.33	-	-	36.33, 1.60
91	1.60	38.90	1.60, 4.31	1.60, 38.92	1.60, 36.33
92	1.63	30.27	1.63, 3.02	1.63, 30.27	1.60, 176.78
93	1.53	36.51	1.53, 3.02	1.56, 36.53	1.53, 37.53
94	1.63	30.27	1.63, 3.02	1.63, 30.27	1.65, 36.65
95	1.63	36.49	1.53, 3.02	1.63, 36.49	1.63, 39.08
96	1.63	30.27	1.63, 3.02	1.63, 30.27	1.63, 38.08
97	1.67	38.94	1.67, 4.31	1.67, 38.94	1.70, 39.10
98	1.63	36.50	1.53, 3.02	1.63, 36.50	1.67, 176.78
99	1.67	38.94	1.67, 4.31	1.67, 38.94	1.67, 176.78

Since the ROESY experiment displays two protons that interact with each other through space within 5 angstroms, it has the ability to show the 3-dimensional structure of the peptide. Interactions of amino acids that are 4 amino acids away are characteristic of α-helix and are medium-range couplings.[5,6] Amino acid residues that are about 10 amino acids apart can only interact through space if they are within 5 angstroms meaning the molecule is bent.[7,8] Table 4.3 shows interactions observed in the ROESY spectrum.

Table 4.3: Determination of tertiary structure of *retro*-DGD-GG-GFOGER-GG-TTK-Adamantane.

Hyp-Arg (α-helix)	Expected Interaction	Observed Interaction	Coupling Range
$d_{\alpha\beta}(i, i + 3)$	4.43, 1.89	4.43, 1.89	medium
$d_{\alpha N}(i, i + 3)$	4.43, 7.69	4.43, 7.69	medium
$d_{NN}(i, i + 3)$	8.32, 7.69	8.32, 7.69	medium
$d_{\alpha N}(i, i + 4)$	4.43, 8.12	4.33, 8.12	medium

The stated interactions for two amino acid residues that are three amino acids apart are characteristic of an α-helical structure. This is in agreement with the circular dichroism experimental result reported in Chapter III. However, no long-range interactions were observed hence the determination of a tertiary structure utilizing computational chemistry revealed a possibility of a helical structure and no other well-defined conformations were detected.

4.2 CONCLUSION

The NMR studies confirmed the existence of the helical structure as detected by the CD measurements and enabled the identification of the amino acids involved in the formation of the helix. This information will be used in the computational binding studies of the *retro*-DGD-GG-GFOGER-GG-TTK-Adamantane-integrin complex.

4.3 REFERENCES

(1) Wüthrich, K. NMR with Proteins and Nucleic Acids. *Europhys News* **1986**, *17* (1), 11–13.

(2) Bax, A. Two-Dimensional NMR and Protein Structure. *Annu Rev Biochem* **1989**, *58*, 223–256.

(3) Oxford Instruments Magnetic Resonance. An Introduction to Total Correlation Spectroscopy (TOCSY).

(4) Zerbe, O.; Bader, R. Peptide NMR. *BioNMR Drug Res* **2002**, 16, 95 – 120.

(5) Shoulders, M. D.; Raines, R. T. Collagen Structure and Stability. *Annu Rev Biochem* **2009**, *78*, 929.

(6) Cavanagh, J.; Fairbrother, W. J.; Palmer III, A. G.; Skelton, N. J. Protein NMR Spectroscopy: Principles and Practice. *Academic press* **1996**.

(7) Wüthrich, K. NMR in Structural Biology. *World Scientific* **1995**, 11–15.

(8) Wüthrich, K. Protein Structure Determination in Solution by NMR Spectroscopy. *J. Biol. Chem.* **1990**, *265* (36), 22059–22062.

CHAPTER V

BINDING PEPTIDES

The chapter describes the synthesis of collagen I mimetic peptides with potentially enhanced integrin-binding properties due to structural modifications of the phenylalanine residue in the *retro*-GG-G[*para*-fluoro-Phe]OGER-GG peptide sequence. The design of the original sequence (*retro*-GG-GFOGER-GG) as well as its interactions with integrins ($\alpha_2\beta_1$, $\alpha_1\beta_1$, $\alpha_{10}\beta_1$, $\alpha_{11}\beta_1$) is described in chapters II and III in detail.

The benzene ring of phenylalanine (F8, Figure 5.1) has an electron density due to resonance in the π-system. The negatively charged cloud interacts with glutamine (Q215) and asparagine (N154) via Van de Walls forces, the hydrophobic interaction is shown in Figure 5.1.

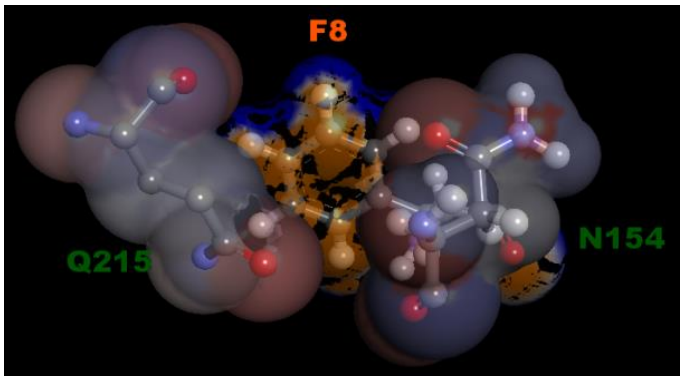

Figure 5.1: Phenylalanine interactions.[1]

The amino acids glutamine (Q215) and asparagine (N154) are neutral polar in nature and can form hydrogen bonds. The introduction of fluorine onto the phenylalanine (F8) was meant to promote hydrogen bonding between the amide proton of the side chains of Q215 and N154 and the fluorine. Hydrogen bonding is stronger than Van de Walls forces and can potentially improve the interaction between *para*-fluoro phenylalanine and Gln215 and Asn154. Due to the high electronegativity of fluorine, it can form strong hydrogen bonds and thereby enhancing the binding interaction.[2] The envisaged structure of the peptide with *para*-fluorophenylalanine is shown in Figure 5.2. Other researchers have studied the binding affinity of phenylalanine in this position by replacing it with other non-polar amino acids such

as leucine (L), methionine (M) and alanine (A) and they concluded that F>L>M>A.[3] Hence phenylalanine was maintained and modified for improved binding.

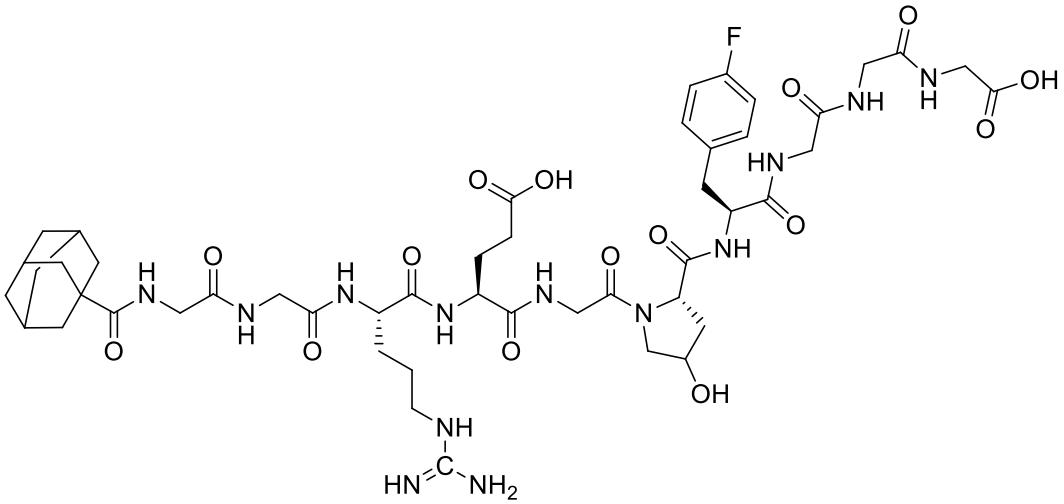

Figure 5.2: Structure of *retro*- *para*-fluorophenylalanine adamantane peptide.

5.1 SYNTHESIS

The *para*-fluorophenylalanine was first protected with an Fmoc protecting group before it was introduced into the sequence {*retro*-GG-G[*para*-fluoro-Phe]OGER-GG-Palmitate and –Adamantane} during solid phase peptide synthesis.

Synthesis of the Fmoc-*para*-fluorophenylalanine was accomplished via an acetylation reaction between 9-fluorenylmethoxycarbonyl chloride (Fmoc-Cl) and *para*-fluorophenylalanine. To a cooled solution of 1.39 g (7.6 mmoles) of *para*-fluorophenylalanine in an ice bath dissolved in 20 mL of 10% aqueous Na_2CO_3 was added with stirring, 1.96 g (7.6 mmoles) of Fmoc-Cl (scheme 5.1).

The mixture was stirred at room temperature for 2 hours, then poured into 400 mL of water and extracted twice with ether to remove small amounts of 9-fluorenylmethanol and the polymer of dibenzofulvene. The aqueous layer was cooled in an ice bath and acidified with concentrated HCl. It was further extracted with ethyl acetate, the extracts were washed with water, dried over $MgSO_4$ and evaporated, and the resulting white residue was recrystallized from methanol. The resulting white solid has a melting point of 184 – 186 °C and a yield of 2 g, 80%. The detailed procedure is outlined in the experimental chapter IX.

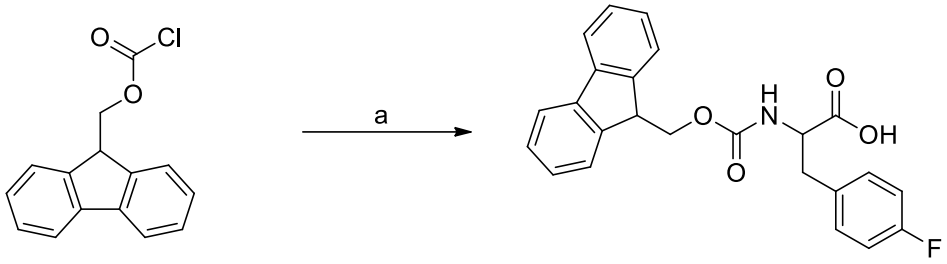

Scheme 5.1: Protection of *para*-fluorophenylalanine.
Reagents and conditions; (a) 0.0076 moles *para*-fluorophenylalanine, 20 mL 10% Na_2CO_3, 25 mL 1,4-dioxane, 2 hrs, r.t., 80 %.

5.2 RESULTS AND DISCUSSION

The reaction follows an S_N2 mechanism where the primary amine acts as a nucleophile, attacking the carbon of the carbonyl thereby displacing chlorine. Displacement of chlorine results in the formation of an amide bond linking the amino acid and the Fmoc protecting group.

^1H NMR spectrum of the product shows the expected number of protons that is commensurate with the calculated number of protons in the aliphatic, aromatic and amide regions of the spectrum Figure 5.3.

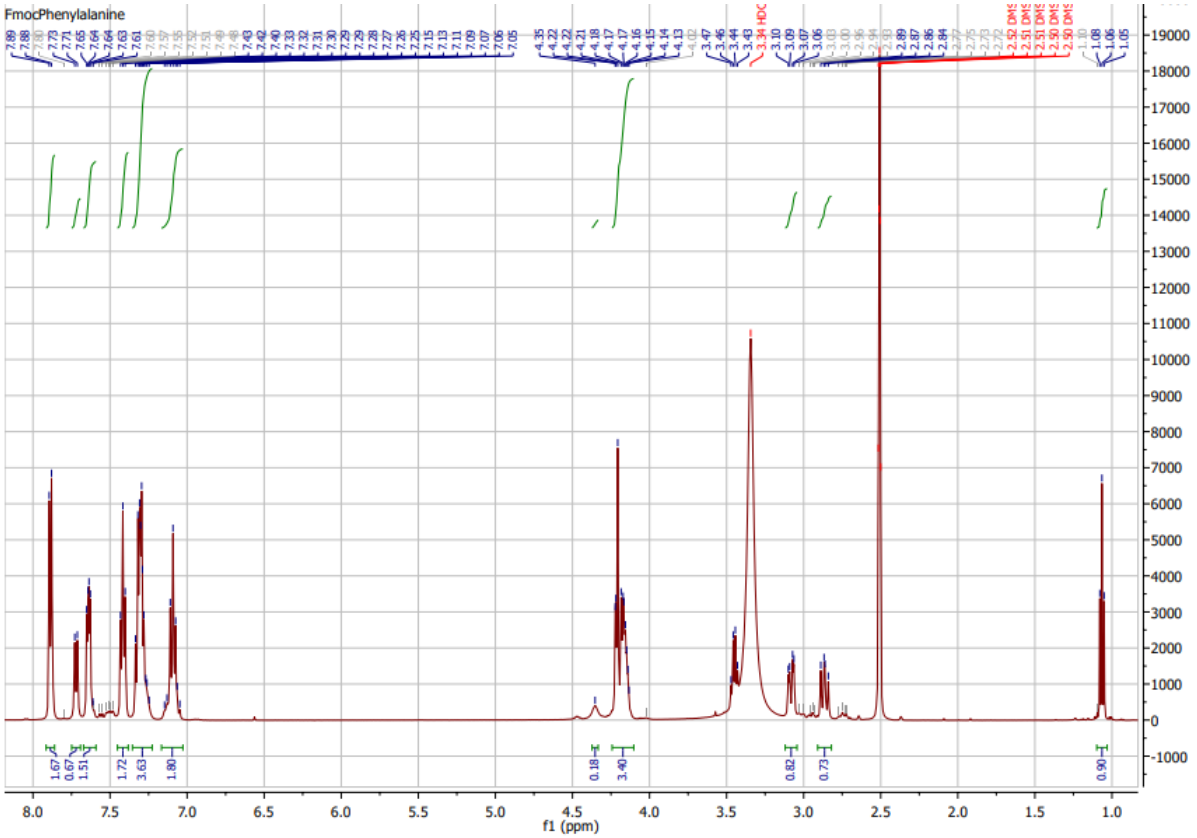

Figure 5.3: ^{1}H NMR of Fmoc-*para*-fluoro phenylalanine.

The multiplets at 2.86 and 3.09 ppm were attributed to phenylalanine H^{β} protons. After being split one by another, each of these protons is further split by the neighboring H^{α} proton-13 resulting in a multiplet.

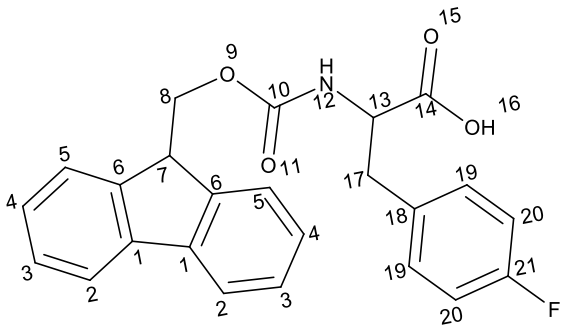

Figure 5.4: Structure of Fmoc-*para* fluoro-phenylalanine.

The four peaks in the region between 4.13 - 4.35 ppm were assigned to the protons of CH – 7, CH_2 – 8 and one CH^{α} – 13 of phenylalanine. The calculated total number of aromatic protons is twelve and the expanded ^{1}H NMR spectrum in Figure 5.4 shows that the peaks integrate to

12 peaks. The peak at 7.72 ppm that integrates for one proton was attributed to the amide proton. Full characterization of the Fmoc-*para*-fluoro phenylalanine is shown in the appendix section.

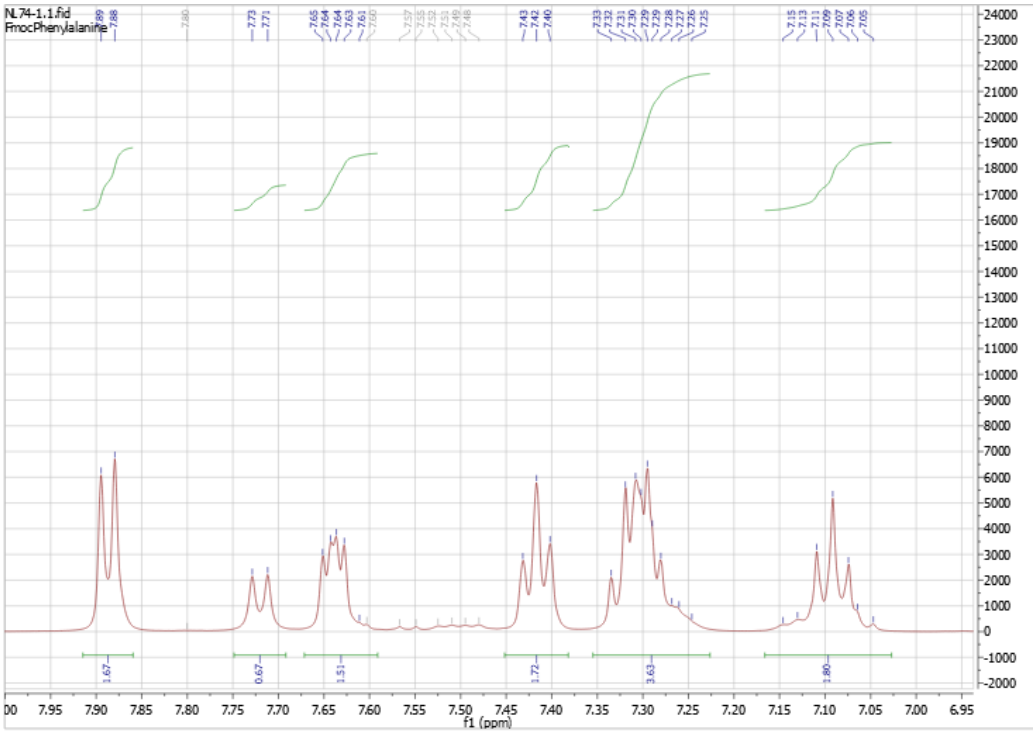

Figure 5.5: Section of ^{1}H NMR spectrum of Fmoc-*para*-fluoro phenylalanine.

The synthesized fmoc-*para*-fluoro phenylalanine was then employed in the synthesis of the peptide GG-G[*para*-fluoroPhe]OGER-GG-Adamantane and -Palmitate as described in the next section.

5.3 SYNTHESIS OF *para*-FLUORO PHENYLALANINE PEPTIDES

The synthesized *para*-fluoro phenylalanine amino acid was incorporated into the already synthesized *retro*-tripeptide, GG-G-NH2 (Scheme 5.2). The tripeptide was synthesized according to the general procedure C for the synthesis of peptides outlined in the experimental chapter IX.

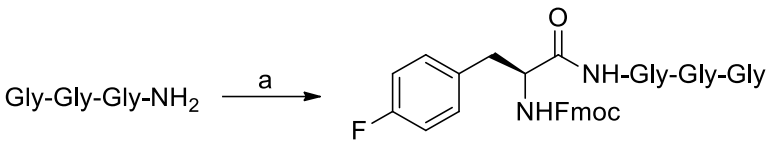

Scheme 5.2: Coupling reaction of *para*-fluorophenylalanine to the tripeptide *retro*-GG-G-NH_2 (Gly = G=Glycine) Reagents and Conditions: (a) 0.2 M *para*-fluorophenylalanine, 1 M DIPEA, 0.19 M HBTU, DMF, 45 min, r.t.

To the already synthesized peptide *retro*-GG-G-NH-Fmoc on a solid support, was added 20% piperidine solution (10 mL) twice for 5 minutes and the mixture was stirred by bubbling nitrogen. The resin was then washed with DMF (3 x 5 mL) followed by DCM (3 x 5 mL) to remove excess reagents.

The *para*-fluorophenylalanine (0.972 g, 0.12 M) and DIPEA (1.26 mL, 1 M) in DMF (10.74 mL) were first mixed and stirred in a shaker for a few minutes before the addition of the coupling reagent, HBTU (0.519 g, 0.11 M). The resultant mixture was added to the resin and stirred by bubbling nitrogen for 45 minutes. Towards the end of the 45 minutes, a few beads were taken from the reaction flask and tested for the presence of free NH_2 using the Ninhydrin Test. According to the test, the reaction was complete at 45 minutes. The solvent was removed and the now coupled *para*-fluorophenylalanine was deprotected by adding 20% piperidine. The reaction mixture was bubbled with nitrogen twice for 5 minutes. The resin was washed with DMF (3 x 5 mL) followed by DCM (3 x 5 mL). The spectrum obtained after addition of ten amino acids showed desired crude peptide mass peak of 923.3897 g/mol at 16 minutes, indicating successful coupling of the amino acids. The high resolution mass spectrum is shown in Figure 5.6.

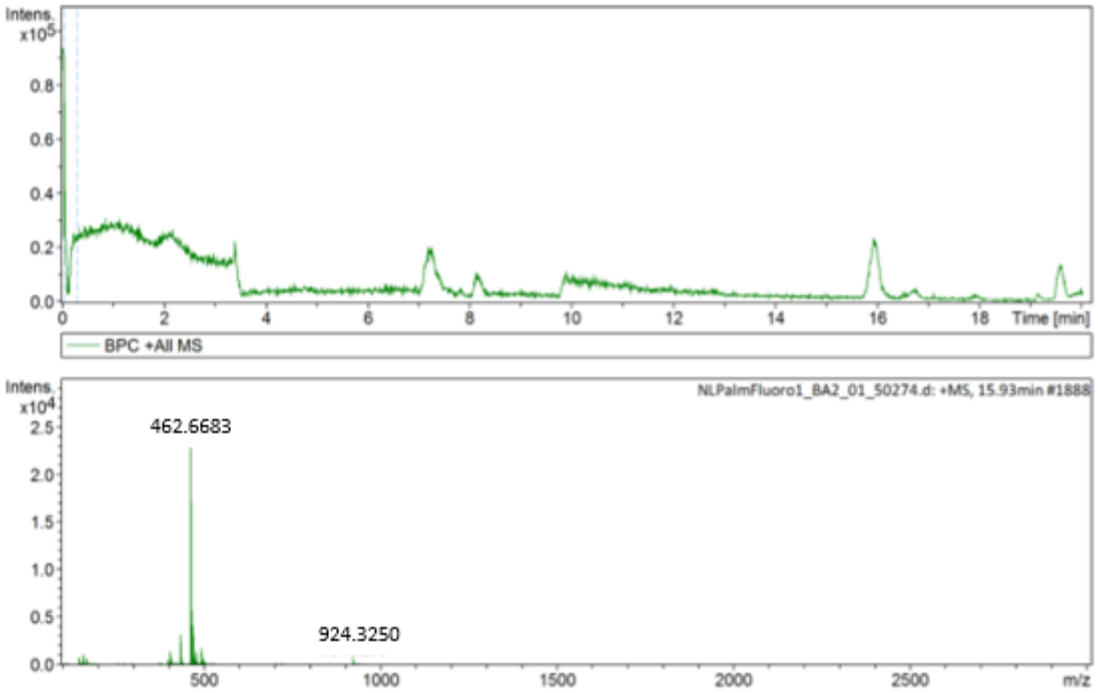

Figure 5.6: Mass spectrum of crude *retro*-GG-G[*para*-fluoroPhe]OGER-GG-NH_2.

The *retro-para*-fluorophenylalanine peptides were synthesized according to Scheme 5.3 shown below.

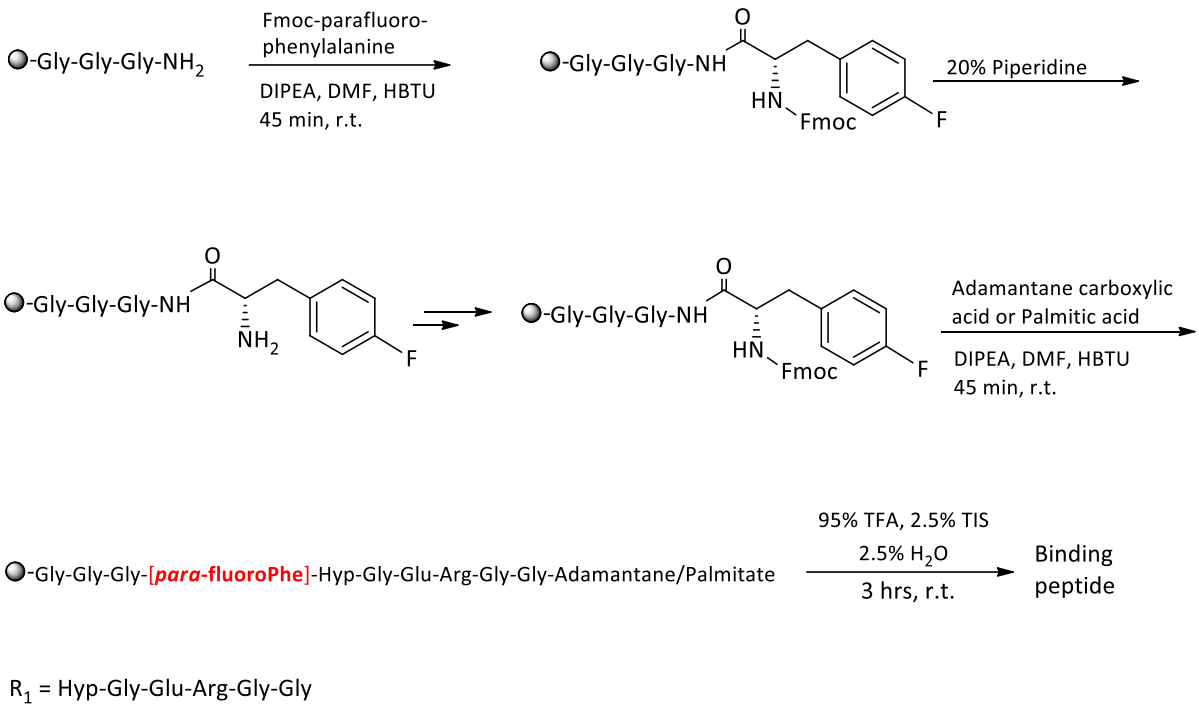

Scheme 5.3: Binding peptide synthetic route.

5.4 RESULTS AND DISCUSSION

The *retro-para*-fluorophenylalanine peptides were successfully synthesized (Table 5.1). The yields were low for the same reasons already outlined in chapter II. Low yield of palmitate peptide could also be attributed to the formation of the foam which indicates low solubility of the reactants.[4]

Table 5.1: Yields of *retro-para*-fluorophenylalanine peptides.

***Para*-fluorophenylalanine peptide**	**Calculated mass (g/mole)**	**Experimental (g/mole)**	**Yield (%)**	**Retention Time (min)**
Palmitate	1161.6194 $C_{53}H_{84}FN_{13}O_{15}$	581.8177 $[M + 2H]^{2+}$	23	15.84
Adamantane	1085.4942 $C_{48}H_{68}FN_{13}O_{15}$	543.7529 $[M + 2H]^{2+}$	28	13.6

When compared to the peptides reported in chapters II and III, *retro*-GG-G[*para*-fluoroPheF]OGER-GG-Palmitate and -Adamantane peptides are more hydrophobic due to the influence of the fluorine in the *para* position of phenylalanine. The peptides, *retro*-GG-

GFOGER-GG-Palmitate and -Adamantane eluted with 80 – 85% acetonitrile but fluorinated peptides eluted with 90 – 95% acetonitrile/water or MeOH (Table 5.1). Increase in hydrophobicity can be good for the peptides in terms of permeability through the hydrophobic cell membrane of the cells.[5] Benzene substituents that have lone pairs donate electrons into benzene ring and increase the electron density and hence its hydrophobicity.[6] Hence the fluorine can donate electrons into the π-system of the benzene and increase its electron density.

The replacement of a hydrogen atom with fluorine brings about a change in the biophysical and chemical properties of bioactives. Due to the fluorine's high electronegativity it can cause low polarizability and a strong covalent bond with carbon.[7,8] Fluorine changes the properties of peptides and influences aspects such as stability, therapeutic properties, peptide folding, peptide-protein interactions,[9–11] metabolic properties, membrane permeability and reactivity.[12–14] Fluorinated peptides's increased hydrophobicity enhances binding affinity.[6] Fluorinated aromatic amino acids destabilize the cation π interactions by altering electrostatics of the aromatic ring whereas their increased hydrophobicity enhances membrane insertion.[6]

For palmitate peptide, retention time that is already high due to non-polar palmitic acid chain is further enhanced by the fluorinated benzene ring causing the retention time to increase as shown in Figure 5.9. Kanao *et al.* also reported the higher retention of molecules due to halogen-π interactions with carbon materials.[15] Increase in the peptides' hydrophobicity due to halogenation has also been reported by Mardirossian *et al*. They also observed an improved stability of fluorinated phenylanine peptides.[16] Chromatograms of crude *retro*-GG-G[*para*-fluoro-Phe]OGER-GG-Palmitate and –Adamantane, shown in Figure 5.7, did not show many impurities.

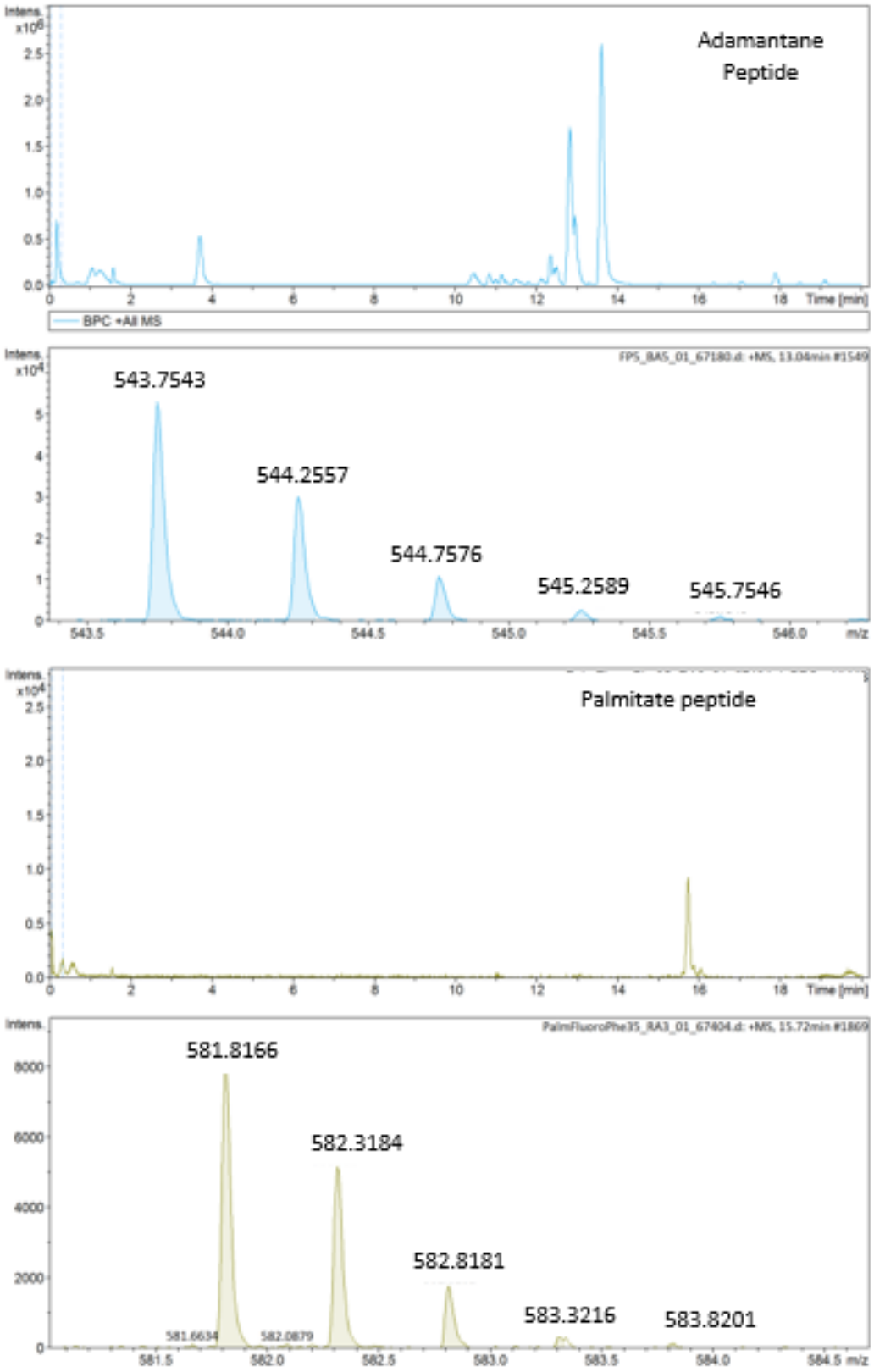

Figure 5.7: Mass spectrum of *retro*-GG-G[*para*-F-Phe]OGER-GG-Adamantane and -Palmitate peptides.

5.4.1 Peptide purification and characterization

The crude adamantane and palmitate derivatives were purified using an Agilent 1260 Infinity semi-preparative instrument on a C18 column. The run time, solvent system and gradient were deduced from the LCMS analysis. The flow rate was set to 15 mL/minute. An acetonitrile/water mobile phase solvent system was used. Each solvent had 0.1 % formic acid (v/v) used as an ion pairing agent. Adamantane peptides were dissolved in milli-Q water whereas palmitate peptide was dissolved in 70% DMSO/water and purified using a solvent gradient method of 5 – 95 % in 10 minutes.

Purification became a challenge when the peptides co-eluted with impurities. The method was changed since the desired peptides eluted with higher acetonitrile percentages. The acetonitrile was allowed to increase from 5 to 30% in 3 minutes and from 30 to 60% in 6 minutes to improve separation from impurities. Thereafter, acetonitrile concentration was increased to 95 % in 1 minute with a hope of a better separation, but the method was unsuccessful. Comparatively 5 – 95 % in 14 minutes was by far the better separation method.

The synthesized peptides will be tested in the future for wound healing activity using the same biological assays described in chapter VII. Computational studies will also be conducted to determine further modifications that can be applied to improve binding. Furthermore, understanding of the distribution of the electron cloud on the aromatic ring is important for binding. Other derivatives such as Fmoc-*meta* fluoro-phenylalanine will also be incorporated in the future.

5.5 CONCLUSION

The fluorinated phenylalanine amino acid was successfully synthesized in satisfactory yield. The *retro*-GG-G[*para*-fluoro-Phe]OGER-GG peptides conjugated to lipophilic molecules were successfully synthesized also. The peptides were more hydrophobic than the original sequences and will be tested for wound healing activity in the future.

5.6 REFERENCES

(1) Discovery Studio. Client 16.1.0. San Diego, CA, USA.

(2) Awad, L. F.; Ayoup, M. S. Fluorinated Phenylalanines: Synthesis and Pharmaceutical Applications. *Beilstein J Org Chem* **2020**, *16*, 1022–1050.

(3) Siljander, P. R.-M.; Hamaia, S.; Peachey, A. R.; Slatter, D. A.; Smethurst, P. A.; Ouwehand, W. H.; Knight, C. G.; Farndale, R. W. Integrin Activation State Determines Selectivity for Novel Recognition Sites in Fibrillar Collagens. *J Biol Chem* **2004**, *279* (46), 47763–47772.

(4) Langevin, D. Coalescence in Foams and Emulsions: Similarities and Differences. *Curr. Opin. Colloid Interface Sci* **2019**, *44*, 23–31.

(5) Kabelka, I.; Vácha, R. Optimal Hydrophobicity and Reorientation of Amphiphilic Peptides Translocating through Membrane. *Biophys J* **2018**, *115* (6), 1045–1054.

(6) He, T.; Gershenson, A.; Eyles, S. J.; Lee, Y. J.; Liu, W. R.; Wang, J.; Gao, J.; Roberts, M. F. Fluorinated Aromatic Amino Acids Distinguish Cation-π Interactions from Membrane Insertion. *J Biol Chem* **2015**, *290* (31), 19334–19342.

(7) Merkel, L.; Budisa, N. Organic Fluorine as a Polypeptide Building Element: In Vivo Expression of Fluorinated Peptides, Proteins and Proteomes. *Org Biomol Chem* **2012**, *10* (36), 7241–7261. https://doi.org/10.1039/c2ob06922a.

(8) Purser, S.; Moore, P. R.; Swallow, S.; Gouverneur, V. Fluorine in Medicinal Chemistry. *Chem Soc Rev* **2008**, *37* (2), 320–330.

(9) Ye, S.; Berger, A. A.; Petzold, D.; Reimann, O.; Matt, B.; Koksch, B. Chemical Aminoacylation of TRNAs with Fluorinated Amino Acids for in Vitro Protein Mutagenesis. *Beilstein J. Org. Chem.* **2010**, *6*.

(10) Tang, Y.; Ghirlanda, G.; Petka, W. A.; Nakajima, T.; DeGrado, W. F.; Tirrell, D. A. Fluorinated Coiled-Coil Proteins Prepared in Vivo Display Enhanced Thermal and Chemical Stability. *Angew Chem Int Ed* **2001**, *40* (8), 1494–1496.

(11) Bilgiçer, B.; Fichera, A.; Kumar, K. A Coiled Coil with a Fluorous Core. *J. Am. Chem. Soc.* **2001***, 123* (19)*,* 4393– 4399.

(12) Bulfield, D.; Huber, S. M. Synthesis of Polyflourinated Biphenyls; Pushing the Boundaries of Suzuki–Miyaura Cross Coupling with Electron-Poor Substrates. *J. Org. Chem.* **2017**, *82* (24), 13188–13203.

(13) Hoffmann, W.; Langenhan, J.; Huhmann, S.; Moschner, J.; Chang, R.; Accorsi, M.; Seo, J.; Rademann, J.; Meijer, G.; Koksch, B.; Bowers, M. T.; von Helden, G.; Pagel, K. An Intrinsic Hydrophobicity Scale for Amino Acids and Its Application to Fluorinated Compounds. *Angew Chem Int Ed* **2019**, *58* (24), 8216–8220.

(14) Lee, K. H.; Lee, H. Y.; Slutsky, M. M.; Anderson, J. T.; Marsh, E. N. G. Fluorous Effect in Proteins: De Novo Design and Characterization of a Four-α-Helix Bundle Protein Containing Hexafluoroleucine. *Biochemistry* **2004**, *43* (51), 16277–16284.

(15) Kanao, E.; Morinaga, T.; Kubo, T.; Naito, T.; Matsumoto, T.; Sano, T.; Maki, H.; Yan, M.; Otsuka, K. Separation of Halogenated Benzenes Enabled by Investigation of Halogen-π Interactions with Carbon Materials. *Chem Sci* **2020**, *11* (2), 409–418.

(16) Mario Mardirossian, M.; Rubini, M.; Adamo, F. A. M.; Scocchi, M.; Saviano, M.; Tossi, A.; Gennaro, R.; Caporale, A. Natural and Synthetic Halogenated Amino Acids-Structural and Bioactive Features in Antimicrobial Peptides and Peptidomimetics. *Molecules* **2021**, *26* (23), 7401.

CHAPTER VI

SYNTHESIS OF PEPTIDOMIMETICS WITH IMPROVED PROTEOLYTIC STABILITY

The chapter describes the synthesis of peptides designed to withstand protease degradation. The peptides are designed with structural modifications that are unfavourable to protease binding. One of the ways this can be achieved is by synthesizing peptides with the opposite stereochemistry to that which the protease is specific to by replacing L-amino acids with D-amino acids. In an alternative approach, resistance to protease degradation can be achieved by alteration of the peptide bond by introducing bulky groups on the backbone nitrogen to sterically hinder the protease from attaching to the peptide to catalyse the hydrolysis of the peptide bond. The synthesized peptides aimed at achieving protease stability are divided into four classes named (1) peptoids, (2) reference peptoids, (3) D-peptides and (4) *N*-methylated peptides. These peptidomimetics have the following main motifs: a dipeptide GG, a *retro*-GFOGER sequence and lipophilic molecules. The function of these motifs and their binding interactions to the integrin are described in detail in Chapters I and II. The GG dipeptide functions as a spacer and reduces steric hindrance around the *retro*-GFOGER sequence which is responsible for binding to the MIDAS region of the integrin. The palmitic and adamantane are lipophilic molecules used to increase the membrane permeability of the peptidomimetics.

6.1 RESULTS AND DISCUSSION

6.1.1 Peptoids

Collagen mimetic peptoids were designed in such a way that they would elicit the properties of the synthesized collagen mimetic peptides described in Chapters II and III but with increased resistance towards protease degradation and different structural properties. To achieve the latter, the side chains of the amino acids were ‘transferred’ onto the amide nitrogen from the *alpha* carbon (Figure 6.1). On the nitrogen atom, the side chains would sterically hinder the protease enzyme from accessing the peptide bond, and since the side chain is exactly the same as the amino acid side chain it can still bind to its original target. Hence, the side chain plays a dual role. The envisaged peptoid structure is shown in Figure 6.1.

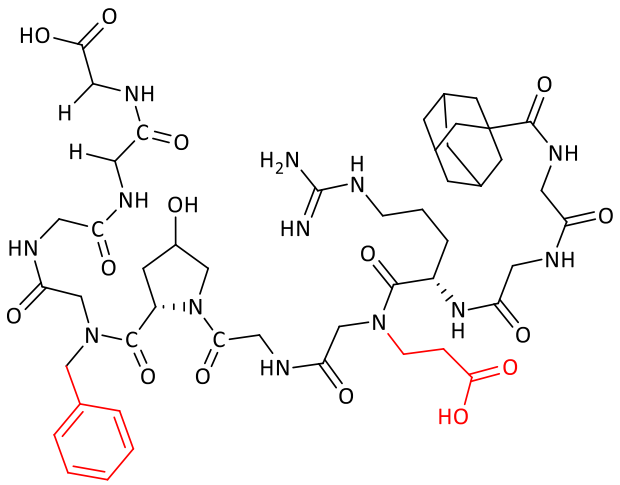

Figure 6.1: *retro*-GG-GFOGER-GG-Adamantane peptoid.

The side chains mimicking glutamic acid (negatively charged) and phenylalanine (aromatic) can also contribute to the formation of a stable conformation according to Fowler *et al*.[1] The aromatic groups on the side chains cause charge-charge repulsion with backbone carbonyls and assist in peptoid folding. This folding can be advantageous since it gives the peptoid a well-defined secondary structure which can be lacking in most peptoids. Peptoids are highly flexible because of the lack of hydrogen bonding and the tertiary nature of the amide bonds that allows them to isomerize between *trans* and *cis* conformations far more readily than secondary amides in peptides and this can result in weak protein-peptoid interactions.[1,2]

Another aspect of these designed peptoids that is important to investigate is peptoid-protein interactions. The information about the behaviour of these peptoids towards the integrin will provide valuable information about the peptoid-protein complexes. In this study, only the peptides were biologically screened (Chapter VII), due to time constraints and the peptoids will be screened in the future.

Literature on peptoid-protein-peptide interactions indicates a need for a more defined backbone that can attain stable structural conformations independent of the main side chains which are needed for the activity. Morimoto *et al.* designed an N– substituted alanine (oligo–NSA) backbone to address the conformational needs of peptoids for better protein binding.[2] They incorporated methyl groups to introduce repulsion and constrain to the normal *N*–substituted glycine (oligo–NSG) peptoid moiety, making oligo-*N*-substituted alanine (oligo-

NSA) backbones which have been demonstrated to be conformationally constrained as shown in Figure 6.2.

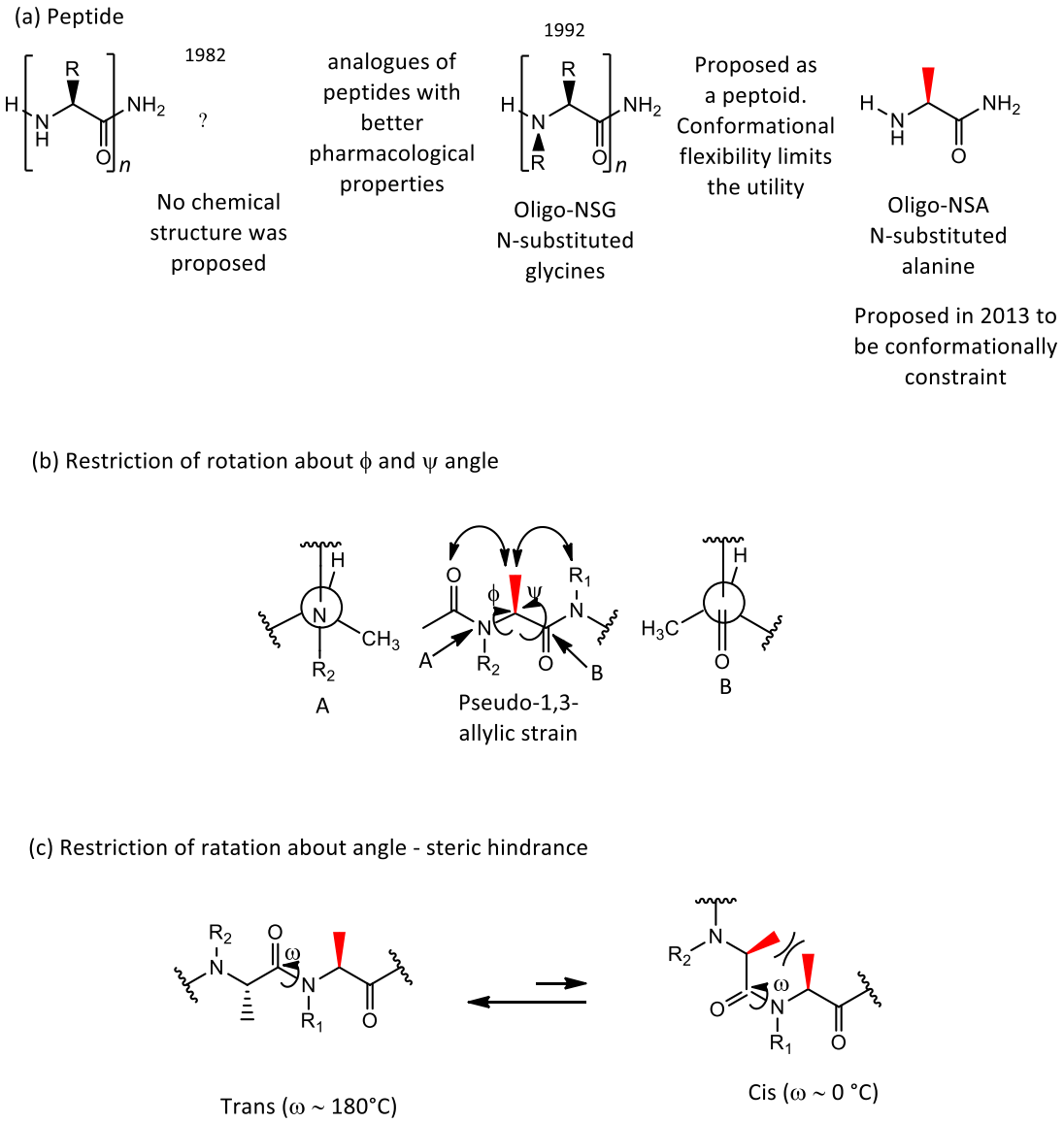

Figure 6.2: Structural differences between the normal *N*– substituted glycine (oligo–NSG) peptoid and oligo-*N*-substituted alanine (oligo-NSA) backbones.[2]

In order to investigate the stability of the backbone of the designed peptoids, reference peptoid analogues were synthesized in which the polar side chains were replaced with methyl groups. The GG dipeptide, lipophilic moiety, the length of the chain and hydrophobic side chains were all kept constant and only the hydrogen bond forming side chains were replaced to investigate the ability of the backbone to attain a stable conformation through

hydrophobic interactions. The synthesis of the reference peptoids is described in section 6.1.2.

6.1.1.1 Synthesis of peptoids

The submonomer method was utilized to synthesize the peptoid oligomers. The aim was to elongate the main chain by acylation with bromoacetic acid followed by the introduction of the side chains via a primary amine.

To the already synthesized peptide, *retro*-GG-G-NH-Fmoc, on a solid resin support was added 20% piperidine solution in DMF (10 mL). The peptide -GG-G-NH-Fmoc was synthesized according to the general procedure C described in the experimental chapter IX section 9.4.3. The resulting mixture was stirred by bubbling nitrogen for approximately 5 minutes (twice) to remove the protecting group. The resin was then washed with DMF (3 x 5 mL) followed by DCM (3 x 5 mL) to remove excess reagents. A mixture of bromoacetic acid (0.2 g, 0.2 M), DIPEA (1.26 mL, 1 M) and N, N'-Diisopropylcarbodiimide (DIC) (0.21 mL, 0.11 M) was added to the deprotected resin peptide, and the reaction was gently mixed by bubbling nitrogen gas into the reaction for 1 hour.

The DIPEA deprotonates the bromoacetic acid which, once deprotonated, reacts with DIC to enhance the electrophilicity of the carbon carbonyl. The resin was then washed with DMF (3 x 5 mL) followed by DCM (3 x 5 mL) to remove excess reagents. Benzylamine (0.16 mL, 0.12 M) in DMF (12 mL) was added and the resin and the reaction were stirred by bubbling nitrogen for 45 minutes. After washing as before, hydroxyproline was coupled to the peptoid. Due to the commercial unavailability of the primary amine mimic of hydroxyproline, the natural amino acid was coupled. Also, the side chain of glycine is made up of only hydrogens and therefore the amino acid was incorporated into the peptide sequence as it is. After deprotection of the glycine Fmoc protecting group, bromoacetic acids was added as described above and then *tert*-butyl 4-amino butanoate (0.38 g, 0.2 M) was coupled to the peptide-peptoid hybrid sequence. Arginine, glycine and glycine (R-GG) and adamantane were then added to the sequence using the procedures outlined in Chapter IX section 9.4.3. The schematic representation of the synthesis of peptoids is shown in Scheme 6.1.

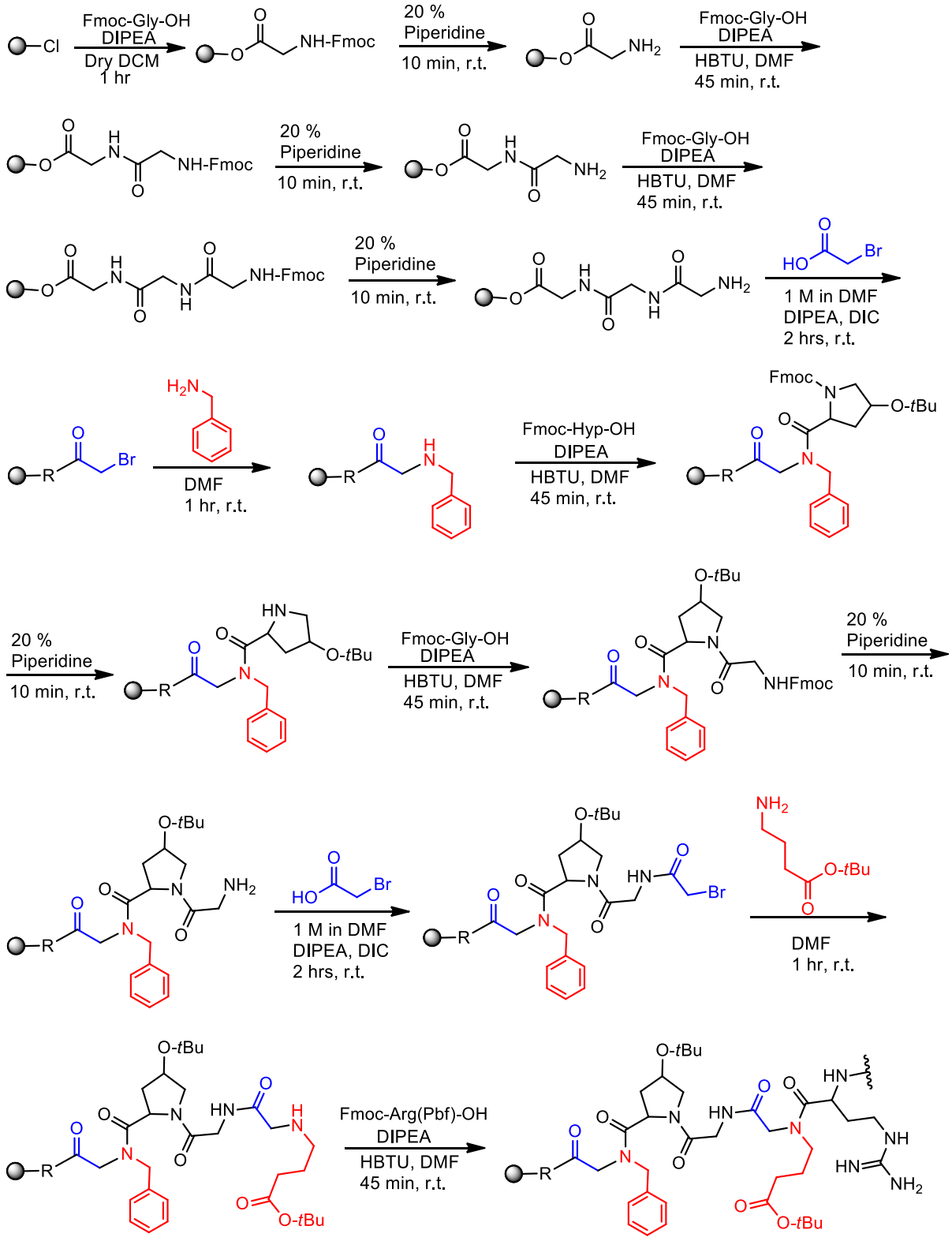

R = Gly-Gly-Gly-

Scheme 6.1: The general synthetic procedure for the synthesis of peptide-peptoid derivatives.

Given that the growing N-terminus of a peptoid chain is a secondary amine, and that it is more hindered, we anticipated lower yields than those of the collagen mimetic peptides. This is

because, despite their higher nucleophilicity, secondary amines have slower coupling reaction times when compared to primary amines because of steric hindrance.

Table 6.1: Yields of synthesized peptoids.

Peptide-peptoid	Calculated mass (g/mole)	Experimental (g/mole)	Yield (%)	Retention Time (min)
retro-GG-G*p*FOG*p*ER-GG-Palmitate (Peptoid)	1143.6367 $C_{53}H_{85}N_{13}O_{15}$	1144.6514 $[M + H]^+$	13	Peak 1 = 8.3 Peak 2 = 8.5
retro-GG-G*p*FOG*p*ER-GG-Adamantane (Peptoid)	1067.5115 $C_{48}H_{69}N_{13}O_{15}$	1068.5189 $[M + H]^+$	17	Peak 1 = 3.5 Peak 2 = 3.6

p = peptoid moiety

The peptoids were purified using a gradient elution method. The procedure is outlined in experimental Chapter IX section 9.4.13.

6.1.1.2 Discussion

The observed low yields were attributed to minor yield losses from multiple reaction steps that lead to the final synthesis of the peptide-peptoid sequences.[3] The losses are compounded over multiple steps, resulting in low yields. In peptoids synthesis, one monomer is coupled over two steps involving acylation and displacement. Even though acylation and displacement reactions on their own are robust and high yielding the small losses accumulate during synthesis.[3] This could be one of the reasons why the yields of peptoids are lower than that of the corresponding peptides.

The high steric hindrance of chiral amines often contributes to their slow reactivity. This seems to suggest that reaction times should be increased during acylation and displacement.[4]

The challenge of low yields in peptoid synthesis remains unresolved even after researchers have investigated possible ways of improving the synthesis. In a study by Zuckermann *et al.*,[3] three haloacetic acids were tested, and bromoacetic (utilized in the current study) gave the highest yield. Performing acylation and displacement at elevated temperatures has also been tested but improvement in yields has proven an elusive goal so far.

Addition of palmitic acid in most reactions resulted in the formation of a foam which indicate poor solubility. The low yield of palmitate peptoids may be further exacerbated by the incomplete coupling of palmitic acid.

6.1.2 Reference peptoids

Reference peptoids were designed to investigate the stability of the backbone as a result of hydrophobic interactions. The motivation for the design is outlined above in section 6.1.1. In order to achieve this goal, all polar hydrogen bond forming side chains were replaced with a methyl group. The envisaged structure is shown in Figure 6.3 below.

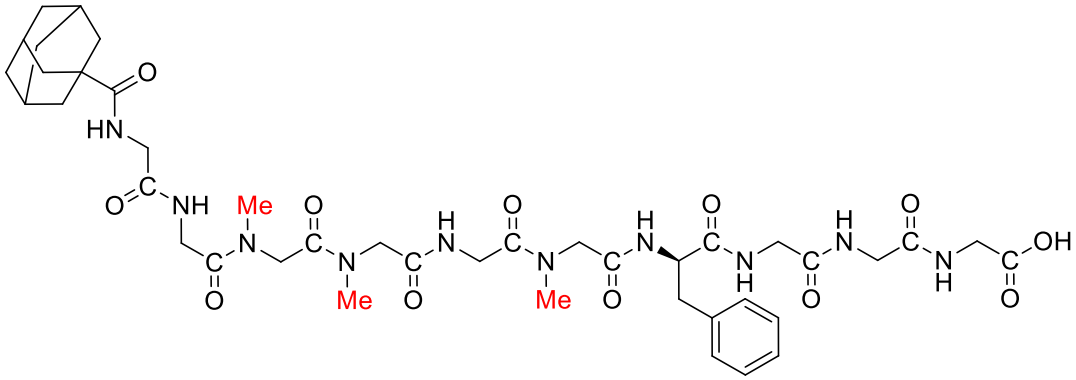

Figure 6.3: Structure of the *retro*-reference peptoid.

6.1.2.1 Synthesis

Bromoacetic acid (0.2 g, 0.2 M) was dissolved in DMF (10.74 mL). The base, DIPEA (1.26 mL, 1 M) was added to the solution and they were stirred together for a few minutes before the addition of *N*, *N*'-Diisopropylcarbodiimide (DIC) (0.21 mL, 0.11 M). The mixture was then added to an already synthesized –GG-GFNH$_2$- (synthesized according to the general procedure C, Chapter IX) on a solid resin support. The resultant reaction mixture was gently mixed by bubbling nitrogen gas into the reaction for 1 hour. The solvent was removed and the resin was washed with DMF (3 x 5 mL) and DCM (3 x 5 mL) to remove excess reagents. In the second step, anhydrous methylamine (0.068 mL, 0.12 M) in dimethyl sulfoxide (DMSO) (12 mL) was added and the mixture and stirred by bubbling nitrogen for 45 minutes. The solvent was drained off and the resin was washed with DMF (3 x 5 mL) followed by DCM (3 x 5 mL). The same procedure was performed for the rest of non-glycine amino acids.

6.1.2.2 Results and Discussion

The introduction of multiple methyl groups led to an increase in hydrophobicity of the peptoids as evidenced by the high retention times. Thus, reference peptoids with increased hydrophobicity were successfully synthesized, albeit, with low yields.

Table 6.2: Yields of synthesized reference peptoids.

Peptide	Calculated mass (g/mole)	Experimental (g/mole)	Yield (%)	Retention Time (min)
retro-GG-GF*p*AG*p*A*p*A-GG-Palmitate (Reference Peptoids)	958.5488 $C_{46}H_{74}N_{10}O_{12}$	959.5500 $[M + H]^+$	16	Peak 1 = 19.2 Peak 2 = 19.3 Peak 3 = 19.4
retro-GG-GF*p*AG*p*A*p*A-GG-Adamantane (Reference Peptoids)	882.4236 $C_{41}H_{58}N_{10}O_{12}$	883.3631 $[M + H]^+$	8	Peak 1 = 16.2 Peak 2 = 16.3

p = peptoid moiety

The reference peptoids were purified using a gradient elution method. The procedure is outlined in experimental Chapter IX section 9.4.13.

6.1.2.3 Discussion

The mass spectra of the reference peptoids showed multiple peaks with the same desired mass and this could be indicative of the presence of isomers. The isomers could result from tertiary amides which form both *cis* and *trans* isomers or conformational isomers. Due to time constraints, the NMR and CD measurements of the peptoids will be obtained in the future to determine the 3D structural conformations formed and the effect of increased hydrophobicity on the conformations. However, judging from the increase in the number of conformations we can conclude that the removed hydrogen bonding side chains of hydroxyproline, arginine and glutamic acid play a major role in the formation of stable conformations of the designed peptoids. Hence, they are necessary not just for binding to the integrin but also for maintaining peptoid folding.

6.1.3 D-Peptides

Proteases specifically hydrolyse peptide bonds of peptides that are made up of L-amino acids because of their ability to optimally bind to the structural conformations formed by L-peptides. Having a collagen mimetic peptide (CMP) with a different stereochemistry from that of L-peptides means that the CMP's proteolytic enzyme stability would be increased. An example of the synthesized D-peptide sequence is shown in Figure 6.4.

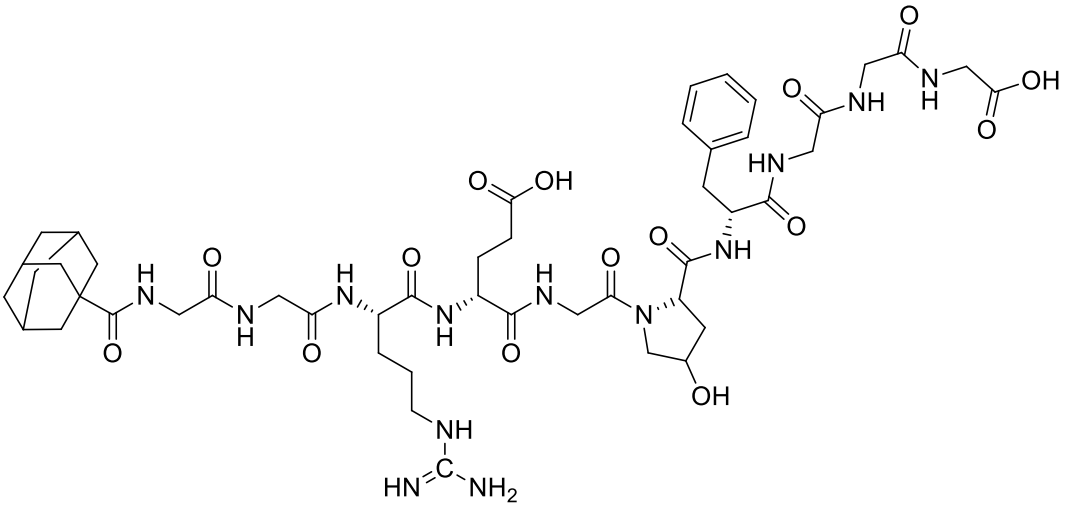

Figure 6.4: *retro*-GG-G$_D$FOG$_D$ER-GG-Adamantane D-Peptide.

6.1.3.1 Synthesis

D-Peptides were synthesized according to the general procedure C for the synthesis of peptides which is outlined in the experimental chapter IX section 9.4.3 and the general scheme shown in Scheme 6.2 below. Glycine, due to its lack of chirality was used as it is. Only phenylalanine and glutamic acid D-amino acids were employed. Hydroxyproline and arginine D-amino acids were not commercially available.

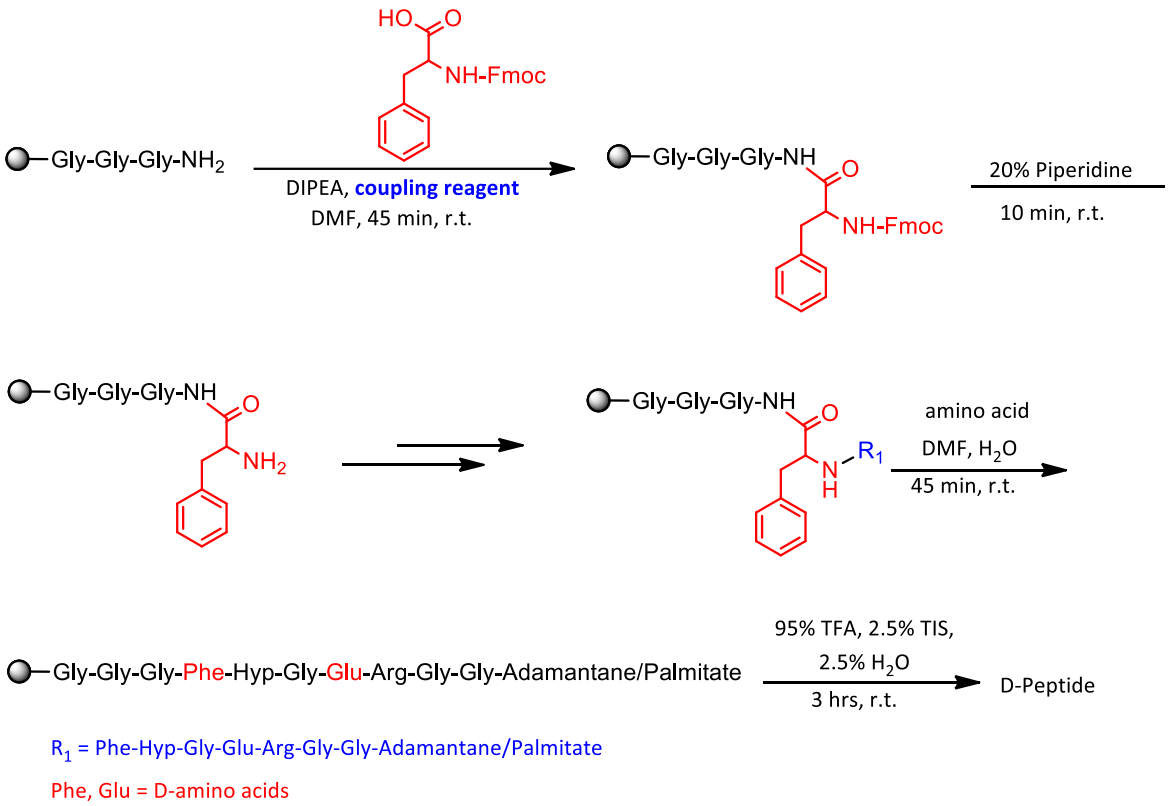

Scheme 6.2: General scheme for the synthesis of *retro*-D-peptides. Coupling reagent = HBTU or HATU.

A noticeable improvement of the yield was observed with D-peptides. The yield increased appreciably as compared to peptoids and reference peptoids. Again, a noticeable decrease in hydrophobicity of the peptides was made as shown in Table 6.3.

Table 6.3: Yields of synthesized D-Peptides.

D-Peptide	Calculated mass (g/mole)	Experimental (g/mole)	Yield (%)	Retention Time (min)
retro-GG-G$_D$FOG$_D$ER-GG-Palmitate (D-Peptide)	1143.6367 $C_{53}H_{85}N_{13}O_{15}$	1144.6556 $[M + H]^+$	33	Peak 1 = 8.2 Peak 2 = 8.3 Peak 3 = 8.5
retro-GG-G$_D$FOG$_D$ER-GG-Adamantane (D-Peptide)	1067.5036 $C_{48}H_{69}N_{13}O15$	1068.5074 $[M + H]^+$	29	Peak 1 = 5.0 Peak 2 = 5.2

$_D$ = *D-amino acids*

6.1.3.2 Discussion

The nucleophilic center is not as sterically hindered as in peptoids hence the yields of D-peptides, relative to reference peptoids and the peptoids, are higher. The amine group of the last amino acid on the peptide anchored on a support is relatively free. Acylation reaction takes place at a higher rate than in peptoids. There is also a reduction in number of reactions per monomer. The absence of the displacement reaction contributed immensely to the improvement of the yields.

An observation was made during the synthesis of D-peptides regarding the difficult/slow coupling between phenylalanine and hydroxyproline as detected by Ninhydrin test. This observation could be due to steric hindrance, aggregation or stereochemistry of the peptide.[5] Hydroxyproline has a cage structure which could sterically hinder amino acid residues from accessing the carbonyl carbon. Aggregation can cause incomplete coupling between peptides.[6,7] As the peptide is elongated, it can form secondary structures that can cause the chain to aggregate resulting in lower reaction rates.[8,9]

Ninhydrin test was employed to monitor the reaction of D-peptides. According to the test, double coupling was necessary for the complete coupling of phenylalanine, hydroxyproline, glutamic acid and arginine. The method for the purification of D-peptides is outlined in Chapter IX section 9.4.13.

6.1.4 *N*-Methylated peptides

Synthesis of *N*-methylated peptides requires the synthesis of Fmoc-*N*-methylated amino acids from the oxazolidinone intermediate.

6.1.4.1 Synthesis of Fmoc-Phenylalanine and Arginine oxazolidinone

Synthesis of phenylalanine and arginine oxazolidinone was achieved according to the reaction scheme shown below (Scheme 6.3).

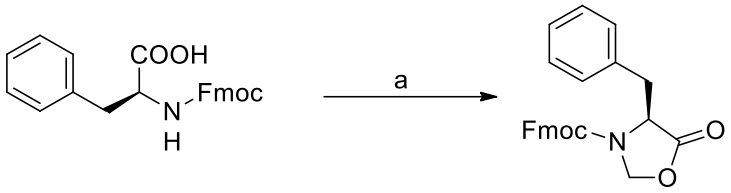

Scheme 6.3: Synthesis of Fmoc-Phe-OH
Reaction reagents and conditions: (a) *p*TsOH (0.006 M), $(CH_2O)n$ (0.3 M), toluene, reflux, 15hr.

The Fmoc amino acid (1.94 g, 0.05 M), paraformaldehyde (1 g, 0.3 M) and *p*-toluenesulphonic acid (0.1 g, 0.006 M) were suspended in toluene (100 mL). The mixture was refluxed in a Dean-Stark setup until no more starting material could be detected by TLC (97.5:2:0.2-$CHCl_3$: MeOH: AcOH). The solution was cooled, washed with saturated $NaHCO_3$ and dried over anhydrous $MgSO_4$. Concentration in vacuo gave a crude product which solidified upon standing. The crude mass spectrum of phenylalanine oxazolidinone is shown in Figure 6.5.

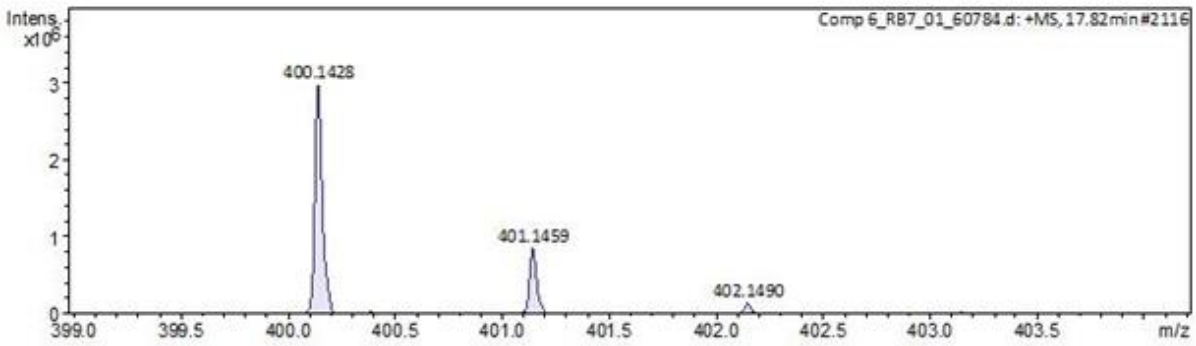

Figure 6.5: Mass spectrum of phenylalanine oxazolidinone.

The observed high retention times could be due to newly introduced methylene group. The crude product was washed with sodium carbonate solution and distilled off *in vacuo* to give a white solid product (phenylalanine oxazolidinone, 85%) and brownish solid (arginine oxazolidinone, 30%) as shown in Table 6.4.

Table 6.4: Yields of oxazolidinone amino acids.

Oxazolidinone	Calculated Mass (g/mol)	Experimental Mass (g/mol)	Yield (%)	Retention time (min)
Phenylalanine	399.1471 ($C_{25}H_{21}NO_4$)	400.1428 $[M + H]^+$	85	17.82
Arginine	660.2618 ($C_{35}H_{40}N_4O_7S$)	663.8386 $[M + 3H]^+$	30	18.58

In the proposed mechanism of formation of the Fmoc amino acids, paraformaldehyde is protonated by *para*-toluenesulfonic acid (*p*TsOH) as the catalyst. Protonation renders the paraformaldehyde carbonyl carbon more electrophilic. The latter is then attacked by nucleophilic oxygen atom of the amino acid hydroxyl group of the amino acid to form an intermediate shown in Scheme 6.4. Abstraction of a proton by the hydroxyl group, resulting in formation of water, makes it a good leaving group. The nucleophilic amine group reacts with electrophilic carbon causing water to leave as a leaving group. This cyclization, accompanied by release of water molecule leads to formation of an oxazolidinone as shown in Scheme 6.4.

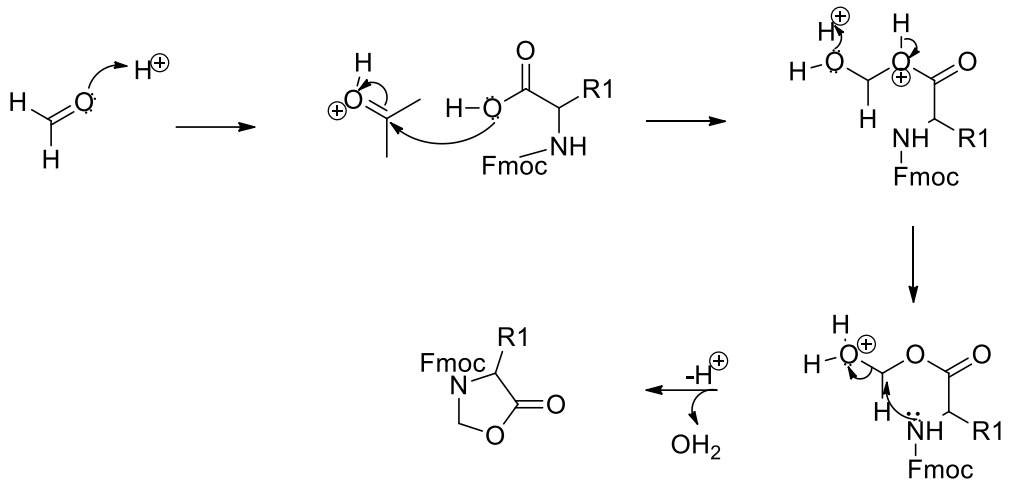

Scheme 6.4: Proposed mechanism for cyclisation of Fmoc-amino acid.

Acylation reaction of arginine amino acid posed a problem due to basicity of its guanidine group. The group presents problems for the oxazolidinone chemistry. Amino acids with reactive side chains such as hydroxyl, sulfur or amino groups do not react to form oxazolidinones nor do they undergo reductive cleavage.[10] This is the case with arginine despite the 2,2,4,6,7-pentamethyl-2,3-dihydrobenzofuran-5-sulfonyl (Pbf) protection. Guanidine has three basic amine groups and only one is protected leaving the other two available to react as nucleophiles. In reaction with formaldehyde, any of the four available amino groups can react with formaldehyde and form undesired products as shown below.

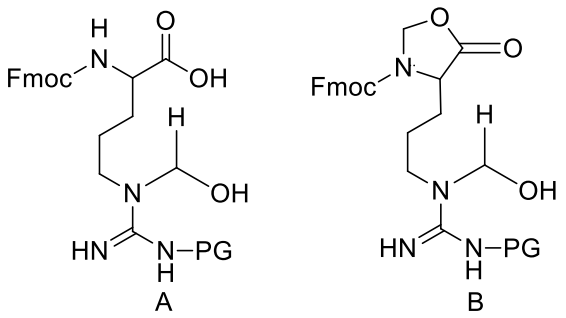

Figure 6.6: Side products of acylation reaction of arginine.

The spectrum of arginine oxazolidinone is in the experimental chapter IX, Figure 9.59.

6.1.4.2 Synthesis of N-methylated phenylalanine and arginine from the oxazolidinone

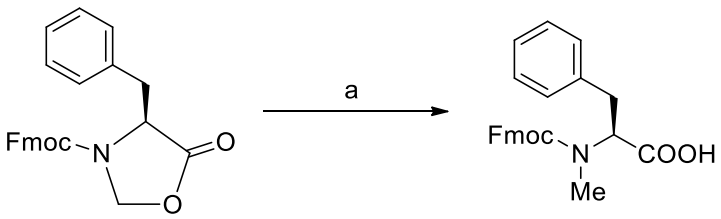

Scheme 6.5: Reductive amination of 5-oxazolidinone.
Reaction reagents and conditions: a = Et_3SiH, $AlCl_3$, CH_2Cl_2, 4 hr, r.t.

To a solution of Fmoc- protected oxazolidinone, (1 equiv.) and anhydrous $AlCl_3$ (2 equiv.) in dry DCM (20 mL/1 mmol oxazolidinone) was added triethylsiliane (TES) (2 equiv.). The reaction was stirred at ambient temperature until TLC (1:3 ethyl acetate/hexane) showed the absence of starting material. An additional amount of DCM (20 mL) was added, and the organic phase was washed with 1 M HCl. The organic phase was dried over anhydrous magnesium sulphate and concentrated *in vacuo*. The crude product was purified via column chromatography on silica gel with (1:19, MeOH: DCM).

The reduction of oxazolidinone with triethylsilane and a Lewis acid, aluminium trichloride facilitated ring opening to give the *N*-methylated Fmoc-amino acid. Thus, *N*-methylated amino acids, phenylalanine and arginine were successfully synthesized. *N*-methylated phenylalanine mass spectrum is shown in Figure 6.7.

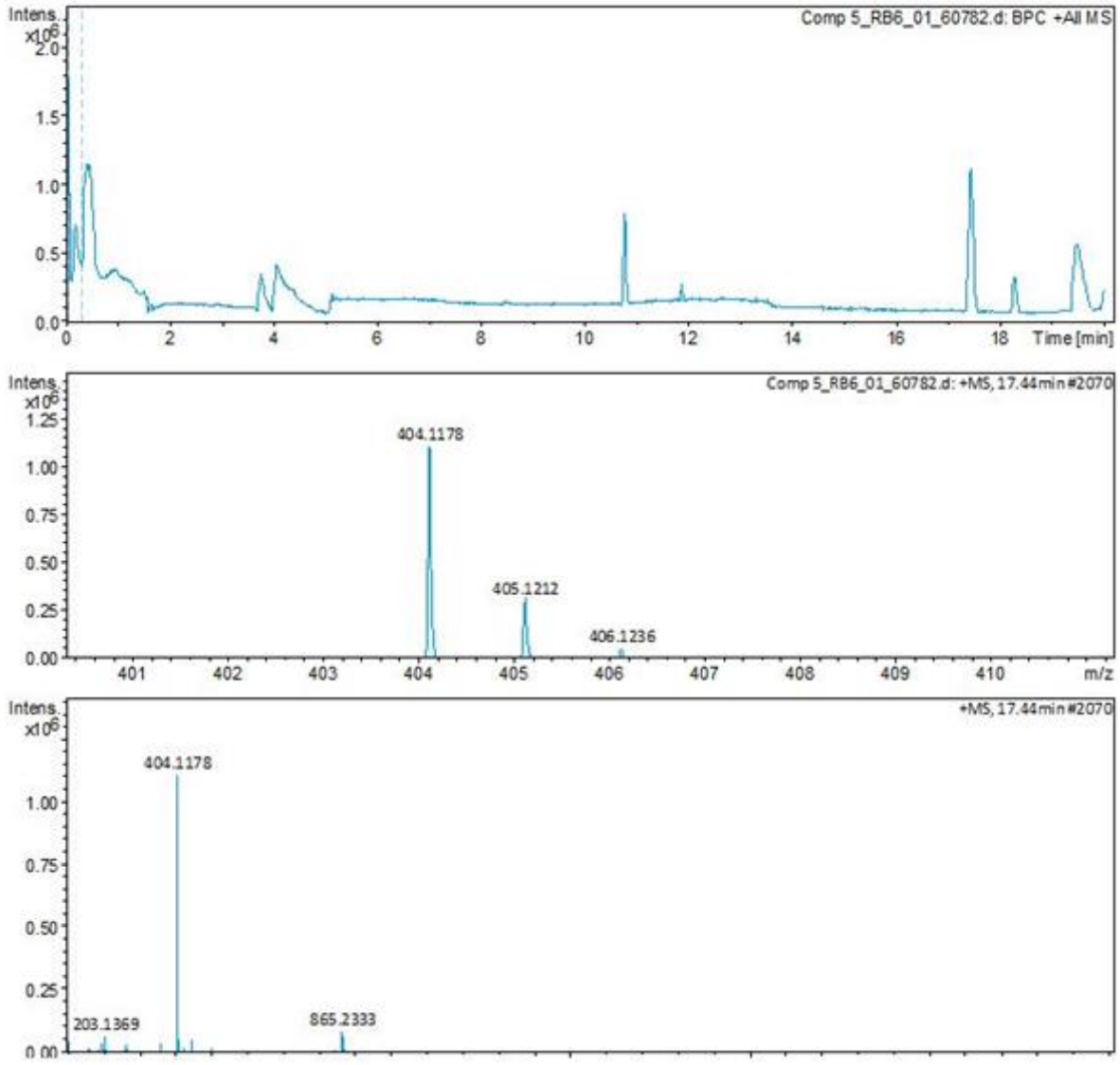

Figure 6.7: Mass spectrum of crude *N*-methylated Fmoc-phenylalanine.

N-Methylated phenylalanine and arginine were protonated three times as indicated in Table 6.5. Triple protonation on phenylalanine could be due to oxygen lone pairs on Fmoc protecting group and the backbone amine group. Triple protonation on arginine is already explained above. The yields of the two *N*-methylated amino acids were respectively 83 and 21%.

Table 6.5: Yields of *N*-methylated amino acids.

N-methylated amino acid	Calaculated Mass (g/mol)	Experimental Mass (g/mol)	Yield (%)	Retention time (min)
Phenylalanine	401.1627 ($C_{25}H_{23}NO_4$)	404.1178 $[M + 3H]^+$	83	17.44
Arginine	662.2774 ($C_{35}H_{42}N_4O_7S$)	665.2470 $[M + 3H]^+$	21	17.94

The retention times are almost the same as for Fmoc-oxazolidinone amino acids. The synthesized *N*-methylated phenylalanine and arginine amino acids were then incorporated into the adamantane, and palmitate *N*-methylated peptides as described in section 6.1.4.3.

6.1.4.3 Synthesis of N-methylated peptide

Employment of the methyl group was influenced by the need to sterically hinder the protease from attaching to the peptide to hydrolyze the peptide bond. The envisaged structures of the peptides are shown in Figures 6.8 and 6.9.

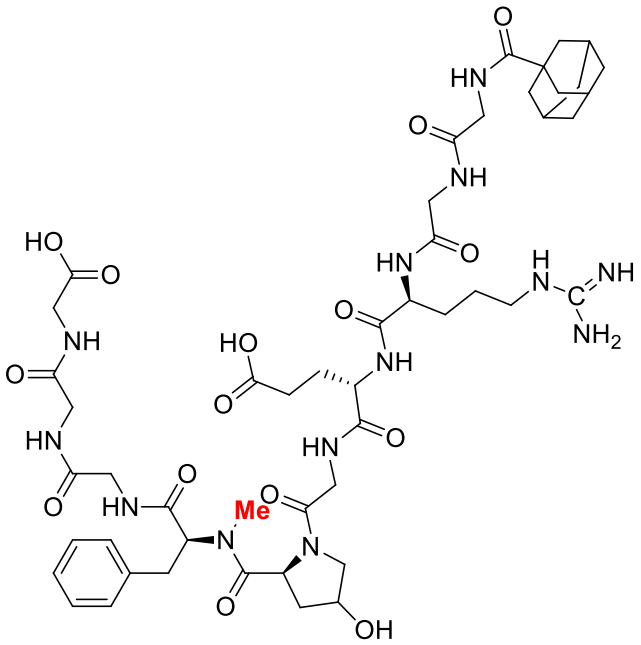

Figure 6.8: Singly substituted *retro*-*N*-methylated peptide.

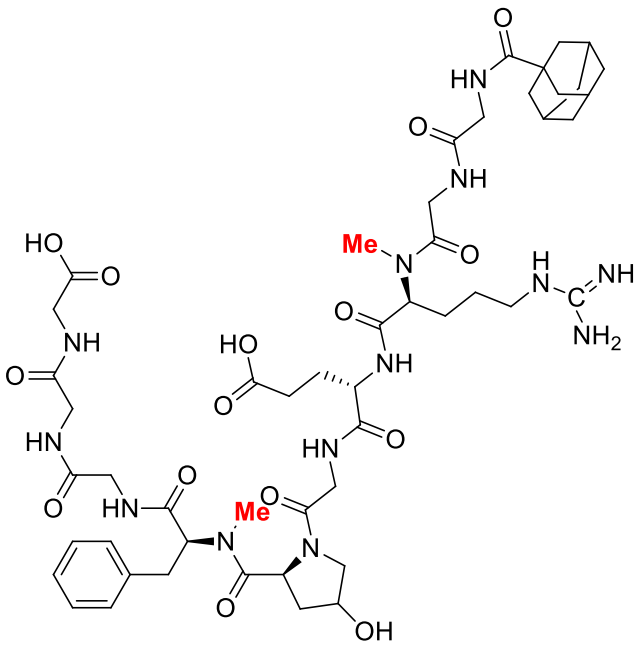

Figure 6.9: Doubly substituted *retro*-*N*-methylated adamantane peptide.

Synthesis

N-Methylated peptides were synthesized according to the general procedure C for the synthesis of peptides which is outlined in the experimental chapter IX section 9.4.3.

To the already synthesized peptide -GG-G-NH-Fmoc on a solid support was added 20% piperidine solution (10 mL). The reaction mixture was bubbled with nitrogen twice for 5 minutes. The resin was then washed with DMF (3 x 5 mL) followed by DCM (3 x 5 mL) to remove excess reagents. A mixture of *N*-methylated phenylalanine (0.578 g, 0.12 M) and DIPEA (1.26 mL, 1 M) in DMF (10.74 mL) was first mixed and stirred in a shaker for a few minutes before the addition of coupling reagent, HBTU (0.519 g, 0.11 M). The resultant mixture was added to the resin and stirred by bubbling nitrogen for 45 minutes. Towards the end of the 45 minutes, a few beads were taken from the reaction flask and tested for completion of reaction using a Ninhydrin Test. According to the test, the reaction was complete. The solvent was removed and the now coupled *N*-methylated phenylalanine was deprotected by adding 10 mL of 20% piperidine. The reaction mixture was bubbled with nitrogen twice for 5 minutes. The resin was washed with DMF (3 x 5 mL) followed by DCM (3 x 5 mL) and the rest of the amino acids in the sequence were coupled.

Results and Discussion

The results of the synthesis of singly substituted *N*-methylated peptide are shown in Table 6.6. The yields of the synthesized peptides are low, and the retention times are reflective of the increased hydrophobicity of the peptides.

Table 6.6: Yields of synthesis of singly substituted *retro*-*N*-methylated peptides.

***N*-methylated Peptide**	**Calculated mass (g/mole)**	**Experimental (g/mole)**	**Yield (%)**	**Retention Time (min)**
retro-GG-G*n*FOGER-GG-Palmitate	1157.6445 $C_{54}H_{87}N_{13}O_{15}$	1158.6289 $[M + H]^+$	12	Peak 1 = 15.8 Peak 2 = 15.9
retro-GG-G*n*FOGER-GG-Adamantane	1081.5193 $C_{49}H_{71}N_{13}O_{15}$	1082.5158 $[M + H]^+$	9	Peak 1 = 12.5 Peak 2 = 12.4 Peak 3 = 12.2

n = N-methylated amino acid

It was observed that the reaction yields were mainly affected by the coupling reagent. In the first attempt of synthesis of singly substituted *N*-methylated peptides, the yields were lower than the ones in Table 6.6. Respectively, palmitate and adamantane peptides yields were 5.2 and 2.7%. A change from HBTU to HATU led to the observed improvement. Doubly *N*-methylated peptide were synthesized using HATU as a coupling reagent and the results are shown in Table 6.7.

Table 6.7: Yields of synthesized doubly substituted *retro*-*N*-methylated peptides.

***N*-methylated Peptide**	**Calculated mass (g/mole)**	**Experimental (g/mole)**	**Yield (%)**	**Retention Time (min)**
retro-GG-G*n*FOGE*n*R-GG-Palmitate	585.3301 $C_{55}H_{89}N_{13}O_{15}$	586.3077 $[M + H]^{2+}$	11	Peak 1 = 15.7 Peak 2 = 15.8
retro-GG-G*n*FOGE*n*R-GG-Adamantane	547.2714 $C_{50}H_{73}N_{13}O_{15}$	548.2816 $[M + H]^{2+}$	14	Peak 1 = 9.7 Peak 2 = 9.8

n = N-Methylated amino acids

The addition of a second methyl did not have much effect on the yield and the hydrophobicity as seen from the retention time that is more or less the same as the singly methylated peptides.

6.2 CONCLUSION

In this chapter the successful synthesis of collagen peptidomimetic and peptide-peptoid hybrids is presented. However, in the future, the employment of fragment convergence synthesis will be considered which will involve the synthesis of at least three fragments, 1. GG-G 2. GFOGER and 3. –GG-lipophilic moiety. Fragment-2 (GFOGER) can then be modified accordingly with *N*-methylation, D-amino acids and peptoid residues before being coupled to fragments 1 and 3. Rinnova *et al.*[11] and Li *et al.*[12] have reported improved yields with the fragment convergence synthesis strategy of peptides. Superior and new coupling additive oxymapure,[13] will also be investigated to improve the yields.

Due to time constraints the NMR spectroscopy and CD measurements of the compounds were not obtained, but will be obtained in the future to determine the 3D structural conformations formed and the effect of increased hydrophobicity on the conformations. Computational studies will also be used to understand the interactions between the compounds and the integrin.

6.3 REFERENCES

(1) Fowler, S. A.; Blackwell, H. E. Structure–Function Relationships in Peptoids: Recent Advances toward Deciphering the Structural Requirements for Biological Function. *Org. Biomol. Chem.,* **2009**, *7* (8), 1508–1524.

(2) Jumpei, Morimoto.; Yasuhiro, Fukuda.; Takumu, Watanabe.; Daisuke, Kuroda.; Kouhei, Tsumo.; Shinsuke Sando. A Peptoid with Extended Shape in Water, **2019**, *141* (37), 14612 – 14623.

(3) Zuckermann, R. N.; Kerr, J. M.; Kent, S. B. H.; Moos, W. H. Efficient Method for the Preparation of Peptoids [Oligo (N-Substituted Glycines)] by Submonomer Solid-Phase Synthesis. *J. Am. Chem. Soc.,* **1992**, *114* (26), 10646–10647.

(4) Rzeigui, M.; Traikia, M.; Jouffret, L.; Kriznik, A.; Khiari, J.; Roy, O.; Taillefumier, C. Strengthening Peptoid Helicity through Sequence Site-Specific Positioning of Amide *Cis*-Inducing NtBu Monomers. *J. Org. Chem.,* **2020**, *85*, 2190–2201.

(5) Paradís-Bas, M.; Tulla-Puche, J.; Albericio, F. The Road to the Synthesis of "Difficult Peptides." *Chem. Soc. Rev.,* **2016**, *45* (3), 631–654.

(6) Kent, S. B. Chemical Synthesis of Peptides and Proteins. *Annu. Rev. Biochem.,* **1988**, *57* (1), 957–989.

(7) Milton, R. D. L.; Milton, S. C.; Adams, P. A. Prediction of Difficult Sequences in Solid-Phase Peptide Synthesis. *J. Am. Chem. Soc.,* **1990**, *112* (16), 6039–6046.

(8) Pugh, K. C.; YORK, E. J.; STEWART, J. M. Effects of Resin Swelling and Substitution on Solid Phase Synthesis. *Int. J. Pept. Protein Res.,* **1992**, *40* (3–4), 208–213.

(9) Atherton, E.; Woolley, V.; Sheppard, R. C. Internal Association in Solid Phase Peptide Synthesis. *J. Chem. Soc. Chem. Commun.,* **1980**, No. 20, 970–971.

(10) Aurelio, L.; Box, J. S.; Brownlee, R. T. C.; Hughes, A. B.; Sleebs, M. M. An Efficient Synthesis of *N*-Methyl Amino Acids by Way of Intermediate 5-Oxazolidinones. *J. Org. Chem.,* **2003**, *68* (7), 2652–2667.

(11) Rinnová, M.; Lebl, M.; Souček, M. Solid-Phase Peptide Synthesis by Fragment Condensation: Coupling in Swelling Volume. *Lett. Pept. Sci.,* **1999**, *6* (1), 15–22.

(12) Li, Y.; Lavey, N. P.; Coker, J. A.; Knobbe, J. E.; Truong, D. C.; Yu, H.; Lin, Y. S.; Nimmo, S. L.; Duerfeldt, A. S. Consequences of Depsipeptide Substitution on the ClpP Activation Activity of Antibacterial Acyldepsipeptides. *ACS Med. Chem. Lett.,* **2017**, *8* (11), 1171–1176.

(13) Manne, S. R.; Sharma, A.; Sazonovas, A.; El-Faham, A.; de la Torre, B. G.; Albericio, F. Understanding OxymaPure as a Peptide Coupling Additive: A Guide to New Oxyma Derivatives. *ACS Omega,* **2022**, *7* (7), 6007–6023.

CHAPTER VII

BIOLOGICAL STUDIES

The chapter describes two important aspects of collagen mimetic peptides. Firstly, their ability to induce cell migration in *in vitro* assays and secondly, their efficiency to induce wound closure in *in vivo* animal models. The peptides were designed not only to mimic collagen (Figure 7.1) in structure but also to mete out the functionalities of collagen. That is, they were designed to facilitate cell adhesion, migration and proliferation of cells and to create an environment conducive to wound healing that consists of macromolecules such as collagen, growth factors and cells such as fibroblasts. Full details about the design are described and presented in Chapter II.

General structure of the designed collagen mimetic peptides

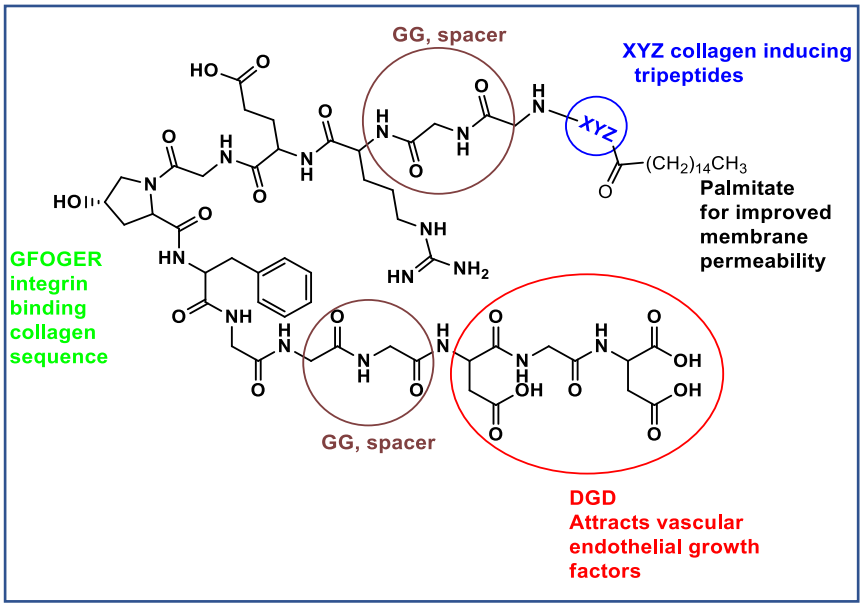

Figure 7.1: Palmitate collagen mimetic peptide.

XYZ = collagen inducing tripeptides TTK / GHK/QPR /EEM.

Three peptides NL008, NL009 and NL010 (Figure 7.2) were selected among the peptides reported in chapters 2 and 3 and submitted for biological screening to the Wits Advanced Drug Delivery Platform (WADDP) Research Unit (Prof Thashree Marimuthu lab).

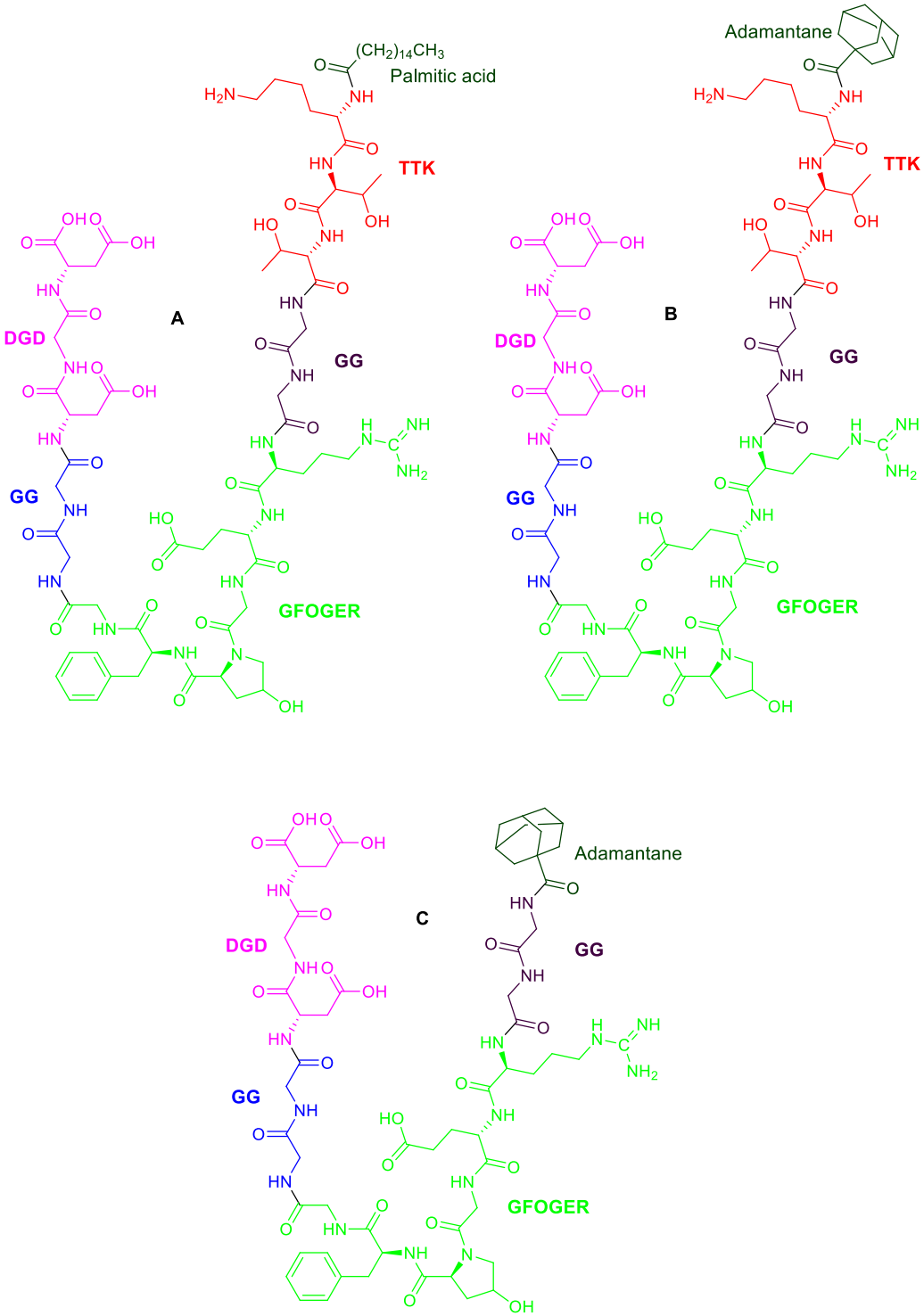

Figure 7.2: A: Chemical structure of the NL009 CMP; B: chemical structure of NL010 CMP; and C: chemical structure of NL008 CMP.

7.1 BIOLOGICAL TESTS

7.1.1 Cytotoxicity

Since the collagen mimetic peptides are meant to be employed in wound healing, their cytotoxicity to other living cells is important. For collagen mimetic peptides to be useful they must have minimal to no toxicity because the destruction of healthy living cells around the wound would have a negative impact on the healing process.

In the current study, trifluoroacetate ions, a common counter ion found after the synthesis and cleavage of peptides was a major concern. Its presence can render the peptides toxic and has also been reported to inhibit the activity of some peptides.[1] Hence, the trifluoroacetate ions were exchanged for HCl by dissolving the peptide in 0.1 M HCl followed by lyophilization. This process had to be performed three times and it is described in detail in chapter IX section 9.4.15.

7.1.1.1 Cell Viability

The HaCaT keratinocytes and NIH 3T3 fibroblasts were seeded onto a 96-well plate at a density of 5×10^4 and incubated for 48 and 72 hours in a humidified incubator at 37°C and 5% CO_2. Following incubation, the cells were treated with varying concentrations of 100, 50, 25, 12.5, and 6.25 µM for the three test peptides (NL008, NL0099, NL010). Treatments were done in triplicate for each test peptide and hydrogel. An amount of 10 µL of 5-fluorouracil (10 µ/mL) was added to untreated wells, in triplicate, to represent a positive control. 10 µL of respective media was added to untreated wells, in triplicate, to act as the negative control. The 48-hour and 72-hour plates were further incubated for 48 and 72 hours, respectively, in a humidified incubator at 37°C and 5% CO_2.

To assess the metabolic activity and viability of the cells, a cell viablity assay was performed. After incubation, 10 µL [3-(4,5-dimethylthiazol)-2-yl]-2,5-diphenyltetrazolium bromide (MTT) reagent was added to each well. The plate was left in the incubator for 3 hours. Following this period, 100 µL MTT solubilising agent was added to each well to dissolve the formazan and the plate was placed back in the humidified incubator at 37°C and 5% CO_2. The colour development was quantified by recording the optical density (OD) at a wavelength of 570 nm in a Perkin Elmer® VICTOR 2030 multilabel plate reader at the respective time points. Cell

viability, relative to the untreated negative control was determined using equation 7.1 below.[2]

$$Cell\ viability\ (\%) = [OD\ treated - OD\ blank\ /OD\ negative\ control] \times 100$$ **Equation 7.1**

7.1.2 Scratch Assay

The scratch assay or wound healing assay is an inexpensive, well-developed, and established technique used to evaluate cell migration *in vitro.*[3] It helps to measure the rate or speed at which cells migrate towards the scratch to close it. The application also allows for the measurement of the size of a scratch or a wound in cultured cells at different points, while the cells are migrating to close the gap of the scratch.

The technique had to be employed in the current study in order to determine the rate at which the peptide would induce or influence the rate of movement of cells. Collagen mimetic peptides possess the ability to influence the migration of cells.

7.1.2.1 Procedure

Human keratinocyte (HaCaT) and murine fibroblasts (NIH-3T3) cell lines were cultured in DMEM and RPMI medium supplemented with 10% fetal bovine serum (FBS) and 1% Penicillin-streptomycin, respectively. The cells were cultured and seeded at a density of 1 × 105 cells/well in 6 well plates. The plates were left in a humidified incubator at 37°C and 5% CO_2 to obtain a confluent monolayer. Following this, a vertical scratch was made with a pipette tip. To remove cell debris, each well was washed with 1 mL PBS. The plate was then treated in triplicates. Treatments comprised of pristine peptides (NL008, NL009 and NL010) at two concentrations of 12.5 and 25. Micrographs of the wound scratch edge were taken using an Olympus® CKX53 microscope at 0, 12, 24, 48 and 72 hours. The rate at which the scratch closed was calculated according to equation 7.2. Areas were obtained using the wound healing plugin of Image J software.[4]

$$Migration\ (\%) = Scratch\ Area(0) - \text{Scratch}\ Area(n) Scratch\ Area(0) / \times 100$$ **Equation 7.2**

7.2 *In vivo* STUDIES

In vivo studies are always considered to be pre-clinical. They inform on clinical studies which normally are conducted in human beings. In the current study, *in vivo* experiments were mainly conducted to corroborate the finding made in *in vitro*. These studies were completed by Ms V. Singh under the supervision of Dr. Marimuthu and are reported here for interpretation of results.

7.2.1 Experimental

7.2.1.1 Materials

Hydrogels (HAgels) and NL010 CMP-hydrogels (NL010-HAgels) were prepared and sterilised and confirmed by antimicrobial streak tests by Ms Variksha Singh under the supervision of Prof Thashree Marimuthu. Commercial 5 mL peptide hydrogel Corning® Puramatrix™ was obtained from Merck (Johannesburg, South Africa). Ethical procedures, animal husbandry, histopathological examinations and statistical analysis are described in detail in Ms Variksha Singh's MSc dissertation submitted to the University of The Witwatersrand's Faculty of Health Sciences in February 2023.

7.2.1.2 Experimental Design

The rats were randomly assigned to groups namely, an experimental group, a control group, a market comparator and a placebo group. There were 3 experimental groups, consisting of 10 rats each. 5 Of the 10 rats in each group, were treated with a comparative formulation, Corning PuraMatrixTM wound gel (1%w/v 0.1-0.2 mL) on the left-sided wound, and with simple gauze on the right-sided wound to serve as a control. On the remaining 5 rats, the left wound area was treated with hyaluronic-CMP (synthesised by Mr. Lesotho under supervision of Dr. Makatini) loaded hydrogel (0.1% w/v, 0.1-0.2 mL), and the right wound area with pristine hyaluronic acid as a drug-free system (2%HA w/v, 0.1- 0.2 mL). A graphical depiction of the experimental design is showcased in Figure 7.3.

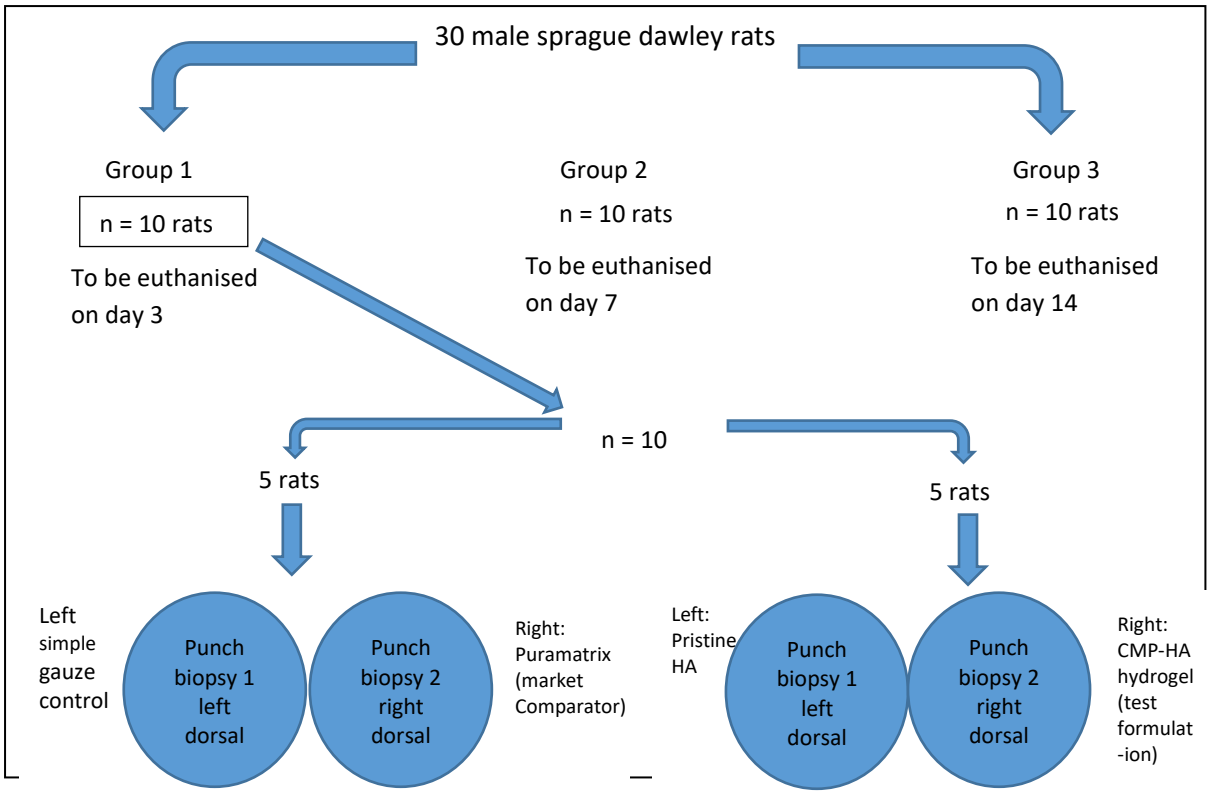

Figure 7.3: Graphical depiction of the experimental design showing the breakdown of the three experimental groups. Group 1 experiment was conducted for 14 days with the rats euthanised on day 14. Group 2 experiment was conducted for 7 days with the rats euthanised on day 7. Group 3 experiment was conducted for 3 days with the rats euthanised on day 3. (Drawn by Ms Variksha Singh).[5]

7.2.1.3 Surgical preparation

The rodents were anaesthetized with Ketamine IM 40 mg/kg/Xylazine 5 mg/kg. Anaesthesia was maintained with isoflurane 2%. The dorsal area was shaved, and surgical fields were outlined with a marking. Following this, the surgical area was prepared and disinfected as per WRAF aseptic techniques. The rat's vital signs were monitored continuously throughout the procedure using a BP monitor.

7.2.1.4 Surgical procedure

Using a skin punch biopsy apparatus, a cutaneous wound (3 mm thick) of 6 mm diameter was induced on the dorsal area of the rat. Two wound areas were punched on the right and left 141 sides of the rat. The original skin plugs were stored in formalin for further histological processing. The induced wound area was wiped with gauze to eliminate excess fluid. The wound areas were assessed for shape, diameter and depth prior to treatment application. All

treatments were previously sterilised and formulated according to strict aseptic techniques. The formulations were evaluated for microbial contamination by streaking the gels on agar plates before treatment on the rats as seen in Figure 7.5 (A and B). The 3 experimental groups consisted of 10 rats each, with 5 of the 10 rats in each group. Wound areas were sealed with gauze and a bandage with adhesive tape. Treatments were applied once-off with bandage changes every 7 days. Surgical preparation and surgical procedures are shown in Figure 7.5 (C-I).

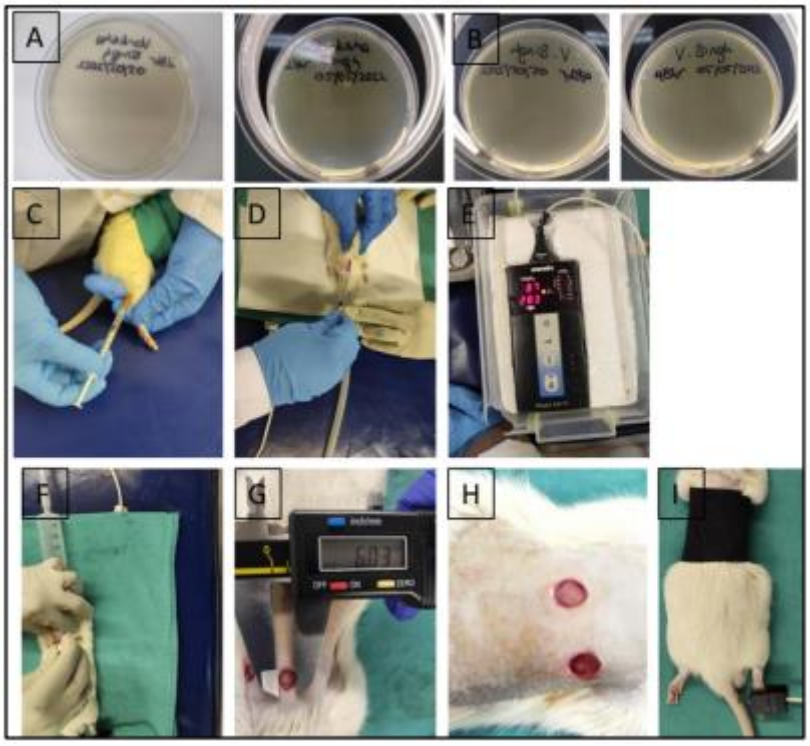

Figure 7.4: Bacterial and fungal evaluation of the treatments on agar plates using the streaking method over A: 24 hrs and B: 48 hrs prior to administration. There is no evidence of bacterial or fungal growth deeming the treatments safe for administration. Surgical preparation and surgical procedures are depicted in images C-I. C: the administration of anaesthesia; D: the administration of prophylactic Tramadol® for pain relief; E: vital sign monitoring by the BP monitor machine; F: punch wound biopsy on the dorsal surface to induce full-thickness wounds of 6 mm diameters; G: wound shape, diameter and depth measurement using digital callipers prior to treatment application; H: treatment application; and, I: bandaging and assessment for consciousness regain. (Obtained from Ms Variksha Singh).[5]

7.2.1.5 Post-operative recovery

The rats were placed back in their individual cages on heating pads for 48 hours after surgery. For post-operative pain relief, Buprenorphine S/C 0.05 mg/kg 2-3 times daily and Tramadol IM 5 mg/kg 2-3 times daily were administered for 48 hours after surgery. Animals were monitored for signs of pain, weight loss or surgical site infections. Each rat was monitored according to a welfare score sheet. The wounds were inspected daily for signs of inflammation and rates of closure on the day of euthanasia. Treatment was applied once off with reapplication if there was a complete loss of treatment upon daily visual inspection, if the animal removes the bandage/treatment or if the hydrogels run off the surface of the wound. Group 1 (14-day study) had treatment reapplied and bandage changes after 7 days. For the remaining groups, the bandages were changed if necessary, using Isofor 1-2% as a method of restraint. The following scenarios constituted bandage changes: removal by the animal, excessive exudate, dirty bandages, discolouration and/or odour.

7.2.1.6 Visual comparative analysis of the wound beds

A visual assessment was carried out using the photographs taken on the days of euthanization to evaluate wound closure rates of all wounds.

7.2.1.7 Macroscopic determination by percentage wound closure evaluation

In order to determine the wound closure rates of the different treatments, percentage wound contraction by wound closure was assessed. The wound beds were measured using digital callipers and photographed on the days of euthanization (days 3, 7 and 14). An object for a scale reference was placed in the pictures. The wound areas were analysed using Image J technologies. The rate of wound closure was evaluated using equation 7.3 below.

$$Wound\ closure\ (\%) = Wound\ area(0) - Wound\ area(n)\ Wound\ area(0) / \times 100$$

Equation 7.3

7.2.1.8 Statistical analysis

All experimental procedures were done in triplicate and repeated at least 3 times. All experimental data were presented as mean ± standard deviation (SD). Statistical analyses were evaluated by one-way ANOVA (OriginPro) and SPSS 18.0 software following the Tukey test for multiple comparisons. Statistical differences of $p < 0.05$ determined significance. *In vitro* scratch closure rates were evaluated using Image J software. Statistical analysis was conducted for cytotoxicity studies and scratch assays and the results were expressed as mean ± SD (p-value). The results are displayed in terms of statistical significance where * represents $p < 0.05$.

7.3 RESULTS

7.3.1 Cell Viability results

All peptides were seen to not only maintain cell viability but also promote cell proliferation as the values increased beyond that of the negative control (Figure 7.5).

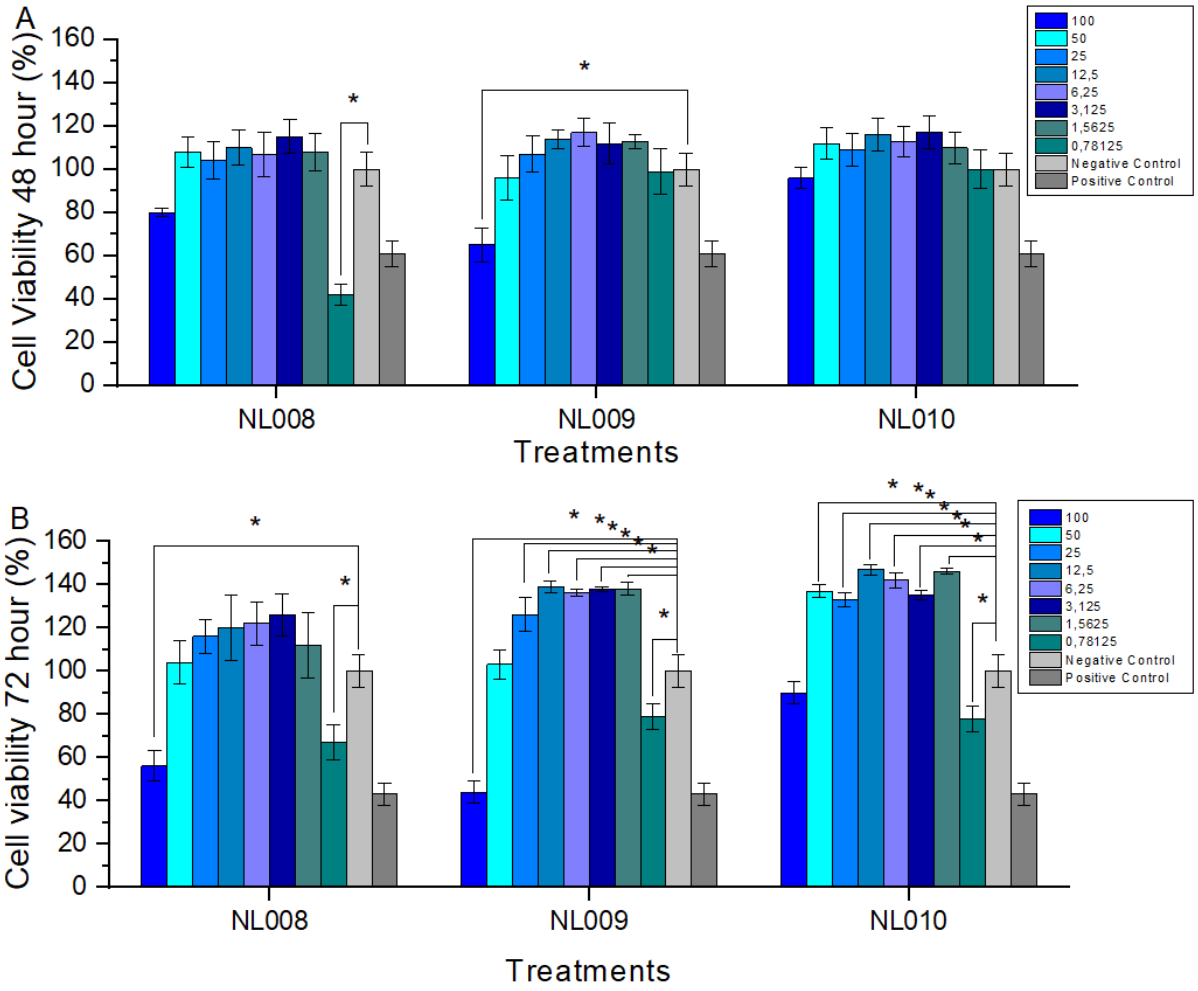

Figure 7.5: Cytotoxicity assays to assess cell viability for 5 concentrations ranging from 100-0.78125 µM over A: 48 hrs and B:72 hrs on HaCaT cells.[5]

Interestingly, the peptides displayed dose-dependent responses, especially seen after 72 hours. Additionally, the peptides did not perform well at a high concentration of 100 µM seeing as the cell viability was often reduced and less than the negative control. A further reduction in viability was noted at T72 for the 100 µM concentration linking to compounded cell hampering over time. At these concentrations, the peptides can be seen as cytotoxic implying that the optimal dosage of peptides should remain relatively low. The CMPs displayed increasing cell viabilities, of direct proportion, from 50 µM to approximately 6.25 µM, whereafter the cell viability began to decrease and tapper off. The greatest cell viability was seen for NL010 at 12.5 µM, promoting its role as an inducer of cell proliferation and growth. For the HaCaT cell line, optimal CMP concentrations of 12.5 and 25 µM were selected from the cytotoxicity data for evaluation on a scratch assay. Herein, scratch closure rates were evaluated to determine the CMP's role in the promotion of cell migration and proliferation.[5]

7.3.2 Scratch Assay results

NL009 and NL010 possess bioactivity due to their ability to induce cell migration and proliferation. NL008 showed minimal bioactivity and cell viability in comparison to NL009 and NL010 across different concentrations and cell lines, Figure 7.6 and 7.7. Owing to this, NL008 was excluded from further studies. The expense of formulating NL008 outweighs its potential for further fabrication into wound healing dressings, especially since it showed undesirable bioactivity.

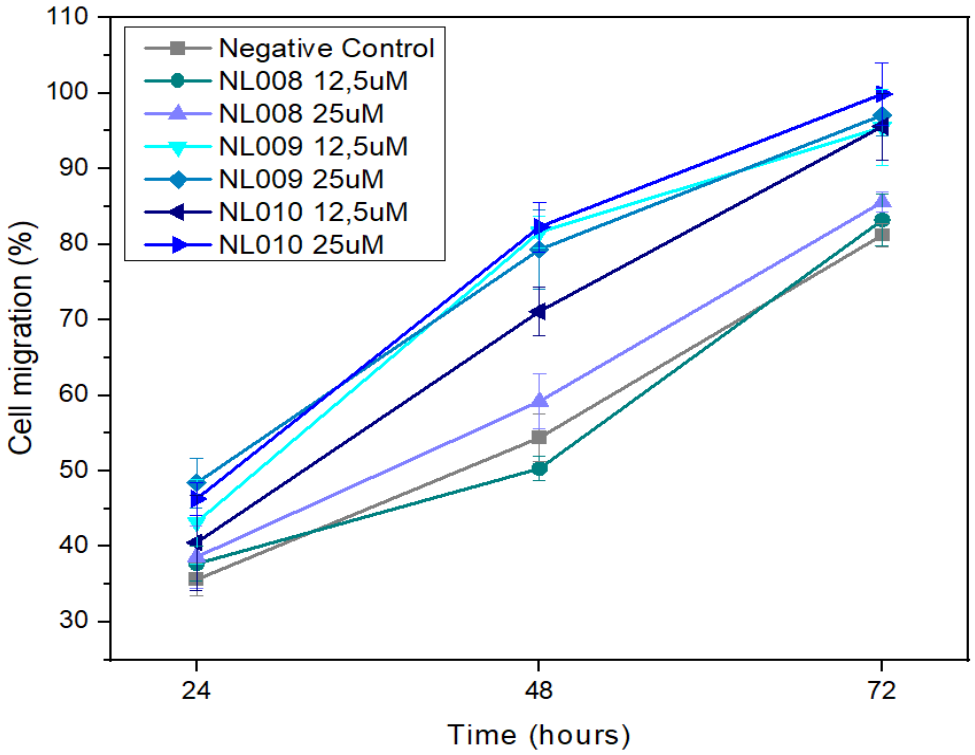

Figure 7.6: Scratch closure rates for the three different CMPs (NL008, NL009 and NL010) at their relative concentrations (12.5 and 25 µM) on the HaCaT cell line expressed as % migration.[5]

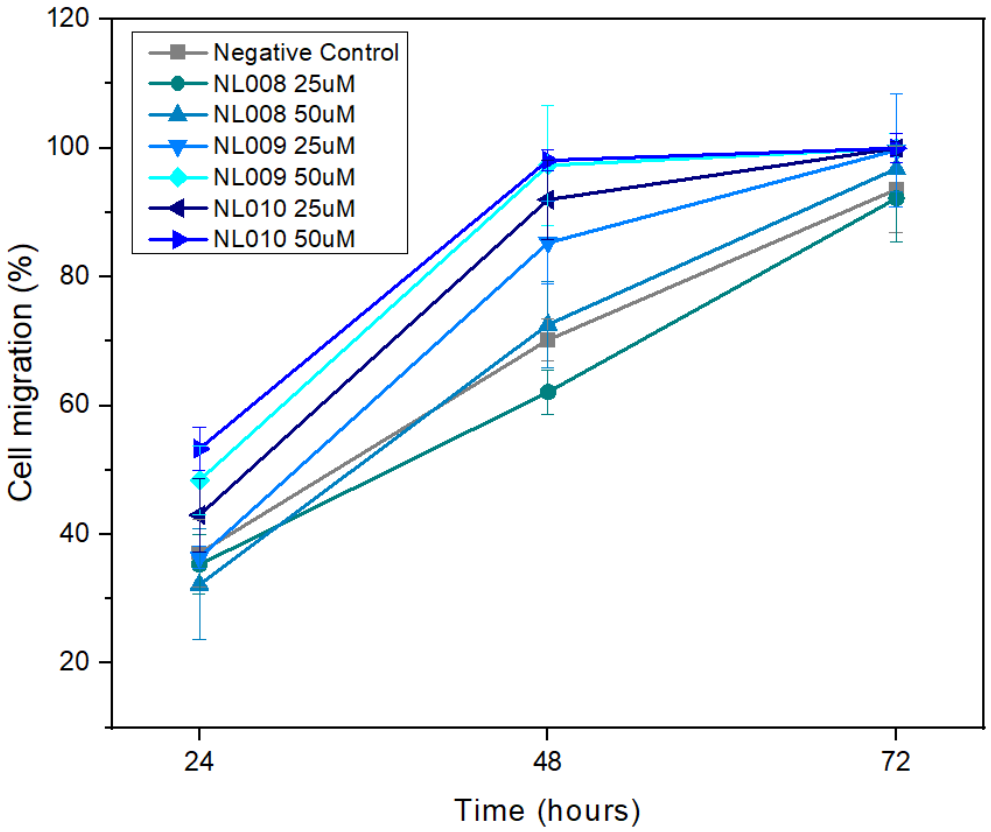

Figure 7.7: Scratch closure rates for the three different CMPs (NL008, NL009 and NL010) at their relative concentrations (25 and 50 µM) on the 3T3 cell line expressed as % migration.[5]

A common trend was noted when considering the bioactivity of the peptides. Scratch closure rates were escalated within the first 24-48 hours of treatment. This was followed by a reduction in the activity of different magnitudes. Peptide degradation is proposed as an explanation for these findings. Pharmaceutical dosing is a critical tool in determining clinical success. Owing to the intense peptide activity noted initially, dosage frequency needs to be thoroughly assessed. The dosing frequency would need to be every 3 days for therapeutic value to be achieved. Alternatively, peptide stability can be improved upon to allow for prolonged administration, as frequent dosing leads to a cost increase. Additionally, formulation techniques can be employed to circumvent this issue.[5] Due to their good *in vitro* activity and low cytotoxicity peptides NL009 and NL010 were formulated into a hydrogel consisting of hyaluronic acid and evaluated in animal studies.

7.3.3 *In vivo* studies

Although the market comparator (Figure 7.8) is noticeably doing well in terms of closing up the wound, the collagen mimetic peptides have also prominently reduced the size of the wound. What this result means is that the collagen mimetic peptide NL010 has managed to create an environment needed for wound healing. DGD tripeptides have managed to attract the growth factors to the wound site and the *retro*-TTK on the other hand has managed to stimulate the production of collagen.

While the rate of closure may not be the same as the one for the market comparator, the designed collagen mimetic peptide has managed to perform the activity it was designed for. Clearly, further modifications in the structure of the peptide, focused mainly at increasing the rate of wound closure would have to be considered. As it is, the peptide has managed to mimic collagen with success. More information on the ability of the peptide to induce fibroblasts is reported in Ms V Singh MSc dissertation.[5]

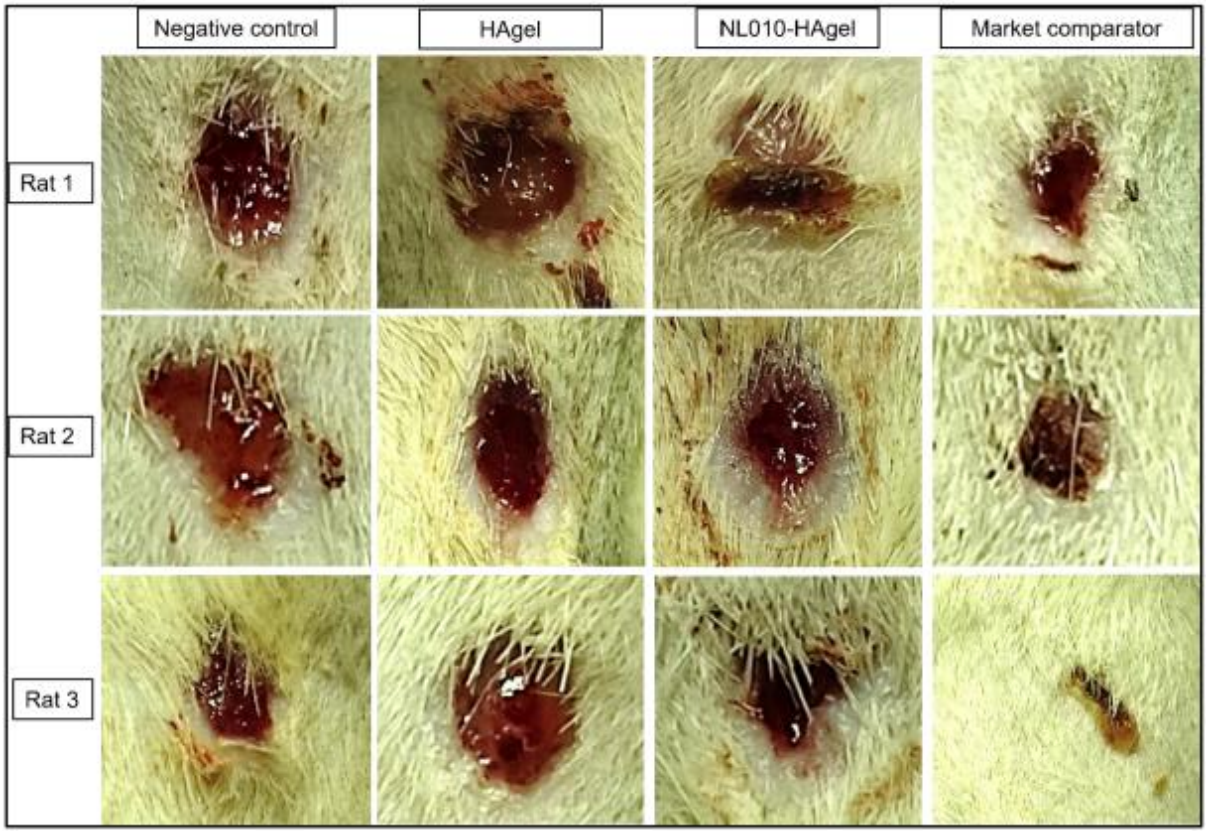

Figure 7.8: 7-day study of three rats treated with the negative control, HAgel, NL010-HAgel and the market comparator.[5]

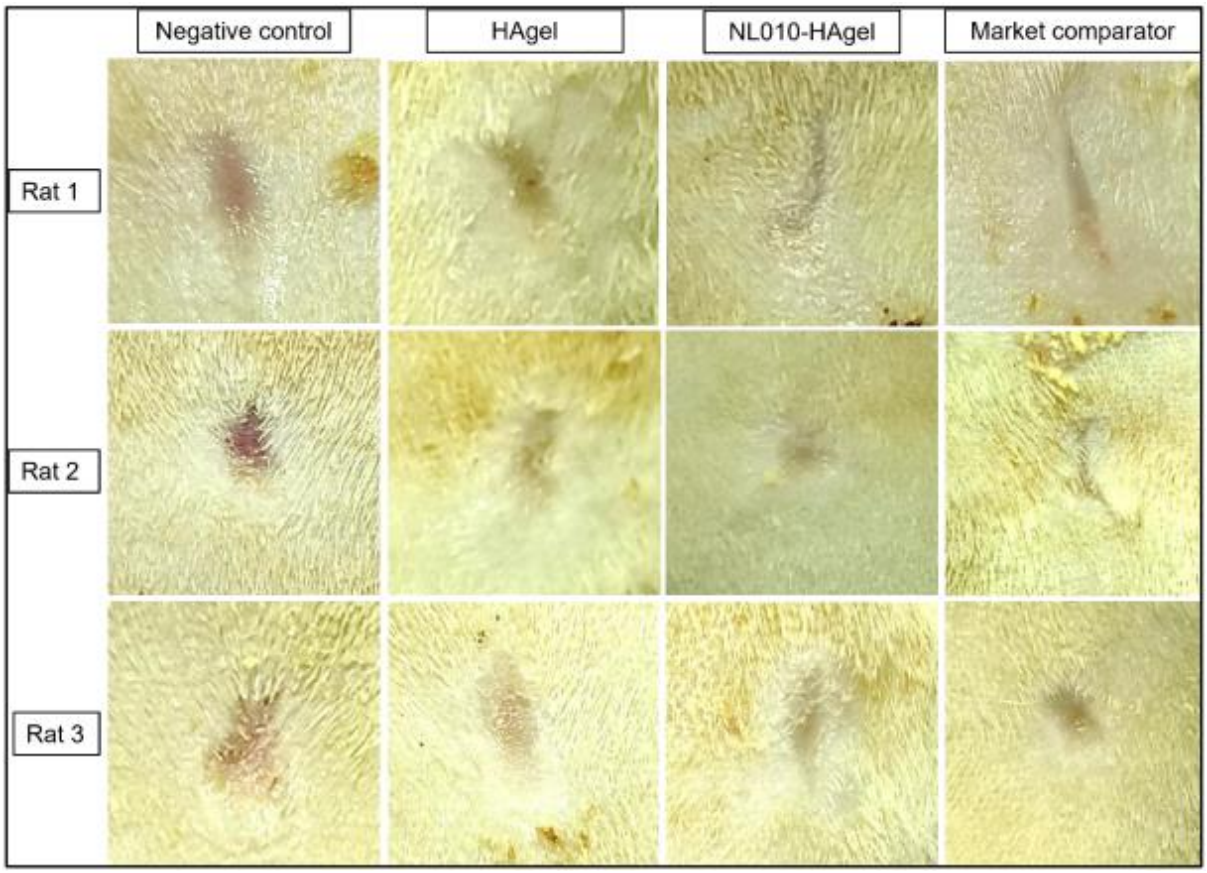

Figure 7.9: 14-day study of three rats treated with the negative control, HAgel, NL010-HAgel and the market comparator.[5]

7.4 CONCLUSION

The peptides *retro*-DGD-GG-GFOGER-GG-TTK-Adamantane and Palmitate possess the properties which they were designed for, that is, properties of collagen I. There is ample room for improvement of these peptides since the 3D structure has been determined (Chapter III). Clearly, the adamantane derivative had better activity when compared to the palmitic derivatives and further analogues will be designed with adamantane as the lipophilic molecule.

7.5 REFERENCES

(1) Sikora, K.; Neubauer, D.; Jaśkiewicz, M.; Kamysz, W. Citropin 1.1 Trifluoroacetate to Chloride Counter-Ion Exchange in HCl-Saturated Organic Solutions: An Alternative Approach. *Int J Pept Res Ther* **2018**, *24* (2), 265–270.

(2) Kamiloglu, S.; Sari, G.; Ozdal, T.; Capanoglu, E. Guidelines for Cell Viability Assays. *Food Front* **2020**, *1* (3), 332–349.

(3) Liang, C. C.; Park, A. Y.; Guan, J. L. In Vitro Scratch Assay: A Convenient and Inexpensive Method for Analysis of Cell Migration in Vitro. *Nat Protoc* **2007**, *2* (2), 329–333.

(4) Felice, F.; Zambito, Y.; Belardinelli, E.; Fabiano, A.; Santoni, T.; di Stefano, R. Effect of Different Chitosan Derivatives on in Vitro Scratch Wound Assay: A Comparative Study. *Int J Biol Macromol* **2015**, *76*, 236–241.

(5) Singh, V. Design and Development of a Collagen Mimetic Peptide (CMP) Instructive Hydrogel for Wound Healing, University of The Witwatersrand, Johannesburg, **2023**.

CHAPTER VIII
CONCLUSION

Collagen mimetic peptides containing the integrin binding motif *retro*-GFOGER, lipophilic moieties (adamantane and palmitic acid for improved membrane permeability), growth factor attracting tripeptide DGD and collagen inducing *retro*-tripeptides namely, Thr-Thr-Lys (TTK), Gly-His-Lys (GHK), Gln-Pro-Arg (QPR) and Glu-Glu-Met (EEM) can be successfully synthesized using the solid phase peptide synthesis strategy.

The *alpha* helical structure of the *retro*-DGD-GG-GFOGER-GG-TTK-Palmitate and *retro*-DGD-GG-GFOGER-GG-TTK-adamantane peptide were successfully characterised by the ROESY and circular dichroism experiments. According to circular dichroism and NMR experiments, the synthesized peptides have three dominant secondary structural conformations, the α-helix, antiparallel and parallel *beta* sheets. Adamantane derivatives mainly consist of parallel conformations while palmitic acid derivatives mainly consist of-helical conformations. These conformations mimic the natural collagen parallel triple-helix structure.

The existence of *trans* isomers, antiparallel/parallel stranded helical conformations indicates that there is a possibility that the synthesized peptides can form a triple helical structure that resembles collagen. The formation of the helical conformation that mimics collagen further implies that the peptides can interact with the integrin in the same way as collagen would.

The *retro*-GG-G[*para*-fluoro-Phe]OGER-GG peptides conjugated to lipophilic molecules were successfully synthesized. The peptides were more hydrophobic than the original sequences and will be tested for wound healing activity in the future. The ability of the phenylalanine fluorine to form hydrogen bonds with the side chain amide groups of the asparagine and glutamine of the integrin will be investigated using computational chemistry in the future.

The last class of compounds that was synthesized consists of moieties that have been reported to improve the peptide's stability against protease degradation. The class comprises of peptoids, D-peptides and *N*-m

ethylated peptides. These compounds were, however obtained in low yields and this was attributed to the acylation reaction involving a secondary sterically hindered amine group with the carboxylic acid of the next amino acid residue or bromoacetic acid (peptoid synthesis). The peptoids and the *N*-methylated peptides, all possess secondary amines which are sterically hindered. The methyl group increases the reactivity of the amine group but also hinders the coupling of the nitrogen atom to the carbonyl carbon, thereby negatively affecting the yield.

In the future, the employment of fragment convergence synthesis will be considered which will involve the synthesis of at least three fragments, 1. GG-G 2. GFOGER and 3. –GG-lipophilic moiety. Fragment-2 (GFOGER) can then be modified accordingly with *N*-methylation, D-amino acids and peptoid residues before being coupled to fragments 1 and 3. Lebl *et al*[1] and Li *et al*[2] have reported improved yields with the fragment convergence synthesis strategy of peptides. Superior and new coupling additive oxymapure,[3] will also be investigated to improve the yields.

The collagen mimetic peptides' ability to induce cell migration can be successfully investigated using the scratch assay. NL009 and NL010 possess bioactivity due to their ability to induce cell migration and proliferation. NL008 showed minimal bioactivity and cell viability in comparison to NL009 and NL010 across different concentrations and cell lines. In the future, the scratch assay and the cytotoxicity assay will be utilized to determine the peptides that can be further studied in animal models. Furthermore, the scratch assay can be used to determine the effect of formulation on cell migration since both the adamantane and palmitic acid derivatives' activity was observed to be enhanced by the presence of hyaluronic acid.

In animal studies, two of the peptides demonstrated an ability to induce wound closure. In an experiment where the peptides were applied to the wounds inflicted on rodents, the peptides' rate of wound closure was satisfactory, by far better than the negative control and hyaluronic acid gel alone. However, the peptide's rate of wound closure was slightly less than that of the market comparator, the Puramatrix® peptide. Hence, further modifications such

as the conjugation of the peptides to nanoparticles will be investigated in the future to improve the activity of adamantane derivatives.

In summary, three novel wound healing peptides have been successfully designed and synthesized and assessed for wound healing properties both in vitro and in vivo. The remaining 14 CMP's that were successfully synthesised have not been assessed for wound healing properties as yet, but will be assessed as future work.

8.1 REFERENCES

(1) Rinnová, M.; Lebl, M.; Souček, M. Solid-Phase Peptide Synthesis by Fragment Condensation: Coupling in Swelling Volume. *Lett. Pept. Sci.* **1999**, *6* (1), 15–22.

(2) Li, Y.; Lavey, N. P.; Coker, J. A.; Knobbe, J. E.; Truong, D. C.; Yu, H.; Lin, Y. S.; Nimmo, S. L.; Duerfeldt, A. S. Consequences of Depsipeptide Substitution on the ClpP Activation Activity of Antibacterial Acyldepsipeptides. *ACS Med Chem Lett* **2017**, *8* (11), 1171–1176.

(3) Manne, S. R.; Sharma, A.; Sazonovas, A.; El-Faham, A.; de la Torre, B. G.; Albericio, F. Understanding OxymaPure as a Peptide Coupling Additive: A Guide to New Oxyma Derivatives. *ACS Omega* **2022**, *7* (7), 6007–6023.

CHAPTER IX
EXPERIMENTAL

9.1 GENERAL INFORMATION

9.1.1 Chemicals and reagents

All organic solvents and reagents were obtained from commercial sources. Fmoc protected amino acids, (1-[bis(dimethylamino)methylene]-1*H*-1,2,3-triazolo[4,5-*b*]pyridinium 3-oxide hexafluorophosphate, Hexafluorophosphate Azabenzotriazole Tetramethyl Uronium) (HATU), *N,N,N',N'*-Tetramethyl-*O*-(1*H*-benzotriazol-1-yl)uraniumhexafluorophosphate (HBTU), and 2-chlorotrityl chloride resin were purchased from DLD scientific. Reagents such as diisopropylethylamine (DIPEA), piperidine, Triisopropylsilane (TIS), formic acid, trifluoroacetic acid (TFA), palmitic acid and adamantane were obtained from Sigma Aldrich (South Africa). Organic solvents such as dimethylformamide (DMF), HPLC grade methanol, HPLC grade acetonitrile, dimethyl sulfoxide, chloroform and diethyl ether were purchased from Radchem and Pyramid Scientific. Organic solvents used for column chromatography such as ethyl acetate, hexane and dichloromethane (DCM), were purchased from DLD Scientific (South Africa). These solvents were dried over calcium hydride and distilled before use to remove non-volatile components.

9.2 INSTRUMENTATION

9.2.1 Ultra-High-Performance Liquid Chromatography Mass Spectrometry (UHPLC-MS)

Analytical LC-MS analysis was performed on an Ultra-High-Performance Liquid Chromatography (Thermo Scientific Ultimate 3000, RS diode array detectors) with a Diode Array (190, 195, 215, 254, and 300 nm) coupled to a Bruker Compact Q-TOF high-resolution mass spectrometer.

9.2.2 Nuclear magnetic resonance (NMR) spectroscopy

Nuclear magnetic resonance (NMR) spectra were recorded on either a Bruker AVANCE 300, 400 or Bruker AVANCE III 500 MHz spectrometer. Peptides were dissolved in deuterated

DMSO, $CDCl_3$ or d_6-acetone. All chemical shift values are reported in parts per million referenced against trimethylsilane which is given an assignment of zero parts per million.

9.2.3 Circular dichroism

The circular dichroism spectra were recorded on a JASCO J-18 spectropolarimeter with the following settings: wavelength scan - 0.1 mm pathlength; 0.1-0.2 mg/mL peptide concentration; 300 µL volume; 1.0 nm bandwidth; 0.5 nm resolution; 8 scans; 4 sec response; 20 nm/minute scan speed; scan range 280 – 160 nm while keeping HT voltage less than 600 V. The wavelength range was set between 190 to 250 nm while the temperature was set to 20 °C. The peptides were prepared in phosphate buffer ph. 8.3 (200 mM) at a concentration of 0.1 mg/mL . A 0.1 cm pathlength cuvette holding 300 µL was used for all CD measurements.

9.2.4 Ultra-violet Visible (UV-Vis)

Absorbance values used to determine the loading capacity of the resin were recorded on the Varian Cary Eclipse (Cary 50) UV-vis spectrophotometer.

9.3 GENERAL TECHNIQUES

9.3.1 UHPLC-MS Analysis

The samples were analysed using a binary solvent system where solvent A consisted of H_2O and 0.1% Formic acid (v/v), and solvent B consisted of Acetonitrile and 0.1% Formic acid (v/v). 20 µL of the sample was injected onto a C18 column (5 µm, 100 Å, 4.60 mm × 150 mm). The system flow rate was set at 0.3 mL/minute in the positive mode. The mass spectrum analysis was processed using the Bruker Daltonics data analysis software. The ultra-pure water used in this study was obtained from the Millipore Direct-Q®3 UV water purification (ZRQSVPO30) system.

The samples were analysed in the positive ionization mode and the MS was scanned at m/z 100-3000 range during separation and detection. Nitrogen gas (N_2) was used as the dry and nebulizer gas. The nebuliser gas was operated at a pressure of 1.8 bars whereas the drying gas was operated at a flow rate of 9 L/minute.

9.3.2 ^{1}H Nuclear Magnetic Resonance (^{1}H NMR) spectroscopy

The chemical shifts (δ) values are reported in parts per million (ppm) relative to deuterated dimethyl sulfoxide (DMSO-d_6, 2.49 ppm) and referenced against the internal standard, tetramethylsilane (TMS, 0.00 ppm). The spectra were analyzed as first order and the values of the coupling constant (J) are reported as Hertz (Hz). Multiplicity of signals is expressed as: s = singlet, br s = broad singlet, d = doublet, dd = double of doublet, t = triplet, q = quartet, m = multiplet.

9.3.3 ^{13}C NMR spectroscopy

The chemical shift values are reported in (ppm) relative to deuterated dimethylsulfoxide (DMSO-d_6, 39.52 ppm) and TMS as an internal standard.

9.3.4 2D NMR spectroscopy

Spectra for COSY, ^{13}C-HSQC, TOCSY, NOESY and ROESY experiments, were recorded at 293, 300, and 308 K on a 500 MHz NMR Bruker III 500 MHz spectrometer. All 2D spectra were recorded at the phase sensitive mode using time proportional phase increment (TPPI). The residual water peak of DMSO-d_6 was suppressed by a pre-saturation pulse of 2.0 s duration. The first NOESY experiments were recorded with mixing time of 150, 200 and 250 ms; ROESY spectra were recorded with mixing times of 100, 150, 154 200, 250 and 300 ms; while TOCSY was recorded with mixing times of 48, 64, 70, 80 and 100 ms; each increment was the sum of 32 scans with a relaxation delay of 2.0 s; 2048 data points were collected per experiment. For conformational analysis, the experiment was conducted at different temperatures such as 300, 323 and 353 K on Bruker AVANCE 400 MHz instrument.

9.4 GENERAL PROCEDURES

9.4.1 General procedure A: Activation and coupling of the first amino acid to 2-chlorotitryl resin.

2-Chlorotrityl-chloride resin (600 mg) was added to a 50 mL tube containing dry DCM (10 mL) and 2 mL of thionyl chloride. The mixture was shaken overnight then filtered using suction and the resin was washed with dry DCM (5 × 4 mL). To avoid deactivation of the water-sensitive resin, DCM (10 mL), 1 mL of DIPEA (1.0 M, 2.0 mL) and the first amino acid (0.987g, 0.2 M) were immediately added to the dry resin in sintered-glass reaction vessel. This mixture

was reacted for 2 hours then dried using suction. Finally, the resin was washed with DCM (3 x 5 mL).

9.4.2 General procedure B: Analysis of the substitution of the first amino acid

The resin, with the first amino acid bonded, was weighed out in duplicate samples of 5 to 10 mg in Eppendorf tubes then 20% piperidine in DMF (1.0 mL) was added to the resin to deprotect the amino acid. The resin was shaken for 20 minutes then centrifuged down. From the centrifuged sample, 100 µL of the supernatant was transferred into a tube with DMF (10.0 mL). The mixture was thoroughly mixed, and the solution (2.0 mL) was pipetted into one cuvette cell and DMF (2.0 mL) was added into another cuvette cell. The cuvette containing DMF was used to zero the spectrophotometer. The sample was checked for absorbance at 301 nm three times and used to calculate the substitution using the following equation:

$$Loading\ capacity\left(\frac{mmol}{g}\right) of\ resin = \frac{(101 \times Average\ Absorbance)}{(7.8 \times mg\ of\ resin\ beads)}$$

The substitution of Fmoc-amino acid loaded was then used to calculate the loading capacity and the theoretical yield:

Theoretical yield = sub (mmol/g) × mass of resin (g) × Mr of peptide (g/mol)

9.4.3 General procedure C: Synthesis of peptides

After the attachment of the first amino acid to the resin, 20% piperidine in DMF (10 mL) was added to the resin and bubbled with nitrogen gas for 5 minutes to deprotect the amino acid. This step was performed twice for the same duration and piperidine was removed using vacuum. The resin was washed first with DMF (3 x 5 mL) followed by DCM (3 × 5 mL). The resin was then mixed with DIPEA (1.26 mL, 0.6 M), HBTU (0.519 g, 0.11 M) and the second amino acid (0.429 g, 0.12 M). This mixture was reacted for 45 minutes then filtered using suction. The resin was washed with DMF (3 × 5 mL) and treated with 20% piperidine in DMF (20.0 mL) twice for 5 minutes and then the resin was then washed again with DMF (3 x 5 mL) and DCM (3 × 5 mL). The resin was then mixed with DIPEA (0.6 M, 1.26 mL), HBTU (0.519 g, 0.11 M) and the next amino acid (0.429 g, 0.12 M). This mixture was reacted for 45 minutes and filtered using suction after which the resin was washed with DMF (3 × 5 mL). This method was repeated until the full peptide was synthesized.

9.4.4 General procedure D: Synthesis of peptides containing adamantane and palmitic acid on the N-terminal.

After all the amino acids in the peptide were coupled using the general synthesis procedure above (section 9.4.3). The resin was treated with 20% piperidine in DMF (10 mL) twice for 5 minutes to deprotect the Fmoc on the last amino acid. The resin was then washed with DMF (3 x 5 mL) and DCM (3 × 5 mL) and dried using suction. Adamantane carboxylic acid (0.260 g, 0.12 M), DIPEA (1.26 mL, 0.6 M) and HBTU (0.519 g, 0.11 M) were then added to the resin attached to the full peptide. This mixture was reacted for 45 minutes, and the resin was washed in DCM (3 × 5 mL) followed by DMF (3 x 5 mL) and finally dried using suction. The analogues with palmitic acid on the N-terminal were synthesized by adding palmitic acid (0.369 g, 0.12 M) and DIPEA (1.26 mL, 0.6 M) and HBTU (0.519 g, 0.11 M) to the resin attached to the full peptide. This mixture was reacted for 45 minutes then the resin was washed with DMF (3 × 5 mL) followed by DCM (3 x 5 mL) and finally dried using suction.

9.4.5 General procedure E: Synthesis of *para*-fluorophenylalanine

Synthesis of the Fmoc-*para*-fluorophenylalanine was accomplished via acetylation reaction of 9-fluorenylmethoxycarbonyl chloride (Fmoc-Cl) and fluorophenylalanine. To a cooled solution of *para*-fluorophenylalanine (1.39 g, 0.0076 moles) dissolved in 20 mL of 10% Na_2CO_3 in an ice bath was added with stirring and a solution of (1.96 g, 0.0076 moles) Fmoc-Cl. The mixture was stirred at room temperature for 2 hours, then poured into 400 mL of water and extracted twice with ether to remove small amounts of 9-fluorenylmethanol and the polymer of dibenzofulvene. The aqueous layer was cooled in an ice bath and acidified with concentrated HCl. It was further extracted with ethyl acetate, the extracts were washed with water, dried over $MgSO_4$ and evaporated, and the resulting white residue was recrystallized from nitromethane (CH_3NO_2) to give the product.

9.4.6 General procedure F: *para*-fluorophenylalanine peptides

The *para*-fluorophenylalanine (0.972 g, 0.12 M) and DIPEA (1.26 mL, 1 M) in DMF (10.74 mL) were first mixed and stirred in a shaker for a few minutes before addition of the coupling reagent, HBTU (0.519 g, 0.11 M). The resultant mixture was added to the resin (with GG-G-NH_2 anchored onto the solid support already) and stirred by bubbling nitrogen for 45 minutes. The solvent was removed and the coupled *para*-fluorophenylalanine was deprotected by

adding 20% piperidine in DMF (20 mL) and bubbling twice with nitrogen for 5 minutes. The resin was washed with DCM (3 x 5 mL) followed by DMF (3 x 5 mL). The rest of the amino acids were coupled according to the general procedure C, for synthesis of peptides.

9.4.7 General procedure G: Synthesis of peptoids

Bromoacetic acid (0.2 g, 0.2 M) was dissolved in DMF (10.74 mL). The base, DIPEA (1.26 mL, 1 M) was added to the mixture and the two were stirred together for a few minutes before adding N, N'-Diisopropylcarbodiimide (DIC) (0.21 mL, 0.11 M). The mixture was added to an already synthesized –GG-G-NH_2- (synthesized according to the general procedure C) on solid support. The resultant reaction mixture was gently mixed by bubbling nitrogen gas into the reaction for 1 hour. The solvent was removed and the resin washed with DCM (3 x 5 mL) and DMF (3 x 5 mL) to remove excess reagents. In the second step, benzylamine (0.16 mL, 0.12 M) in dry DMF (12 mL) was added and the mixture and stirred by bubbling nitrogen for 45 minutes. Due to commercial unavailability of primary amine of hydroxyproline, the latter was used as it is. Also, the 'R' group of glycine is only hydrogen and therefore the amino acid was incorporated into the peptide as it is. The deprotected glycine coupled to the resin was allowed to react again with activated bromoacetic (0.2 g, 0.2 M). Once bromoacetic acid was coupled to the resin and the latter washed as stated already, γ-amino butyric acid (4-amino butanoic acid) (0.25g, 0.2 M) was coupled to the peptide. As mentioned already, the amino acid was deprotected and the washing of the resin ensued.

9.4.8 General procedure H: Synthesis of D-Peptides

D – peptides were synthesized according to the general procedure C. However, D - amino acids were utilized in place of L – amino acids.

9.4.9 General procedure I: Synthesis of Singly *N*-methylated peptides

To the already synthesized peptide -GG-G-NH-Fmoc on a solid support was added 20% piperidine solution (10 mL) and bubbled with nitrogen twice for 5 minutes. The resin was then washed with DMF (3 x 5 mL) followed by DCM (3 x 5 mL) to remove excess reagents. *N*-Methylated phenylalanine (0.578 g, 0.12 M) and DIPEA (1.26 mL, 1 M) in DMF (10.7 mL) were first mixed and stirred in a shaker for a few minutes before the addition of the coupling reagent, HBTU (0.519 g, 0.11 M). The resultant mixture was added to the resin and stirred by bubbling nitrogen for 45 minutes. The solvent was removed and the coupled *N*-methylated

phenylalanine was deprotected by adding 20% piperidine in DMF (20 mL) by bubbling with nitrogen twice for 5 minutes. The resin was washed with DCM (3 x 5 mL) followed by DMF (3 x 5 mL). The rest of the amino acids were coupled as stipulated in general procedure C to yield the peptide.

9.4.10 General procedure J: Synthesis of doubly *N*-methylated peptides

To the already synthesized peptide -GG-G[*N*-methPhe]OGE-NH-Fmoc, on a solid support, was added 20% piperidine solution (10 mL) twice for 5 minutes. The resin was then washed with DMF (3 x 5 mL) followed by DCM (3 x 5 mL) to remove excess reagents. *N*-methylated Fmoc-Arg(Pbf)-OH (0.954 g, 0.12 M) and DIPEA (1.26 mL, 1 M) in DMF (10.7 mL) were first mixed and stirred in a shaker for a few minutes before the addition of the coupling reagent, HATU (0.50 g, 0.11 M). The resultant mixture was added to the resin and stirred by bubbling nitrogen for 45 minutes. The solvent was removed and the coupled second *N*-methylated phenylalanine was deprotected by adding 20% piperidine in DMF (20 mL) and bubbling with nitrogen twice for 5 minutes. The resin was washed with DCM (3 x 5 mL) followed by DMF (3 x 5 mL). The rest of the amino acids were coupled to yield the desired peptide following the general procedure C.

9.4.11 General procedure K: Monitoring of the reaction

Reagent A:

16.5 mg of KCN was dissolved in 25 mL of distilled water. 1.0 mL of this solution was diluted with 49 mL of pyridine (freshly distilled from ninhydrin). The solution was then poured into a small reagent bottle labelled “A”.

Reagent B:

1.0 g of ninhydrin was dissolved in 20 mL of *n*-butanol. The resulting solution was poured into a small reagent bottle labelled “B”.

Reagent C:

40 g of phenol was dissolved in 20 mL of *n*-butanol. The solution was poured into a small reagent bottle and labelled “C”.

Approximately fifteen beads of resin from the reaction mixture were transferred to a dry test tube and labelled ‘S’. No beads were added to another test tube, ‘R’ (reference). To each tube

was added 3 drops of Reagent A, 3 drops of Reagent B and 3 drops of Reagent C. Both test tubes were heated at 110°C for 5 minutes. Resulting colour in test tube 'S' was compared to the colour in reference tube. Different colours have different meaning. Colourless or faint blue colour: complete coupling (proceed with synthesis). Dark blue solution with colourless beads: nearly complete coupling (extend coupling). Light blue solution with dark blue beads: coupling incomplete (recouple). Intense blue solution with all blue beads: failed coupling (check amino acid, reagents, then recouple). Completion of coupling reactions of hydroxyproline was indicated by a less intense red brown colour.

9.4.12 General procedure L: Cleavage of the peptides from the resin

The resin attached to the peptide was then washed with DCM (3 x 5.0 mL) then DMF (3 x 5.0 mL) and dried under suction. A cleavage mixture was prepared by mixing 95:2.5:2.5 % (v/v) TFA: H_2O: TIS in a 50 mL tube. The dry resin was then transferred into the 50 mL centrifuge tube containing 20 mL of the cleavage mixture and was placed in a shaker for 3 hours. The resin was filtered and washed with 5 mL of the cleavage mixture. The filtrate was divided into two portions. This step was followed by the addition of 60 mL of cold diethyl ether (which caused the peptide to precipitate). The resulting mixture was centrifuged at 5000 rpm for 10 minutes, after which the supernatant was decanted off. The remaining white solid was washed twice more with the same amount of cold diethyl ether. The white precipitate was then dissolved in 10 mL (40/60; H_2O/DMSO) for further analysis and purification.

9.4.13 General procedure M: Purification of the peptides

Semi-preparative HPLC was carried out on an Agilent 1260 Infinity instrument equipped with a UV/VIS detector and an automated fraction collector. Purification was achieved via reverse phase chromatography. A Phenomenex Kinetex® XB-C18 column (5 µm B-C18, 100 Å, 250 mm × 230 nm x 21.2 mm) was used to separate the compounds with a flow rate of 15 mL/minute. For the mobile phase, a two-buffer system consisting of 0.1 % formic acid/H_2O (v/v) (Buffer A) and 0.1 % formic acid/acetonitrile (v/v) (Buffer B) was utilized. A flow rate of 15 mL/minute and UV wavelengths of 215 and 254 nm were utilized. The formic acid was used as an ion pairing agent. The peptide derivatives were eluted using a gradient method of 5 – 95 % Buffer B in 14 minutes, unless stated otherwise. Detection of the peptides also was performed at wavelengths 215 and 254 nm.

9.4.14 General procedure N: Removal of TFA from synthetic peptides using HCl

The peptide was dissolved in distilled water at 1 mg (weight) per 1 mL of solvent. (Phosphate buffer (50 mM phosphate and 100 mM NaCl) can be used instead of water). 100 mM acqueous HCl was added to the peptide solution for a final HCl concentration between 2 mM and 10 mM. HCl concentration below 2 mM or higher than 10 mM may result in incomplete TFA exchange or modified peptides. The solution was allowed to stand at room temperature for at least a minute. The solution was frozen in liquid nitrogen and then lyophilized overnight to remove all liquid. The peptide was re-dissolved in an HCl solution, frozen again and then lyophilized overnight. The latter steps were repeated at least two times. After final lyophilization step the peptide was stored in the fridge at 4 °C in a tightly sealed glass container.

9.4.15 General procedure O: Synthesis of oxazolidinone

The Fmoc amino acid (1.94 g, 0.05 M), paraformaldehyde (1 g, 0.3 M) and *p*-toluenesulfonic acid (0.1 g, 0.006 M) were suspended in toluene (100 mL). The mixture was refluxed in a Dean-Stark setup until no more starting material could be detected by TLC (97.5:2:0.2-$CHCl_3$: MeOH: AcOH). The solution was cooled, washed with saturated acqueous $NaHCO_3$ and dried over anhydrous $MgSO_4$. Concentration under vacuum gave the crude product which in most cases solidified upon standing.

9.4.16 General procedure P: Synthesis of *N*-methylated amino acids

To a solution of Fmoc- protected oxazolidinone, (1 equiv.) and anhydrous $AlCl_3$ (2 equiv.) in dry DCM (20 mL/1 mmol oxazolidinone) was added triethylsiliane (TES) (2 equiv.). The reaction was stirred at ambient temperature until TLC (1:3 ethyl acetate/hexane) showed the absence of starting material. An additional amount of DCM (20 mL) was added, and the organic phase was washed with 1 M HCl. The organic phase was dried over anhydrous magnesium sulphate and concentrated *in vacuo*. The crude product was purified via column chromatography on silica gel with (1:19, MeOH: DCM).

9.5 SUMMARY OF SYNTHESIZED COMPOUNDS

9.5.1 *Retro*-DGRGOF-Palmitate

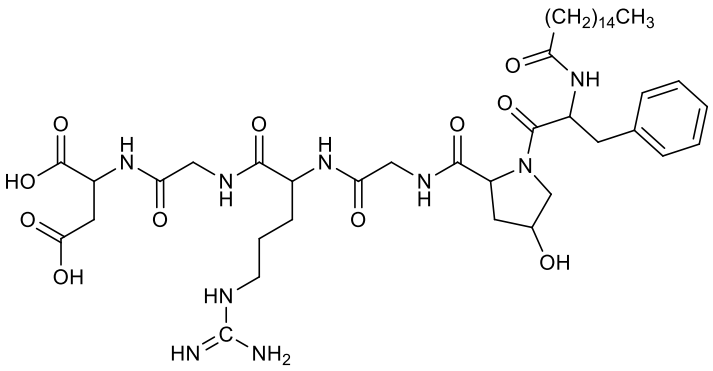

Figure 9.1: *retro*-DGRGOF-Palmitate peptide.

UHPLC (Thermo Scientific Dionex Ultimate 3000) Peak 9.61 minutes

HRMS (ESI) (Bruker Compact Q-TOF): Calculated for $C_{44}H_{71}N_9O_{11}$ = 901.5273; found 902.5413 ($[M + H]^+$).

9.5.2 *Retro*-DGRGOF-Adamantate

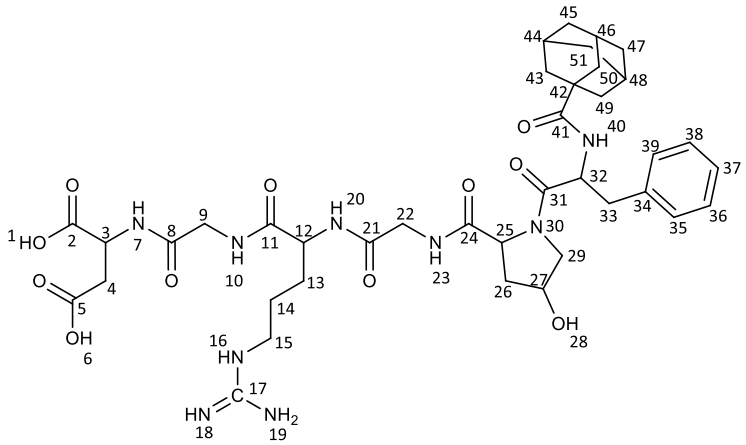

Figure 9.2: *Retro*-DGRGOF-Adamantate peptide.

UHPLC (Thermo Scientific Dionex Ultimate 3000) Peak 5.79 minutes

HRMS (ESI) (Bruker Compact Q-TOF): Calculated for $C_{39}H_{55}N_9O_{11}$ = 825.4021; found 826.4111 ($[M + H]^+$).

^{1}H NMR (400 MHz, DMSO) δ_H = 8.97 (1H, *b s*, guanidyl), 8.53 (1H, *s*, NH amide), 8.30 (1H, *s*, NH amide), 8.18 (1H, *s*, NH amide), 7.92 (2H, *d*, NH amide, *J* = 6 Hz), 7.28 (1H, *d*, guanidyl, *J* = 3 Hz), 7.24 (5H, *s*, benzene *o, m, p* H), 7.17 – 7.19 (2H, *m*, guanidyl NH_2), 4.67 – 4.69 (1H, *m*, H^α Asp), 4.38 – 4.40 (1H, *m*, H^α), 4.34 – 4.36 (1H, *m*, H^α), 4.29 – 4.31 (1H, *m*, H^α), 4.19 – 4.21 (1H, *m*, H^α), 3.89 – 3.91 (1H, m, H^α), 3.74 (2H, H^α, *d*, *J* = 3 Hz), 3.60 - 3.62 (3H, *m*, H), 3.52 – 3.53 (4H, *m*, H), 3.11 – 3.12 (1H, *m*, H), 2.97 – 2.99 (3H, *m*, H), 2.85 – 2.87 (2H, *m*, H), 2.39 – 2.41 (2H, *m*, H), 2.01 – 2.03 (2H, *m*, H), 1.90 (2H, *s*, H), 1.31 – 1.62 (15H, *m*, adamantane)

^{13}C NMR (400 MHz, DMSO) δ_C = 176.20 (C = O), 173.40 (C = O), 173.29 (C = O), 171.83 (C = O), 171.63 (C = O), 170.21 (C = O), 168.69 (C = O), 163.44 (C = O), 157.01 (C = N, guanidyl), 137.63 (ArC), 129.54 (ArC), 127.88 (ArC), 126.20 (ArC), 68.81 (HO-*C*-H), 58.93 (C^α), 54.85 (C^α), 52.09 (C^α), 51.61 (C^α), 48.90 (C^α), 42.00 (C^α), 40.57 (C^α), 39.50 (C^β), 38.45 (C^β), 37.48 (C^β), 36.32 (C^β), 36.02 (C^β), 29.79 (C^γ), 27.57 (C^γ), 24.59 (C^γ)

9.5.3 *Retro*-GOP-GFOGER-GOP-Palmitate

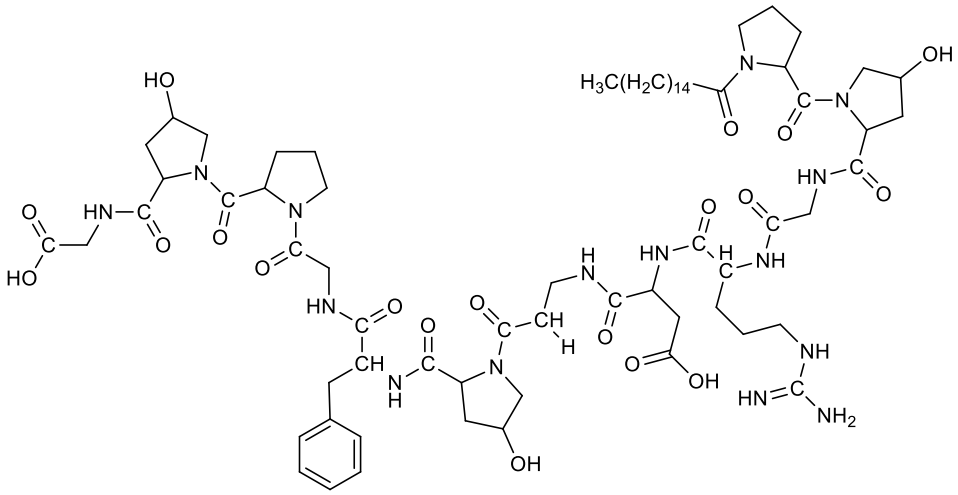

Figure 9.3: *Retro*-GOP-GFOGER-GOP-Palmitate.

UHPLC (Thermo Scientific Dionex Ultimate 3000) Peak 8.20 minutes

HRMS (ESI) (Bruker Compact Q-TOF): Calculated for $C_{69}H_{107}N_{15}O_{19}$ = 1449.7868; found 1451.7978 ($[M + H]^+$).

9.5.4 *Retro*-GOP-GFOGER-GOP-Adamantane

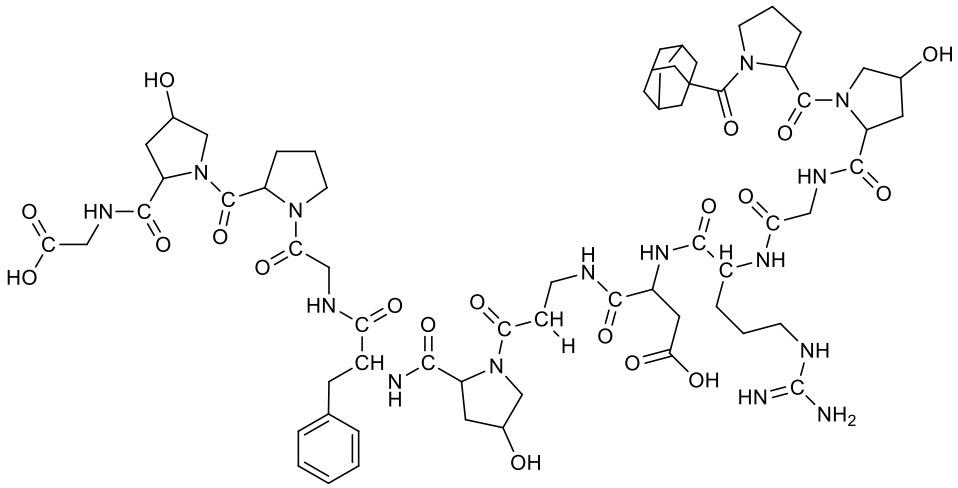

Figure 9.4: *Retro*-GOP-GFOGER-GOP-Adamantate.

UHPLC (Thermo Scientific Dionex Ultimate 3000) Peak 8.29 minutes

HRMS (ESI) (Bruker Compact Q-TOF): Calculated for $C_{64}H_{91}N_{15}O_{19}$ = 1143.6367; found 1144.6346 ($[M + H]^+$).

9.5.5 *Retro*-GG-GFOGER-GG-Palmitate

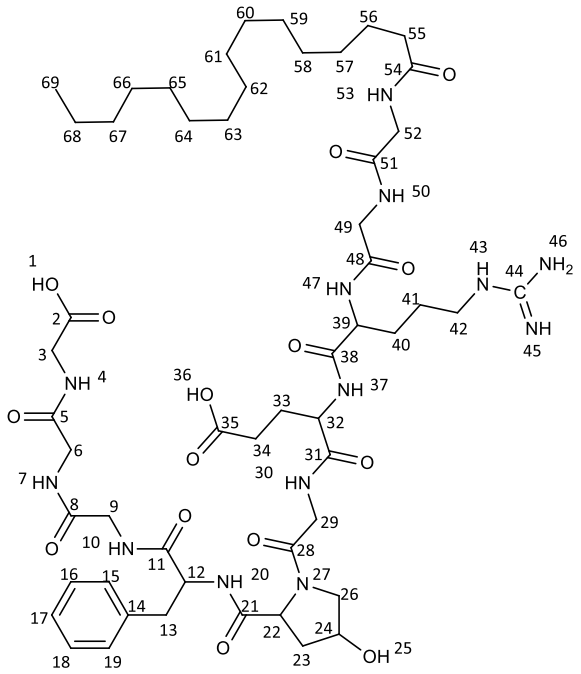

Figure 9.5: *Retro*-GG-GFOGER-GG-Palmitate.

UHPLC (Thermo Scientific Dionex Ultimate 3000) Peak 8.33 minutes

HRMS (ESI) (Bruker Compact Q-TOF): Calculated for $C_{53}H_{85}N_{13}O_{15}$ = 1430.7042; found 1431.7201 ($[M + H]^+$).

9.5.6 *Retro*-GG-GFOGER-GG-Adamantane

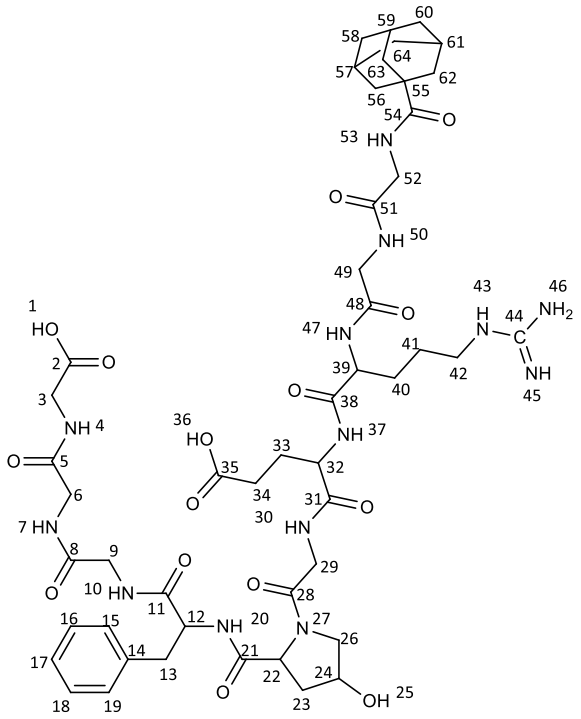

Figure 9.6: *Retro*-GG-GFOGER-GG-Adamantate.

UHPLC (Thermo Scientific Dionex Ultimate 3000) Peak 6.42 minutes

HRMS (ESI) (Bruker Compact Q-TOF): Calculated for $C_{48}H_{69}N_{13}O_{15}$ = 1760.9421; found 881.4604 ($[M + 2H]^{2+}$).

^{1}H NMR (400 MHz, DMSO) δ_H = 8.97 (1H, *m*, guanidyl), 8.55 (4H, *m*, NH amide), 8.53 (1H, *m*, NH amide), 8.30 (1H, *m*, NH amide), 7.96 (1H, *m*, NH amide), 7.91 (1H, *m*, NH amide), 7.29 (1H, *m*, NH amide), 7.26 (1H, *m*, ArH), 7.19 (1H, *m*, ArH), 7.12 (1H, *m*, ArH), 4.69 (1H, *m*, H^{α}), 4.39 (2H, *m*, H^{α}), 4.31 (1H, *m*, H^{α}), 4.20 (1H, *m*, H^{α}), 3.89 (3H, *m*, H^{α}), 3.73 (1H, *m*, H^{α}), 3.61 (1H, *m*, H^{α}), 3.52 (2H, *m*, H^{α}), 3.00 (1H, *m*, H^{α}), 2.96 (1H, *m*, H^{α}), 2.85 (1H, *m*, H^{α}), 2.56 (1H, *m*, H^{α}), 2.44 (1H, *m*, H^{α}), 1.92 (1H, *m*, H^{α}), 1.91 (1H, *m*, H^{α}), 1.51 (1H, *m*, H^{β}), 1.60 (15H, *m*, adamantane)

^{13}C NMR (400 MHz, DMSO) δ_C = 176.66 (C = O), 176.50 (C = O), 172.41 (C = O), 172.18 (C = O), (C = O), 170.56 (C = O), 169.12 (C = O), 168.98 (C = O), 163.96 (C = O), 157.01 (C = NH), 137.57 (ArC), 129.49 (ArC), 127.84 (ArC), 126.15 (ArC), 69.28 (OH-C-H), 69.26 (C^{α}), 59.46 (C^{β} Hyp), 59.42 (C^{α}), 55.35 (C^{α}), 55.28 (C^{α}), 52.68 (C^{α}), 52.13 (C^{α}), 49.32 (C^{α}), 49.61 (C^{α}), 42.54 (C^{α}), 42.45

(C^{α}), 42.38 (C^{α}), 40.16 (C^{α}), 38.94 (C-Aliphatic), 38.90 (C-Aliphatic), 38.80 (C-Aliphatic), 38.03 (C-Aliphatic), 36.85 (C-Aliphatic), 36.51 (C-Aliphatic), 36.50 (C-Aliphatic), 30.27 (C-Aliphatic), 29.16 (C-Aliphatic), 28.03 (C-Aliphatic)

Table 9.1: Characterization table of *retro*-GG-GFOGER-GG-Adamantane.

No.	δ ^{1}H	δ ^{13}C	δ COSY	δ HSQC	δ HMBC
1	11	-	-	-	-
2	-	172.18	-	-	3.89, 172.18
3	3.89	42.45	3.89, 8.55	3.89, 42.45	3.89, 172.18
4	8.53		8.53, 3.89	-	8.53, 172.13
5	-	172.18	-	-	-
6	3.52	55.28	3.52, 8.55	3.52, 55.28	3.52, 172.18
7	8.55	-	8.55, 3.52	-	8.55, 172.18
8	-	172.18	-	-	3.89, 172.18
9	3.89	42.45	3.89, 8.55	3.89, 42.45	3.89, 172.18
10	8.55	-	8.55, 3.89	-	8.55, 172.18
11	-	170.56	-	-	2.85, 170.79 2.96, 170.64
12	4.69	52.13	(2.86, 4.69), (4.69, 7.29)	4.69, 52.13	4.69, 170.56
13	2.85, 2.96	36.85	2.85, 4.69	2.85, 36.85	(2.85, 138.21), (2.85 & 2.96, 169.12)
14	-	137.57	-	-	2.85, 138.21
15	7.14	127.84	7.14, 7.27	7.14, 126.71	7.14, 126.71, 36.92, 138.11
16	7.27	129.49	7.27, 7.17	7.27, 129.39	-
17	7.17	126.15	7.17, 7.27	7.17, 128.86	-
18	7.27	129.49	7.27, 7.17	7.27, 129.39	-
19	7.14	127.84	7.14, 7.27	7.14, 126.71	7.14, 126.71, 36,85, 138.11
20	7.29	-	7.29, 4.69	-	7.29, 170.56
21	-	172.41	-	-	1.97, 172.40
22	4.39	69.26	4.36, 1.97	4.36, 69.29	4.39, 172.41
23	1.97 1.92	38.03	1.97, 4.36	1.97, 38.03	1.92, 172.40
24	4.39	69.28	4.39, 3.56 4.39, 1.97	4.39, 69.25	4.39, 69.26
25	3.52	-	-	-	3.52, 69.23
26	3.56 3.90	42.54	3.56, 4.39	3.56, 42.54	3.52, 172.29
27	-	-	-	-	-
28	-	168.98	-	-	3.74, 168.98
29	3.73	42.38	3.73, 8.30	3.73, 42.38	3.73, 168.98
30	8.30	-	8.30, 3.73	-	-
31		163.96	-	-	4.20, 165.97
32	4.20	49.32	4.20, 2.53	4.20, 49.32	4.20, 163.96
33	2.53 2.44	40.16	2.53, 4.20	2.53, 40.16	2.53, 49.32
34	1.66 2.02	38.80	2.37, 2.52	2.37, 38.80	2.02, 40.16

No.	δ ^{1}H	δ ^{13}C	δ COSY	δ HSQC	δ HMBC
35		176.66			2.38, 176.66
36	11.0	-	-	-	-
37	7.96	-	7.96, 4.20	-	7.96, 49.32
38		169.12	-	-	4.31, 169.12
39	4.31	52.68	4.31, 1.62	4.31, 52.68	4.31, 169.12
40	1.89 1.97	28.03	1.89, 4.31 1.62, 4.31	1.89, 52.68	1.92, 169.12
41	1.51 1.62	59.42	1.51, 1.89	1.51, 59.42	1.51, 28.03
42	3.00 3.13	55.35	3.02, 1.51	3.02, 55.35	3.02, 59.42
43	8.97	-	8.97, 3.02	-	8.97, 55.35
44	8.56		-		
45		157.01	-	8.53, 172.18	
46	8.56		-		
47	7.91	-	7.91, 4.31	-	7.91, 52.68
48	-	172.18	-	-	8.55, 172.18
49	3.89	42.45	3.89, 8.55	3.89, 42.45	3.89, 172.18
50	8.55	-	8.55, 3.89	-	8.55, 42.45
51		172.18			
52	3.52	55.28	3.52, 8.55	3.52, 55.28	3.52, 172.18
53	8.55	-	8.53, 3.89		8.53, 172.13, 59.46
54	-	176.50	-	-	-
55	-	59.46	-	-	-
56	1.60	38.90	1.60, 4.31	1.60, 38.92	1.60, 176.78
57	1.63	30.27	1.63, 3.02	1.63, 30.27	-
58	1.53	36.51	1.53, 3.02	1.56, 36.53	-
59	1.63	30.27	1.63, 3.02	-	-
60	1.63	36.49	1.53, 3.02	-	-
61	1.63	30.27	1.63, 3.02	-	-
62	1.67	38.94	1.67, 4.31	-	1.67, 176.78
63	1.63	36.50	1.53, 3.02	-	
64	1.67	38.94	1.67, 4.31	-	1.67, 176.78

9.5.7 *Retro*-DGD-GG-GFOGER-GG-Palmitate

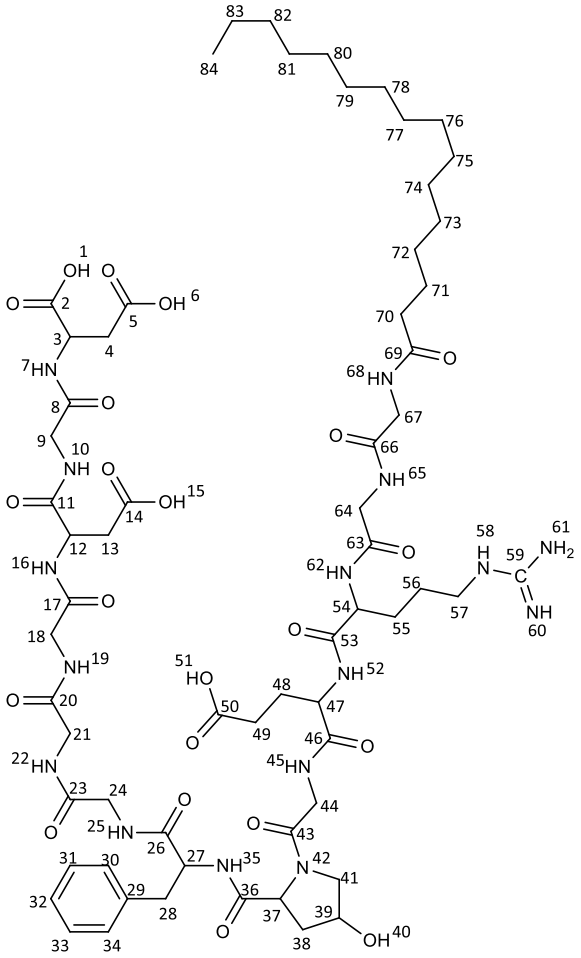

Figure 9.7: *Retro*-DGD-GG-GFOGER-GG-Palmitate.

UHPLC (Thermo Scientific Dionex Ultimate 3000) Peak 8.33 minutes

HRMS (ESI) (Bruker Compact Q-TOF): Calculated for $C_{63}H_{98}N_{16}O_{22}$ = 1430.7042; found 1431.7201 ($[M + H]^+$).

9.5.8 *Retro*-DGD-GG-GFOGER-GG-Adamantane

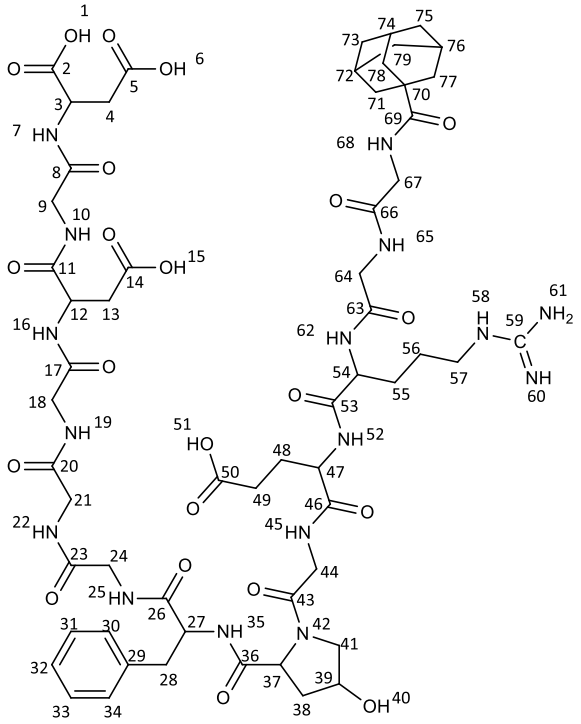

Figure 9.8: *Retro*-DGD-GG-GFOGER-GG-Adamantate.

UHPLC (Thermo Scientific Dionex Ultimate 3000) Peak 4.91 minutes

HRMS (ESI) (Bruker Compact Q-TOF): Calculated for $C_{58}H_{82}N_{16}O_{22}$ = 1354.5790; found 1355.5960 ([M + H^+]).

^{1}H NMR (400 MHz, DMSO) δ_H = 8.66 (1H, *m*, NH amide), 8.53 (1H, *m*, NH amide), 8.27 (1H, *m*, NH amide), 8.26 (1H, *m*, NH amide), 8.25 (2H, *m*, NH amide), 8.09 (1H, *m*, NH amide), 8.08 (2H, *m*, NH amide), 8.01 (2H, *m*, NH amide), 7.94 (1H, *m*, NH amide), 7.78 (1H, *m*, NH amide), 7.26 (1H, *m*, ArH), 7.19 (1H, *m*, ArH), 7.14 (1H, *m*, ArH), 4.72 (1H, *m*, H^{α} Phe), 4.65 (1H, *m*, H^{α} Asp), 4.64 (1H, *m*, H^{α} Asp), 4.58 (1H, *m*, H^{α} Gly), 4.44 (1H, *m*, H^{α} Hyp), 4.41 (1H, *m*, H^{α} Gly), 4.33 (1H, *m*, H^{α} Arg), 4.30 (1H, *m*, H^{α} Gly), 4.24 (1H, *m*, H^{α} Hyp), 4.02 (1H, *m*, H^{α} Gly), 3.78 (1H, *m*, H^{α} Gly), 3.71 (1H, *m*, H^{α} Gly), 3.67 (1H, *m*, H^{α} Gly), 3.60 (1H, *m*, H^{α} Hyp), 3.59 (1H, *m*, H^{α} Glu), 3.34 (1H, *m*, H^{β} Glu), 3.10 (2H, *m*, H^{β} Asp), 3.10 (1H, *m*, H^{β} Asp), 3.09 (1H, *m*, H^{β} Arg), 2.87 (1H, *m*, H^{β} Glu), 2.79 (1H, *m*, H^{β} Phe), 1.91 (1H, *m*, H^{γ} Hyp), 1.86 (1H, *m*, H^{γ} Hyp), 1.65 (2H, *m*, Adamantane), 1.63 (3H, *m*, Adamantane), 1.62 (3H, *m*, Adamantane), 1.59 (2H, *m*, Adamantane), 1.57 (2H, *m*, Adamantane), 1.51 (2H, *m*, H^{β} Arg)

^{13}C NMR (400 MHz, DMSO) δ_C = 174.78 (C = O), 173.86 (C = O), 172.92 (C = O), 172.62 (C = O), 172.05 (C = O), 171.79 (C = O), 171.76 (C = O), 171.53 (C = O), 170.99 (C = O), 170.51 (C = O), 169.62 (C = O), 169.35 (C = O), 169.19 (C = O), 168.41 (C = O), 163.90 (*C* = NH), 129.61 (ArC), 128.50 (ArC), 129.50 (ArC), 69.02 (OH-*C*-H), 66.99 (C^{α}), 66.38 (C^{β} Hyp), 56.50 (C^{α}), 52.79 (C^{α}), 52.45 (C^{α}), 42.53 (C^{α}), 36.60 (C^{β}), 30.80 (C^{β}), 31.01 (C^{β}), 29.60 (C-Aliphatic), 28.10 (C-Aliphatic), 27.06 (C-Aliphatic), 22.83 (C-Aliphatic), 20.07 (C-Aliphatic), 19.81 (C-Aliphatic), 19.01 (C-Aliphatic), 15.63 (C-Aliphatic)

Table 9.2: Characterization table of *retro*-DGD-GG-GFOGER-GG-Adamantane.

No.	δ ^{1}H	δ ^{13}C	δ COSY	δ HSQC	δ HMBC
1	11	-	-	-	-
2	-	54.30	-	54.30, 4.64	54.30, 8.66
3	4.64	54.30	4.64, 8.66	4.64, 54.30	4.64, 162.49
4	3.10	37.40	3.10, 4.65	3.10, 37.40	3.10, 165.43
5					165.43, 3.10
6	11	-	-	-	-
7	8.66	-	8.66, 4.64	-	8.66, 169.98
8					166.56, 4.41
9	4.41	58.01	4.41, 8.58	4.41, 58.01	4.41, 166.56
10	8.53	-	8.53, 4.41	-	8.53, 166.23
11					175.64, 4.65
12	4.65	54.30	4.65, 3.10	4.65, 54.30	4.64, 162.49
13	3.10	37.40	3.10, 4.65	3.1037.40	3.10, 165.43
14					165.43, 3.10
15	11	-	-	-	-
16	8.27	-	8.27, 4.65	-	8.26, 169.28
17					169.58, 3.78
18	3.78	42.39	3.78, 8.26	3.78, 42.39	3.78, 169.42
19	8.26	-	8.26, 3.78	-	8.26, 169.28

No.	δ ^{1}H	δ ^{13}C	δ COSY	δ HSQC	δ HMBC
20					169.66, 3.71
21	3.71	54.30	3.71, 8.09	3.71, 54.30	3.71, 169.42
22	8.09	-	8.09, 3.71	-	8.09, 169.02
23					172.69, 4.58
24	4.58	49.66	4.58, 8.08	4.58, 49.66	4.58, 171.82
25	8.08	-	8.08, 4.58	-	8.08, 171.29
26					165.18, 4.76
27	4.76	60.00	4.76, 3.10	4.65, 60.00	4.76, 165.18
28	3.10 2.86	36.57	3.10, 4.65	3.10, 36.57	2.82, 168.47
29	-	138.51	-	-	138.51, 7.26
30	7.14	126.66	7.14, 7.26	7.14, 126.15	7.14, 138.51
31	7.26	129.66	7.26, 7.14	7.26, 129.45	7.26, 138.51
32	7.18	128.50	7.18, 7.26	7.18, 127.84	7.18, 138.51
33	7.26	129.66	7.26, 7.14	7.26, 129.45	7.26, 138.51
34	7.14	126.66	7.14, 7.26	7.14, 126.15	7.26, 138.51
35	8.03	-	8.03, 4.72	-	8.05, 171.60
36					168.65, 4.17
37	4.17	67.35	4.17, 1.89	4.17, 67.35	4.17, 168.65
38	1.85	38.03	1.85, 4.24	1.85, 38.03	1.85, 172.40
39	4.24	69.00	4.24, 3.60	4.24, 69.00	4.24, 33.73
40	3.54				3.54, 69.38
41	3.60	54.33	3.60, 4.24	3.60, 54.33	3.61, 69.95
42	-	-	-	-	-
43	-		-	-	171.79, 4.17
44	4.30	59.23	4.30, 8.25	4.30, 59.23	4.30, 171.79
45	8.25	-	8.25, 4.30	-	8.25, 169.28-
46	-	-	-	-	168.68, 3.59

No.	δ ^{1}H	δ ^{13}C	δ COSY	δ HSQC	δ HMBC
47	3.59	54.47	3.59, 7.78	3.59, 54.47	3.59, 168.68
48	2.43	37.32	2.43, 3.59	2.43, 37.32	2.43, 54.39
49	3.34	54.48	3.34, 2.87	3.34, 54.48	3.35, 37.56
50	-	-	-	-	170.75, 3.32
51	11	-	-	-	-
52	7.79	-	7.79, 3.59	-	7.79, 168.53-
53	-	-	-	-	171.91, 4.33-
54	4.33	52.34	4.33, 8.01	4.33, 52.34	4.33, 171.91
55	1.91 1.97	37.92	1.91, 4.33	1.91, 37.92	1.95, 28.25
56	1.51 1.62	29.25	1.51, 1.91	1.51, 29.25	1.55, 36.75
57	3.09	40.77	3.09, 7.54	3.09, 40.77	3.09, 28.25
58	7.54		7.54, 3.09		7.56, 158.20
59	-	157.31	-	-	-
60	-	-	-	-	-
61	-	-	-	-	-
62	8.01	-	8.01, 4.33	-	8.01, 169.33
63					165.75, 4.01
64	4.01 3.84	42.02	4.02, 8.00	4.01, 42.02	4.01, 165.75
65	8.01	-	8.01, 4.04	-	8.01, 169.33
66					170.22, 3.67
67	3.67	49.08	4.53, 8.48	4.53, 49.08	4.55, 172.97
68	7.94	-	7.94, 3.67	-	7.94, 170.19
69					176.78, 1.60
70		36.33	-	-	36.33, 1.60
71	1.60	38.90	1.60, 4.31	1.60, 38.92	1.60, 176.78
72	1.63	30.27	1.63, 3.02	1.63, 30.27	1.63, 39.11

No.	δ ^{1}H	δ ^{13}C	δ COSY	δ HSQC	δ HMBC
73	1.53	36.51	1.53, 3.02	1.56, 36.53	1.53, 36.72

9.5.9 *Retro*-DGD-GG-GFOGER-GG-TTK-Palmitate

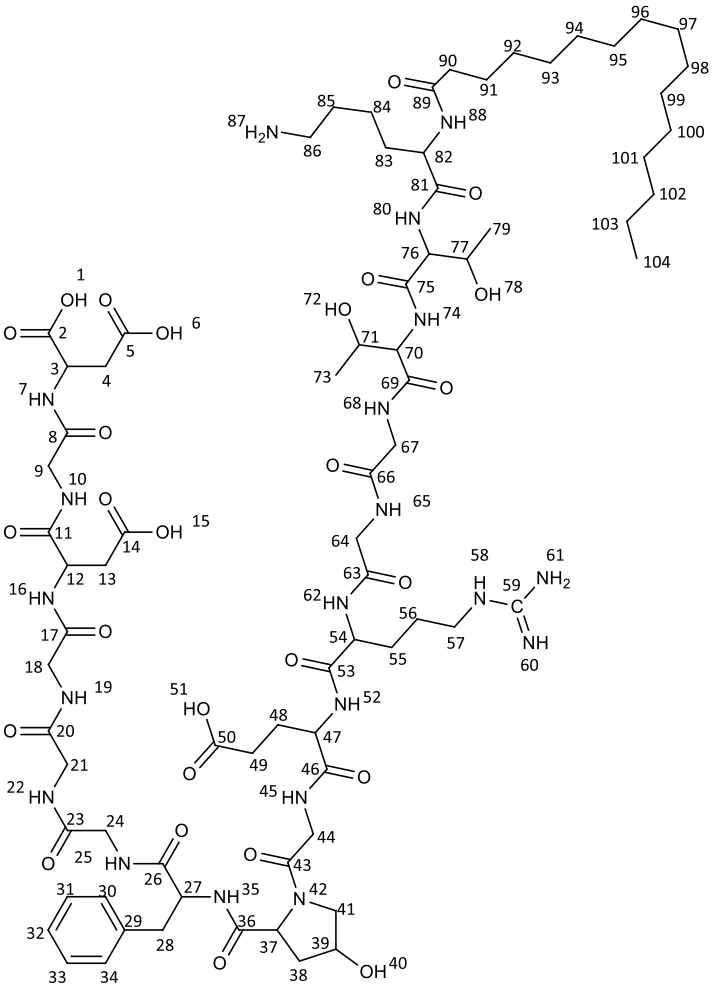

Figure 9.9: *Retro*-DGD-GG-GFOGER-GG-TTK-Palmitate.

UHPLC (Thermo Scientific Dionex Ultimate 3000) Peak 6.42 minutes

HRMS (ESI) (Bruker Compact Q-TOF): Calculated for $C_{77}H_{124}N_{20}O_{27}$ = 1760.8945; found 881.4604 ($[M + 2H]^{2+}$).

^{1}H NMR (400 MHz, DMSO) δ_H = 8.66 (1H, *m*, NH amide), 8.35 (1H, *m*, NH amide), 8.27 (1H, *m*, NH amide), 8.18 (1H, *m*, NH amide), 8.16 (1H, *m*, NH amide), 8.17 (1H, *m*, NH amide), 7.79

(1H, *m*, NH amide), 7.73 (1H, *m*, NH amide), 8.02 (1H, *m*, NH amide), 7.79 (1H, *m*, NH amide), 7.82 (1H, *m*, NH amide), 8.22 (1H, *m*, NH amide), 8.22 (1H, *m*, NH amide), 7.98 (1H, *m*, NH amide), 7.14 (1H, *m*, ArH), 7.27 (1H, *m*, ArH), 7.17 (1H, *m*, ArH), 7.27 (1H, *m*, ArH), 7.14 (1H, *m*, ArH), 4.63 (1H, *m*, H^{α} Asp), 4.33 (1H, *m*, H^{α} Gly), 4.55 (1H, *m*, H^{α} Asp), 3.73 (1H, *m*, H^{α} Gly), 3.70 (1H, *m*, H^{α} Gly), 4.58 (1H, *m*, H^{α} Gly), 4.74 (1H, *m*, H^{α} Phe), 4.36 (1H, *m*, H^{α} Hyp), 4.16 (1H, *m*, H^{α} Gly), 4.25 (1H, m, H^{α} Glu), 4.36 (1H, m, H^{α} Arg), 4.17 (1H, *m*, H^{α} Gly), 3.59 (1H, *m*, H^{α} Gly), 3.75 (2H, *m*, H^{α} Thr), 4.29 (1H, m, H^{α} Lys), 2.83 (1H, m, H^{β} Asp), 2.56 (1H, *m*, H^{β} Glu), 2.85 (1H, *m*, H^{β} Phe), 1.90 (1H, *m*, H^{β} Hyp), 4.23 (1H, m, H^{γ} Hyp), 3.65 (1H, m, H^{γ} Hyp), 2.56, 2.37 (2H, m, H^{β} Glu), 3.05 (1H, m, H^{γ} Hyp), 1.89, 1.97 (1H, *m*, H^{β} Arg), 1.51, 1.62 (1H, *m*, H^{γ} Arg), 3.00, 3.13 (1H, *m*, H^{δ} Arg), 8.97 (1H, m, NH guanidyl), 8.56 (), 4.08 (1H, *m*, H^{β} Thr), 5.41 (1H, m, OH), 1.08 (1H, *m*, H^{β} Thr), 4.08 (1H, *m*, H^{β} Thr), 5.41 (1H, m, OH), 1.08 (1H, *m*, H^{β} Thr), 1.88 (1H, *m*, H^{β} Lys), 1.57 (1H, *m*, H^{γ} Lys), 1.73 (1H, *m*, H^{δ} Lys), 2.27 (1H, *m*, H^{ε}Lys)

^{13}C NMR (400 MHz, DMSO) δ_C = 172.65 (C = O), 171.82 (C = O), 170.62 (C = O), 169.66 (C = O), 169.33 (C = O), 164.33 (C = O), 138.69 (C = NH), 129.60 (ArC), 128.50 (ArC), 129.50 (ArC), 73.06 (OH-C-H), 69.00 (C^{α}), 65.38 (C^{β} Hyp), 58.58 (C^{α}), 56.50 (C^{α}), 54.54 (C^{α}), 54.46 (C^{α}), 52.67 (C^{α}), 50.29 (C^{α}), 49.61 (C^{α}), 42.62 (C^{α}), 42.56 (C^{α}), 41.96 (C^{α}), 39.14 (C-Aliphatic), 35.61 (C-Aliphatic), 31.75 (C-Aliphatic), 31.15 (C-Aliphatic), 29.47 (C-Aliphatic), 29.43 (C-Aliphatic), 29.29 (C-Aliphatic), 29.16 (C-Aliphatic), 27.14 (C-Aliphatic), 25.77 (C-Aliphatic), 22.71 (C-Aliphatic), 22.56 (C-Aliphatic), 20.02 (C-Aliphatic), 19.01 (C-Aliphatic), 15.63 (C-Aliphatic), 14.42 (C-Aliphatic)

Table 9.3: Characterization table of *retro*-DGD-GG-GFOGER-GG-TTK-Palmitate.

No.	δ ^{1}H	δ ^{13}C	δ COSY	δ HSQC	δ HMBC
1	11.0	-	-	-	-
2	-	-	-	-	177.47, 4.63
3	4.63	54.27	4.63, 8.66	4.63, 54.27	4.63, 42.51
4	2.83	42.44	2.83, 4.63	2.83, 42.44	2.83, 54.24
5	-	-	-	-	165.03, 2.83
6	11.0	-	-	-	-
7	8.66	-	8.66, 4.63	-	8.65, 165.02,
8	-				179.30, 4.33
9	4.33	54.91	4.33, 8.35	4.33, 54.91	4.32, 179.30
10	8.35		8.35, 4.33	-	8.35, 178.65
11	-				165.01, 4.55
12	4.55	54.35	4.55, 8.27	4.55, 54.35	4.55, 42.51
13	2.56	42.44	2.56, 4.55	2.56, 42.44	2.56, 54.35
14	-	-	-	-	164.43, 2.56-
15	11.0	-	-	-	-
16	8.27	-	8.27, 4.55	-	8.26, 171.26
17	-	-	-	-	169.89, 3.73-
18	3.73	42.52	3.73, 8.36	3.72, 42.52	3.74, 54.54
19	8.18	-	8.18, 3.74	-	8.18, 169.43
20	-	-	-	-	169.71, 3.70-
21	3.70	52.92	3.70, 8.14	3.70, 52.92	3.69, 51.78
22	8.16	-	8.16, 3.70	-	8.16, 169.36
23	-	-	-	-	166.74, 4.58-
24	4.58	42.52	4.58, 8.14	4.58, 42.45	4.59, 43.57
25	8.17	-	8.15, 4.59	-	8.15, 177.49
26	-	-	-	-	180.27, 4.74-
27	4.74	52.13	4.74, 8.37	4.74, 52.13	4.73, 57.47
28	2.85	38.25	2.85, 4.74	2.85, 38.25	2.85, 179.66
29	-	138.19	-	-	138.19, 7.19
30	7.14	127.84	7.14, 7.27	7.14, 126.71	7.14, 129.66 36.92, 138.11
31	7.27	129.49	7.27, 7.17	7.27, 129.39	7.27,

No.	δ ^{1}H	δ ^{13}C	δ COSY	δ HSQC	δ HMBC
32	7.17	126.15	7.17, 7.27	7.17, 128.86	7.17,
33	7.27	129.49	7.27, 7.17	7.27, 129.39	7.27,
34	7.14	127.84	7.14, 7.27	7.14, 126.71	7.14, 126.71 36,85, 138.11
35	8.14	-	8.14, 4.74	-	8.14, 171.16
36	-				166.92, 4.36
37	4.36	68.22	4.36, 1.88	4.36, 68.22	4.36, 58.39
38	1.90	37.82	1.90, 4.22	1.90, 37.82	2.04, 172.81
39	4.23	69.02	4.22, 1.90	4.23, 69.02	4.23, 37.51
40	3.64	-	-	-	
41	3.65	54.71	3.60, 4.38	3.65, 54.71	3.68, 169.16
42	No N**H**-	-	-	-	
43	-				172.53, 4.16
44	4.16	43.78	4.17, 7.80	4.17, 42.38	4.17, 170.73
45	7.79	-	7.79, 4.17	-	7.79, 171.94
46					171.59, 4.25
47	4.25	49.32	4.25, 7.86	4.25, 49.32	4.24, 57.72
48	2.56, 2.37	37.92	2.56, 4.25	2.56, 37.92	2.56, 39.53
49	3.05, 2.02	40.68	3.05, 2.56	3.05, 40.68	2.04, 172.81
50	-	-	-	-	177.92, 3.05-
51	11.0	-	-	-	
52	7.73	-	7.73, 4.33	-	7.73, 168.00
53	-	-	-	-	177.53, 4.36-
54	4.36	52.56	4.36, 8.02	4.36, 52.56	4.36, 177.53
55	1.89, 1.97	28.03	1.89, 4.31, 1.62, 4.31	1.89, 52.68	1.92, 169.12
56	1.51, 1.62	59.42	1.51, 1.89	1.51, 59.42	1.51, 28.03
57	3.00, 3.13	55.35	3.02, 1.51	3.02, 55.35	3.02, 59.42
58	8.97	-	8.97, 3.02	-	8.97, 55.35
59	8.56		-		
60		157.01	-	8.53, 172.18	
61	8.56		-		
62	8.02		8.02, 4.36		8.02,
63					172.28, 4.17

No.	δ ^{1}H	δ ^{13}C	δ COSY	δ HSQC	δ HMBC
64	4.17	43.78	4.17, 7.79	4.17, 43.78-	4.17, 172.28
65	7.79		7.79, 3.59	-	7.79,
66					172.94, 3.59
67	3.59	55.28	3.58, 7.82	3.59, 55.28	3.56, 50.22
68	7.82	-	7.82, 3.57	-	7.82,
69					169.86, 3.75
70	3.75	44.94	3.74, 8.22	3.75, 44.94	3.75, 169.86
71	4.08	66.91	4.05, 1.08	4.05, 66.91	4.08, 44.94
72	4.32				4.32, 66.57
73	1.08	19.90	1.08, 4.08	1.08, 19.90-	1.08, 66.91
74	8.22	-	8.22, 3.73		8.18, 169.43
75					169.86, 3.75
76	3.75	44.94	3.74, 8.22	3.75, 44.94	3.75, 169.86
77	4.08	66.91	4.05, 1.08	4.05, 66.91	4.08, 44.94
78	4.32				4.32, 66.57
79	1.08	19.90	1.08, 4.08	1.08, 19.90-	1.08, 66.91
80	8.22	-	8.22, 3.73		8.18, 169.43
81					172.94, 4.29
82	4.29	52.62-	4.29, 7.98	4.29, 52.62	4.28, 50.45
83	7.98		7.98, 4.29		7.98,172.94
84	1.88	37.91	1.88, 4.29	1.88, 37.91	1.88, 37.23
85	1.57	37.65	1.57, 1.88	1.57, 37.65	1.57, 36.64
86	1.73	29.14	1.73, 1.57	1.73, 29.14	1.73, 40.50
87	2.27	31.08	2.27, 1.73	2.27, 31.08	2.27, 25.33
88	-	-	-	-	-
89					172.31, 2.05
90	2.05	40.53	2.06, 1.53	2.05, 40.53	2.05, 27.50
91	1.53	27.01	1.53, 1.32	1.53, 27.01	1.53, 41.59
92	1.29	25.03	1.29, 1.24	1.29, 25.03	1.31, 28.00
93	1.23	29.35	1.23, 1.23	1.23, 29.35	1.23, 26.87
94	1.23	29.35	1.23, 1.23	1.23, 29.35	1.23, 26.87
95	1.23	29.35	1.23, 1.23	1.23, 29.35	1.23, 26.87
96	1.23	29.35	1.23, 1.23	1.23, 29.35	1.23, 26.87

No.	δ ^{1}H	δ ^{13}C	δ COSY	δ HSQC	δ HMBC
97	1.23	29.35	1.23, 1.23	1.23, 29.35	1.23, 26.87
98	1.23	29.35	1.23, 1.23	1.23, 29.35	1.23, 26.87
99	1.23	29.35	1.23, 1.23	1.23, 29.35	1.23, 26.87
100	1.23	29.35	1.23, 1.23	1.23, 29.35	1.23, 26.87
101	1.23	29.35	1.23, 1.23	1.23, 29.35	1.23, 26.87
102	1.09	15.57	1.09, 1.11	1.09, 15.5	1.09, 20.05
103	1.05	19.93	1.05, 0.88	1.05, 19.93	1.05, 29.25
104	0.88	14.31	0.88, 1.05	0.88, 14.31	0.88, 19.93

9.5.10 *Retro*-DGD-GG-GFOGER-GG-TTK-Adamantane

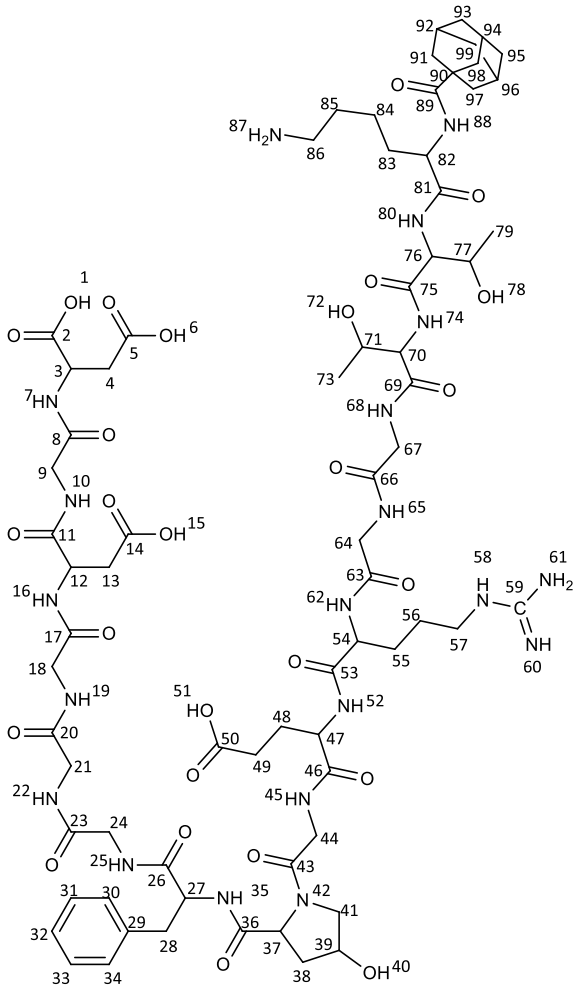

Figure 9.10: *Retro*-DGD-GG-GFOGER-GG-TTK-Adamantate.

UHPLC (Thermo Scientific Dionex Ultimate 3000) Peak 6.01 minutes

HRMS (ESI) (Bruker Compact Q-TOF): Calculated for $C_{72}H_{108}N_{20}O_{27}$ = 1684.7693; found 843.3929 ($[M + 2H]^{2+}$).

^{1}H NMR (400 MHz, DMSO) δ_H = 8.60 (1H, m, NH amide), 8.54 (1H, *m*, NH amide), 8.60 (1H, *m*, NH amide), 8.36 (1H, *m*, NH amide), 8.13 (1H, *m*, NH amide), 8.15 (1H, *m*, NH amide), 8.14 (1H, *m*, NH amide), 8.32 (1H, *m*, NH amide), 8.23 (1H, *m*, NH amide), 7.69 (2H, *m*, NH amide), 8.12 (1H, *m*, NH amide), 7.79 (1H, *m*, NH amide), 7.79 (1H, *m*, NH amide), 7.99 (1H, *m*, NH amide), 7.14 (2H, *m*, ArH), 7.27 (2H, *m*, ArH), 7.17 (1H, *m*, ArH), 4.63 (2H, *m*, H^{α} Asp), 4.41 (1H, *m*, H^{α} Gly), 3.80 (1H, *m*, H^{α} Gly), 3.77 (1H, *m*, H^{α} Gly), 4.54 (1H, *m*, H^{α} Gly), 4.66 (1H, *m*, H^{α} Phe), 4.43 (1H, *m*, H^{α} Hyp), 4.27 (1H, *m*, H^{α} Gly), 4.33 (1H, *m*, H^{α} Glu), 4.31 (1H, *m*, H^{α} Arg), 4.06 (1H, *m,* H^{α} Gly), 4.24 (1H, *m*, H^{α} Gly), 3.82 (2H, *m*, H^{α} Thr), 4.35 (1H, m, H^{α} Lys), 2.81 (2H, m, H^{β} Asp), 2.85 (1H, *m,* H^{β} Phe), 1.90 (1H, *m*, H^{β} Arg), 4.23 (1H, *m*, H^{γ} Hyp), 3.61 (1H, *m*, H^{δ} Hyp), 2.53 (1H, *m*, H^{β} Glu), 3.05 (1H, m, H^{γ} Glu), 1.89 (1H, m, H^{α} Arg), 1.51 (1H, *m*, H^{β} Arg), 3.00 (1H, *m*, H^{γ} Arg), 8.82 (1H, *m*, NH guanidyl), 4.04 (2H, *m*, $H^{\boldsymbol{\beta}}$ Thr), 4.32 (2H, m, OH Thr), 1.04 m, (2H, *m*, H^{γ} Thr), 1.88 (1H, *m*, H^{β}), 1.57 (1H, *m*, H^{γ}), 1.73 (1H, *m*, H^{δ}), 2.27 (1H, *m*, H^{ε})

^{13}C NMR (400 MHz, DMSO) δ_C = 174.78 (C = O), 172.72 (C = O), 172.67 (C = O), 172.05 (C = O), 171.80 (C = O), 170.99 (C = O), 170.51 (C = O), 169.35 (C = O), 169.19 (C = O), 168.41 (C = O), 163.90 (C = O), 129.61 (ArC), 128.50 (ArC), 69.02 (C^{α}), 66.99 (C^{α}), 65.38 (C^{α}), 56.50 (C^{α}), 52.80 (C^{α}), 52.45 (C^{α}), 42.53 (C^{β}), 40.88 (C^{β}), 39.18 (C - Aliphatic), 38.98 (C - Aliphatic), 36.56 (C - Aliphatic), 31.07 (C - Aliphatic), 30.80 (C - Aliphatic), 29.60 (C - Aliphatic), 28.10 (C - Aliphatic), 27.06 (C - Aliphatic), 22.83 (C - Aliphatic), 20.07 (C - Aliphatic), 19.80 (C - Aliphatic), 19.01 (C - Aliphatic), 15.63 (C - Aliphatic)

Table 9.4: *Retro*-DGD-GG-GFOGER-GG-TTK-Adamantane characterization table.

No.	δ ^{1}H	δ ^{13}C	δ COSY	δ HSQC	δ HMBC
1	11.0	-	-	-	-
2	-	-	-	-	165.63, 4.63-
3	4.63	54.22	4.63, 8.60	4.63, 54.22	4.63, 165.63
4	2.81	40.77	2.81, 4.63	2.81, 40.77	2.81,54.66
5	-	-	-	-	170.30, 2.83-
6	11.0	-	-	-	-
7	8.60	-	8.59, 4.63	-	8.56, 171.72
8	-				166.73, 4.41
9	4.41	54.47	4.41, 8.54	4.41, 54.47	4.41, 166.68
10	8.54		8.54, 4.41	-	8.54, 179.77
11	-				165.63, 4.63
12	4.63	54.22	4.63, 8.60	4.63, 54.22	4.63,135.63
13	2.81	40.77	4.63, 2.81	2.81, 40.77	2.81, 54.66
14	-	-	-	-	170.30, 2.83-
15	11.0	-	-	-	
16	8.60		8.60, 4.63	-	8.60, 171.15
17	-				171.97, 3.80
18	3.80	49.33	3.80, 8.36	3.80, 49.33	3.80, 171.97
19	8.36	-	8.36, 3.80	-	8.36, 163.90
20	-	-	-	-	169.85, 3.77-
21	3.77	44.91	3.77, 8.13	3.77, 44.91	3.77, 169.88
22	8.13	-	8.13, 3.77	-	8.13, 171.26
23	-	-	-	-	171.48, 4.54-
24	4.54	50.22	4.54, 8.15	4.54, 50.22	4.54, 171.36
25	8.15	-	8.15, 4.54	-	8.15, 177.49
26	-	-	-	-	171.34, 4.66-
27	4.66	58.53	4.66, 8.14	4.66, 58.64	4.66, 178.07
28	2.85	38.25	2.81, 4.65	2.85, 38.25	2.85, 179.66
29	-	138.19	-	-	138.19, 7.19
30	7.14	127.84	7.14, 7.27	7.14, 126.71	7.14, 126.71, 36.92, 138.11
31	7.27	129.49	7.27, 7.17	7.27, 129.39	
32	7.17	126.15	7.17, 7.27	7.17, 128.86	
33	7.27	129.49	7.27, 7.17	7.27, 129.39	
34	7.14	127.84	7.14, 7.27	7.14, 126.71	7.14, 126.71
35	8.14	-	8.14, 4.66	-	8.14, 171.16
36	-				172.69, 4.43
37	4.43	54.47	4.43, 8.32	4.43, 54.47	4.53, 171.85
38	1.90	37.53	1.90, 4.23	1.90, 37.53	1.89, 69.04
39	4.23	69.03	4.23, 3.61	4.23, 69.03	4.23, 67.03
40	3.58	-	-	-	3.55, 69.21
41	3.61	54.48	3.61, 4.23	3.61, 54.48	3.62, 65.08
42	-	-	-	-	
43	-				

No.	δ ^{1}H	δ ^{13}C	δ COSY	δ HSQC	δ HMBC
44	4.27	49.35	4.27, 8.32	4.27, 49.35	4.27, 172.20
45	8.32	-	8.32, 4.27	-	8.32, 175.43
46	-				172.31, 4.32
47	4.33	52.51	4.33, 8.23	4.33, 52.51	4.33, 172.03
48	2.53	40.16	2.53, 4.20	2.53, 40.16	2.53, 49.32
49	3.05	40.77	3.05, 2.52	3.05, 40.77	2.02, 40.16
50	-	-	-	-	165.94, 3.04-
51	11.0	-	-	-	
52	8.23	-	8.23, 4.33	-	8.23, 170.07
53	-	-	-	-	170.55, 4.31-
54	4.31	52.51	4.31, 7.69	4.31, 52.51	4.31, 172.29
55	1.89	28.03	1.89, 4.31	1.89, 52.68	1.92, 169.12
56	1.51	59.42	1.51, 1.89	1.51, 59.42	1.51, 28.03
57	3.00	55.35	3.02, 1.51	3.02, 55.35	3.02, 59.42
58	8.82	-	8.82, 3.07	-	8.82, 55.35
59	-	-	-	-	156.80, 8.82
60	-	-	-	-	-
61	-	-	-	-	-
62	7.69	-	7.69, 4.31	-	7.69, 170.62
63	-	-	-	-	174.00, 4.07
64	4.06	52.60	4.06, 7.69	4.06, 52.60	4.06, 170.53
65	7.69	-	7.69, 4.07	-	7.69, 170.62
66	-	-	-	-	170.88, 4.23
67	4.24	58.76	4.24, 8.12	4.24, 58.76	4.24, 171.09
68	8.12	-	8.12, 4.24	-	8.12, 173.58
69	-	-	-	-	169.58, 3.82-
70	3.82	52.90	3.82, 7.99	3.82, 52.90	3.82, 169.68
71	4.04	66.87	3.82, 4.04	4.04, 66.87	4.04,
72	4.32				4.32, 66.87
73	1.04	19.79	1.04, 4.04	1.04, 19.79	1.04, 66.87
74	7.79	-	7.79, 3.82	-	7.79, 179.67
75	-	-	-	-	169.58, 3.82--
76	3.82	52.90	3.82, 7.99	3.82, 52.90	3.82, 169.58
77	4.04	66.87	3.82, 4.04	4.04, 66.87	4.04,
78	4.32				4.32, 66.87
79	1.04	19.79	1.04, 4.04	1.04, 19.79	1.04, 66.87
80	7.79	-	7.79, 3.82	-	7.79, 179.67
81	-	-	-	-	-
82	4.35	59.45	4.35, 7.99	4.35, 59.45	4.35, 172.31
83	7.99	-	7.99, 4.35	-	7.79, 179.67
84	1.88	37.91	1.88, 4.29	1.88, 37.91	1.88, 37.23
85	1.57	37.65	1.57, 1.88	1.57, 37.65	1.57, 36.64
86	1.73	29.14	1.73, 1.57	1.73, 29.14	1.73, 40.50
87	2.27	31.08	2.27, 1.73	2.27, 31.08	2.27, 25.33
88	-	-	-	-	-
89	-	-	-	-	178.05, 1.60

No.	δ ^{1}H	δ ^{13}C	δ COSY	δ HSQC	δ HMBC
90	-	36.33	-	-	36.33, 1.60
91	1.60	38.90	1.60, 4.31	1.60, 38.92	1.60, 36.33
92	1.63	30.27	1.63, 3.02	1.63, 30.27	1.60, 176.78
93	1.53	36.51	1.53, 3.02	1.56, 36.53	1.53, 37.53
94	1.63	30.27	1.63, 3.02	1.63, 30.27	1.65, 36.65
95	1.63	36.49	1.53, 3.02	1.63, 36.49	1.63, 39.08
96	1.63	30.27	1.63, 3.02	1.63, 30.27	1.63, 38.08
97	1.67	38.94	1.67, 4.31	1.67, 38.94	1.70, 39.10
98	1.63	36.50	1.53, 3.02	1.63, 36.50	1.67, 176.78
99	1.67	38.94	1.67, 4.31	1.67, 38.94	1.67, 176.78

9.5.11 *Retro*-DGD-GG-GFOGER-GG-GHK-Palmitate

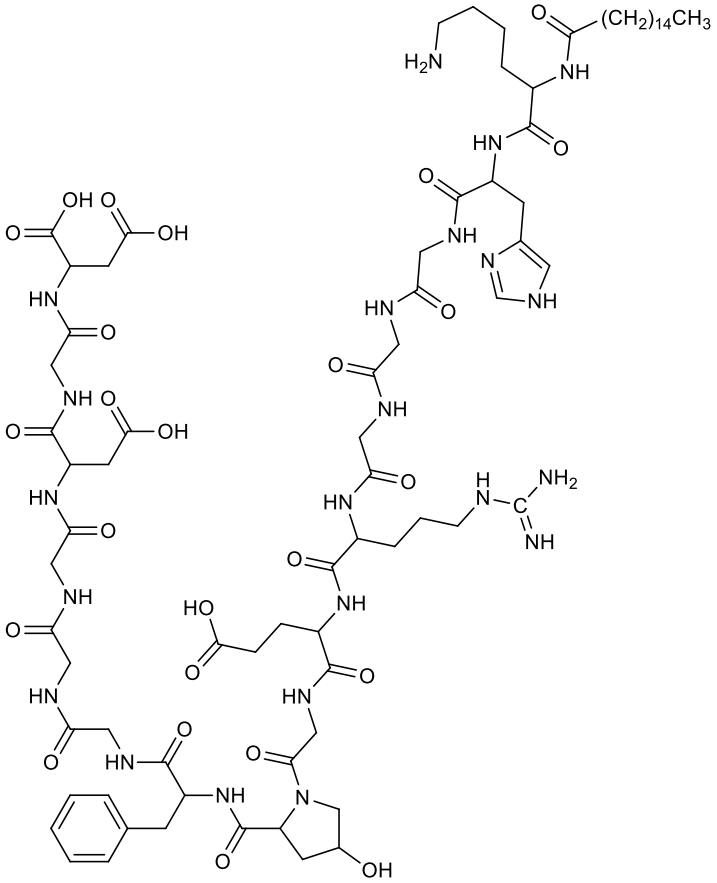

Figure 9.11: *Retro*-DGD-GG-GFOGER-GG-GHK-Palmitate.

UHPLC (Thermo Scientific Dionex Ultimate 3000) Peak 6.00 minutes

HRMS (ESI) (Bruker Compact Q-TOF): Calculated for $C_{77}H_{120}N_{22}O_{25}$ = 1752.8795; found 877.4499 ($[M + 2H]^{2+}$]).

^{1}H NMR (400 MHz, DMSO) δH = 9.20 (1H, m, NH amide), 8.81 (1H, *m*, NH amide), 8.59 (1H, *m*, NH amide), 8.19 (1H, *m*, NH amide), 7.90 (1H, *m*, NH amide), 7.57 (1H, *m*, NH amide), 7.30 (1H, *m*, NH amide), 7.33 (1H, *m*, NH amide), 8.23 (1H, *m*, NH amide), 7.69 (2H, *m*, NH amide), 8.12 (1H, *m*, NH amide), 7.79 (1H, *m*, NH amide), 7.79 (1H, *m*, NH amide), 7.99 (1H, *m*, NH amide), 7.14 (2H, *m*, ArH), 7.27 (2H, *m*, ArH), 7.17 (1H, *m*, ArH), 4.63 (2H, *m*, Hα Asp), 4.41 (1H, *m*, Hα Gly), 3.80 (1H, *m*, Hα Gly), 3.77 (1H, *m*, Hα Gly), 4.54 (1H, *m*, Hα Gly), 4.66 (1H, *m*, Hα Phe), 4.43 (1H, *m*, Hα Hyp), 4.27 (1H, *m*, Hα Gly), 4.33 (1H, *m*, Hα Glu), 4.31 (1H, *m*, Hα Arg), 4.06 (1H, *m,* Hα Gly), 4.24 (1H, *m*, Hα Gly), 3.82 (2H, *m*, Hα Gly), 4.90 (2H, *m*, Hα His), 4.35 (1H, m, Hα Lys), 2.81 (2H, m, Hβ Asp), 2.85 (1H, *m,* Hβ Phe), 1.90 (1H, *m*, Hβ Arg), 4.23 (1H, *m*, Hγ Hyp), 3.61 (1H, *m*, Hδ Hyp), 2.53 (1H, *m*, Hβ Glu), 3.05 (1H, m, Hγ Glu), 1.89 (1H, m, Hα Arg), 1.51 (1H, *m*, Hβ Arg), 3.00 (1H, *m*, Hγ Arg), 8.80 (1H, *m*, NH guanidyl), 3.20 (2H, *m*, Hβ His), 7.70 (1H, *m*, C-H, His), 8.67 m, (1H, *m*, C-H, His), 8.03 (1H, *m*, NH, His), 1.79 (2H, *m*, Hβ Lys), 1.29 (2H, *m*, Hγ Lys), 1.52 (2H, *m*, Hδ Lys), 2.71 (2H, *m*, Hε Lys), 5.14 (2H, *m*, NH_2 Lys)

^{13}C NMR (400 MHz, DMSO) δC = 174.78 (C = O), 172.72 (C = O), 172.67 (C = O), 172.05 (C = O), 171.80 (C = O), 170.99 (C = O), 170.51 (C = O), 169.35 (C = O), 169.19 (C = O), 168.41 (C = O), 163.90 (C = O), 129.61 (ArC), 128.50 (ArC), 69.02 (Cα), 66.99 (Cα), 65.38 (Cα), 56.50 (Cα), 52.80 (Cα), 52.45 (Cα), 42.53 (Cβ), 40.88 (Cβ), 39.18 (C - Aliphatic), 38.98 (C - Aliphatic), 36.56 (C - Aliphatic), 31.07 (C - Aliphatic), 30.80 (C - Aliphatic), 29.60 (C - Aliphatic), 28.10 (C - Aliphatic), 27.06 (C - Aliphatic), 22.83 (C - Aliphatic), 20.07 (C - Aliphatic), 19.80 (C - Aliphatic), 19.01 (C - Aliphatic), 15.63 (C - Aliphatic)

9.5.12 *Retro*-DGD-GG-GFOGER-GG-GHK-Adamantane

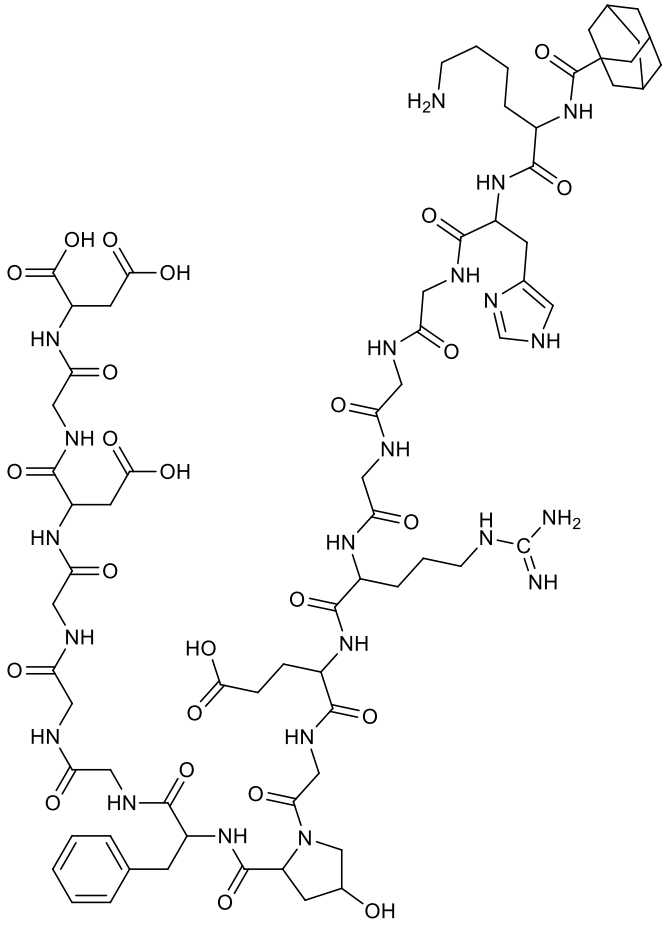

Figure 9.12: *Retro*-DGD-GG-GFOGER-GG-GHK-Adamantate.

UHPLC (Thermo Scientific Dionex Ultimate 3000) Peak 3.52 minutes

HRMS (ESI) (Bruker Compact Q-TOF): Calculated for $C_{72}H_{104}N_{22}O_{25}$ = 1676.7543; found 839.2885 ($[M + 2H]^{2+}$).

^{1}H NMR (400 MHz, DMSO) δH = 9.49 (1H, m, NH amide), 9.10 (1H, *m*, NH amide), 8.88 (1H, *m*, NH amide), 8.48 (1H, *m*, NH amide), 8.19 (1H, *m*, NH amide), 7.86 (1H, *m*, NH amide), 7.59 (1H, *m*, NH amide), 7.62 (1H, *m*, NH amide), 8.52 (1H, *m*, NH amide), 7.98 (2H, *m*, NH amide), 8.41 (1H, *m*, NH amide), 8.08 (1H, *m*, NH amide), 8.08 (1H, *m*, NH amide), 8.28 (1H, *m*, NH amide), 7.29 (2H, *m*, ArH), 7.40 (2H, *m*, ArH), 7.27 (1H, *m*, ArH), 4.61 (2H, *m*, Hα Asp), 4.40 (1H, *m*, Hα Gly), 3.82 (1H, *m*, Hα Gly), 3.80 (1H, *m*, Hα Gly), 4.53 (1H, *m*, Hα Gly), 4.66 (1H, *m*, Hα Phe), 4.43 (1H, *m*, Hα Hyp), 4.27 (1H, *m*, Hα Gly), 4.30 (1H, *m*, Hα Glu), 4.31 (1H, *m*, Hα Arg), 4.07 (1H, *m,* Hα Gly), 4.23 (1H, *m*, Hα Gly), 3.84 (2H, *m*, Hα Gly), 4.92 (2H, *m*, Hα His),

4.32 (1H, *m*, Hα Lys), 2.81 (2H, m, Hβ Asp), 2.85 (1H, *m,* Hβ Phe), 1.90 (1H, *m*, Hβ Arg), 4.23 (1H, *m*, Hγ Hyp), 3.61 (1H, *m*, Hδ Hyp), 2.53 (1H, *m*, Hβ Glu), 3.05 (1H, *m*, Hγ Glu), 1.89 (1H, *m*, Hα Arg), 1.51 (1H, *m*, Hβ Arg), 3.00 (1H, *m*, Hγ Arg), 8.82 (1H, *m*, NH guanidyl), 3.17 (2H, *m*, Hβ His), 7.66 (1H, *m*, C-H, His), 8.73 (1H, *m*, C-H, His), 8.03 (1H, *m*, NH, His), 1.79 (2H, *m*, Hβ Lys), 1.29 (2H, *m*, Hγ Lys), 1.55 (2H, *m*, Hδ Lys), 2.65 (2H, *m*, Hε Lys), 5.11 (2H, *m*, NH_2 Lys)

^{13}C NMR (400 MHz, DMSO) δC = 177.87 (C = O), 172.65 (C = O), 172.54 (C = O), 172.07 (C = O), 171.70 (C = O), 170.59 (C = O), 169.80 (C = O), 169.35 (C = O), 158.67 (C = O), 157.30 (C = O), 134.09 (C = O), 129.65 (ArC), 129.48 (ArC), 128.49 (ArC), 117.47, 116.43, 69.03 (Cα), 54.44 (Cα), 53.06 (Cα), 51.95 (Cα), 50.00 (Cα), 48.99 (Cα), 42.47 (Cβ), 40.87 (Cβ), 39.52 (C - Aliphatic), 39.07 (C - Aliphatic), 38.91 (C - Aliphatic), 36.53 (C - Aliphatic), 28.09 (C - Aliphatic), 27.02 (C - Aliphatic), 25.39 (C - Aliphatic), 22.88 (C - Aliphatic)

9.5.13 *Retro*-DGD-GG-GFOGER-GG-QPR-Palmitate

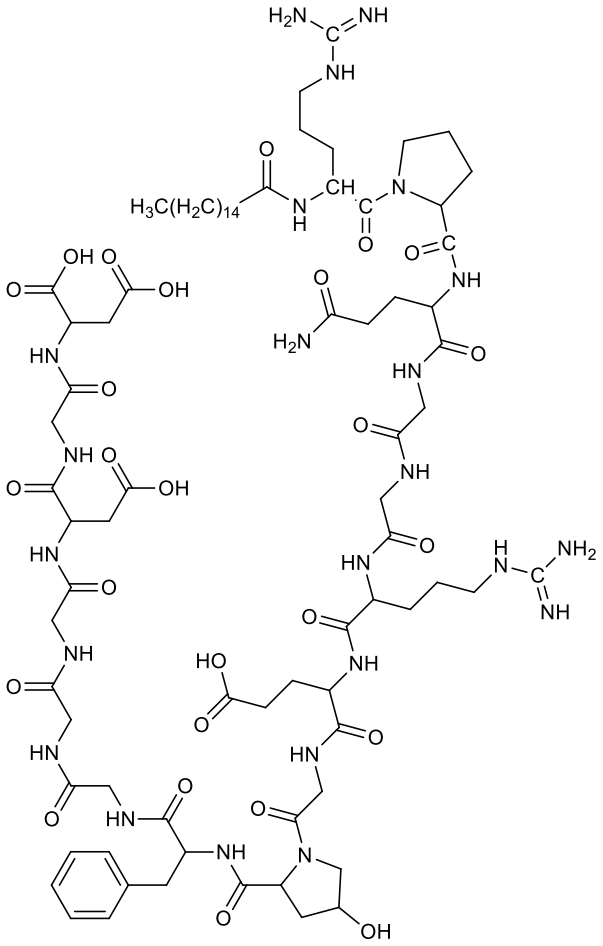

Figure 9.13: *Retro*-DGD-GG-GFOGER-GG-QPR-Palmitate.

UHPLC (Thermo Scientific Dionex Ultimate 3000) Peak 6.54 minutes

HRMS (ESI) (Bruker Compact Q-TOF): Calculated for $C_{79}H_{125}N_{23}O_{26}$ = 1811.9166; found 907.0723 ($[M+2H]^{2+}$).

9.5.14 *Retro*-DGD-GG-GFOGER-GG-QPR-Adamantane

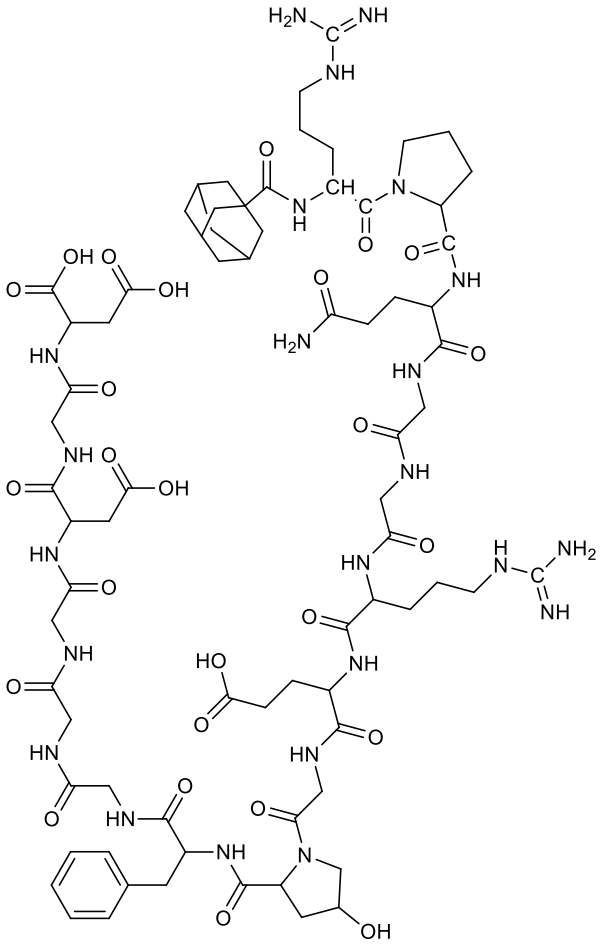

Figure 9.14: *Retro*-DGD-GG-GFOGER-GG-QPR-Adamantate.

UHPLC (Thermo Scientific Dionex Ultimate 3000) Peak 3.87 minutes

HRMS (ESI) (Bruker Compact Q-TOF): Calculated for $C_{74}H_{109}N_{23}O_{26}$ = 1735.7914; found 868.9049 ($[M + 2H]^{2+}$).

9.5.15 *Retro*-DGD-GG-GFOGER-GG-EEM-Palmitate

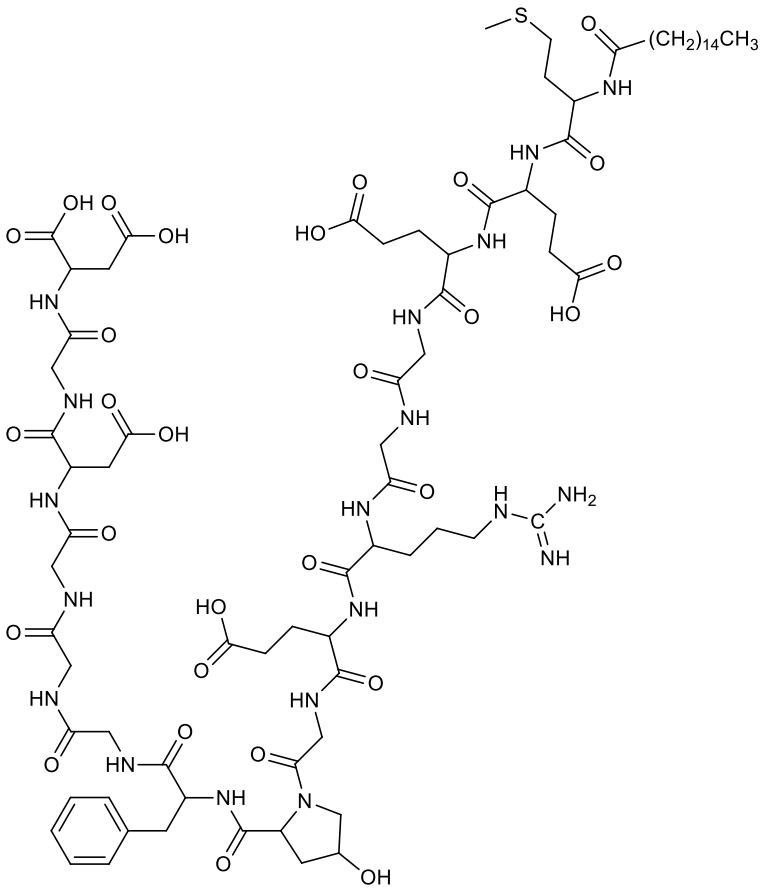

Figure 9.15: *Retro*-DGD-GG-GFOGER-GG-EEM-Palmitate.

UHPLC (Thermo Scientific Dionex Ultimate 3000) Peak 9.00 minutes

HRMS (ESI) (Bruker Compact Q-TOF): Calculated for $C_{78}H_{121}N_{19}O_{29}S$ = 1819.8298; found 1821.8628 ($[M + H]^{2+}$).

9.5.16 *Retro*-DGD-GG-GFOGER-GG-EEM-Adamantate

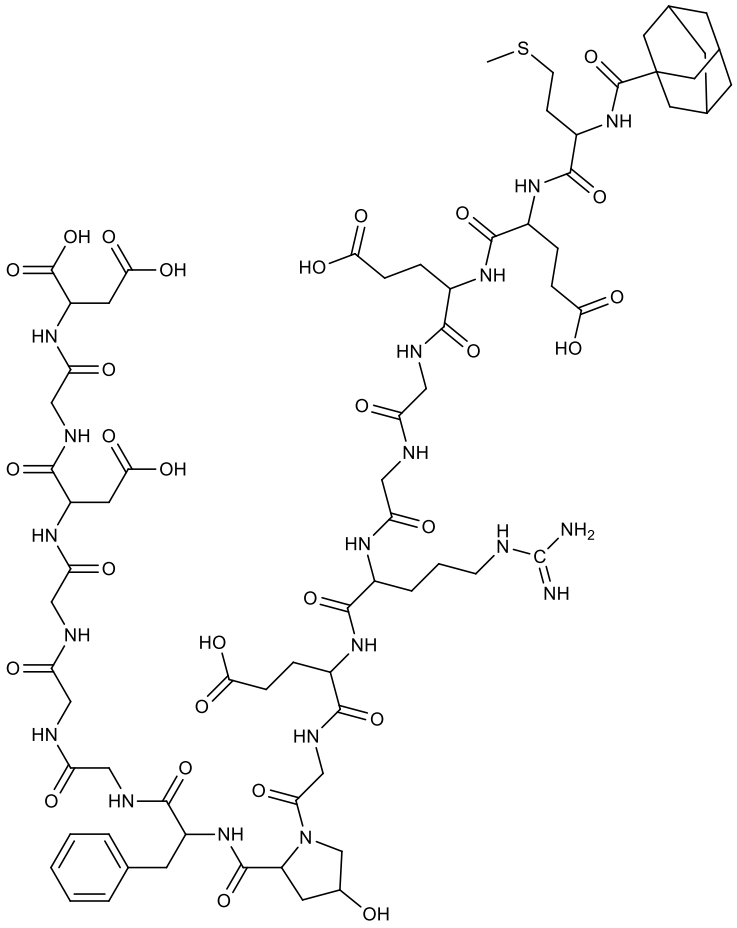

Figure 9.16: *Retro*-DGD-GG-GFOGER-GG-EEM-Adamantate.

UHPLC (Thermo Scientific Dionex Ultimate 3000) Peak 5.98 minutes

RMS (ESI) (Bruker Compact Q-TOF): Calculated for $C_{73}H_{105}N_{19}O_{29}S$ = 1743.7046; found 872.8559 ($[M + 2H]^{2+}$).

9.5.17 *Retro*-GG-GF(*para*-fluoro)OGER-GG-Palmitate

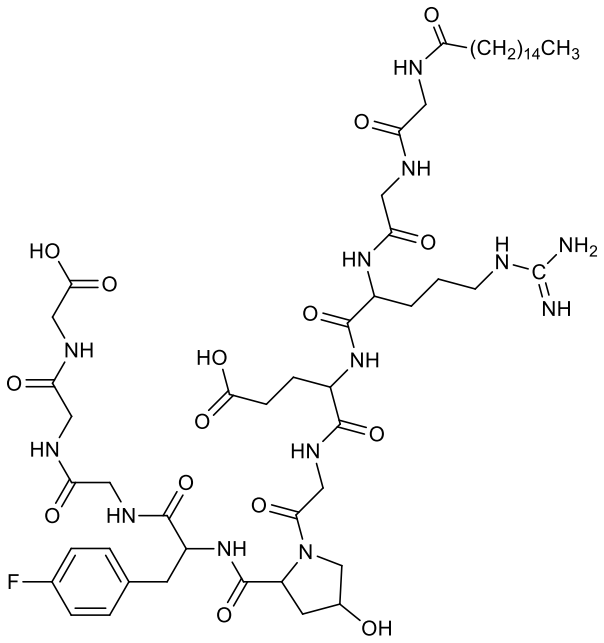

Figure 9.17: *Retro*-GG-GF(*para*-fluoro)OGER-GG-Palmitate.

UHPLC (Thermo Scientific Dionex Ultimate 3000) Peak 15.75 minutes

HRMS (ESI) (Bruker Compact Q-TOF): Calculated for $C_{53}H_{84}FN_{13}O_{15}$ = 1161.6194; found 581.8177 ($[M + 2H]^{2+}$).

9.5.18 *Retro*-GG-GF(*para*-fluoro)OGER-GG-Adamantane

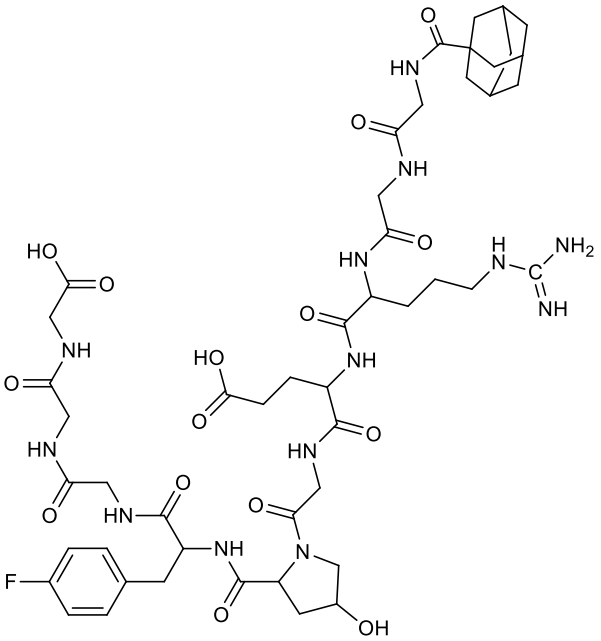

Figure 9.18: *Retro*-GG-GF(*para*-fluoro)OGER-GG-Adamantane.

UHPLC (Thermo Scientific Dionex Ultimate 3000) Peak 12.12 minutes

HRMS (ESI) (Bruker Compact Q-TOF): Calculated for $C_{48}H_{68}FN_{13}O_{15}$ = 1085.4942; found 543.7530 ($[M + 2H]^{2+}$).

9.5.19 *Retro*-GG-GFOGER-GG-Palmitate (D-Peptide)

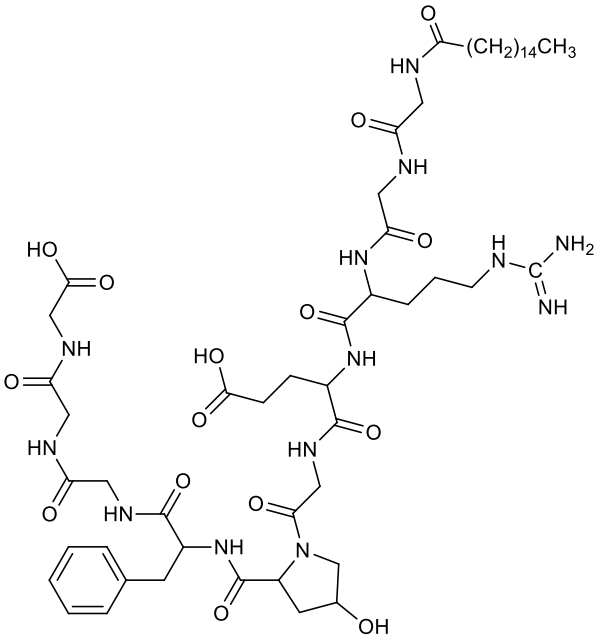

Figure 9.19: *Retro*-GG-GFOGER-GG-Palmitate (D-Peptide).

UHPLC (Thermo Scientific Dionex Ultimate 3000) Peak 8.39 minutes

HRMS (ESI) (Bruker Compact Q-TOF): Calculated for $C_{53}H_{85}N_{13}O_{15}$ = 1143.6288; found 1144.6556 ($[M + H]^+$).

9.5.20 *Retro*-GG-GFOGER-GG-Adamantane (D-Peptide)

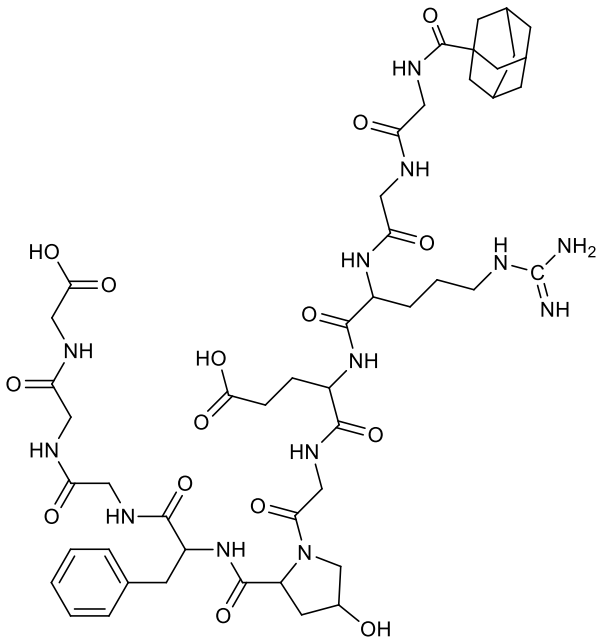

Figure 9.20: *Retro*-GG-GFOGER-GG-Adamantane (D-Peptide).

UHPLC (Thermo Scientific Dionex Ultimate 3000) Peak 5.10 minutes

HRMS (ESI) (Bruker Compact Q-TOF): Calculated for $C_{48}H_{69}N_{13}O_{15}$ = 1067.5036; found 1068.5074 ($[M + H]^+$).

9.5.21 *Retro*-GG-GFOGER-GG-Palmitate (Reference peptoid)

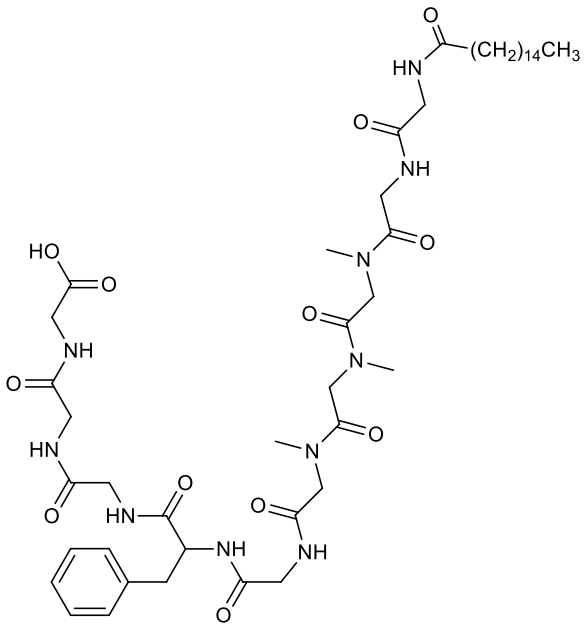

Figure 9.21: *Retro*-GG-GFOGER-GG-Palmitate (Reference peptoid).

UHPLC (Thermo Scientific Dionex Ultimate 3000) Peak 19.38 minutes

HRMS (ESI) (Bruker Compact Q-TOF): Calculated for $C_{46}H_{74}N_{10}O_{12}$ = 958.5488; found 959.5500 ($[M + H]^+$).

9.5.22 *Retro*-GG-GFOGER-GG-Adamantane (Reference peptoid)

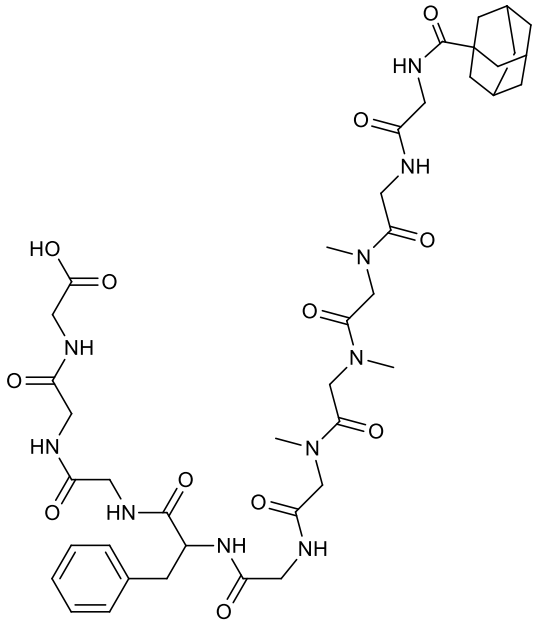

Figure 9.22: *Retro*-GG-GFOGER-GG-Adamantane (Reference peptoid).

UHPLC (Thermo Scientific Dionex Ultimate 3000) Peak 16.46 minutes

HRMS (ESI) (Bruker Compact Q-TOF): Calculated for $C_{41}H_{58}N_{10}O_{12}$ = 882.4236; found 883.3631 ($[M + H]^+$).

9.5.23 *Retro*-GG-GFOGER-GG-Palmitate (peptoid)

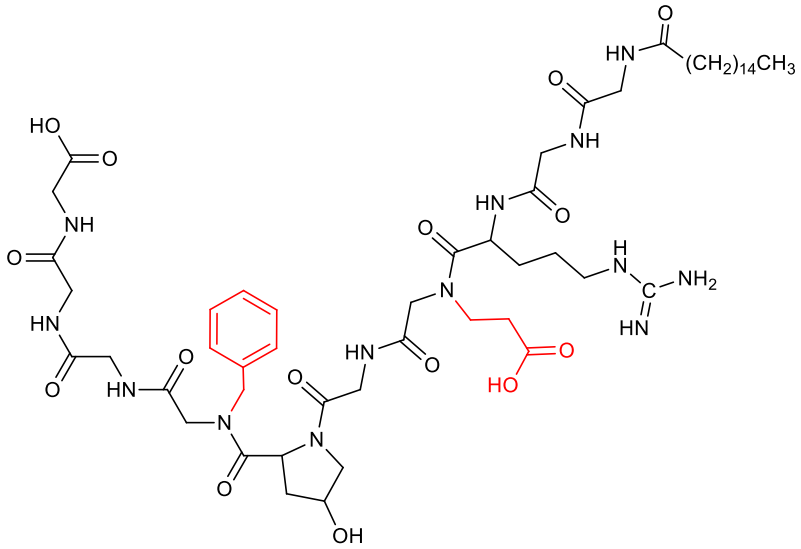

Figure 9.23: *Retro*-GG-GFOGER-GG-Palmitate (peptoid).

UHPLC (Thermo Scientific Dionex Ultimate 3000) Peak 8.34 minutes

HRMS (ESI) (Bruker Compact Q-TOF): Calculated for $C_{53}H_{85}N_{13}O_{15}$ = 1143.6288; found 1144.6514 ($[M + H]^+$).

9.5.24 *Retro*-GG-GFOGER-GG-Adamantane (peptoid)

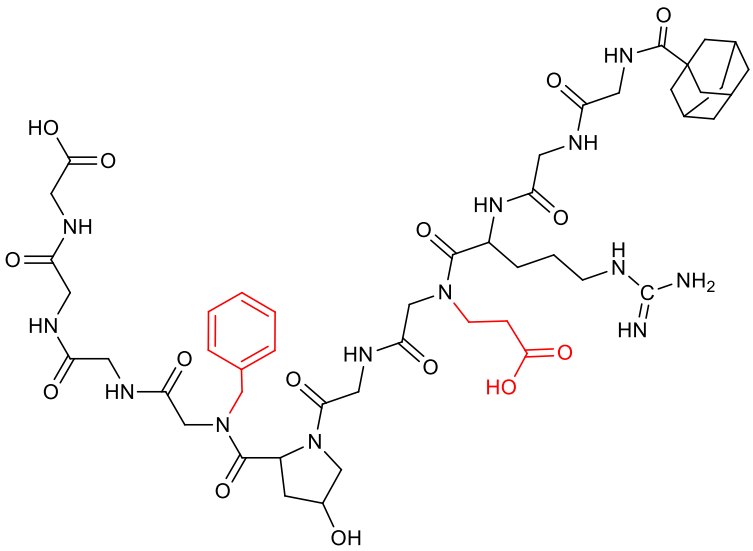

Figure 9.24: *Retro*-GG-GFOGER-GG-Adamantane (peptoid).

UHPLC (Thermo Scientific Dionex Ultimate 3000) Peak 3.47 minutes

HRMS (ESI) (Bruker Compact Q-TOF): Calculated for $C_{48}H_{69}N_{13}O_{15}$ = 1067.5036; found 1068.5189 ($[M + H]^+$).

9.5.25 Fmoc-Phe-OH oxazolidinone

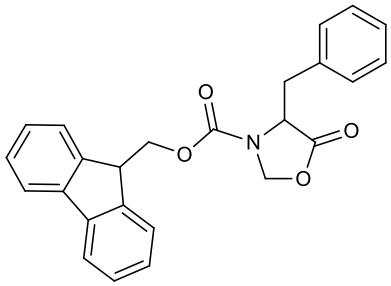

Figure 9.25: Fmoc-Phe-OH oxazolidinone.

UHPLC (Thermo Scientific Dionex Ultimate 3000) Peak 17.82 minutes

HRMS (ESI) (Bruker Compact Q-TOF): Calculated for $C_{25}H_{21}NO_4$ = 399.1471; found 400.1428 ($[M + H]^+$).

9.5.26 Fmoc-Arg-OH oxazolidinone

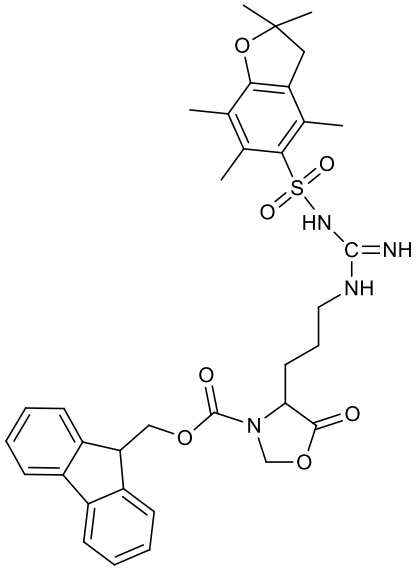

Figure 9.26: Fmoc-Arg-OH oxazolidinone.

UHPLC (Thermo Scientific Dionex Ultimate 3000) Peak 18.58 minutes

HRMS (ESI) (Bruker Compact Q-TOF): Calculated for $C_{35}H_{40}N_4O_7S$ = 660.2618; found 663.83 ($[M + H]^+$).

9.5.27 *N*-Methylated Fmoc-Phe-OH

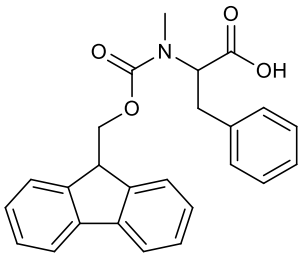

Figure 9.27: *N*-Methylated Fmoc-Phe-OH.

UHPLC (Thermo Scientific Dionex Ultimate 3000) Peak 3.47 minutes

HRMS (ESI) (Bruker Compact Q-TOF): Calculated for $C_{25}H_{23}NO_4$ = 401.1627; found 404.1178 ($[M + H]^+$).

9.5.28 *N*-Methylated Fmoc-Arg(Pbf)-OH

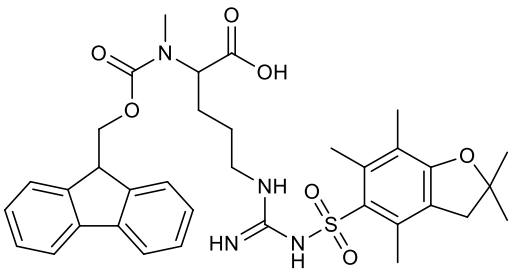

Figure 9.28: *N*-Methylated Fmoc-Arg(Pbf)-OH.

UHPLC (Thermo Scientific Dionex Ultimate 3000) Peak 3.47 minutes

HRMS (ESI) (Bruker Compact Q-TOF): Calculated for $C_{35}H_{42}N_4O_7S$ = 662.2774; found 665.2470($[M + H]^+$).

9.5.29 *Retro*-GG-GF(Me)OGER-GG-Palmitate (Singly *N*-methylated)

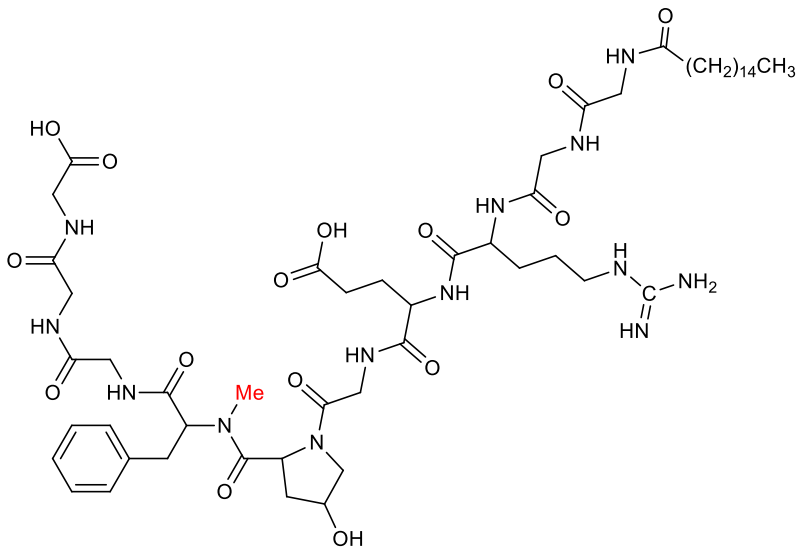

Figure 9.29: *Retro*-GG-GF(Me)OGER-GG-Palmitate (Singly *N*-methylated).

UHPLC (Thermo Scientific Dionex Ultimate 3000) Peak 15.55 minutes

HRMS (ESI) (Bruker Compact Q-TOF): Calculated for $C_{54}H_{87}N_{13}O_{15}$ = 1157.6445; found 1158.6289 ($[M + H]^+$).

9.5.30 *Retro*-GG-GF(Me)OGER-GG-Adamantane (Singly

9.5.31 ethylated)

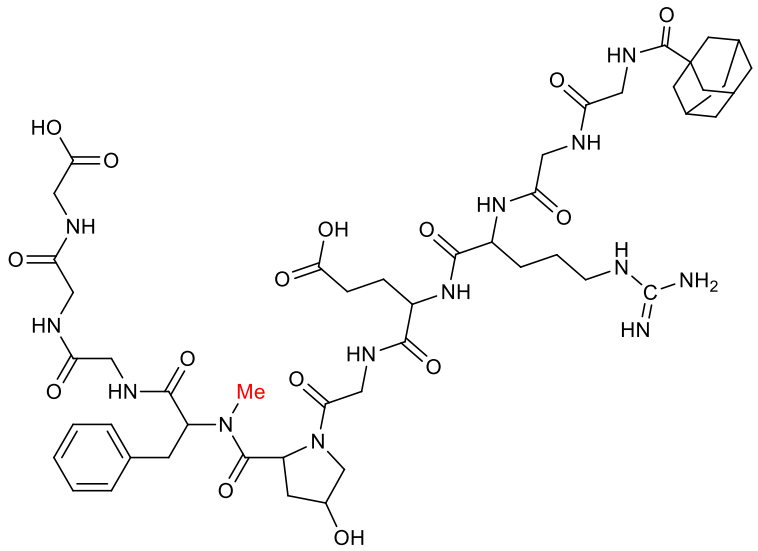

Figure 9.30: *Retro*-GG-GF(Me)OGER-GG-Palmitate (Singly *N*-methylated).

UHPLC (Thermo Scientific Dionex Ultimate 3000) Peak 12.09 minutes

HRMS (ESI) (Bruker Compact Q-TOF): Calculated for $C_{49}H_{71}N_{13}O_{15}$ = 1081.5193; found 1082.5158 ($[M + H]^+$).

9.5.32 *Retro*-GG-GF(Me)OGER(Me)-GG-Palmitate (Doubly *N*-methylated peptide)

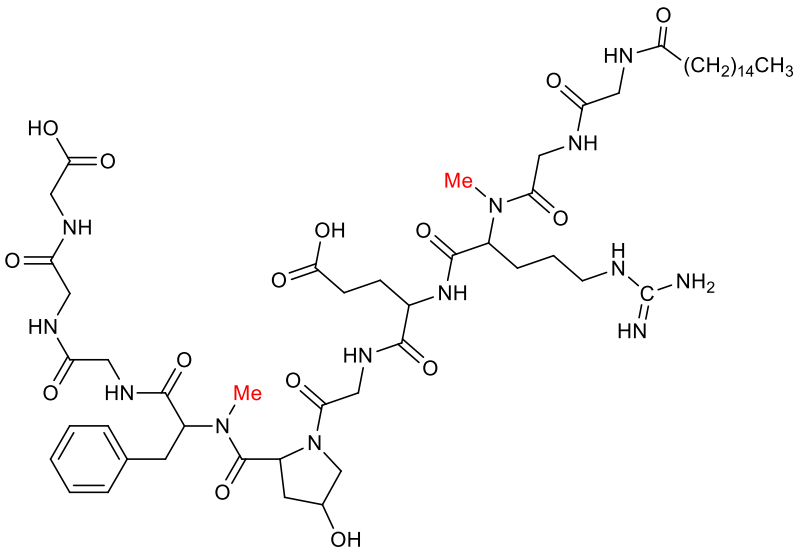

Figure 9.31: *Retro*-GG-GF(Me)OGER(Me)-GG-Palmitate (Doubly *N*-methylated peptide).

UHPLC (Thermo Scientific Dionex Ultimate 3000) Peak 16.36 minutes

HRMS (ESI) (Bruker Compact Q-TOF): Calculated for $C_{55}H_{89}N_{13}O_{15}$ = 1171.6601; found 1172.6175 ($[M + H]^+$).

9.5.33 *Retro*-GG-GF(Me)OGER(Me)-GG-Adamantane (Doubly *N*-methylated peptide)

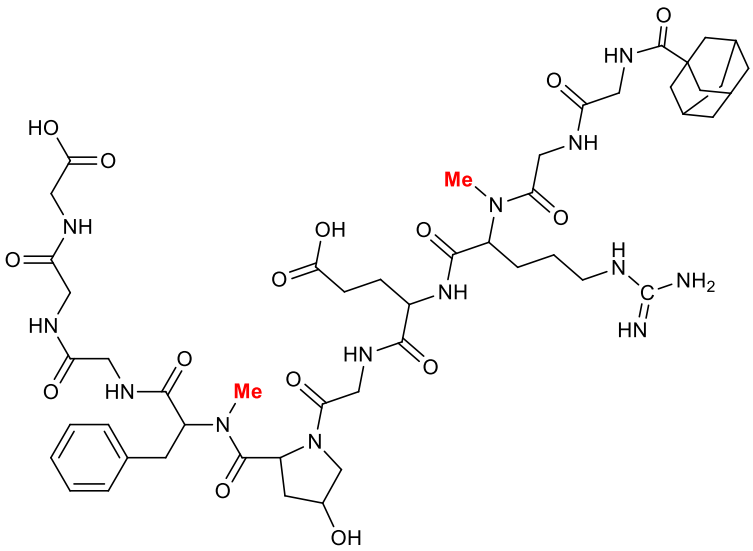

Figure 9.32: *Retro*-GG-GF(Me)OGER(Me)-GG-Adamantane (Doubly *N*-methylated peptide).

UHPLC (Thermo Scientific Dionex Ultimate 3000) Peak 9.81 minutes

HRMS (ESI) (Bruker Compact Q-TOF): Calculated for $C_{50}H_{73}N_{13}O_{15}$ = 1095.5349; found 548.2862 ($[M + 2H]^{2+}$).

9.6 MASS SPECTRA OF SELECTED PEPTIDES

9.6.1 *Retro*-DGRGOF-Palmitate

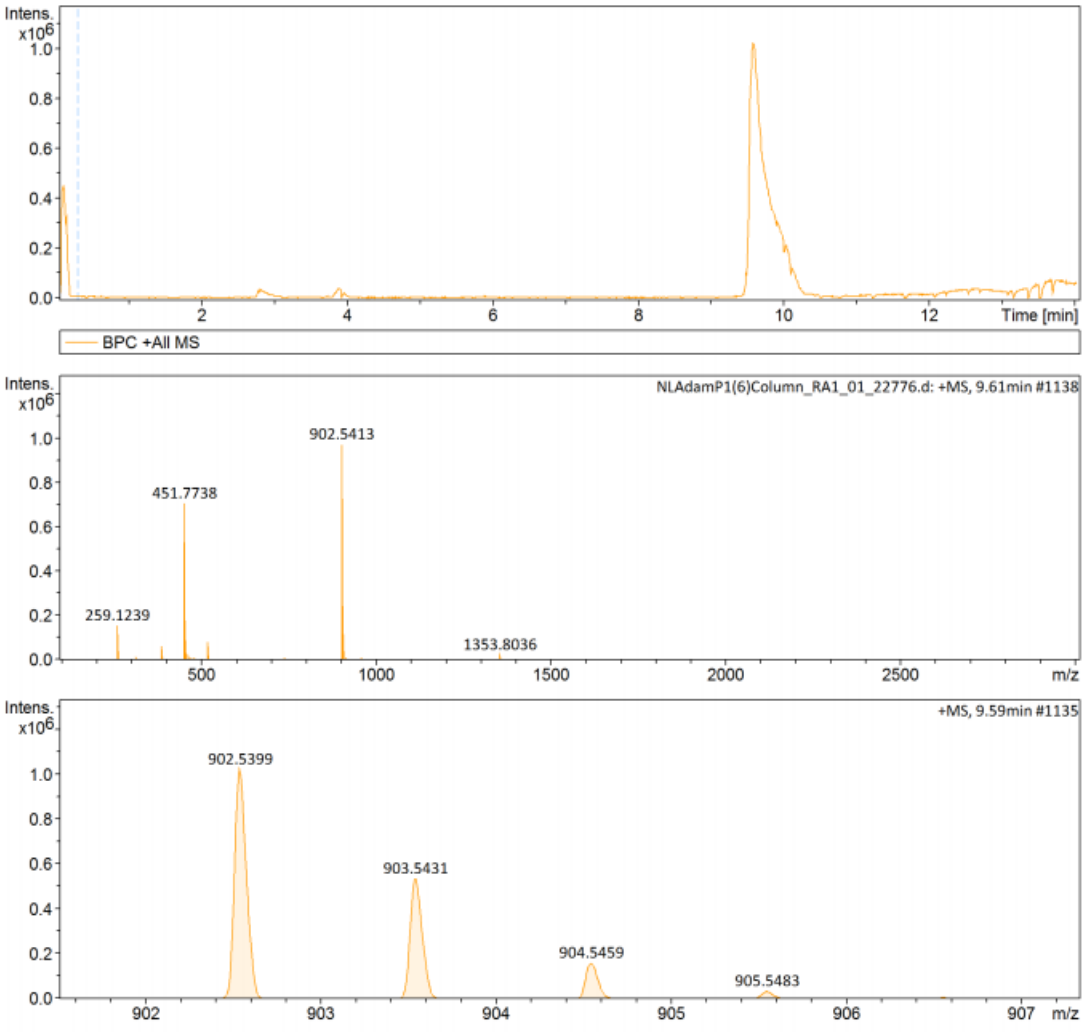

Figure 9.33: Mass spectrum of *retro*-DGRGOF-Palmitate.

9.6.2 *Retro*-DGRGOF-Adamantate

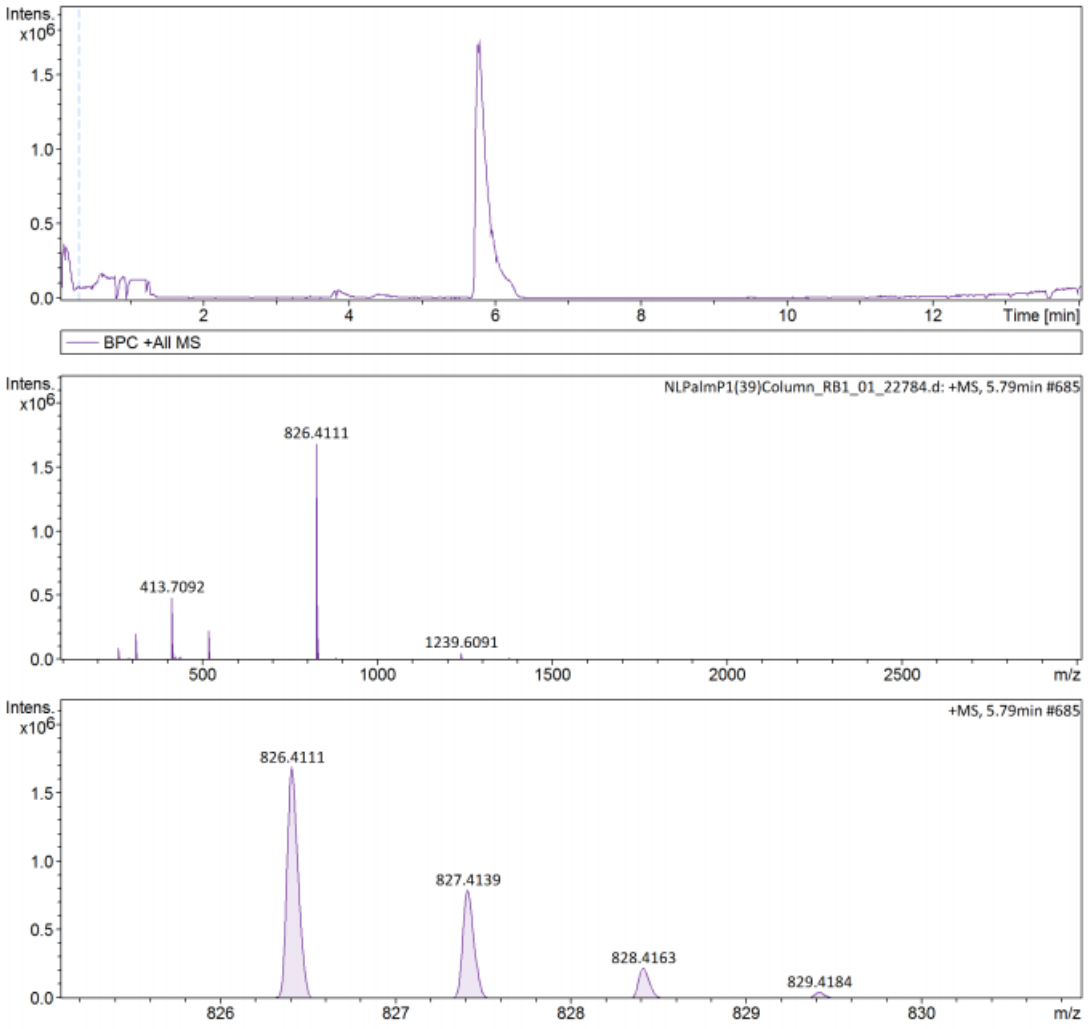

Figure 9.34: Mass spectrum of *retro*-DGRGOF-Adamantate.

9.6.3 *Retro*-GOP-GFOGER-GOP-Palmitate

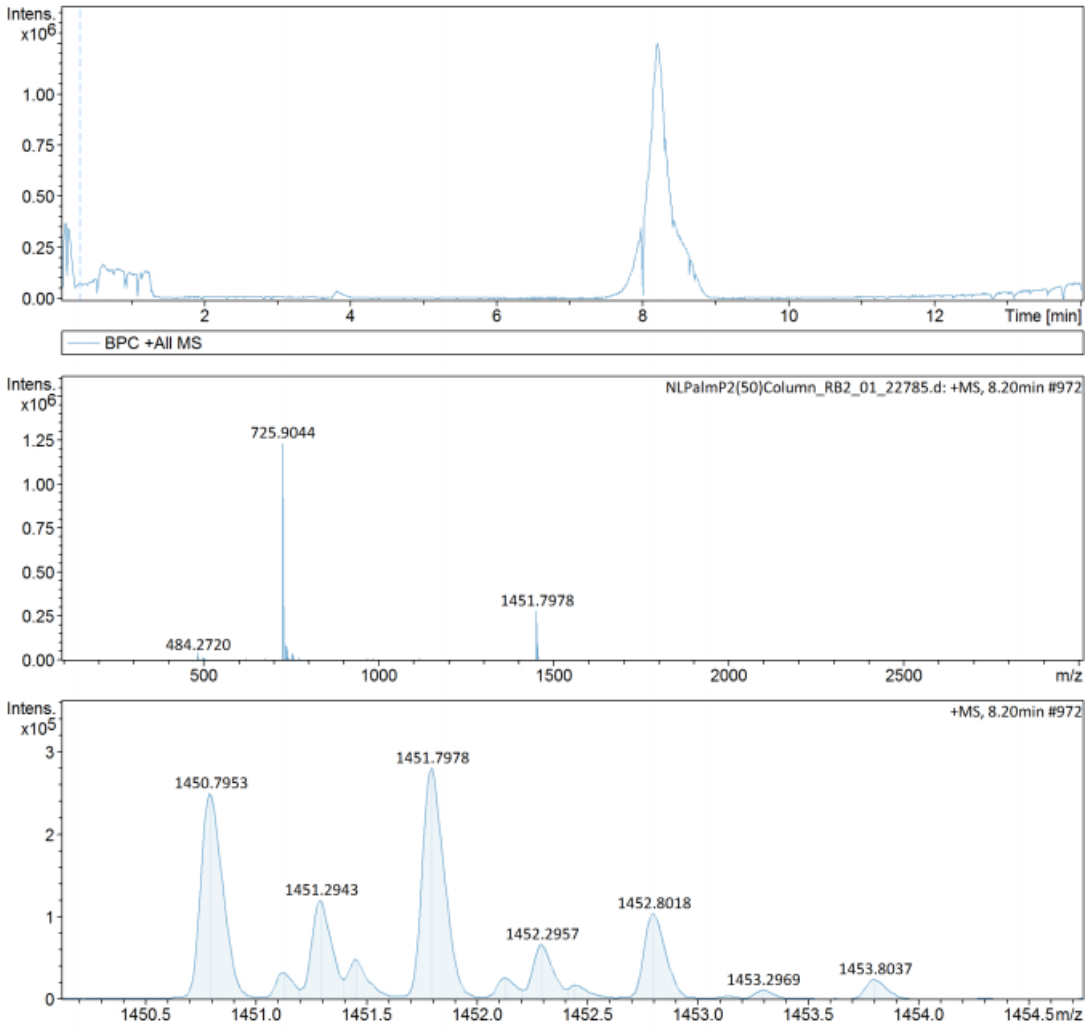

Figure 9.35: Mass spectrum of *retro*-GOP-GFOGER-GOP-Palmitate.

9.6.4 *Retro*-GOP-GFOGER-GOP-Adamantate

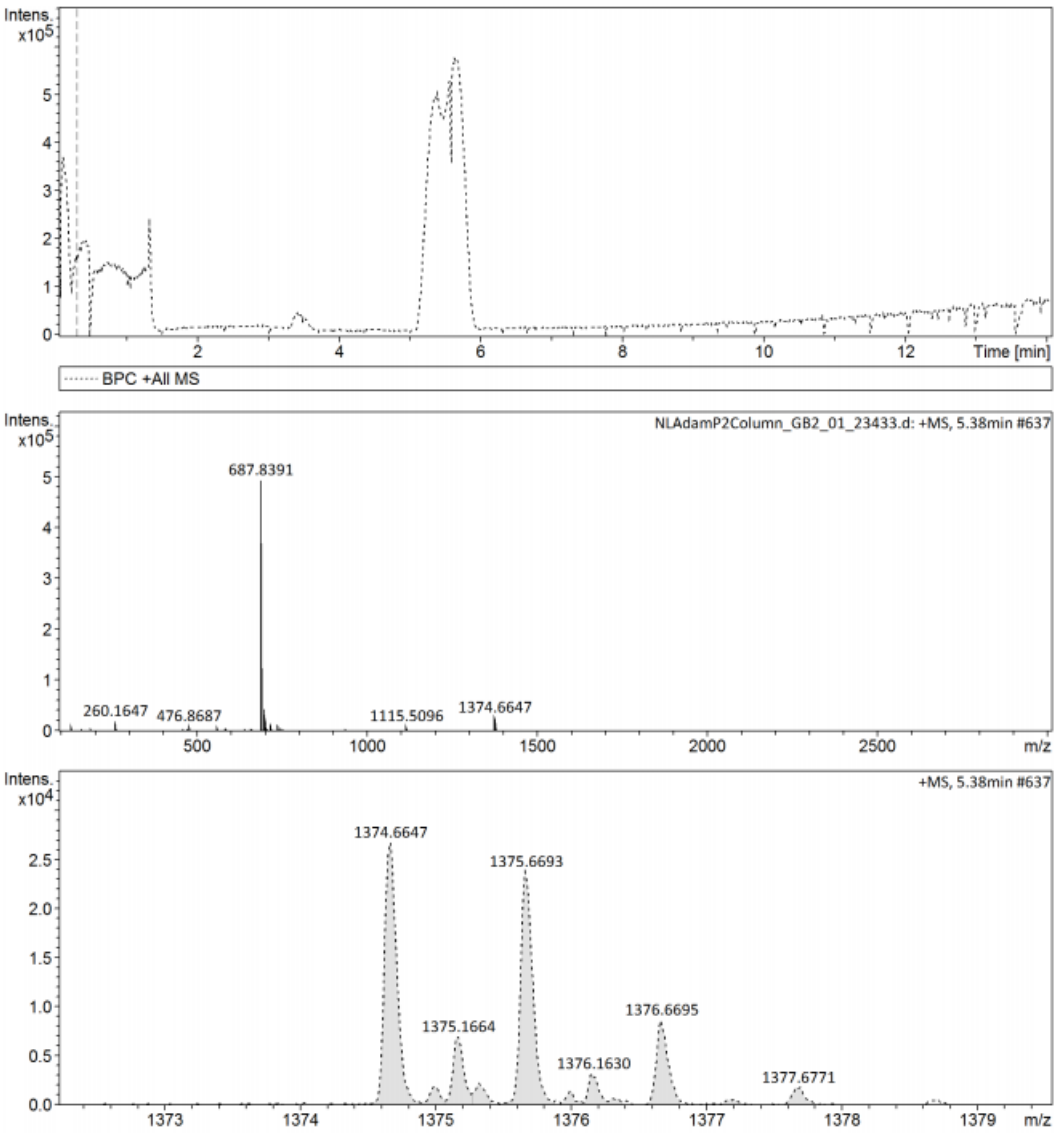

Figure 9.36: Mass spectrum of *retro*-GOP-GFOGER-GOP-Adamantate.

9.6.5 *Retro*-GG-GFOGER-GG-Palmitate

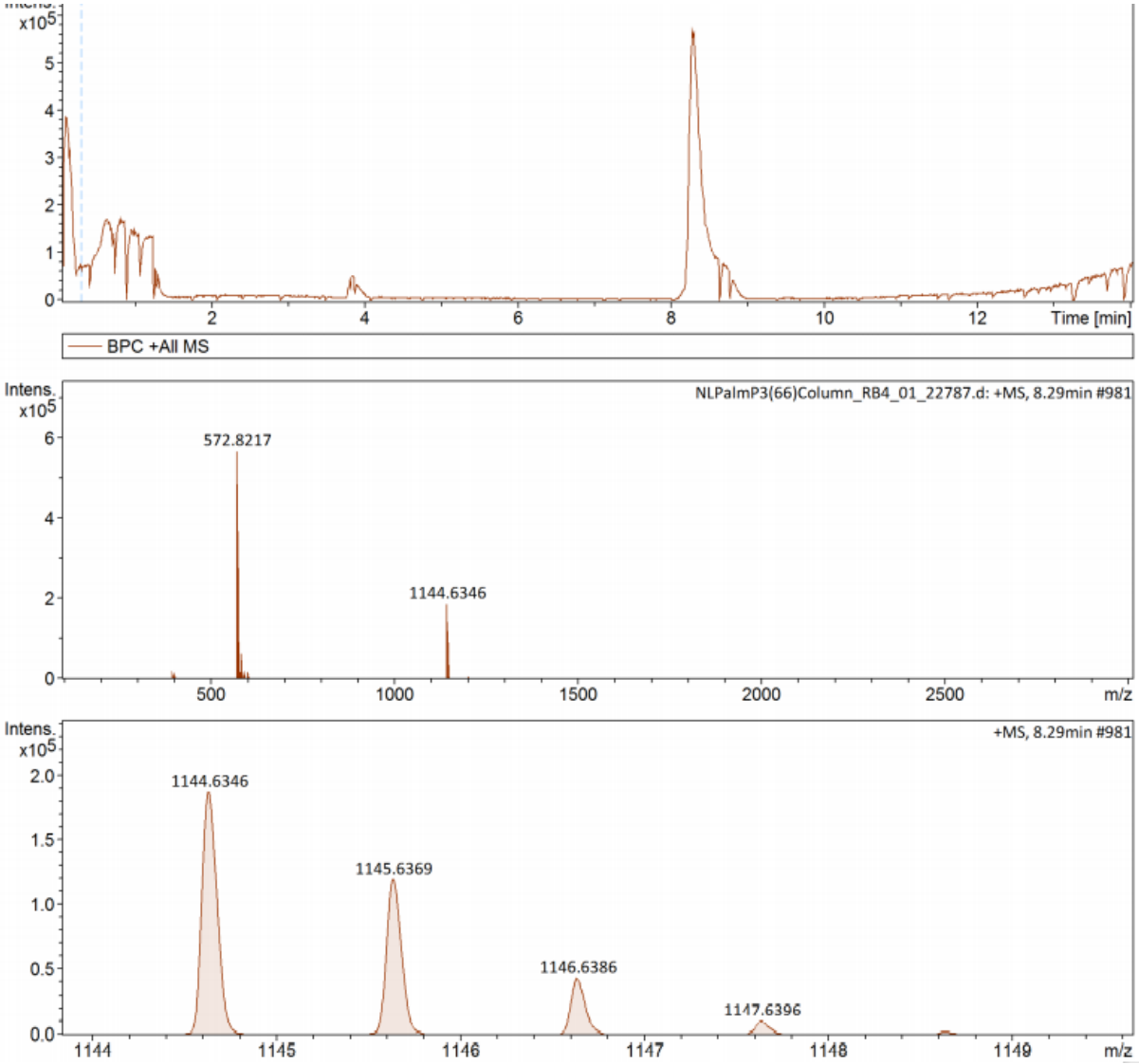

Figure 9.37: Mass spectrum of *retro*-GG-GFOGER-GG-Palmitate.

9.6.6 *Retro*-GG-GFOGER-GG-Adamantate

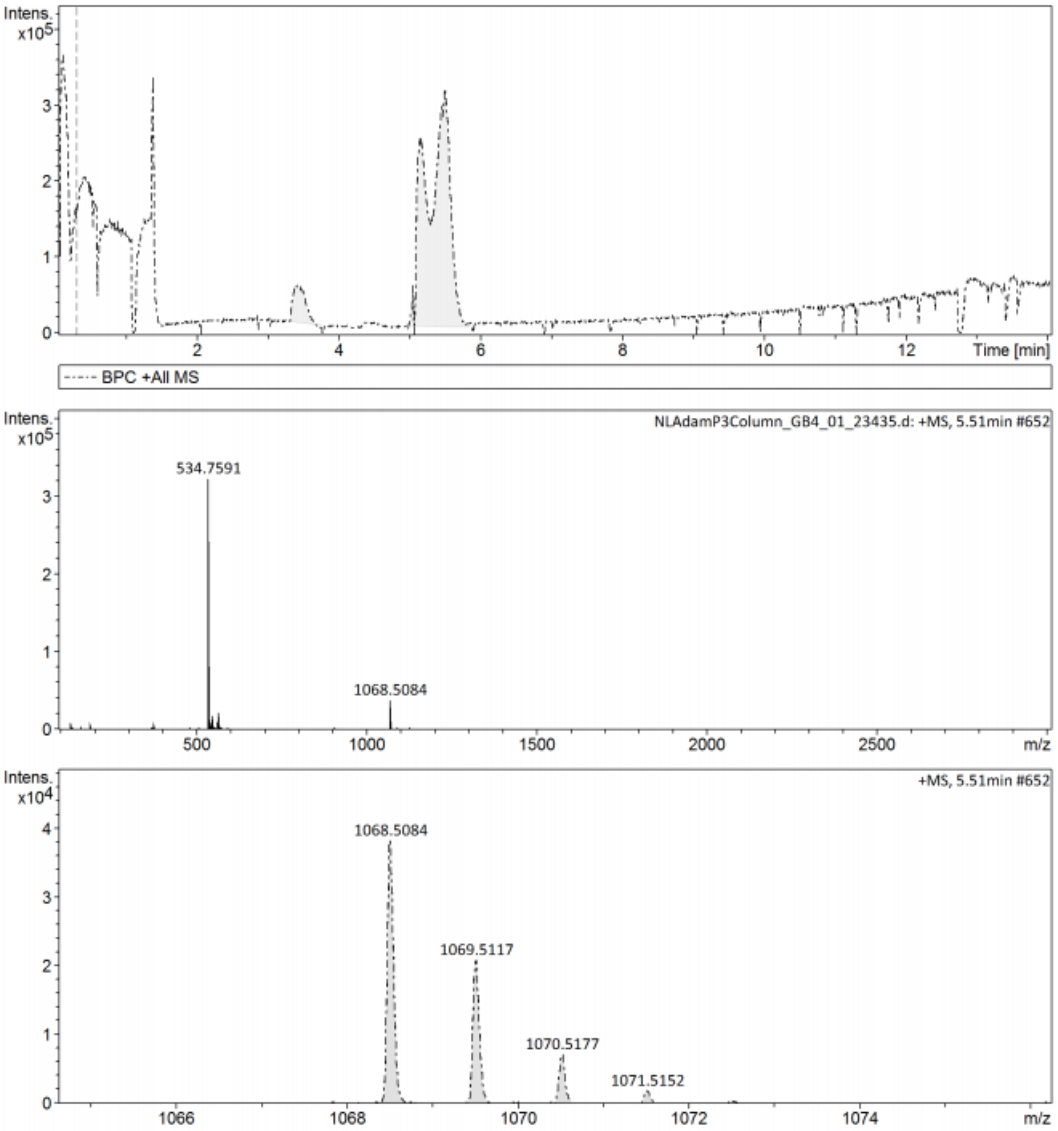

Figure 9.38: Mass spectrum of *retro*-GG-GFOGER-GG-Adamantate.

9.6.7 *Retro*-DGD-GG-GFOGER-GG-Palmitate

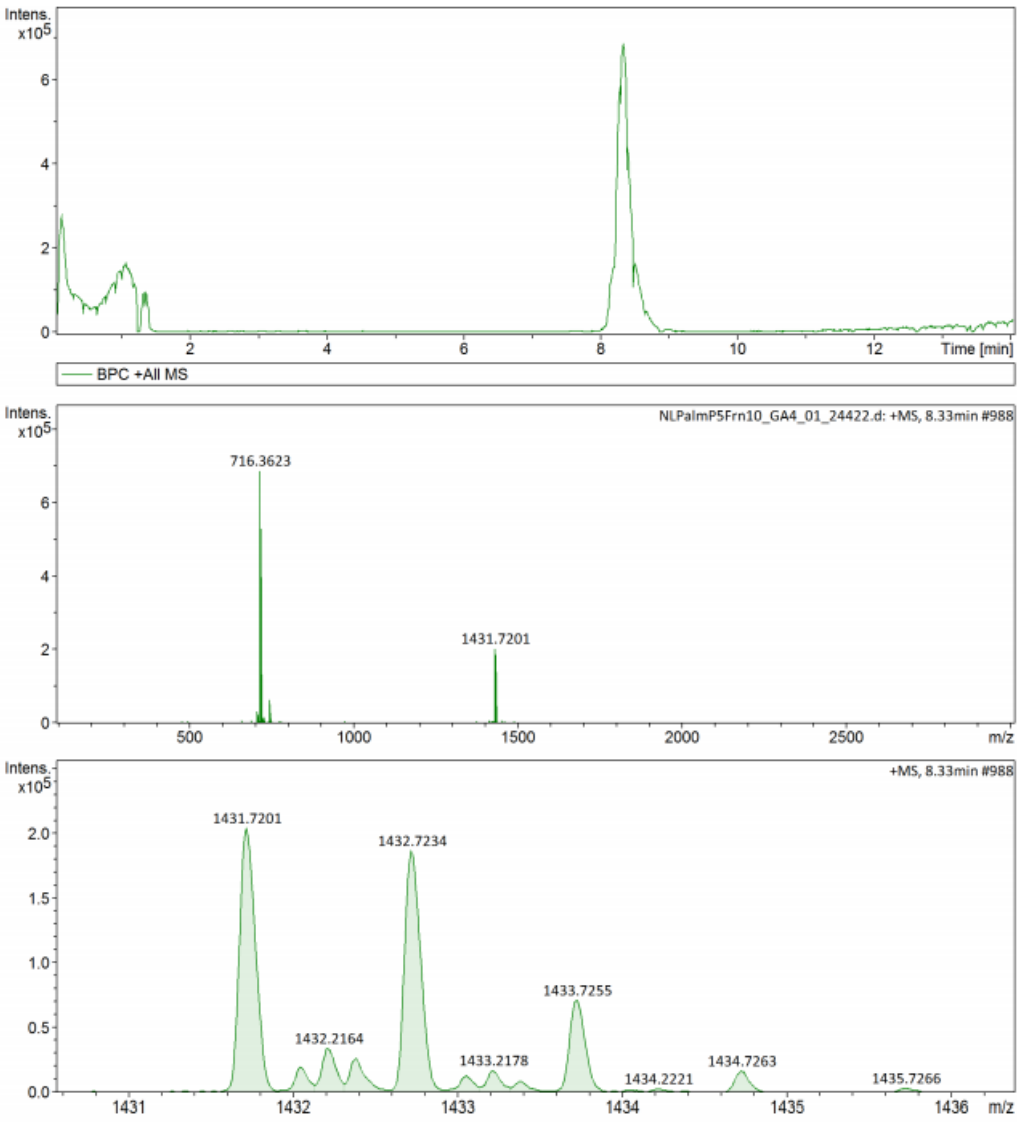

Figure 9.39: Mass spectrum of *retro*-DGD-GG-GFOGER-GG-Palmitate.

9.6.8 *Retro*-DGD-GG-GFOGER-GG-Adamantate

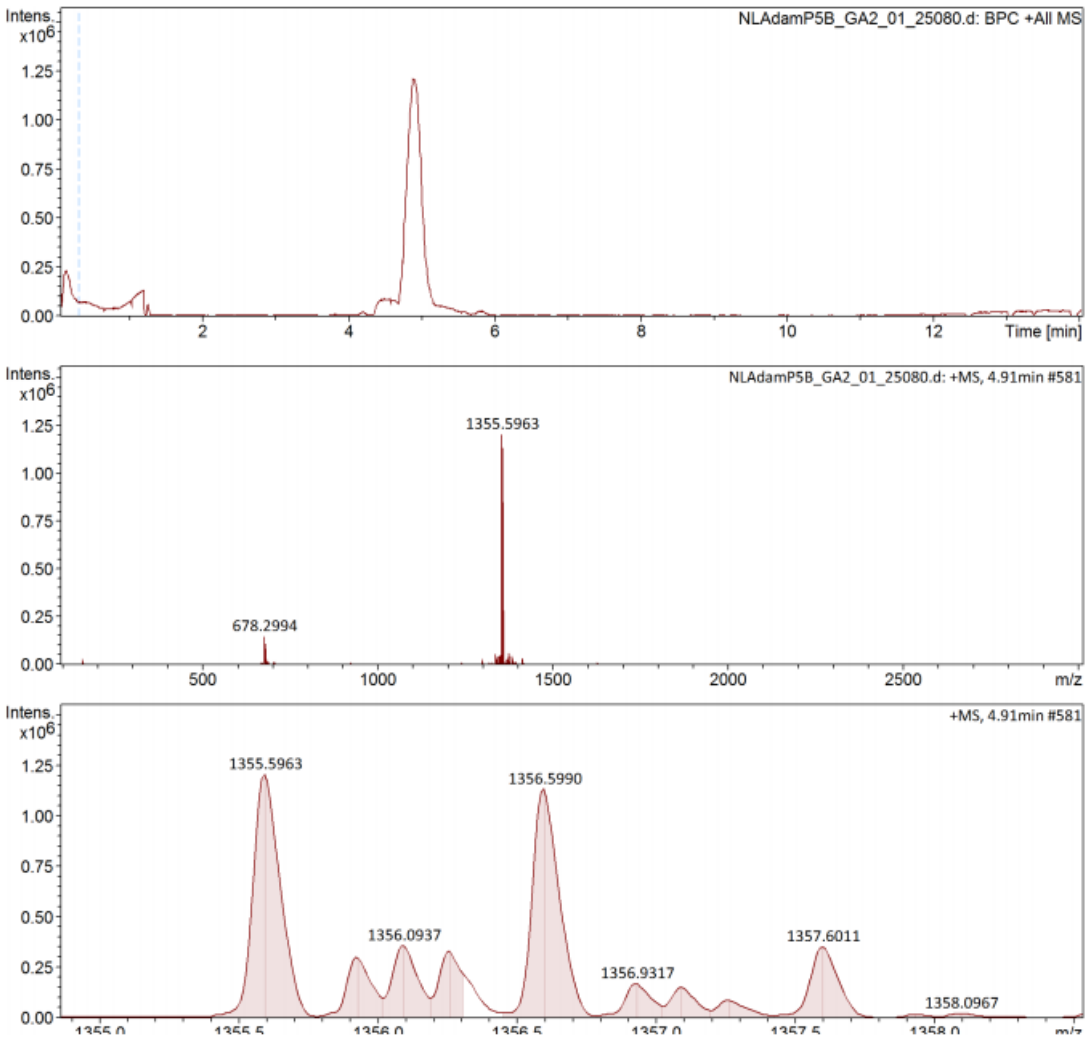

Figure 9.40: Mass spectrum of *retro*-DGD-GG-GFOGER-GG-Adamantate.

9.6.9 *Retro*-DGD-GG-GFOGER-GG-TTK-Palmitate

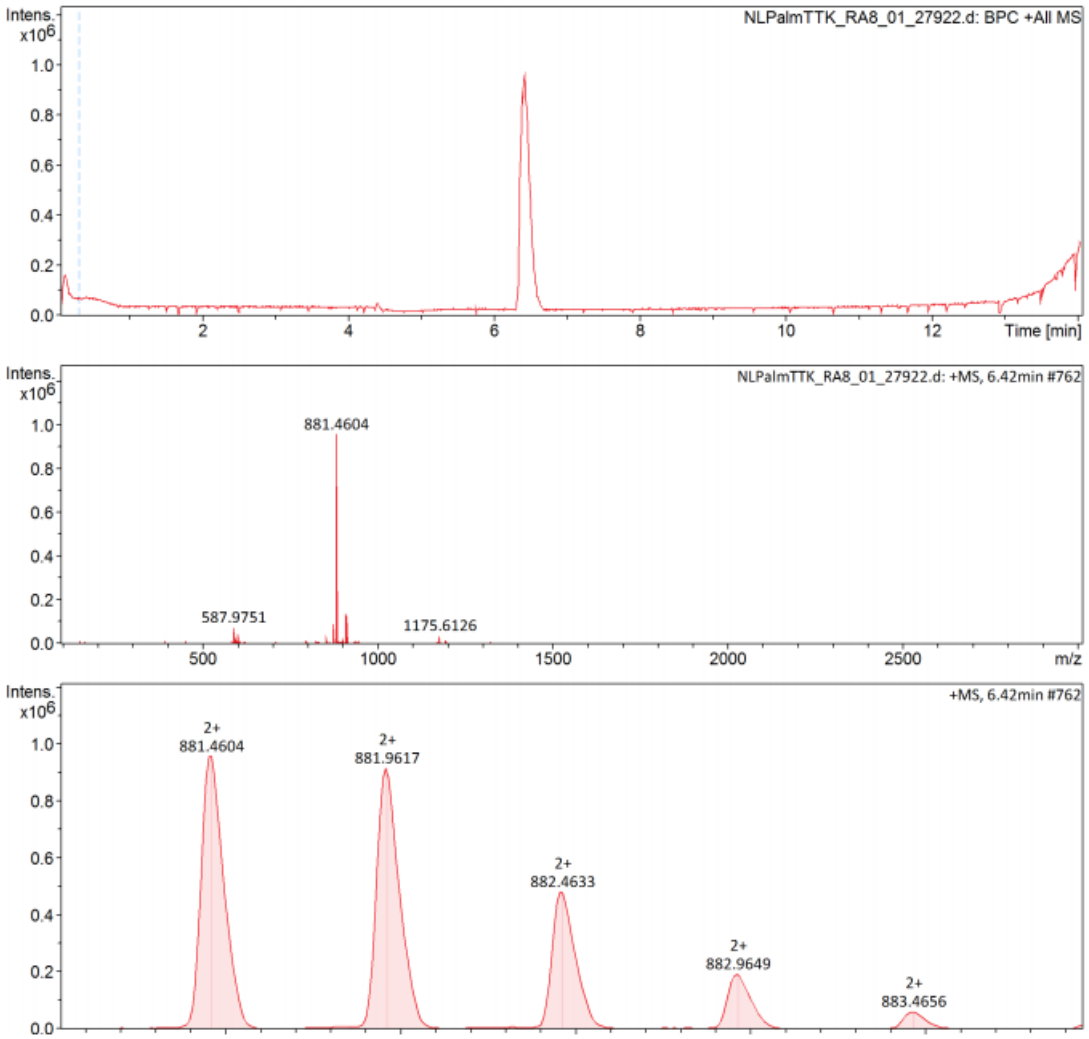

Figure 9.41: Mass spectrum of *retro*-DGD-GG-GFOGER-GG-TTK-Palmitate.

9.6.10 *Retro*-DGD-GG-GFOGER-GG-TTK-Adamantate

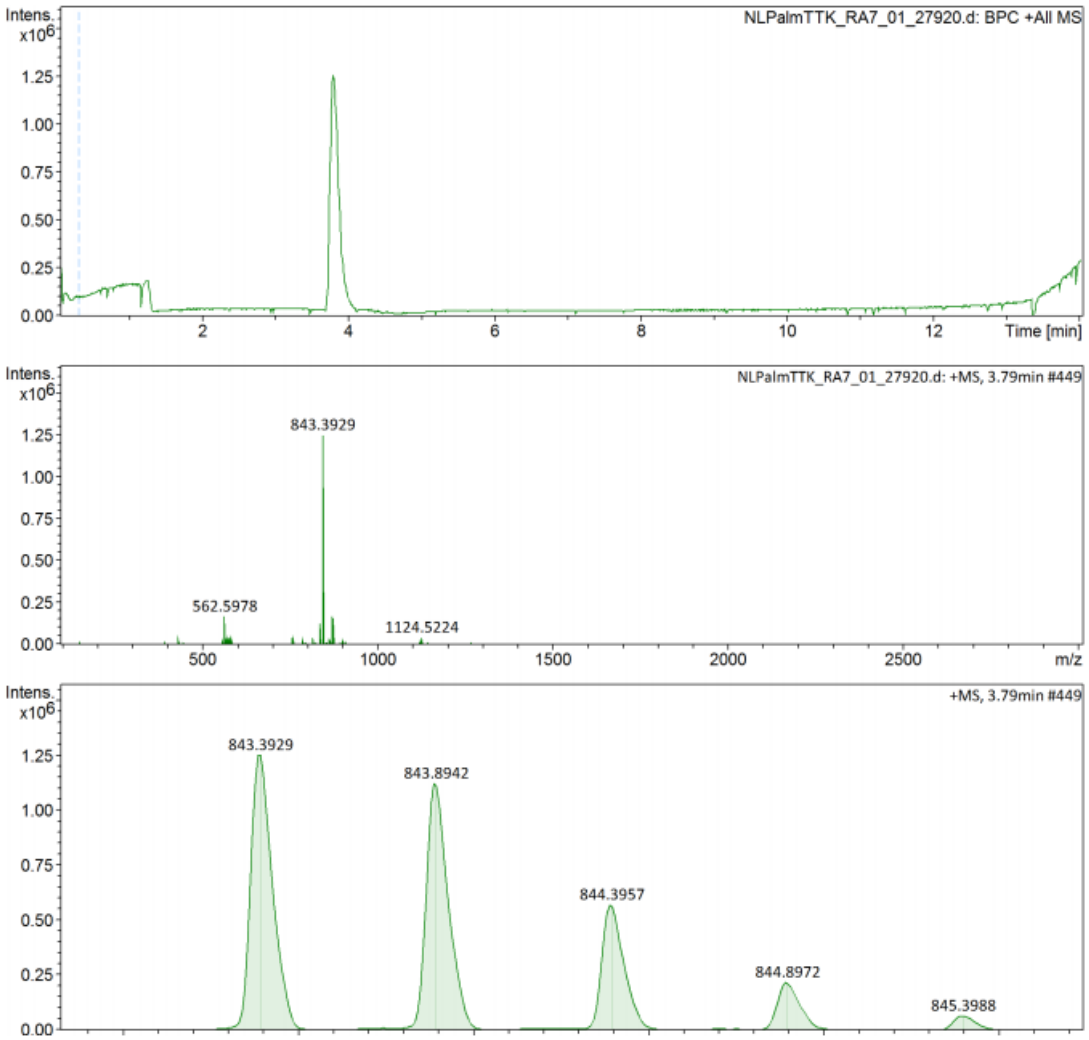

Figure 9.42: Mass spectrum of *retro*-DGD-GG-GFOGER-GG-TTK-Adamantate.

9.6.11 *Retro*-DGD-GG-GFOGER-GG-GHK-Palmitate

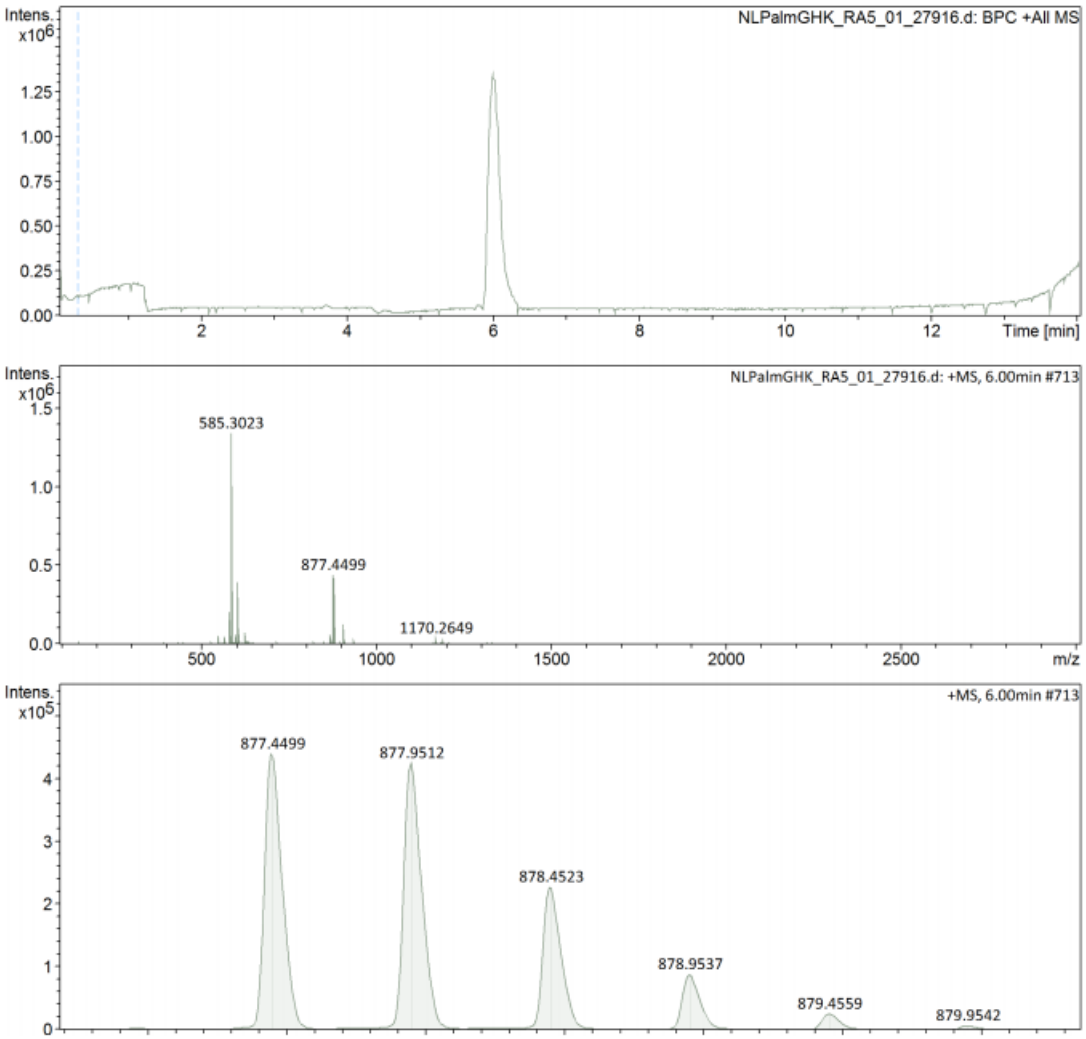

Figure 9.43: Mass spectrum of *retro*-DGD-GG-GFOGER-GG-GHK-Palmitate.

9.6.12 *Retro*-DGD-GG-GFOGER-GG-GHK-Adamantate

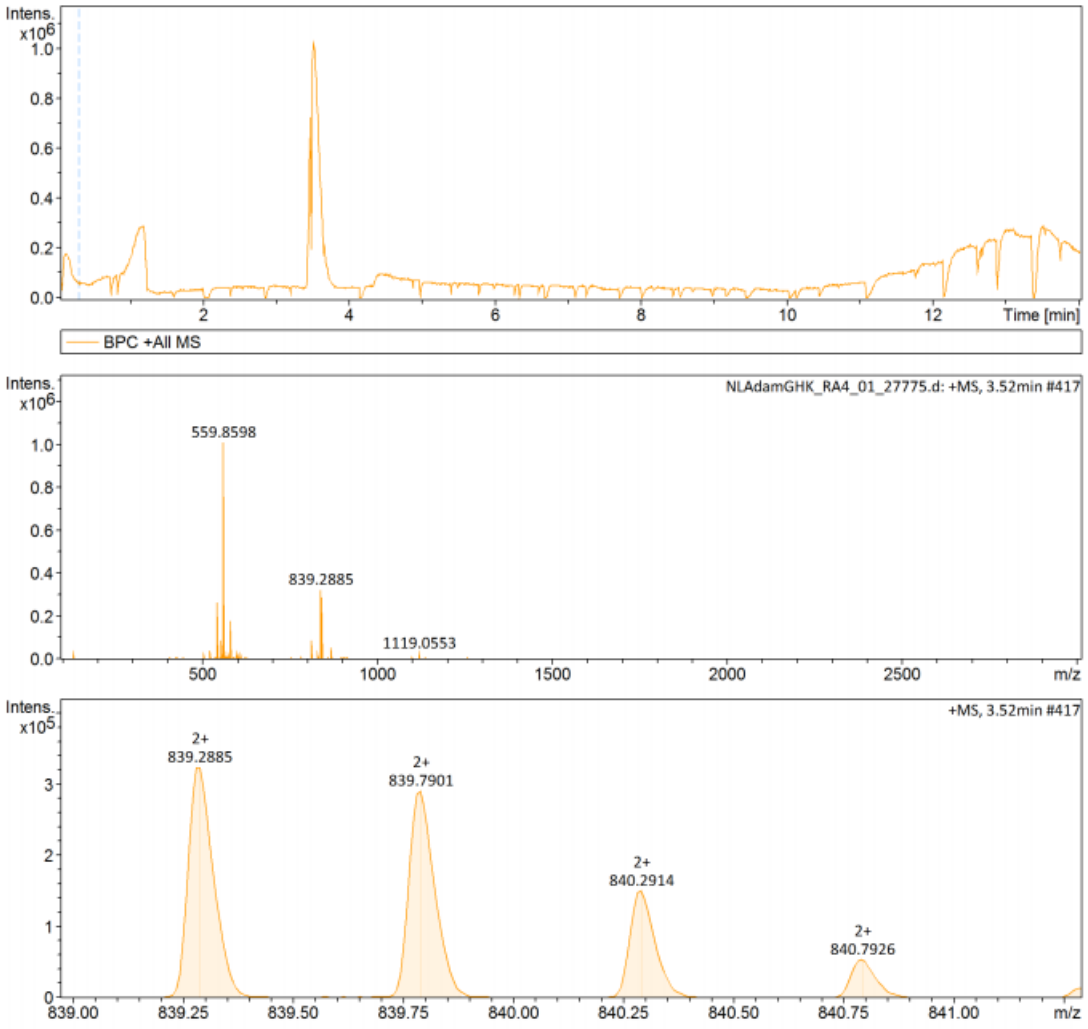

Figure 9.44: Mass spectrum of *retro*-DGD-GG-GFOGER-GG-GHK-Adamantate.

9.6.13 *Retro*-DGD-GG-GFOGER-GG-QPR-Palmitate

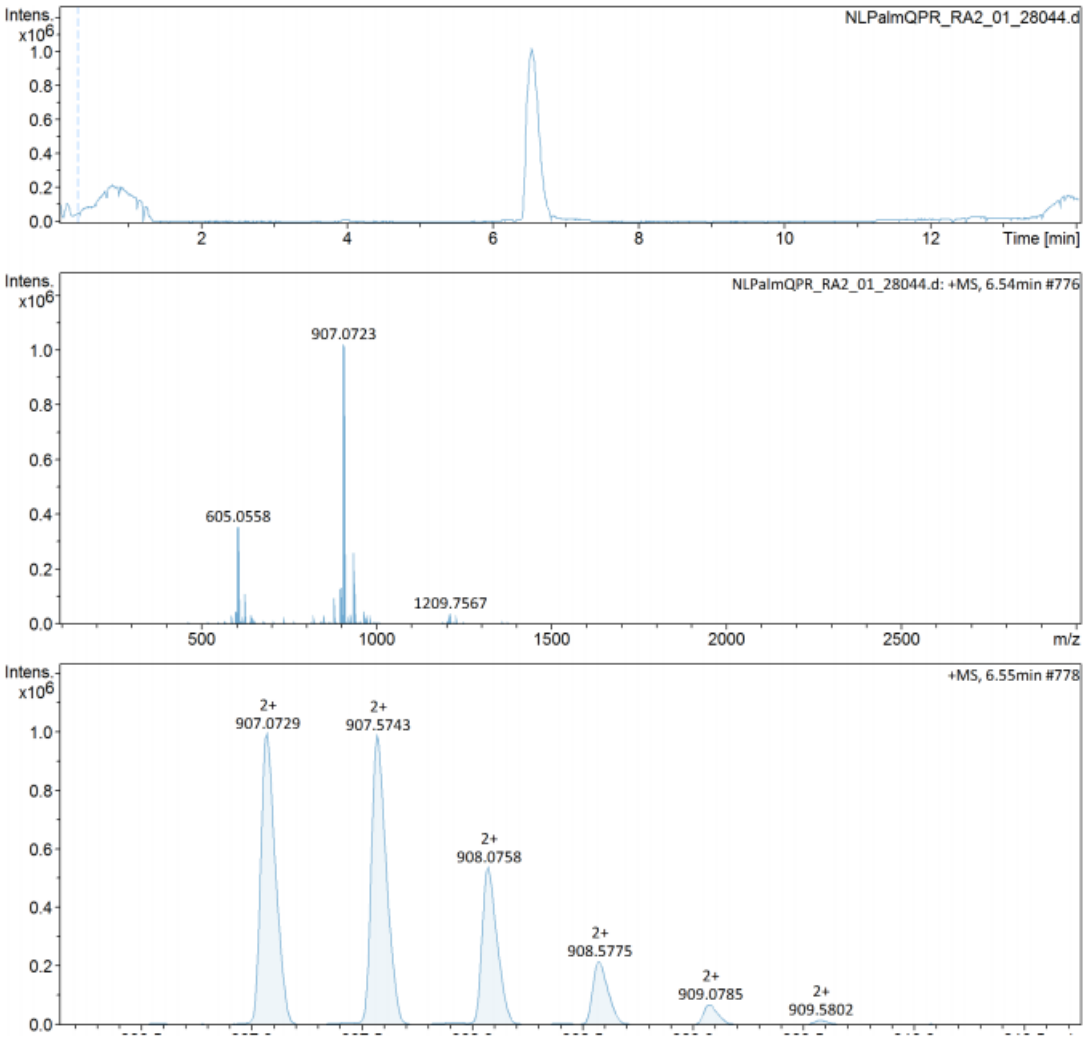

Figure 9.45: Mass spectrum of *retro*-DGD-GG-GFOGER-GG-QPR-Palmitate.

9.6.14 *Retro*-DGD-GG-GFOGER-GG-QPR-Adamantate

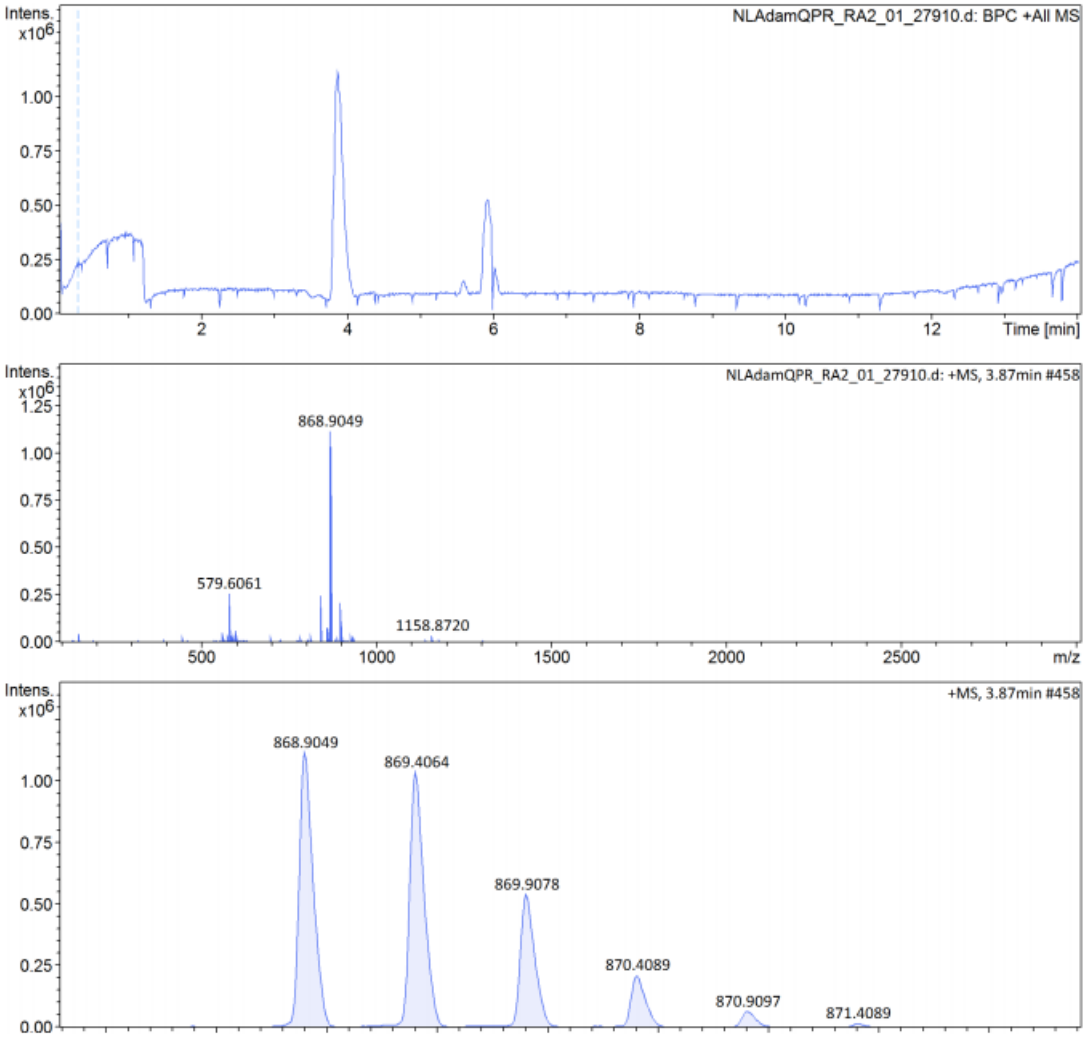

Figure 9.46: Mass spectrum of *retro*-DGD-GG-GFOGER-GG-QPR-Adamantate.

9.6.15 *Retro*-DGD-GG-GFOGER-GG-EEM-Palmitate

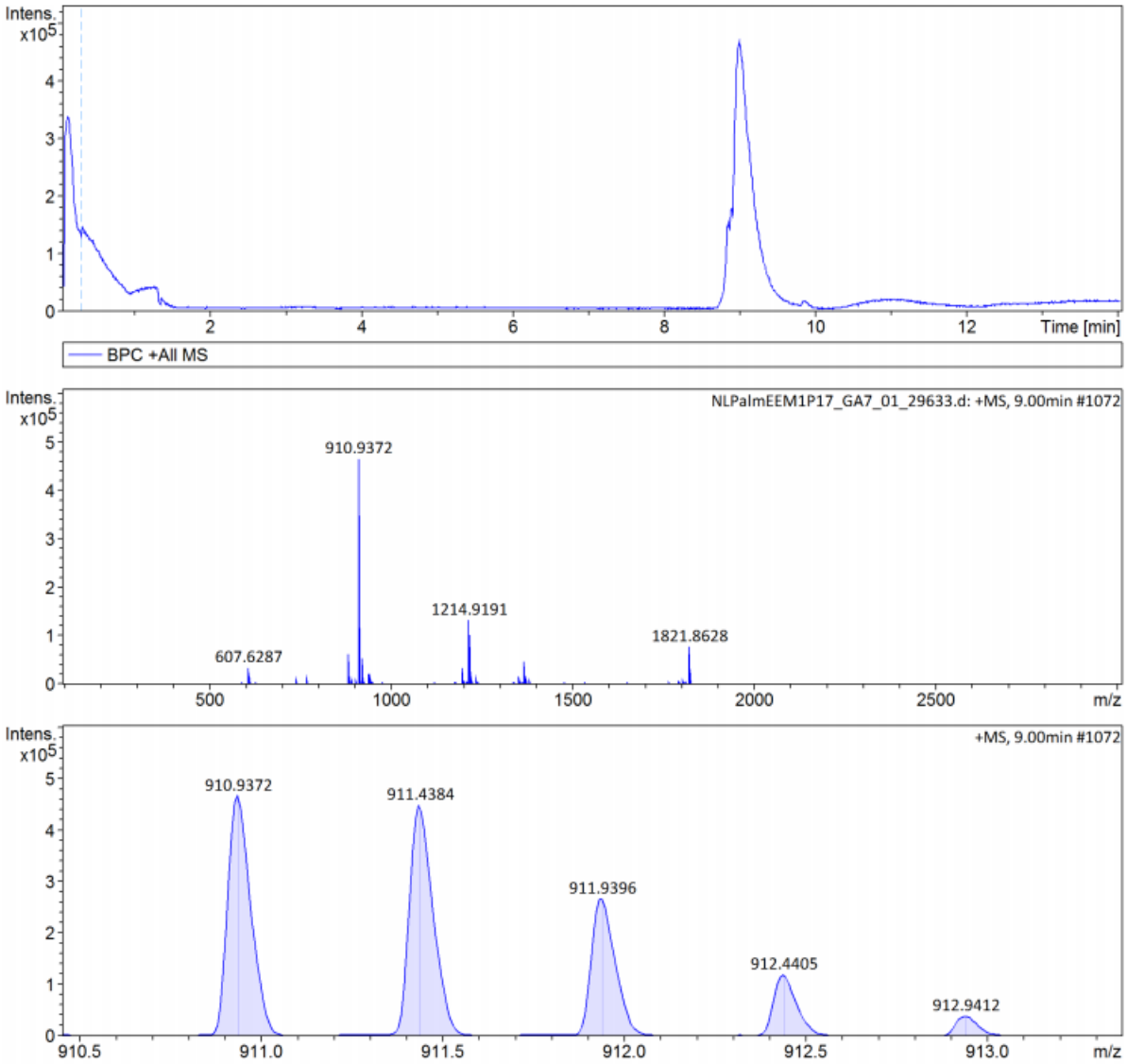

Figure 9.47: Mass spectrum of *retro*-DGD-GG-GFOGER-GG-EEM-Palmitate.

9.6.16 *Retro*-DGD-GG-GFOGER-GG-EEM-Adamantate

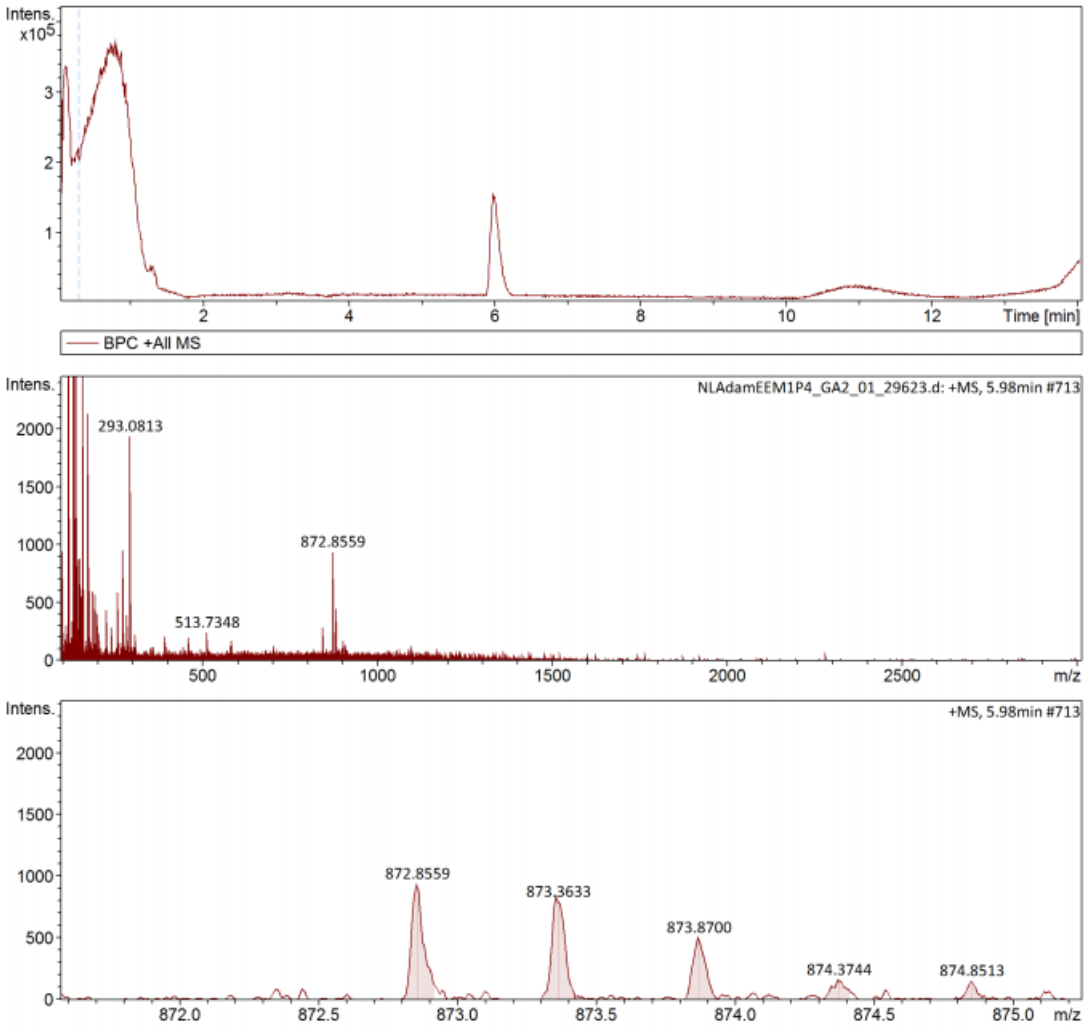

Figure 9.48: Mass spectrum of *retro*-DGD-GG-GFOGER-GG-EEM-Adamantane.

9.6.17 *Retro*-GG-G[*para*-fluoro phenylalanine]OGER-GG-Palmitate (*para*-fluoro phenylalanine peptide)

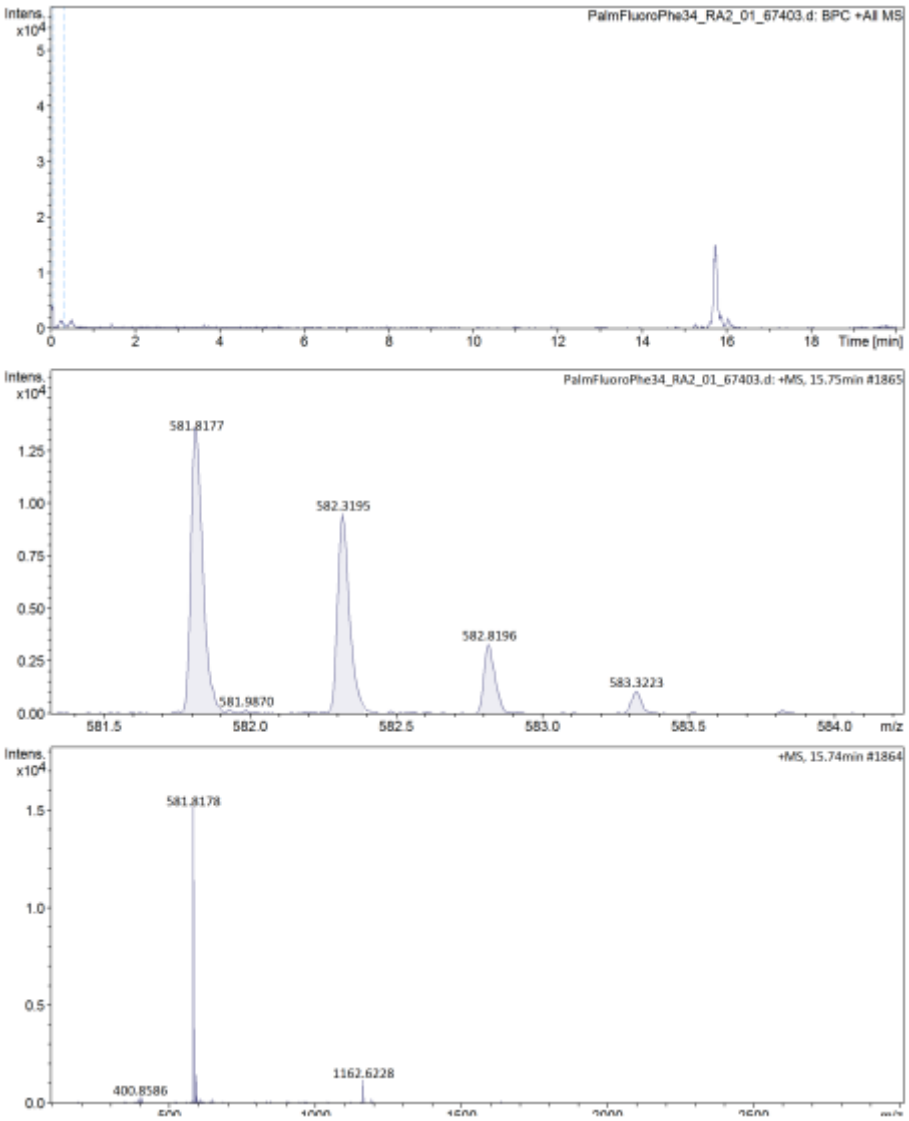

Figure 9.49: Mass spectrum of *retro*-*para*-fluorophenyl adamantane peptide.

9.6.18 *Retro*-GG-G[*para*-fluoro phenylalanine]OGER-GG-Adamantane (*para*-fluoro phenylalanine peptide)

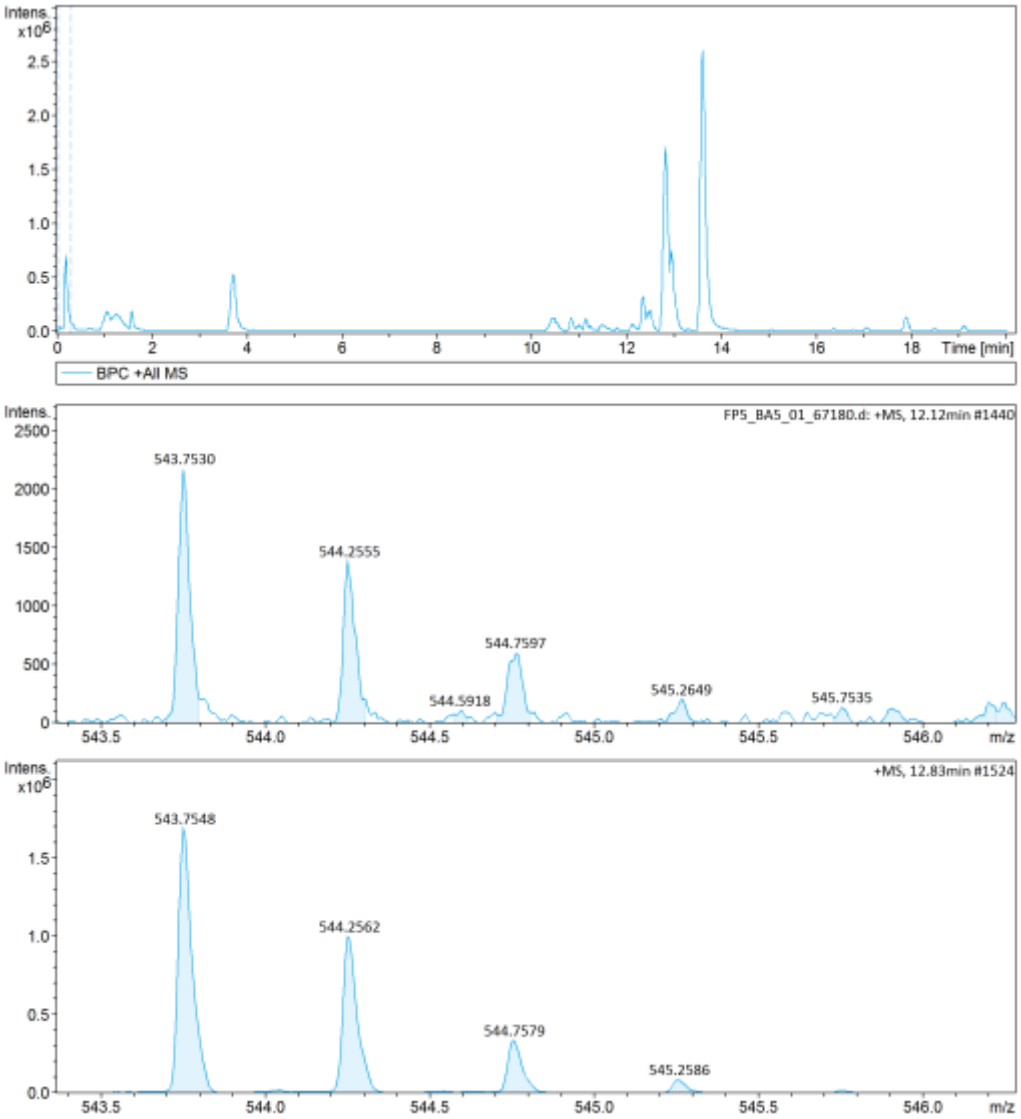

Figure 9.50: Mass spectrum of *retro*-*para*-fluorophenyl adamantane peptide.

9.6.19 *Retro*-GG-GFOGER-GG-Adamantane (D-Peptide)

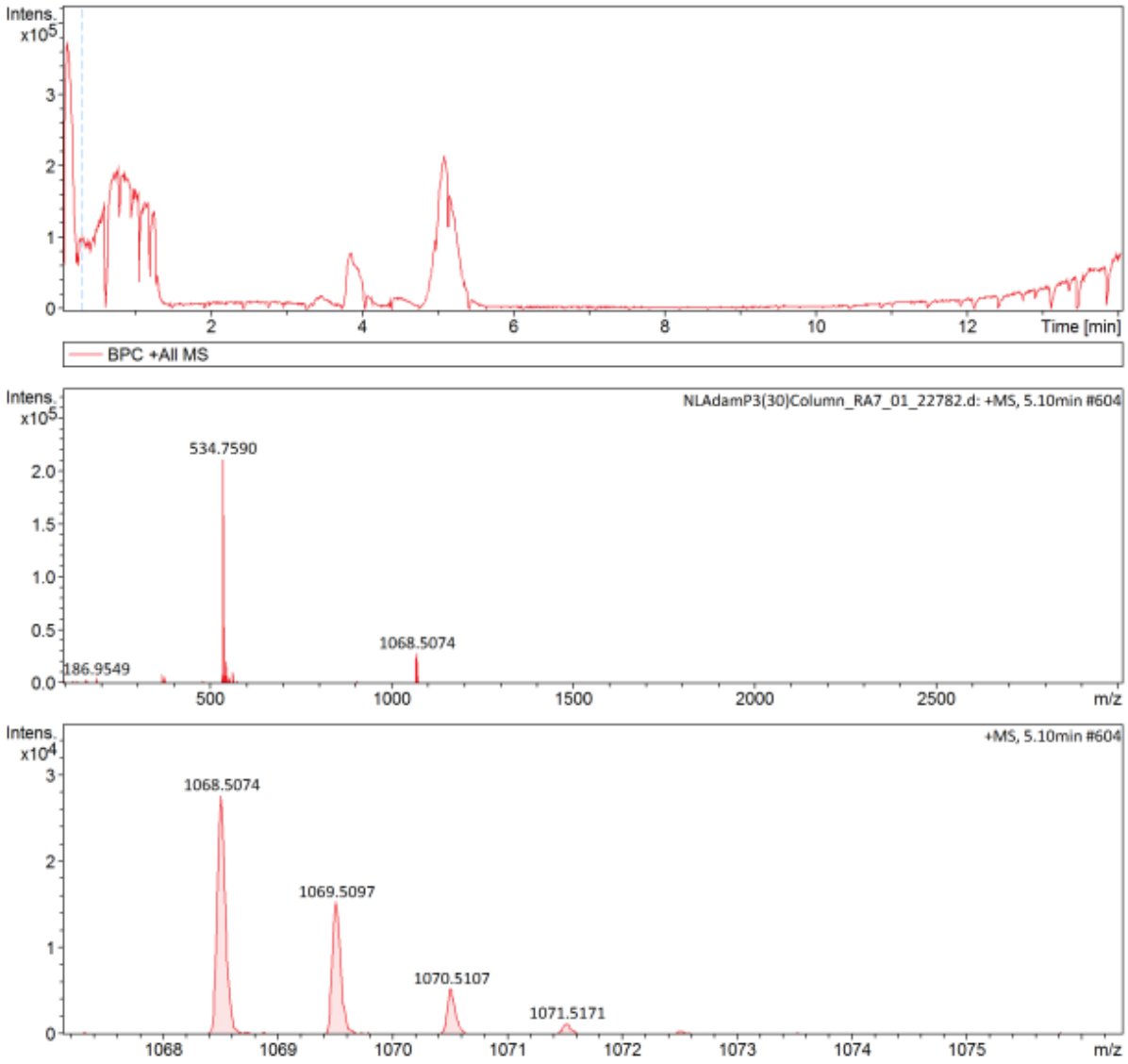

Figure 9.51: Mass spectrum of *retro*-GG-GFOGER-GG-Adamantane (D-Peptide).

9.6.20 *Retro*-GG-GFOGER-GG-Palmitate (D-Peptide)

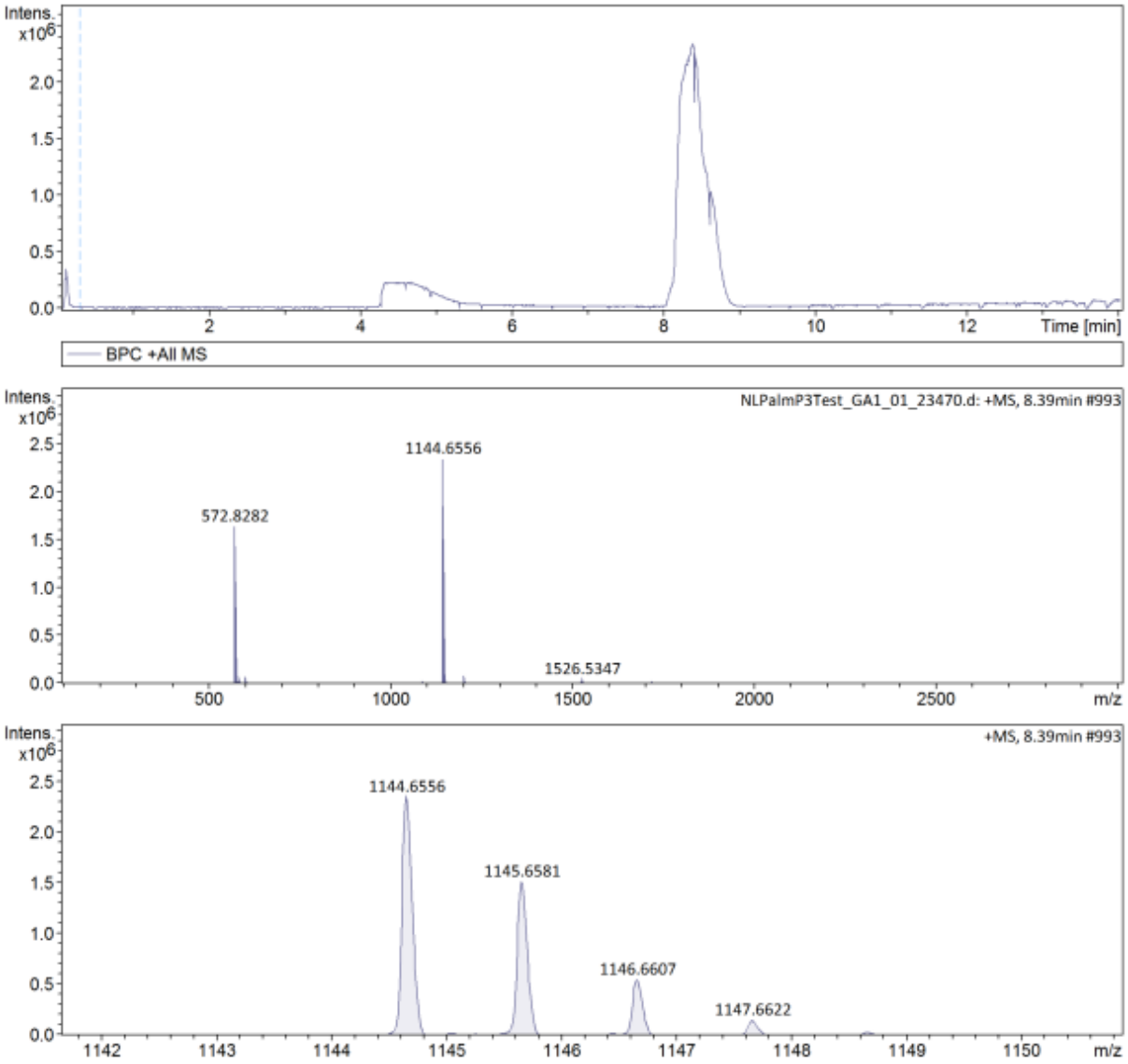

Figure 9.52: Mass spectrum of *retro*-GG-GFOGER-GG-Palmitate (D-Peptide).

9.6.21 *Retro*-GG-GF[G-Me]G[G-Me][G-Me]-GG-Adamantate (Reference Peptoid)

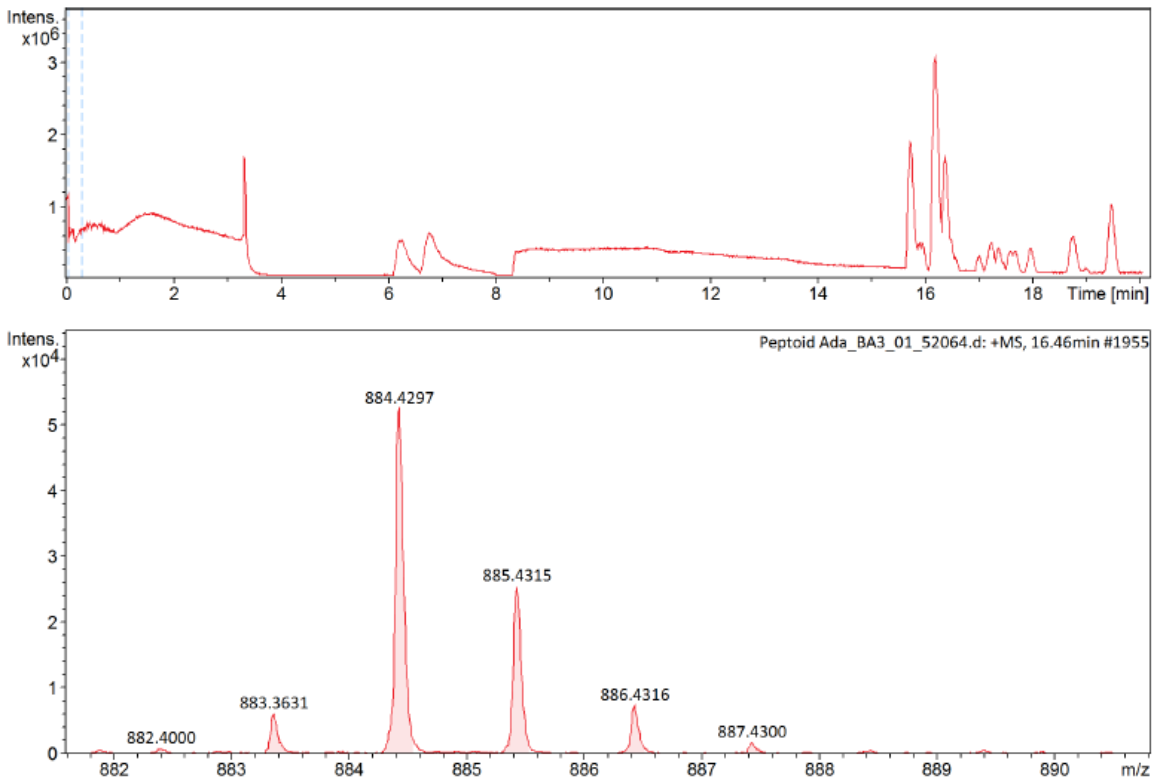

Figure 9.53: Mass spectrum of *retro*-GG-GF[G-Me]G[G-Me][G-Me]-GG-Adamantate (Reference Peptoid).

9.6.22 *Retro*-GG-GF[G-Me]G[G-Me][G-Me]-GG-Palmitate (Reference Peptoid)

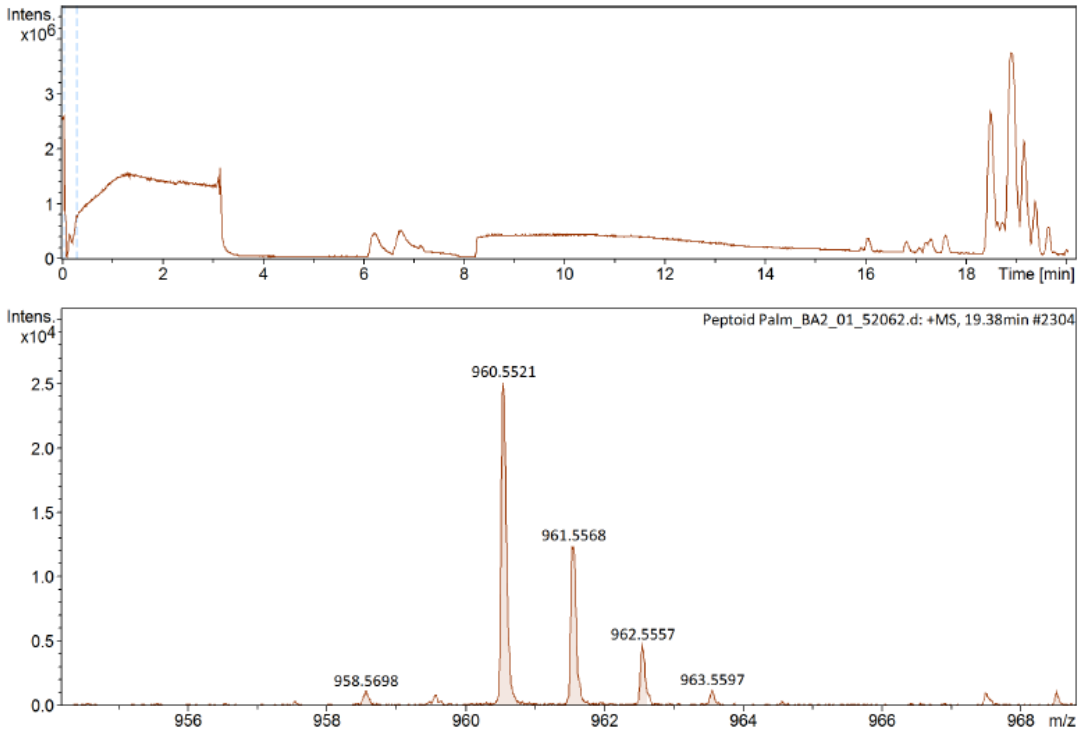

Figure 9.54: Mass spectrum of *retro*-GG-GF[G-Me]G[G-Me][G-Me]-GG-Palmitate (Reference Peptoid).

9.6.23 *Retro*-GG-GFOGER-GG-Adamantane (Peptoids)

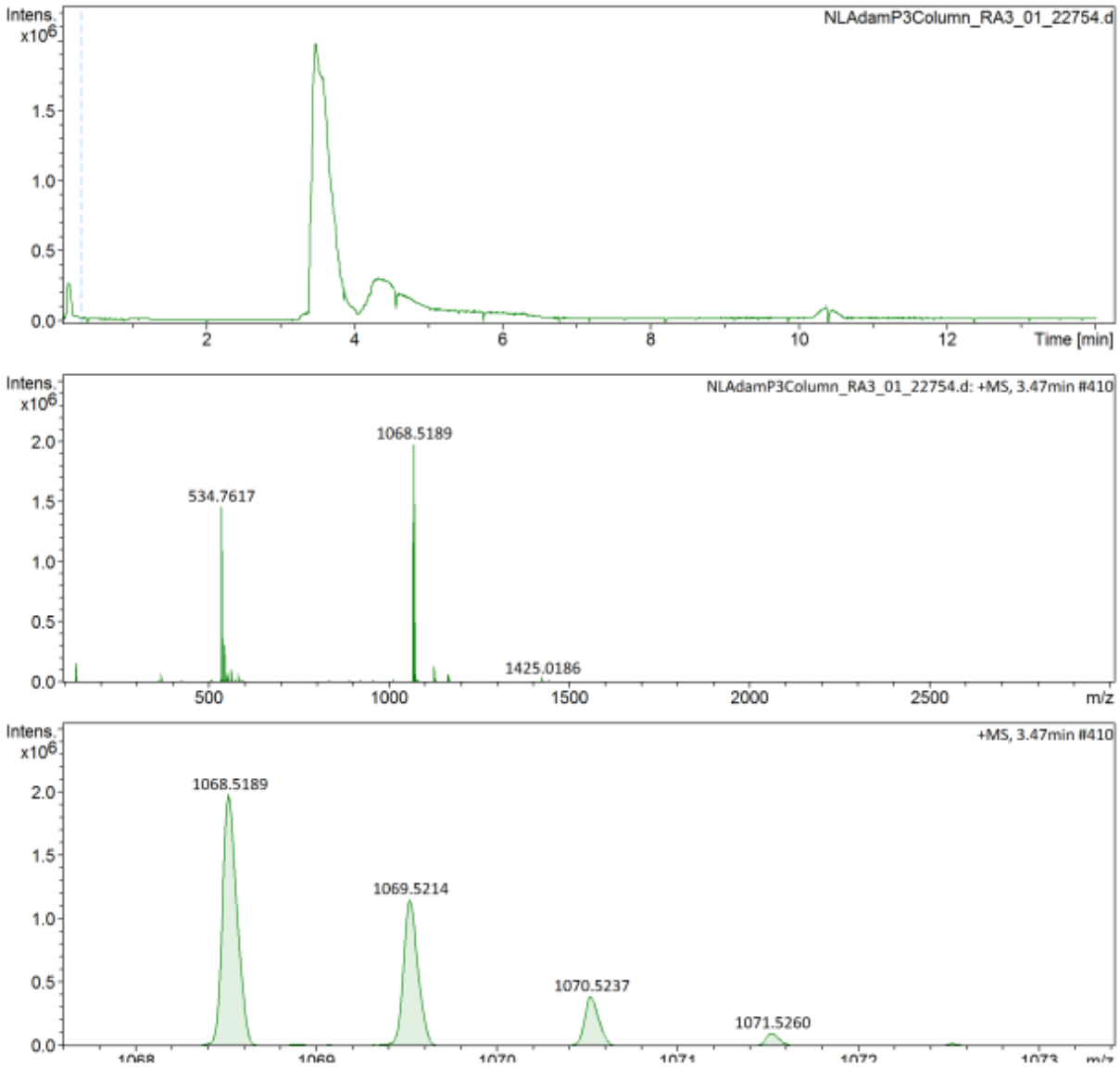

Figure 9.55: Mass spectrum of *retro*-GG-GFOGER-GG-Adamantane (Peptoids).

9.6.24 *Retro*-GG-GFOGER-GG-Palmitate (Peptoids)

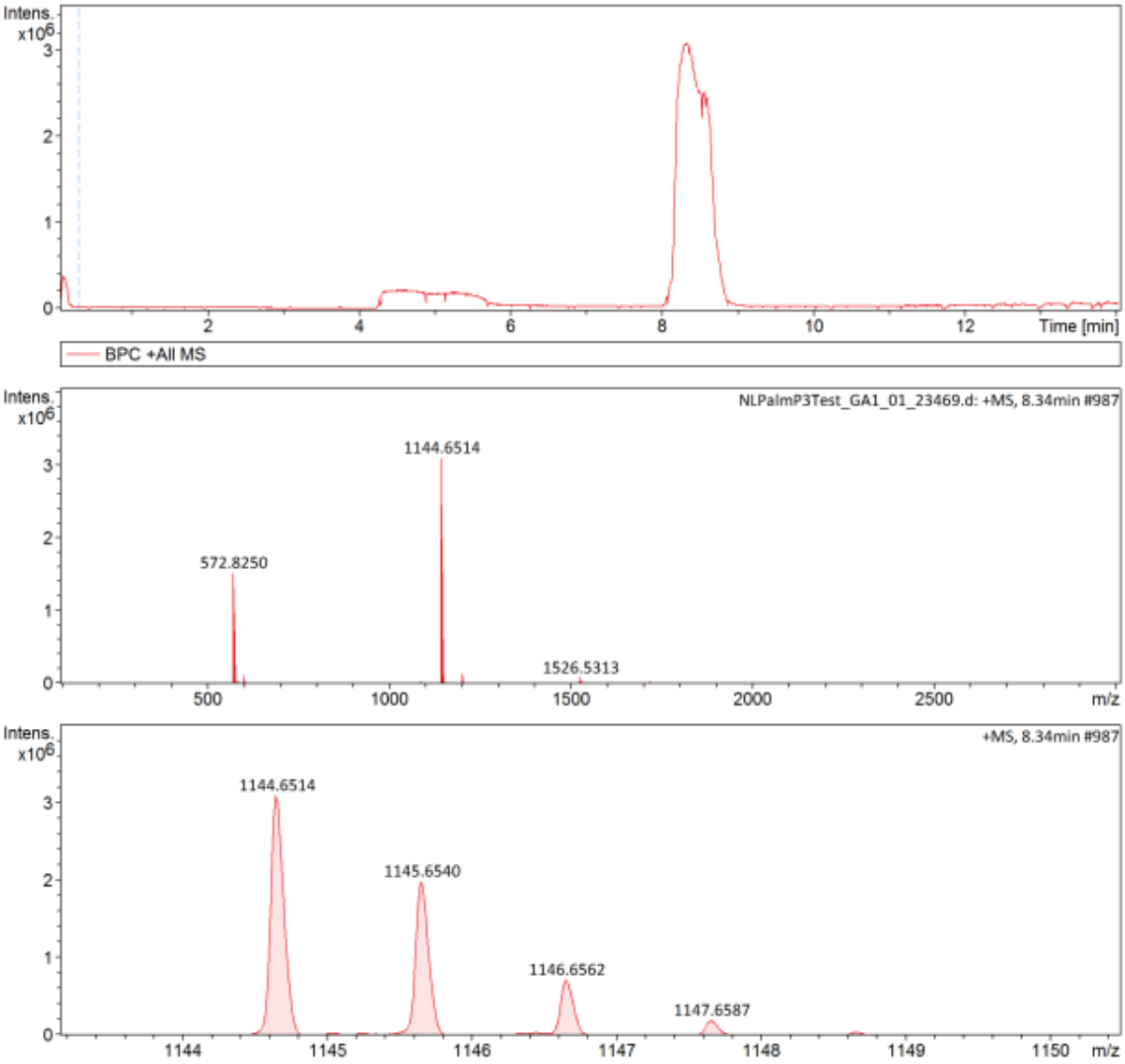

Figure 9.56: Mass spectrum of *retro*-GG-GFOGER-GG-Palmitate (Peptoids).

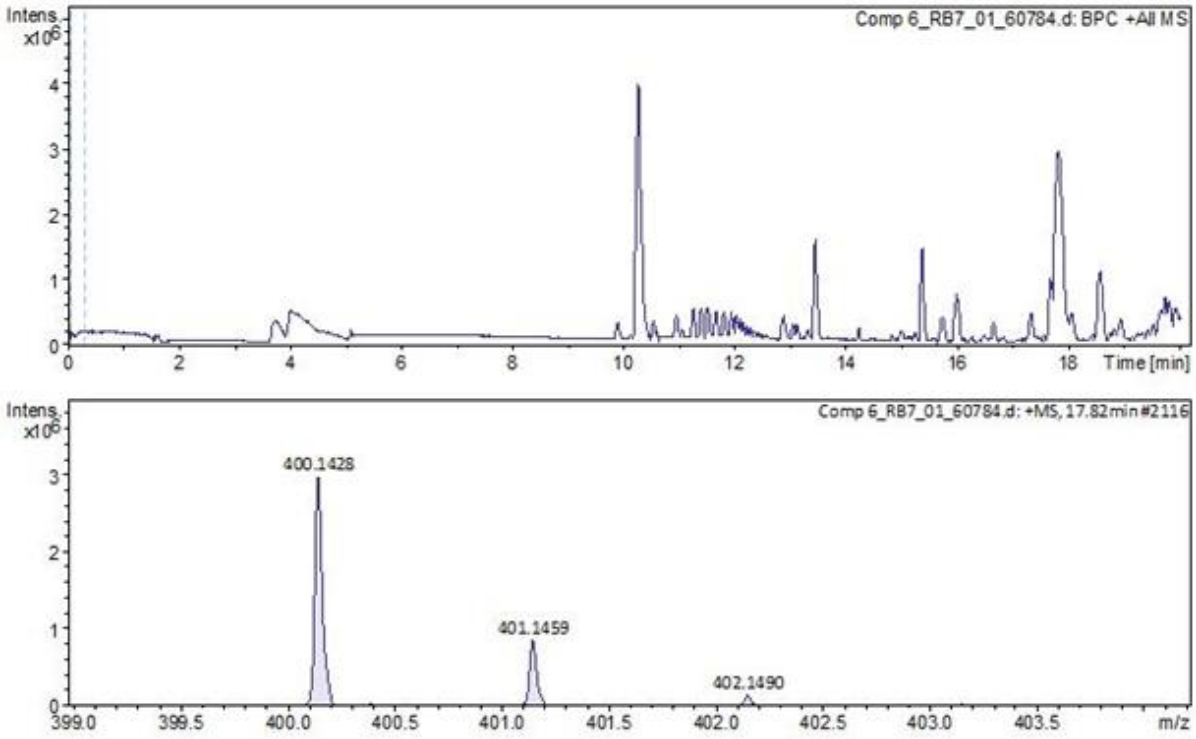

Figure 9.57: Mass spectrum of crude phenylalanine oxazolidinone.

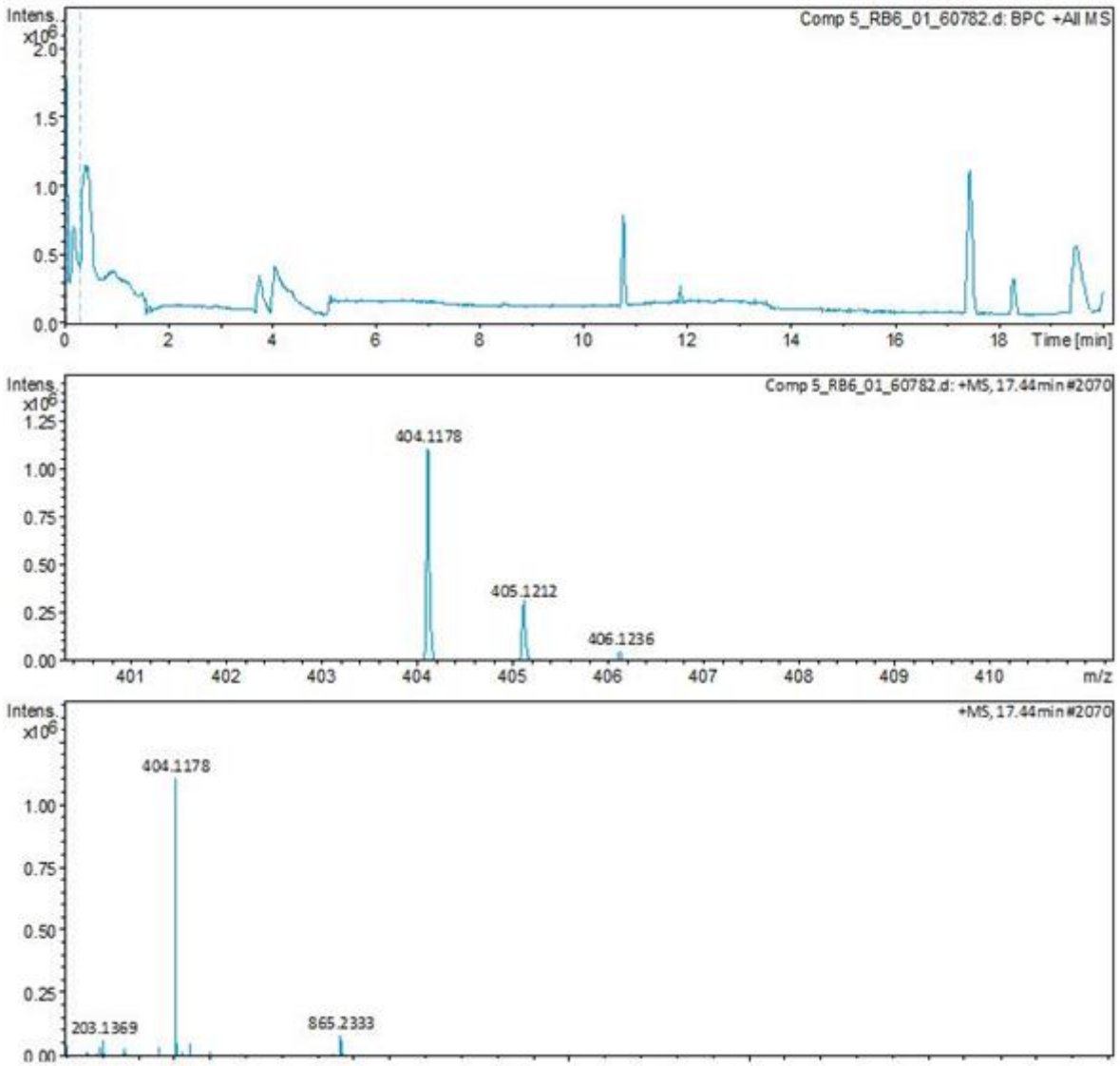

Figure 9.58: Mass spectrum of crude *N*-methylated phenylalanine.

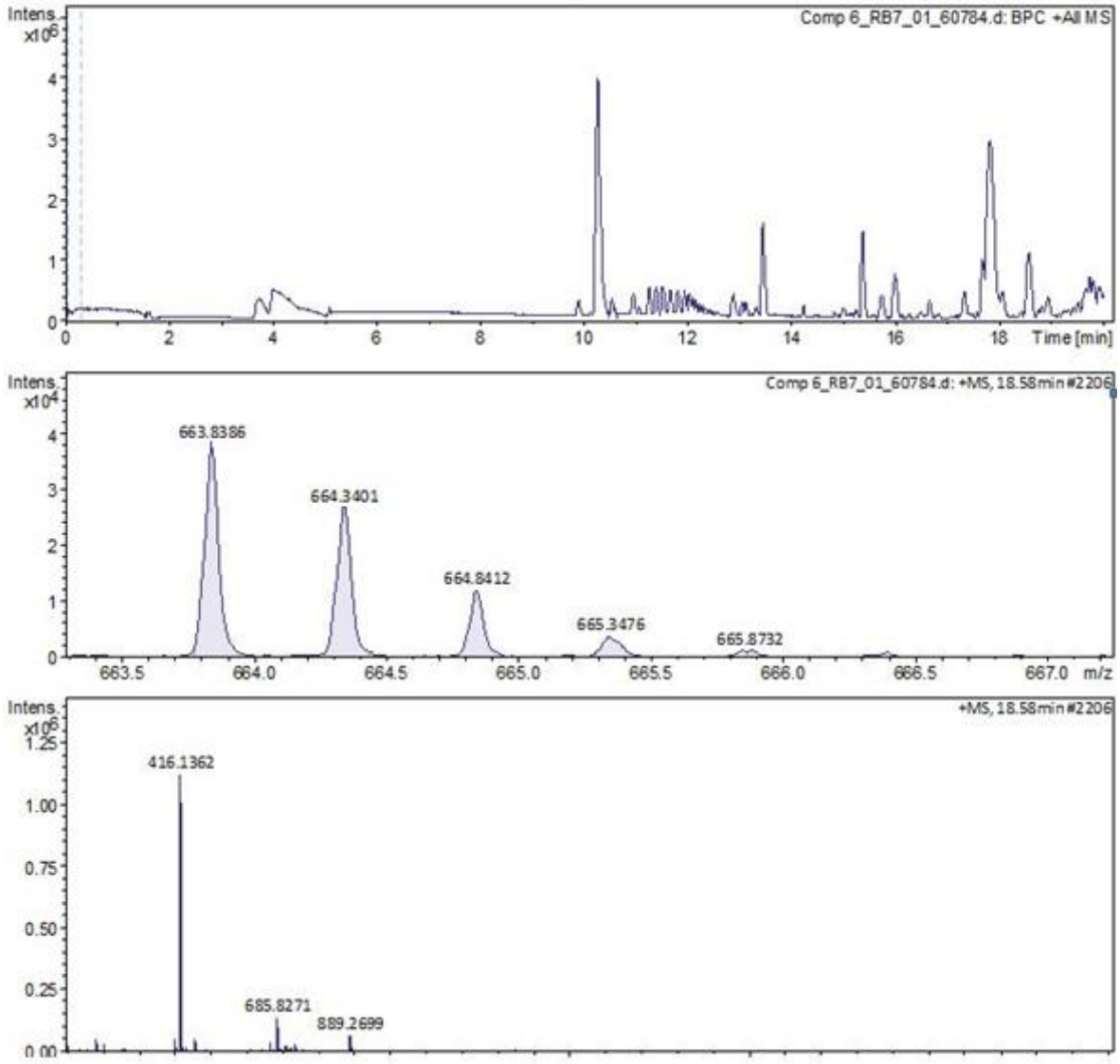

Figure 9.59: Mass spectrum of crude Fmoc- arginine oxazolidinone.

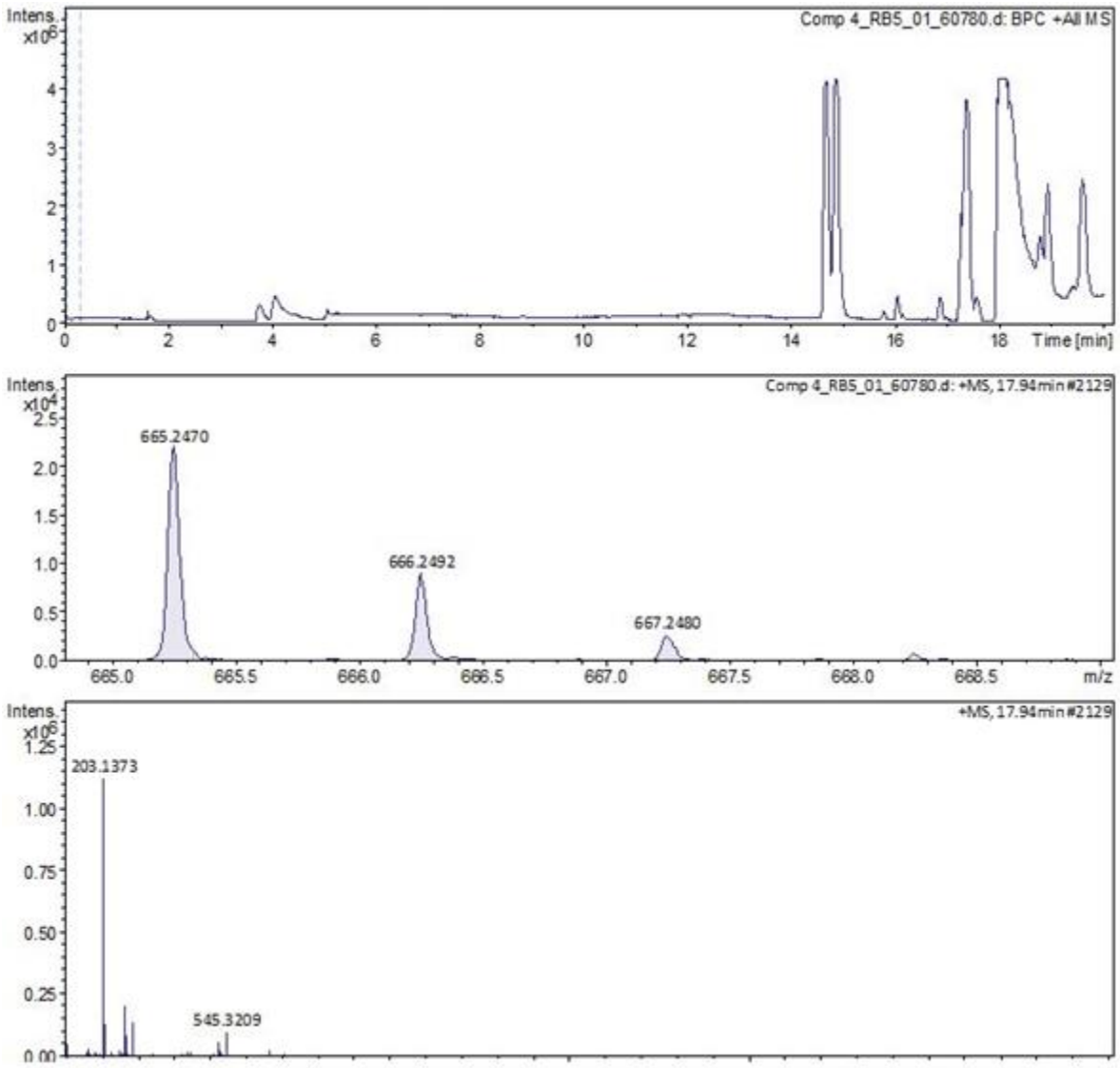

Figure 9.60: Mass spectrum of crude *N*-methylated arginine.

9.6.25 *Retro*-GG-GFOGER-GG-Adamantane (Singly Methylated)

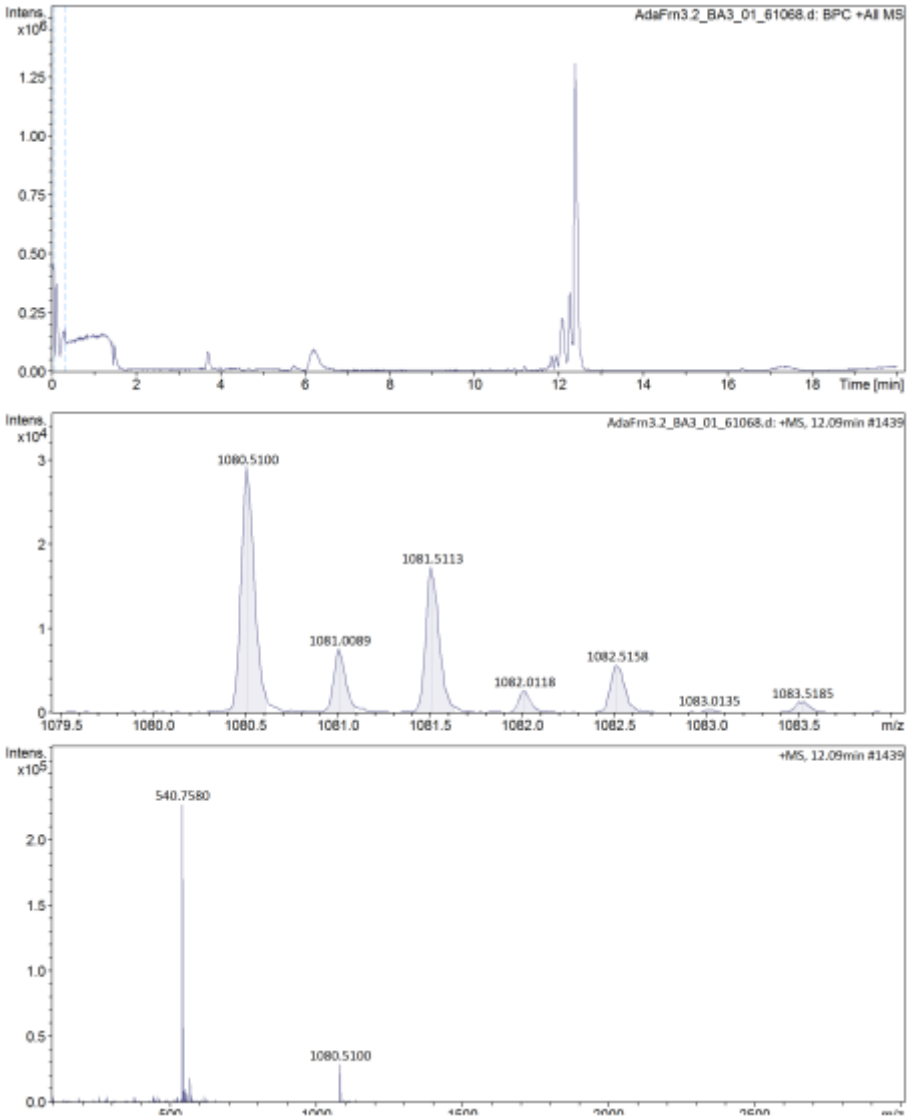

Figure 9.61: Mass spectrum of *retro*-GG-GFOGER-GG-Adamantane (Singly Methylated).

9.6.26 *Retro*-GG-GFOGER-GG-Palmitate (Singly Methylated)

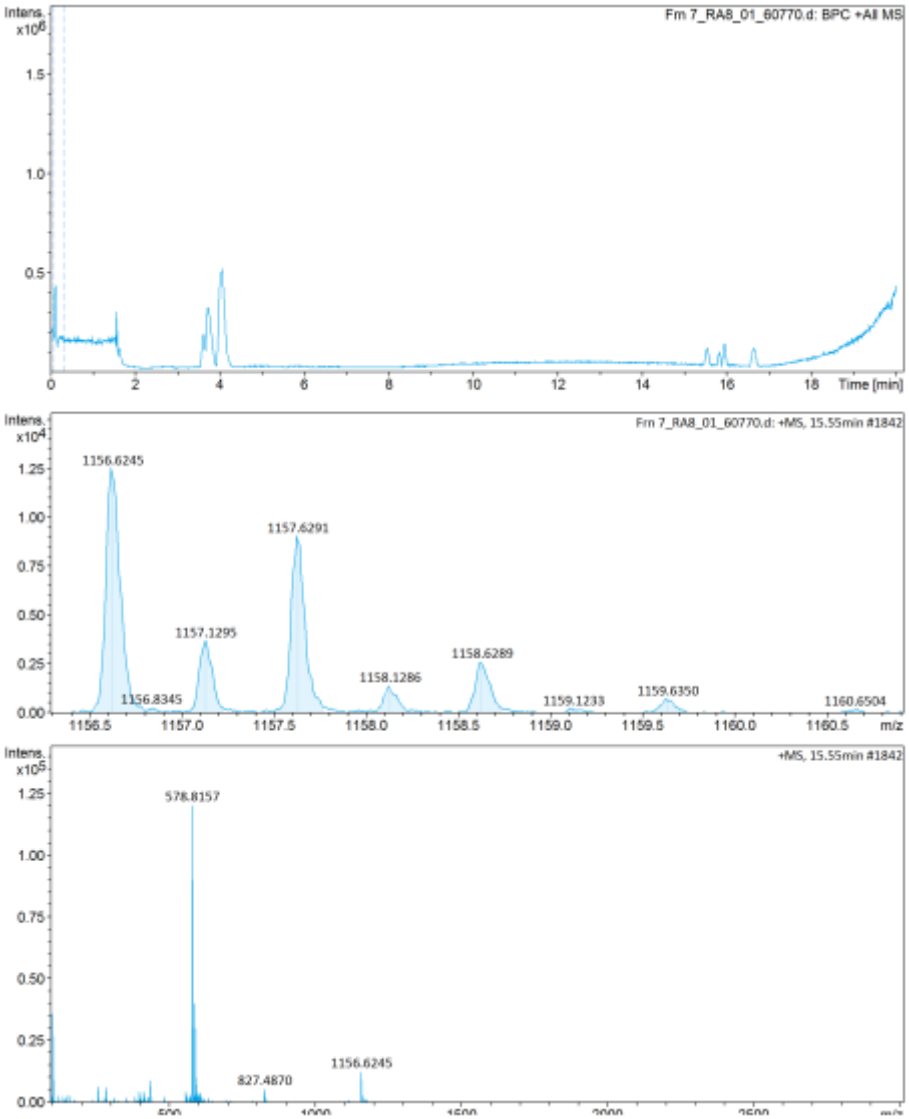

Figure 9.62: Mass spectrum of *retro*-GG-GFOGER-GG-Palmitate (Singly Methylated).

9.6.27 *Retro*-GG-GFOGER-GG-Adamantane (Doubly Methylated)

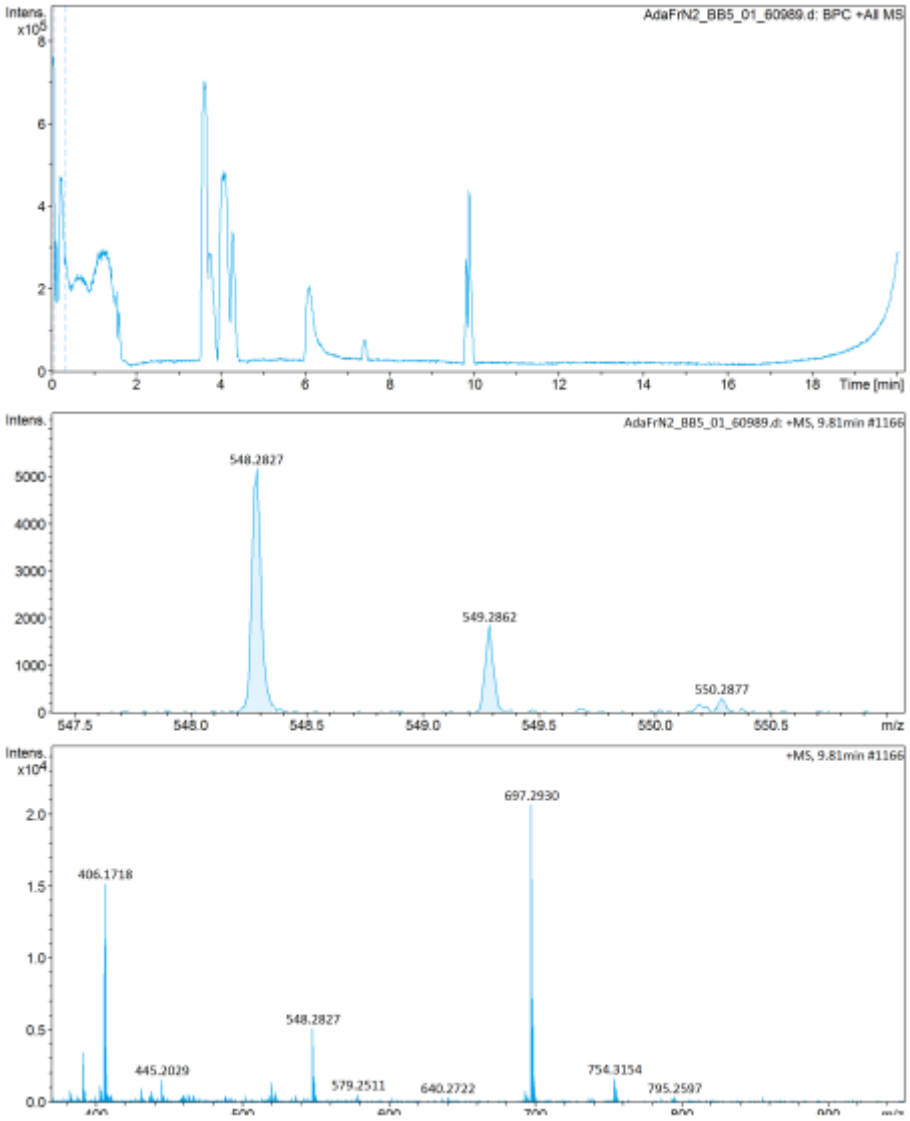

Figure 9.63: Mass spectrum of *retro*-GG-GFOGER-GG-Adamantane (Doubly Methylated).

9.6.28 *Retro*-GG-GFOGER-GG-Palmitate (Doubly Methylated)

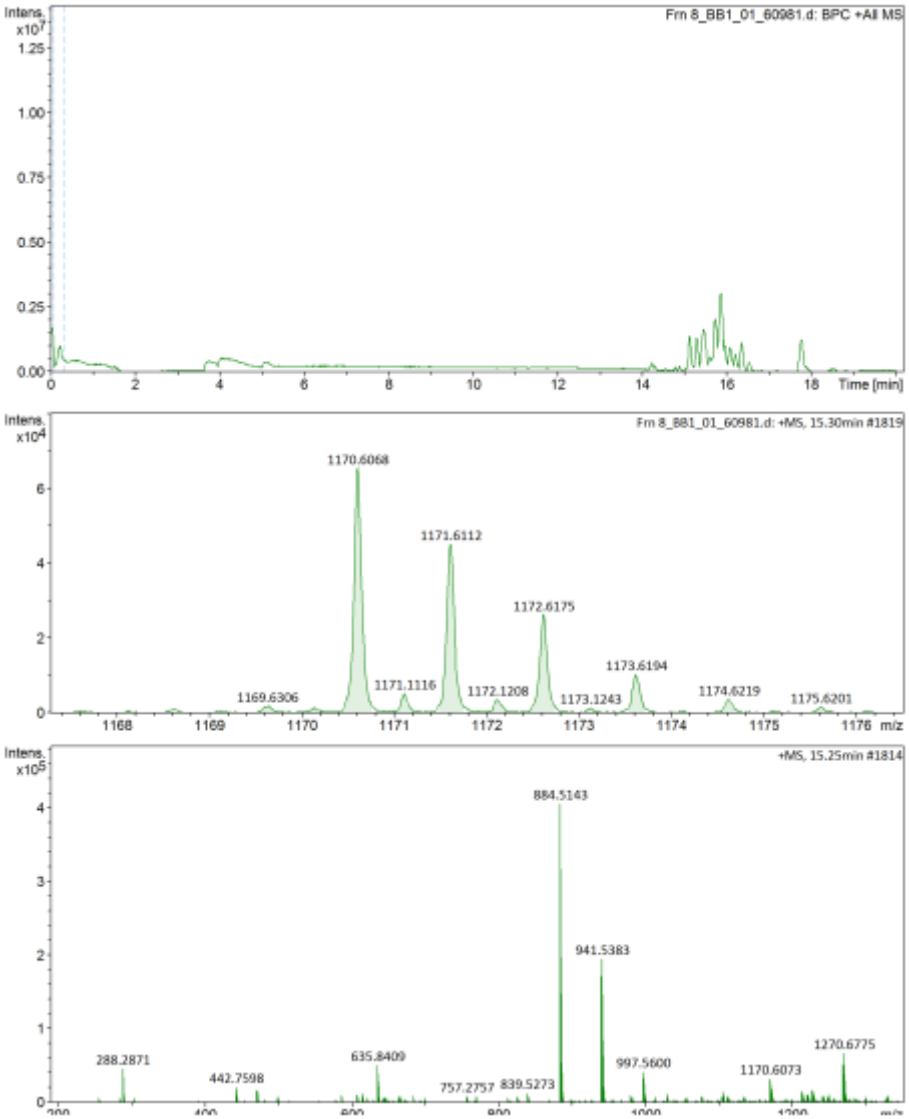

Figure 9.64: Mass spectrum of *retro*-GG-GFOGER-GG-Palmitate (Doubly Methylated).

9.7 NMR SPECTRA OF SELECTED PEPTIDES

9.7.1 ^{1}H NMR spectrum of *retro*-DGRGOF-Adamantate

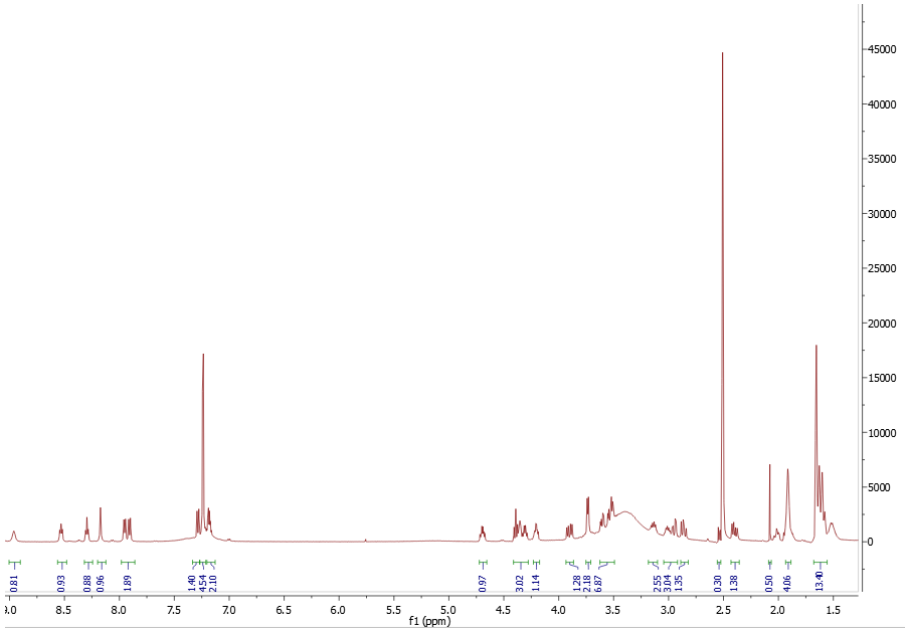

Figure 9.65: ^{1}H NMR spectrum of *retro*-DGRGOF-Adamantate.

9.7.2 ^{13}C NMR spectrum of *retro*-DGRGOF-Adamantane

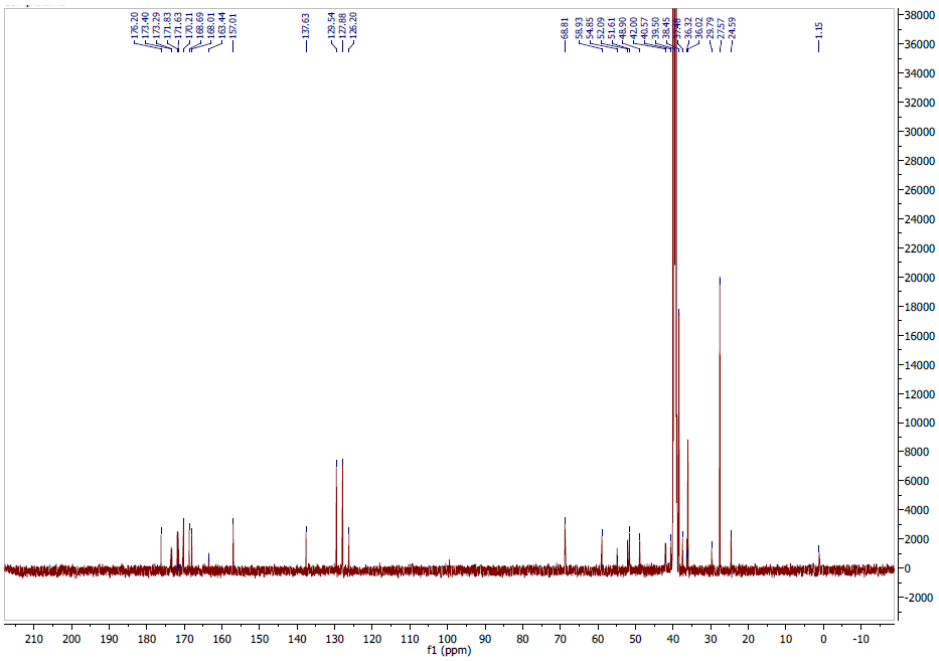

Figure 9.66: ^{13}C NMR spectrum of *retro*-DGRGOF-Adamantane.

9.7.3 DEPT 135 spectrum of *retro*-DGRGOF-Adamantane

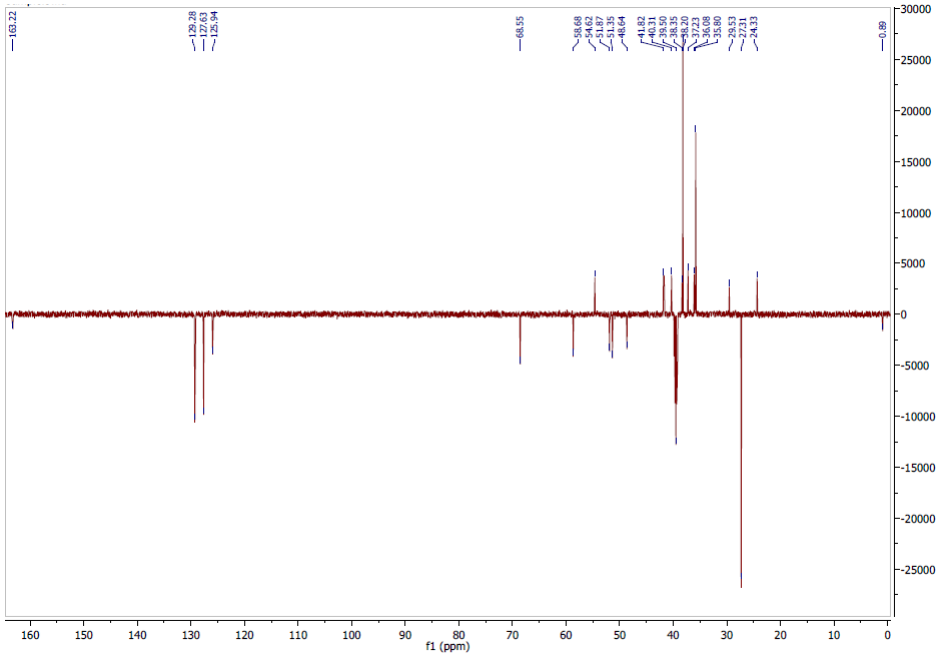

Figure 9.67: DEPT 135 spectrum of *retro*-DGRGOF-Adamantane.

9.7.4 COSY spectrum of *retro*-DGRGOF-Adamantane

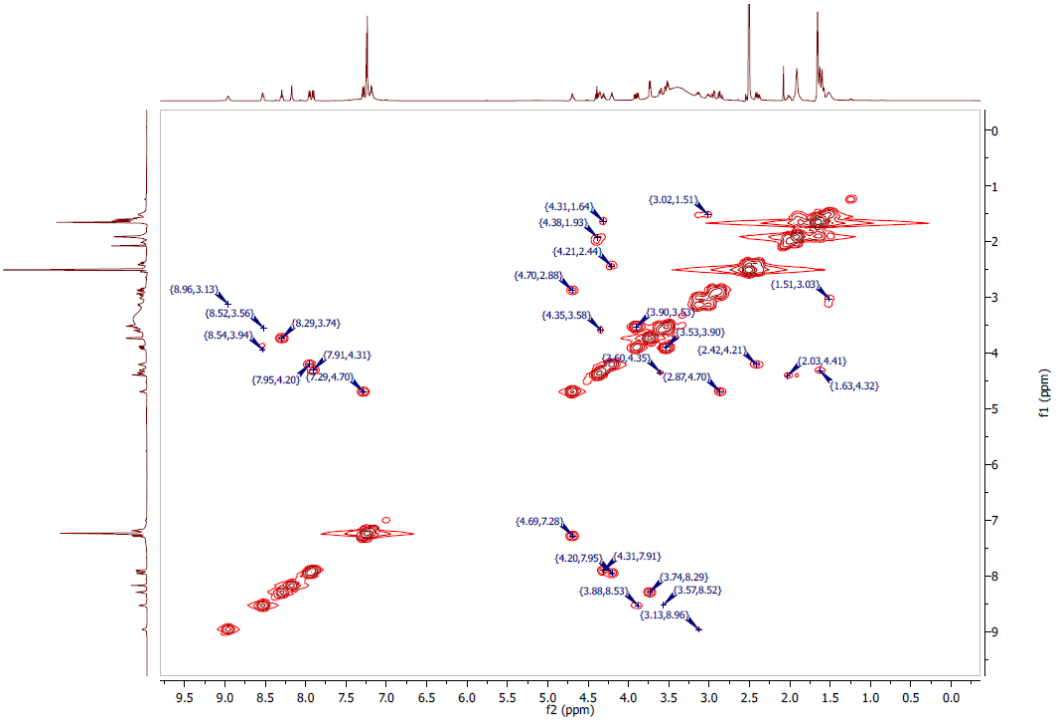

Figure 9.68: COSY spectrum of *retro*-DGRGOF-Adamantane.

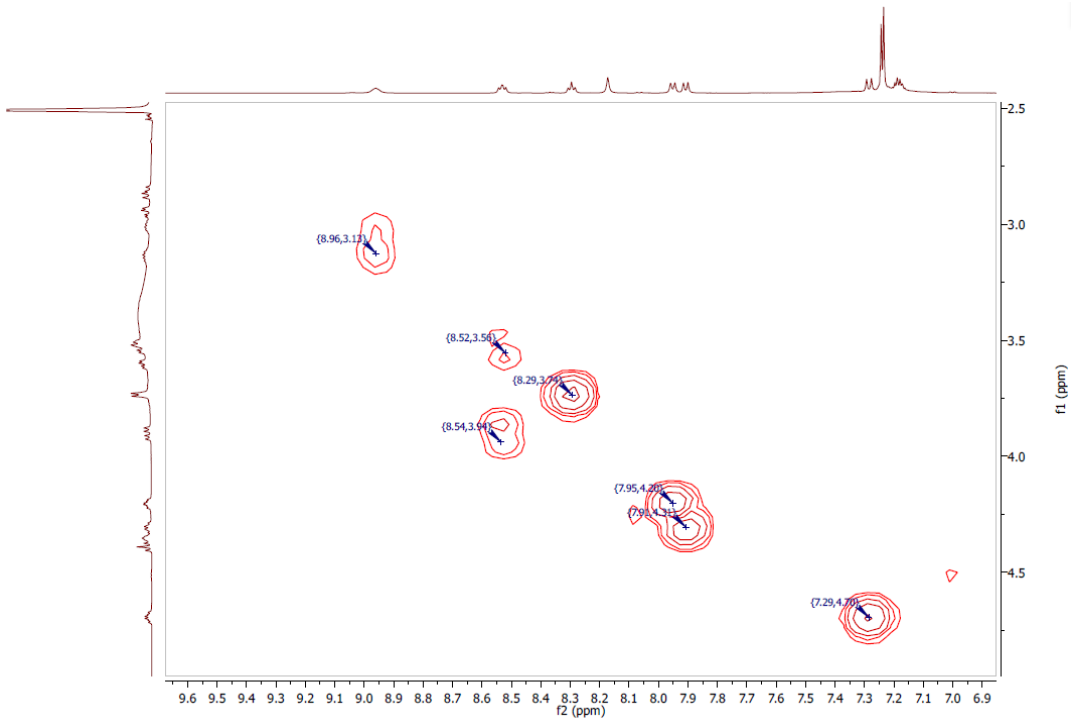

Figure 9.69: COSY *alpha*-amide section of spectrum of *retro*-DGRGOF-Adamantane.

9.7.5 HSQC spectrum of *retro*-DGRGOF-Adamantane

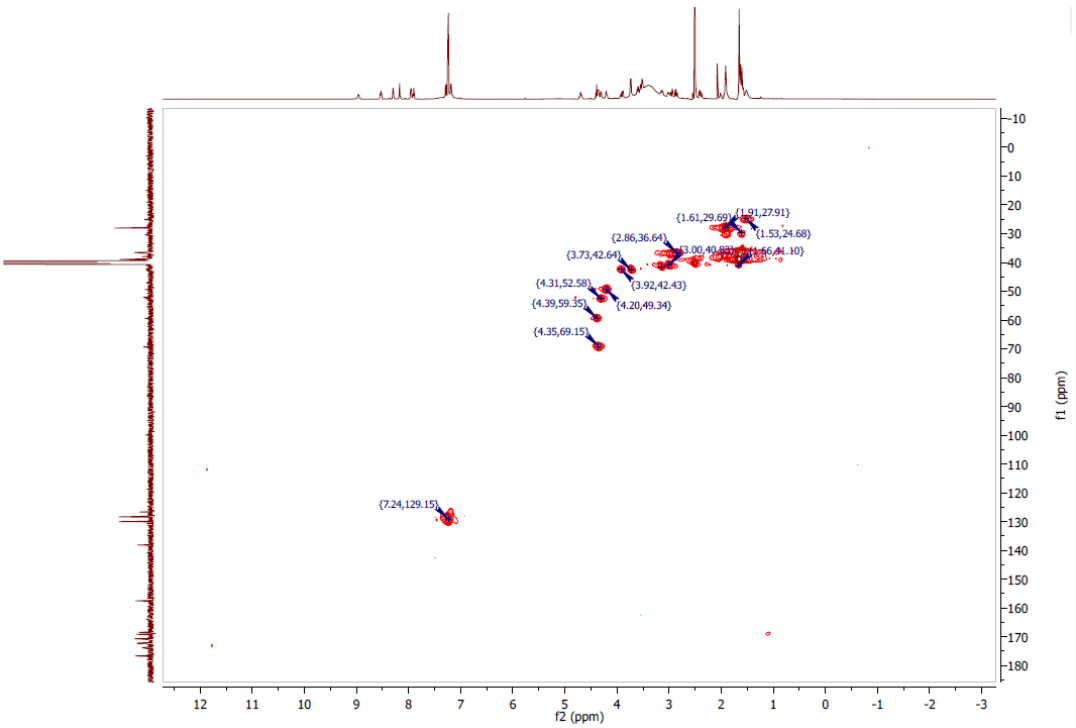

Figure 9.70: HSQC spectrum of *retro*-DGRGOF-Adamantane.

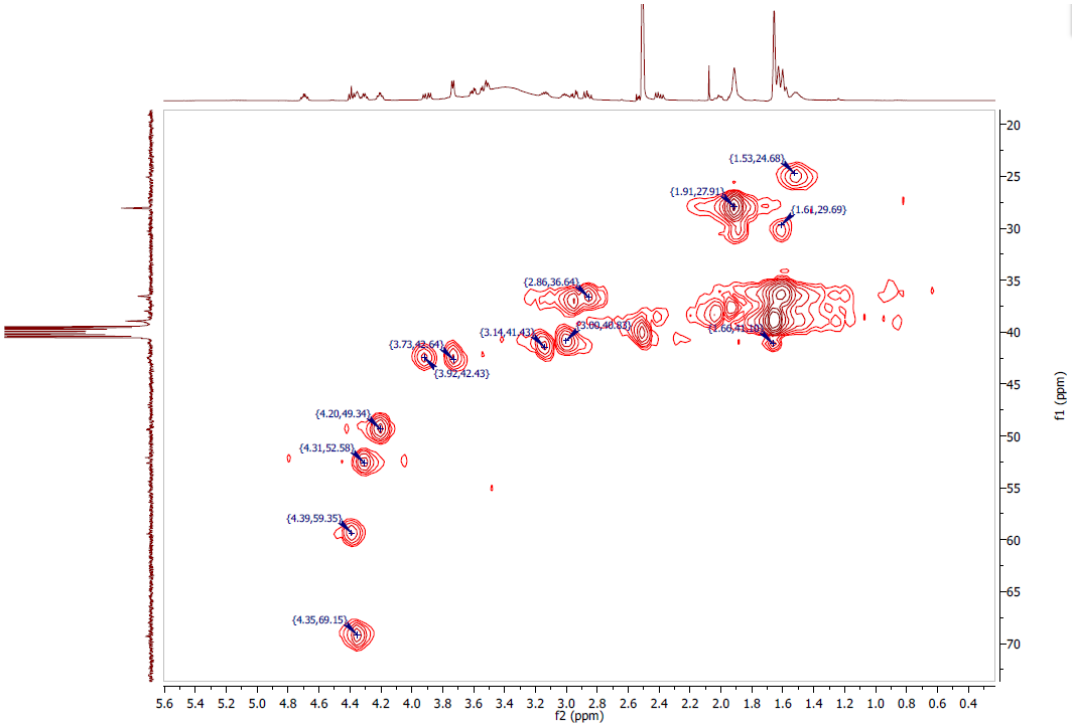

Figure 9.71: HSQC *alpha* section of spectrum of *retro*-DGRGOF-Adamantane.

9.7.6 ROESY spectrum of *retro*-DGRGOF-Adamantane

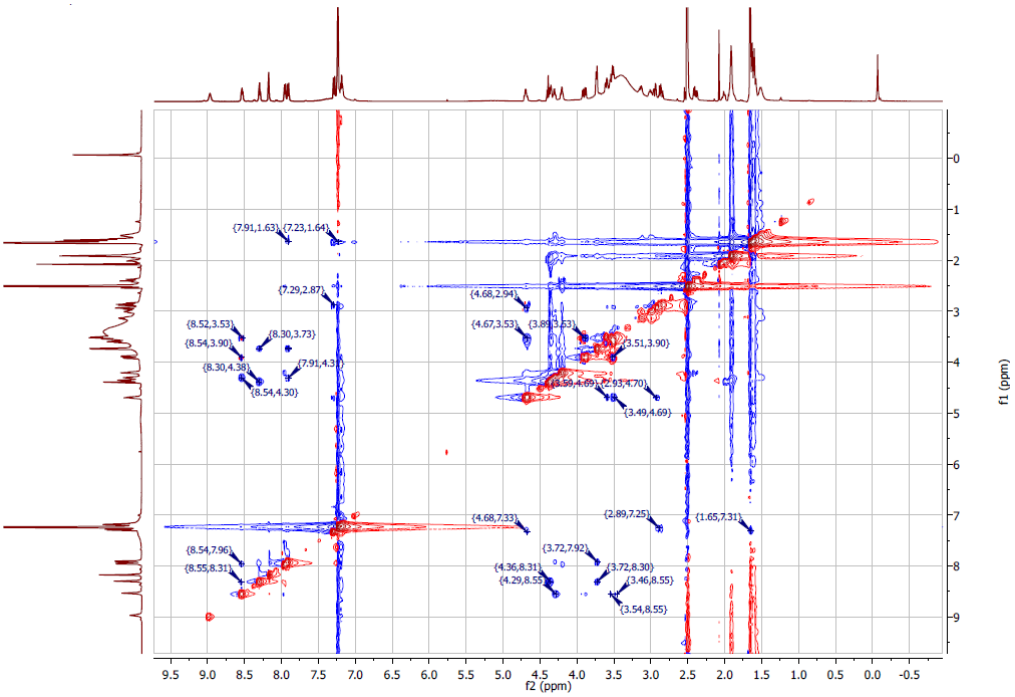

Figure 9.72: ROESY spectrum of *retro*-DGRGOF-Adamantane.

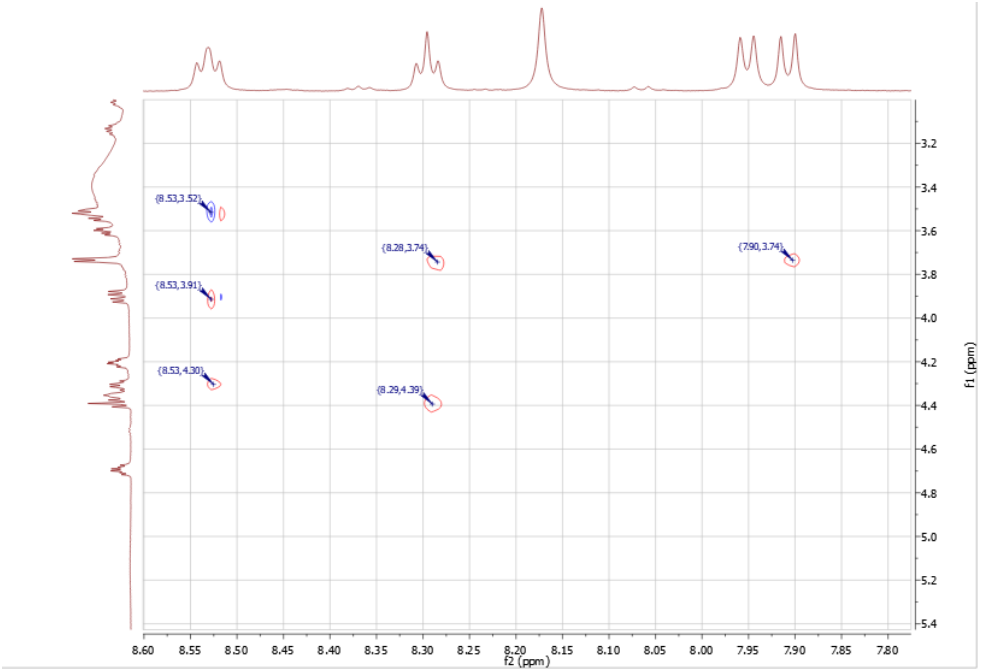

Figure 9.73: ROESY *alpha*-amide section of spectrum of *retro*-DGRGOF-Adamantane.

9.7.7 ^{1}H NMR Spectrum of *retro*-GG-GFOGER-GG-Adamantane

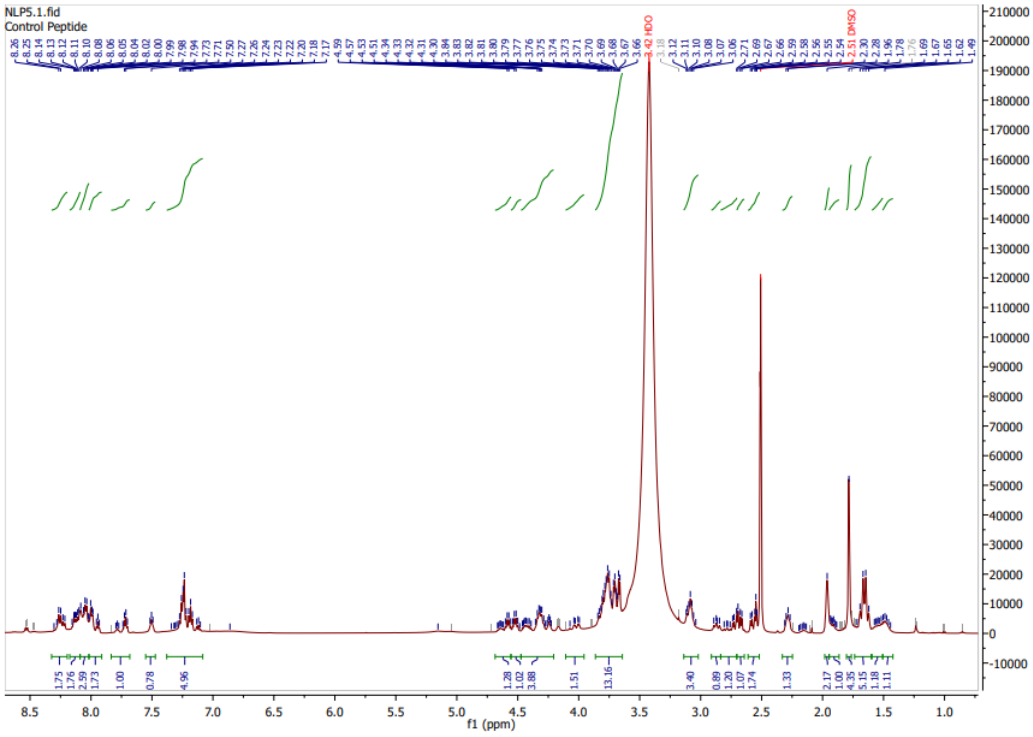

Figure 9.74: ^{1}H NMR spectrum of *retro*-GG-GFOGER-GG-Adamantane.

9.7.8 ^{13}C NMR spectrum of *retro*-GG-GFOGER-GG-Adamantane

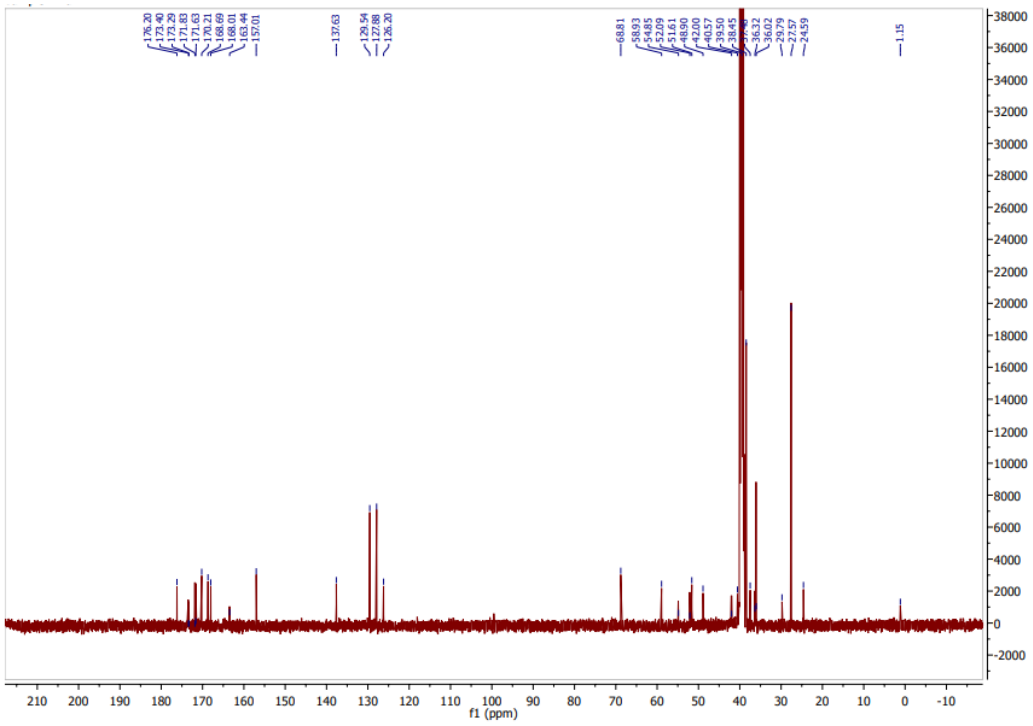

Figure 9.75: ^{13}C NMR spectrum of *retro*-GG-GFOGER-GG-Adamantane.

9.7.9 DEPT 135 spectrum of *retro*-GG-GFOGER-GG-Adamantane

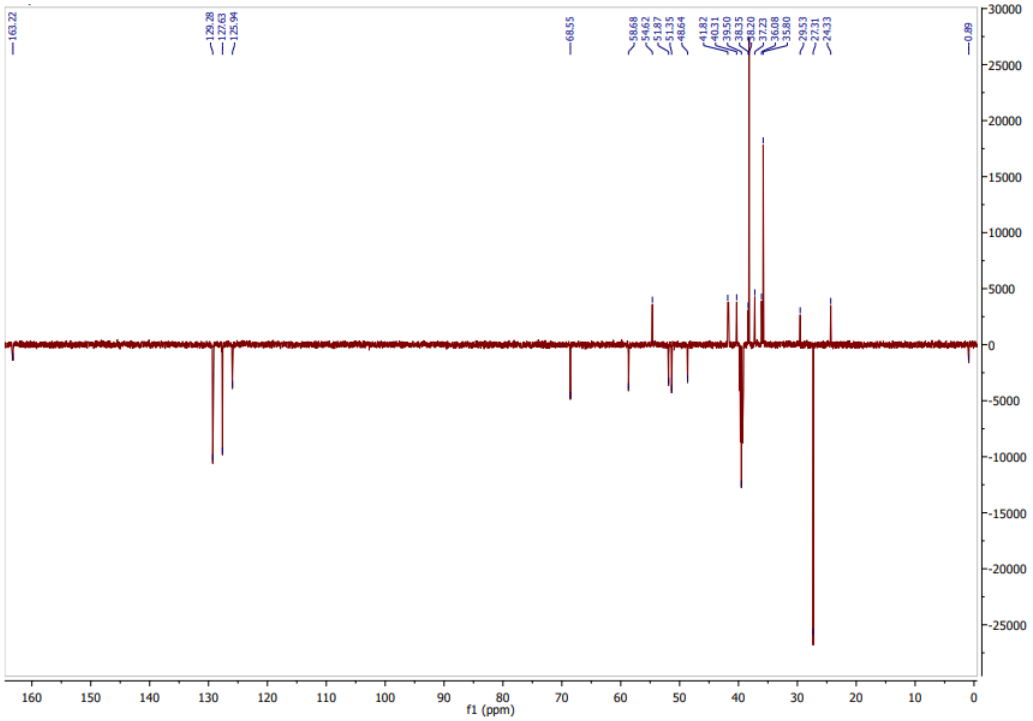

Figure 9.76: DEPT 135 spectrum of *retro*-GG-GFOGER-GG-Adamantane.

9.7.10 COSY spectrum of *retro*-GG-GFOGER-GG-Adamantane

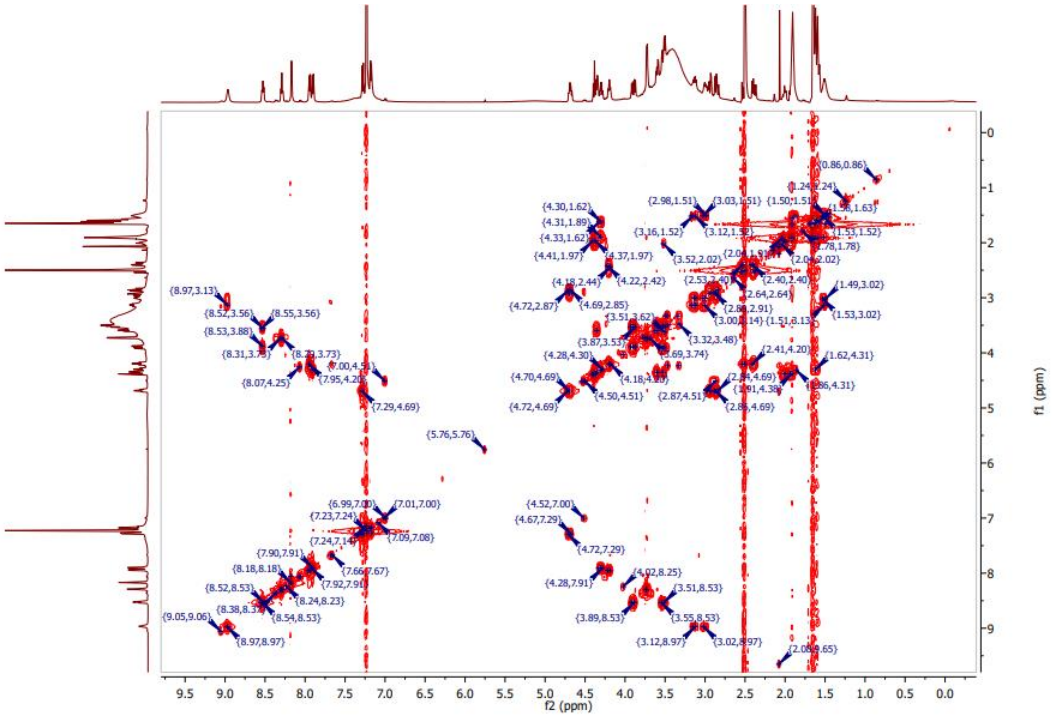

Figure 9.77: COSY spectrum of *retro*-GG-GFOGER-GG-Adamantane.

9.7.11 HSQC spectrum of *retro*-GG-GFOGER-GG-Adamantane

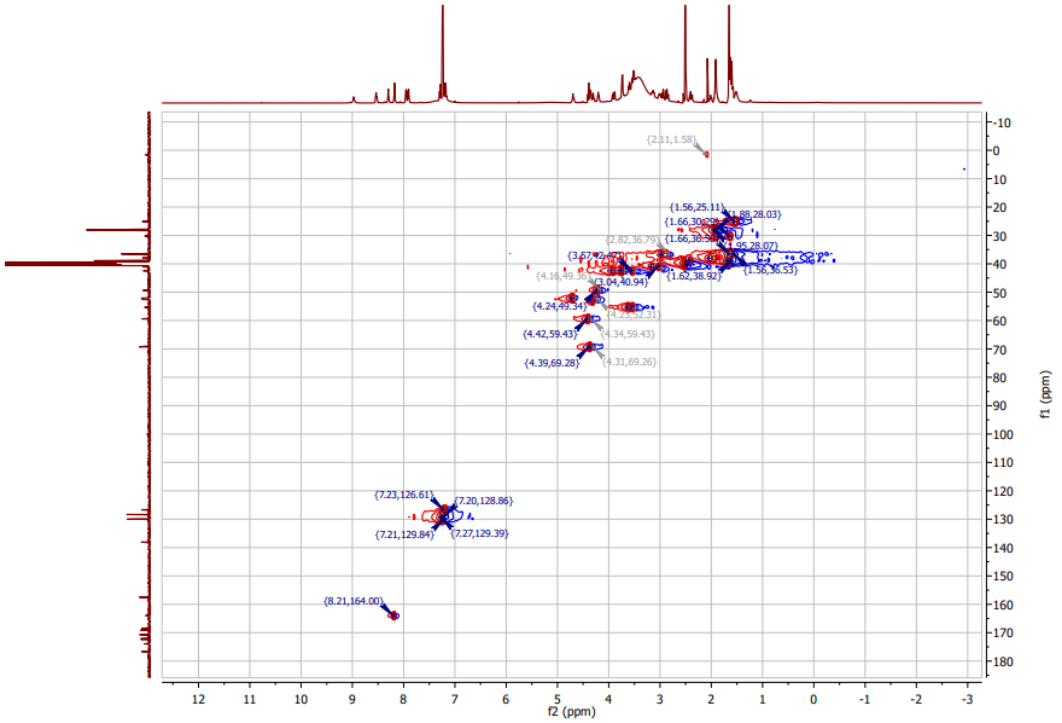

Figure 9.78: HSQC spectrum of *retro*-GG-GFOGER-GG-Adamantane.

9.7.12 HMBC spectrum of *retro*-GG-GFOGER-GG-Adamantane

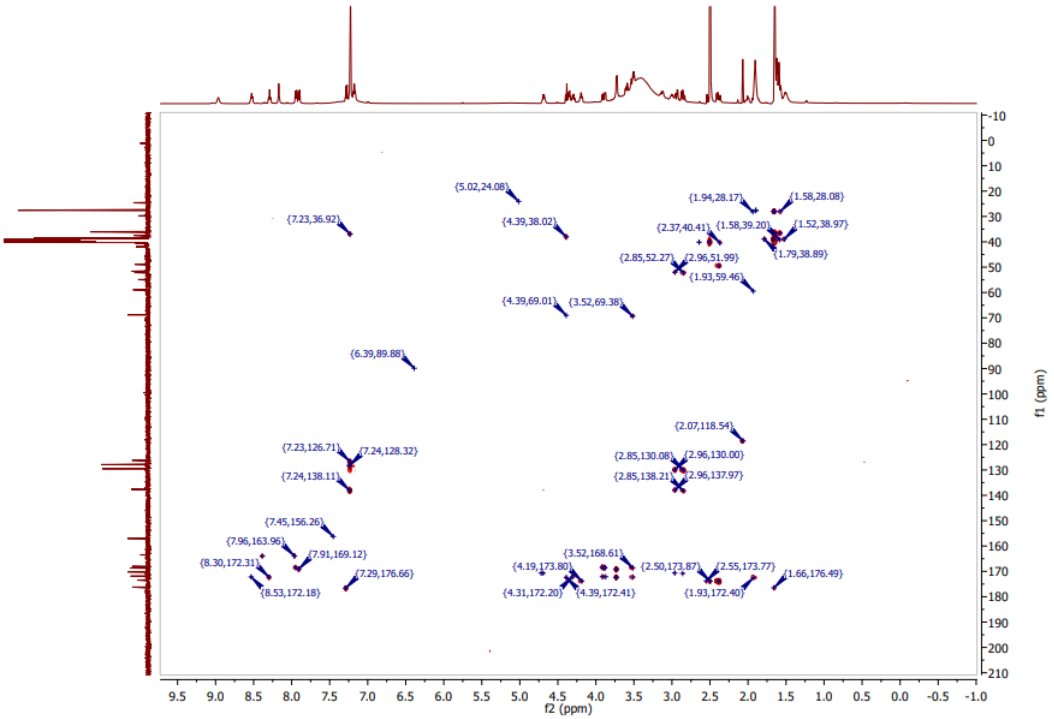

Figure 9.79: HMBC spectrum of *retro*-GG-GFOGER-GG-Adamantane.

9.7.13 TOCSY spectrum of *retro*-GG-GFOGER-GG-Adamantane

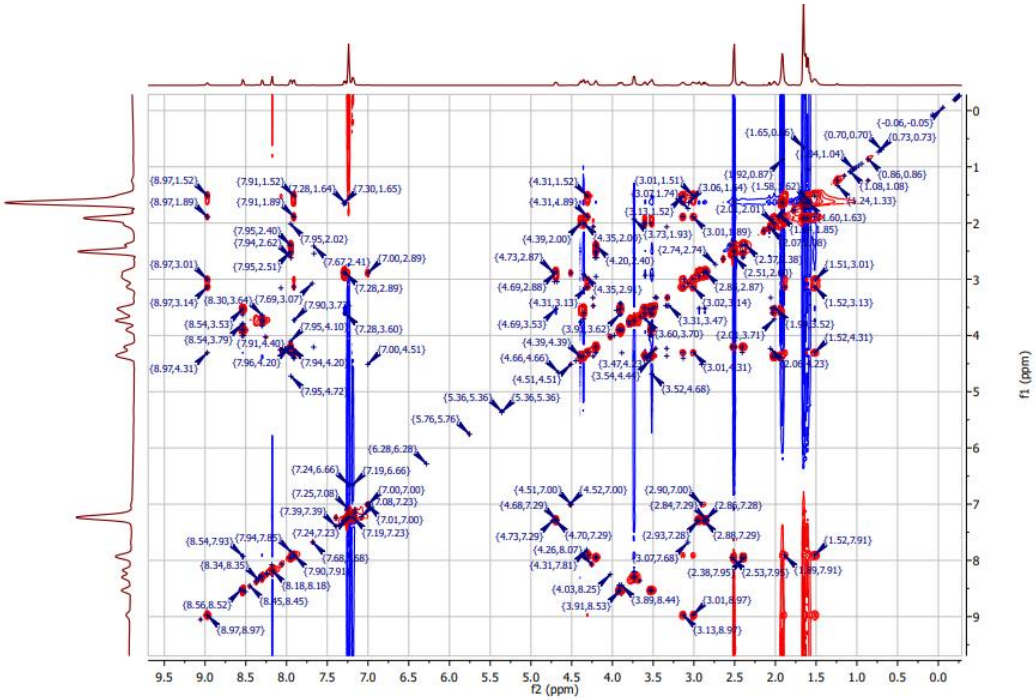

Figure 9.80: TOCSY spectrum of *retro*-GG-GFOGER-GG-Adamantane.

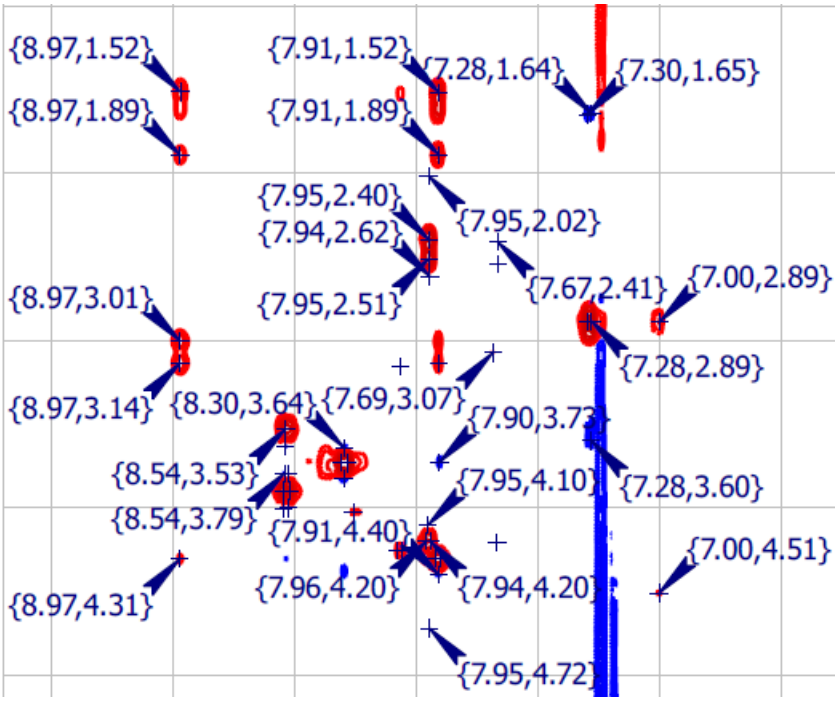

Figure 9.81: Section of TOCSY spectrum of *retro*-GG-GFOGER-GG-Adamantane.

9.7.14 ROESY spectrum of *retro*-GG-GFOGER-GG-Adamantane

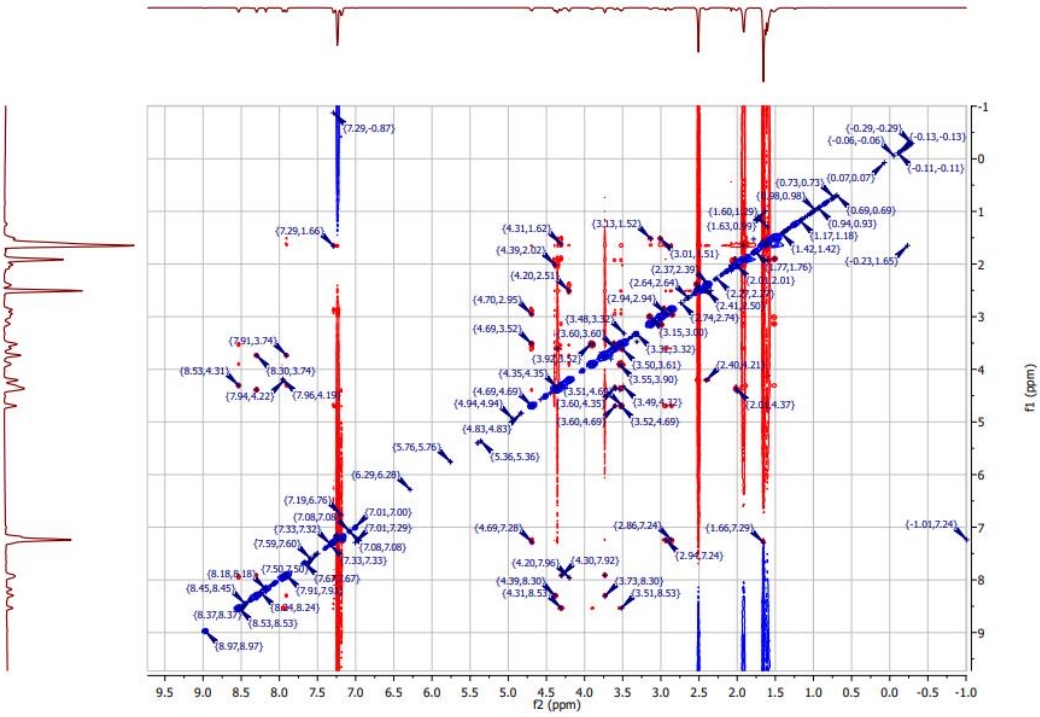

Figure 9.82:ROESY spectrum of *retro*-GG-GFOGER-GG-Adamantane.

9.7.15 ^{1}H NMR Spectrum of *retro*-DGD-GG-GFOGER-GG-Adamantane

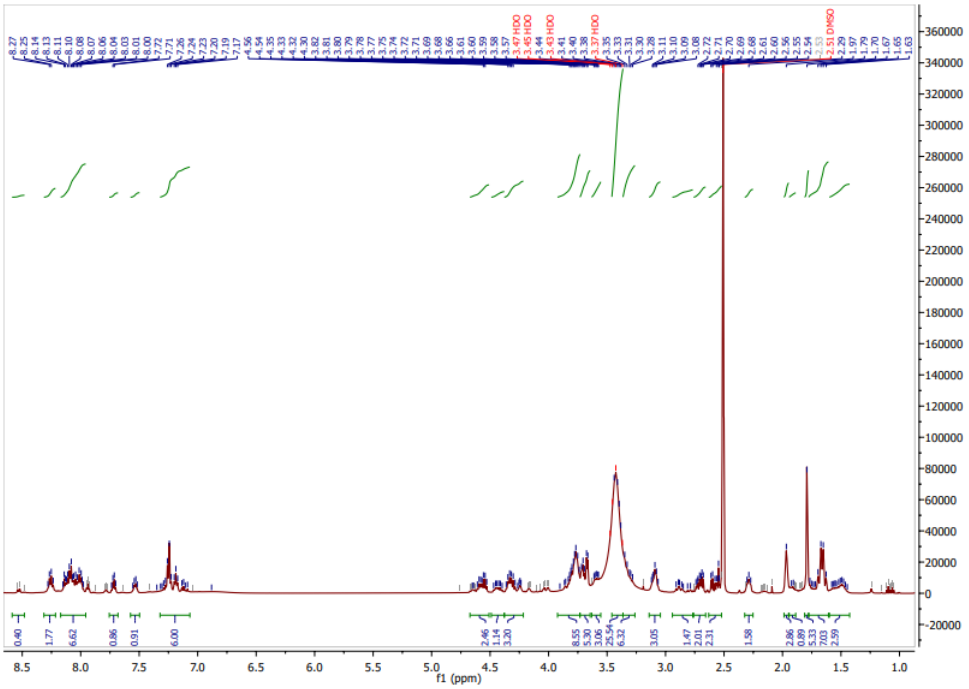

Figure 9.83: ^{1}H NMR spectrum of *retro*-DGD-GG-GFOGER-GG-Adamantane.

9.7.16 ^{13}C NMR spectrum of *retro*-DGD-GG-GFOGER-GG-Adamantane

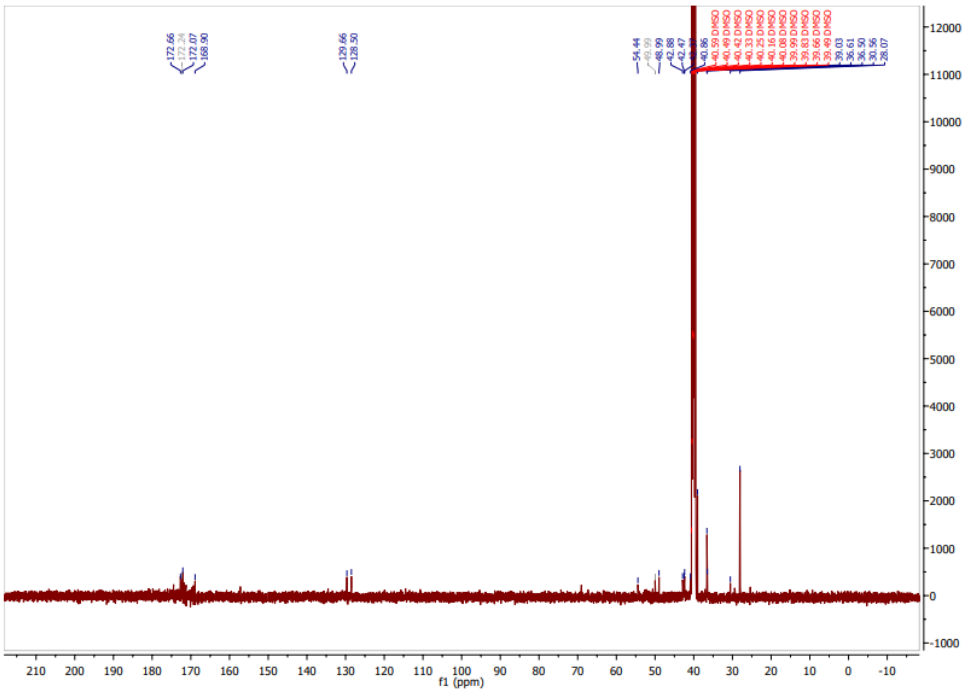

Figure 9.84: ^{13}C NMR spectrum of *retro*-DGD-GG-GFOGER-GG-Adamantane.

9.7.17 DEPT135 spectrum of *retro*-DGD-GG-GFOGER-GG-Adamantane

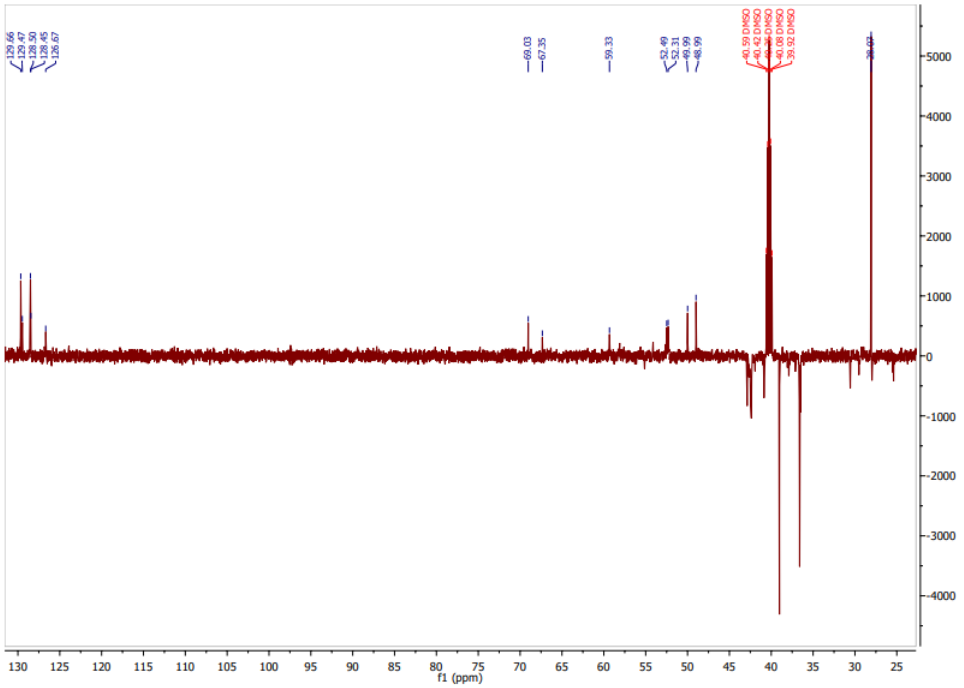

Figure 9.85: DEPT 135 spectrum of *retro*-DGD-GG-GFOGER-GG-Adamantane.

9.7.18 COSY spectrum of *retro*-DGD-GG-GFOGER-GG-Adamantane

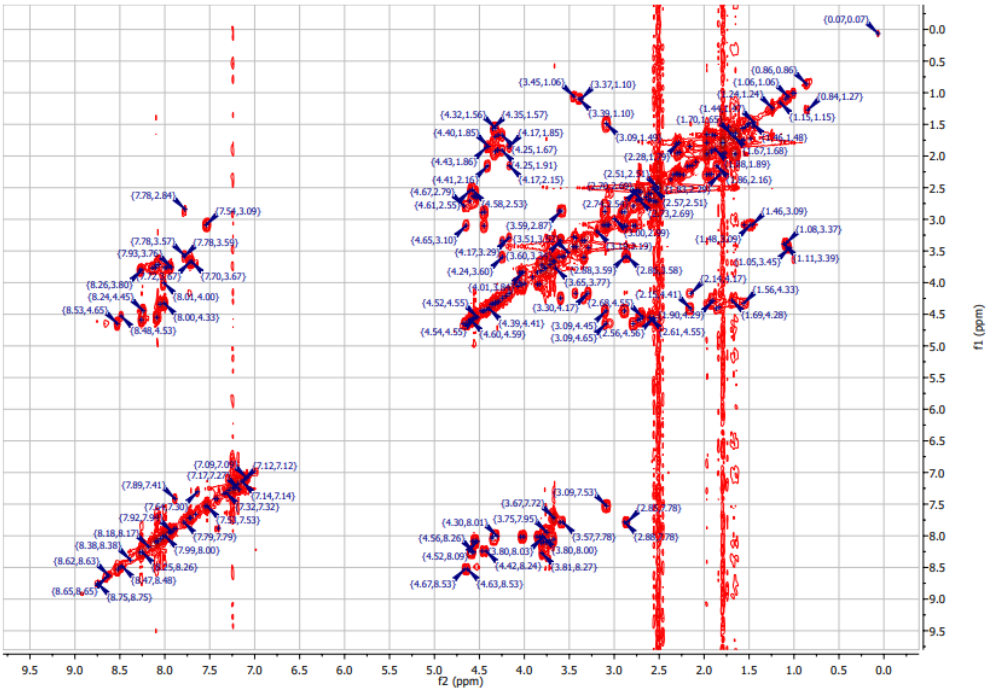

Figure 9.86: COSY spectrum of *retro*-DGD-GG-GFOGER-GG-Adamantane.

9.7.19 HSQC spectrum of *retro*-DGD-GG-GFOGER-GG-Adamantane

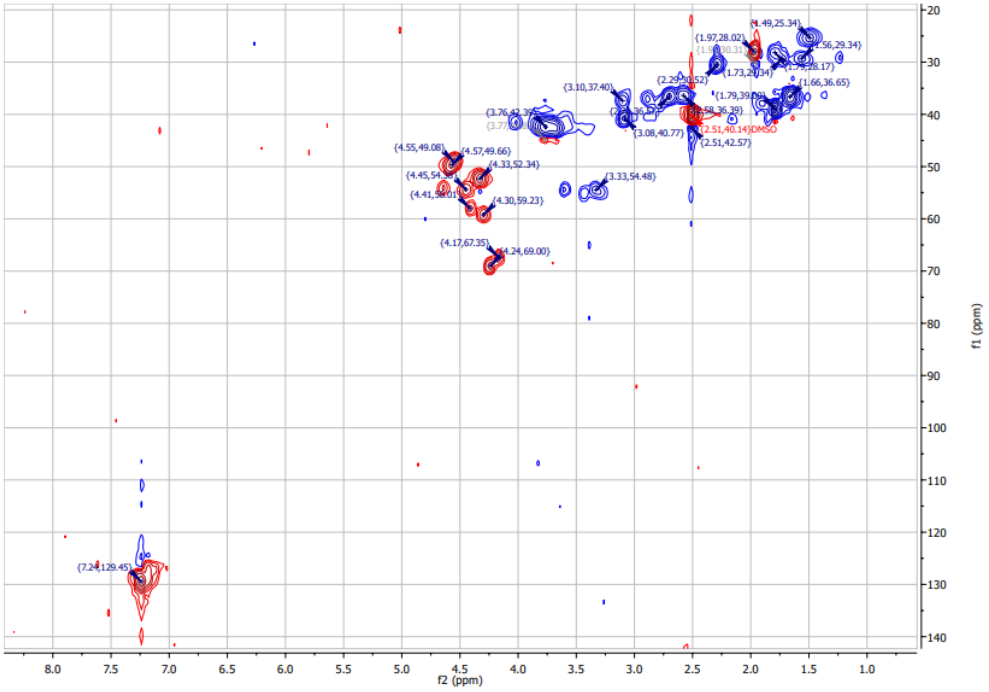

Figure 9.87: HSQC spectrum of *retro*-DGD-GG-GFOGER-GG-Adamantane.

9.7.20 HMBC spectrum of *retro*-DGD-GG-GFOGER-GG-Adamantane

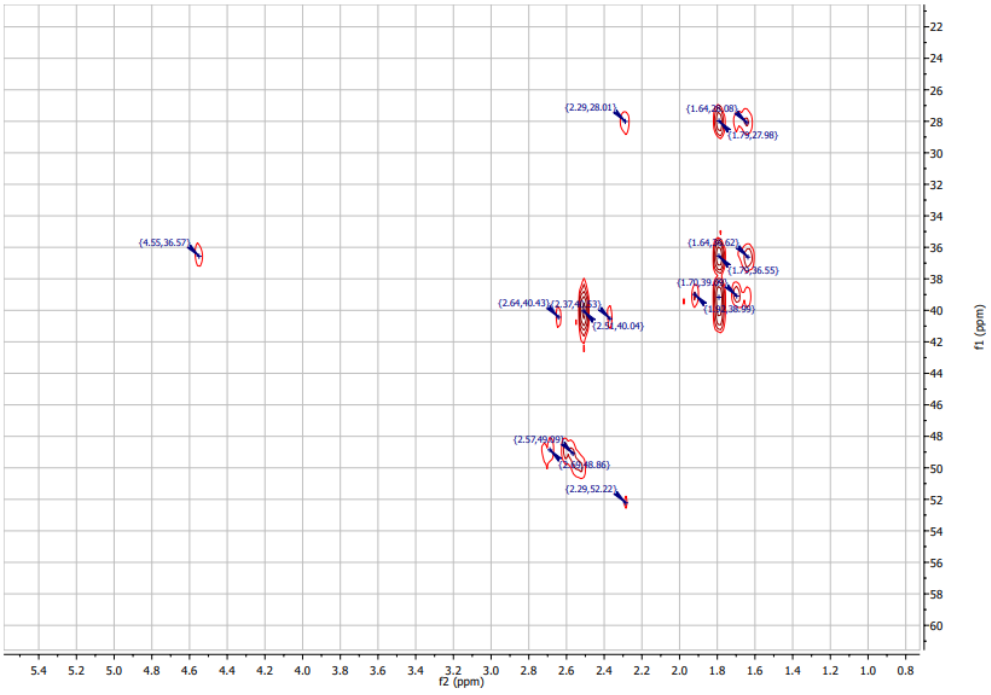

Figure 9.88: HMBC spectrum of *retro*-DGD-GG-GFOGER-GG-Adamantane.

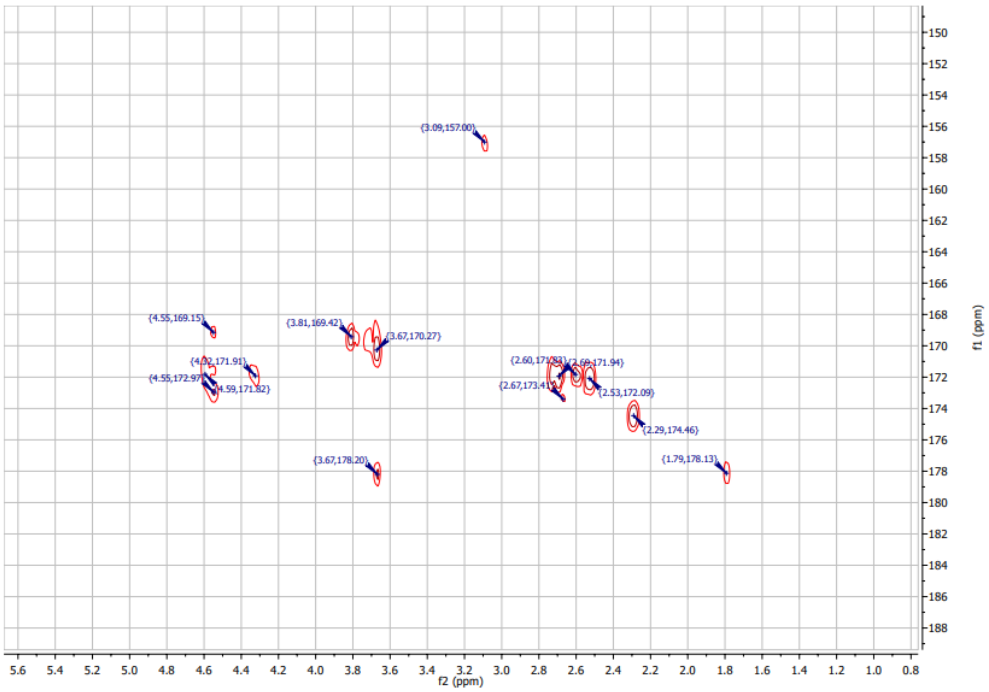

Figure 9.89: Aliphatic section of HMBC spectrum of *retro*-DGD-GG-GFOGER-GG-Adamantane.

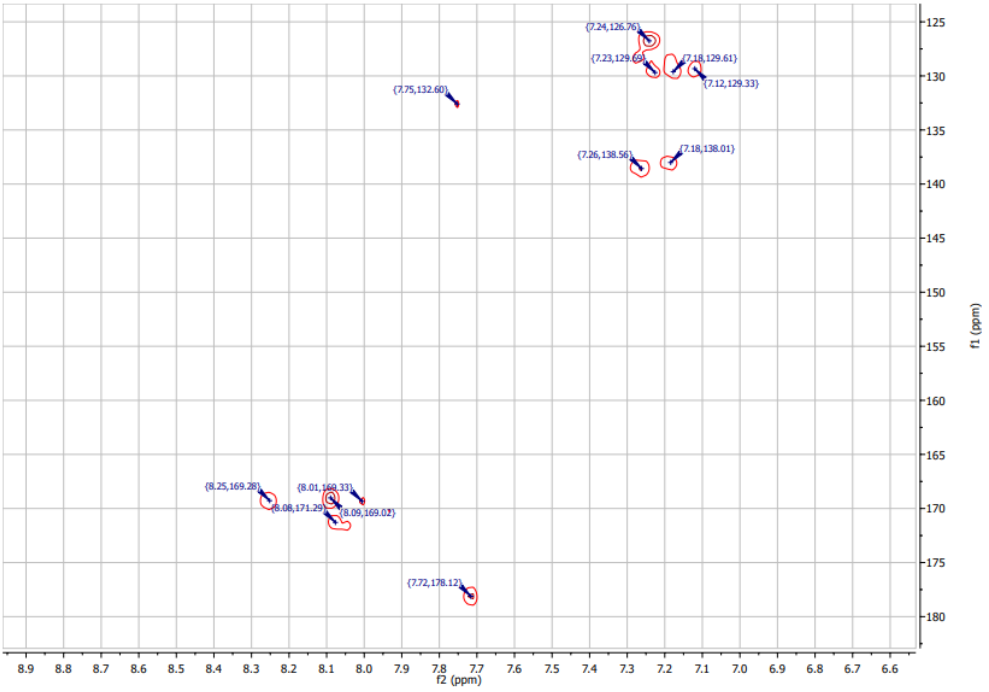

Figure 9.90: Amide-aromatic section of spectrum of *retro*-DGD-GG-GFOGER-GG-Adamantane.

9.7.21 TOCSY spectrum of *retro*-DGD-GG-GFOGER-GG-Adamantane

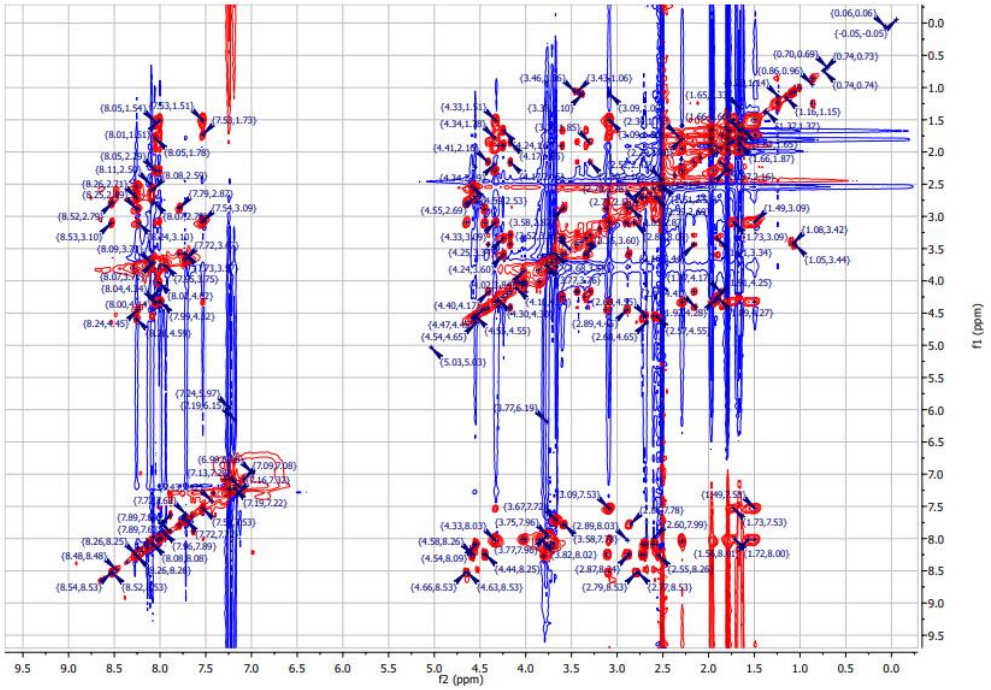

Figure 9.91: TOCSY spectrum of *retro*-DGD-GG-GFOGER-GG-Adamantane.

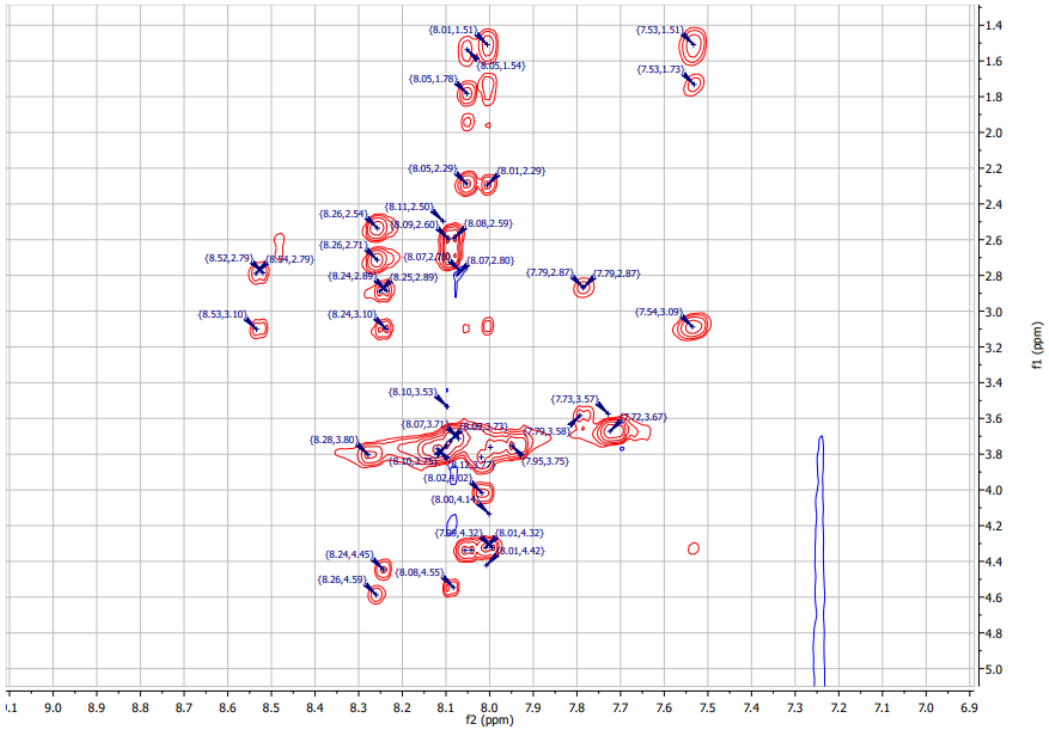

Figure 9.92: Amide section of TOCSY spectrum of *retro*-DGD-GG-GFOGER-GG-Adamantane.

9.7.22 ROESY spectrum of *retro*-DGD-GG-GFOGER-GG-Adamantane

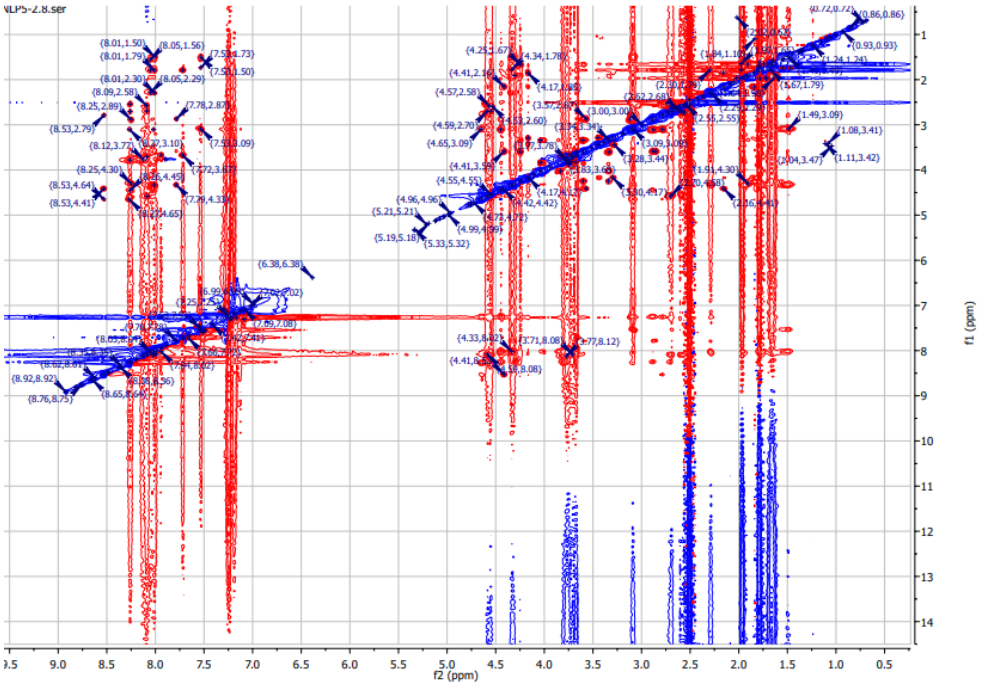

Figure 9.93: ROESY spectrum of *retro*-DGD-GG-GFOGER-GG-Adamantane.

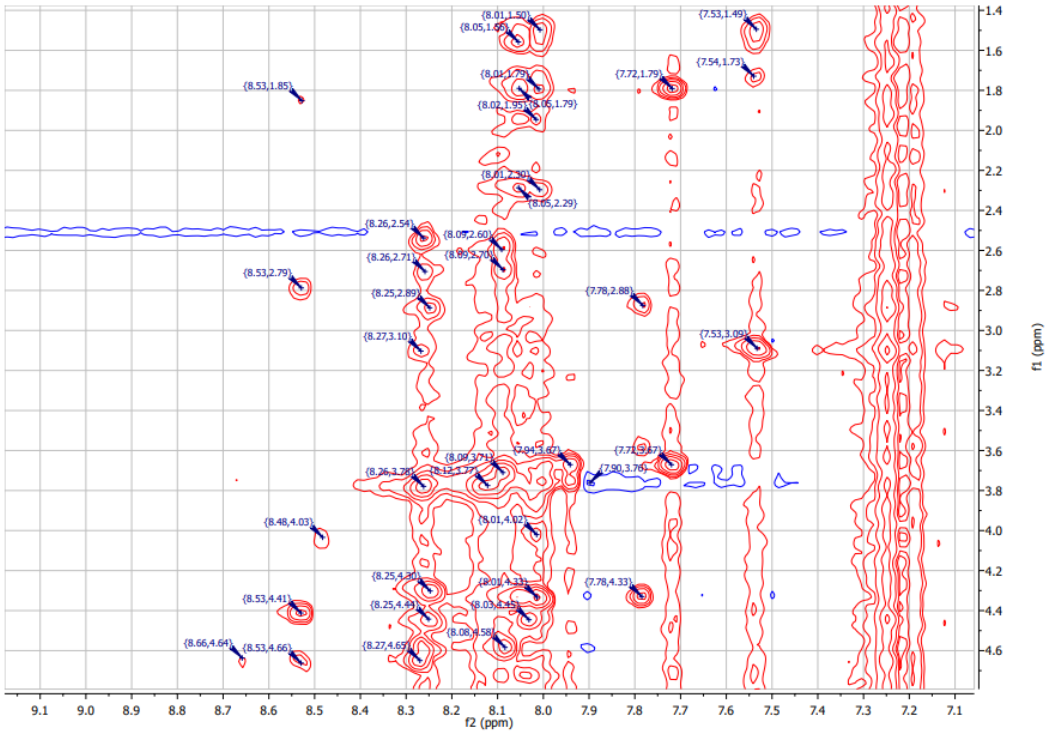

Figure 9.94: Amide section of ROESY spectrum of *retro*-DGD-GG-GFOGER-GG-Adamantane.

9.7.23 ^{1}H NMR spectrum of *retro*-DGD-GG-GFOGER-GG-TTK-Adamantane

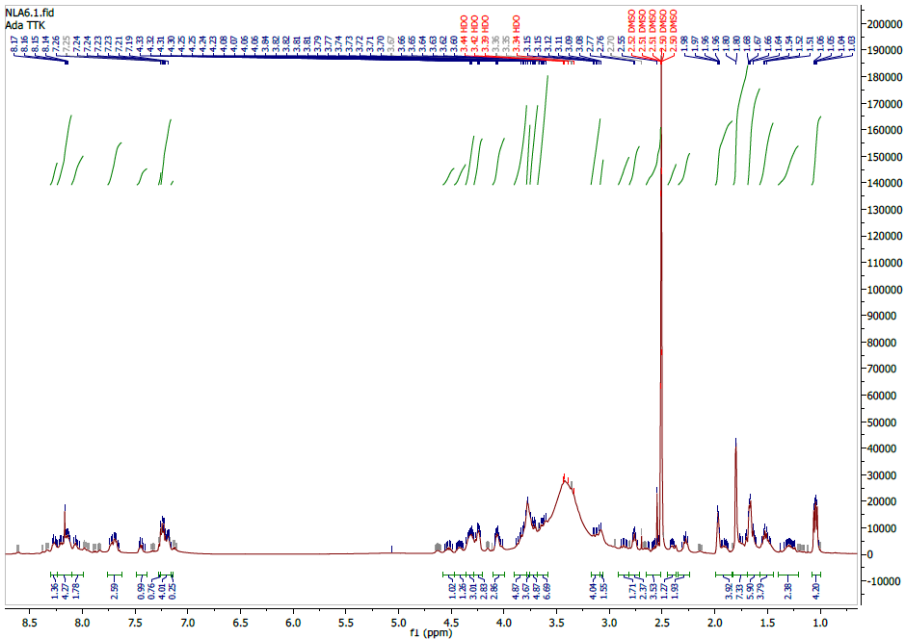

Figure 9.95: ^{1}H NMR spectrum of *retro*-DGD-GG-GFOGER-GG-TTK-Adamantane.

9.7.24 ^{13}C NMR spectrum of *retro*-DGD-GG-GFOGER-GG-TTK-Adamantane

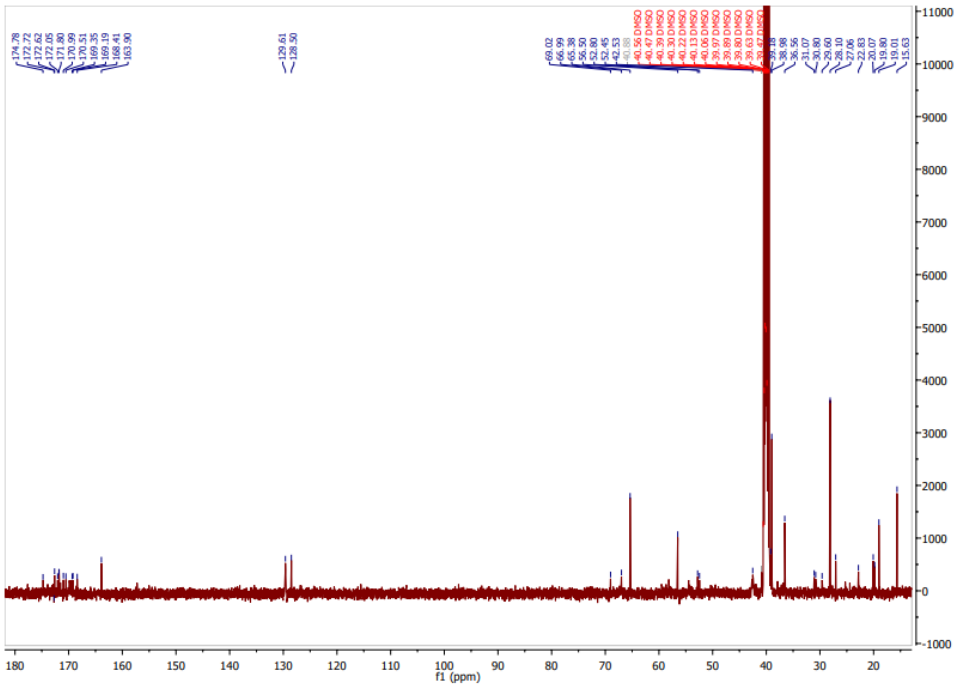

Figure 9.96:.^{13}C NMR spectrum of *retro*-DGD-GG-GFOGER-GG-TTK-Adamantane.

9.7.25 DEPT135 spectrum of *retro*-DGD-GG-GFOGER-GG-TTK-Adamantane

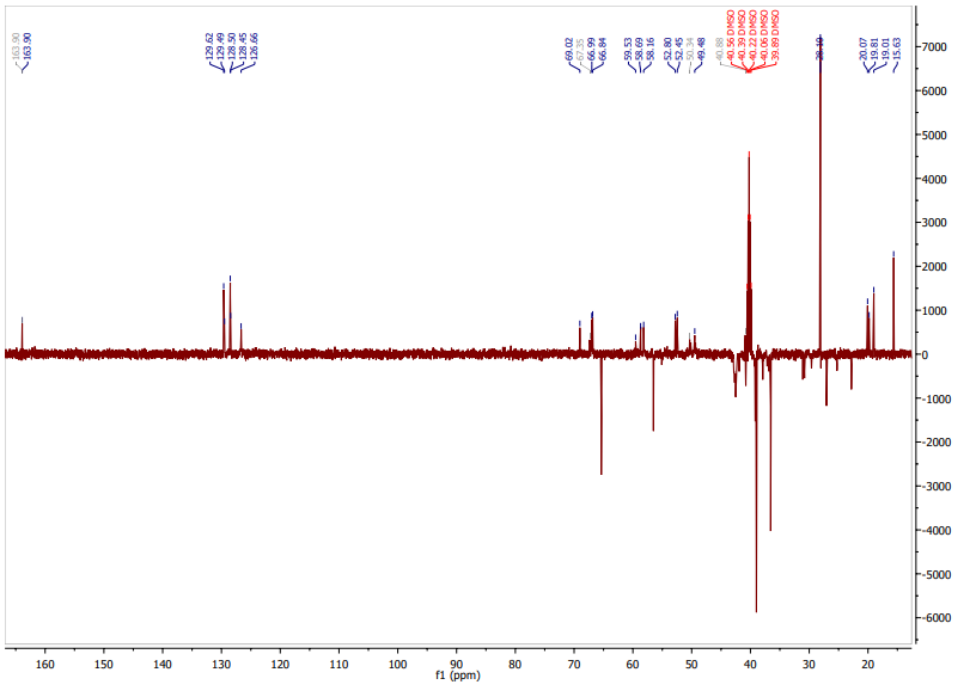

Figure 9.97: DEPT 135 spectrum of *retro*-DGD-GG-GFOGER-GG-TTK-Adamantane.

9.7.26 COSY spectrum of *retro*-DGD-GG-GFOGER-GG-TTK-Adamantane

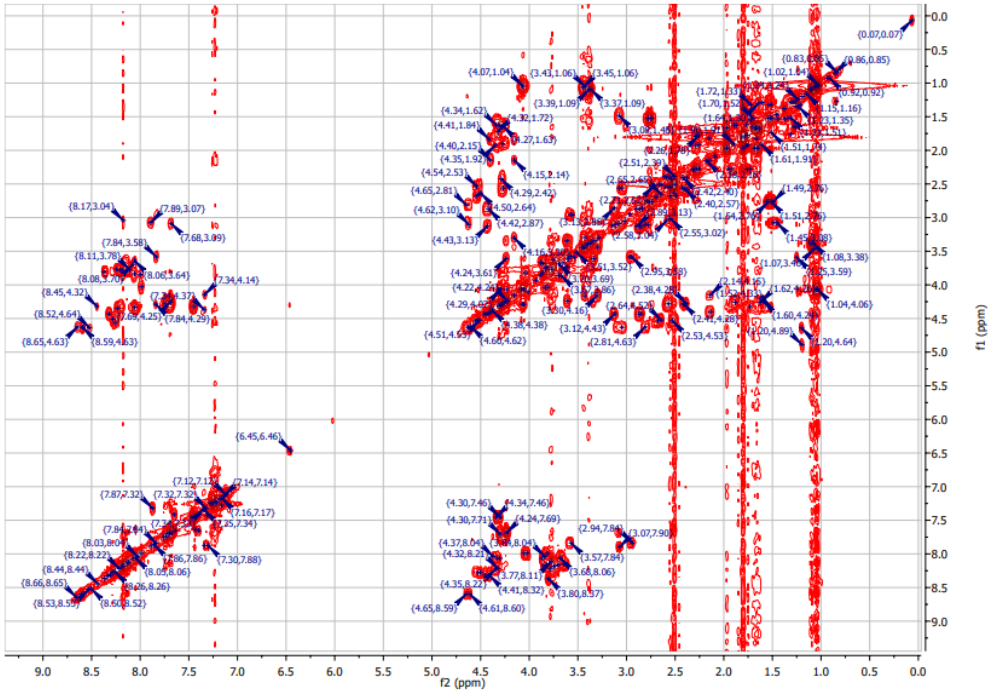

Figure 9.98: COSY spectrum of *retro*-DGD-GG-GFOGER-GG-TTK-Adamantane.

9.7.27 HSQC spectrum of *retro*-DGD-GG-GFOGER-GG-TTK-Adamantane

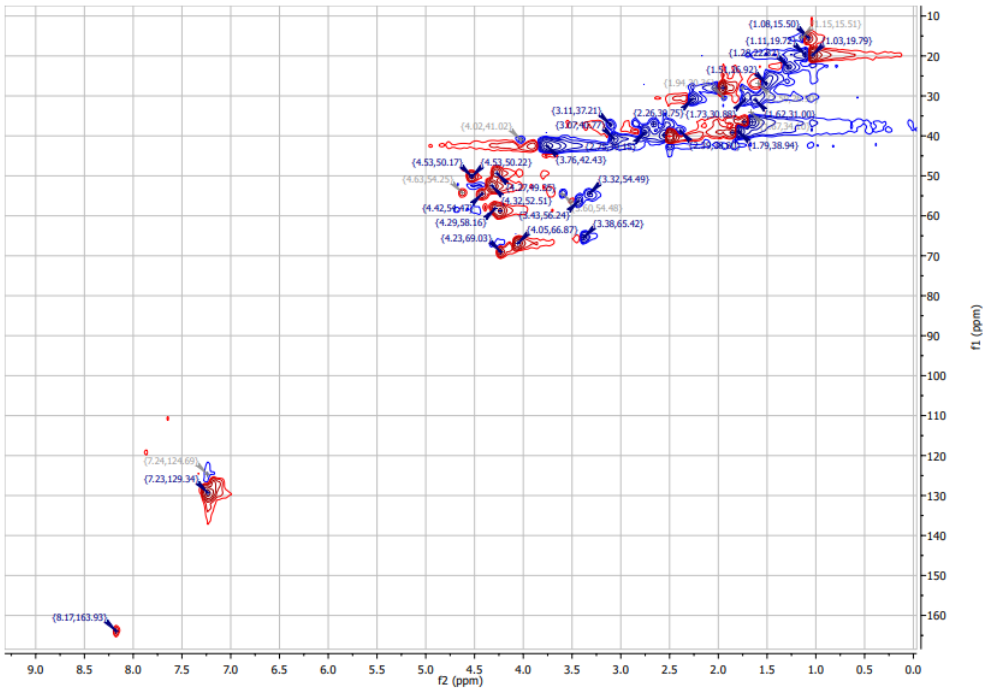

Figure 9.99: HSQC spectrum of *retro*-DGD-GG-GFOGER-GG-TTK-Adamantane.

9.7.28 HMBC spectrum of *retro*-DGD-GG-GFOGER-GG-TTK-Adamantane

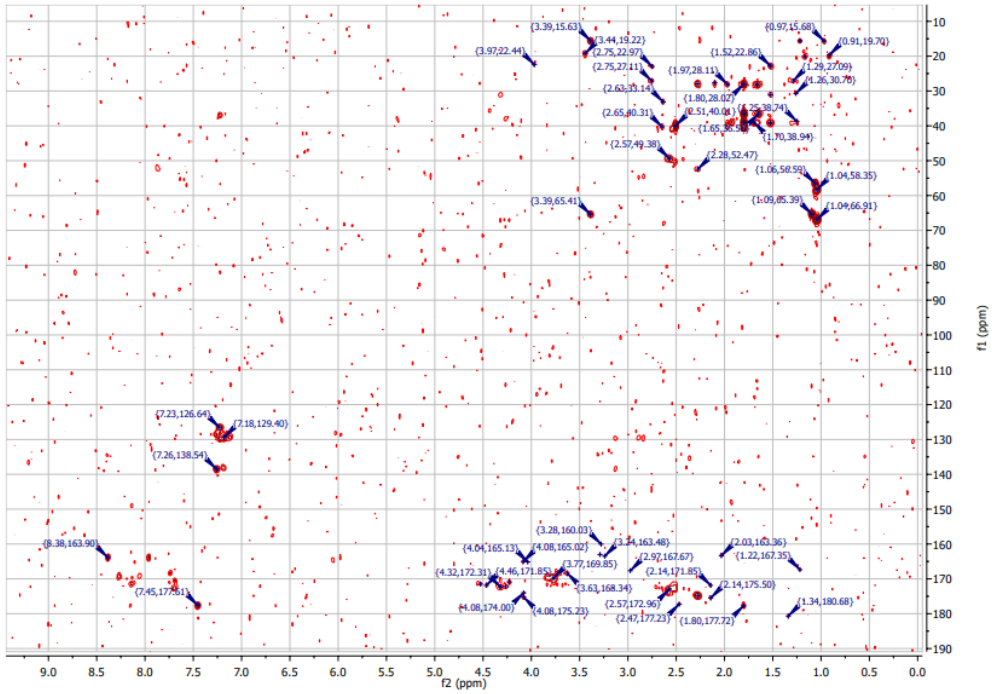

Figure 9.100: HMBC spectrum of *retro*-DGD-GG-GFOGER-GG-TTK-Adamantane.

9.7.29 TOCSY spectrum of *retro*-DGD-GG-GFOGER-GG-TTK-Adamantane

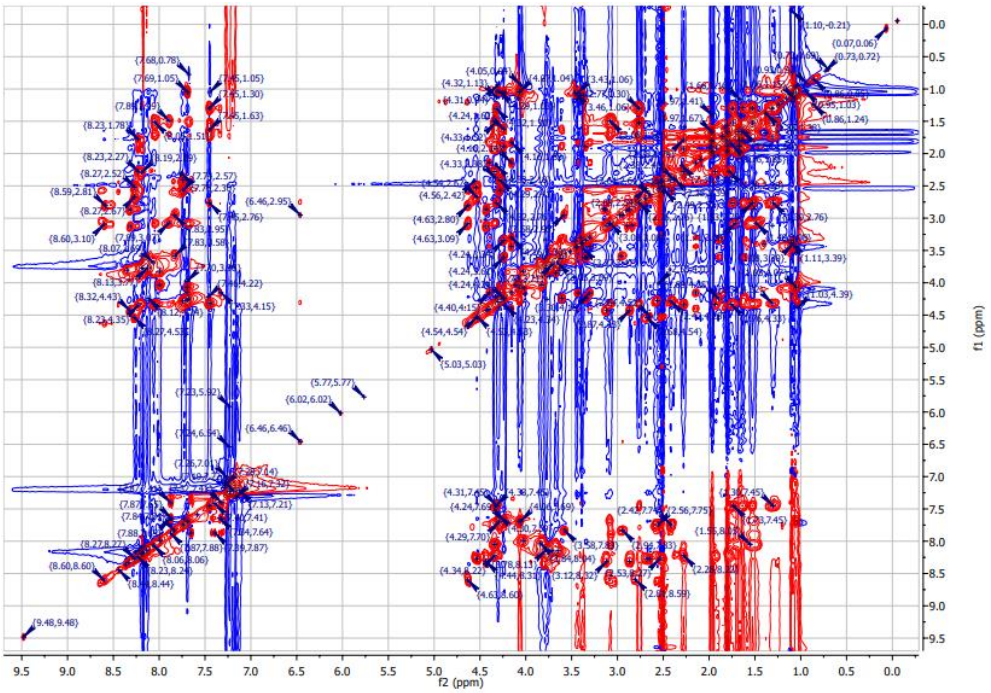

Figure 9.101: TOCSY spectrum of *retro*-DGD-GG-GFOGER-GG-TTK-Adamantane.

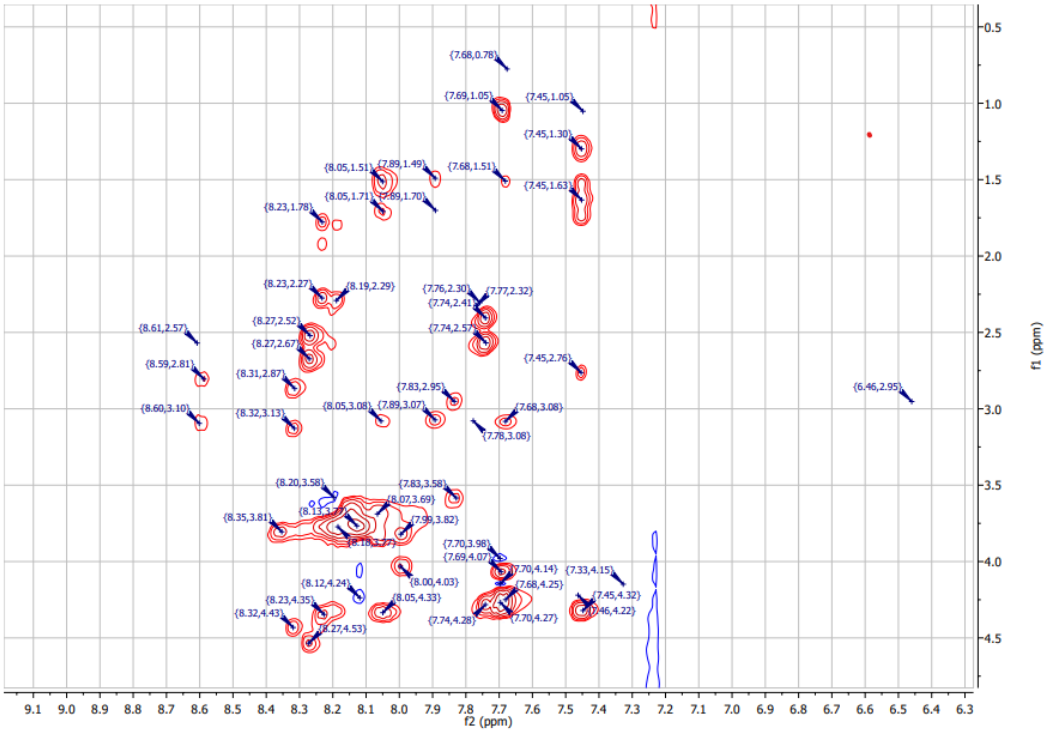

Figure 9.102: Amide section of TOCSY spectrum of *retro*-DGD-GG-GFOGER-GG-TTK-Adamantane.

9.7.30 ROESY spectrum of *retro*-DGD-GG-GFOGER-GG-TTK-Adamantane

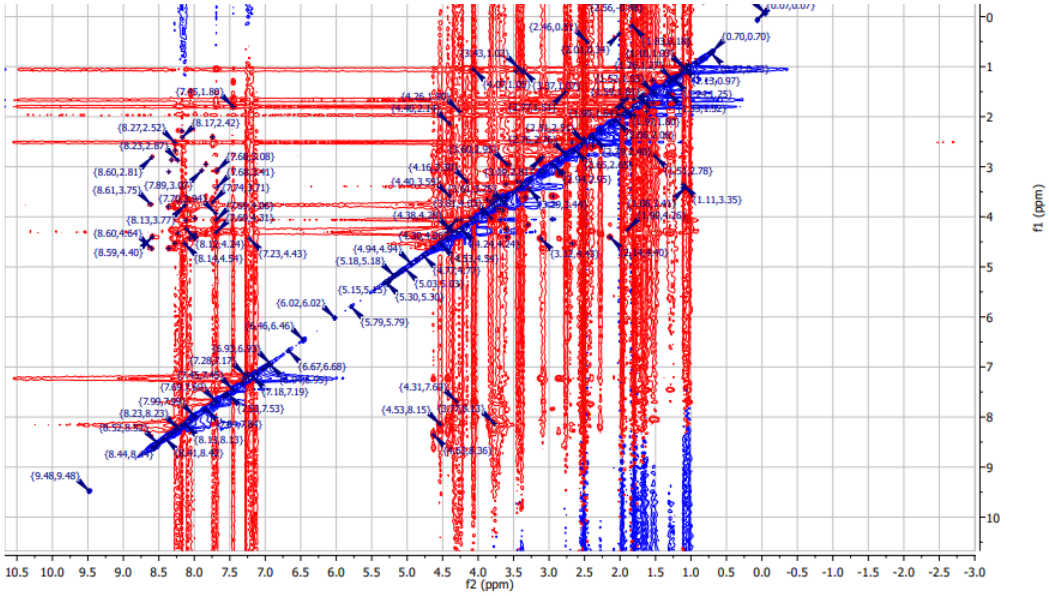

Figure 9.103: ROESY spectrum of *retro*-DGD-GG-GFOGER-GG-TTK-Adamantane.

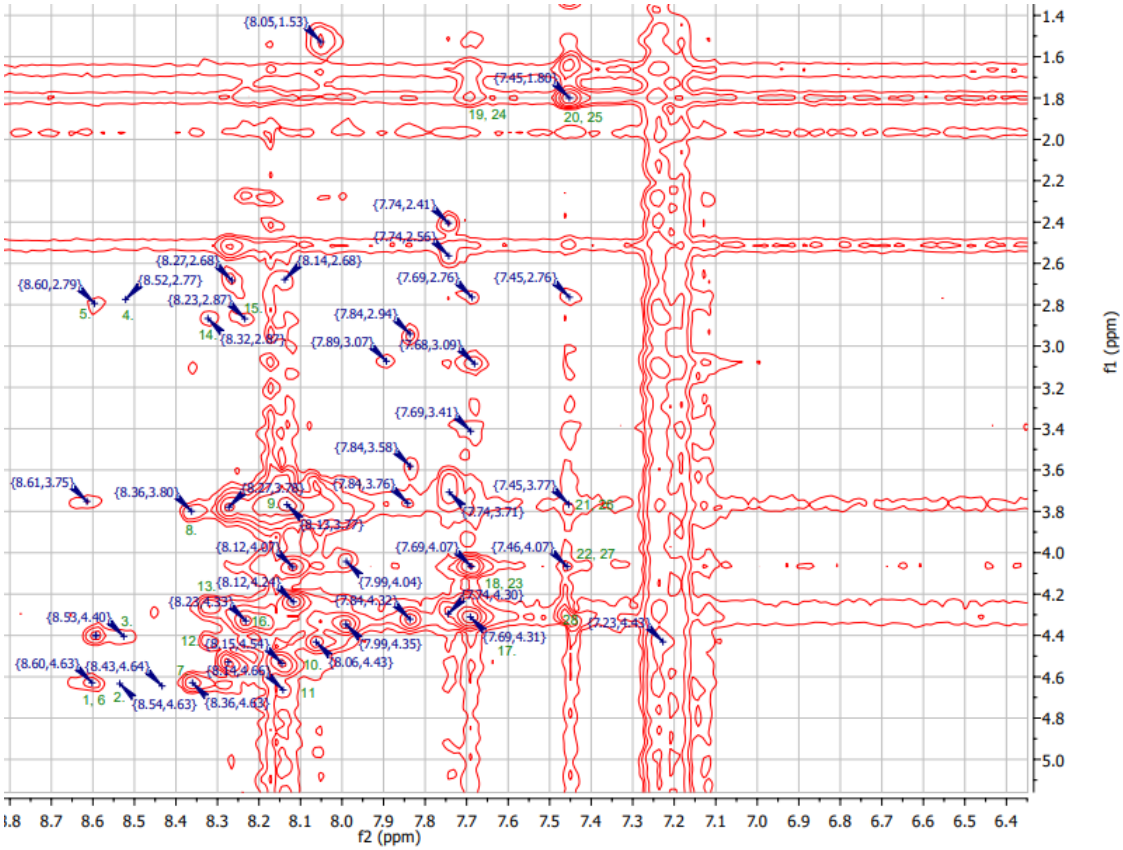

Figure 9.104: Amide section of spectrum of *retro*-DGD-GG-GFOGER-GG-TTK-Adamantane.

9.7.31 ^{1}H NMR spectrum of *retro*-DGD-GG-GFOGER-GG-TTK-Palmitate

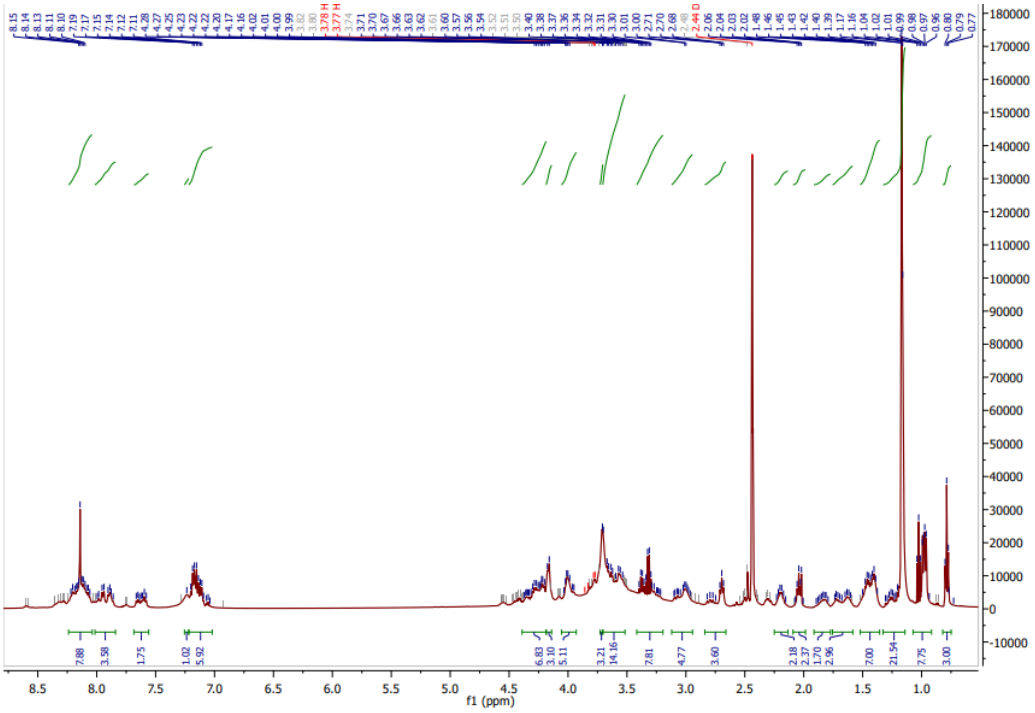

Figure 9.105: ^{1}H NMR spectrum of *retro*-DGD-GG-GFOGER-GG-TTK-Palmitate.

9.7.32 ^{13}C NMR spectrum of *retro*-DGD-GG-GFOGER-GG-TTK-Palmitate

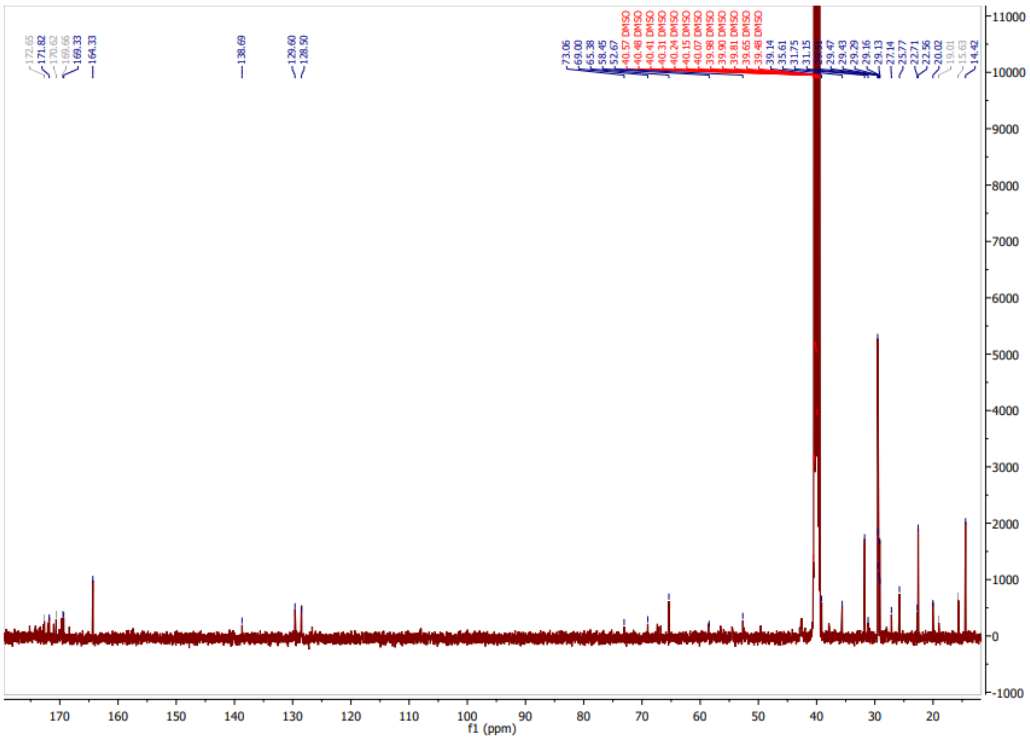

Figure 9.106: ^{13}C NMR spectrum of *retro*-DGD-GG-GFOGER-GG-TTK-Palmitate.

9.7.33 DEPT Spectrum of *retro*-DGD-GG-GFOGER-GG-TTK-Palmitate

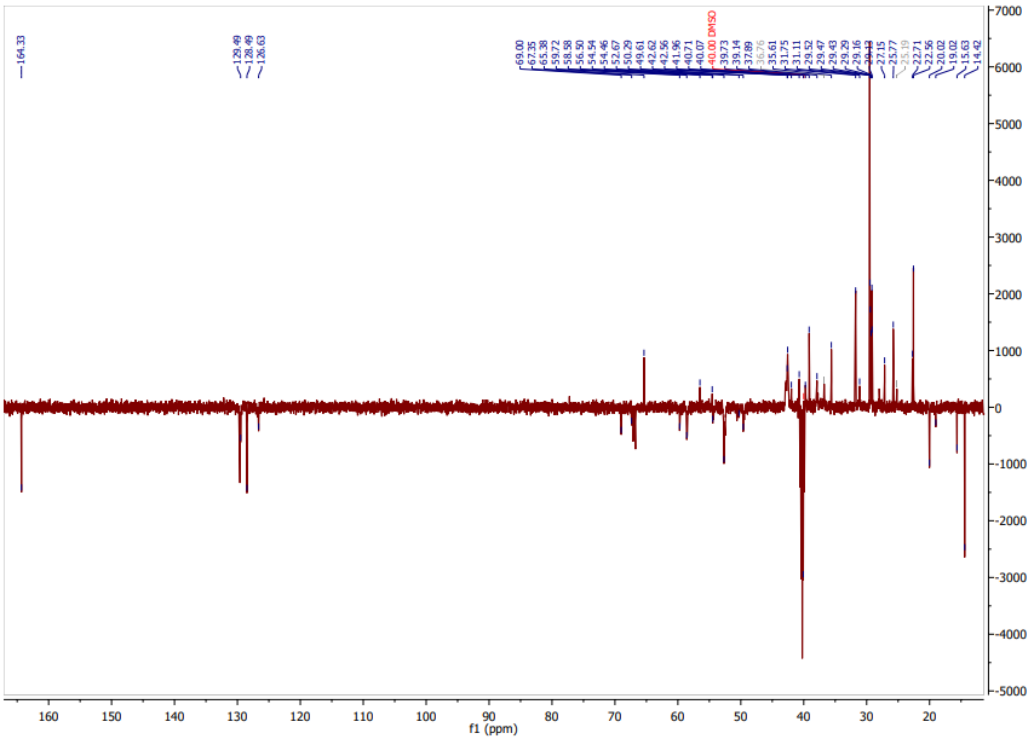

Figure 9.107: DEPT 135 Spectrum of *retro*-DGD-GG-GFOGER-GG-TTK-Palmitate.

9.7.34 COSY Spectrum of *retro*-DGD-GG-GFOGER-GG-TTK-Palmitate

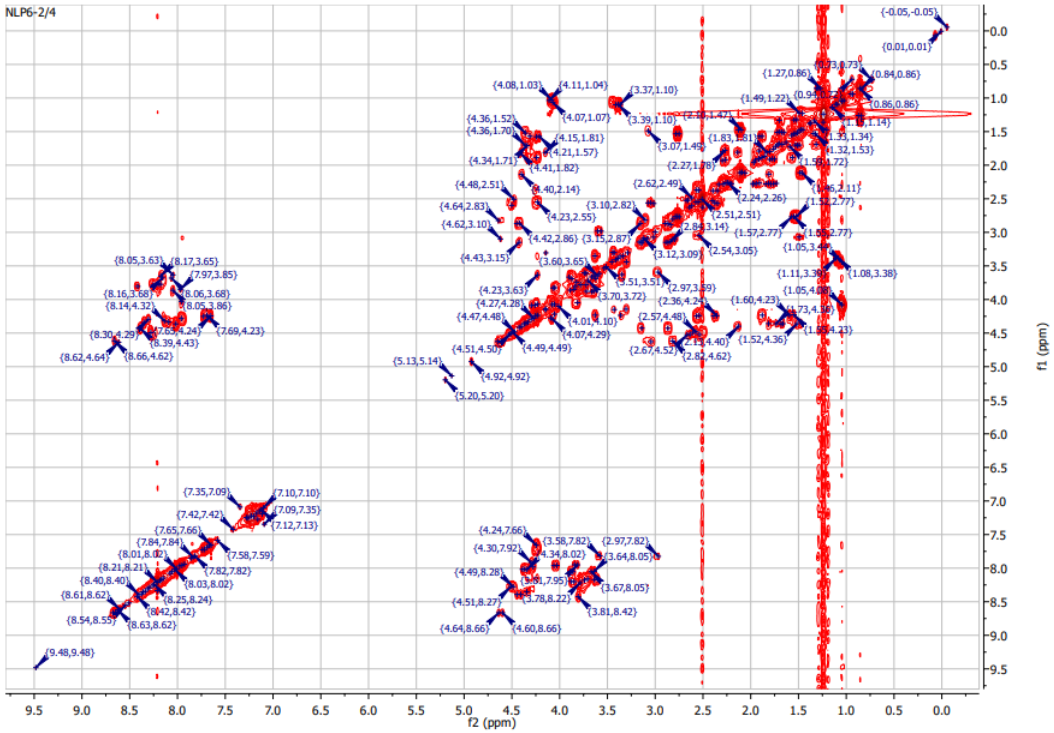

Figure 9.108: COSY Spectrum of *retro*-DGD-GG-GFOGER-GG-TTK-Palmitate.

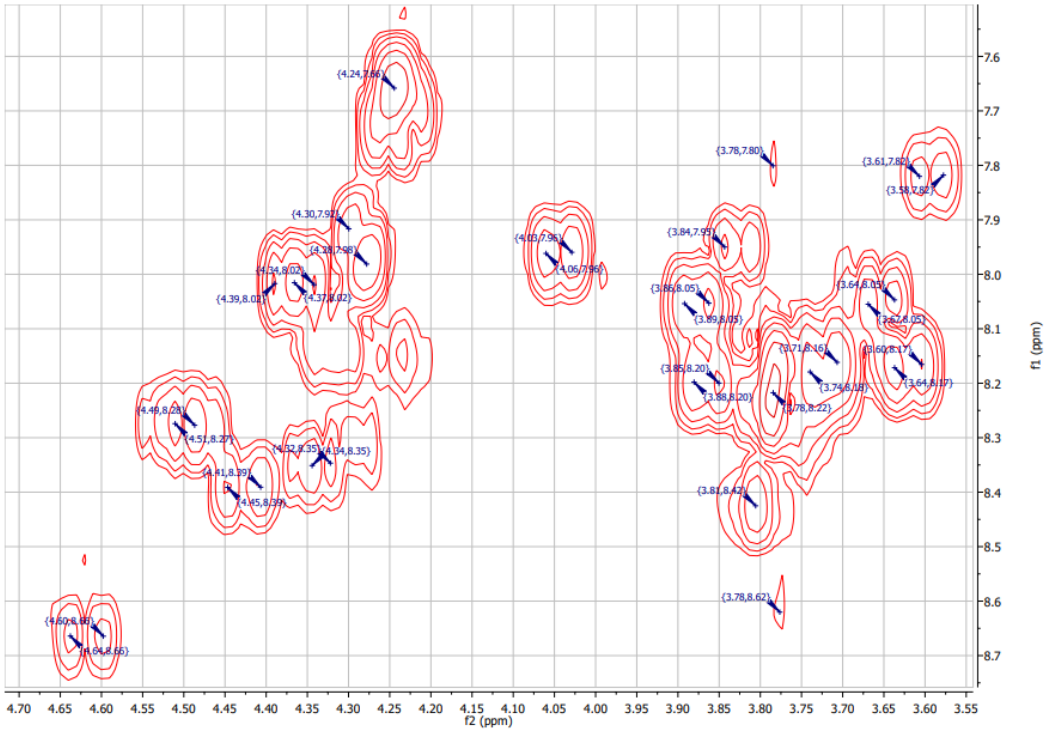

Figure 9.109: COSY *alpha*-amide section of *retro*-DGD-GG-GFOGER-GG-TTK-Palmitate.

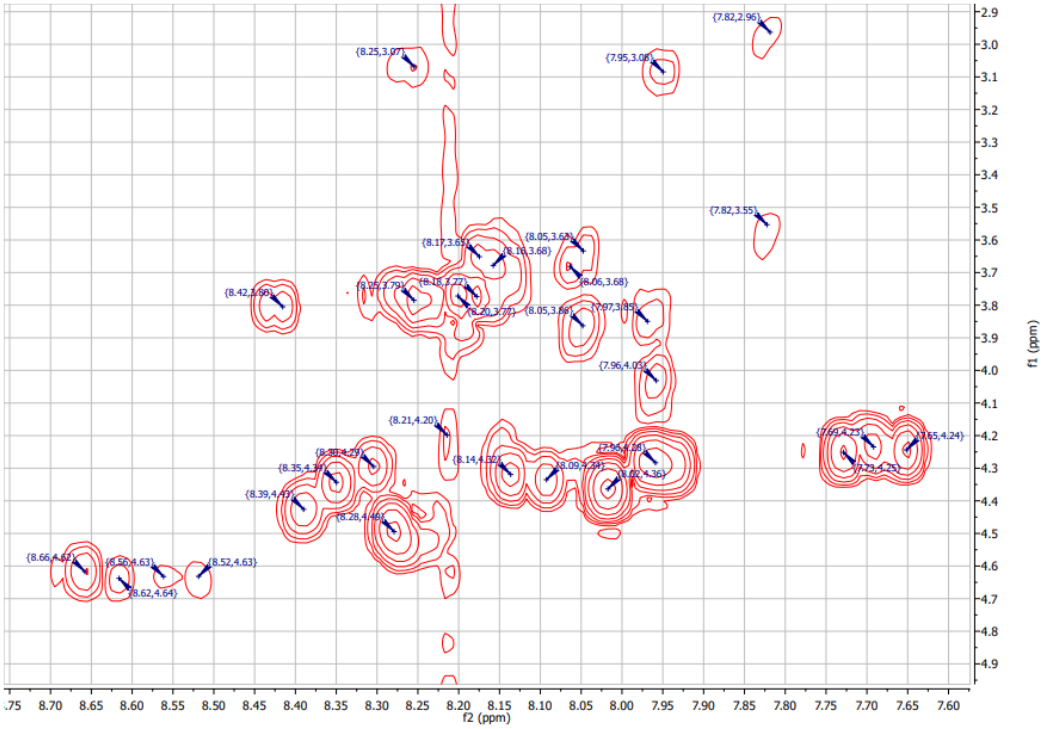

Figure 9.110: Section of COSY spectrum of *retro*-DGD-GG-GFOGER-GG-TTK-Palmitate.

9.7.35 HSQC spectrum of *retro*-DGD-GG-GFOGER-GG-TTK-Palmitate

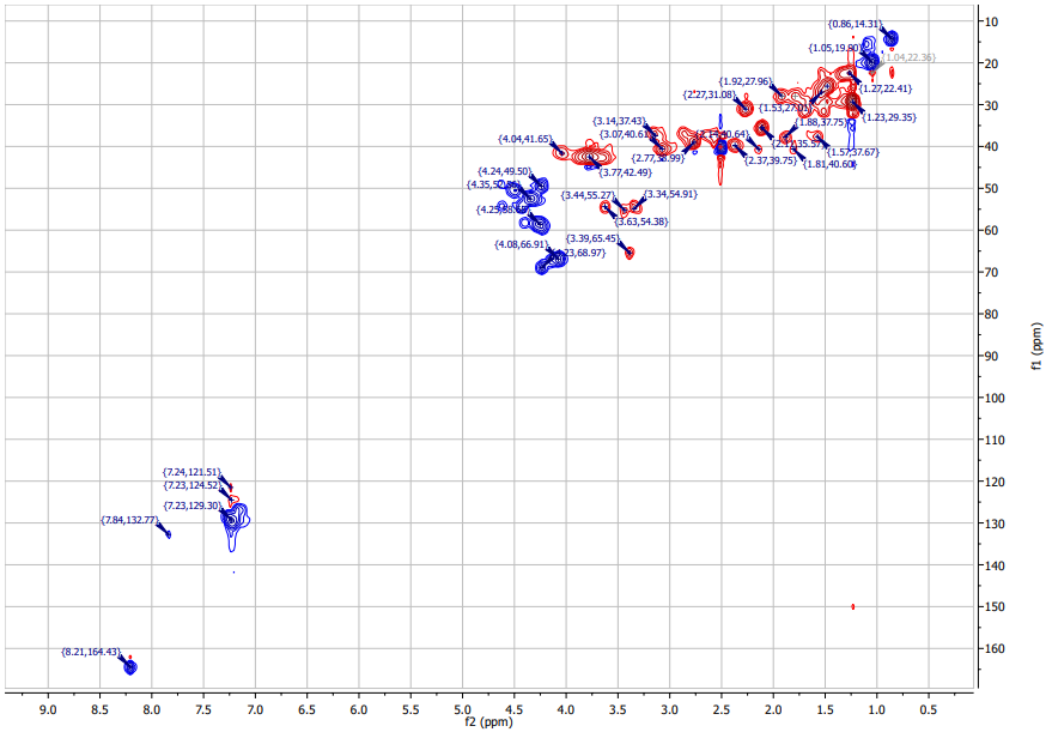

Figure 9.111: HSQC spectrum of *retro*-DGD-GG-GFOGER-GG-TTK-Palmitate.

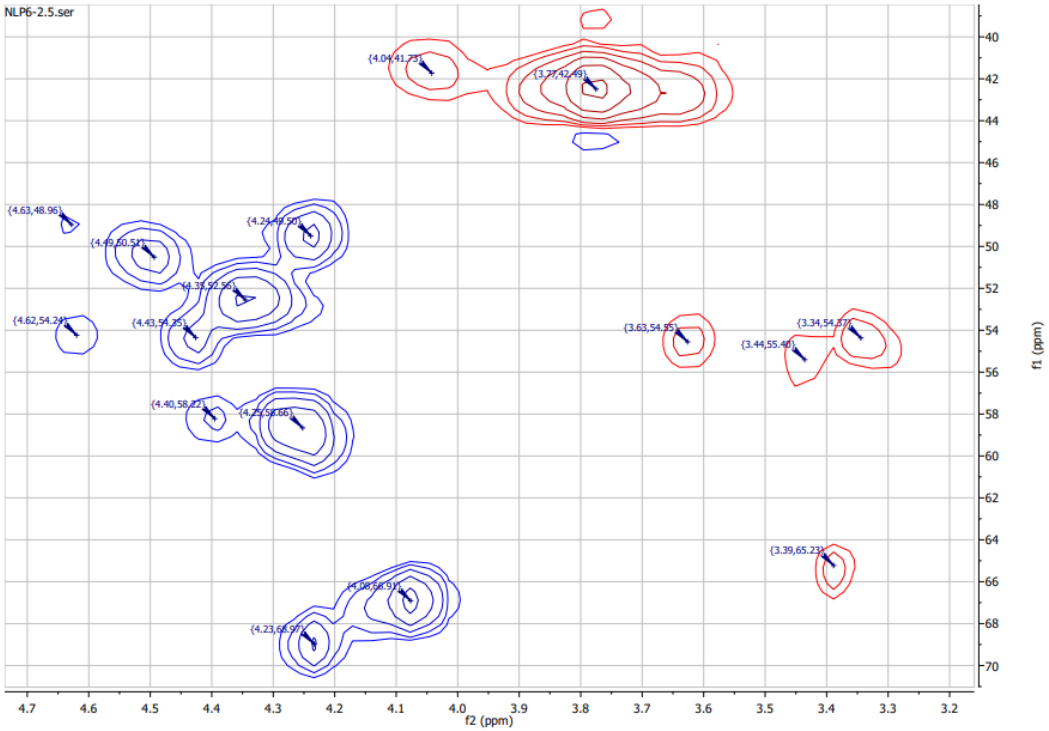

Figure 9.112: HSQC section of spectrum of *retro*-DGD-GG-GFOGER-GG-TTK-Palmitate.

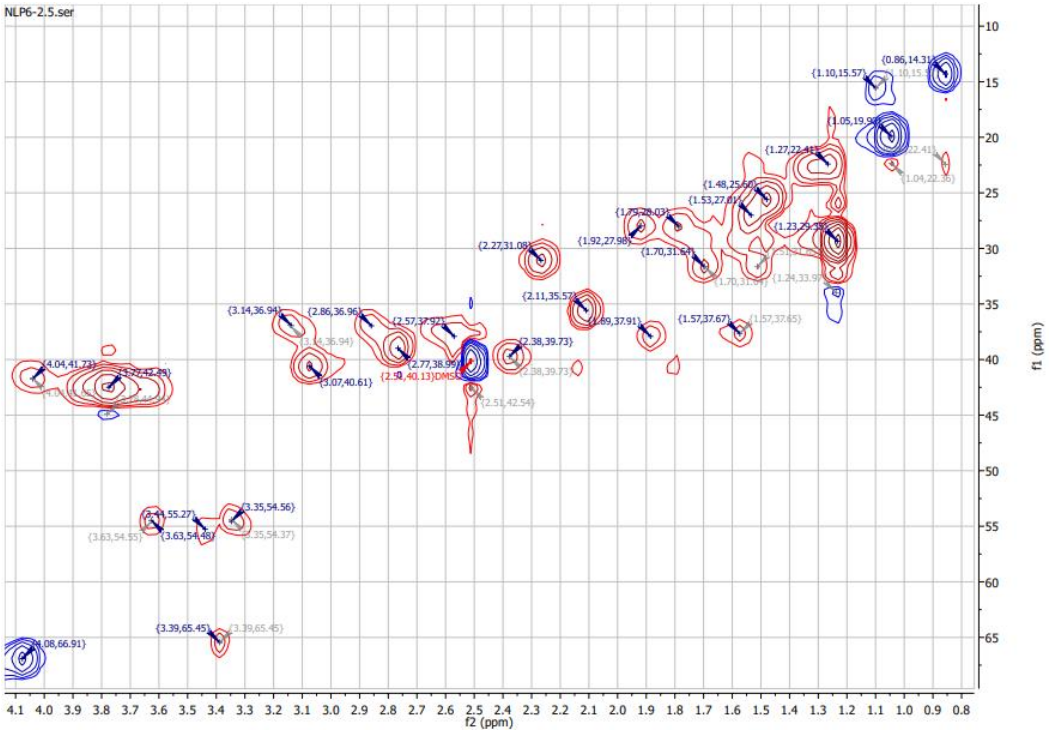

Figure 9.113: HSQC section of spectrum of *retro*-DGD-GG-GFOGER-GG-TTK-Palmitate.

9.7.36 HMBC spectrum of *retro*-DGD-GG-GFOGER-GG-TTK-Palmitate

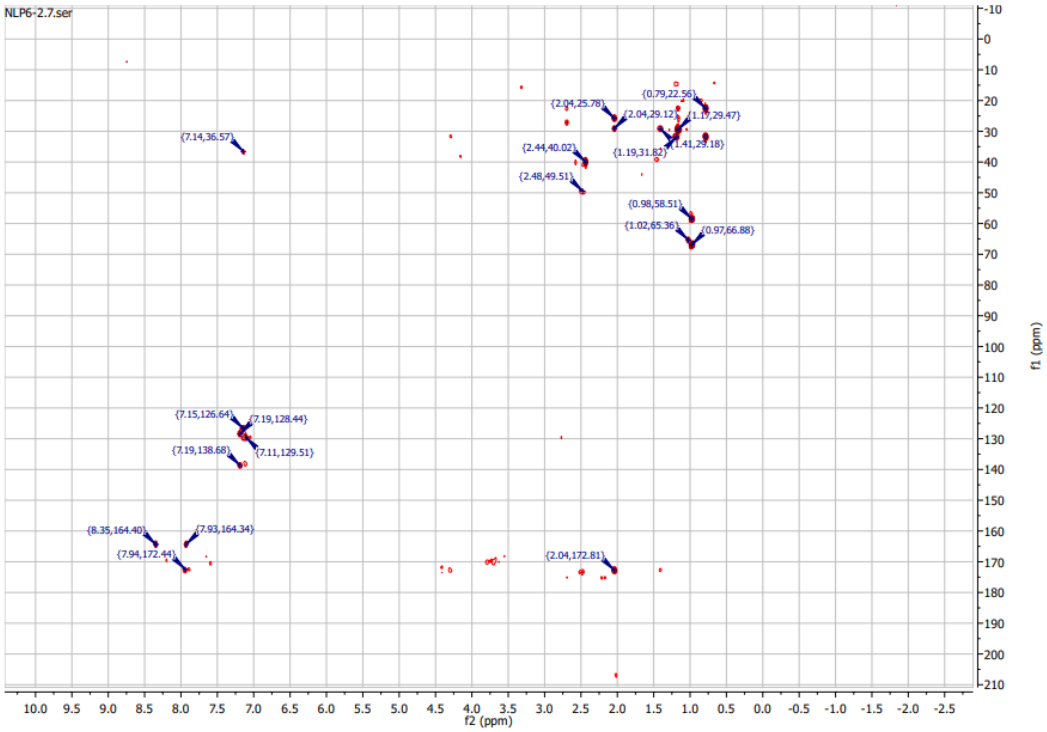

Figure 9.114: HMBC spectrum of *retro*-DGD-GG-GFOGER-GG-TTK-Palmitate.

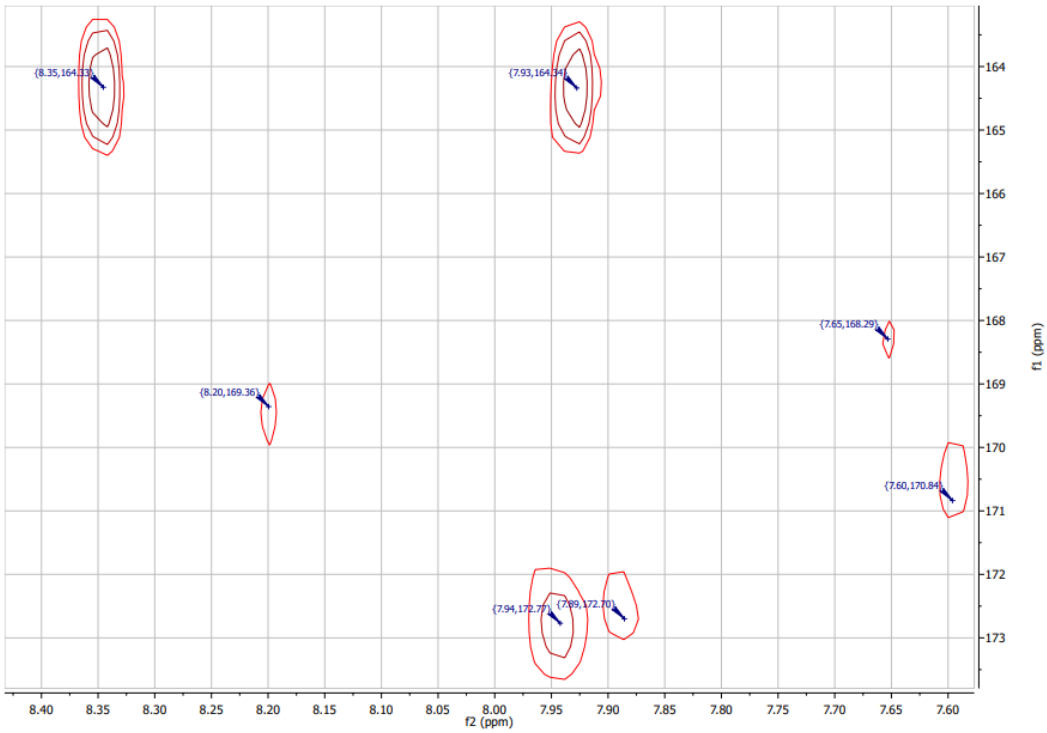

Figure 9.115: HMBC amide section of spectrum of *retro*-DGD-GG-GFOGER-GG-TTK-Palmitate.

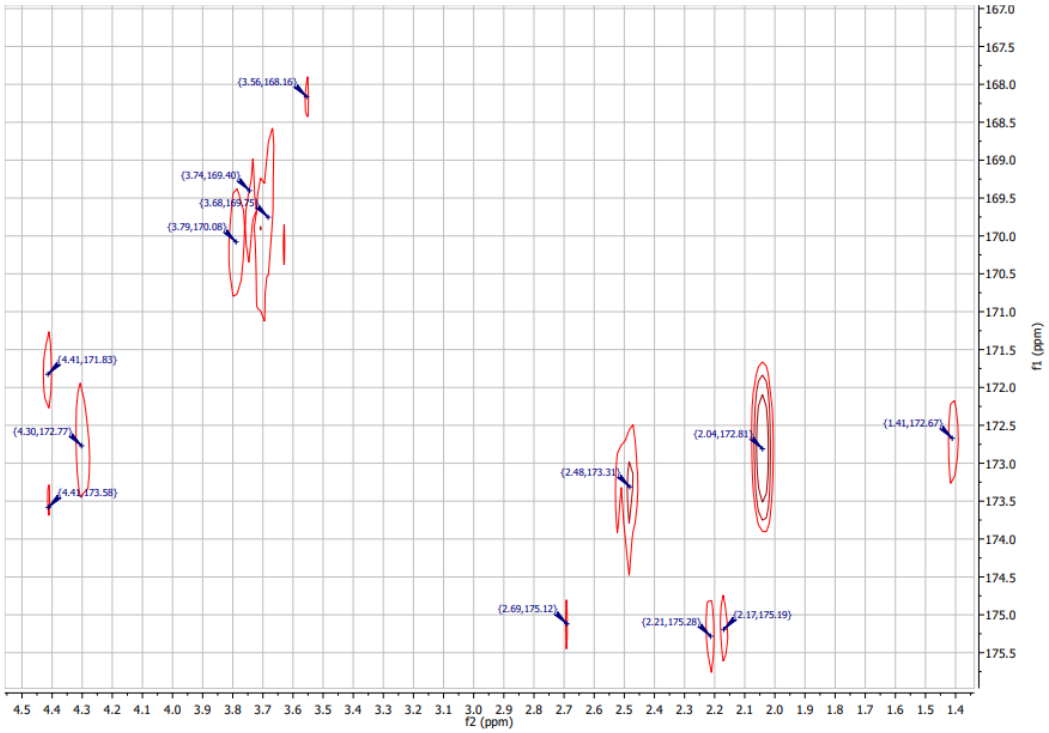

Figure 9.116: HMBC aliphatic section of spectrum of *retro*-DGD-GG-GFOGER-GG-TTK-Palmitate.

9.7.37 TOCSY spectrum of *retro*-DGD-GG-GFOGER-GG-TTK-Palmitate

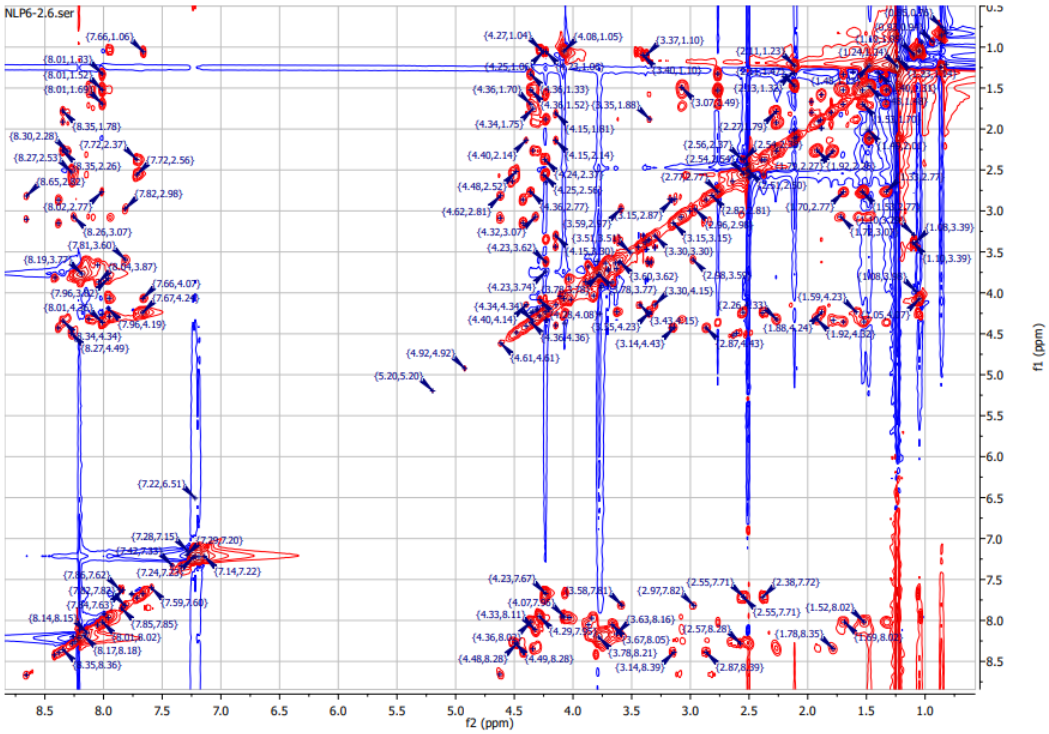

Figure 9.117: TOCSY spectrum of *retro*-DGD-GG-GFOGER-GG-TTK-Palmitate.

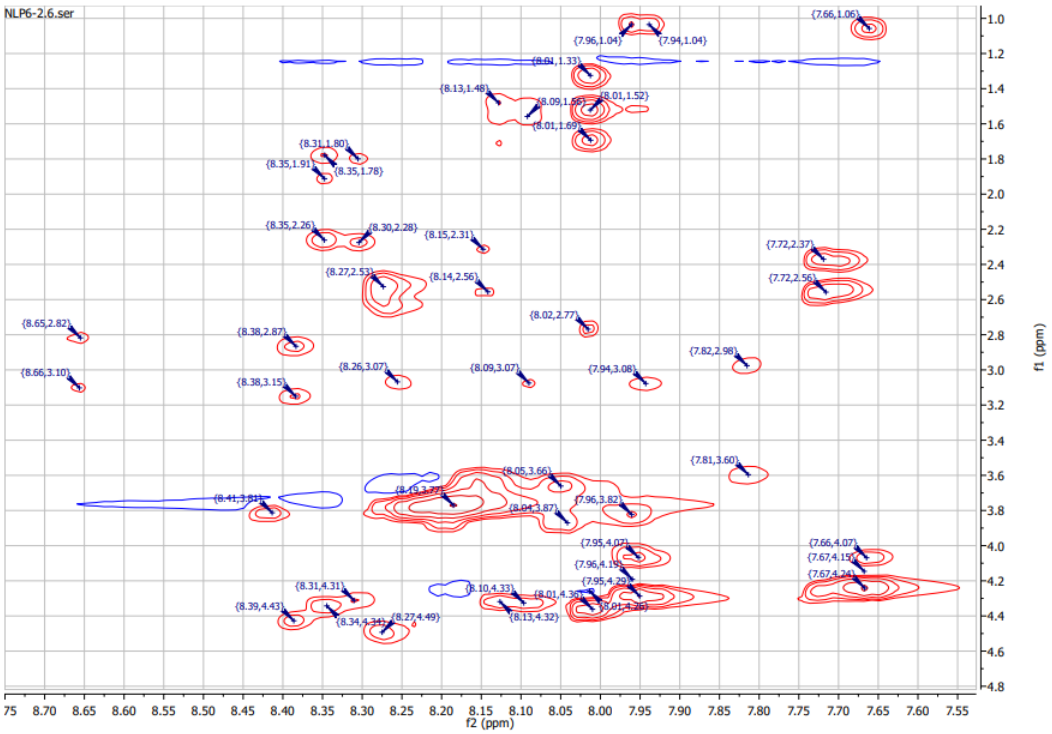

Figure 9.118: TOCSY aliphatic-amide section of spectrum of *retro*-DGD-GG-GFOGER-GG-TTK-Palmitate.

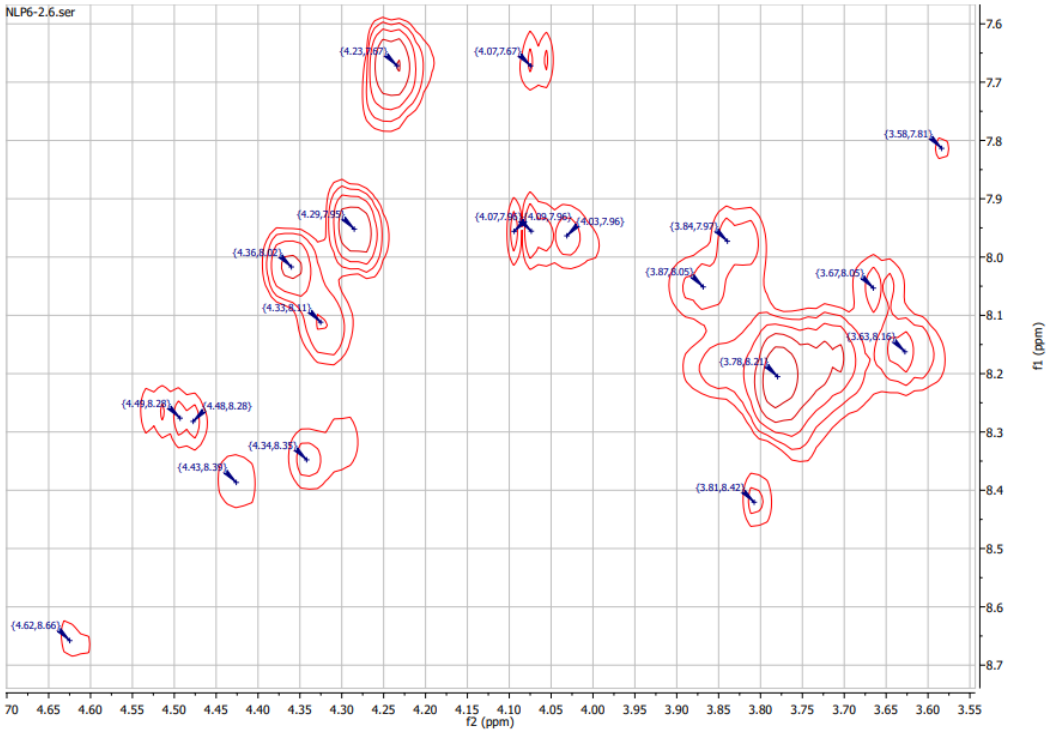

Figure 9.119: TOCSY *alpha*-amide section of spectrum of *retro*-DGD-GG-GFOGER-GG-TTK-Palmitate.

9.7.38 ROESY spectrum of *retro*-DGD-GG-GFOGER-GG-TTK-Palmitate

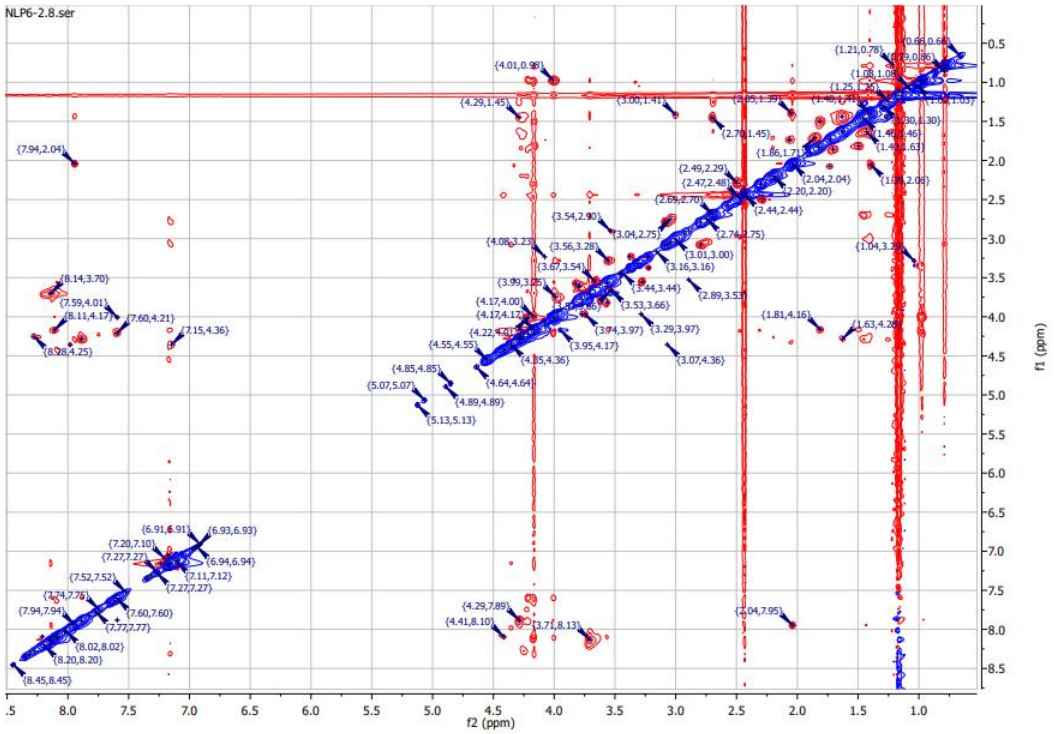

Figure 9.120: ROESY spectrum of *retro*-DGD-GG-GFOGER-GG-TTK-Palmitate.

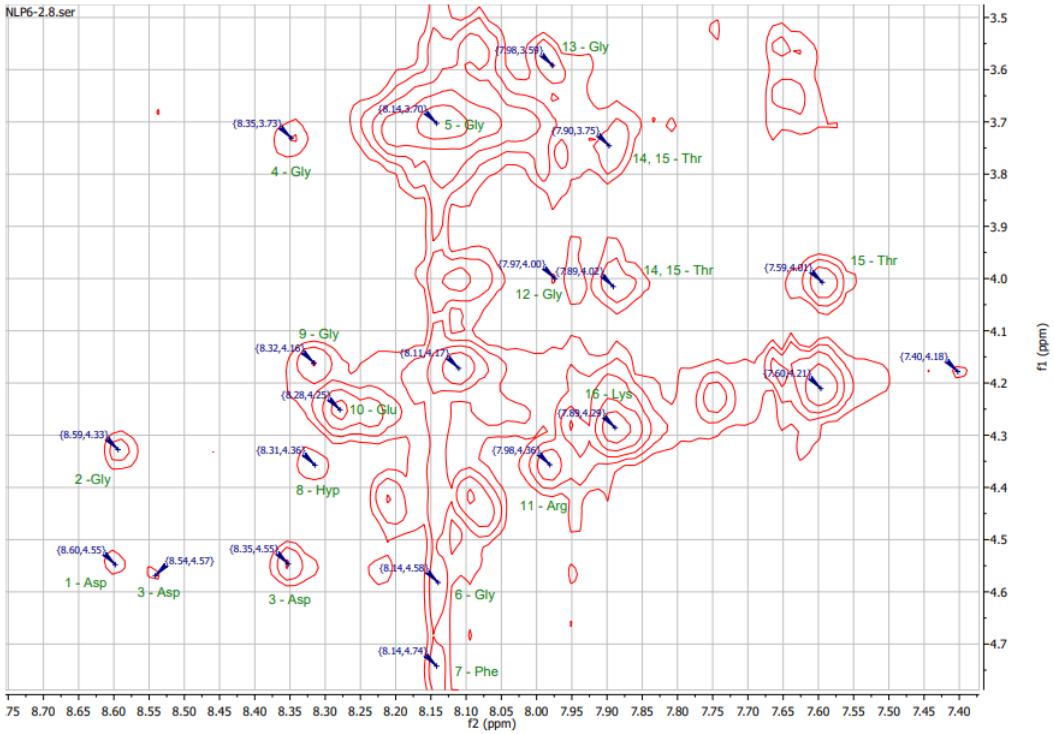

Figure 9.121: ROESY *alpha*-amide section of spectrum of *retro*-DGD-GG-GFOGER-GG-TTK-Palmitate.

9.7.39 ^{1}H NMR spectrum of *para*-fluorophenylalanine

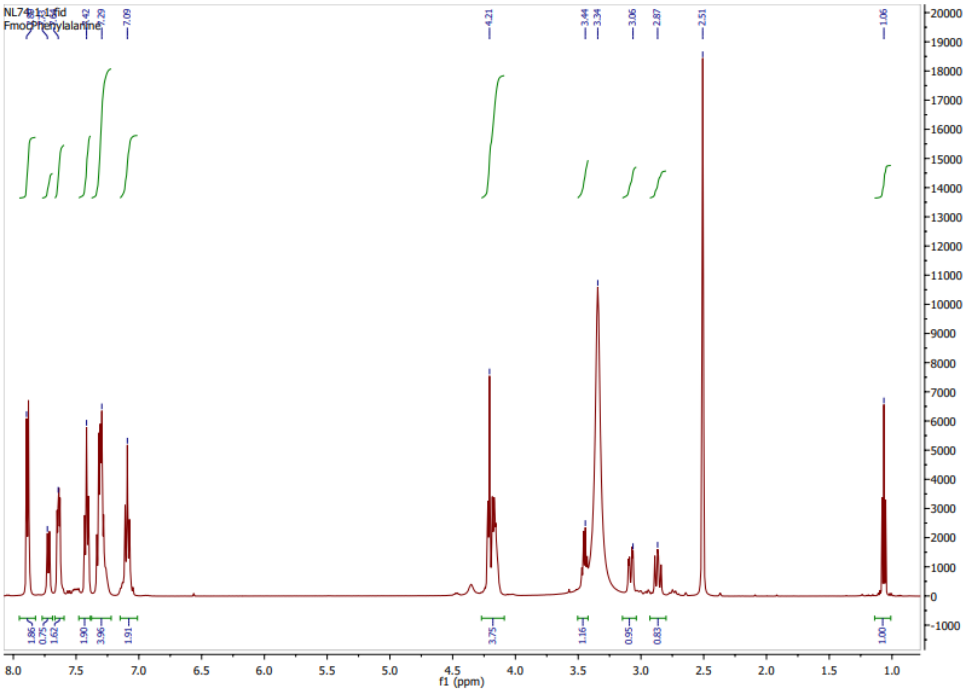

Figure 9.122: ^{1}H NMR spectrum of *para*-fluorophenylalanine spectrum.

9.7.40 ^{1}H NMR spectrum of phenylalanine oxazolidinone

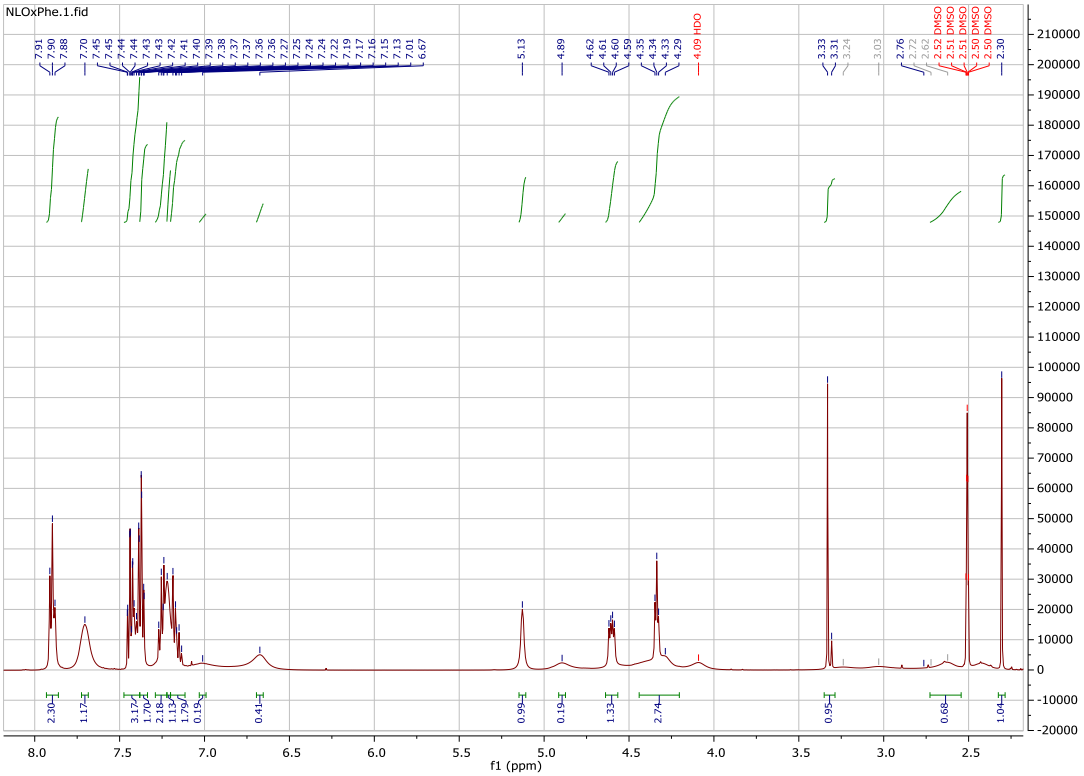

Figure 9.123: ^{1}H NMR spectrum of phenylalanine oxazolidinone.

9.8 CIRCULAR DICHROISM (CD) OF SELECTED PEPTIDES

9.8.1 CD spectrum of *retro*-DGD-GG-GFOGER-GG-TTK-Palmitate peptide

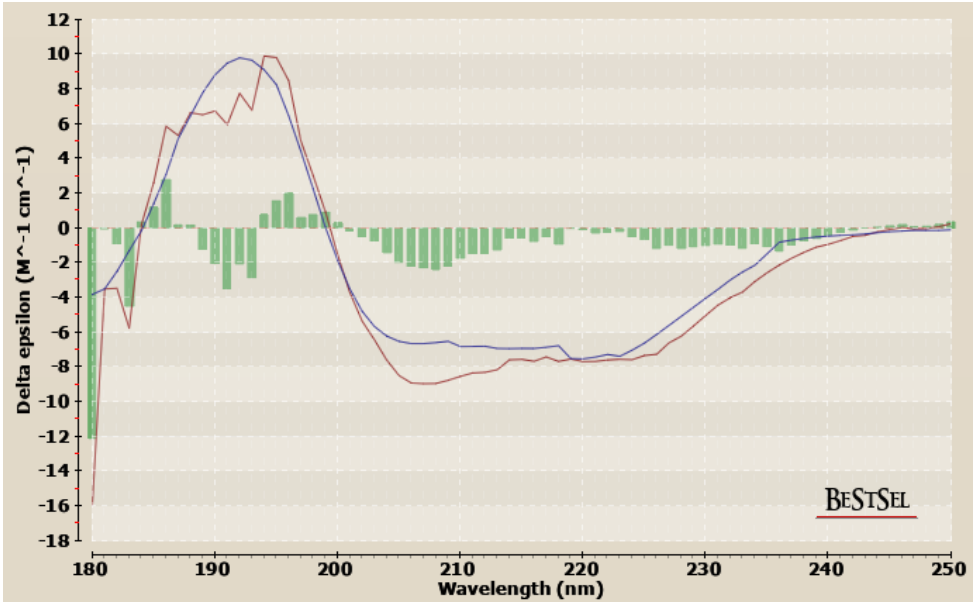

Figure 9.124: CD spectrum of *retro*-DGD-GG-GFOGER-GG-TTK-Palmitate peptide (brick red = experimental; blue = fitted).

9.8.2 *Retro*-DGD-GG-GFOGER-GG-GHK-Palmitate peptide

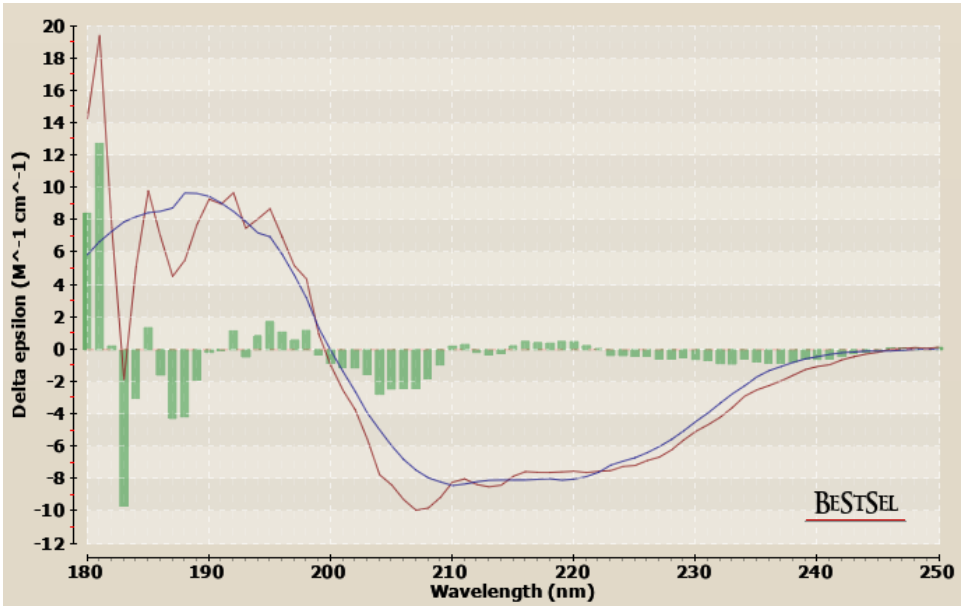

Figure 9.125: CD spectrum of *retro*-DGD-GG-GFOGER-GG-GHK-Palmitate peptide (brick red = experimental; blue = fitted).

9.8.3 *Retro*-DGD-GG-GFOGER-GG-QPR-Palmitate peptide

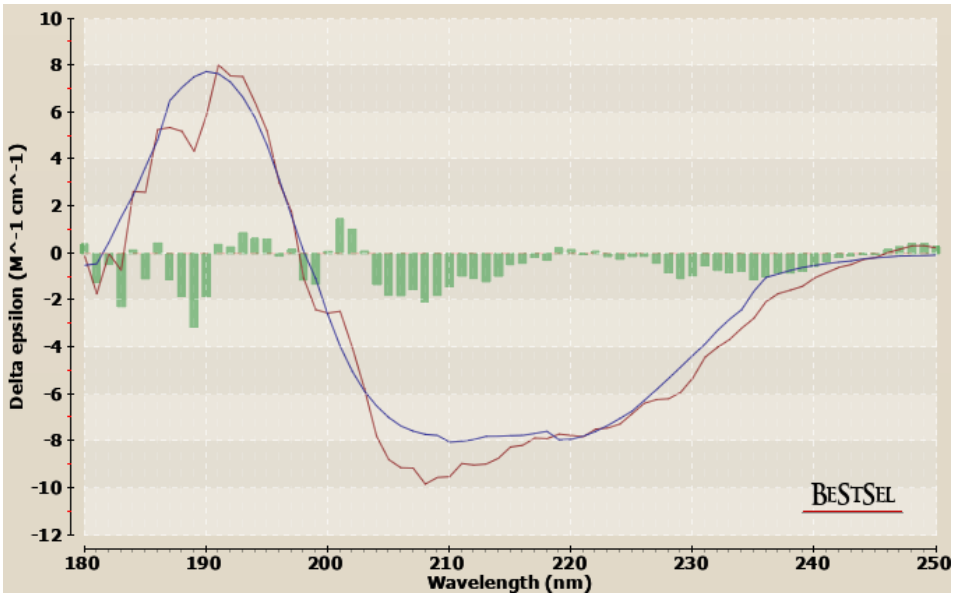

Figure 9.126: CD spectrum of *retro*-DGD-GG-GFOGER-GG-QPR-Palmitate peptide (brick red = experimental; blue = fitted).

9.8.4 *Retro*-DGD-GG-GFOGER-GG-EEM-Palmitate peptide

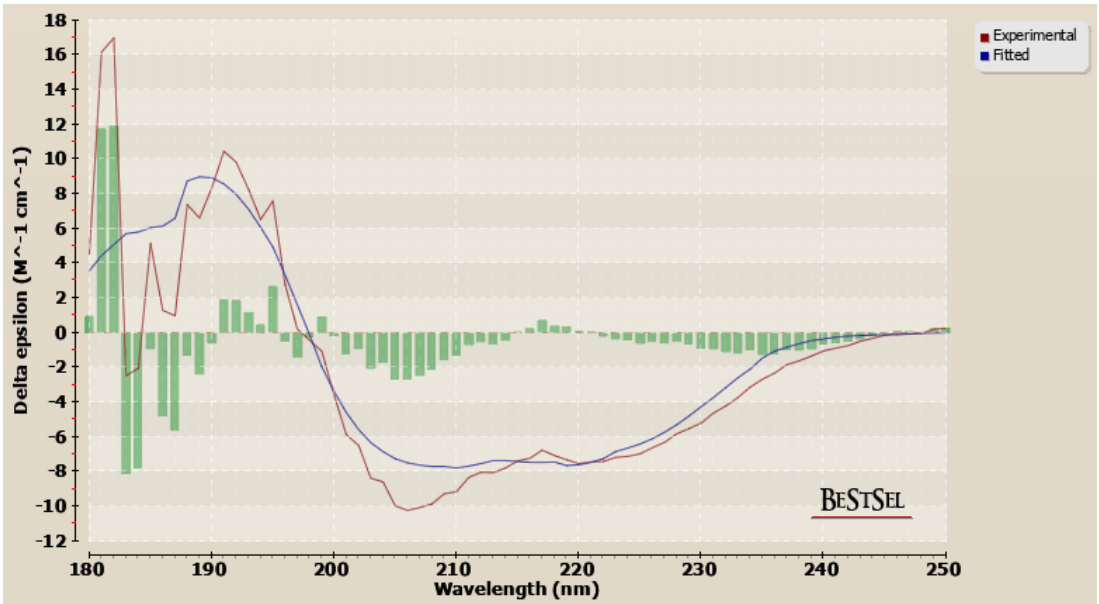

Figure 9.127: CD spectrum of *retro*-DGD-GG-GFOGER-GG-EEM-Palmitate peptide.

9.8.5 *Retro*-DGD-GG-GFOGER-GG-TTK-Adamantane peptide

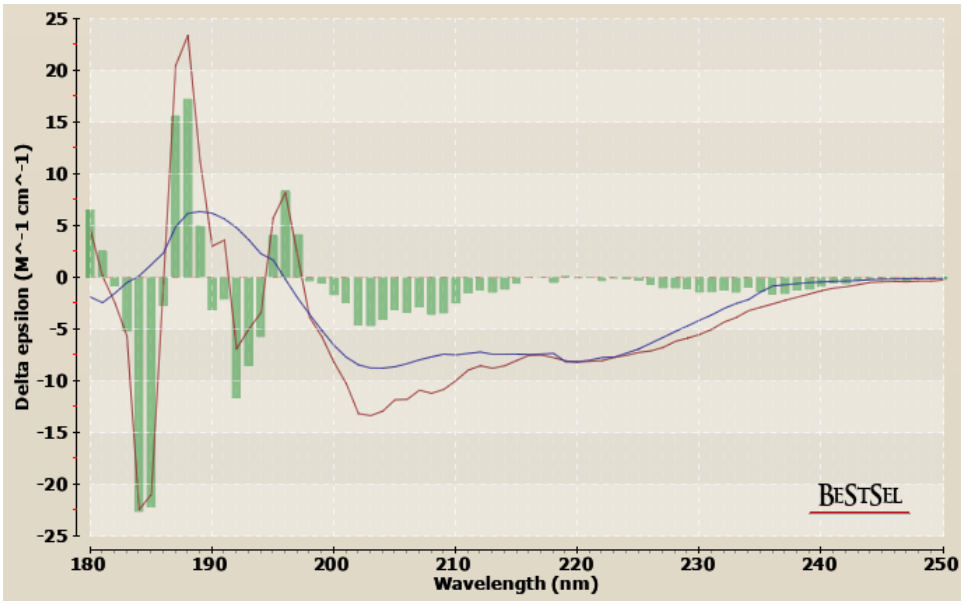

Figure 9.128: CD spectrum of *retro*-DGD-GG-GFOGER-GG-TTK-Adamantane peptide (brick red = experimental; blue = fitted).

9.8.6 *Retro*-DGD-GG-GFOGER-GG-GHK-Adamantane peptide

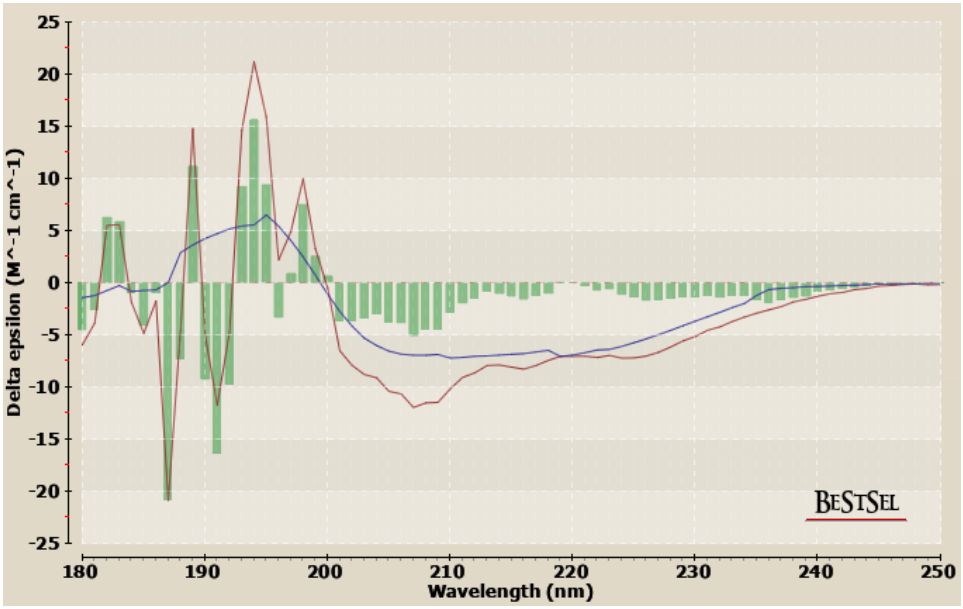

Figure 9.129: CD spectrum of *retro*-DGD-GG-GFOGER-GG-GHK-Adamantane peptide (brick red = experimental; blue = fitted).

9.8.7 *Retro*-DGD-GG-GFOGER-GG-EEM-Adamantane peptide

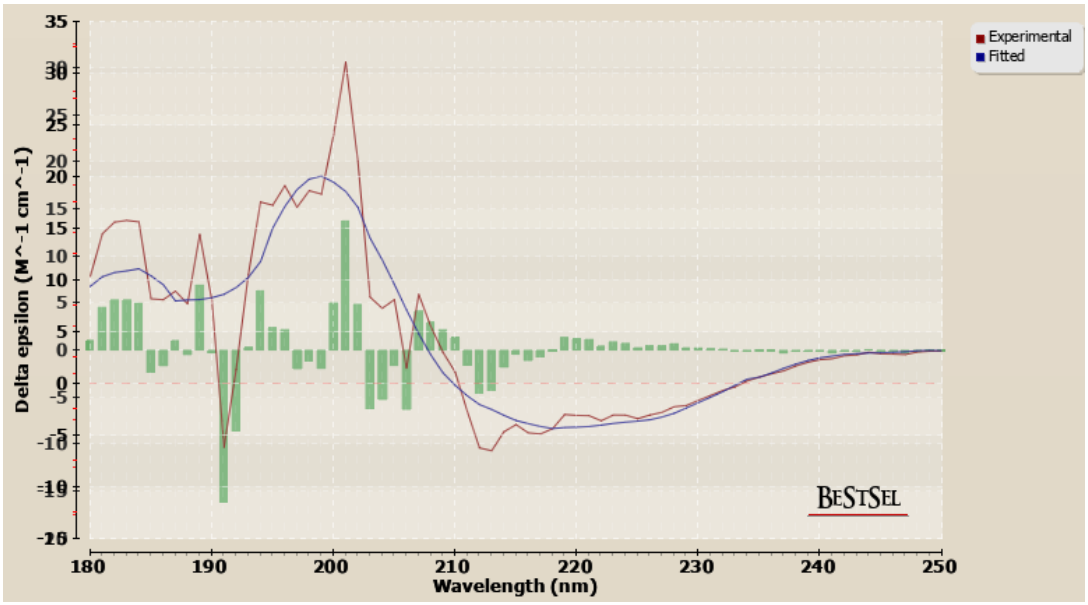

Figure 9.130: CD spectrum of *retro*-DGD-GG-GFOGER-GG-EEM-Adamantane peptide.

APPENDIX

10.1 CHARACTERIZATION TABLES

10.1.1 *Retro*-GG-GFOGER-GG-Adamantane

Table 10.1: TOCSY/ROESY amide and *alpha* protons chemical shifts of *retro*-GG-GFOGER-GG-Adamantane.

TOCSY Spin System	Amide (NH, *i*)		*Alpha* (H^{α}, *i* – 1)	
	COSY	ROESY	COSY	ROESY
3.89 (Gly)	8.53, 3.89	8.53, 3.52	3.52, 8.55	3.52, 8.53
3.52 (Gly)	8.55, 3.52	8.55, 3.89	3.89, 8.55	3.89, 8.55
3.89 (Gly)	8.55, 3.89	8.55, 4.69	4.69, 7.29	4.69, 8.55
4.69 (Phe)	7.29, 4.69	7.29, 4.39	4.39, -	4.39, 7.29
4.39 (Hyp)	- , 4.39	- , 3.73	3.73, 8.30	3.73, -
3.73 (Gly)	8.30, 3.73	8.30, 4.20	4.20, 7.96	4.20, 8.30
4.20 (Glu)	7.96, 4.20	7.96, 4.31	4.31, 7.91	4.31, 7.96
4.31 (Arg)	7.91, 4.31	7.91, 3.89	3.89, 8.55	3.89, 7.91
3.89 (Gly)	8.55, 3.89	8.55, 3.52	3.52, 8.55	3.52, 8.55
3.52 (Gly)	8.55, 3.52	8.55, -	-	-

Table 10.2: Correlations between dipeptides observed in the ROESY spectrum of *retro*-GG-GFOGER-GG-Adamantane.

TOCSY Spin system		ROESY		Dipeptide
H^{α}	H^{β}, H^{γ}, H^{δ} ,H^{ϵ}	$H^{\alpha}1$, $H^{\alpha}2$	H^{β}, H^{γ}, H^{δ}, H^{ϵ}	
3.89	-	3.89, 3.52	-	Gly-Gly
3.52	-	3.52, 3.89	-	Gly-Gly
3.89	-	3.89, 4.69	2.85, 2.96, 7.12, 7.26, 7.19	Gly-Phe
4.69	2.85, 2.96, 7.12, 7.26, 7.19	4.69, 4.39	2.85, 2.96, 7.12, 7.26, 7.19, 1.92, 4.39, 3.61	Phe-Hyp
4.39	1.92, 4.39, 3.61	4.39, 3.73	1.92, 4.39, 3.61	Hyp-Gly
3.73	-	3.73, 4.20	2.56, 2.44	Gly-Glu
4.20	2.56, 2.44	4.20, 4.31	2.56, 2.44, 3.00, 1.51, 1.91,	Glu-Arg
4.31	3.00, 1.51, 1.91	4.31, 3.89	3.00, 1.51, 1.91	Arg-Gly
3.89	-	3.89, 3.52	-	Gly-Gly
3.52	-			

Table 10.3: Tertiary structure determination of *retro*-GG-GFOGER-GG-Adamantane.

Hyp-Arg (α-helix)	Expected Interaction	Observed Interaction	Coupling Range
$d_{\alpha\beta}(I, I + 3)$	4.39, 1.90/1.97	4.39, 1.90	medium
$d_{\alpha N}(I, I + 3)$	4.39, 7.91	4.39, 8.30	medium
$d_{NN}(I, I + 3)$	7.95	No NH	-
$d_{\alpha N}(I, I + 4)$	4.39, 8.55	4.39, 8.30	medium

10.1.2 *Retro*-DGD-GG-GFOGER-GG-Adamantane (NL008)

Table 10.4: ROESY correlations of dipeptide of NL008.

TOCSY Spin System		ROESY		Dipeptide
H^{α}	H^{β}, H^{γ}, H^{δ} ,H^{ϵ}	$H^{\alpha}1$, $H^{\alpha}2$	H^{β}, H^{γ}, H^{δ}, H^{ϵ}	
4.63	3.10, 2.80	4.63, 4.41	3.10, 2.80	Asp-Gly
4.41	-	4.41, 4.63	3.10, 2.80	Gly-Asp
4.63	3.10, 2.80	4.63, 3.89	3.10, 2.80	Asp-Gly
3.89	-	3.89, 3.52	-	Gly-Gly
3.52	-	3.52, 3.89	-	Gly-Gly
3.89	-	3.89, 4.69	2.85, 2.96, 7.12, 7.26, 7.19	Gly-Phe
4.69	2.85, 2.96, 7.12, 7.26, 7.19	4.69, 4.39	2.85, 2.96, 7.12, 7.26, 7.19, 1.92, 4.39, 3.61	Phe-Hyp
4.39	1.92, 4.39, 3.61	4.39, 3.73	1.92, 4.39, 3.61	Hyp-Gly
3.73	-	3.73, 4.20	2.56, 2.44	Gly-Glu
4.20	2.56, 2.44	4.20, 4.31	2.56, 2.44, 3.00, 1.51, 1.91,	Glu-Arg
4.31	3.00, 1.51, 1.91	4.31, 3.89	3.00, 1.51, 1.91	Arg-Gly
3.89	-	3.89, 3.52	-	Gly-Gly

Table 10.5: TOCSY/ROESY amide and *alpha* proton chemical shifts of *retro*-DGD-GG-GFOGER-GG-Adamantane.

TOCSY Spin System	Amide (NH, *i*)		*Alpha* (H^{α}, *i* – 1)	
	COSY	ROESY	COSY	ROESY
4.64 (Asp)	8.66, 4.64	8.66, 4.41	4.41, 8.53	4.41, 8.66
4.41 (Gly)	8.53, 4.41	8.53, 4.65	4.65, 8.27	4.65, 8.53
4.65 (Asp)	8.27, 4.65	8.27, 3.78	3.78, 8.26	3.78, 8.27
3.78 (Gly)	8.26, 3.78	8.26, 3.71	3.71, 8.09	3.71, 8.26
3.71 (Gly)	8.09, 3.71	8.09, 4.58	4.58, 8.08	4.58, 8.09
4.58 (Gly)	8.08, 4.58	8.08, 4.72	4.72, 8.03	4.72, 8.08
4.72 (Phe)	8.03, 4.72	8.03, 4.44	4.44, -	4.44, 8.03
4.44 (Hyp)	- , 4.44	- , 4.30	4.30, 8.25	4.30, -
4.30 (Gly)	8.25, 4.30	8.25, 3.59	3.59, 7.78	3.59, 8.25
3.59 (Glu)	7.78, 3.59	7.78, 4.33	4.33, 8.01	4.33, 7.78
4.33 (Arg)	8.01, 4.33	8.01, 4.02	4.02, 8.01	4.02, 8.01
4.02 (Gly)	8.01, 4.02	8.01, 3.67	3.67, 7.94	3.67, 8.01
3.67 (Gly)	7.94, 3.67	7.94, -	-	-

Table 10.6: ROESY correlations for the tertiary structure determination of *retro*-DGD-GG-GFOGER-GG-Adamantane.

Hyp-Arg (α-helix)	Expected Interaction	Observed Interaction	Coupling Range
$d_{\alpha\beta}(i, i + 3)$	4.72, 4.20	Not observed	-
$d_{\alpha N}(i, i + 3)$	4.72, 7.78	Not observed	-
$d_{NN}(i, i + 3)$	8.03, 7.78	8.03, 7.78	medium
$d_{\alpha N}(i, i + 4)$	4.72, 8.01	Not observed	-

10.1.3 *Retro*-DGD-GG-GFOGER-GG-TTK-Adamantane

Table 10.7: Amide proton interactions in *retro*-DGD-GG-GFOGER-GG-TTK-Adamantane.

TOCSY Spin System	Amide (NH, *i*)		*Alpha* (H^{α}, *i* – 1)	
	COSY	ROESY	COSY	ROESY
4.63 (Asp)	8.60, 4.63	8.60, 4.41	4.41, 8.53	4.41, 8.60
4.41 (Gly)	8.53, 4.41	8.53, 4.63	4.63, 8.60	4.63, 8.53
4.63 (Asp)	8.60, 4.63	8.60, 3.80	3.80, 8.36	3.80, 8.60
3.80 (Gly)	8.36, 3.80	8.36, 3.77	3.77, 8.13	3.77, 8.36
3.77 (Gly)	8.13, 3.77	8.13, 4.54	4.54, 8.15	4.54, 8.13
4.54 (Gly)	8.15, 4.54	8.15, 4.66	4.66, 8.14	4.66, 8.15
4.66 (Phe)	8.14, 4.66	8.14, 4.43	4.43, -	4.43, 8.14
4.43 (Hyp)	- , 4.43	- , 4.27	4.27, 8.32	4.27, -
4.27 (Gly)	8.32, 4.27	8.32, 4.33	4.33, 8.23	4.33, 8.32
4.33 (Glu)	8.23, 4.33	8.23, 4.31	4.31, 7.96	4.31, 8.23
4.31 (Arg)	7.96, 4.31	7.96, 4.06	4.06, 7.69	4.06, 7.96
4.06 (Gly)	7.69, 4.06	7.69, 4.24	4.24, 8.12	4.24, 7.69
4.24 (Gly)	8.12, 4.24	8.12, 3.82	3.82, 7.99	3.82, 8.12
3.82 (Thr)	7.99, 3.82	7.99, 3.82	3.82, 7.99	3.82, 799
3.82 (Thr)	7.99, 3.82	7.99, 4.35	4.35, 7.99	4.35, 7.99
4.35 (Lys)	7.99, 4.35	7.99, -	-	-

10.1.4 *Retro*-DGD-GG-GFOGER-GG-TTK-Palmitate (NL009)

Table 10.8: TOCSY/ROESY amide and *alpha* protons correlations of NL009.

TOCSY Spin System	Amide (NH, *i*)		*Alpha* (H^{α}, *i* – 1)	
	COSY	ROESY	COSY	ROESY
4.63 (Asp)	8.66, 4.63	8.66, 4.33	4.33, 8.53	4.33, 8.66
4.33 (Gly)	8.35, 4.33	8.35, 4.63	4.63, 8.66	4.63, 8.35
4.63 (Asp)	8.66, 4.63	8.66, 3.73	3.73, 8.14	3.73, 8.66
3.73 (Gly)	8.14, 3.73	8.14, 3.70	3.70, 8.16	3.70, 8.14
3.70 (Gly)	8.16, 3.70	8.16, 4.58	4.58, 8.17	4.58, 8.16
4.58 (Gly)	8.17, 4.58	8.17, 4.74	4.74, 8.14	4.74, 8.17
4.74 (Phe)	8.14, 4.74	8.14, 4.36	4.36, -	4.36, 8.14
4.36 (Hyp)	- , 4.36	- , 4.17	4.17, 7.97	4.36, -
4.17 (Gly)	7.97, 4.17	7.97, 4.25	4.25, 7.73	4.25, 7.97
4.25 (Glu)	7.73, 4.25	7.73, 4.36	4.36, 8.02	4.36, 7.73
4.36 (Arg)	8.02, 4.36	8.02, 4.01	4.01, 7.82	4.01, 8.02
4.01 (Gly)	7.82, 4.01	7.82, 3.57	3.57, 7.83	3.57, 7.82
3.57 (Gly)	7.83, 3.57	7.83, 3.73	3.73, 8.14	3.73, 7.83
3.73 (Thr)	8.14, 3.73	8.14, 3.73	3.73, 8.14	3.73, 8.14
3.73 (Thr)	8.14, 3.73	8.14, 4.29	4.29, 8.53	4.29, 8.14
4.29 (Thr)	8.53, 4.29	8.53, -	-	-

10.2 CIRCULAR DICHROISM

10.2.1 *Retro*-DGD-GG-GFOGER-GG-TTK-Palmitate

Table 10.9: Helix content of *retro*-DGD-GG-GFOGER-GG-TTK-Palmitate.

Helix	Content (%)
Helix 1 (regular)	24.7
Helix 2 (distorted)	3.7
Anti 1 (left-twisted)	0.0
Anti 2 (relaxed)	0.0
Anti 3 (right-twisted)	0.0

10.2.2 *Retro*-DGD-GG-GFOGER-GG-GHK-Palmitate

Table 10.10: Helix content of *retro*-DGD-GG-GFOGER-GG-GHK-Palmitate.

Helix	Content (%)
Helix 1 (regular)	54.0
Helix 2 (distorted)	19.9
Anti 1 (left-twisted)	0.0
Anti 2 (relaxed)	0.0
Anti 3 (right-twisted)	11.1

10.2.3 *Retro*-DGD-GG-GFOGER-GG-QPR-Palmitate

Table 10.11: Helix content of *retro*-DGD-GG-GFOGER-GG-QPR-Palmitate.

Helix	Content (%)
Helix 1 (regular)	27.0
Helix 2 (distorted)	7.0
Anti 1 (left-twisted)	0.0
Anti 2 (relaxed)	0.0
Anti 3 (right-twisted)	4.5

10.2.4 *Retro*-DGD-GG-GFOGER-GG-EEM-Palmitate

Table 10.12: Helix content of *retro*-DGD-GG-GFOGER-GG-EEM-Palmitate.

Helix	Content (%)
Helix 1 (regular)	43.6
Helix 2 (distorted)	8.9
Anti 1 (left-twisted)	0.0
Anti 2 (relaxed)	0.0
Anti 3 (right-twisted)	12.3

10.2.5 *Retro*-DGD-GG-GFOGER-GG-TTK-Adamantane

Table 10.13: Helix content of *retro*-DGD-GG-GFOGER-GG-TTK-Adamantane.

Helix	Content (%)
Helix 1 (regular)	18.1
Helix 2 (distorted)	0.0
Anti 1 (left-twisted)	0.0
Anti 2 (relaxed)	0.0
Anti 3 (right-twisted)	6.5

10.2.6 *Retro*-DGD-GG-GFOGER-GG-GHK-Adamantane

Table 10.14: Helix content of *retro*-DGD-GG-GFOGER-GG-GHK-Adamantane.

Helix	Content (%)
Helix 1 (regular)	31.8
Helix 2 (distorted)	13.7
Anti 1 (left-twisted)	0.0
Anti 2 (relaxed)	0.0
Anti 3 (right-twisted)	0.0

10.2.7 *Retro*-DGD-GG-GFOGER-GG-EEM-Adamantane

Table 10.15: Helix content of *retro*-DGD-GG-GFOGER-GG-EEM-Adamantane.

Helix	Content (%)
Helix 1 (regular)	6.2
Helix 2 (distorted)	44.5
Anti 1 (left-twisted)	33.1
Anti 2 (relaxed)	2.7
Anti 3 (right-twisted)	0.0

10.3 SUPPLEMENTARY INFORMATION FOR THE PUBLISHED ARTICLE

Contents

1. GENERAL INFORMATION 254

2. INSTRUMENTATION 254

3. GENERAL TECHNIQUES 255

4. GENERAL PROCEDURES 257

5. SUMMARY OF SYNTHESIZED COMPOUNDS 260

6. MASS SPECTRA 274

7. NMR SPECTRA OF SELECTED PEPTIDES 283

Electronic Supplementary Information

Design, Synthesis and Characterization of Type I Collagen Mimetic Peptides.

Ntlama Lesotho[1], Thabo Peme[1], Maya Makatini[1*]

[1]*Molecular Sciences Institute, School of Chemistry, University of the Witwatersrand, Private Bag 3, PO WITS, 2050, South Africa.*

Email: maya.makatini@wits.ac.za, Tel: +27 11 717 6708

1. GENERAL INFORMATION

1.1 Chemicals and reagents

All organic solvents and reagents were obtained from commercial sources. Fmoc protected amino acids, (1-[Bis(dimethylamino)methylene]-1H-1,2,3-triazolo[4,5-b]pyridinium 3-oxide hexafluorophosphate, Hexafluorophosphate Azabenzotriazole Tetramethyl Uronium) (HATU), N,N,N',N'-Tetramethyl-O-(1H-benzotriazol-1-yl)uraniumhexafluorophosphate (HBTU), and 2-chlorotrityl chloride resin were purchased from DLD scientific. Reagents such as diisopropylethylamine (DIPEA), piperidine, Triisopropylsilane (TIS), formic acid, trifluoroacetic acid (TFA), palmitic acid and adamantane were obtained from Sigma Aldrich (South Africa). Organic solvents such as dimethylformamide (DMF), HPLC grade methanol, HPLC grade acetonitrile, dimethylsulfoxide and diethylether were purchased from Radchem and Pyramid scientific.

2. INSTRUMENTATION

2.1 Ultra-High-Performance Liquid Chromatography Mass Spectrometry (UHPLC-MS)

Analytical LC-MS analysis was performed on an Ultra-High-Performance Liquid Chromatography (Thermo Scientific Ultimate 3000, RS diode array detectors) with a Diode Array (190, 195, 215, 254, and 300 nm) coupled to a Bruker Compact Q-TOF high-resolution mass spectrometer.

2.2 Spectroscopic and physical data

Nuclear magnetic resonance (NMR) spectra were recorded on either a Bruker AVANCE 300, 400 or Bruker AVANCE III 500 MHz spectrometer. Peptides were dissolved in deuteurated DMSO, $CDCl_3$ or d_6-acetone. Coupling constant (J-values are given in Hertz (Hz)). All chemical

shift values are reported in parts per million referenced against trimethylsilane which is given an assignment of zero parts per million.

For conformational analysis, the experiment was conducted at different temperatures such as 300, 323 and 353 K on Bruker AVANCE 400 MHz instrument. For 2D experiments such as COSY, HSQC, HMBC, TOCSY, NOESY and ROESY, the spectra were recorded at the phase-sensitive mode using time proportional phase increment (TPPI) on a Bruker III 500 MHz spectrometer. The NOESY experiments were recorded with mixing times of 150, 200 and 250 ms; the ROESY spectrum was recorded with mixing times of 100, 150, 200, 250 and 300 ms; while TOCSY was recorded with mixing times of 48, 64, 70, 80 and 100 ms. The residual water peak of DMSO-d6 was suppressed by a presaturation pulse of 2 s duration. 2048 data points were collected per experiment.

2.3 Circular dichroism

The circular dichroism spectra were recorded on a JASCO J-18 spectropolarimeter with the following settings; wavelength scan - 0.1 mm pathlength; 0.2 mg/mL protein concentration; 225 µl volume; 1.0 nm bandwidth; 0.5 nm resolution; 8 scans; 4 secs response; 20 nm/minute scan speed; scan range 280 – 160 nm while keeping HT voltage less than 600 V. The wavelength range was set between 190 to 250 nm while the temperature was set to 20 °C. The peptides were prepared in phosphate buffer at a concentration of 0.1 mg/mL. A 0.1 cm pathlength cuvette holding 300 µl was used for all CD measurements.

2.4 Ultra-violet Visible (UV-Vis)

Absorbance values used to determine the loading capacity of the resin were recorded on the Varian Cary Eclipse (Cary 50) UV-vis spectrophotometer.

3. GENERAL TECHNIQUES

3.1 UHPLC-MS Analysis

The samples were analysed using a binary solvent system where solvent A consisted of H_2O and 0.1% Formic acid (v/v), and solvent B consisted of Acetonitrile and 0.1% Formic acid (v/v). 20 µL of the sample was injected into a C18 column (5 µm, 100 Å, 4.60 mm × 150 mm). The system flow rate was set at 0.3 mL/minute in the positive mode. The mass spectrum analysis

was processed using the Bruker Daltonics data analysis software. The ultra-pure water used in this study was obtained from the Millipore Direct-Q®3 UV water purification (ZRQSVPO30) system.

The samples were analysed in the positive ionization mode and the MS was scanned at m/z 100-3000 range during separation and detection. Nitrogen gas (N_2) was used as the dry and nebulizer gas. The nebuliser gas was operated at a pressure of 1.8 bars whereas the drying gas was operated at a flow rate of 9 L/minute.

3.2 ^{1}H Nuclear Magnetic Resonance (^{1}H NMR)

The chemical shifts (δ) values are reported in parts per million (ppm) relative to deuterated dimethyl sulfoxide (DMSO-d_6, 2.49 ppm) and referenced against the internal standard, tetramethylsilane (TMS, 0.00 ppm). The spectra were analyzed as first order and the values of the coupling constant (J) are reported as Hertz (Hz). Multiplicity of signals is expressed as: s = singlet, br s = broad singlet, d = doublet, dd = double of doublet, t = triplet, q = quartet, m = multiplet.

3.3 ^{13}C NMR

The chemical shift values are reported in (ppm) relative to deuterated (DMSO-d_6, 39.52 ppm) and TMS as an internal standard.

3.4 2D NMR

Spectra for COSY, ^{13}C-HSQC, TOCSY, NOESY and ROESY experiments, were recorded at 293, 300, and 308 K on a 500 MHz NMR Bruker III 500 MHz spectrometer. All 2D spectra were recorded at the phase-sensitive mode using time proportional phase increment (TPPI). The residual water peak of DMSO-d_6 was suppressed by a pre-saturation pulse of 2.0 *s* duration. The first NOESY experiments were recorded with mixing time of 150, 200 and 250 ms; the ROESY spectrum was recorded with mixing times of 100, 150, 154 200, 250 and 300 ms; while TOCSY was recorded with mixing times of 48, 64, 70, 80 and 100 ms; each increment was the sum of 32 scans with a relaxation delay of 2.0 s; 2048 data point were collected per experiment.

4. GENERAL PROCEDURES

4.1 General procedure A: Activation and coupling of the first amino acid to 2-chlorotitryl resin.

2-Chlorotrityl-chloride resin (600 mg, 0.174 mmol/g) was added to a 50 mL centrifuge tube. Dry DCM (10 mL) and 2mL of thionyl chloride were added to the tube. The mixture was shaken overnight then filtered using suction and washed with dry DCM (5 × 4 mL). To avoid deactivation of the water-sensitive resin, DCM (10 mL), 1 mL of DIPEA (1.0 M, 2.0 mL) and the first amino acid (0.987g, 0.2 M) were immediately added to the dry resin in a sintered-glass reaction vessel. This mixture was reacted for 2 hours and then dried using suction. Finally, the resin was washed with DCM (3 x 5 mL).

4.2 General procedure B: Analysis of the substitution of the first amino acid

The resin, with the first amino acid bonded, was weighed out in duplicate samples of 5 to 10 mg in Eppendorf tubes then 20% piperidine in DMF (1.0 mL) was added to the resin to deprotect the amino acid. The resin and was shaken for 20 minutes then centrifuged down. From the centrifuged sample, 100 µL of the supernatant was transferred into a tube with DMF (10.0 mL). The mixture was thoroughly mixed, and the solution (2.0 mL) was pipetted into one cuvette cell and DMF (2.0 mL) was added into another cuvette cell. The cuvette containing DMF was used to zero the spectrophotometer. The sample was checked for absorbance at 301 nm three times and used to calculate the substitution using the following equation:

$$Loading\ capacity\left(\frac{mmol}{g}\right) of\ resin = \frac{(101 \times Average\ Absorbance)}{(7.8 \times mg\ of\ resin\ beads)}$$

The substitution of fmoc-amino acid loaded was then used to calculate the loading capacity and the theoretical yield:

Theoretical yield = sub (mmol/g) × mass of resin (g) × Mr of peptide (g/mol)

4.3 General procedure C: Synthesis of peptides

After the attachment of the first amino acid to the resin, 20% piperidine in DMF (10 mL) was added to the resin and bubbled with nitrogen gas for 5 minutes to deprotect the amino acid. This step was performed twice for the same duration and piperidine was drained off using vacuum. The resin was washed first with DCM (3 x 5 mL) followed by DMF (3 × 5 mL). The resin was then mixed with DIPEA (1.26 mL, 0.6 M), HBTU (0.519 g, 0.11 M) and the second amino acid (0.429 g, 0.12 M). This mixture was reacted for 45 minutes and then dried using suction. The resin was washed with DMF (3 × 5 mL) and treated with 20% piperidine in DMF (20.0 mL) twice for 5 minutes and then the resin was then washed again with DCM (3 x 5 mL) and DMF (3 × 5 mL). The resin was then mixed with DIPEA (0.6 M, 1.26 mL), HBTU (0.519 g, 0.11 M) and the next amino acid (0.429 g, 0.12 M). This mixture was reacted for 45 minutes and dried using suction after which the resin was washed with DMF (3 × 5 mL). This method was repeated until the full peptide was synthesized.

4.4 General procedure D: Synthesis of peptides containing adamantane and palmitic acid on the N-terminal.

The resin attached to the first amino acid was treated with 20% piperidine in DMF (20.0 mL) twice for 5 minutes to deprotect the amino acid. The resin was then washed with DCM (3 x 15.0 mL) and DMF (3 × 15.0 mL) and mixed with DIPEA (1.0 M, 20.0 mL), HBTU (0.863 g) and the second amino acid (2.0 M). This mixture was reacted for 45 minutes and dried using suction. The resin was washed with DMF (3 × 15.0 mL) and treated with 20% piperidine in DMF (20.0 mL) twice for 5 minutes to deprotect the amino acid and again washed with DCM (3 x 15.0 mL) and DMF (6 × 15.0 mL). The resin was then mixed with DIPEA (1.0 M, 20 mL), HBTU (0.863 g) and the next amino acid (2.0 M). This mixture was reacted for 45 minutes and dried using suction. The resin was washed with DMF (3 × 15.0 mL). This method was repeated until all the amino acids in the peptide were coupled. The resin was treated with 20% piperidine in DMF (20.0 mL) twice for 5 minutes to deprotect the amino acid and washed again with DCM (3 x 15.0 mL) and DMF (3 × 15.0 mL) and dried using suction.

Adamantane carboxylic acid (2 M, 443 mg), DIPEA (1.0 M, 20.0 mL) and HBTU (0.863 g) were then added to the resin attached to the full peptide. This mixture was reacted for 45 minutes, and the resin was washed in DMF (3 × 15.0 mL) and finally dried using suction.

The analogues with palmitic acid on the N-terminal were synthesized by adding palmitic acid (2.0 M, 615 mg) and DIPEA (1.0 M, 20.0 mL) and HBTU (0.863 g) to the resin attached to the full peptide. This mixture was reacted for 45 minutes then the resin was washed in DMF (3 × 15.0 mL) and finally dried using suction.

4.5 General procedure E: Cleavage of the peptides from the resin

The resin attached to the peptide was then washed with DCM (3 x 5.0 mL) then DMF (3 x 5.0 mL) and dried under suction. A cleavage mixture was prepared by mixing 95:2.5:2.5 % (v/v) TFA: H_2O: TIS in a 50 mL centrifuge tube. The dry resin was then transferred into the 50 mL centrifuge tube containing 20 mL of the cleavage mixture and was placed in a shaker for 3 hours. The resin was filtered and washed with 5 mL of the cleavage mixture. The filtrate was divided into two portions. This step was followed by the addition of 60 mL of cold diethyl ether (which caused the peptide to precipitate). The resulting mixture was centrifuged at 5000 rpm for 10 minutes, after which the supernatant was decanted off. The remaining white solid was washed twice more with the same amount of cold diethyl ether. The white precipitate was then dissolved in 10 mL (40/60; H_2O/DMSO) for further analysis and purification.

4.6 General procedure F: Purification of the peptides

Semi-preparative HPLC was carried out on an Agilent 1260 Infinity instrument equipped with a UV/VIS detector and an automated fraction collector. Purification was achieved via the reverse phase chromatography. A Phonomenex Kinetex® XB-C18 column (5 µm B-C18, 100 Å, 250 mm × 230 nm x 21.2 mm) was used to separate the compounds with a flow rate of 15 mL/minute. For the mobile phase, a two-buffer system consisting of 0.1 % formic acid/H_2O (v/v) (Buffer A) and 0.1 % formic acid/acetonitrile (v/v) (Buffer B) was utilized. A flow rate of 15 mL/minute and UV wavelengths of 215 and 254 nm were utilized.

The formic acid was used as an ion pairing agent. The peptide derivatives were eluted using a gradient method of 5 – 95 % Buffer B in 14 minutes, unless stated otherwise. Detection of the peptides also was performed at wavelengths 215 and 254 nm.

5. SUMMARY OF SYNTHESIZED COMPOUNDS

5.1 DGRGOF-Palmitate

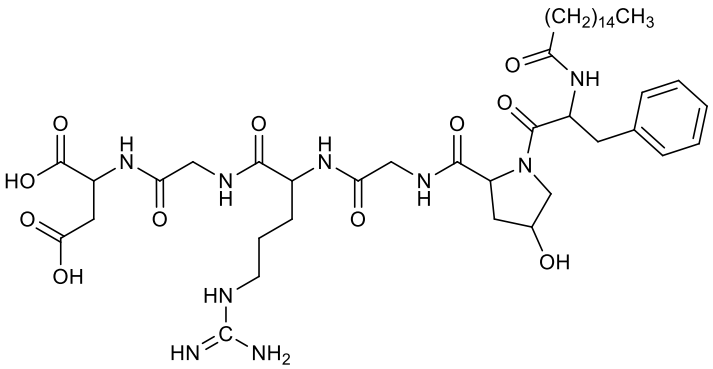

Figure 1: DGRGOF-Palmitate peptide.

UHPLC (Thermo Scientific Dionex Ultimate 3000) Peak 9.61 minutes

HRMS (ESI) (Bruker Compact Q-TOF): Calculated for $C_{44}H_{71}N_9O_{11}$ = 901.5273; found 902.5413 ($[M + H]^+$).

Fragments: 1353.8036, 451.7738, 259.1239.

5.2 DGRGOF-Adamantate

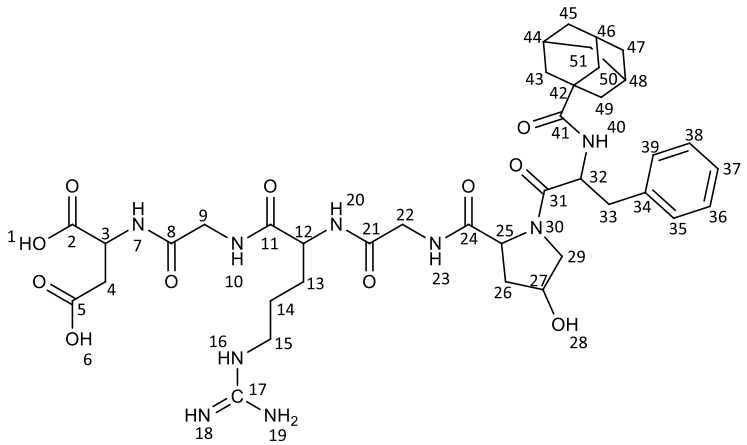

Figure 2: DGRGOF-Adamantate peptide.

UHPLC (Thermo Scientific Dionex Ultimate 3000) Peak 5.79 minutes

HRMS (ESI) (Bruker Compact Q-TOF): Calculated for $C_{39}H_{55}N_9O_{11}$ = 825.4021; found 826.4111 ($[M + H]^+$).

Fragments: 1239.6091, 413.7092.

^{1}H NMR (400 MHz, DMSO) δ_H = 8.97 (1H, *b s*, guanidyl), 8.53 (1H, *s*, NH amide), 8.30 (1H, *s*, NH amide), 8.18 (1H, *s*, NH amide), 7.92 (2H, *d*, NH amide, *J* = 6 Hz), 7.28 (1H, *d*, guanidyl, *J* = 3 Hz), 7.24 (5H, *s*, benzene *o, m, p* H), 7.17 – 7.19 (2H, *m*, guanidyl NH_2), 4.67 – 4.69 (1H, *m*, H^{α} Asp), 4.38 – 4.40 (1H, *m*, H^{α}), 4.34 – 4.36 (1H, *m*, H^{α}), 4.29 – 4.31 (1H, *m*, H^{α}), 4.19 – 4.21 (1H, *m*, H^{α}), 3.89 – 3.91 (1H, m, H^{α}), 3.74 (2H, H^{α}, *d*, *J* = 3 Hz), 3.60 - 3.62 (3H, *m*, H), 3.52 – 3.53 (4H, *m*, H), 3.11 – 3.12 (1H, *m*, H), 2.97 – 2.99 (3H, *m*, H), 2.85 – 2.87 (2H, *m*, H), 2.39 – 2.41 (2H, *m*, H), 2.01 – 2.03 (2H, *m*, H), 1.90 (2H, *s*, H), 1.31 – 1.62 (15H, *m*, adamantane)

^{13}C NMR (400 MHz, DMSO) δ_C = 176.20 (C = O), 173.40 (C = O), 173.29 (C = O), 171.83 (C = O), 171.63 (C = O), 170.21 (C = O), 168.69 (C = O), 163.44 (C = O), 157.01 (C = N, guanidyl), 137.63 (ArC), 129.54 (ArC), 127.88 (ArC), 126.20 (ArC), 68.81 (HO-*C*-H), 58.93 (C^{α}), 54.85 (C^{α}), 52.09 (C^{α}), 51.61 (C^{α}), 48.90 (C^{α}), 42.00 (C^{α}), 40.57 (C^{α}), 39.50 (C^{β}), 38.45 (C^{β}), 37.48 (C^{β}), 36.32 (C^{β}), 36.02 (C^{β}), 29.79 (C^{γ}), 27.57 (C^{γ}), 24.59 (C^{γ})

5.3 GOP-GFOGER-GOP-Palmitate

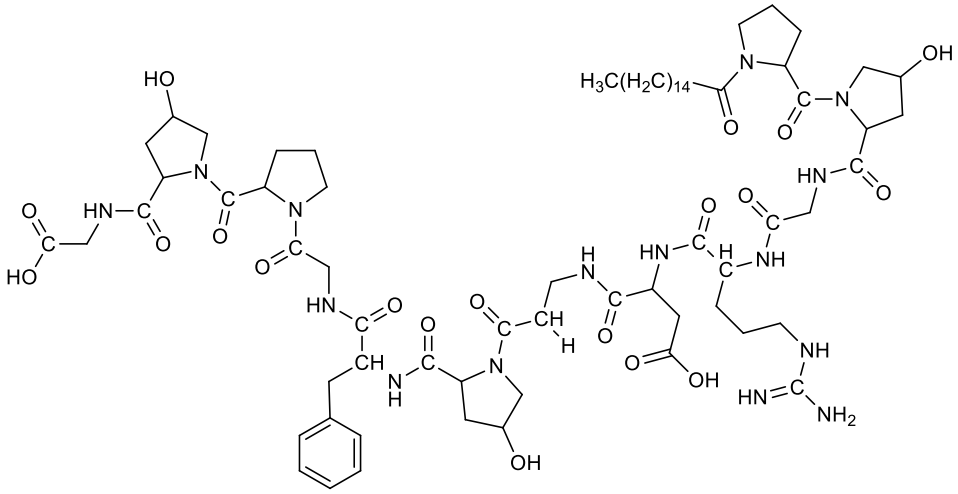

Figure 3: GOP-GFOGER-GOP-Palmitate.

UHPLC (Thermo Scientific Dionex Ultimate 3000) Peak 8.20 minutes

HRMS (ESI) (Bruker Compact Q-TOF): Calculated for $C_{69}H_{107}N_{15}O_{19}$ = 1449.7868; found 1451.7978 ($[M + H]^+$).

Fragments: 1451.7960, 725.9020, 484.2700.

5.4 GG-GFOGER-GG-Palmitate

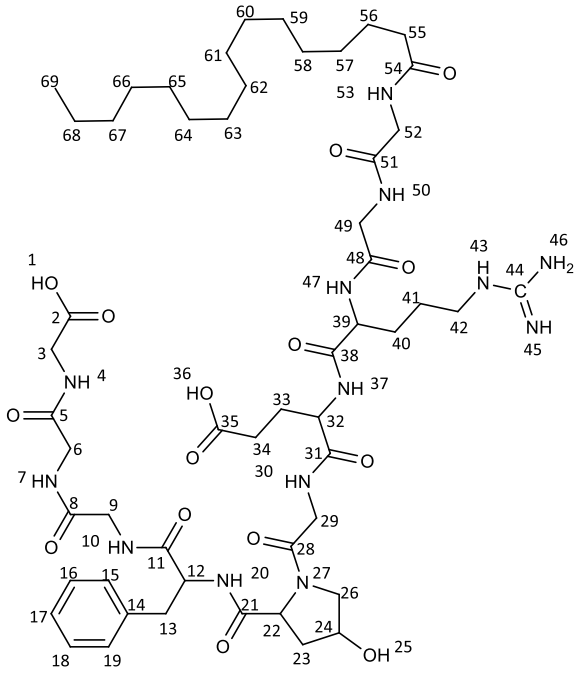

Figure 4: GG-GFOGER-GG-Palmitate.

UHPLC (Thermo Scientific Dionex Ultimate 3000) Peak 8.29 minutes

HRMS (ESI) (Bruker Compact Q-TOF): Calculated for $C_{53}H_{85}N_{13}O_{15}$ = 1143.6288; found 1144.6346 ($[M + H]^+$).

Fragment: 572.8217

5.5 DGD-GG-GFOGER-GG-Palmitate

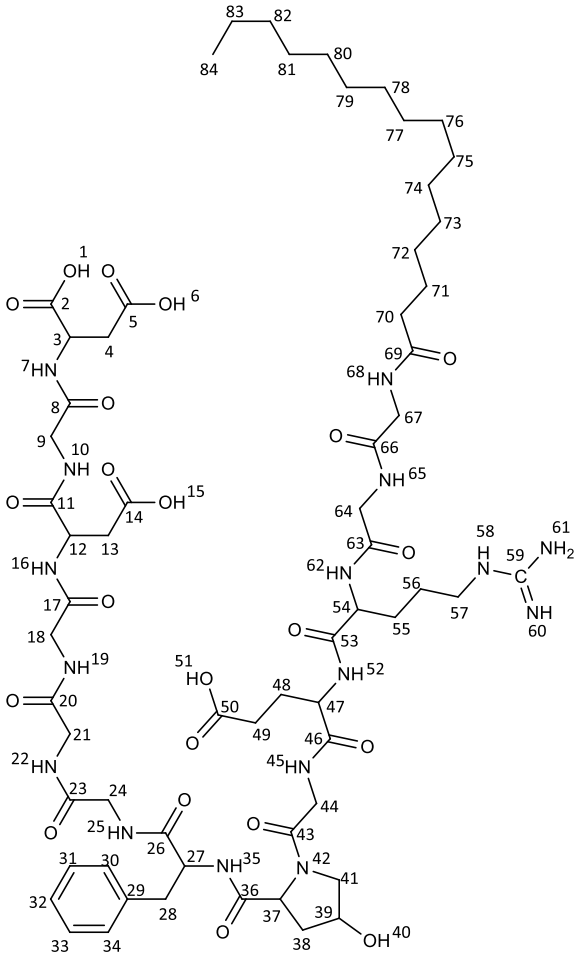

Figure 5: DGD-GG-GFOGER-GG-Palmitate.

UHPLC (Thermo Scientific Dionex Ultimate 3000) Peak 8.33 minutes

HRMS (ESI) (Bruker Compact Q-TOF): Calculated for $C_{63}H_{98}N_{16}O_{22}$ = 1430.7042; found 1431.7201 ($[M + H]^+$).

Fragment: 716.3623.

5.6 DGD-GG-GFOGER-GG-TTK-Palmitate

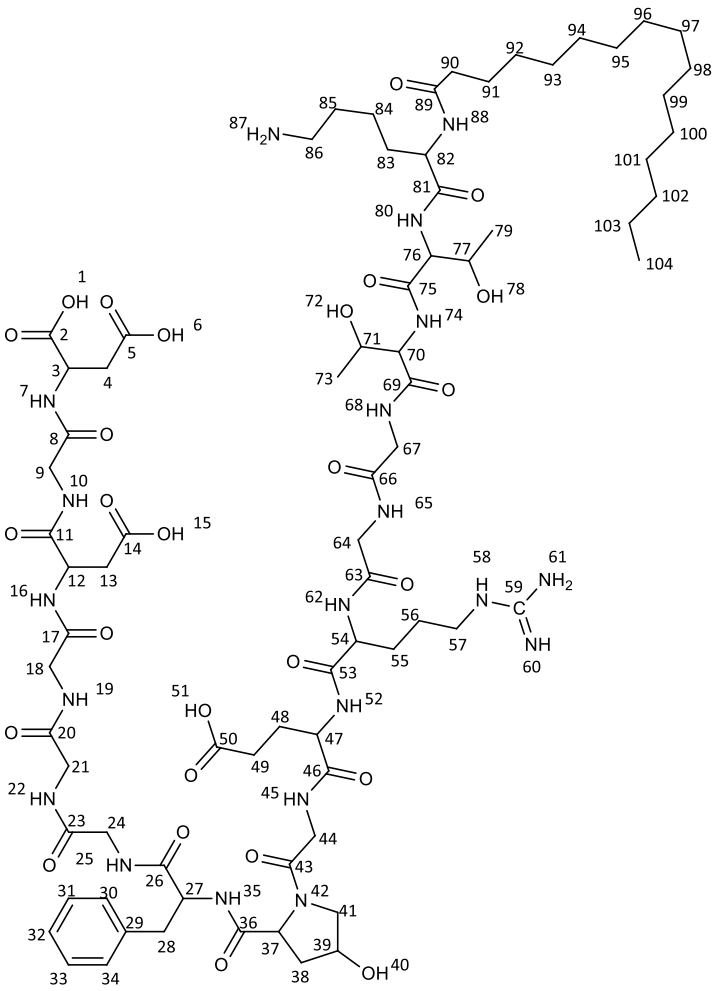

Figure 6: DGD-GG-GFOGER-GG-TTK-Palmitate.

UHPLC (Thermo Scientific Dionex Ultimate 3000) Peak 6.42 minutes

HRMS (ESI) (Bruker Compact Q-TOF): Calculated for $C_{77}H_{124}N_{20}O_{27}$ = 1760.9421; found 881.4604 ([M + 2H]$^{2+}$).

Fragments: 1175.6126, 587.9751

^{1}H NMR (400 MHz, DMSO) δ_H = 8.66 (1H, *m*, NH amide), 8.35 (1H, *m*, NH amide), 8.27 (1H, *m*, NH amide), 8.18 (1H, *m*, NH amide), 8.16 (1H, *m*, NH amide), 8.17 (1H, *m*, NH amide), 7.79 (1H, *m*, NH amide), 7.73 (1H, *m*, NH amide), 8.02 (1H, *m*, NH amide), 7.79 (1H, *m*, NH amide), 7.82 (1H, *m*, NH amide), 8.22 (1H, *m*, NH amide), 8.22 (1H, *m*, NH amide), 7.98 (1H, *m*, NH amide), 7.14 (1H, *m*, ArH), 7.27 (1H, *m*, ArH), 7.17 (1H, *m*, ArH), 7.27 (1H, *m*, ArH), 7.14 (1H, *m*, ArH), 4.63 (1H, *m*, H$^{\alpha}$ Asp), 4.33 (1H, *m*, H$^{\alpha}$ Gly), 4.55 (1H, *m*, H$^{\alpha}$ Asp), 3.73 (1H, *m*, H$^{\alpha}$ Gly), 3.70 (1H, *m*, H$^{\alpha}$ Gly), 4.58 (1H, *m*, H$^{\alpha}$ Gly),

4.74 (1H, *m*, H^{α} Phe), 4.36 (1H, *m*, H^{α} Hyp), 4.16 (1H, *m*, H^{α} Gly), 4.25 (1H, m, H^{α} Glu), 4.36 (1H, m, H^{α} Arg), 4.17 (1H, *m*, H^{α} Gly), 3.59 (1H, *m*, H^{α} Gly), 3.75 (2H, *m*, H^{α} Thr), 4.29 (1H, m, H^{α} Lys), 2.83 (1H, m, H^{β} Asp), 2.56 (1H, *m*, H^{β} Glu), 2.85 (1H, *m*, H^{β} Phe), 1.90 (1H, *m*, H^{β} Hyp), 4.23 (1H, m, H^{γ} Hyp), 3.65 (1H, m, H^{γ} Hyp), 2.56, 2.37 (2H, m, H^{β} Glu), 3.05 (1H, m, H^{γ} Hyp), 1.89, 1.97 (1H, *m*, H^{β} Arg), 1.51, 1.62 (1H, *m*, H^{γ} Arg), 3.00, 3.13 (1H, *m*, H^{δ} Arg), 8.97 (1H, m, NH guanidyl), 8.56 (), 4.08 (1H, *m*, H^{β} Thr), 5.41 (1H, m, OH), 1.08 (1H, *m*, H^{β} Thr), 4.08 (1H, *m*, H^{β} Thr), 5.41 (1H, m, OH), 1.08 (1H, *m*, H^{β} Thr), 1.88 (1H, *m*, H^{β} Lys), 1.57 (1H, *m*, H^{γ} Lys), 1.73 (1H, *m*, H^{δ} Lys), 2.27 (1H, *m*, H^{ϵ}Lys)

^{13}C NMR (400 MHz, DMSO) δ_C = 172.65 (C = O), 171.82 (C = O), 170.62 (C = O), 169.66 (C = O), 169.33 (C = O), 164.33 (C = O), 138.69 (C = NH), 129.60 (ArC), 128.50 (ArC), 129.50 (ArC), 73.06 (OH-C-H), 69.00 (C^{α}), 65.38 (C^{β} Hyp), 58.58 (C^{α}), 56.50 (C^{α}), 54.54 (C^{α}), 54.46 (C^{α}), 52.67 (C^{α}), 50.29 (C^{α}), 49.61 (C^{α}), 42.62 (C^{α}), 42.56 (C^{α}), 41.96 (C^{α}), 39.14 (C-Aliphatic), 35.61 (C-Aliphatic), 31.75 (C-Aliphatic), 31.15 (C-Aliphatic), 29.47 (C-Aliphatic), 29.43 (C-Aliphatic), 29.29 (C-Aliphatic), 29.16 (C-Aliphatic), 27.14 (C-Aliphatic), 25.77 (C-Aliphatic), 22.71 (C-Aliphatic), 22.56 (C-Aliphatic), 20.02 (C-Aliphatic), 19.01 (C-Aliphatic), 15.63 (C-Aliphatic), 14.42 (C-Aliphatic)

Table 4: Characterization table of DGD-GG-GFOGER-GG-TTK-Palmitate.

No.	δ ^{1}H	δ ^{13}C	δ COSY	δ HSQC	δ HMBC
1	11.0	-	-	-	-
2	-	-	-	-	177.47, 4.63
3	4.63	54.27	4.63, 8.66	4.63, 54.27	4.63, 42.51
4	2.83	42.44	2.83, 4.63	2.83, 42.44	2.83, 54.24
5	-	-	-	-	165.03, 2.83
6	11.0	-	-	-	-
7	8.66	-	8.66, 4.63	-	8.65, 165.02,
8	-				179.30, 4.33
9	4.33	54.91	4.33, 8.35	4.33, 54.91	4.32, 179.30
10	8.35		8.35, 4.33	-	8.35, 178.65
11	-				165.01, 4.55
12	4.55	54.35	4.55, 8.27	4.55, 54.35	4.55, 42.51
13	2.56	42.44	2.56, 4.55	2.56, 42.44	2.56, 54.35
14	-	-	-	-	164.43, 2.56-
15	11.0	-	-	-	-
16	8.27	-	8.27, 4.55	-	8.26, 171.26
17	-	-	-	-	169.89, 3.73-

No.	δ ^{1}H	δ ^{13}C	δ COSY	δ HSQC	δ HMBC
18	3.73	42.52	3.73, 8.36	3.72, 42.52	3.74, 54.54
19	8.18	-	8.18, 3.74	-	8.18, 169.43
20	-	-	-	-	169.71, 3.70-
21	3.70	52.92	3.70, 8.14	3.70, 52.92	3.69, 51.78
22	8.16	-	8.16, 3.70	-	8.16, 169.36
23	-	-	-	-	166.74, 4.58-
24	4.58	42.52	4.58, 8.14	4.58, 42.45	4.59, 43.57
25	8.17	-	8.15, 4.59	-	8.15, 177.49
26	-	-	-	-	180.27, 4.74-
27	4.74	52.13	4.74, 8.37	4.74, 52.13	4.73, 57.47
28	2.85	38.25	2.85, 4.74	2.85, 38.25	2.85, 179.66
29	-	138.19	-	-	138.19, 7.19
30	7.14	127.84	7.14, 7.27	7.14, 126.71	7.14, 129.66 36.92, 138.11
31	7.27	129.49	7.27, 7.17	7.27, 129.39	7.27,
32	7.17	126.15	7.17, 7.27	7.17, 128.86	7.17,
33	7.27	129.49	7.27, 7.17	7.27, 129.39	7.27,
34	7.14	127.84	7.14, 7.27	7.14, 126.71	7.14, 126.71 36,85, 138.11
35	8.14	-	8.14, 4.74	-	8.14, 171.16
36	-				166.92, 4.36
37	4.36	68.22	4.36, 1.88	4.36, 68.22	4.36, 58.39
38	1.90	37.82	1.90, 4.22	1.90, 37.82	2.04, 172.81
39	4.23	69.02	4.22, 1.90	4.23, 69.02	4.23, 37.51
40	3.64	-	-	-	
41	3.65	54.71	3.60, 4.38	3.65, 54.71	3.68, 169.16
42	No N**H**-	-	-	-	
43	-				172.53, 4.16
44	4.16	43.78	4.17, 7.80	4.17, 42.38	4.17, 170.73
45	7.79	-	7.79, 4.17	-	7.79, 171.94
46					171.59, 4.25
47	4.25	49.32	4.25, 7.86	4.25, 49.32	4.24, 57.72
48	2.56, 2.37	37.92	2.56, 4.25	2.56, 37.92	2.56, 39.53
49	3.05, 2.02	40.68	3.05, 2.56	3.05, 40.68	2.04, 172.81
50	-	-	-	-	177.92, 3.05-

No.	δ ^{1}H	δ ^{13}C	δ COSY	δ HSQC	δ HMBC
51	11.0	-	-	-	
52	7.73	-	7.73, 4.33	-	7.73, 168.00
53	-	-	-	-	177.53, 4.36-
54	4.36	52.56	4.36, 8.02	4.36, 52.56	4.36, 177.53
55	1.89, 1.97	28.03	1.89, 4.31, 1.62, 4.31	1.89, 52.68	1.92, 169.12
56	1.51, 1.62	59.42	1.51, 1.89	1.51, 59.42	1.51, 28.03
57	3.00, 3.13	55.35	3.02, 1.51	3.02, 55.35	3.02, 59.42
58	8.97	-	8.97, 3.02	-	8.97, 55.35
59	8.56		-		
60		157.01	-	8.53, 172.18	
61	8.56		-		
62	8.02		8.02, 4.36		8.02,
63					172.28, 4.17
64	4.17	43.78	4.17, 7.79	4.17, 43.78-	4.17, 172.28
65	7.79		7.79, 3.59	-	7.79,
66					172.94, 3.59
67	3.59	55.28	3.58, 7.82	3.59, 55.28	3.56, 50.22
68	7.82	-	7.82, 3.57	-	7.82,
69					169.86, 3.75
70	3.75	44.94	3.74, 8.22	3.75, 44.94	3.75, 169.86
71	4.08	66.91	4.05, 1.08	4.05, 66.91	4.08, 44.94
72	4.32				4.32, 66.57
73	1.08	19.90	1.08, 4.08	1.08, 19.90-	1.08, 66.91
74	8.22	-	8.22, 3.73		8.18, 169.43
75					169.86, 3.75
76	3.75	44.94	3.74, 8.22	3.75, 44.94	3.75, 169.86
77	4.08	66.91	4.05, 1.08	4.05, 66.91	4.08, 44.94
78	4.32				4.32, 66.57
79	1.08	19.90	1.08, 4.08	1.08, 19.90-	1.08, 66.91
80	8.22	-	8.22, 3.73		8.18, 169.43
81					172.94, 4.29
82	4.29	52.62-	4.29, 7.98	4.29, 52.62	4.28, 50.45
83	7.98		7.98, 4.29		7.98,172.94

No.	δ ^{1}H	δ ^{13}C	δ COSY	δ HSQC	δ HMBC
84	1.88	37.91	1.88, 4.29	1.88, 37.91	1.88, 37.23
85	1.57	37.65	1.57, 1.88	1.57, 37.65	1.57, 36.64
86	1.73	29.14	1.73, 1.57	1.73, 29.14	1.73, 40.50
87	2.27	31.08	2.27, 1.73	2.27, 31.08	2.27, 25.33
88	-	-	-	-	-
89					172.31, 2.05
90	2.05	40.53	2.06, 1.53	2.05, 40.53	2.05, 27.50
91	1.53	27.01	1.53, 1.32	1.53, 27.01	1.53, 41.59
92	1.29	25.03	1.29, 1.24	1.29, 25.03	1.31, 28.00
93	1.23	29.35	1.23, 1.23	1.23, 29.35	1.23, 26.87
94	1.23	29.35	1.23, 1.23	1.23, 29.35	1.23, 26.87
95	1.23	29.35	1.23, 1.23	1.23, 29.35	1.23, 26.87
96	1.23	29.35	1.23, 1.23	1.23, 29.35	1.23, 26.87
97	1.23	29.35	1.23, 1.23	1.23, 29.35	1.23, 26.87
98	1.23	29.35	1.23, 1.23	1.23, 29.35	1.23, 26.87
99	1.23	29.35	1.23, 1.23	1.23, 29.35	1.23, 26.87
100	1.23	29.35	1.23, 1.23	1.23, 29.35	1.23, 26.87
101	1.23	29.35	1.23, 1.23	1.23, 29.35	1.23, 26.87
102	1.09	15.57	1.09, 1.11	1.09, 15.5	1.09, 20.05
103	1.05	19.93	1.05, 0.88	1.05, 19.93	1.05, 29.25
104	0.88	14.31	0.88, 1.05	0.88, 14.31	0.88, 19.93

Table 5: Dipeptides couplings observed from the ROESY spectrum.

TOCSY Spin System		ROESY		Dipeptide
H^{α}	H^{β}, H^{γ}, H^{δ} ,H^{ϵ}	$H^{\alpha}1$, $H^{\alpha}2$	H^{β}, H^{γ}, H^{δ}, H^{ϵ}	
4.63	3.10, 2.80	4.63, 4.33	3.10, 2.80	Asp-Gly
4.33	-	4.33, 4.63	3.10, 2.80	Gly-Asp
4.63	3.10, 2.80	4.63, 3.73	-	Asp-Gly
3.73	-	3.73, 3.70	-	Gly-Gly
3.70	-	3.70, 4.59	-	Gly-Gly
4.59	-	4.59, 4.74	2.86, 3.13, 7.12, 7.26, 7.19	Gly-Phe
4.74	2.86, 3.13, 7.12, 7.26, 7.19	4.74, 4.36	2.86, 3.13, 7.12, 7.26, 7.19, 1.90, 4.23, 3.61	Phe-Hyp
4.36	1.92, 4.23, 3.61	4.36, 4.16	1.92, 4.39, 3.61	Hyp-Gly
4.16	-	4.16, 4.25	2.56, 2.44	Gly-Glu
4.25	2.56, 2.44	4.25, 4.36	2.56, 2.44, 3.00, 1.51, 1.91,	Glu-Arg
4.36	3.00, 1.51, 1.91	4.36, 3.59	3.00, 1.51, 1.91	Arg-Gly
3.59	-	3.59, 3.57	-	Gly-Gly
3.57	-	3.57, 3.73	4.05, 0.94	Gly-Thr
3.73	4.05, 3.58, 0.94	3.73, 3.73	4.05, 0.94	Thr-Thr
3.73	4.05, 3.58, 0.94	3.73, 4.29	4.05, 0.94, 1.92, 1.51, 1.33, 2.76	Thr-Lys
4.29	1.92, 1.51, 1.33, 2.76	4.29	1.92, 1.51, 1.33, 2.76	

5.7 DGD-GG-GFOGER-GG-GHK-Palmitate

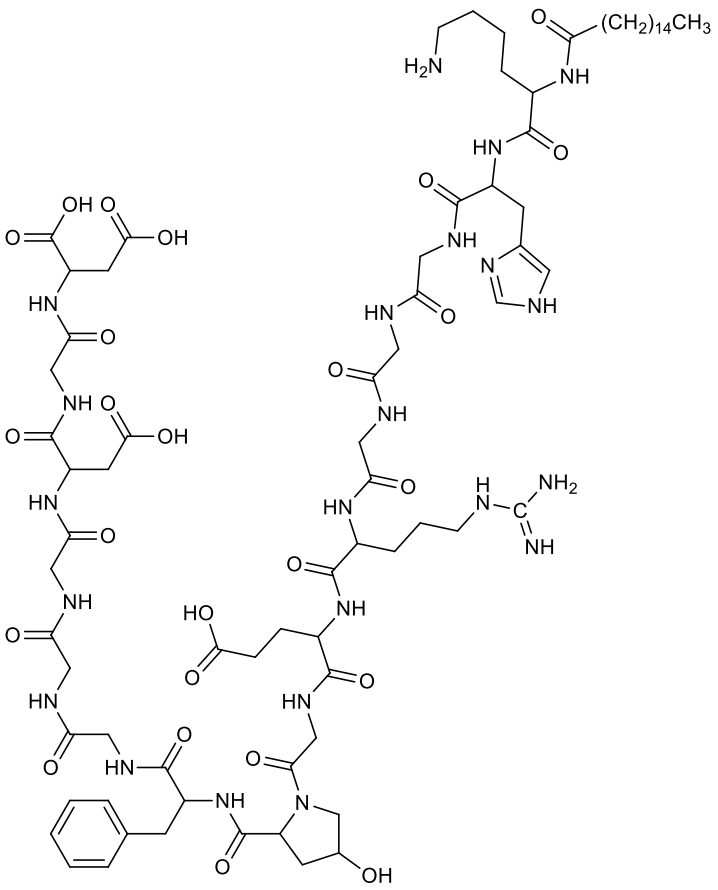

Figure 7: DGD-GG-GFOGER-GG-GHK-Palmitate.

UHPLC (Thermo Scientific Dionex Ultimate 3000) Peak 6.00 minutes

HRMS (ESI) (Bruker Compact Q-TOF): Calculated for $C_{77}H_{120}N_{22}O_{25}$ = 1752.8795; found 877.4499 ([M + H]$^{2+}$).

Fragments: 1170.2649, 877.4499, 585.3023

^{1}H NMR (400 MHz, DMSO) δH = 9.20 (1H, m, NH amide), 8.81 (1H, *m*, NH amide), 8.59 (1H, *m*, NH amide), 8.19 (1H, *m*, NH amide), 7.90 (1H, *m*, NH amide), 7.57 (1H, *m*, NH amide), 7.30 (1H, *m*, NH amide), 7.33 (1H, *m*, NH amide), 8.23 (1H, *m*, NH amide), 7.69 (2H, *m*, NH amide), 8.12 (1H, *m*, NH amide), 7.79 (1H, *m*, NH amide), 7.79 (1H, *m*, NH amide), 7.99 (1H, *m*, NH amide), 7.14 (2H, *m*, ArH), 7.27 (2H, *m*, ArH), 7.17 (1H, *m*, ArH), 4.63 (2H, *m*, Hα Asp), 4.41 (1H, *m*, Hα Gly), 3.80 (1H, *m*, Hα Gly), 3.77 (1H, *m*, Hα Gly), 4.54 (1H, *m*, Hα Gly), 4.66 (1H, *m*,

Hα Phe), 4.43 (1H, *m*, Hα Hyp), 4.27 (1H, *m*, Hα Gly), 4.33 (1H, *m*, Hα Glu), 4.31 (1H, *m*, Hα Arg), 4.06 (1H, *m,* Hα Gly), 4.24 (1H, *m*, Hα Gly), 3.82 (2H, *m*, Hα Gly), 4.90 (2H, *m*, Hα His), 4.35 (1H, m, Hα Lys), 2.81 (2H, m, Hβ Asp), 2.85 (1H, *m,* Hβ Phe), 1.90 (1H, *m*, Hβ Arg), 4.23 (1H, *m*, Hγ Hyp), 3.61 (1H, *m*, Hδ Hyp), 2.53 (1H, *m*, Hβ Glu), 3.05 (1H, m, Hγ Glu), 1.89 (1H, m, Hα Arg), 1.51 (1H, *m*, Hβ Arg), 3.00 (1H, *m*, Hγ Arg), 8.80 (1H, *m*, NH guanidyl), 3.20 (2H, *m*, Hβ His), 7.70 (1H, *m*, C-H, His), 8.67 m, (1H, *m*, C-H, His), 8.03 (1H, *m*, NH, His), 1.79 (2H, *m*, Hβ Lys), 1.29 (2H, *m*, Hγ Lys), 1.52 (2H, *m*, Hδ Lys), 2.71 (2H, *m*, Hε Lys), 5.14 (2H, *m*, NH_2 Lys)

^{13}C NMR (400 MHz, DMSO) δC = 174.78 (C = O), 172.72 (C = O), 172.67 (C = O), 172.05 (C = O), 171.80 (C = O), 170.99 (C = O), 170.51 (C = O), 169.35 (C = O), 169.19 (C = O), 168.41 (C = O), 163.90 (C = O), 129.61 (ArC), 128.50 (ArC), 69.02 (Cα), 66.99 (Cα), 65.38 (Cα), 56.50 (Cα), 52.80 (Cα), 52.45 (Cα), 42.53 (Cβ), 40.88 (Cβ), 39.18 (C - Aliphatic), 38.98 (C - Aliphatic), 36.56 (C - Aliphatic), 31.07 (C - Aliphatic), 30.80 (C - Aliphatic), 29.60 (C - Aliphatic), 28.10 (C - Aliphatic), 27.06 (C - Aliphatic), 22.83 (C - Aliphatic), 20.07 (C - Aliphatic), 19.80 (C - Aliphatic), 19.01 (C - Aliphatic), 15.63 (C - Aliphatic)

5.8 DGD-GG-GFOGER-GG-QPR-Palmitate

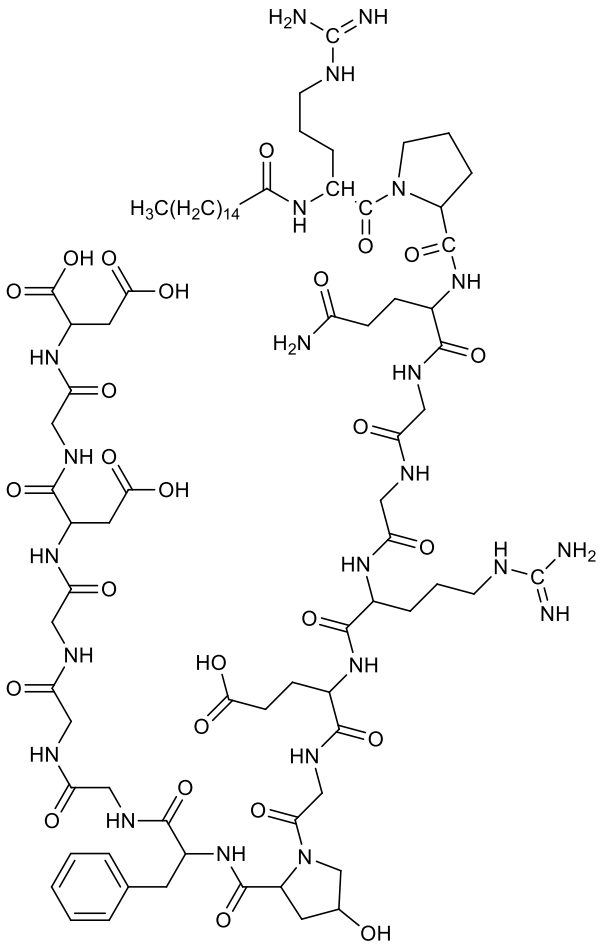

Figure 8: DGD-GG-GFOGER-GG-QPR-Palmitate.

UHPLC (Thermo Scientific Dionex Ultimate 3000) Peak 6.54 minutes

HRMS (ESI) (Bruker Compact Q-TOF): Calculated for $C_{79}H_{125}N_{23}O_{26}$ = 1811.9166; found 907.0723 ([M + $2H^+$]$^{2+}$).

Fragments: 1209.7567, 605.0558

5.9 DGD-GG-GFOGER-GG-EEM-Palmitate

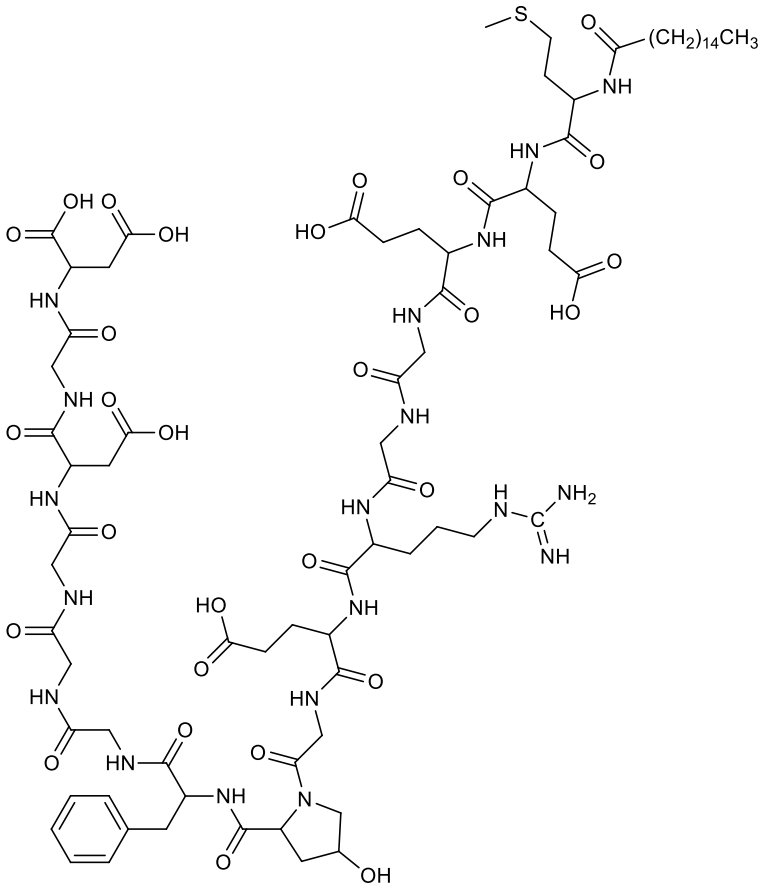

Figure 9: DGD-GG-GFOGER-GG-EEM-Palmitate.

UHPLC (Thermo Scientific Dionex Ultimate 3000) Peak 9.00 minutes

HRMS (ESI) (Bruker Compact Q-TOF): Calculated for $C_{78}H_{121}N_{19}O_{29}S$ = 1819.8298; found 1821.8628 ($[M + 2H^+]^{2+}$) .

Fragments: 1214.9191, 910.9372, 607.6287

6. MASS SPECTRA

6.1 DGRGOF-Palmitate

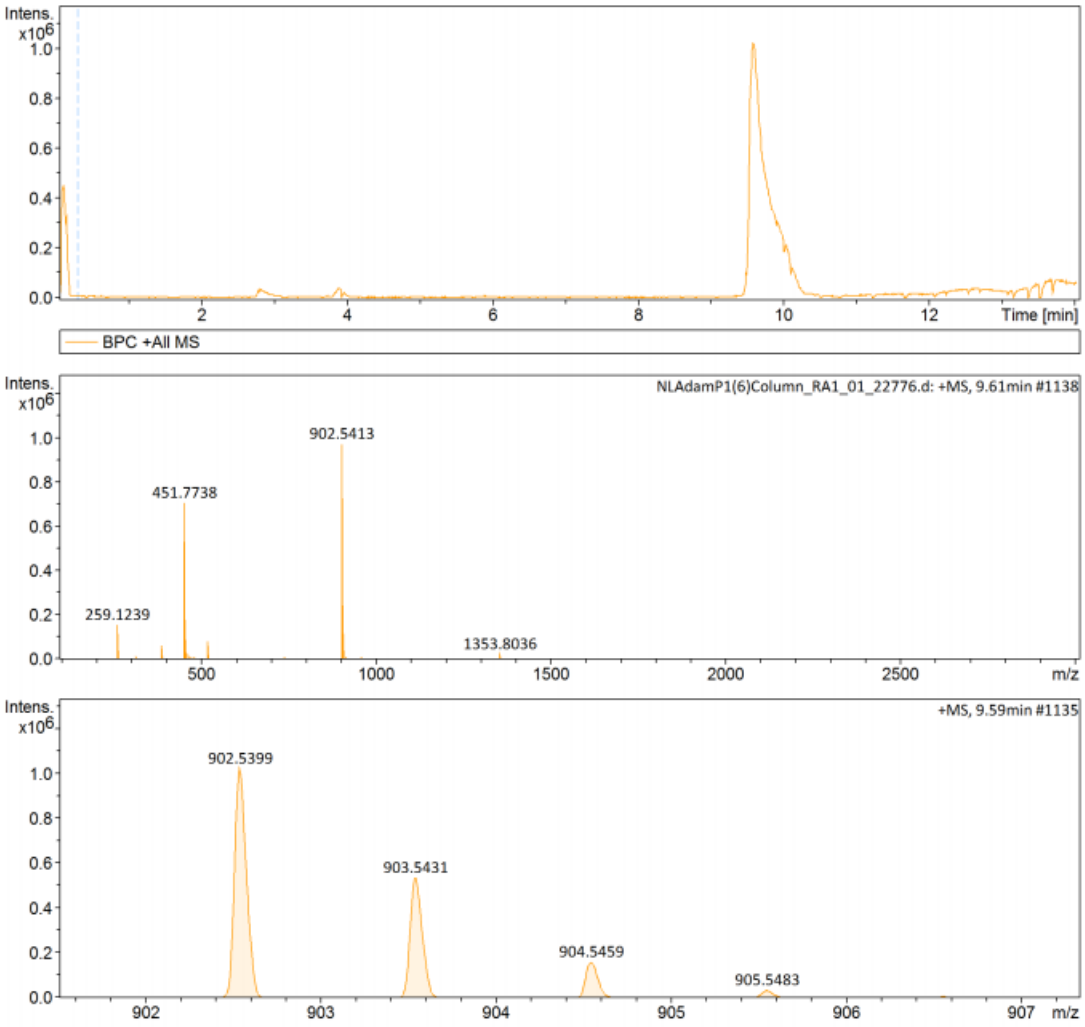

Figure 10: Mass Spectrum of DGRGOF-Palmitate.

6.2 DGRGOF-Adamantate

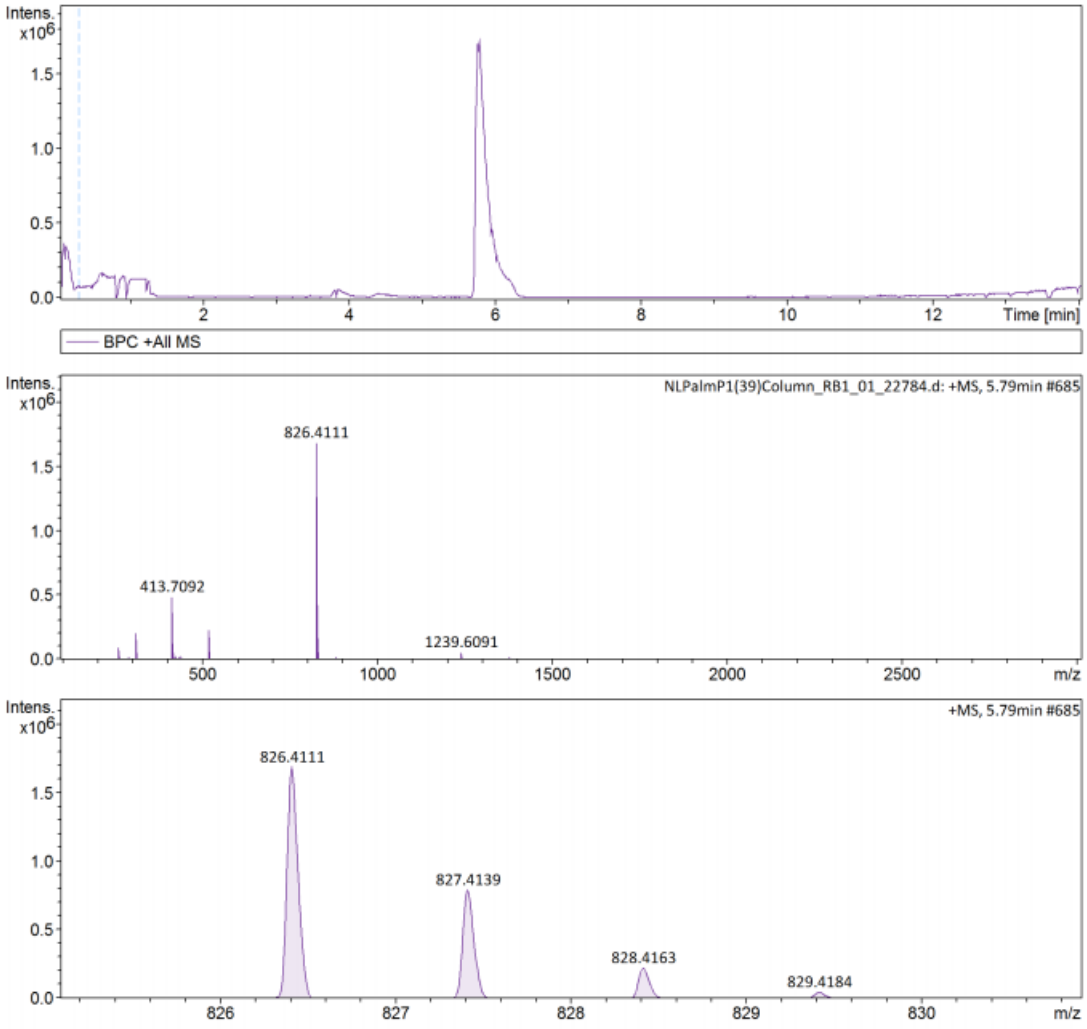

Figure 11: Mass Spectrum of DGRGOF-Adamantate**.**

6.3 GOP-GFOGER-GOP-Palmitate

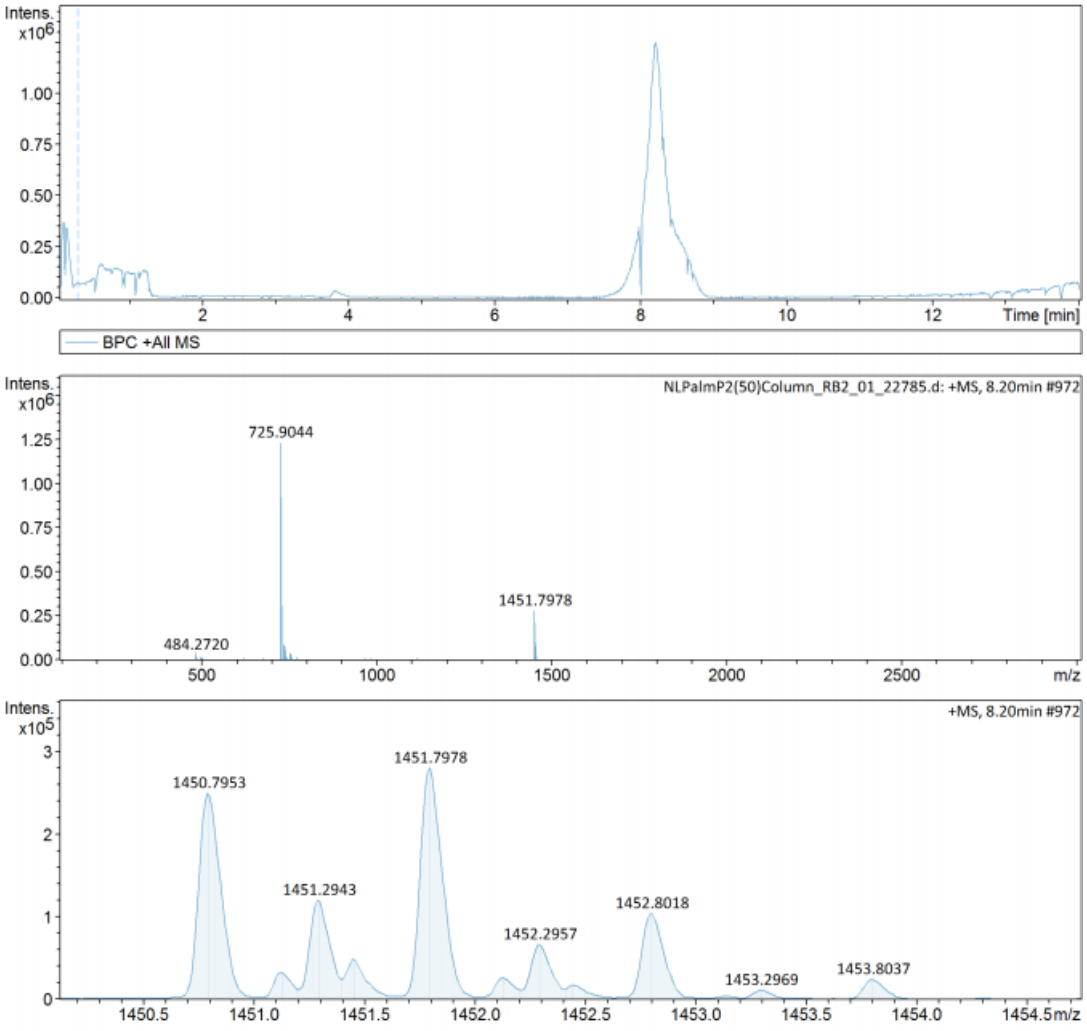

Figure 12: Mass Spectrum of GOP-GFOGER-GOP-Palmitate**.**

6.4 GG-GFOGER-GG-Palmitate

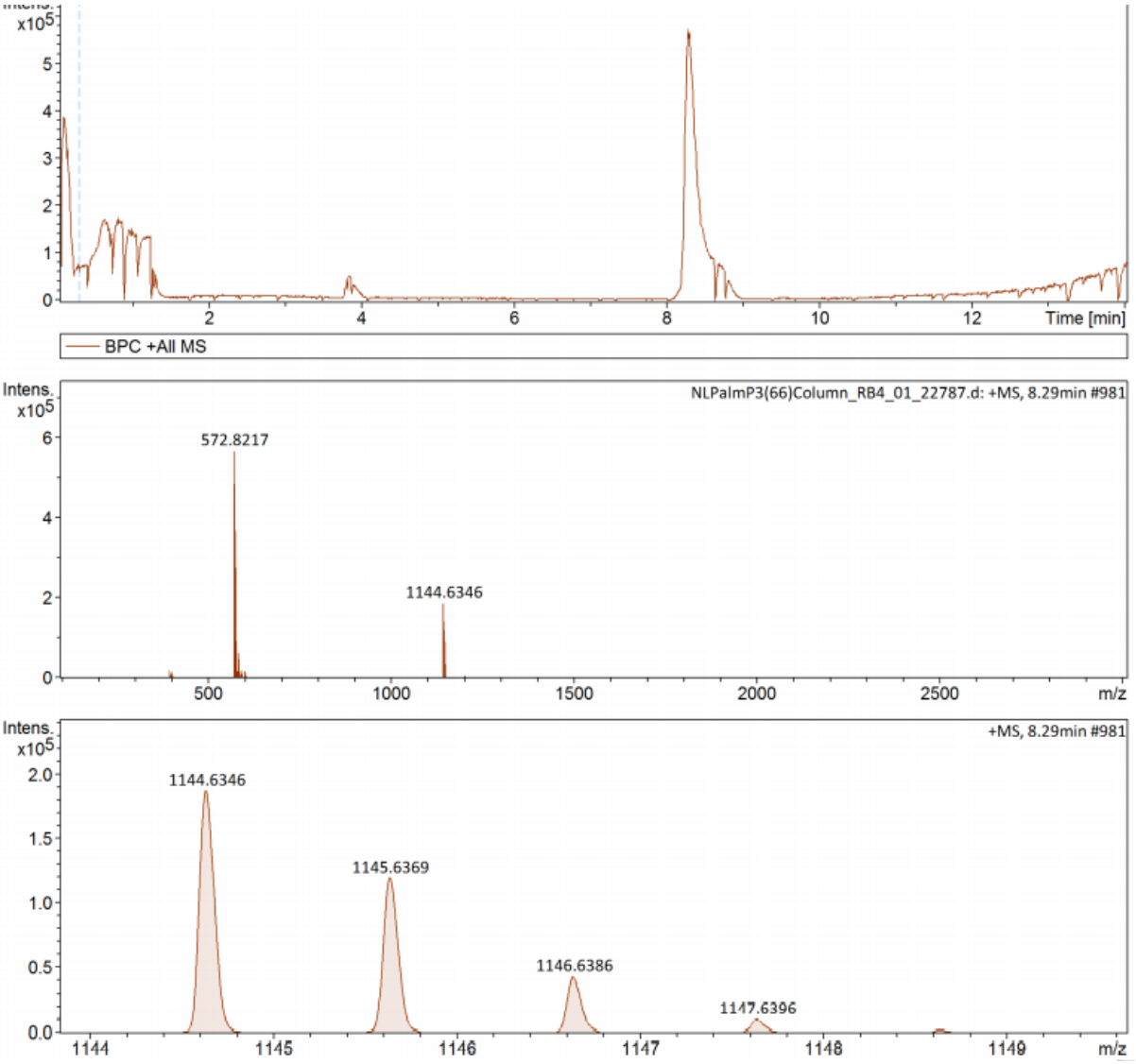

Figure 13: Mass Spectrum of GG-GFOGER-GG-Palmitate.

6.5 DGD-GG-GFOGER-GG-Palmitate

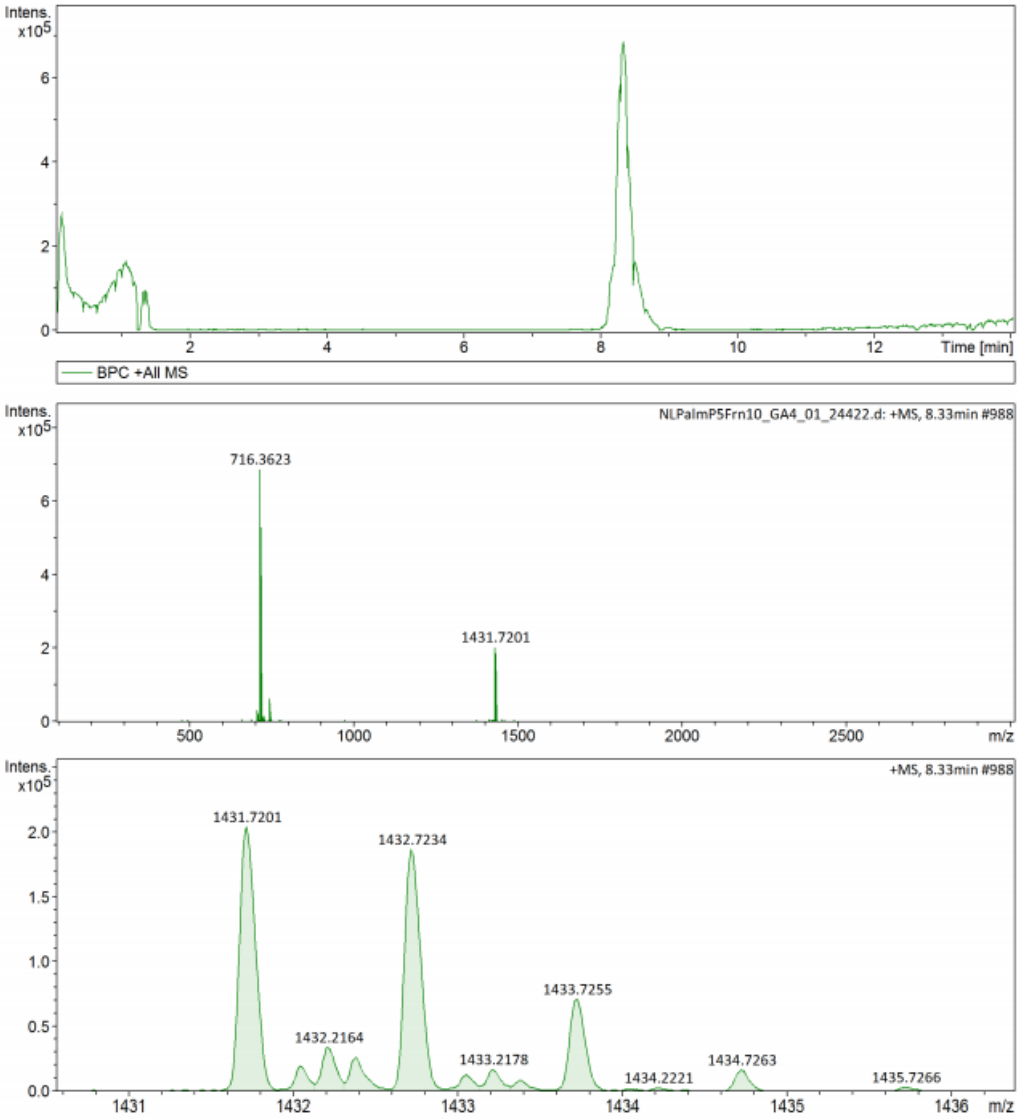

Figure 14: Mass Spectrum of DGD-GG-GFOGER-GG-Palmitate.

6.6 DGD-GG-GFOGER-GG-TTK-Palmitate

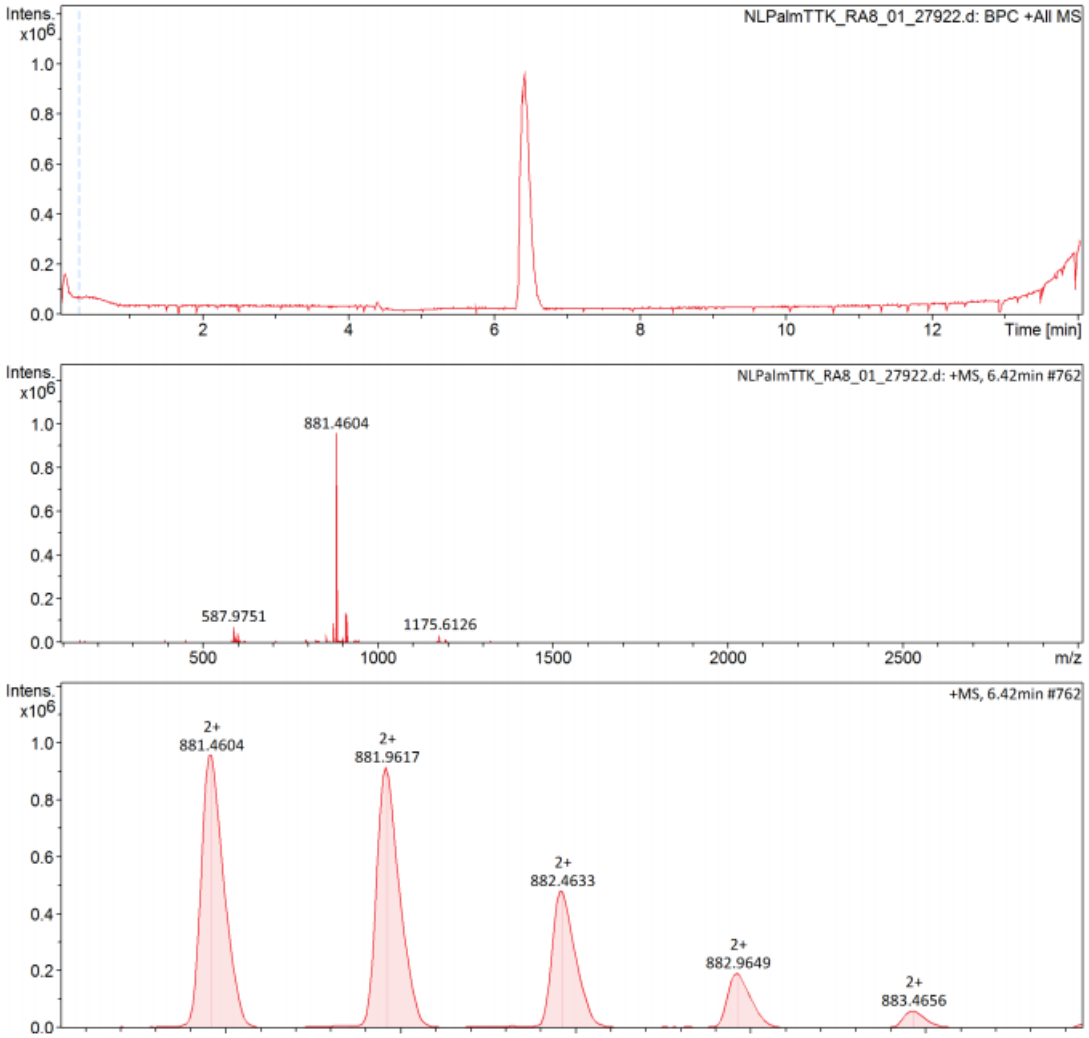

Figure 15: Mass Spectrum of DGD-GG-GFOGER-GG-TTK-Palmitate.

6.7 DGD-GG-GFOGER-GG-GHK-Palmitate

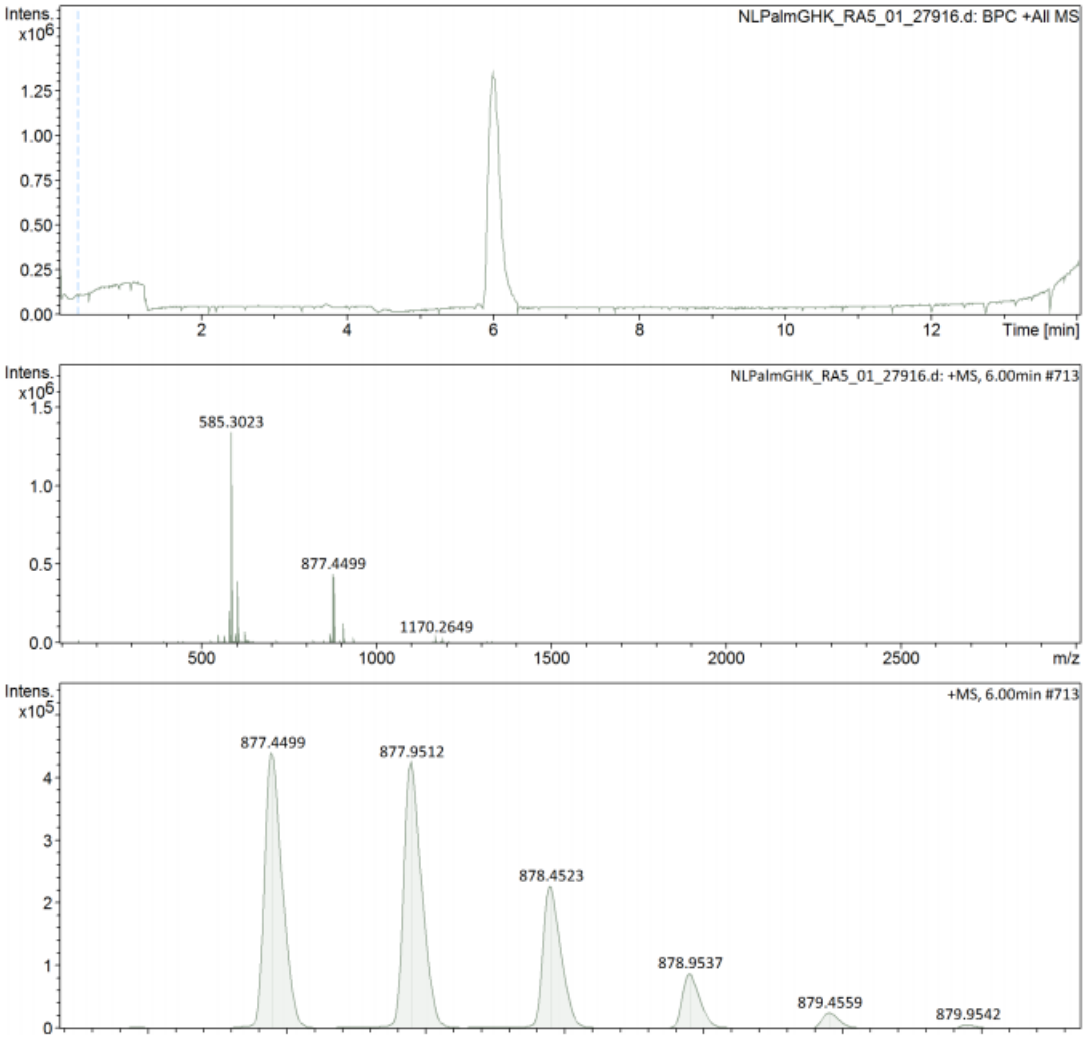

Figure 16: Mass Spectrum of DGD-GG-GFOGER-GG-GHK-Palmitate.

6.8 DGD-GG-GFOGER-GG-QPR-Palmitate

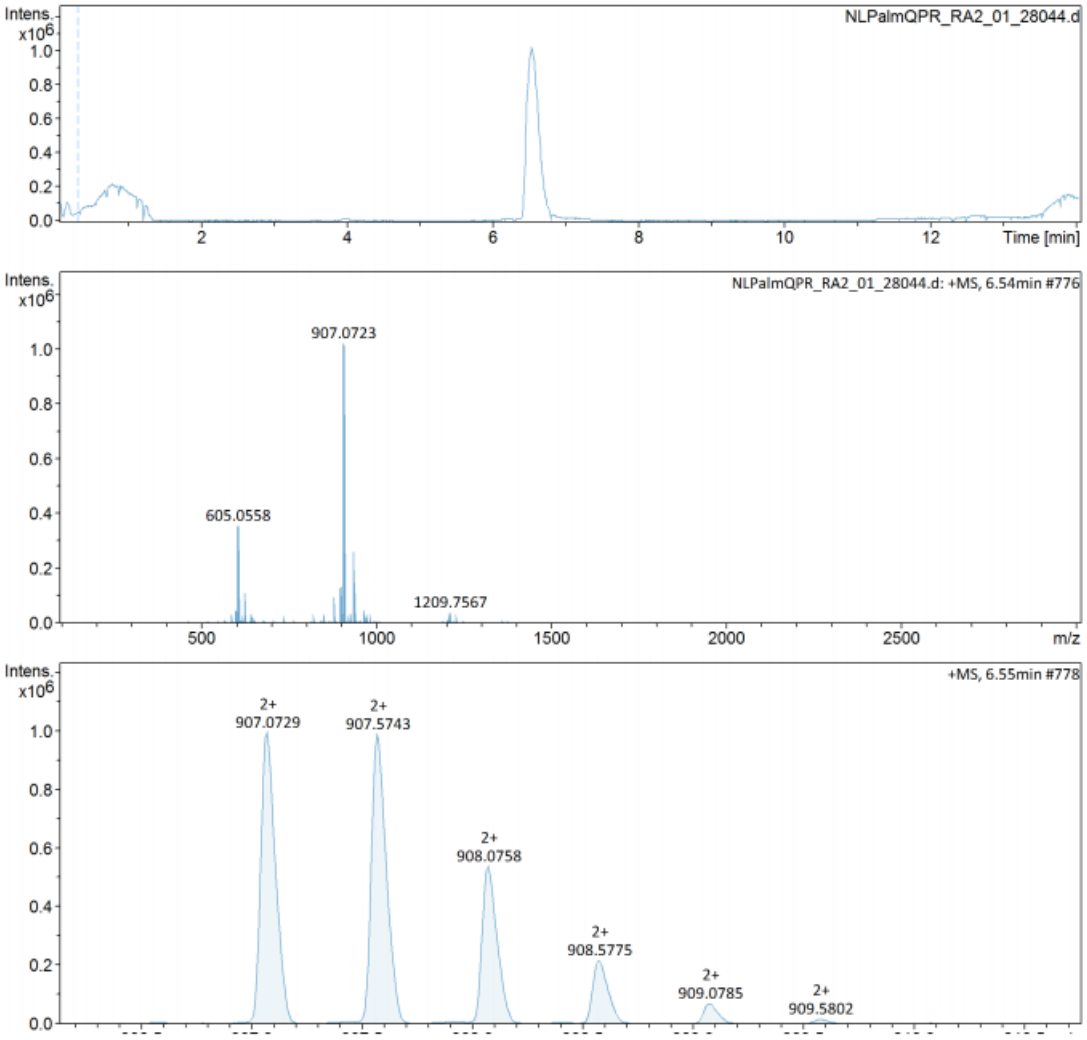

Figure 17: Mass Spectrum of DGD-GG-GFOGER-GG-QPR-Palmitate.

6.9 DGD-GG-GFOGER-GG-EEM-Palmitate

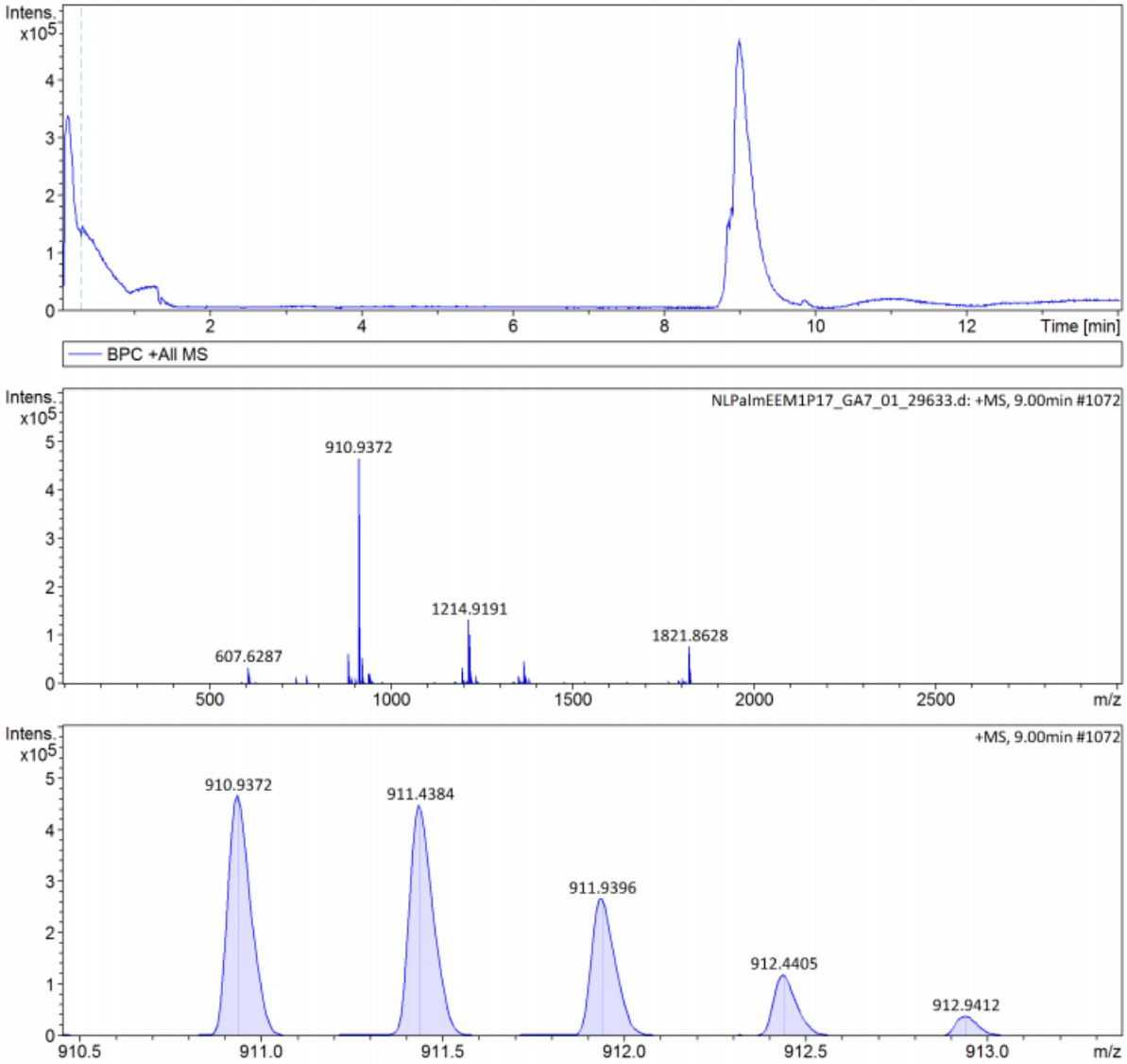

Figure 18: Mass Spectrum of DGD-GG-GFOGER-GG-EEM-Palmitate.

7. NMR SPECTRA OF SELECTED PEPTIDES

7.1 DGRGOF-Adamantate

7.1.1 ^{1}H NMR

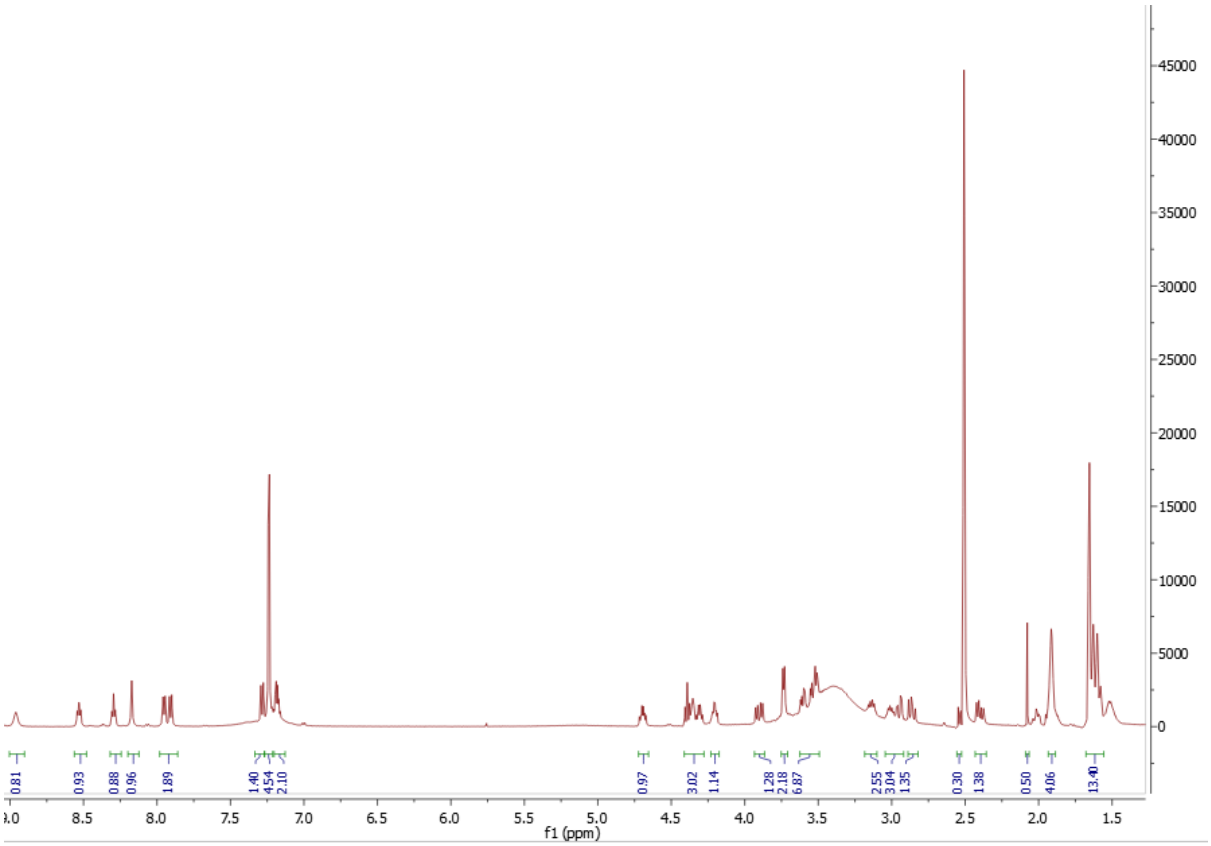

Figure 19: ^{1}H NMR spectrum of DGRGOF-Adamantate.

7.1.2 ^{13}C NMR

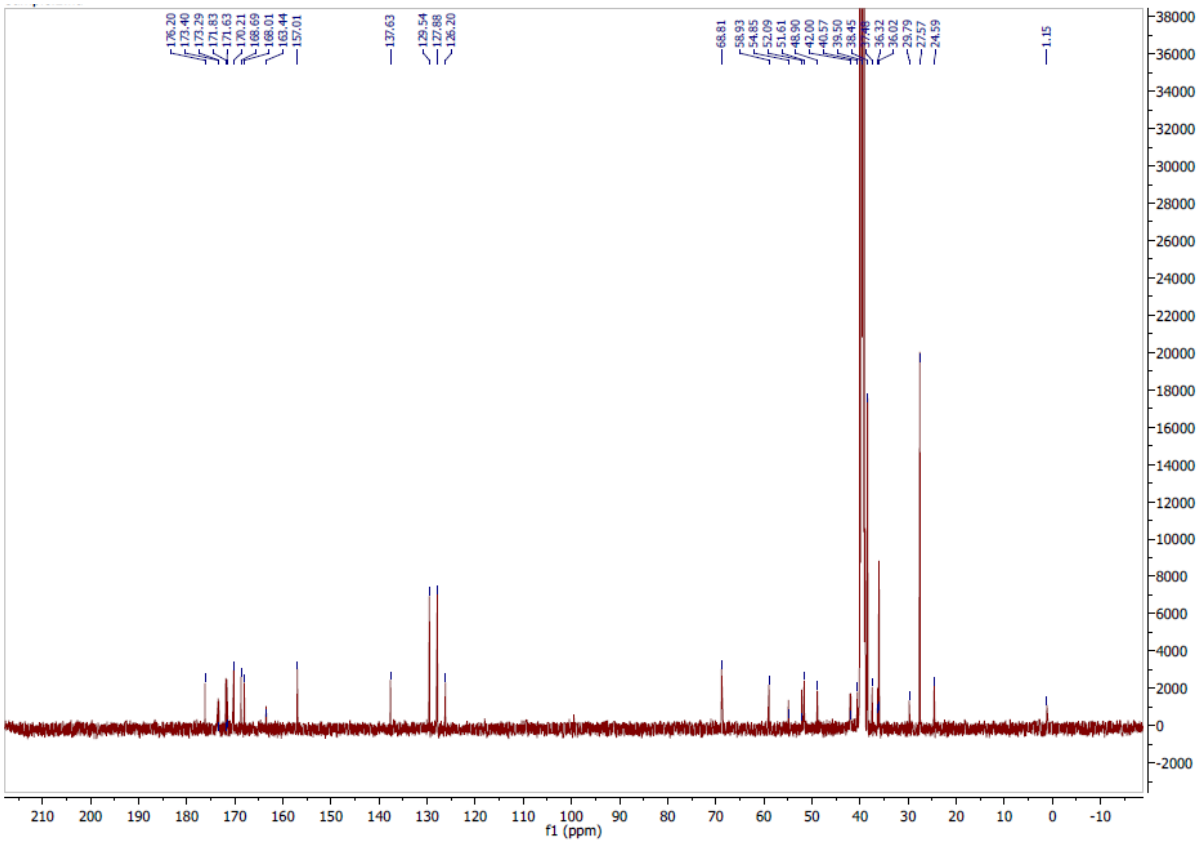

Figure 20: ^{13}C NMR spectrum of DGRGOF-Adamantane.

7.1.3 DEPT 135

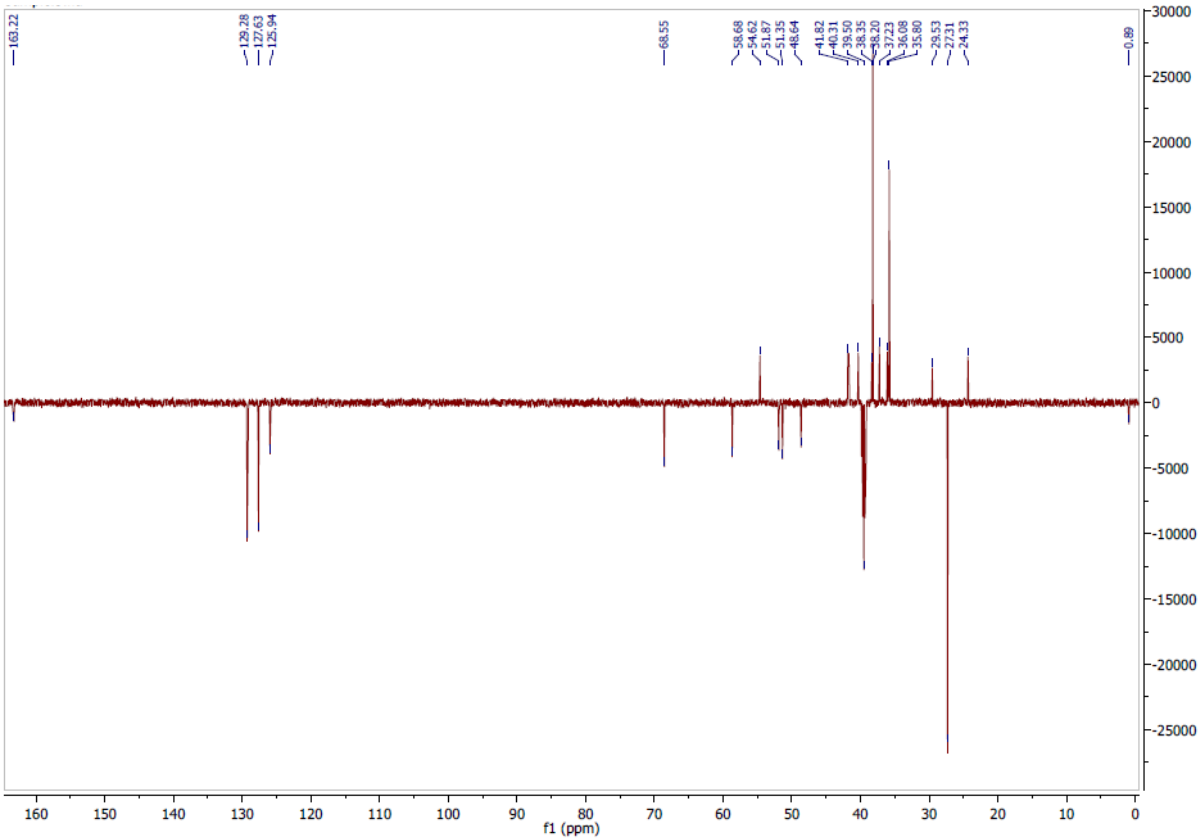

Figure 21: DEPT 135 spectrum of DGRGOF-Adamantane.

7.1.4 COSY

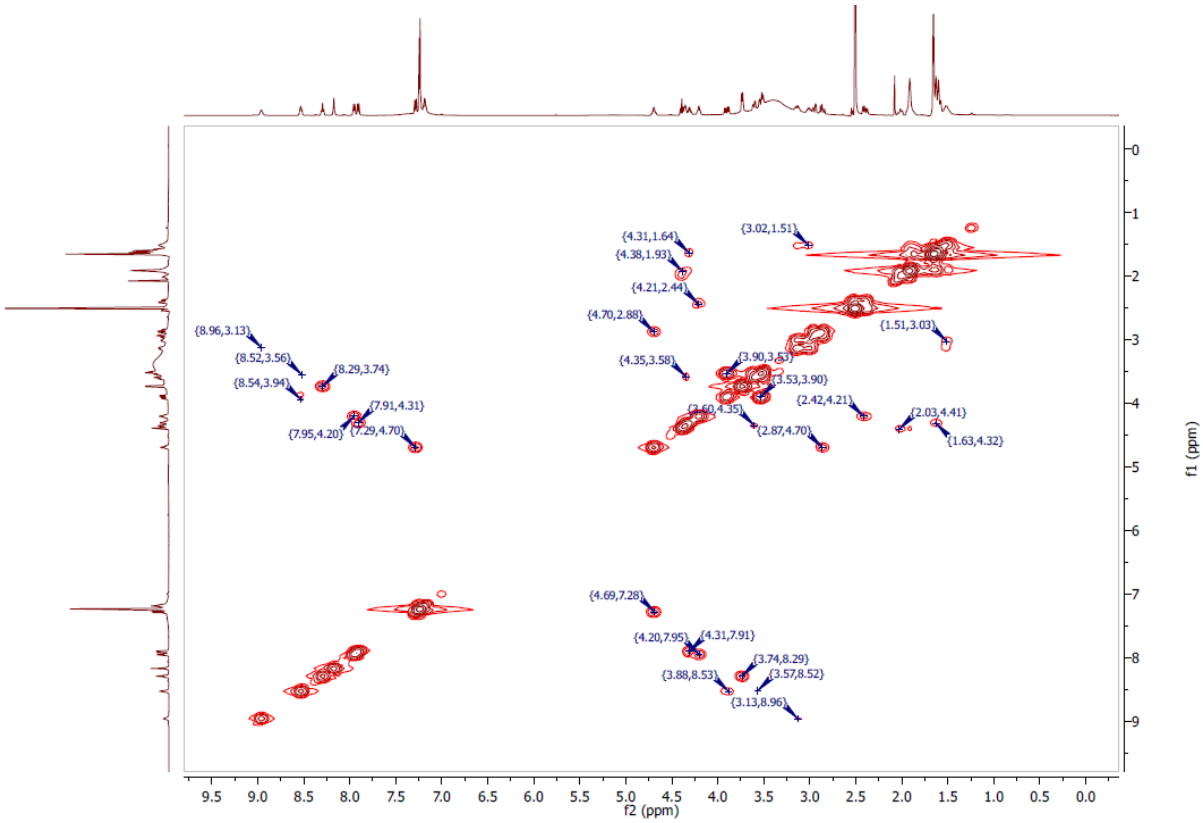

Figure 22: COSY spectrum of DGRGOF-Adamantane.

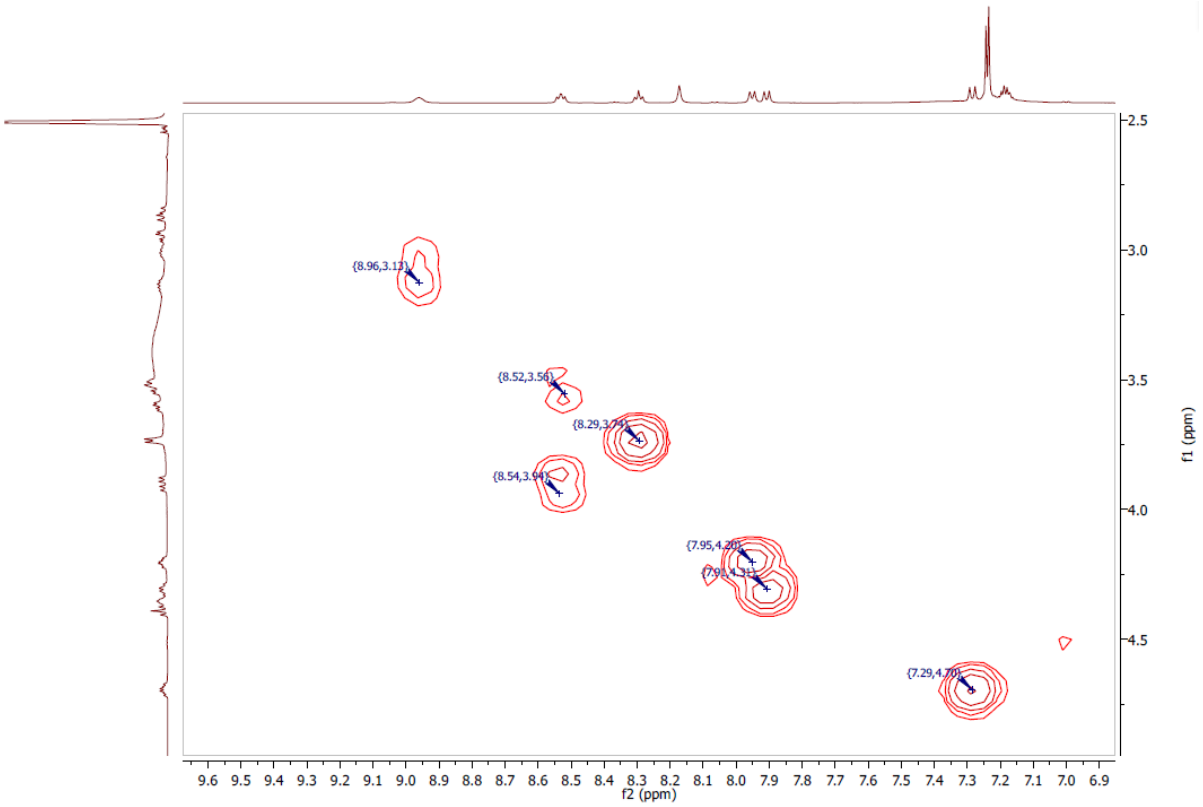

Figure 23: Expanded alpha-amide region from the COSY spectrum of DGRGOF-Adamantane.

7.1.5 HSQC

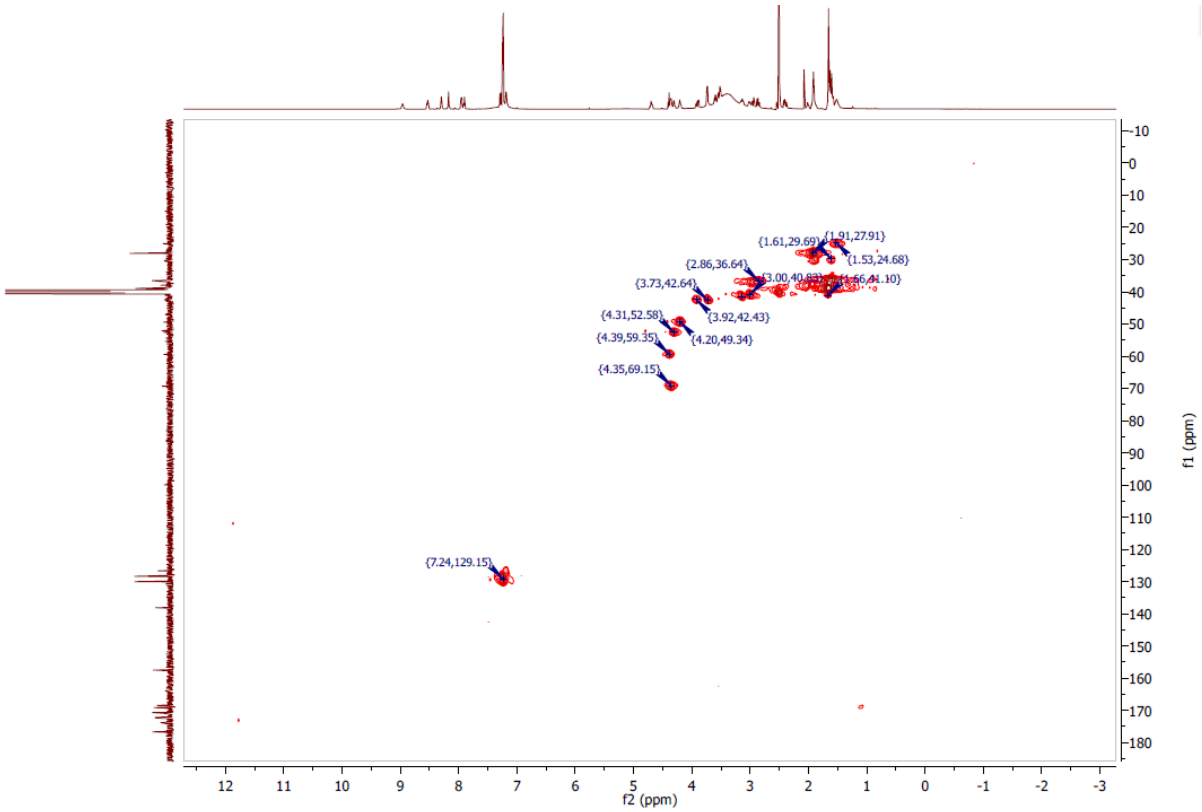

Figure 24: HSQC spectrum of DGRGOF-Adamantane.

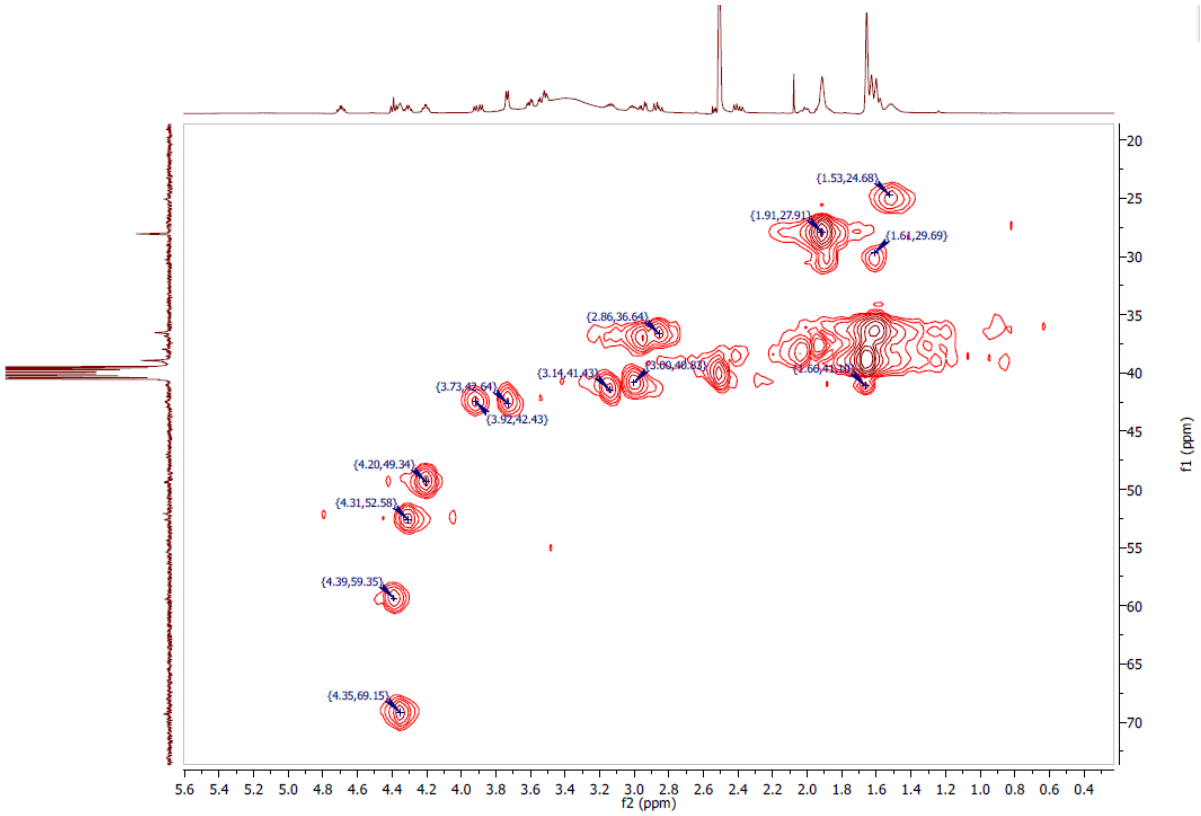

Figure 25: Expanded alpha region from the HSQC spectrum of DGRGOF-Adamantane.

7.1.6 ROESY

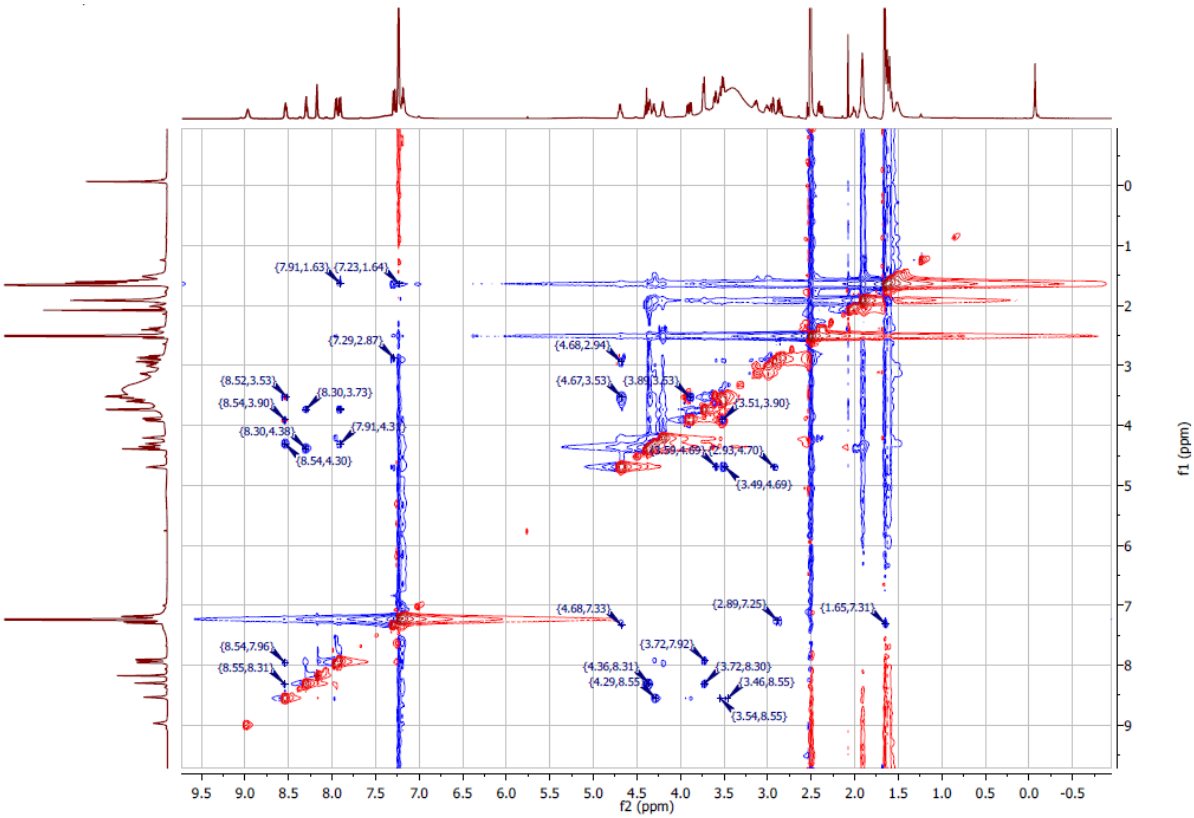

Figure 26: ROESY spectrum of DGRGOF-Adamantane.

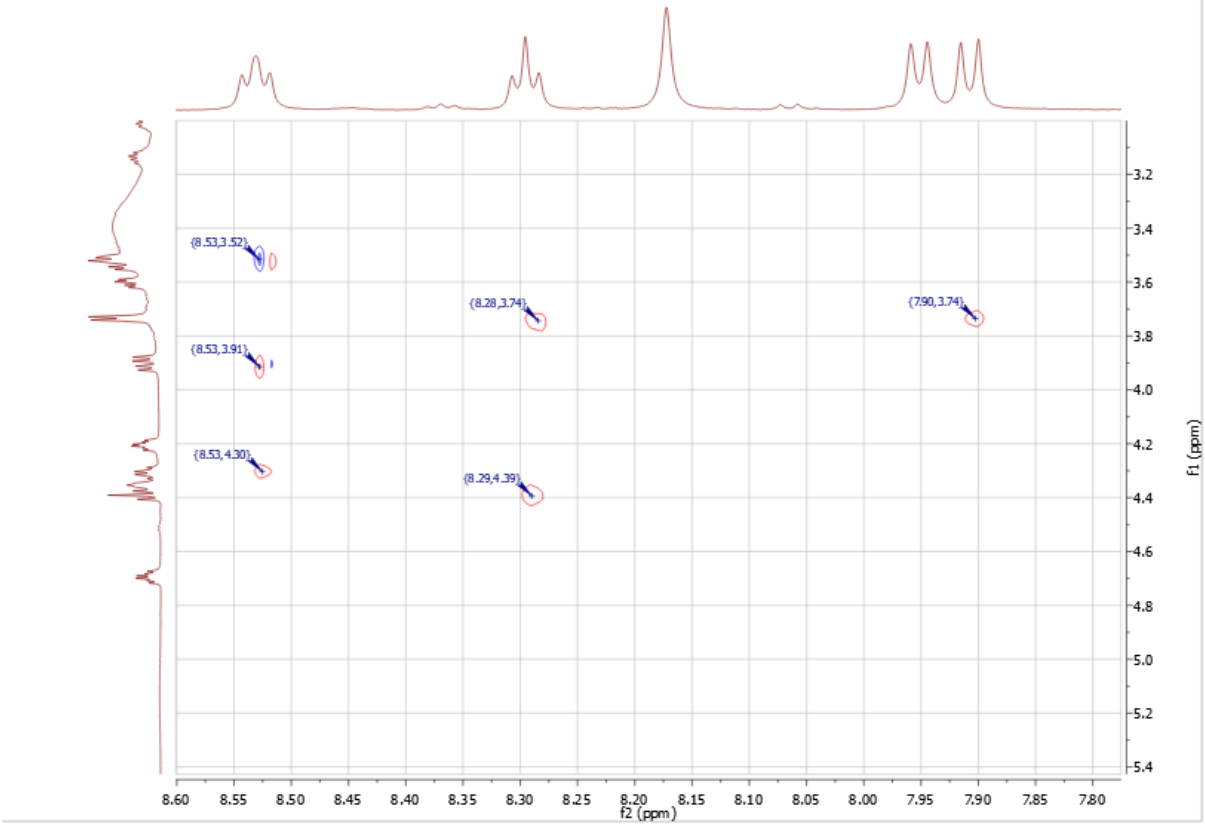

Figure 27: Expanded alpha-amide region from the ROESY spectrum of DGRGOF-Adamantane.

7.2 DGD-GG-GFOGER-GG-TTK-Palmitate

7.2.1 ^{1}H NMR

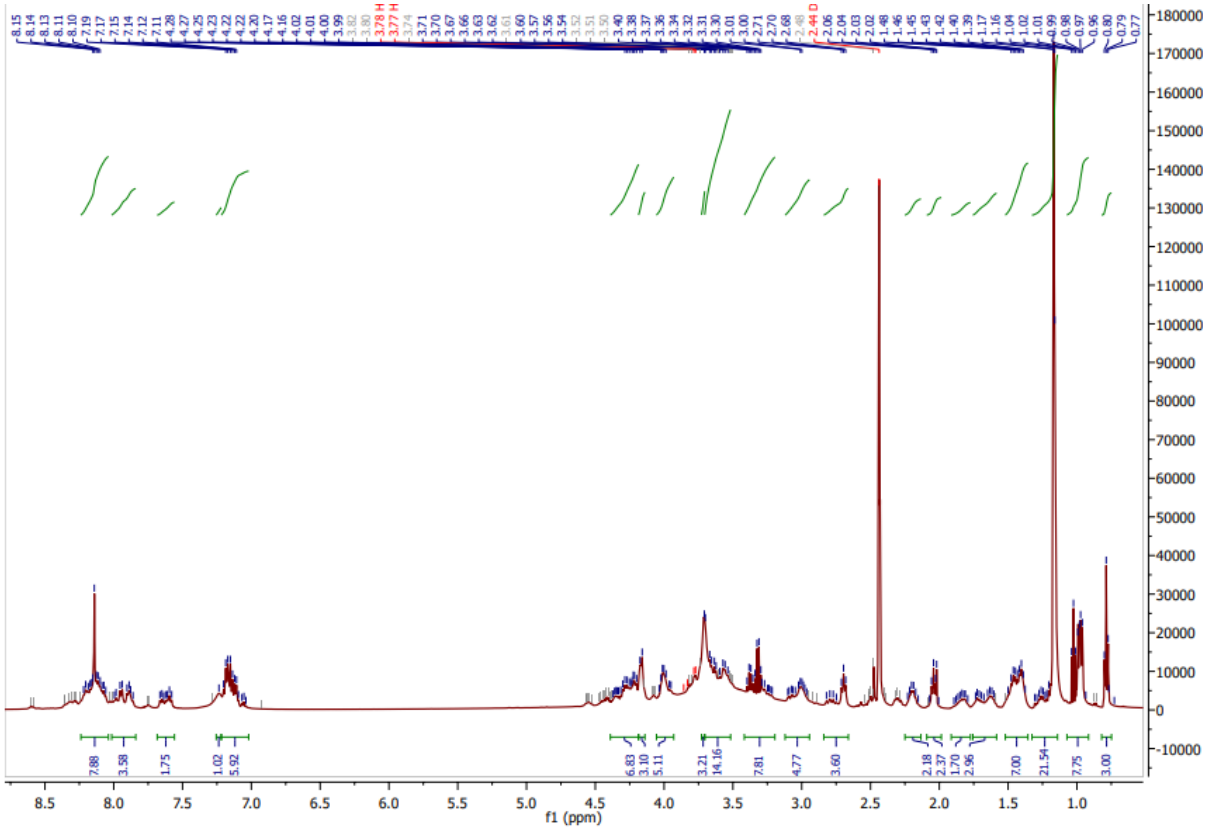

Figure 28: ^{1}H NMR DGD-GG-GFOGER-GG-TTK-Palmitate.

7.2.2 ^{13}C NMR

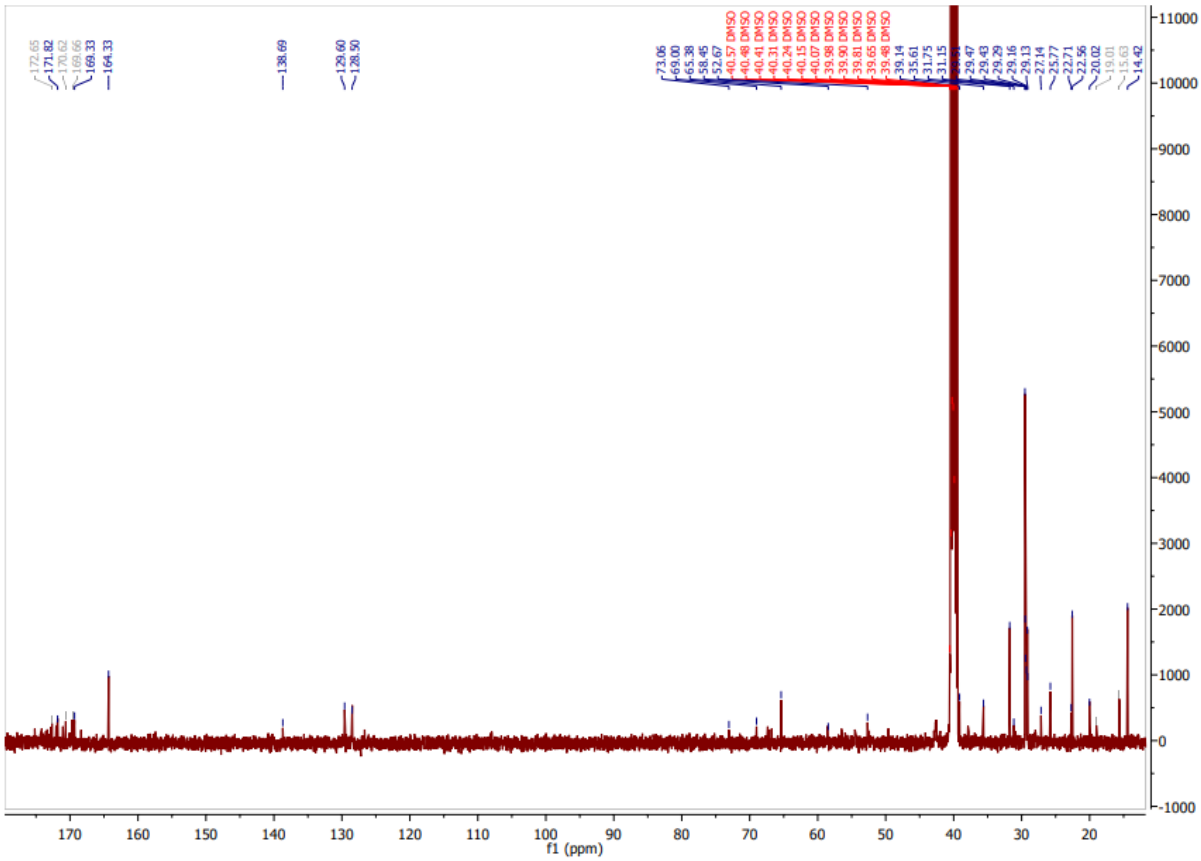

Figure 29: ^{13}C NMR of DGD-GG-GFOGER-GG-TTK-Palmitate.

7.2.3 DEPT

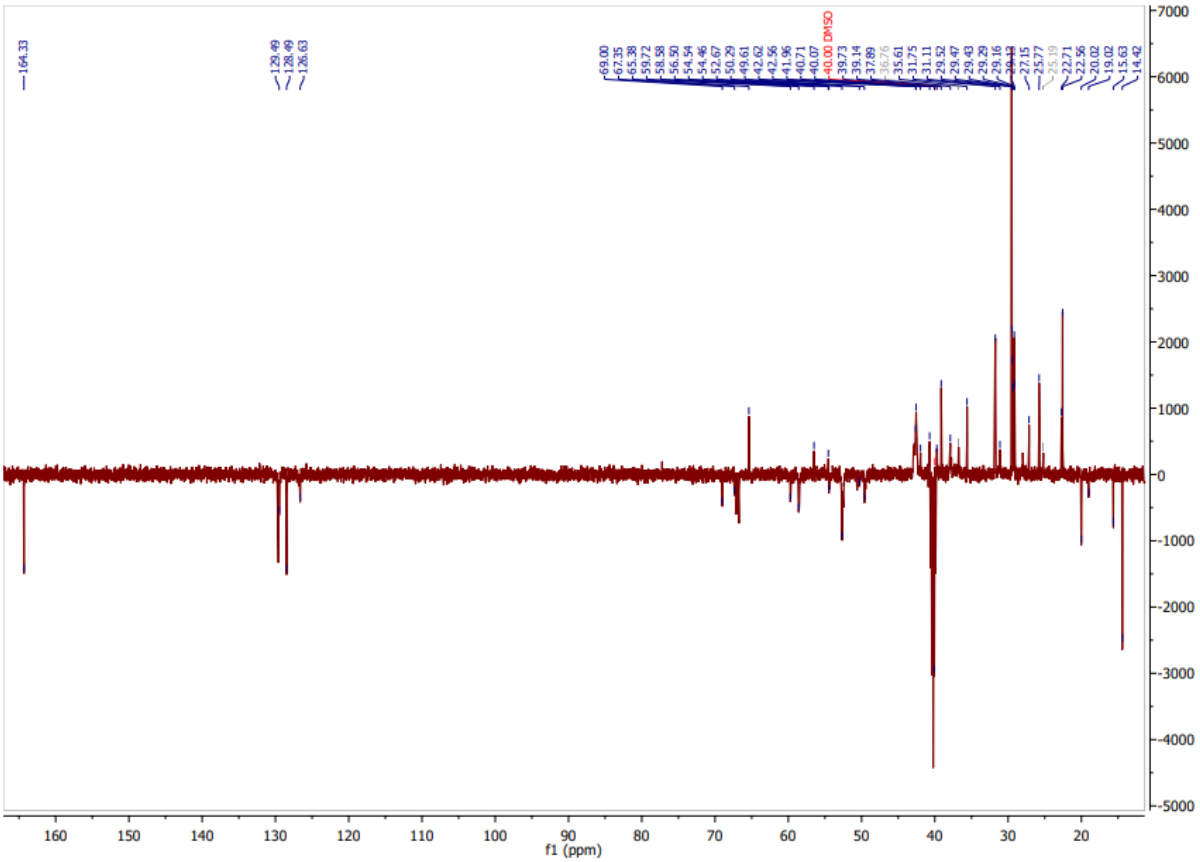

Figure 30: DEPT Spectrum of DGD-GG-GFOGER-GG-TTK-Palmitate.

7.2.4 COSY

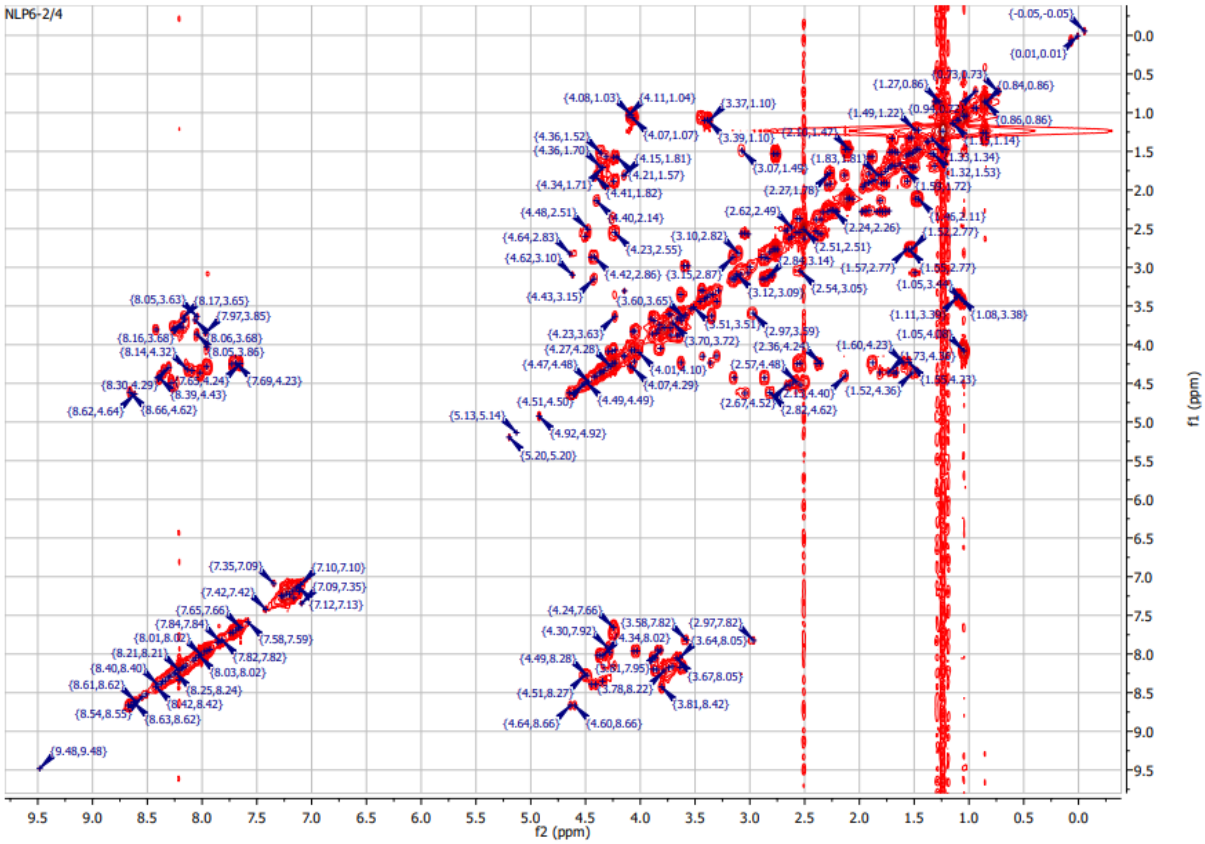

Figure 31: COSY Spectrum of DGD-GG-GFOGER-GG-TTK-Palmitate.

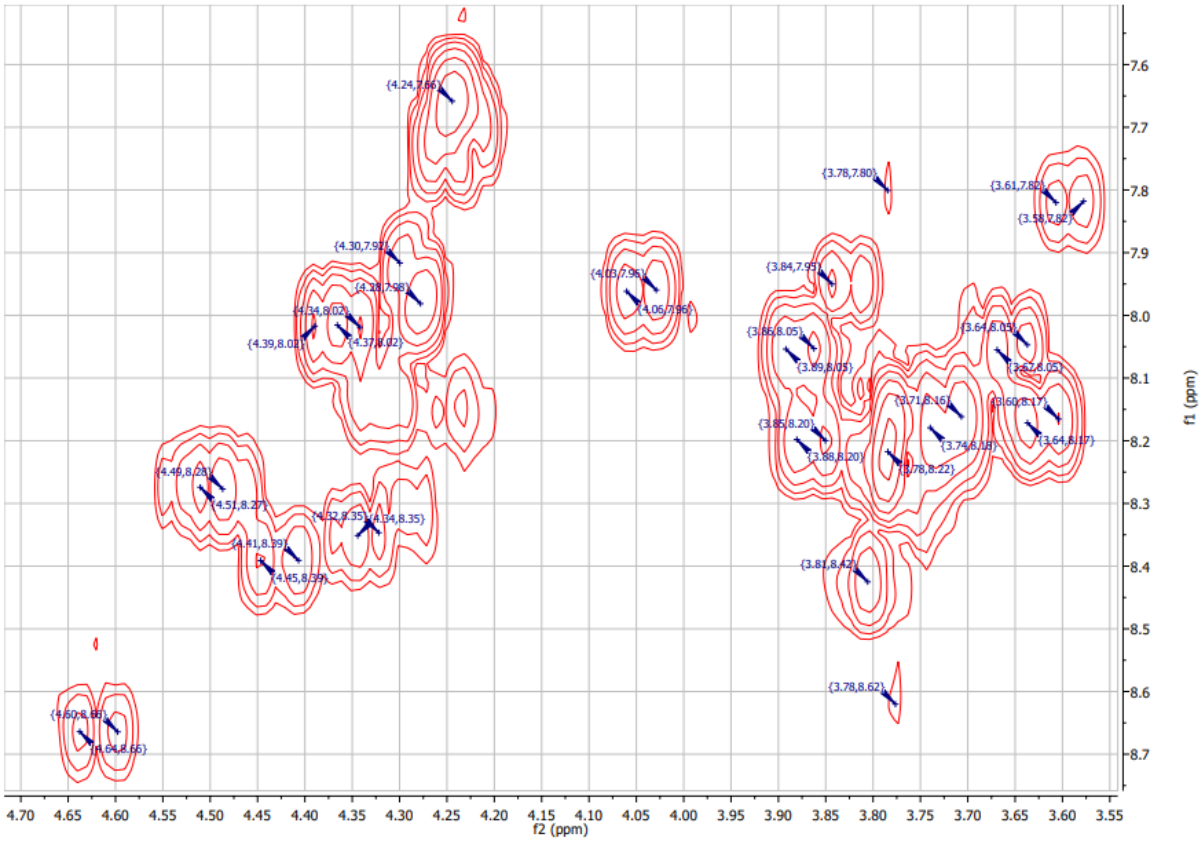

Figure 32: COSY spectrum alpha-amide region of DGD-GG-GFOGER-GG-TTK-Palmitate.

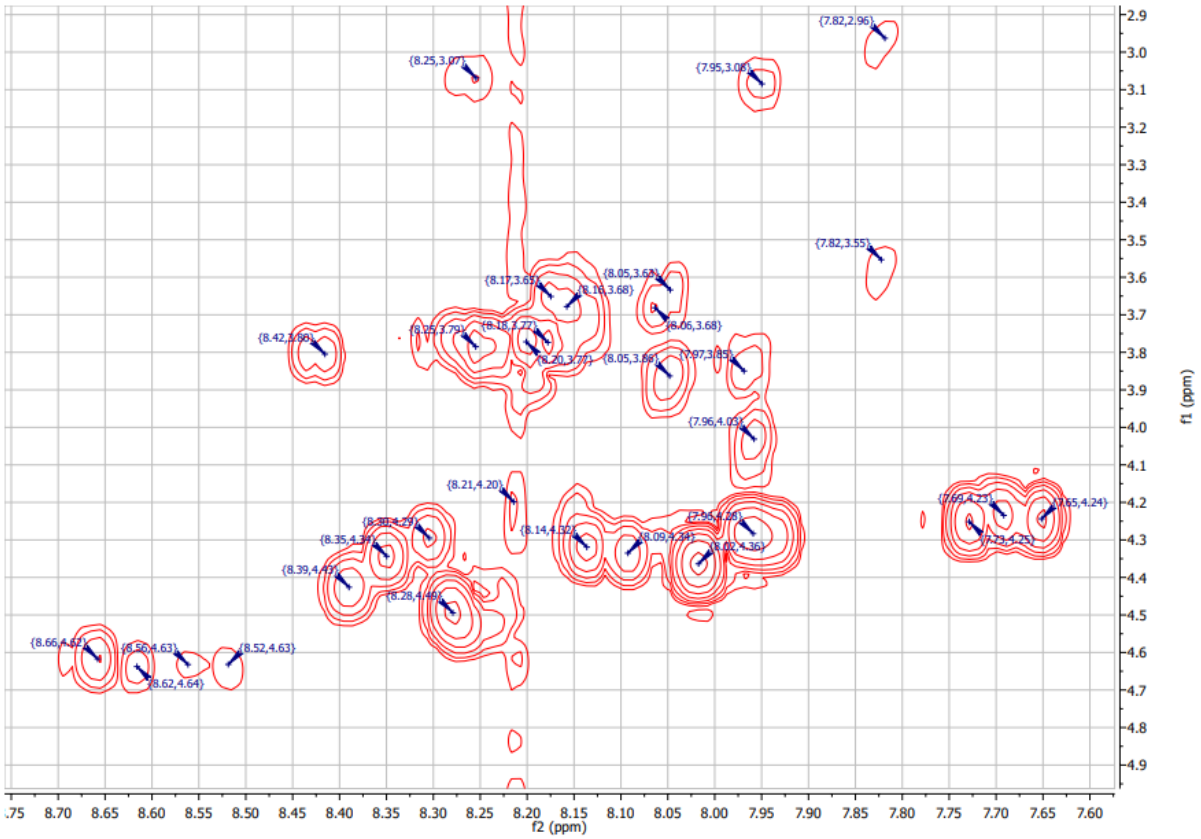

Figure 33: Expanded COSY spectrum of DGD-GG-GFOGER-GG-TTK-Palmitate.

7.2.5 HSQC

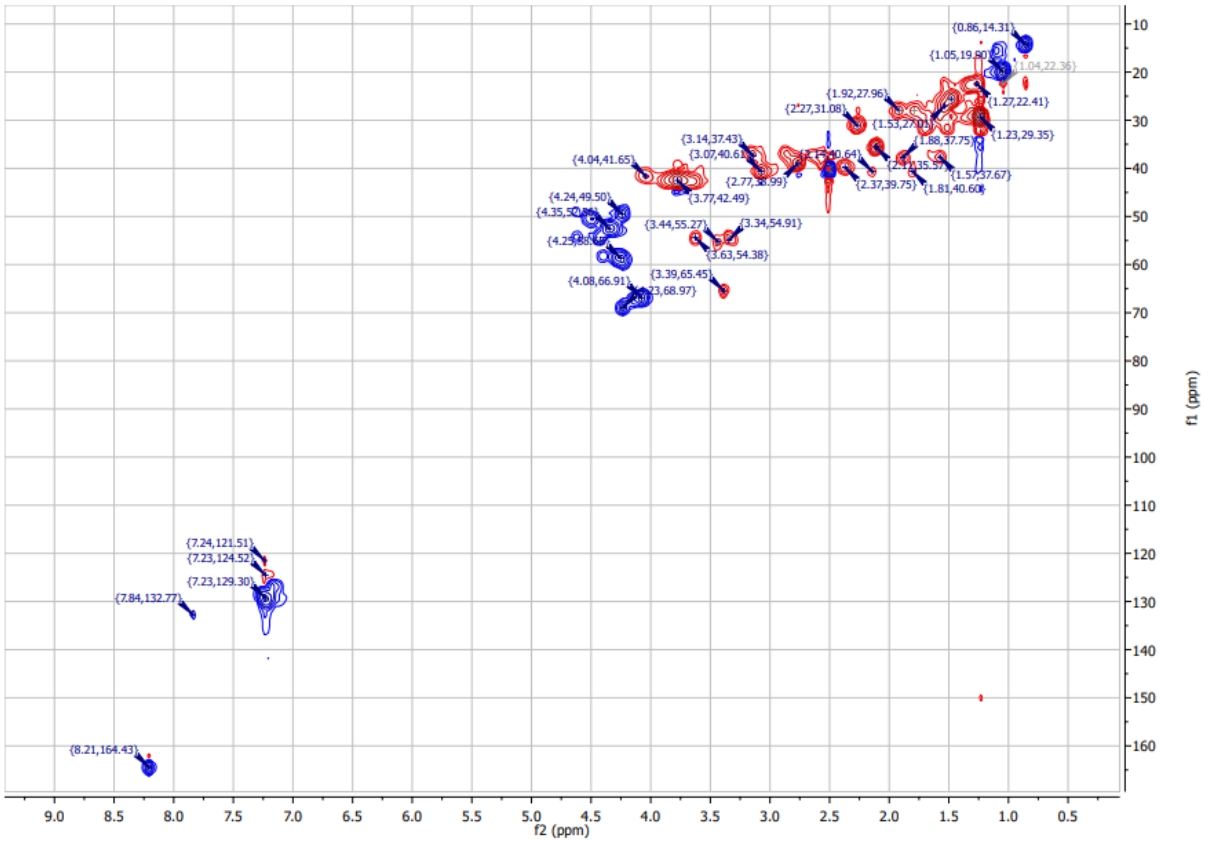

Figure 34: HSQC spectrum of DGD-GG-GFOGER-GG-TTK-Palmitate.

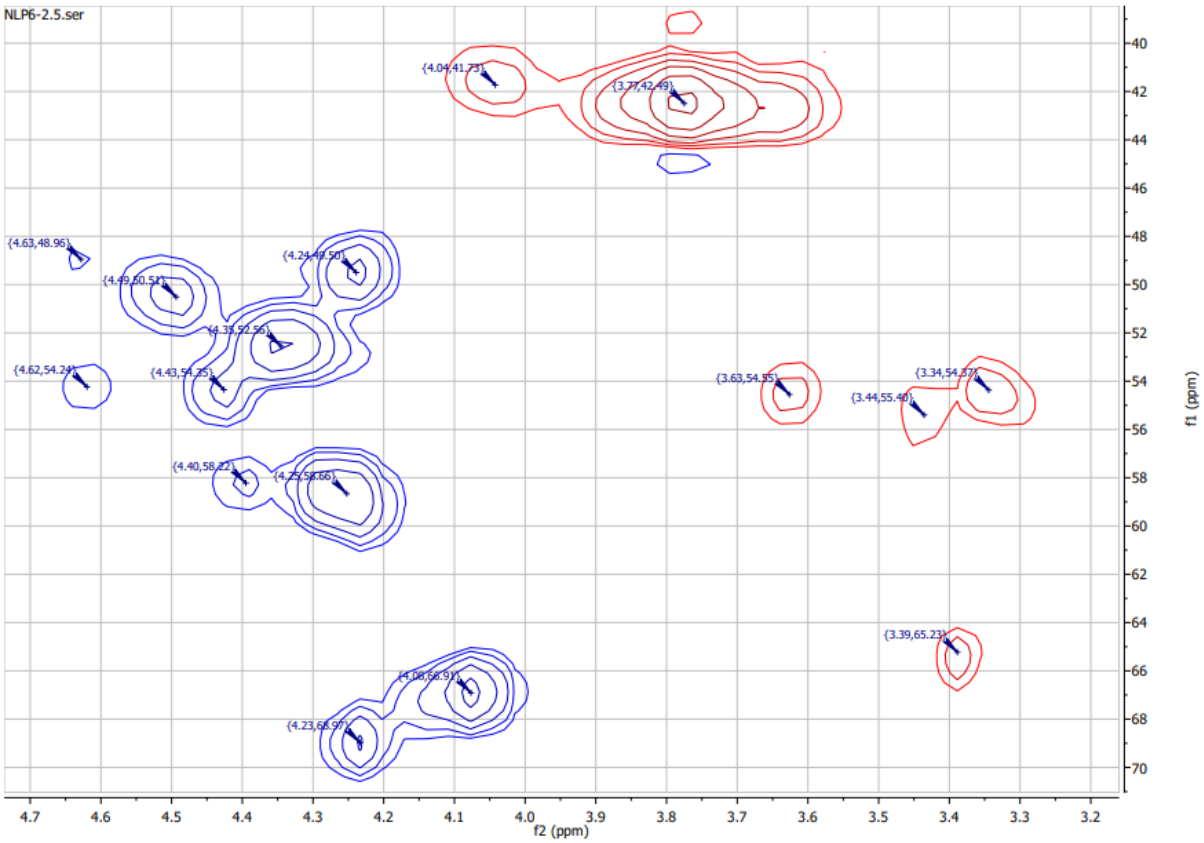

Figure 35: Expanded HSQC spectrum of DGD-GG-GFOGER-GG-TTK-Palmitate.

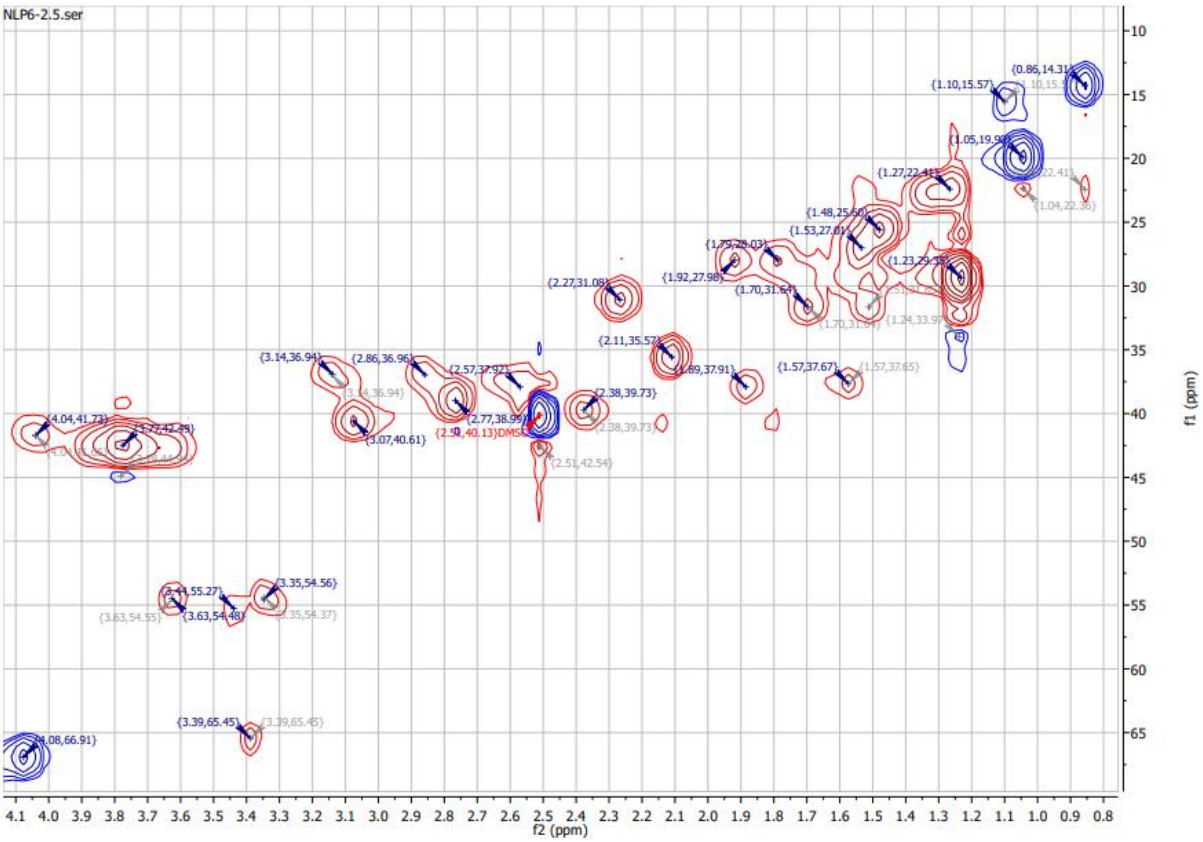

Figure 36: Expanded HSQC spectrum of DGD-GG-GFOGER-GG-TTK-Palmitate.

7.2.6 HMBC

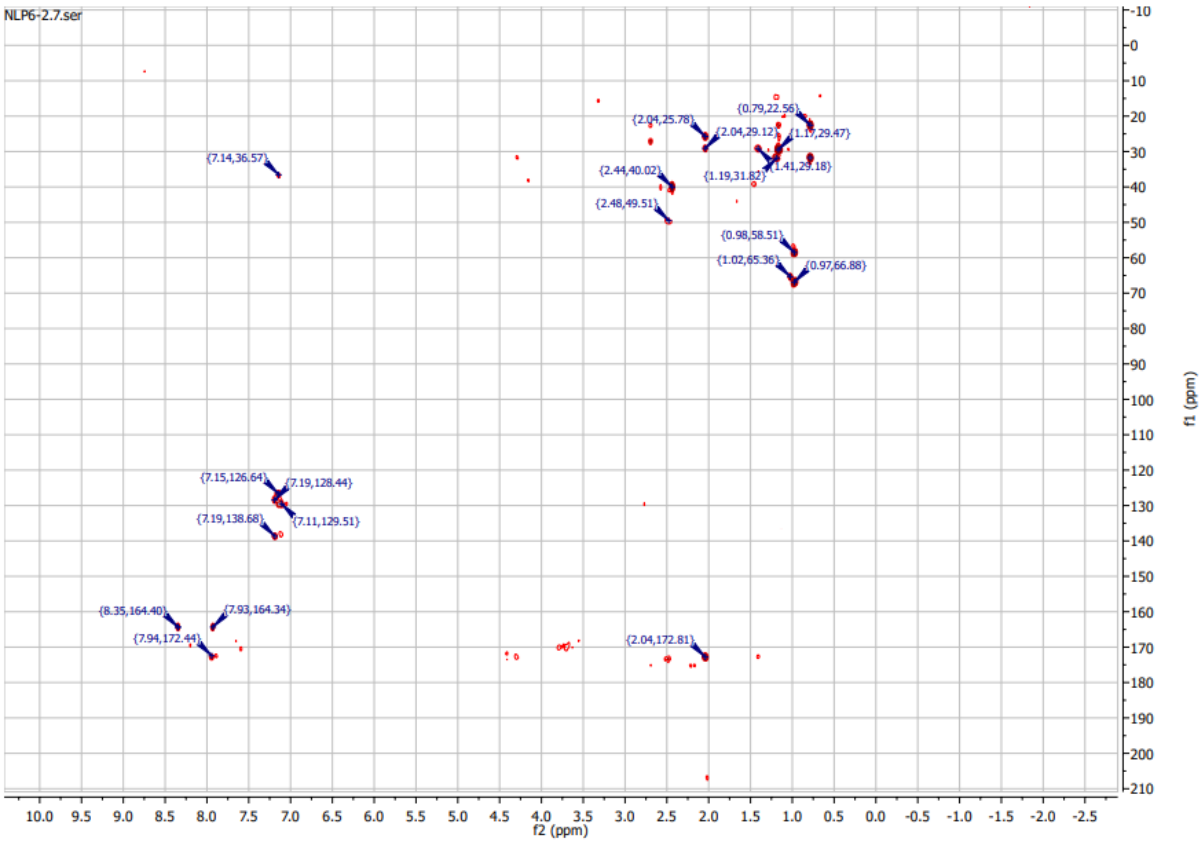

Figure 37: HMBC spectrum of DGD-GG-GFOGER-GG-TTK-Palmitate.

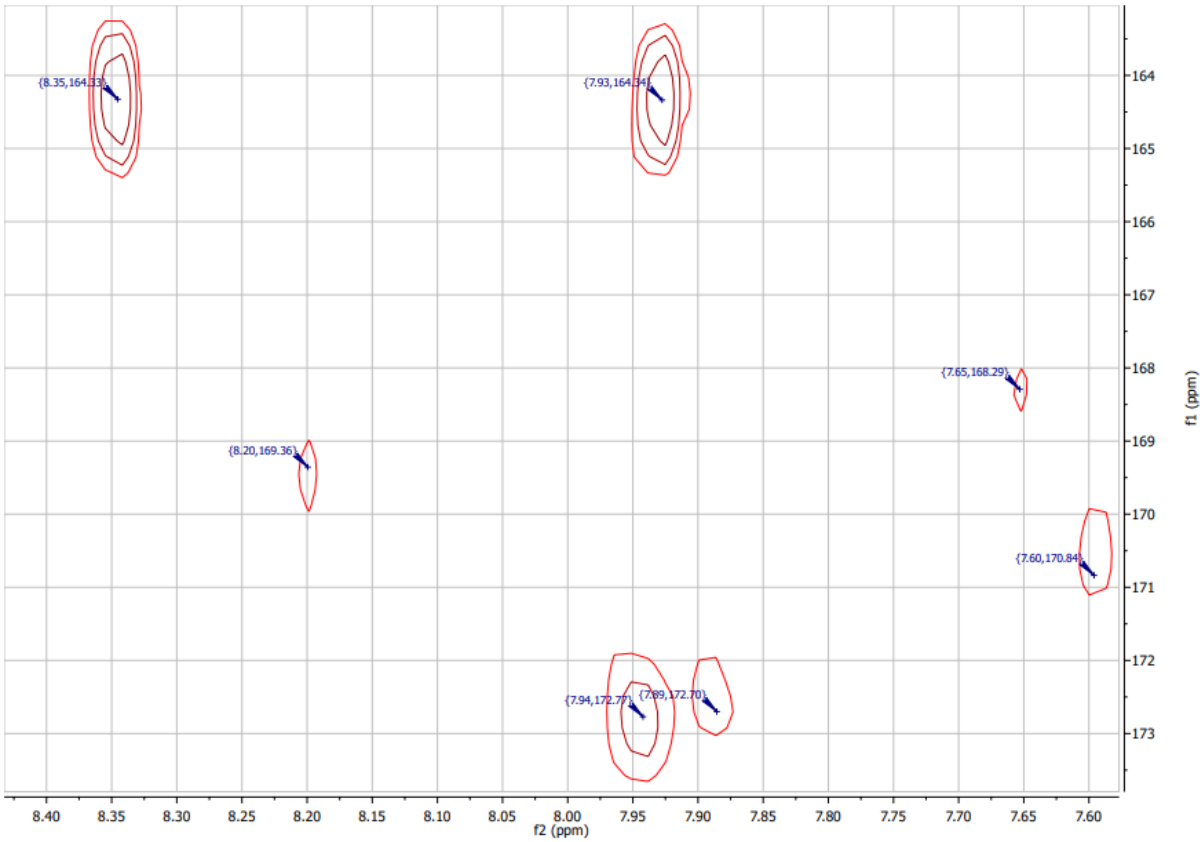

Figure 38: Expanded amide region from the HMBC spectrum of DGD-GG-GFOGER-GG-TTK-Palmitate.

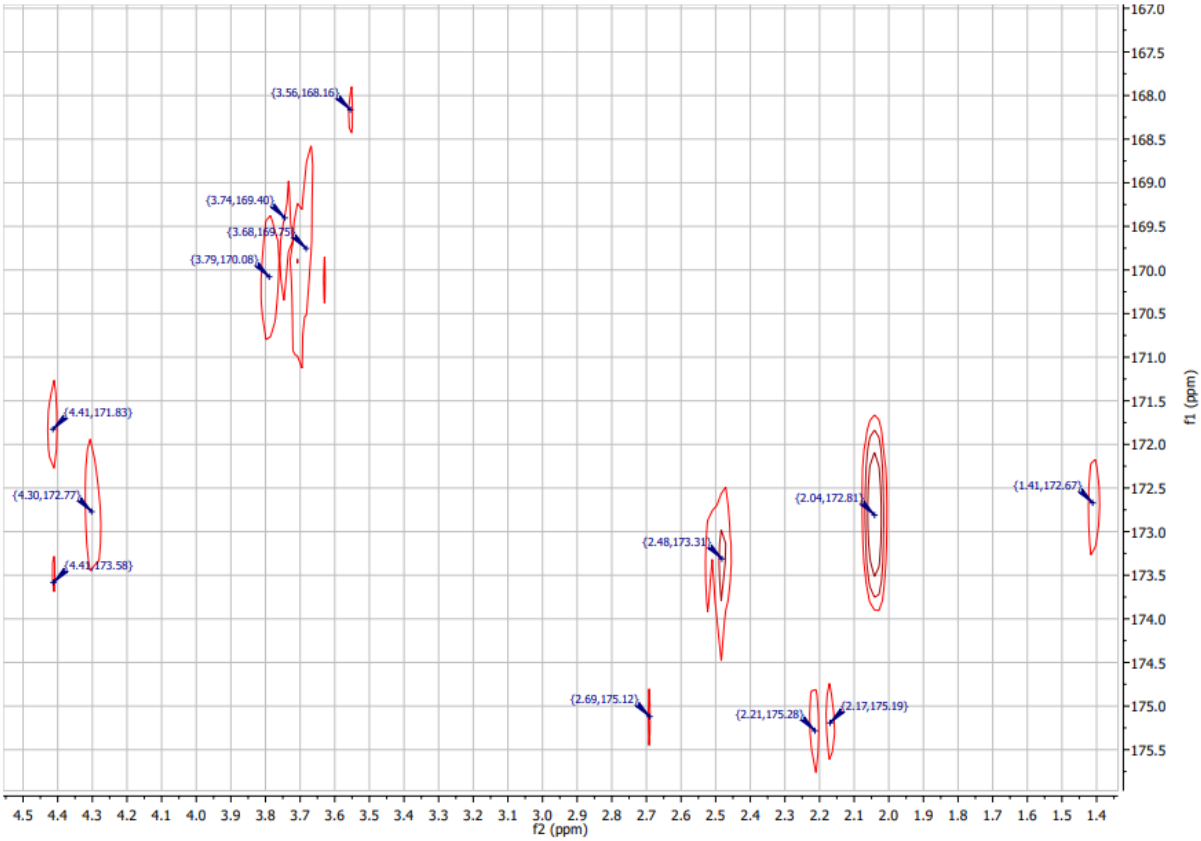

Figure 39: Aliphatic region from the HMBC spectrum of DGD-GG-GFOGER-GG-TTK-Palmitate.

7.2.7 TOCSY

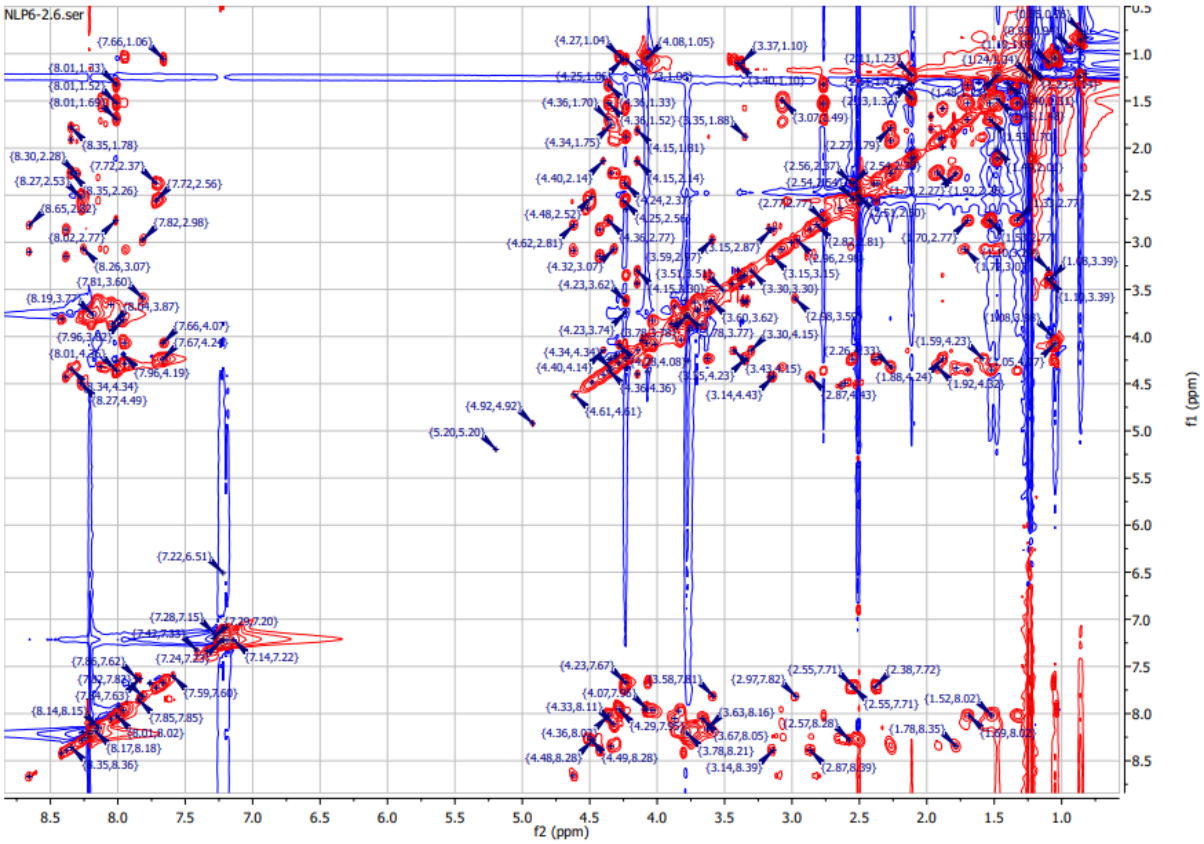

Figure 40: TOCSY spectrum of DGD-GG-GFOGER-GG-TTK-Palmitate.

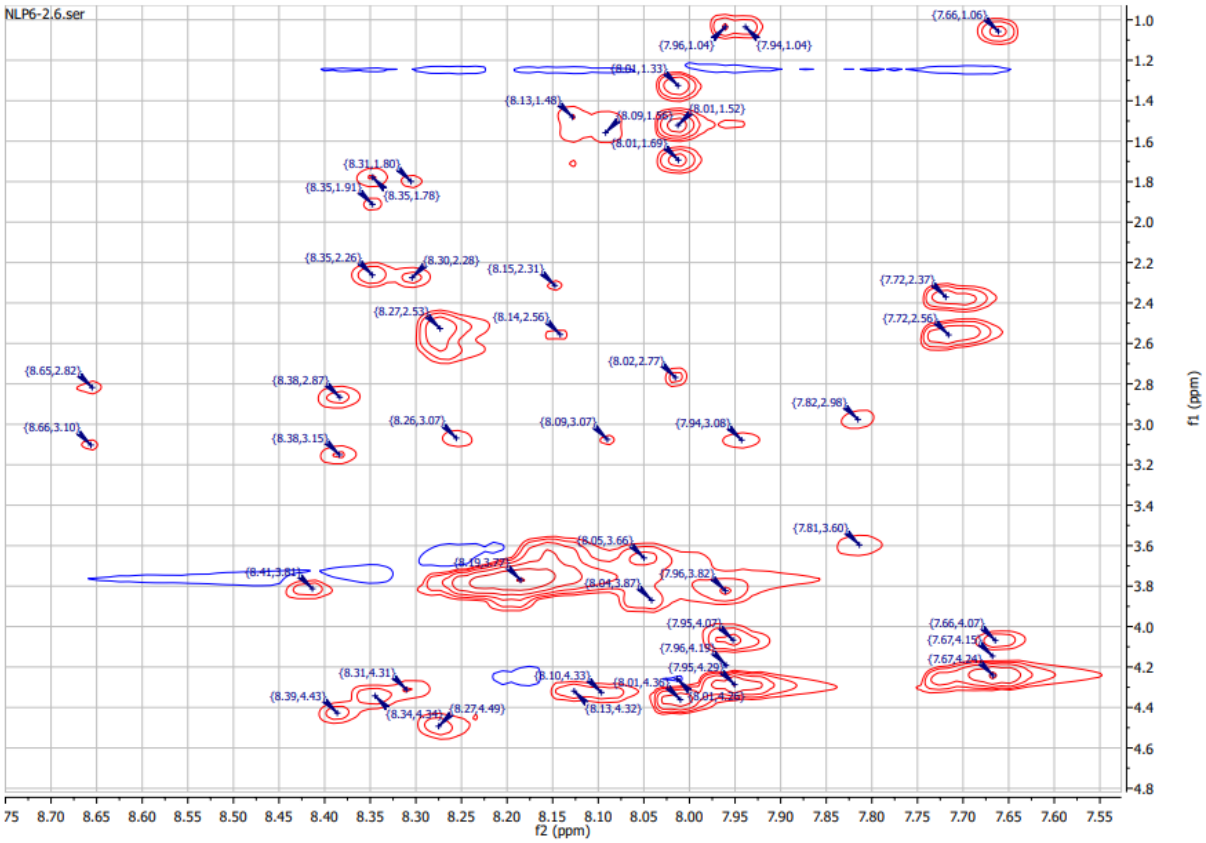

Figure 41: Aliphatic-amide region from the TOCSY spectrum of DGD-GG-GFOGER-GG-TTK-Palmitate.

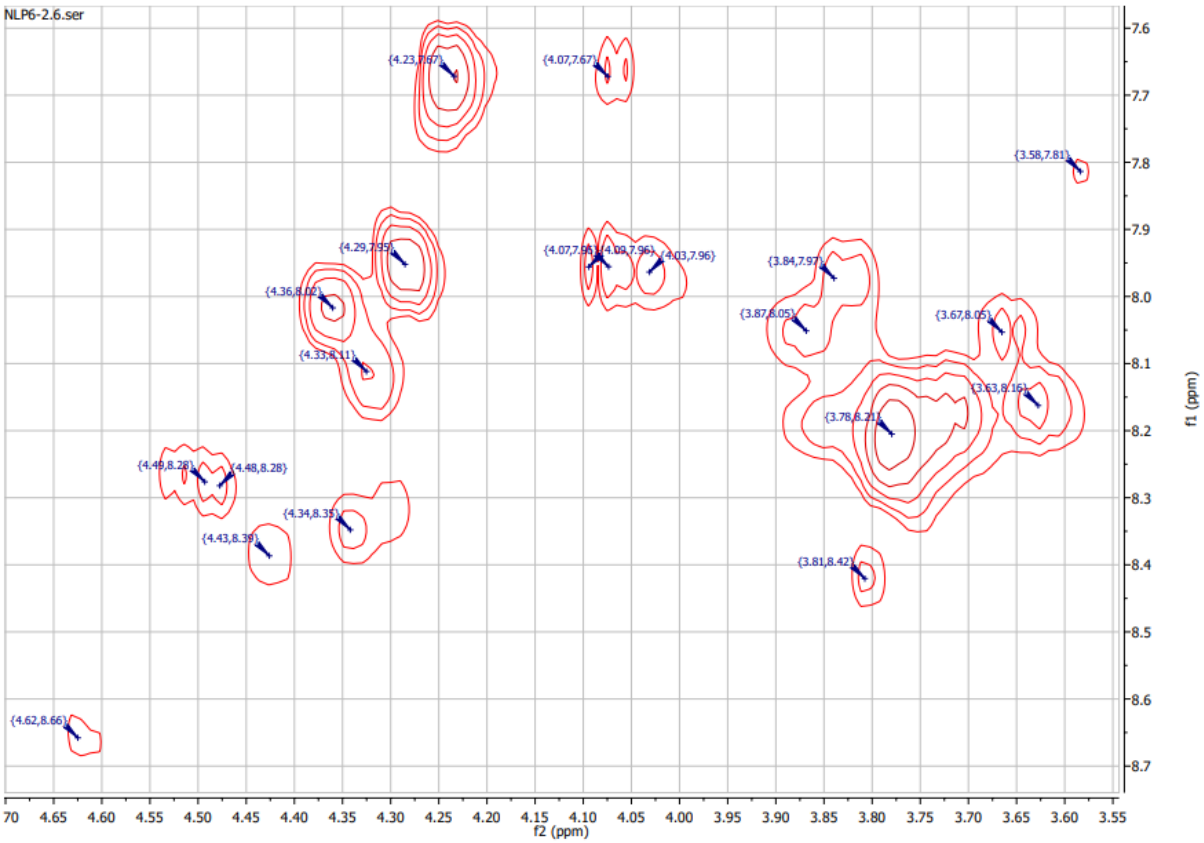

Figure 42: Alpha-amide region from the TOCSY spectrum of DGD-GG-GFOGER-GG-TTK-Palmitate.

7.2.8 ROESY

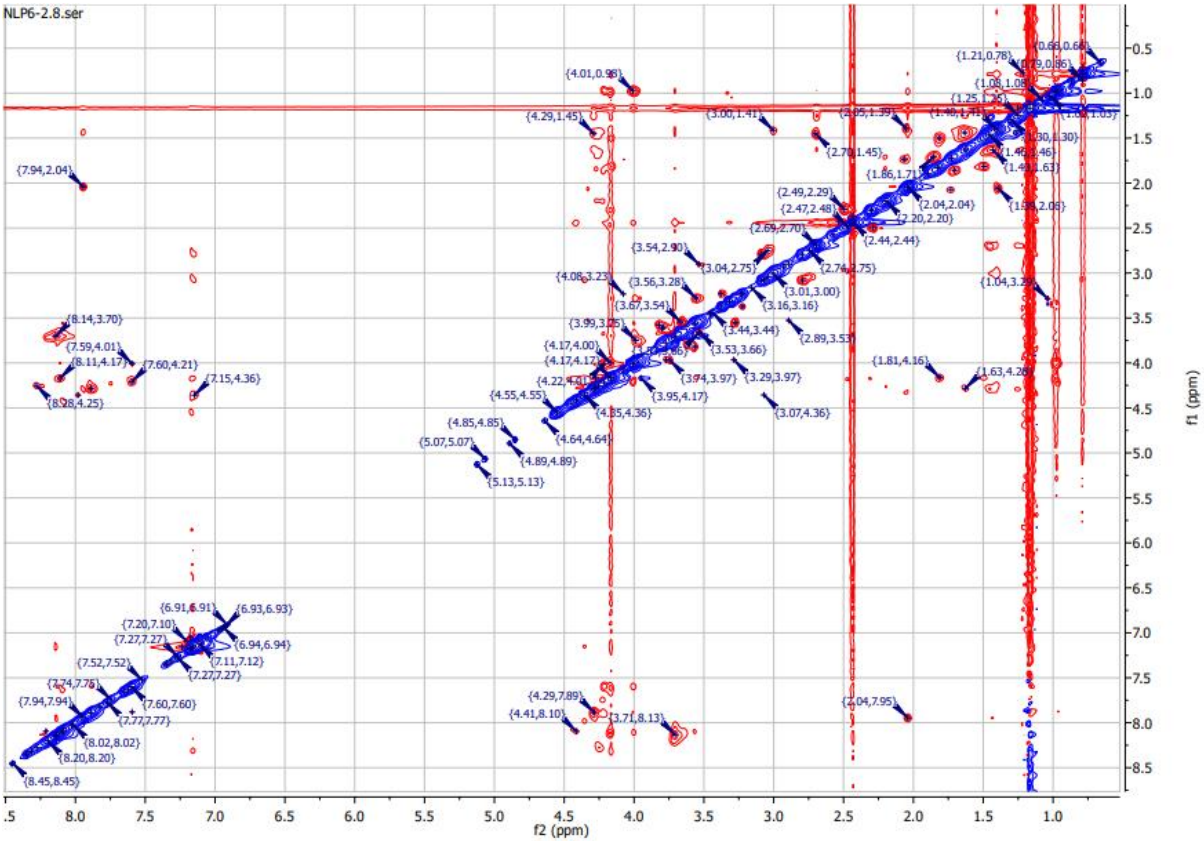

Figure 43: ROESY spectrum of DGD-GG-GFOGER-GG-TTK-Palmitate.

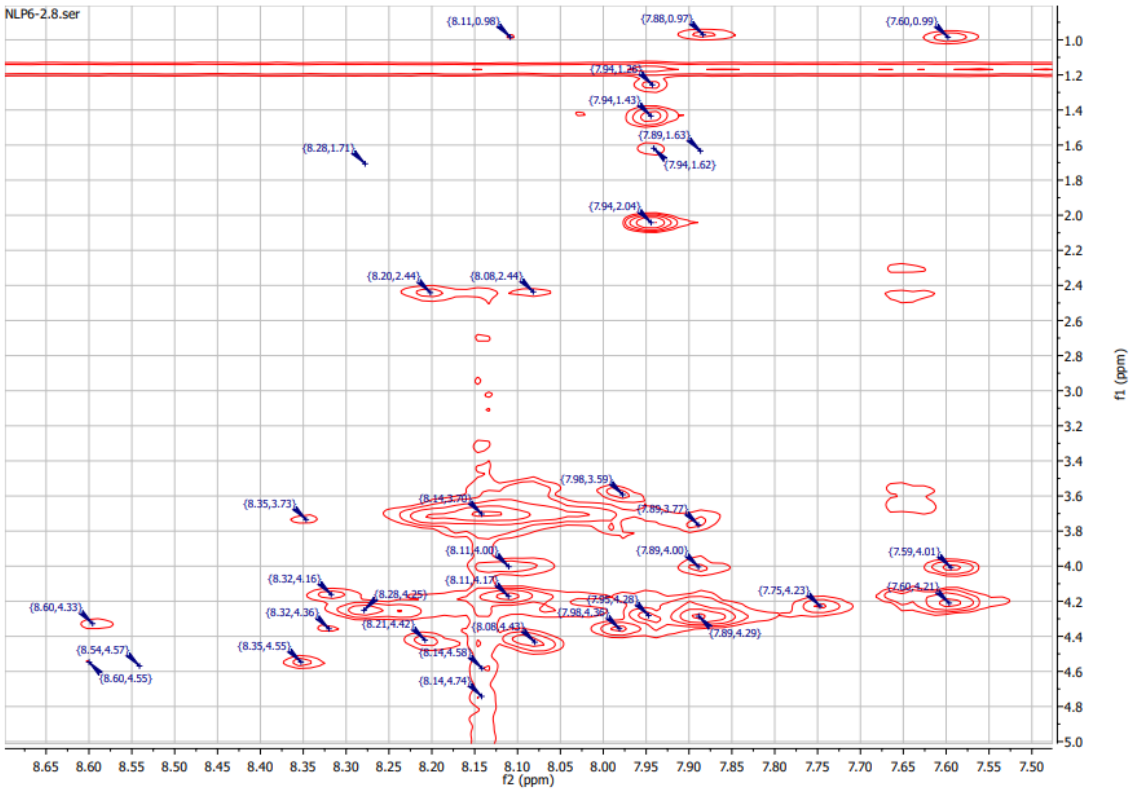

Figure 44: Amide region from the ROESY spectrum of DGD-GG-GFOGER-GG-TTK-Palmitate.

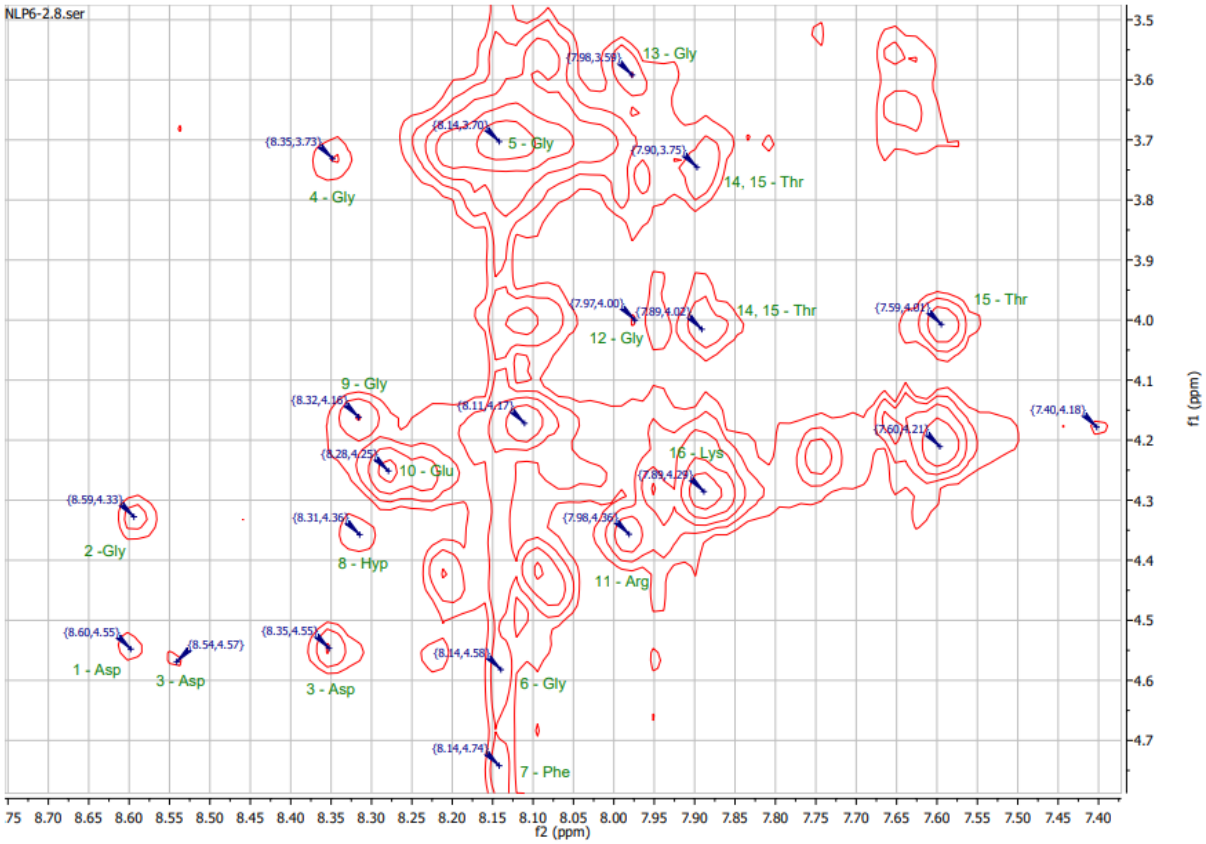

Figure 45: Expanded alpha-amide region from the ROESY spectrum of DGD-GG-GFOGER-GG-TTK-Palmitate.